MICROMECHANICS OF AGGLOMERATE DAMAGE PROCESSES

MARCEL TEODOR CIOMOCOS, BSc, MSc, MSc

Doctor of Philosophy

THE UNIVERSITY OF ASTON IN BIRMINGHAM

July 1996

The University of Aston in Birmingham

MICROMECHANICS OF AGGLOMERATE DAMAGE PROCESSES

Marcel Teodor Ciomocos, BSc, MSc (Civil Engineering),
MSc (Software Engineering)

Thesis submitted for the degree of Doctor of Philosophy
1996

SUMMARY

This thesis reports a detailed investigation of the micromechanics of agglomerate behaviour under free-fall impact, double (punch) impact and diametrical compression tests using the simulation software TRUBAL. The software is based on the discrete element method (DEM) which incorporates the Newtonian equations of motion and contact mechanics theory to model the interparticle interactions. Four agglomerates have been used: three dense (differing in interface energy and contact density) and one loose. Although the simulated agglomerates are relatively coarse-grained, the results obtained are in good agreement with laboratory test results reported in the literature.

The computer simulation results show that, in all three types of test, the loose agglomerate cannot fracture as it is unable to store sufficient elastic energy. Instead, it becomes flattened for low loading-rates and shattered or crushed at higher loading-rates. In impact tests, the dense agglomerates experience only local damage at low impact velocities. Semi-brittle fracture and fragmentation are produced over a range of higher impact velocities and at very high impact velocities shattering occurs. The dense agglomerates fracture in two or three large fragments in the diametrical compression tests. Local damage at the agglomerate-platen interface always occurs prior to fracture and consists of local bond breakage (microcrack formation) and local dislocations (compaction). The fracture process is dynamic and much more complex than that suggested by continuum fracture mechanics theory. Cracks are always initiated from the contact zones and propagate towards the agglomerate centre. Fracture occurs a short time after the start of unloading when a fracture crack "selection" process takes place. The detailed investigation of the agglomerate damage processes includes an examination of the evolution of the fracture surface. Detailed comparisons of the behaviour of the same agglomerate in all three types of test are presented. The particle size distribution curves of the debris are also examined, for both free-fall and double impact tests.

Key words: computer simulation
fracture
impact
diametrical compression
particle technology

To my parents, Felicia and Teodor

and

in the memory of my grandparents, Alexandru, Ilie, Floare and Elisabeta.

ACKNOWLEDGEMENTS

I would like to thank my research supervisor, Dr. Colin Thornton, for his enthusiasm, encouragement and support throughout the duration of my research work on this project. I am grateful for his help in organising the project, for his advice, guidance and for his patience during the preparation of the thesis. I also wish to thank Professor Michael J. Adams of Unilever Research, Port Sunlight Laboratories for his useful advice and encouragement.

I am grateful to Unilever Research Port Sunlight Laboratories for financial support and to the Committee of Vice-Chancellors and Principals of the Universities of the U.K. for the three-year Overseas Research Studentship award.

I am also indebted to my parents, Professor Felicia D. S. Ciomocos and Dr. Teodor Ciomocos, for their generous financial support during most of the writing up of this thesis and for their encouragement in the most difficult moments of the project.

I appreciate the help and co-operation of Dr. David Kafui, who also provided technical assistance during the project. As to my other fellow colleagues - Dr. K. Yin, Dr. G. Sun, Dr. Z. Ning, Dr. G. Lian and L. Toland - I value their encouragement and support on numerous occasions during the project.

My appreciation also goes to Dr. Roger Kettle (ex-Head of the Department of Civil Engineering) for the support provided when I first started research at Aston University. I finally wish to acknowledge that I enjoyed working and living in Great Britain during my research programme.

CONTENTS

LIST OF FIGURES

LIST OF TABLES

CHAPTER 1

INTRODUCTION

1.1 PARTICULATE MATERIALS AND AGGLOMERATES

Mankind has benefited from particulate systems since its beginnings. The early production of ceramic handicraft (pottery) and milling of flour represented chief industries for thousands of years. Mining and mineral processing has increased our familiarity with particulates, whereas the understanding of soils and construction materials has played an important role in the development of civil engineering (Ennis et al, 1994).

Particulate materials are nowadays critical to most industrial products. As an example, a dominant percentage of the products manufactured by Unilever are powders, granules/agglomerates, dispersions, flakes, slurries, pastes, or heterogeneous solids incorporating particulates. Particle technology is vital to the chemical and pharmaceutical industries, but also to other sectors including food and detergent processing, advanced materials, mining, minerals processing, agriculture, munitions, energy and the environment.

There is an increasing interest in the behaviour and strength of particulates in the four main industrial stages they experience: processing (creation of products from particulate material - including mixing, agglomeration, crushing), transportation and handling, storage and utilisation of the end-product. Whereas transportation and storage are usually concerned with attrition of particulate material (trying to prevent their unwanted degradation/breakage), processing and end-use are also concerned with comminution, as often the particulate material needs to be reduced in size.

There are two distinct states of powder (particulate material): dispersed (single particles) or flocculated. In the dispersed condition, being separated from each other, the system of particles behaves similar to a fluid. In the flocculated states particles are in contact with each other, in chain structures, as agglomerates, aggregates or powder compacts. These structures behave similar to bulk solids, exhibiting elasticity, plasticity, fracture and shear failure under applied loads.

Due to dynamic effects and to a multitude of adhesion forces and mechanisms, very small particles of different materials usually form clusters, or agglomerates. These "naturally" formed agglomerates are generally coarse-grained (have a relatively small number of constituent particles) and loose. Many industries (including mineral processing, pharmaceuticals, detergent and food industries) favour agglomerated products to fine powders, mainly because they flow easier and are less prone to dust formation (see Adams

et al, 1989). Many agglomerates are, therefore, created artificially in industry through forcibly bringing together very small particles. The three main categories of agglomeration processes are cumulative granulation, pressing and crystallisation.

In cumulative granulation (or size enlargement) processes - such as mixing, pelletization, nodulizing, drumming, sieving or collision of particles in a gas fluidized bed - particles deposit themselves on one another due to environmental forces (gravity, inertia, drag, etc.) and interparticle attraction forces. Agglomerates so formed are usually spherical. As adhesion decreases with size, attractive forces will be sufficient only in the case of small particles; for granulating large particles binders are commonly used.

Pelletization, or balling, is today used on a very large scale in the processing of ores, creation of most ceramics, preparation of cement, minerals, fertilisers, dyestuffs, chemicals, pharmaceuticals, foodstuffs, fodder, fluorspar, etc. (Kapur and Fuerstenau, 1967, Rumpf, 1990, Kelly and Macmillan, 1986). Pelletization consists of the following main processes: creation of green pellets (by rotating and mixing particles or powder in a drum, usually in the presence of a binding agent), drying, sintering (firing or burning) and sometimes shaping (into more perfect spheres - mainly for testing samples). The last three processes are also known as after-treatment, or strengthening of agglomerates. Creation of ceramics almost always involves firing of green bodies. The porosity of pellets varies largely with particle material, but is usually around 0.25-0.40. In pelletization, due to wanted or unwanted processes, binding material is sometimes concentrated in the outer shell of the agglomerate (Capes, 1970/71).

In the pressing processes particles, or even particle agglomerates, are either compressed (using large forces) in dies (generally cylindrical) or compacted by isostatic compression, roller milling compaction, or extrusion. A feature of most powder compacts is that binders for conferring strong bonds are not added (but only, sometimes, ingredients to ease compaction). A typical example is the process of developing pharmaceutical tablets, where fine powders are first converted into granules (agglomerates) by mixing them with binders, granulating and drying them. Agglomerates are then compressed in a die cavity to form tablets (Jarosz and Parrot, 1983). The compression of a powder (very small particles) to form a tablet is composed of several stages. At the start, the compressive load causes particles to rearrange to a closer packing; additional compressive force produces both elastic deformation and plastic deformation of particles - plus local crushing, fracture and/or fragmentation. The products obtained by die compaction of particulate material are sometimes also referred to as agglomerates; usually they are cylindrical or cubical.

Another process of creating particle agglomerates is crystallisation, or grain growth, where moist material is granulated, dissolved in liquid and then dried. However, it is often the case that crystallisation leads to heterogeneous solids.

Compared with disperse particle systems, agglomerated products have many advantages: no or low dust content; improved storage, handling, metering and dosing; less segregation; increased bulk density; defined shape and weight; improved product appeal and sale value. However, agglomerates present two main problems: attrition (unwanted breakage or material loss) and comminution (energy has to be consumed to break down agglomerates in small fragments, for size reduction).

1.2 BONDING MECHANISMS AND ADHESION

To keep particles in agglomerate form, external forces (gravity, inertia, drag, applied forces, etc.) acting opposite to adhesive forces should be smaller than the latter. The adhesion tendency increases with decreasing particle size of at least one of the adhesion partners (mainly because the surface of smaller particles is less rough). For example, gold spheres of 10 μm diameter develop an adhesion force 10000 larger than the particle weight (Pietsch, 1991).

Compared to homogeneous solids, particle agglomerates are usually weaker and less brittle. In some agglomerates the interparticle bond is so weak that an external force is not transmitted throughout the agglomerate's volume - but just dissipates locally, close to the point of its application, due to fast local shearing apart of particles (Kapur and Fuerstenau, 1967). The interparticle bonds, therefore, determine the strength of agglomerates much more than the properties of the individual constituent particles.

The bonding between two particles constituting a particulate material can be of two types: localised bonding and bonding consisting of strength-transferring material. According to their nature, the localised bondings can be due to attraction between particles, or to adhesional and cohesional forces in bonding bridges which are not freely movable. Attraction between particles can be due to van der Waals (molecular), electrostatic, ionic or metallic forces, or of covalent or chemical nature. The adhesional and cohesional forces in bonding bridges which are not freely movable can be due to chemical reactions (e.g. ore pellets, briquettes), melting (almost always a bridge of molten material is formed at the point of particle contact), and crystallisation of dissolved materials. The bondings consisting of strength-transferring material can consist of movable liquid, non-movable fluid (viscous binders or adsorption binders), completely filled void volume, or solid bridges.

Pietsch (1991) categorised the bonding mechanisms of particulate material into five types: solid bridges, binder bridges, liquid bridges, attraction forces between particles and interlocking bonds. Solid bridges usually give the strongest bonding and can even "transform" the particulate material into continuous heterogeneous material. If the interparticle bonds are stronger than the particles, breakage (failure) can even occur through constituent particles (intragranular), making the fracture surface less rough and more planar. Certain particle shapes (long and/or flat) give strong interlocking bonds; nevertheless, compression and shear forces must usually act on the system for these interlocking bonds to be maintained. Binder and solid bridges are probably the most common in particulate materials.

Adhesion between powders plays an important role in many industrial processes; it is indispensable for some, but can also create unwanted effects. Interparticle adhesion is due to forces (van der Waals, electrostatic, electrical double layer formation, capillary) or interfacial mechanisms (bridges, contact melting, mechanical interlocking and shearing of particles, sintering effects), but usually a complicated mixture of these, acting concurrently or successively (Lam and Newton, 1991). The strength of the adhesive bond is dependent on different factors: surface roughness, cleanliness, size, shape and mechanical properties of particles, size of contact area. Adhesion increases with increasing contact compressive force, as this increases the contact area (Tabor, 1987). Observed adhesion may be much larger than the calculated value due to viscoelastic energy dissipation. Charge separation at interfaces may sometimes produce large electrostatic forces that increase adhesion. Surface roughness may greatly reduce adhesion, especially with hard high-modulus materials (ceramics). Over the years, different experimental techniques have been devised to measure adhesion; the most used one in the pharmaceutical industry is the centrifuge technique.

1.3 TESTS FOR ATTRITION, COMMINUTION AND STRENGTH MEASUREMENT/DETERMINATION

Testing techniques to predict material attrition (unwanted damage) have been devised to analyse and compare attrition of different materials, and to predict material behaviour during their usage (Bemrose and Bridgwater, 1987). The testing techniques for comminution were mainly devised to analyse the results of fracture/fragmentation and optimise the amount of energy input needed. Both types of testing techniques can be single-sample (usually tension, compression, impact or shear tests) or multi-sample. The multi-sample tests (e.g. fluidized bed, shear cell, rotating drum, grindability, vibration, drop shatter, paddle wheel, enhanced shieving - for attrition; and milling, grinding, drop shatter - for comminution) closely imitate the real processes materials go through, but they are primarily empirical in nature. The single-sample tests help the understanding of sample behaviour under different (usually

well-defined) external forces, but are more difficult to compare with the materials' behaviour observed in practice (where the applied load is usually very complex).

Friability is a widely-accepted concept for defining strength of particular materials; it is more useful than, for example, tensile strength. Friability is an important property of particulate material as it measures an agglomerates' tendency to break down in size during storage and handling. There is wide diversity in the methods used to measure friability, from the well defined applied-stress methods (diametrical compression and impact tests), to the methods where the particulate material is subjected to a random series of stresses. As the strength/friability of most agglomerates is very variable, many workers stressed that large numbers of agglomerates should be tested for obtaining representative mean values. For example, the international standard for iron ore pellets (ISO/DIS 4700) recommended that a minimum of 60 "clone" pellets to be tested. To simplify the testing procedure, several multi-particle tests have been devised. Workers developed tests where a number of pellets were compressed in a steel cylinder and showed that the weight of the debris obtained could give a good measure of the material's friability. Meyers and Tantevee (1986) devised a similar test for iron-ore pellets, but they went further and analysed the way in which each pellet behaved. Other multi-particle friability tests devised for particulate materials include the following: multi-particle impact, shear, tumbler, vibration and fluidized beds. Multi-particle friability tests offer very similar conditions to those in industrial situations but have the main disadvantage that they cannot explain, show and rationalise the intimate details of the micro-mechanics of agglomerate failure.

Agglomerate strength is a major factor of concern in the industries manufacturing or utilising agglomerated products. Single-sample tests for measuring "strength" are common: the diametrical compression test is widely used to determine an agglomerates' tensile/failure strength, while impact tests are often employed to determine the agglomerate strength in terms of the energy needed for agglomerate failure.

1.4 COMPUTER SIMULATION

The application of computer simulation to engineering problems has increased considerably over the past several years - to the extent that computational techniques have become as important as theoretical analysis and laboratory experiments.

It is very difficult in the laboratory to determine what happens inside a specimen, to accurately measure forces, stresses, displacements, etc. and sometimes, even to eliminate the effects of the test devices from the test results. In the same way, it is very difficult to "catch" exactly the moment when something of major interest happens or when the test or a

load should be halted. Also, it is impossible to re-produce exactly the same experiment, or to "freeze" an experiment at a certain important moment.

The major advantage of simulations over experiments is that they can offer more intimate details of what is actually going on. The level of detail that can be portrayed by experimental results is usually more limited. Another advantage of simulations is their repeatability: any test can be repeated any number of times and, moreover, exactly the same specimen can be re-tested an infinite number of times, under different loads and test conditions.

The computer simulations' problem is that they produce "good" results only if they follow a realistic theory. The better the principles, methods and approximations they are based on, the more reliable the simulations are. As opposed to experiments, simulations can follow theory so well that they can even demonstrate, by simply analysing results of particular cases, whether the theory is good or wrong. The inconsistencies that occur when applying theory to testing disappear with computer simulations, as these represent the equations and methodologies used in the implementation.

In contrast to solid samples, the behaviour of agglomerates is strongly affected by the total number of interparticle contacts in the agglomerate, by the evolution of their state (i.e. rigid, more degrees of freedom, sliding, broken, re-adhered) and of the contact force. In agglomerates, it is enough to know the magnitude of all interparticle-contact forces for determining the load transmission through the agglomerate and the amount of elastic energy stored within the agglomerate. However, in the laboratory it is extremely difficult, usually impossible, to measure the number of bonds within an agglomerate, let alone measure the interparticle forces. Computer simulation packages can provide the number and the values of these contact forces any time during the testing of an agglomerate.

In the area of particulate materials, simulation techniques to model more and more realistically the physical behaviour are continuously developing. The early continuum techniques are too mathematically complex for particulates and thus present large limitations. Discrete simulation techniques are conceptually much simpler and realistic; they can be divided in three categories: classical Newtonian dynamics models, statistical models and hybrid models. The dynamic models for particulates involve the application of the Newtonian dynamics equations to each particle from a system of particles, including keeping track of all the forces and the moments acting on each particle at every time-step. Cundall and Strack's (1979a,b) distinct element model (DEM) is the best known and the most utilised model. The only disadvantage of this model is the large computational resources required. The statistical mechanic models use statistical approaches (generally the Monte Carlo ideas of statistical mechanics) for determining the state of the particles. Although these models are simple and efficient, they are inflexible, as there is little control over most

parameters, and not too accurate. The hybrid models combine the ideas from both the deterministic and statistical approaches - see Hogue and Newland (1994).

The object of this research project is to examine in detail the agglomerate damage processes (especially their fracturing) by means of computer simulation. The (numerical) simulation software is called TRUBAL, a program based on the DEM (see more details in Cundall and Strack, 1979a,b, paragraph 5.1 and Appendix A) which has been extensively used, improved and validated in different granular/particulate material applications in the last 15 years. Each of the agglomerates used in this project consisted of a random distribution of 4000 primary particles. The tests simulated were the free-fall normal impact, double impact and diametrical compression.

In the area of computer simulation, this research extends into three dimensions the two-dimensional free-fall impact and diametrical compression work of Yin (1992) and Potapov and Campbell (1994) and complements the three-dimensional simulation of Kafui (1996) on the free-fall impact of FCC and BCC agglomerates. At the time the present project started, there were no reports of any diametrical compression and double impact test simulations on three-dimensional agglomerates.

The work carried out in this project is relevant to agglomerates having localised bondings, but also (approximately) to agglomerates having weak and short solid bridges. It is not pertinent to agglomerates having liquid bridges or large solid bridges. The constituent particles of the agglomerates simulated in this project present no surface roughness (they are perfect spheres), are impossible to break and, moreover, only suffer elastic deformations.

1.5 STRUCTURE OF THE THESIS

Chapters 2, 3 and 4 provide critical reviews of the previous research work relevant to the topic of this research project. Chapter 2 presents the main fracture mechanics concepts and briefly describes the methods of fracture analysis in laboratory experiments. It also summarises the latest developments in indentation testing related to the work in this project. A review of the previous theoretical and experimental work on diametrical compression of various spherical, cylindrical and disc-shaped samples is presented in Chapter 3. Chapter 4 reviews the single-sample impact test, considering the research work results obtained in both free-fall (single) and double (restricted) types of impact test. The emphasis is on spherical samples.

Chapter 5 presents preliminary results of diametrical compression test simulations on agglomerates having particles arranged in body-centred cubic (BCC) and face-centred cubic (FCC) packings and on the first random agglomerate.

Detailed analyses and results of computer simulated tests on one loose and three dense agglomerates (each consisting of 4000 random-distributed particles) are provided in Chapters 6 and 7. Chapter 6 only deals with normal free-fall impact tests, whereas Chapter 7 is concerned with both the double impact and diametrical compression tests. The impact velocity was varied in both impact tests; the mass of the impacting platen was also varied in the double impact test. Comparisons with experimental results on agglomerates can be found at the end of each chapter.

The fracture of the dense agglomerates in the impact and diametrical compression tests is closely examined in Chapter 8. Three-dimensional computer graphics reveal an interesting insight into the actual fracture mechanisms, including the formation of microcracks, crack initiation and the propagation of the cracks up to the fracture moment and beyond.

Chapter 9 provides additional details of the behaviour of the randomly distributed agglomerates in impact and diametrical compression tests. It also presents a comparison between the results obtained in all the three types of test, including analyses of fragment size distributions, average crack velocity, wave propagation, load transmission and energy variation. Finally, a summary and the main conclusions resulting from all the simulation work carried out in this project are discussed in Chapter 10. Further work on the topic is also suggested.

Appendix A presents more information about the software TRUBAL. Appendix B is a user manual for the new variant of TRUBAL used in this project's simulations.

1.6 TERMINOLOGY AND CONVENTIONS ADOPTED (ALPHABETICAL)

Agglomerate - an assemblage of particles which are either loosely or rigidly joined together (Bemrose and Bridgwater, 1987). In this project an agglomerate is a roughly spherical cluster of spherical particles brought together (prepared) by inducing a centripetal gravity field.

- *BCC agglomerate* - agglomerate consisting of particles arranged in a body-centre-cubic packing.
- *FCC agglomerate* - agglomerate consisting of particles arranged in a face-centre-cubic packing.
- *Random agglomerate* - agglomerate consisting of particles located at random.

Clusters - isolated assemblage of particles resulting from the failure of an agglomerate. The smallest cluster has 1 particle and is called a singlet. Particles in a cluster do not have any contacts with particles in other clusters.

Coordination number of an agglomerate - the average number of interparticle contacts per particle.

Contact force - the force developed at the contact between two particles or at the contact between a particle and a platen. The contact force can be decomposed into the normal contact force (perpendicular to the plane of contact, along the line uniting the two particles' centres), and the tangential contact force (orthogonal to the normal contact force and tangent to the contact plane).

Crack - a fault within an agglomerate which provides a preferential site for breakage or fragmentation. In agglomerates the smallest crack represents the breakage of an interparticle contact.

- *Microcrack* - similar, but without necessarily being a preferential site for breakage or fragmentation.
- *Local crack* - crack that only develops locally.
- *Fracture crack* - crack that when completely developed contributes to the fracture/fragmentation of the agglomerate

Damage of an agglomerate - term usually used in this project to denote the breakage of interparticle contacts within the agglomerate.

- *Attrition* - the unwanted breakdown of agglomerates within a process (includes abrasion and fragmentation).
- *Comminution* - the intentional size reduction (breakdown) of agglomerates by any means.

Damage ratio - the ratio of the broken bonds to the initial number of bonds at start of the test.

Debris ratio - ratio of the mass of debris (fragments of under 2.5% mass of the initial agglomerate mass) produced to the mass of agglomerate at the start of the test.

Diametrical compression test - a unidirectional compression test where a sample (usually discoidal, spherical or cylindrical) is very slowly compressed between two platens (it is often called the "Brazilian" test). A diametrical compression test is, according to the standard "APPIE/G001" a form of slow compression test carried out at a strain-rate lower than 20 mm/min.

Fragment - assemblage of particles usually produced by the fracture or fragmentation of an agglomerate. As opposed to a cluster, particles in a fragment can occasionally have one or a few contacts with other particles outside the fragment (usually due to an interlocking mechanism). However, a fragment behaves as an individual entity (e.g. all particles in a fragment move together).

- *Large fragment* - a fragment having over 10% from the total number of particles in the original agglomerate (over 400 particles).

- *Medium-sized fragment* - a fragment having between 2.5% and 10% from the total number of particles in the original agglomerate (100 - 400 particles).
- *Small fragment or Debris* - a fragment having under 2.5% from the total number of particles in the original agglomerate (under 100 particles).
- *Fines* - finest debris (smallest fragments) - clusters consisting of under 8 particles each (under 0.2% of the mass of the original agglomerate).

Fracture - breakage of the agglomerate into under 7 large fragments (usually 2, 3 or 4).

Fragmentation - breakage of the agglomerate into over 6 large or medium-sized fragments.

Friability - the tendency to break down in storage and handling under the influence of small forces.

Microcrack - see *Crack.*

Particle - a piece of material which is an entity in itself and has not been formed by joining together two or more smaller pieces of material. All the particles simulated in this project are perfectly elastic spheres of about 60 μm diameter.

Particulate/granular material - a material (system of particles) made of individual discrete particles. In contrast to heterogeneous porous materials, the voids in particulate materials are not isolated.

Platens/walls - in this project they are planar, rigid and perfect elastic.

Powder - system of discrete particles with a maximum dimension of less than 1 mm.

Toughness - material's resistance to crack growth.

TRUBAL-ACI - a variant of the TRUBAL software (Aston University version) specially developed for the simulations of dry agglomerates carried out in this project.

CHAPTER 2

FRACTURE CONCEPTS AND INDENTATION TESTING

When subjected to sufficient load, an agglomerate - similar to a solid specimen - will either deform, erode, fracture, fragment or (completely) disintegrate. Many scientists describe the fracture of particulate materials in terms of the same mechanisms as used for solids: through a crack initiation and propagation process conforming to traditional fracture mechanics theory. They believe that, also in the case of particulate materials, fracture initiates from a structural pre-existing flaw, so that this flaw determines failure. However, from indentation test results on heterogeneous solids, it seems that the more heterogeneous (discontinuous) a material, the more complex its fracture/failure mechanism is. Indentation tests have shown that microcracks develop prior to the failure/fracture of many heterogeneous solids and that pre-existing flaws do not determine the fracture of these materials.

2.1 FRACTURE MECHANICS CONCEPTS

The criterion for fracture based on the attainment of some characteristic maximum stress has been extensively used in the case of samples that present brittle fracture. This criterion's main problem is that it starts from an unrealistic point of view - that the material is homogeneous and behaves perfectly elastic up to the point of failure. Moreover, the criterion only addresses part of the necessary and sufficient conditions for fracture, giving no consideration to the fracture mechanism: fracture is assumed to occur at the very moment when a certain stress (usually tensile) exceeds a particular value.

Fracture mechanics theory deals with crack propagation and failure mechanisms: it quantitatively describes the transformation of an intact specimen into a fractured one through a crack growth theory. During loading, before the crack starts propagating, the load charges the material with elastic strain energy - the same as energy in a spring. When a critical state is reached, the crack begins to grow/extend; the crack propagation process may be violently fast or slow and consumes part of the strain energy stored in the material.

For elastic materials, fracture mechanics theory was developed by Griffith (1920). He stated that there is an energy balance in a crack: fracture (the crack's propagation) occurs only if the available stored strain energy for a differential advance of a crack is bigger than the necessary surface energy for creating new surfaces. Instability arises because the available strain energy is proportional to the length of the crack, while the specific energy

consumption remains constant. As a result, beyond a critical crack length there is an excess of energy and the crack can suddenly extend without being arrested. Although Griffith formulated his criterion for fracture in terms of macroscopic thermodynamical quantities, he also considered the molecular level events, stating that the maximum stress at the tip of an equilibrium crack must correspond to the theoretical tensile strength of the solid. This gave an indication of the strength of ideal "strong" solids. Observing that the strength of real materials was lower by about two orders of magnitude than the predictions, Griffith concluded that the typical brittle solids must contain sub-microscopic flaws too small to be detected by ordinary means (nowadays called "Griffith flaws"). Griffith's energy-balance concept (pertaining to crack propagation) and flaw hypothesis (pertaining to crack initiation) represent the foundation of a general theory of fracture.

Fracture mechanics was originally applied to brittle-behaving solids - for which the fracture behaviour is supposed to be mainly affected by the presence (pre-existence) of bulk imperfections (flaws). Real solid bodies are not perfect in their structure: they possess structural flaws. Inglis (1913) discovered that an elliptical cavity in a stressed plate acts as a stress concentrator. His work suggests that, under loading, flaws are potential sources of weakness in solids, as the stresses developed around these flaws can be several times that of the applied stress. Fracture mechanics theory supports the idea that cracks are initiated at structural flaws (micro-cracks, pores, defects, etc.); the larger these are the more they endanger the material. The fracture process is a matter of energetics, as energy is needed to create new surfaces. Most of this energy comes from the applied stress and/or from the stored elastic strain energy in the body. The fracture's consumption of energy is due mainly to irreversible deformation in the immediate neighbourhood of the crack tip.

Griffith based his model on the notion of an ideally brittle solid, in which the creation of new fracture surface by the rupture of cohesive (molecular) bonds constitutes the sole mode of energy dissipation. In real materials crack growth is accompanied by irreversible processes, so that a much larger amount of (mechanical) energy may be consumed in the process of separating the material. Stroh (1954a) showed that, although the Griffith theory gives satisfactory predictions for some materials such as glass, it seems unlikely that a pre-existing crack can play any important part in the fracture of a metal. Stroh (1954b) showed how piled-up groups of dislocations can also generate (initiate) a crack. Irwin (1958) and Orowan (1949) analysed the stress field close to the crack tip and developed failure criteria for inelastic solids, in which the plastic deformation complicated the equations (an additional criterion was needed to define ductility).

The Griffith concept needed functional quantities that characterise the driving force for fracture, namely the stress-intensity factor K and the mechanical-energy-release rate G - which is also referred to as the crack extension energy, or the amount of energy loss, and is

equal to half of the new crack surface. The value of G is also equal to the energy offered from the stress field to propagate the crack. The critical values of K and G at crack propagation are related by the expression

$$K^2 = E \cdot G \tag{2.1}$$

where E is the modulus of elasticity. Fracture mechanics usually attempts to describe the crack response in terms of K, or some other equivalent parameter.

There are three basic modes of crack-surface displacement that determine the fracture mode: *Mode I* (opening mode) - corresponds to normal separation of the crack walls under the action of tensile stresses, *Mode II* (sliding mode) - corresponds to longitudinal shearing of the crack walls in a direction normal to the crack front and *Mode III* (tearing mode) - corresponds to lateral shearing parallel to the crack front. Of the three modes the first is by far the most pertinent to crack propagation in brittle solids, as there is always a tendency for a brittle crack to seek an orientation that minimises the shear loading (e.g. crack extension by progressive stretching and rupture of cohesive bonds across the crack plane). Pure shear fractures occur, for example, in the constrained propagation of cracks along weak interfaces (cleavage planes in monocrystals, grain or interphase boundaries in polycrystals, etc.) inclined to the principal stress axes, or in the rupture of metals and polymers where ductile tearing is favoured (Lawn, 1993).

2.2 APPLICATION OF FRACTURE MECHANICS

Observing that the strength of brittle-behaving solids decreases with increasing sample size, Weibull (1951) suggested that this was only due to more "dangerous" (pre-existing) bulk flaws in larger samples, due to an increased probability of having weak spots (critical flaws). He developed a theory giving a probabilistical explanation of the size effect. For two specimens of volume V_1 and V_2 (of same material), he established the tensile strength σ_1 and σ_2 to be in relationship:

$$\frac{\sigma_1}{\sigma_2} = \left(\frac{V_2}{V_1}\right)^{\frac{1}{m}} \tag{2.2}$$

where ***m*** is a material constant. Using this relationship, ***m*** can be determined from just two experiments and the tensile strength can then be predicted for any other sample size for the same material. Although widely applied, Weibull's work is only valid for some materials and only within certain size limits - mainly because there are additional factors affecting the strength/size effect.

Sammis and Ashby (1986) carried out several compression tests, on glass and PMMA plates and resin cylinders, to help them build their theoretical model of crack propagation in compressed porous brittle solids. Their diametrical compression tests showed that microcracks initiate from pores and propagate in a direction which is approximately parallel to the direction of the largest principal compression stress. Subsequently, the microcracks start to link creating a network of cracks which finally causes the macroscopic failure of the sample. In the samples having arrays of holes, the interaction caused them to nucleate earlier and grow further from the small holes rather than from the large ones. When the cracks were large, they deviated towards each other and finally linked. In the resin cylinder, cracks initiated and propagated from a spherical hole even when the hole was not in the loading plane. The crack initiated from a pore suddenly (with an audible "pop") and then grew in a stable manner as the load was increased further. Sammis and Ashby's experiments also revealed the fact that cracks interact with the surfaces of a finite sample in a way which causes them to grow faster than they do in an infinite medium.

Inferring that hard agglomerates fail by the propagation of cracks that may initiate at surface flaws, Adams (1985), Kendall et al (1987) and Kendall (1988) developed theoretical predictions of agglomerate strength. Adams et al (1989) developed a fracture mechanics model for agglomerates formed with small quantities of binder. Abdel-Ghani et al (1991) interpreted data obtained from experiments on powder compacts in terms of fracture mechanics in order to determine the effective elastic modulus and fracture energy. They also analysed the data in terms of the theoretical models of Rumpf (1962), Schubert et al (1975) and Kendall (1988) and suggested that the three theories overestimated the elastic modulus and underestimated the fracture energy by orders of magnitude. The large differences were attributed to the complexities of real particle systems. Abdel-Ghani et al (1991) argued that, because stresses are transmitted in discrete chains of particles in a way that produces many redundant interparticle contacts, the elastic modulus was overestimated, and suggested that the underestimation of the fracture energy was because the major component of energy is dissipated in a plastic "processing zone" ahead of the crack tip.

Analysing the fracture of alumina and zirconia (polycrystalline ceramics) in combined mode I and II on pre-cracked disc specimens, Singh and Shetty (1989) showed that crack-surface resistances arising from grain interlocking and abrasion were the main sources of the increased fracture resistance in mode II - compared to the predictions of fracture mechanics

theory. Wu et al (1994) also pointed out that heterogeneous solids (blends) show increasing fracture toughness due to crack-interface bridging mechanisms.

Most experimentalists applying fracture mechanics theory analyse the fracture behaviour of different materials using the method of introducing artificial defects (holes, notches, chevrons - all to represent cracks) into them prior to testing. They then analyse how fracture evolves from these artificial defects. Examination of crack propagation can sometimes provide insight into the macro-failure of materials, but cannot explain the mechanism of microcrack formation and crack initiation under loading. The way a sample fails should not be artificially "directed" by introducing initial notches/cracks as, in reality, materials do not have initial cracks (of artificial sizes and shapes) in "key" positions. Moreover, experimentalists often changed the sample's shape and even the test conditions (they generally used bend, split-cell and indentation tests) to determine more easily the fracture parameters.

One of the best definitions of fracture is due to Rudnick et al (1963): fracture starts when the stress reaches a critical value at a (real) flaw which is in an appropriate location and orientation to initiate a crack.

2.3 FRACTURE PATTERN FORECASTING AND ANALYSIS

The process of fragmentation is largely a unresolved problem (Grady, 1990), as too few physical and geometric constraints have been found in this process. It is very difficult to make a quantitative analysis of fragmentation parameters, such as energy consumption, fragment sizes, or distribution of fragments. In a way, fragmentation is a consequence of cracks branching, diverging and interacting. Grady (1990) showed that examination of network formation can sometimes provide insight into the inherent relationship between the mechanism of microcrack formation and the macro-failure of materials. However, the final fracture pattern of a sample cannot solely depend on the inherent distribution of flaws, but must also be influenced by the particular test conditions, the stresses induced, the shape of sample and the sample material.

Over the years, better and better methods have been developed for the "post-mortem" analysis of the results of fracture, i.e. the fragments that constituted the sample. Some devices were developed to automatically record the shape and size of fragments, others - usually optical instruments or the scanning electron microscope - have been created to closely analyse the fracture surface. Using fractography techniques, markings on the fracture surface can provide a route map to the fracture origin; measurements of fracture mirror radii (see Kelly and Macmillan, 1986) as a function of strength can indicate sizes of

critical flaws and fracture toughness. The fracture surface of a fragment can reveal how planar or rough the fracture is, whether fracture happened intragranular or intergranular, but also the approximate temperature of fracture and the degree of local melting. Fractal geometry is a non-Euclidean geometry which has been developed to infer the fracture surface generation mechanism from the analysis of irregular or fractional shapes. Determining the fractal dimension of successively sectioned fracture surfaces (of different alumina and glasses), Mecholsky et al (1989) found that the fracture surface increases in roughness as the toughness increases.

2.4 HARDNESS AND INDENTATION TESTING

2.4.1 Generalities And Definition

Being simple, quick and only requiring a small and easily prepared sample, hardness testing is an important tool in the study of the mechanical behaviour of solids and in characterising their intrinsic mechanical properties. Hardness testing (Kelly and Macmillan, 1986) also gives less scatter than other tests (e.g. bend or diametrical compression tests). Microhardness (indentation) tests have become very popular due to their increased precision. Hardness testing - utilising high-precision, small-scale (indentation) devices - is nowadays used to measure Young's modulus, flow stress, fracture toughness, contact-induced strength degradation and crack growth. The indenter generates a stress field in the sample that, although complex, produces well-defined deformation-fracture patterns. Indentation can thus give a good indication of a material's elastic or plastic, brittle or ductile nature and of its toughness and strength.

Hardness tests have been extensively used to measure the resistance of a solid to indenting it with a hard material; using different indenter shapes and definitions, a series of standards were defined - e.g. Meyer hardness, Brinell, Vickers, and Knopp hardness numbers. Hardness is estimated from the dimensions of the recovered indentation (its form may differ significantly from the form imposed by the indenter at maximum load, due to reversible deformation). In contrast with the blunt (usually spherical) indenters, the sharp (pyramidal or conical) indenters, having tip radii of a few microns only, produce irreversible (plastic) deformation in any sample from the very moment of coming into contact with it.

2.4.2 Relevance Of The Indentation Tests For This Project

Indentation tests use and try to expand the theories of fracture mechanics and contact mechanics. There are several reasons why indentation testing is relevant to the work done in this project. First of all, indentation testing - same as diametrical compression and impact tests - uses compression loads on the samples. Secondly, its theoretical relationships are also based on contact mechanics theory. Thirdly, the indentation tests - being more precise and closely-analysed than other tests - can give a clearer idea as to why, where and how the cracks are generated in the diametrical compression and impact tests. Fourthly, for some materials, workers have found close similarities between indentation tests and the way in which the conical (or wedge-shaped) zone of compacted material (formed at the contact with the platen/target) is pushed into the sample in the diametrical compression and impact tests.

Carrying out diametrical compression on ferrite spherical agglomerates, Tanaka et al (1985) found that fracture crack initiation follows a similar process to that in indentation crack

initiation - the plastic-deformed contact regions adjacent to the platens acting as indenters pushing into the agglomerates. Using the Hertzian theory to calculate, at the failure point, the average contact pressures, they found comparable values with the Vickers hardness as measured on plates of the same material.

2.4.3 Behaviour Of Solids Under Indentation Tests

Extensive indentation testing has been carried out mainly on glasses and ceramics. Under sharp indenters, even glass and other brittle homogeneous materials develop first a plastically deformed (approximately hemispherical) zone. Above a threshold load level (which was found to be rate-dependent) cracks initiate and start propagating from the deformation zone where a high stress concentration exists (Lawn, 1985). Cracks grow spontaneously but stop at a certain length (equal to several contact area diameters) primarily determined by the material's toughness.

Under spherical indentations, homogeneous brittle solids (glasses, single crystals, etc.) usually exhibit a classical ring-conical fracture: the ring crack initiates in the weakly tensile region just outside the contact circle and propagates downwards as a surface-truncated cone, arresting at a depth approximately equal to the contact radius. The very shape of the cracks generated by the local loading in indentation testing can give an indication of the material's nature. Under spherical indenters, formation of Hertzian ring-cone or of circumferential cracks indicates brittle failure, whereas creation of radial, lateral, meridian-vent or conical cracks denotes semi-brittle failure (Ghadiri et al, 1990).

Residual stresses were found to have an important role in driving the fracture process. Lawn and Wilshaw (1975) showed the formation of a vent crack under point (maximum sharpness) indentation: the median vent forms during loading, whereas the lateral vent forms during unloading. Lawn (1985) suggests that faults are actually formed by deformation and that crack initiation is a two-step process consisting of shear faulting followed by tensile microcrack development. Deformation is thus an integral part of the mechanism of crack formation; it is also a determining factor in the (crack) propagation stage of fracture. In glasses, for different-angle conical indenters, it has also been found that the central zone under an indenter is undeformed and uncracked for angles less than 130° and larger than 150° (Van der Zwaag and Hagan, 1985).

Cai et al (1994) added mica to the composition of glass and used spherical indenters to test samples made of this material. Mica weakened the samples, but also granted them considerable ductility which increased their resistance to strength degradation at high contact loads. Section views showed a transition from the classical cone fracture in the pure glass to accumulated subsurface deformation/microfracture in the glass-ceramic. This clearly

demonstrates that microstructure plays an important role in the failure of heterogeneous materials. Cai et al (1994) attributed the subsurface deformation to the shear-driven sliding between the mica flakes and the glass matrix. They observed that the microcracks initiate at the shear-fault interfaces and propagate inside the sample, finally coalescing with neighbours at adjacent mica flakes and producing easy material removal.

Examining the behaviour of different strength-controlling flaw types in ceramics, Bennison and Lawn (1989) showed that polycrystalline materials show "flaw tolerance": their strength is almost insensitive to the initial size of flaw (totally insensitive for initial flaws smaller than 100 μm). This contradicts Griffith theory and common belief that, in all materials showing brittle behaviour, failure occurs spontaneously from some pre-existing "Griffith" flaw when a critical applied stress is reached. Many ceramics display an increasing resistance with continued crack extension (Mai and Lawn, 1987); they do not fail spontaneously but failure occurs only after a period of stable growth (often over a considerable distance) of the critical flaw (Swanson et al, 1987, Cook et al, 1987). Elimination of all flaws, however, should not be the ultimate objective of strong-material fabrication. The crack stabilisation of many ceramics has the advantage that it can provide early warning of any impending failure. Varying the grain size of alumina ceramics (2 to 80 μm), Chantikul et al (1990) showed that smaller grains give higher strength, but larger ones confer higher toughness by making crack growth more stable.

Using spherical indenters, Guiberteau et al (1994) showed that no microcracking was developed in fine alumina specimens (2.5 μm grain size). For alumina samples having 23 μm grain size, damage did not initiate in the surface region of weak tension outside the contact but in the subsurface region of high compression and shear beneath the contact. Microfracture damage increased with increasing grain size from 3 μm (when almost Hertzian cone cracks developed as in ideally homogeneous solids) to 48 μm (when the partial cone crack arrested at the very first subsurface grain boundary intersection). For 48 μm grain size it was shown (Guibereau et al, 1994) how the fully developed damage zone was made up of an accumulation of microstructurally discrete events, each consisting of some kind of intragranular shear faulting accompanied by intergrain microcracking. Guiberteau et al (1994) illustrated this deformation-microfracture behaviour by a simple model: shear stresses (developed during loading) initiate intragrain lamellae which "pop-in" intergrain microcracks at their ends. It is very interesting that, although the (indentation test) failure mechanism is so different for alumina samples having 3 μm and 48 μm grain size, their indentation stress-strain curves were almost identical.

Brittleness measures the relative susceptibility of a material to two competing mechanical responses - deformation and fracture. Lawn and Marshall (1979) concluded that the present knowledge of the factors which determine a material's brittleness is largely empirical. Based

on indentation mechanics they proposed the ratio H/K_c - where H is hardness (resistance to deformation) and K_c is toughness (resistance to fracture) - as an index for brittleness.

One of the most important conclusions derived from indentation testing is that microstructure plays a critical role in the fracture behaviour of heterogeneous solids. Depending on the contact geometry and material, individual cracks may initiate from pre-existing flaws, but also from precursor plastic deformation - where both initiation and propagation of cracks is preceded by plastic deformation (Lawn, 1993). For concentrated loads (sharp indenters), cracks always initiate from the inelastic deformation zone.

2.5 SUMMARY

Fracture mechanics theories were originally developed to explain the fracture of brittle elastic solids such as glass. Subsequently, researchers have modified the original theory in order to try to explain the behaviour of other types of solid. However, the work of Lawn and co-workers on indentation testing of alumina clearly demonstrates that the conventional fracture mechanics concepts do not apply to heterogeneous particulate solids. Therefore, attempts to model the fracture of agglomerates based on traditional fracture mechanics theories should be treated with caution.

CHAPTER 3

TENSILE STRENGTH AND DIAMETRICAL COMPRESSION TESTS

Over the years it was found that failure of materials under different external loads occurs mainly due to the tensile stresses developed inside them. Most materials, but especially the brittle ones, have tensile strengths much smaller than compressive and shear strengths. Diametrical compression is the most utilised test for determining the tensile strength of a specimen. It was the very reason why the test was actually devised.

3.1 DIRECT METHODS FOR DETERMINING THE TENSILE STRENGTH

The uniaxial tension test, which provides the basis for the definition of the tensile strength, is the only direct and correct way of determining how resistant to tensile stresses a sample is. For homogeneous solids there are two kinds of fracture in tensile tests (Timoshenko, 1958): cohesive fracture - when fracture is brittle without substantial plastic flow (e.g. rock salt) - and shear fracture, when large plastic deformations consisting of sliding along certain crystallographic planes precede fracture (e.g. metals). The relationship between resistance to separation (cohesive fracture) and resistance to sliding in shear is not a material constant but varies with strain-rate and temperature.

For particulate materials, Rumpf (1961) developed a well-known theoretical method of predicting the order of magnitude of the tensile strength of agglomerates. His theory was based on a mono-sized system of spheres which did not take into account the actual structure of the agglomerate. The model permitted the nature of the predominant bonding mechanism to be considered. He differentiated between localised bonds (where a bond is localised at the point of contact between particles) and bonds where the space between particles is filled with strength-transferring material. For agglomerates with localised bondings, he resolved the tensile strength as:

$$\sigma_t = \frac{9ZH(1-n)}{8\pi d^2} \tag{3.1}$$

where H is the bonding force per point of contact, d is the diameter of a constituent particle, n is the agglomerate porosity, and Z is the mean coordination number. This estimation of agglomerate tensile strength seems to be very useful as it only demands knowledge of the

nature of the bond between particles, particle dimensions, agglomerate porosity and coordination number. No mechanical test would thus be required - values of d and n can be obtained from the size distribution analysis and from the agglomerate density. Rumpf gave details of how expression (3.1) changes in the case of liquid bridges and solid bridges. For his theoretical predictions, Rumpf found good agreement with results of limestone agglomerate experiments. However, Rumpf's theory was based on assumptions that are not physically realistic. Not only are real agglomerates heterogeneous in structure and do not fail exactly through a cross-section, but the mechanism of tensile failure is much different. In reality, agglomerates do not fail by simultaneous rupture of particle contacts (bonds) but by a progressive mechanism of crack initiation and propagation.

Pietsch (1991) distinguished between tensile testing methods for strongly and weakly bonded agglomerates. The measured tensile strength was reported to vary too much even for samples having the same properties. The eternal problem of such tests is the method of transferring load via the platen/sample interface.

3.2 THE INDIRECT TENSILE STRENGTH - DIAMETRICAL COMPRESSION TESTS

Direct tensile tests are too difficult, laborious and expensive for routine applications to a large number of specimens. Consequently scientists tried to find indirect, but more convenient, alternatives for measuring the tensile strength. Most of these were based on diametrical compression tests. Other popular indirect tensile tests include the bend (flexure) test and the indentation test. As indicated by Peltier (1954), the justifications for using indirect tests for determining the tensile strength are the following: freedom from sensitivity to surface conditions and fabrication problems, uniformity of the internal stress distribution, avoidance of problems with collinearity of machine and specimen axes and lower coefficients of variation in the results.

Diametrical compression tests devised for measuring the tensile strength generally use samples having cylindrical, discoidal or spherical shapes; these tests are also known as Brazilian tests.

Various testing methods were used for diametrically compressing samples (British Materials Handling Board, 1987). The simplest test utilised was the manual test - employed in the pharmaceutical and steel industries to assess the strength of (weak) tablets and iron-ore pellets (from the amount of pressure required to break the agglomerate between the finger and thumb). A diversity of commercial devices/instruments have been designed for diametrical compression, most of them using two parallel platens (one fixed and one

moving) between which the sample was compressed. The initial devices were merely able to record the maximum force on the platens, whereas the most modern ones can plot the force versus strain curve, can move the platen at a constant velocity (rather than just apply a constant force or pressure) and can stop automatically at sample fracture. As the experimentalists observed that the measured maximum force on the platens varies with the loading rate, the devices were improved to use very low (called "quasi-static") loading rates. For measuring the strength of agglomerates (British Materials Handling Board, 1987), either the loading-rate, or the velocity of the moving platen were standardised.

3.3 CYLINDRICAL SAMPLES

The story of the diametrical compression test started in 1943 when Carneiro and Barcellos (1953) proposed the use of cylindrical samples for the routine determination of the tensile strength of concrete (see also Akazawa, 1953). In the original Brazilian test a right circular cylindrical specimen is compressed diametrically between two flat parallel platens. As a result of the applied compression, maximum tensile stresses are developed in a direction normal to the loading direction across the loaded diameter. These tensile stresses are proportional to the applied load. Under proper (test) conditions, the tensile stresses cause the cylinder to fracture along the diametrically loaded plane. Only in this case is the test considered valid and the tensile strength can then be computed from the load at the moment of fracture using the relationship

$$\sigma_t = \frac{2P}{\pi DL} \tag{3.2}$$

where P is the load at failure, D and L are the diameter and length of the cylinder.

Although Carneiro and Barcellos (1953) developed their theory for the diametrical compression testing of cylindrical samples between parallel rigid-hard platens, they recommended the use of square sectioned softwood strips between the platens and the sample in order to obtain a "better" distribution of stress. Many experiments have demonstrated the practicability of the cylinder splitting test, which has become established as a convenient means of testing a wide variety of materials (mainly concrete, ceramics, pharmaceutical tablets) and is now used in many national and international standards specifications.

Observing that line loading induced extremely high compressive stresses at the cylinder's regions of contact with the platens, Peltier (1954) made a substantial analysis of the padding influence over the induced stresses. His results showed that the tensile stresses can be held uniform over a reasonable proportion of the loaded diameter D if the width of the bearing

area is $\geq D/5$. Peltier (1954) developed a relationship for determining the minimum width of load distribution, and insisted that padding was needed in order to avoid "premature crack initiation" leading to invalid tests.

Following the elastic theory of Timoshenko and Goodier (1951) and the work of Frocht (1948), Hondros (1959) theoretically calculated the principal strains for both plane strain (cylindrical sample) and plane stress (discoidal sample). The calculations indicated distinct bimodal radial tensile strain distributions on the vertical diameter, the peaks being situated at $D/6$ or $D/7$ from the platens for $\nu = 0.3$. Experimental results confirmed Hondros's theory for both steel and concrete.

Rudnick et al (1963) made a complete analytical comparison between line and distributed loading for the cylinder splitting test. In the case of ideal line loading, the compressive and shear stresses were found to vary in magnitude along the loaded diameter, from a minimum at its centre to infinitely high values immediately under the platens. For the failure to initiate in tension and not in shear or compression, the high compressive and shear stresses from under the platens must be reduced. When the loads are distributed over a certain width (using paddings), Rudnick et al (1963) found that the stress distribution immediately under the loads changes: tensile stresses are eliminated and the compressive and shear stresses become finite. However, they found that it is not convenient for the load to be distributed over too great an area as the stresses in the centre of the specimen will be affected. The length along the loaded diameter over which the tensile stresses are constant does not only depend on load width but also on the mechanical properties of the specimen and platens/paddings. Rudnick et al (1963) explicitly demonstrated that proper choice of padding (width and material) is crucial for the cylinder splitting test to be successful. Concerning the variation of experimentally determined tensile strength with sample size, they explained that this is normal, as no direct or indirect test can determine the "true" tensile strength of a material. The strength values obtained under any set of conditions are "true" values only for those conditions.

Four main assumptions are normally invoked in the theoretical treatment of the cylindrical samples in diametrical compression tests, namely: {1} the material is homogenous, {2} Hooke's law is obeyed up to failure, {3} a state of plane stress (or plane strain) is induced, and {4} the material is isotropic. Assumption {1} is rarely true, whereas assumption {2} is certainly not true for concrete and many other materials tested in this way. Assumption {3} is only valid for thin discs or very long cylinders. Wijk (1978) showed that, to avoid peak tensile stresses near the generators, the cylinder should be either very long (to achieve a plane strain state), or have the length $L < D/6$ (to achieve a plane stress state). This condition was probably never adopted in the cylinder splitting tests; the majority of

cylindrical samples used were not long enough, as they had $L = 2D$. Assumption {4} is approximately obeyed by most of the materials used.

As the cylinder splitting test was mainly used for determining the tensile strength, the failure of the cylindrical samples under diametrical compression was almost always inferred to initiate due to the tensile stresses acting on the cylinder's diametral loading plane, at a point near the centre of sample. Three main types of failure were reported: half-half, single- and multi-cleft, and fragmentation/shattering. Mitchell (1961) presented end-result photographs from tests of all these three types and classified the fracture types according to the load distribution considered - see Fig. 3.1a,b,c.

Most workers considered that all the failure types are tensile (e.g. Freiman and Hench, 1972), although only the first type (half-half fracture, Fig. 3.1b) was normally used for tensile strength determination utilising relationship (3.2). In the case when the failure occurred by fragmentation it was incorrect for some experimentalists to assume that failure was due to tensile stresses. Several workers showed that failure in this case was due to shear (cleavage or inclined shear - see Mitchell, 1961, and Rudnick et al, 1963), or compressive stresses (Mitchell, 1961), or both. While some workers believed that this "invalid" type of failure occurs due to the insufficient distribution of the applied loading (Fig. 3.1a), others believed that fragmentation was specific for several brittle materials such as glass where failure is explosive (see Freiman and Hench, 1972). Mitchell (1961) found that "valid" half-half rupture only occurs for a certain load width (Fig. 3.1b). For narrow (linear) load distribution he argued that the high compressive stresses under the platens produced heavy shattering whereas too wide load widths led to high shear stresses usually resulting in "double-cleft" fracture in his tests. However, the mechanisms of failure were not always examined in detail. Few researchers reported the failure strain, how the applied load varied with strain, or the extent of crushing in the zones near the platens prior to failure.

Carrying out experiments on concrete cylinders of different sizes, Wright (1955) found that an increase in specimen size leads to a reduction in the observed strength and more consistent results, and that the tensile strength values obtained were 1.5 higher than the values obtained in the direct tensile strength. Wright's findings were confirmed by Chapman's (1968) experimental work, but the latter also showed that distributing the load over a certain width by using hardboard strips led to more reliable results.

3.4 DISC-SHAPED SAMPLES

In principle, if the material maintains perfect elastic behaviour up to failure, the stress field which induces tensile failure in a diametrically compressed disc can be fully determined. The stress solution for diametrically compressed discs was first obtained by Hertz (1895), and later refined by Mitchell (1961). Hondros (1959) developed a complete stress solution for the case of the load being distributed over finite-width strips (arcs). His relationships for determining the principal stresses - the stress component normal to the loading diameter $\sigma\theta(\theta=0)$ and the stress component along the loading diameter $\sigma_{r(\theta=0)}$ are the following:

$$\sigma_{\theta_{(\theta=0)}} = \frac{P}{\pi R t a}\left(\frac{1-\frac{r^2}{R^2}\sin(2a)}{1-2\frac{r^2}{R^2}\cos(2a)+\frac{r^4}{R^4}} - \tan^{-1}\frac{1-\frac{r^2}{R^2}\sin(2a)}{1-2\frac{r^2}{R^2}} \right) \tag{3.3}$$

$$\sigma_{r_{(\theta=0)}} = \frac{P}{\pi R t a}\left(\frac{1-\frac{r^2}{R^2}\sin(2a)}{1-2\frac{r^2}{R^2}\cos(2a)+\frac{r^4}{R^4}} + \tan^{-1}\frac{1-\frac{r^2}{R^2}\sin(2a)}{1-2\frac{r^2}{R^2}} \right) \tag{3.4}$$

where P is the applied load, R is the disc radius, t is the disc thickness, $2a$ is the angular distance over which P is assumed to be distributed radially, and r is the distance from the centre of the disc.

Griffith (1920) developed a widely accepted failure criterion that, in the case of the Brazilian test, predicts that failure will occur when

$$\sigma_1 = \sigma_T \qquad \text{if} \qquad 3\sigma_1 + \sigma_3 \geq 0 \tag{3.5}$$

where σ_1 is the major (tensile) principal stress, σ_3 is the minor principal stress, and σ_T is the uniaxial tensile strength of the material. Theoretically, according to the Griffith criterion, the only point where the conditions for tensile failure are satisfied is at the centre of the disc where

$$\sigma_\theta \approx \frac{P}{\pi R t} \tag{3.6}$$

$$\sigma_r \approx -\frac{3P}{\pi R t} \tag{3.7}$$

Griffith (1920) claimed that, for any material, the ratio ρ of compressive strength to tensile strength is constant and equal to 8. However, it was later demonstrated that this was too simplistic and was only relevant to crack initiation. Mellor and Hawkes (1971) and others

have shown that not all materials obey the rule that $\rho = 8$. Moreover, later studies showed that ρ varies significantly with the geometry of the specimen. Fairhurst (1964) generalised the Griffith criterion to account for the variation of the compression/tension strength ratio ρ from the Griffith constant of *8*. He defined a parameter *S* (the stress severity) as the ratio of the theoretical load at the most stressed point to the load required to cause failure at any point in the specimen considered. Fairhurst (1964) restated the failure conditions and concluded that failure may occur in one or two regions of the loaded diameter. His theoretical results showed that it is necessary to spread the applied load over a contact arc of 20° or more in order to assure fracture initiation near to the specimen's centre. A narrow contact strip was found to increase the probability that the fracture will not traverse the specimen's centre. Fairhurst's criterion predicts peak severity near *D/8* from the platens for materials having $\rho \leq 10$ when the width of the loaded area was equal to *D/12*.

Using photoelasticity in different diametrical compression tests, Rudnick et al (1963) found that very similar stress fields develop in discs and cylinders of same diameter. On rock (granite and dolerite) disc-shaped samples, Colback (1966) used high-speed photography of photoelastic patterns to aid the detection of fracture initiation and propagation. For distributed loading, he believed that failure always initiated at or near to the centre of the specimen, from a pre-existing "Griffith" crack, due to the tensile stresses. His published photographs, however, do not quite support this affirmation. Analysing results of more tests, Colback (1966) concluded that half-half (diametral, Fig. 3.2b) is always the primary fracture; all the other fractures (e.g. producing triple-cleft failure, Fig. 3.2e) occur subsequently and are secondary (probably due to the fact that the applied load could not be halted and thus the disc's half-half fragments fractured individually due to the continuing of loading). It is interesting that the secondary fractures are described as propagating from the platens inwards, although the primary fracture were thought to have propagated from the centre towards the platens. For elastic (steel) platens and line loading, Colback (1966) showed that fracture originates near one of the loading points but does not propagate quite along the loaded diameter (but along a curved path, Fig. 3.2f). Rudnick et al (1963) also reported that fracture starts at an angle to the loaded diameter if the initiation of failure is due to shear stresses.

Ridgway (1960) presented five different types of failure which occurred in his diametrical compression tests on pharmaceutical tablets (see Fig. 3.2a-e). He inferred that (*a*) represents failure initiated under the platens due to compressive stresses; (*b*) is the ideal tensile failure obtained with the optimum distribution of load; (*c*) represents failure initiated under the platens, due to shear stresses - sometimes this is caused by too wide a load distribution; (*d*) is failure along maximum shear loci for point loading; (*e*) represents the triple-cleft fracture due to transfer of load to each half-disc after breakage in (*b*). Fell and Newton (1970) also presented fragmentation (Fig. 3.2i) and the shattering case (Fig. 3.2k) -

that could occur due to a more complex process and was usually found in brittle materials. Similar failure modes to the ones in Fig. 3.2b,e,k. were found by Rudnick et al (1963) for several "brittle" materials. For alumina discs Marion and Johnstone (1977) also found the breakage forms presented in Fig.3.2g,h.

Mellor and Hawkes (1971) carried out diametrical compression and direct tensile tests on three rocks, two plastics, glass and ice. For the rocks, the disc specimens gave good agreement with the values obtained from the direct tensile test, for plastics the disc's tensile strength was lower and the ice's disc tensile strength was far lower than its direct tensile strength. It is interesting that, in order to distribute the load, Mellor and Hawkes (1971) used curved-jaw platens. Different rock samples generally exhibited half-half break-up (Fig. 3.2.b.) and thus "valid" tensile fracture. The fracture cracks were reported not to initiate at the platen contacts, but at or near the points predicted by theory (i.e. in the centre of sample). Cracks then propagated along the diametrical loading plane. In many tests the cracks even terminated at about *D/10* from the outer boundary. The variation in the width of the diametral cracks suggested that failure started in the discs' mid-section. If loading was continued after primary failure a variety of secondary crack patterns were formed. For the glass discs the mode of failure could not be determined, as the central portion of the specimen was always completely shattered. Nevertheless, they suspected again that failure initiated at the centre of sample. The discrepancy found between the direct tensile strength and the disc tensile strength for ice showed that the compressive stresses in the disc play a part in the failure process. Only the failure of the plastic (Lucite) disc was considered "invalid", as gross deformation (10% strain) occurred prior to failure. Final collapse of the Lucite sample occurred when a pair of symmetrical crescending cracks formed between the outer edges of the platen contact; there was no diametrical crack. Mellor and Hawkes (1971) concluded that the disc test is relatively insensitive to inelastic behaviour and gives a good approximation of the uniaxial tensile strength for "Griffith-type" materials.

Large differences have been found by many workers between the tensile strength determined in diametrical compression tests on disc specimens, and the direct tension tests or other methods (e.g. the bend test). As a result, several workers applied corrections to the measured tensile strength based on fracture mechanics theory and Weibull's probabilistic theory of critical flaws in brittle materials, e.g. Vardar and Finnie (1975). Marion and Johnstone (1977) and other workers, reported that the area over which the load should be distributed for a "valid" tensile failure depends on sample material. Patel and Staniforth (1987) observed that the behaviour of pharmaceutical tablets is very sensitive to the strain-rate. For soil discs, Krishnayya and Eisenstein (1994) argued that the Brazilian test can lead to considerable errors in estimating the tensile strength.

The diametrical compression test has been extensively used in the pharmaceutical industry to determine the crushing or tensile strength of tablets and of other disc-shaped samples made of powder material - see Edicott et al (1969), Rees and Shotton (1969), Fell and Newton (1968), Ridgway (1970), Fell and Newton (1970), Newton et al (1971), York and Pilpel (1973), Esezobo and Pilpel (1975), Britten and Pilpel (1978), Lautenschlager et al (1976), Jarosz and Parrott (1982), Ferracane and Greener (1986), Doelker et al (1989). Many workers insisted that only when the tablet splits into two equal halves along the loaded diametral plane is the fracture load valid to use for determination of the tensile strength. In order to obtain "valid" tensile failure for hard samples, they noted that paddings are necessary to reduce the high local compressive and tensile stresses under loading; the choice of material and width of paddings is best made from experimental observations (i.e. trial and error). For less hard (lower elastic modulus) samples, many (e.g. Fell and Newton, 1970) observed that paddings are not needed, as flattening of the sample prior to failure is sufficient to prevent line loading and obtain the "valid" form of sample failure. However, the wedge-like regions formed under the platens suggest that fracture could not be pure tensile in this case, even though samples finally split into two halves. Shotton and Ganderton (1960) described in detail the observed failure of sodium chloride tablets in which the wedges formed eventually produced a sudden failure by cleaving the sample across the diameter (*Fig. 3.2.j*). Newton et al (1972) proposed the utilisation of a different shape of samples: discoidal, but already flattened at two poles - to eliminate the need for paddings to distribute the load.

Shinohara and Capes (1979) analysed the effect of load distribution by comparing four different loading widths and obtained results similar to those of Rudnick et al (1963). Supporting the need for padding to distribute the load (for a tensile failure) they proposed an alternative solution for particle agglomerates and other weak samples: compaction of the sample in the region of load application, prior to testing it. They concluded that this would result in a distributed load and would considerably increase the chances of a "pure" tensile failure (as in Fig. 3.2c).

Shinohara et al (1982) developed a theoretical model to predict the effect on agglomerate tensile strength of variations in bulk powder properties and other parameters due to pre-flattening of samples. Their simplified model is based on the mechanical properties of powders (compaction behaviour, cohesion). The idea was that, prior to testing, the disc-shaped agglomerate was to be flattened by applying a certain amount of loading on it - which increased its bulk density and cohesive strength and to "prepare" it for tensile fracturing in the test. Assuming an exponential relationship between bulk density and pressure, Shinohara et al (1982) calculated the compaction force needed for the initial flattening of the discoidal agglomerate. The decomposition of failure of agglomerates into two distinct parts: yielding and compaction of contact regions, and then tensile failure is an

interesting idea. However, the real behaviour of weak materials in a diametrical compression test is a little different: failure follows the flattening, but there should be no interruption of loading in between. Unfortunately, the model has not been tested against experimental data.

Shinohara et al (1982) also analysed the effect of the shape of the applied load distribution. They found that if the load is spread more evenly, the stress distribution curve deviates more from that of the line loading and the stresses in the zones close to the platens become smaller. Investigating the effect of varying the number of individual (point) loads, they showed that having a smaller number of loads leads to considerable fluctuation of the tensile stress in the vicinity of the loading points. In trying to link the mathematical parameters describing the distributed loading to real experiments, they proposed two interesting connections: the width and the shape of the distributed loading relates to the stiffness of the platens and the sample, and the number of individual loads relates to the surface roughness of the platens/sample.

3.5 SPHERICAL SOLID SAMPLES

Diametrical compression tests have been performed on spherical specimens for mainly three reasons: to determine the tensile strength, to determine the "crushing" or "compressive" strength, or to examine the mode (brittle, elastic, etc.) and the mechanism of fracture, fragmentation or crushing. Most of the theories for the diametrical compression of spherical samples assumed perfect elastic behaviour before failure and brittle fracture behaviour; the majority of the work in this area was carried out on brittle solids (e.g. glass, rock, brittle ceramics).

3.5.1 Theoretical Considerations

Frocht and Guernsey (1952) investigated the stress within diametrically loaded spheres using experimental photoelastic results. They found that the maximum tensile stress, σ_t occurs at the centre of sphere, and is directly proportional to the load P and inversely proportional with the square of sphere's diameter D

$$\sigma_t = 0.573\frac{P}{D^2} \tag{3.8}$$

Rogowski (1964) assumed that diametrically loaded elastic aggregates of soil fail by tensile cracking according to the Griffith (1920) theory of crack initiation and propagation (i.e. the strength of a material is governed by the presence of naturally occurring cracks). Using the theory of Sternberg and Rosenthal (1952) and Frocht (1948), Rogowski (1964) worked out the tensile yield stress as

$$\sigma_t = 0.5762\frac{P}{D^2} \tag{3.9}$$

Lur'e (1964) mathematically analysed the case of an elastic sphere compressed by concentrated loads at its two poles. For the tensile stress in the centre of the sphere he obtained the relationship

$$\sigma_t = \frac{P}{\pi R^2}\left[\frac{21}{28+20\nu}\right] \tag{3.10}$$

or, for $\nu = 0.25$

$$\sigma_t = 0.81\frac{P}{D^2} \tag{3.11}$$

where P is the applied load and R is the sphere's radius.

Using the maximum tensile strain as a failure criterion Shaw et al (1975) worked out the failure tensile stress as

$$\sigma_t = \frac{P}{\pi R^2}\left[\left(\frac{21}{28+20\nu}\right)(1-\nu)+\left(\frac{42+15\nu}{14+10\nu}\right)\nu\right] \tag{3.12}$$

or, for $\nu = 0.25$

$$\sigma_t = 1.17\frac{P}{\pi R^2} = 1.49\frac{P}{D^2} \tag{3.13}$$

which is about twice the prediction of the previous authors.

Using their theoretical results and their diametrical compression experiments on rocks, Hiramatsu and Oka (1966) obtained the following expression for calculating the fracture stress of failure in tension along the loaded diameter

$$\sigma_t = K\frac{P_f}{\pi D_f^2} \qquad \text{where } K = 0.9 \tag{3.14}$$

The expression only needs the values of the load at fracture Pf and of the diameter of the spherical sample at the instant of fracture Df. This relationship became famous and was extensively used by experimentalists who assumed tensile failure of their samples (in diametrical compression tests).

Shipway and Hutchings (1993a,b,c) were the first to analyse and emphasise the significant effect of the contact load distribution (and platen material) in diametrical compression tests on spherical samples. They corrected Hiramatsu and Oka's (1966) solution for the internal stresses and extended Dean et al's (1952) solution to diametrical compression. Giving numerical values to their theoretical relationships, they obtained useful stress distributions that predict the tensile stresses along the loading axis, the maximum values of the axial and surface tensile stresses, and the shear stresses - all for a wide range of contact radius (width) values. The maximum values of the tensile and shear stresses on the loaded axis and the surface tensile stresses can be easily determined from these graphs (distributions), if the force and the contact radius is known at fracture. Although the solutions assume a uniform pressure over the loaded area and perfect elastic spheres, they still provide an idea of the stresses developed in non-idealised conditions.

3.5.2 Behaviour Before The Final Failure/Fracture

The behaviour of elastic spheres in diametrical compression tests was usually inferred to be perfect brittle - i.e. they suffered only elastic deformation until a final sudden failure. Detailed test observations were rarely obtained and/or published. Most of the few workers who did report the observed behaviour described that elastic spherical samples suffer local damage by the platens at the start of the diametrical compression test, before general failure. Glass samples (0.05 - 25 mm diameter) were reported to develop ring-cracks and/or cone-cracks near one or both areas of contact with the platens - see Bergstrom and Sollenberger (1961), Arbiter et al (1969), Rumpf and Schönert (1972), Shipway and Hutchings (1993). Other elastic samples (metal, glass-reinforced amalgam, sapphire) behaved similarly in the initial stages of the tests - see Schönert (1973), Verall (1976), Shipway and Hutchings (1993b,c), Kienzler and Schmitt (1990). The surface cracks often managed to spall off thin flakes from the spheres' poles. Bergstrom and Sollenberger (1961) believed that these encircling spalling fractures are due to (initiated by) the local tensile stresses, whereas Arbiter et al (1969) inferred that local shear stresses are alone responsible for them. Kschinka et al (1986) were among the workers reporting that no cracks at all formed around the contact zones of their glass spheres.

For elastic samples, some workers reported the development of inverted conical regions of densified material at the sphere's loaded poles. Arbiter et al (1969) reported that compressive stresses comminuted the material in the cones before final failure, whereas Rumpf (1990) argued that the cone's comminution (transformation into fines) happened at the moment of final failure. A few other workers identified two unbroken cones at the very end of test - see Bergstrom and Sollenberger (1961), Bergstrom et al (1961), Gilvarry and Bergstrom (1961), Shipway and Hutchings (1993b,c). Unbroken cones were usually seen as a

reflection of the more elasto-plastic character of the material. If the platens were plastic, no local contact damage before final fracture was found by Shipway and Hutchings (1993) for glass and sapphire spheres. The samples instead formed indentations into the platens. This significantly increased the area of load distribution.

Irrespective of platens material workers reported that the load-strain/displacement curve presented a steady increase until a sudden drop at the final failure. Although very few published the experimental curves most workers argued that, for elastic spheres, the curves showed elastic behaviour up to failure. The load-strain curve published by Verall (1976) for dental amalgam spheres (concave at the very start and straight afterwards) would, however, suggest that pure elastic behaviour only occurs in the very first moments of the test. Verrall (1976) believed that the small amount of initial curvature of the load-strain curve was due to local crushing at contacts with platens, due to the Hertzian-type cone cracks, and not due to the initial elastic behaviour of sample.

For plastic spheres, the initial local plastic deformation by the poles was reported to mainly consist of flattening. The material in the compression zones adjacent to the platens is compacted and forms two opposite cone-shaped zones of higher density - Rumpf and Schönert (1972), Schönert (1973), Rumpf (1990), Kienzler and Schmitt (1990). Plastic samples deformed (flattened) much more than the elastic ones before the occurrence of final failure. Diametrical compression tests, therefore, lasted much longer for plastic than for elastic spheres.

3.5.3 Final Failure And Inferred Mode Of Failure

Failure of brittle-elastic spheres was generally reported to occur at low strains - e.g. Arbiter et al (1969) reported failure strains of about 0.1% for their glass spheres. Local deformation/cracking by contacts did not stop most workers believing that final failure initiation in diametrical compression tests on spherical elastic-brittle samples was only due to internal tensile stresses. They suggested that fracture began from an internal flaw (defect) located somewhere near the centre of sample, where the tensile stresses were largest. That was why these workers used relationships similar to that of Hiramatsu and Oka to calculate a solid sphere's tensile strength from the fracture load and sample diameter.

Brittle-elastic samples were generally reported to fracture. The usual exceptions were the glass specimens, whose failure was sometimes that explosive that only small debris remained at the very end of the tests. Gilvarry and Bergstrom (1961) and other workers regarded shattering failure mode as (presumptive) evidence for the pre-existence of internal cracks inside samples. For elastic samples, Gilvarry and Bergstrom (1961) differentiated between single and multiple fracture. Fracture of a brittle solid by an external stress system

which is removed instantly when fracture is initiated was defined as single (primary) fracture. Multiple fracture consists of a single fracture followed by a sequence of only a few secondary fractures. With glass spheres, multiple fracture was reported to occur mainly because the large fragments resulted from primary fracture broke further due to high-velocity impacts with testing device's walls. Bergstrom and Sollenberger (1961) and Gilvarry and Bergstrom (1961a, 1961b) managed to eliminate secondary fractures by placing the specimen in gelatine during test.

Generally, the reported surfaces over which primary fracture of elastic spheres occurred were meridional. Exceptions to these are the observations of Rumpf and Schönert (1973) and Schönert (1973) who described that failure occurred along curved surfaces, similar to onion layers. Whereas no cracks developed along meridional planes in their tests, high surface tensile stresses in the neighbourhood of one of the contact areas created cracks that propagated along onion layers-like surfaces and destroyed the glass sample. Also, from the theoretical treatment of a steel ball, Schönert (1973) concluded that no cracks parallel to the meridional planes could be expected. Another exception is the observation of Kschinka et al (1986) who reported that failure of their glass samples occurred in an explosive-like manner with the glass sphere completely disintegrating into a powder. Kschinka et al (1986) inferred that their specimens failed from volume (internal) flaws due to the internal tensile stresses on the loaded diameter.

3.5.3.1 Glass Spheres

The reports of most workers revealed that final failure of glass samples usually produced large lune-shaped or wedge-shaped fragments, similar to orange slices - see Bergstrom and Sollenberger (1961), Bergstrom et al (1961), Gilvarry and Bergstrom (1961), Arbiter et al (1969), Shipway and Hutchings (1993b,c). Apart from these, they also reported small irregular fragments and, sometimes, two medium-sized conical fragments (cones) consisting of compacted (densified) fine particles (debris) with the flattened sample-platen contact areas as their base. The lune-shaped fragments were observed to fly outwards at high velocities so that, at the moment of fracture, very little material remained in the original location. Bergstrom and Sollenberger (1961) inferred that internal shear stresses are responsible for this type of failure. They believed that, when the sphere fractures, each fragment slips and pushes against its neighbours and that the lune-shaped fragments are driven apart due to an interplay of forces. Arbiter et al's (1969) observations were somewhat similar. However, they showed that tensile stresses also play a major role: shear deformation on conical planes produces hoop tension which in turn causes the opening of the cracks in the central region (starting from platens). This finally leads to the splitting of the sphere along several meridional fracture planes. Arbiter et al (1969) explained in detail that the very high

compressive stresses along loading axis and approximately uniform tension (normal to the loading axis) are responsible for disintegration of material in the sample's core.

Shipway and Hutchings (1993b,c) obtained similar results for rigid-*elastic platens.* They believed that the internal shear stresses initiated the final failure, pointing out that the conical fragments are a proof of that. From the measured and calculated contact radius at fracture, Shipway and Hutchings (1993b,c) determined the values of the stresses of interest at failure for the 15 different platen materials (some elastic, some plastic) that they used. Although testing identical glass spheres, they found great variation in the behaviour and failure load values for each platen material. For the elastic platens Shipway and Hutchings (1993b,c) found that the values of the surface tensile stresses varied much more than those of the internal shear stresses and were too low to cause fracture from surface flaws. The internal shear stresses exhibited much more constant (consistent) values (around 2 GPa, which is sufficient to cause fracture), thereby demonstrating that fracture was initiated by a local internal shear failure. Nevertheless, they concluded that the failure mechanism is a complex process and that propagation of the cracks, once initiated, is also affected by the internal tensile stresses - which are higher than the surface tensile stresses.

For soft or *plastic platens,* Shipway and Hutchings (1993b,c) reported that the spheres indented the platens as the load was increased, that very little or no crushing was produced at contacts with the platens (no cone-shaped fragments were found), that the resulting fragments were larger and had the shape of hemispheres or sphere segments. Shipway and Hutchings (1993b,c) showed that the surface tensile stresses initiated final failure of glass samples in the case of plastic platens. The maximum values of the surface tensile stresses were only slightly lower and varied less than those of the internal tensile stresses. Knowing that the surface strength of glass is much lower than the internal strength, they concluded that the failure must have been initiated at a critical value of the surface stresses (at around 0.2 GPa). Supporting this conclusion were also the results obtained with glass spheres having abraded surfaces, where the fracture loads were reduced dramatically (by the increase in density and severity of surface flaws).

3.5.3.2 Other-Than-Glass "Elastic" Spheres

For brittle-elastic materials other than glass, workers have reported breakage/fracture of spherical specimens into two halves or sometimes into three, four or five lunar segments, with little or no fines at the contacts with the platens - e.g. Hiramatsu and Oka (1966) and Oka and Majima (1970) for rock samples, Verall (1976) for dental amalgam spheres. Most workers believed that these specimens fracture due to internal tensile stresses and, therefore, used diametrical compression tests mainly to determine the tensile strength with equations similar to (3.14). However, several workers have recently shown that the meridional

fracturing of elastic samples (other than glass) is due to the pushing towards the inside of the sample of the two conical densified zones that form at the contacts - see Kienzler and Schmitt (1990), Shipway and Hutchings (1993b) for sapphire samples.

Based on finite element analysis, Kienzler and Schmitt (1990) claimed that no meridional cracks can initiate exactly from the contact areas as the circumferential stresses are compressive. Nevertheless, since the tangential component is singular at sufficiently high loads, ring cracks may initiate at the contact surface. The contact area increases and then, if the available energy is high enough, there are two possible modes of behaviour. If the crack keeps its original direction and follows the trajectories of principal shear stress, two opposite macroscopic convergent cone cracks are created. The cones are pushed farther into the sphere and meridional cracks occur. If, however, the crack is deep enough to get into the region of tensile principal stresses in the meridional plane, it will deviate from its initial orientation and follow the trajectories of principal compressive stresses. In this case, Kienzler and Schmitt (1990) stated that divergent cone cracks develop which, if not arrested, will split off fragments when they will arrive at the free surface.

For different platen materials, Shipway and Hutchings (1993b) found much more variation in the failure loads for sapphire than glass spheres. For stiff, elastic platens, sapphire spheres developed shear cones that led Shipway and Hutchings (1993b) to conclude that the fracture was initiated by internal shear failure. However, they concluded that the failure of the sapphire spheres might have been governed by propagation rather than by initiation of fracture - which was the case with glass samples. Sapphire spheres with abraded surfaces proved to be a special case: Shipway and Hutchings (1993b) could not discern any conical region with either plastically or elastically deforming platens. Fracture apparently initiated from the surface of the sample, although it was not clear where this occurred with respect to the platens.

From a wide range of laboratory test results, Rumpf (1990) gave a different explanation for the failure mechanism for all elastic spheres subjected to diametrical compression. He reported two fracture phases. In the primary fracture phase, curved fracture trajectories run from one contact zone to the opposite one. The fractures approximately follow the principal compressive stress direction. The secondary fracture phase is determined by dynamic stress fields which are produced by the rapidly advancing fractures. If these primary fractures relieve the stresses in the compression zones adjacent to the platens rapidly enough, vibrations are induced in the material and these vibrations result in tensile stresses or even secondary fractures. Rumpf (1990) also remarked that the compression contact zones possess the highest energy density before fracture begins and when this energy is released it results in the production of mainly fine material.

3.5.3.3 "Plastic" Spheres

For plastic spheres, the relatively large conical zones formed from contacts with platens seem to have played a very important role in the failure mechanism. Rumpf and Schönert (1972) explained that the conical (indenter-shaped) zones cause plastic flow when pushed into the material by the applied load.

Schönert (1973) investigated the diametrical compression behaviour of a 50 mm PMMA sphere and of polymer samples of diameter 30 μm - 5 mm. Measuring the strains induced on the surface of the PMMA sample, he found very high latitudinal tensile strains up to the neighbourhood of the contact area (he found much lower latitudinal strains in elastic spheres). Schönert (1973) explained that this was because, beneath the contact area, a cone-shaped part of the material was driven into the sample, pushing off the surrounding material which flew outwards and stressed the sample's outer shell similar to internal pressure. He argued that, due to the high latitudinal tensile stresses, cracks are initiated and run parallel to the meridional planes, dividing the sample into two or more fragments - similar to orange slices. His 50 mm PMMA sphere was split into two halves by a meridional crack. Polystyrene samples larger than 0.35 mm developed meridional cracks: the larger the sample, the more cracks were developed. The cracks developed at a much lower speed (and at larger strains) than in elastic materials and needed further loading to propagate. Further loading usually also resulted in the initiation and propagation of new cracks. Breakage of polystyrene did not occur, not even for the largest (5 mm diameter) sample at 60% strain. At large strains, polystyrene samples exhibited very high levels of damage but could not be broken. The failure was not explosive at all and the force was continuously increasing on the platens - with one or more drops corresponding to crack formations. Lower temperatures caused a little "embrittlement" but not a change in the fracture mode. Polystyrene samples equal or smaller than 0.35 mm in diameter presented very ductile behaviour: they did not even crack.

For samples which deform plastically, Rumpf (1990) described the behaviour under diametrical compression as comprising of two main phases. In the primary phase, the material in the compression zones adjacent to the platens deforms plastically and forms two opposite cone-shaped zones of higher density. In the secondary fracture phase, the two opposite cone-shaped zones are pushed into the centre of the sample, thus forcing the material to the side of them outwards. These movements of material generate peripheral (or hoop) tensile stresses perpendicular to the load direction. As a consequence, the sphere fractures by breaking up into pieces like segments of an orange. Rumpf (1990) also noted that it is a characteristic of plastic material not to produce fines. Although tensile stresses are also produced in the contact zones of high energy density, these are superimposed on the compressive stresses during loading, with the result that no local crushing occurs. Another

particularity of plastic spheres noted by Rumpf (1990) is that, when the load is released, fractures are produced due to tensile stresses caused by plastic deformation and stored energy inside the sample.

For an ideal homogenous solid of elasto-plastic material, Kienzler and Schmitt (1990), using finite-element analysis, found that the peak tangential stress components diminish due to plastic flow. The region of high circumferential stresses spreads towards the surface, whereas the hoop stresses increase, become tensile at sample-platen contacts and finally control the whole fracture process. Meridional (orange-slice) cracks develop and produce (first) orange-sliced fragments which may be further comminuted by subsequent ring cracks.

3.5.4 Other Observations

Investigating the behaviour of a wide range of small quartz and limestone samples (1-100 μm in diameter) Steier and Schönert (1972) found that the smaller the size, the more ductile and plastically they behave. The number of radial cracks increased with decreasing sample size (from 100 to 5 μm), due to larger plastic deformations in the centre of the sample. However, below 3-5 μm size the number of radial cracks decreased again, such that they expected the samples smaller than 1 μm to deform without fracture (i.e. purely ductile). Hess and Schönert (1981) found analogous results for black coal, boron, boron-carbide, cane sugar, cement clinker, limestone, marble, potassium chloride and quartz samples. The so-called micro-plasticity of small brittle materials was characterised by a failure composed of a series of fracture events, reflected in a multi-peak (fluctuating) load-displacement curve. Using samples of decreasing size, Hess and Schönert (1981) found that the transition from brittle to ductile behaviour occurs between 20 μm and 10 μm sample diameter. Similar transitions were reported by other workers for small glass samples.

Many workers, especially those interested in comminution, have tried to determine the input strain energy required for creating new surfaces (for size reduction) of a sample in the diametrical compression tests. Many size-reduction theories have been developed both empirically and theoretically. Rittinger (1867) postulated that the work consumed for the reduction of particle size is directly proportional to the new surface produced. Kick (1885) hypothesised that, irrespective of the original size, the work required for crushing a given quantity of material is constant for the same reduction ratio. Bond (1952) attempted to produce a practical unifying principle for comminution in all size ranges. Charles (1957) developed a general equation relating energy and size reduction of brittle and semi-brittle materials which has a different form for each comminution process. Charles showed that the previous three hypotheses (of Rittinger, Kick and Bond) can be derived as special cases of this general equation. However, the variable exponent in the equation should be determined

directly from experimental tests. Charles (1957) was the first to base his theory on the strain energy of elastic deformation, showing that it is the energy stored in the sample which produces fracture (size reduction). He showed that for impacts of elastic systems, the maximum fraction of kinetic energy absorbed as strain energy is mainly dependent on the geometry of system and only slightly on the input energy. In fracture by high velocity impacts, Charles (1957) found that if the input energy is doubled, the energy useful to fracture is doubled. Gilvarry (1961a) proposed a theory based on the stress activation of flaws in Griffith-type material samples, whereas Oka and Majima (1970) developed a theory of size reduction based on the concepts of material strength and suggested that the energy required for size reduction is proportional to the second order of the tensile strength, the third order of the particle size and inversely proportional to Young's modulus.

Most of the input energy in elastic samples is transformed into strain energy and then (after fracture) into kinetic energy of the fragments. For glass spheres Bergstrom and Sollenberger (1961) found that 45% of the initial energy was converted into kinetic energy of the fragments but, due to air drag, most of this is eventually converted into thermal energy (if fragments did not impact other surfaces). They stated that dissipation of energy into other forms (e.g. surface energy, sonic energy, vibrational energy) represents a very small fraction of the initial input energy.

3.5.5 "Fast" Diametrical Compression

In order to determine the (tensile) strength of spherical samples many workers carried out "fast" diametrical compression tests, but still at a platen velocity where they could not observe significant strain-rate effects. Jaeger (1967) tested different rocks (Carrara marble, bowral trachyte, sandstone and limestone) in "rapid" diametrical compression. He applied Hiramatsu and Oka (1966) relationship (3.14) to determine the samples' tensile strength (using different values of the coefficient K for each type of rock). He only noted some strain-rate effects for marble. As in most cases the calculated maximum tensile stresses on the loading axes were of the order of the material's uniaxial tensile strength, Jaeger (1967) inferred that failure initiated in the sample's centre due to internal tensile stresses. Other workers using (3.14) for calculating the tensile strength from fast diametrical compression tests inferred the same initiation and failure mechanism, without closely analysing the fracture behaviour during the tests.

Jaeger (1967) reported slight differences in the failure of hard rocks. Although several "harder" trachyte samples shattered (broke down suddenly into many small fragments), the trachyte samples usually broke up into two or three approximately equal "lunes". The sandstone, marble and limestone samples generally fractured into two hemispheres. Apart from large fragments, Jaeger (1967) also noted some debris (fines). In some cases, a while

after the primary fracture, one of the hemispheres was further divided in two roughly equal parts. Jaeger (1967) described the mechanism of failure for the fast diametrical compression test as "an extension fracture in a single diametral plane".

From fast diametrical compression experiments on rock samples (Oka and Majima, 1970) and on cement-mortar, marble and on sandstone samples (Kobayashi, 1965) it was found that fracture load increases with increasing compression velocity. Samples of the same material thus seemed stronger for higher load-rates. From their different strain-rate diametrical compression and free-fall impact tests on spherical soil samples, Hadas and Wolf (1984) concluded that, below a specific loading rate - suspected to equal the stress wave velocity specific to that soil (e.g. 3 m/s for one of the soils) - soil strength (and thus fracture load) is independent of the loading rates.

Bergstrom et al (1961) and Gilvarry and Bergstrom (1961b) carried out diametrical compression tests at variable strain-rates on spherical glass samples (of 3-76 mm diameter). The mechanism of breakage for "fast" compression seemed to remain the same as for the "slow" compression as they could not find any statistically reliable evidence of an effect of the rate of loading on the form of the distribution function for fragment size. Similar conclusions were drawn by Arbiter et al (1969) from comparing their slow load-rate double impact and slow compression tests on glass spheres.

For sapphire and polycrystalline samples (3 - 25 mm), Bergstrom et al (1961) studied the efficiency of the crushing operation through variable strain-rate compression tests. They found similar results to the ones they obtained with glass samples and to the ones obtained by Charles (1957): the energy input per unit mass required for fracture was inversely proportional to the product size. They also showed that smaller samples required greater energy per unit mass for fracture.

3.6 SPHERICAL AGGLOMERATES

Diametrical compression testing has been applied to agglomerates in order to determine their tensile strength (for "brittle" samples) or their crushing strength (for weakly-bonded agglomerates). Neglecting their particulate nature, many workers have inferred that brittle agglomerates fracture in the same manner as homogeneous brittle solids. These workers even used equations similar to (3.14) to determine the agglomerate tensile strength from measuring the fracture load and diametral area.

3.6.1 Theoretical Considerations

Most researchers considered agglomerate porosity to be the main factor which controls the tensile strength. Ashton et al (1965) expressed agglomerate tensile strength as a function of porosity and particle density, whereas Cheng (1968) suggested a more complicated relationship in which the tensile strength varied with porosity, coordination number, relative mean particle surface, interparticle force and platen interface details. Rumpf (1962) calculated the tensile strength for agglomerates of monosized spheres as a function of the porosity n, coordination number Z, the mean interparticle force F_{av} and the surface area of a particle S_p

$$\sigma_t = Z(1-n)\frac{F_{av}}{S_p} \tag{3.15}$$

Tsunakawa and Aoki (1972) believed that tensile strength also varies with the shape and size of the constituent particles. Schubert (1975) concluded that a practical relationship for the tensile strength must consider all the above factors plus the elasticity of particles, as it determines the force-displacement behaviour at the interparticle contacts. Testing different powder agglomerates in tensile splitting tests, Schubert (1975) found that Rumpf's equation (3.15) overestimated the tensile strength by an order of magnitude because, he believed, it superimposed the interparticle adhesion forces.

Fracture mechanics workers have shown that flaws change the (local) stress distributions in samples. Hertzberg (1976) gave a relationship to account for the increase in stress caused by a flaw with sharp edges

$$\sigma_{max} = \sigma(1+k\sqrt{\pi a}) \tag{3.16}$$

where σ is the stress not influenced by flaws, $2a$ is the flaw length and k is a constant. Meyers and Meyers (1984) used (3.16) to determine the tensile stress causing fracture from a flaw in the centre of a pellet

$$\sigma_t = \frac{8P_f(1+k\sqrt{\pi a})}{\pi^2 D^2} \tag{3.17}$$

where D is the pellet's diameter and P_f the rupture (fracture) load.

Breval et al (1987) claimed that, when fracture initiates in a uniform stress field, due to a crack propagating in Mode I perpendicular to the internal tensile stresses, failure occurs at a stress value that does not depend on the magnitude of the stresses acting in the plane of the crack. In this case the failure tensile stress σ_t is given by

$$\sigma_t = \frac{K_{Ic}\sqrt{\pi}}{2\sqrt{c}} \tag{3.18}$$

where K_{Ic} is the Mode I fracture toughness and c the pore radius. They obtained good agreement with (3.18) from their diametrical tests on proppants and sand samples having different sizes of internal pores.

Capes (1970/71, 1971/72) investigated the crushing of spherical agglomerates having hardened shells. He created a theoretical model which would fail when the tensile strength of the bonds (considered constant per unit area) would be exceeded by the compressive stress created by the squashing of the sample under the platens. Using the studies of Rumpf (1962) and Pietsch (1969), he developed a relationship in which the load required to crush the agglomerate was equal to the tensile strength of the bonds multiplied by that part of the failure cross-section where the binder (hardening material) was present.

For an agglomerate in which perfect-elastic rubber-beads ("evatane" resin, ICI) particles (of 3 mm diameter each) were kept together only by van der Waals forces (according to JKR theory), Kendall and Weihs (1992) estimated the fracture strength as

$$\sigma_f = 15.6\frac{\varphi^4 \Gamma_b^{5/6} \Gamma^{1/6}}{\sqrt{dc}} \tag{3.19}$$

where φ is the volume fraction of the agglomerate, d is the average diameter of the constituent particles, Γ_b is the work of adhesion measured by fracturing contacts between particles, Γ is the equilibrium value of adhesion energy measured in elastic modulus tests, and c is the flaw size within the agglomerate.

3.6.2 Behaviour Before The Final Failure/Fracture

Most investigations reported in the literature suggest that agglomerates behave like plastic solid spheres in that they exhibit relatively large strains along the loading axis before final failure. Straining is mainly due to the compaction and/or plastic deformation of the sample-platen contact zones. This occurs despite the fact that the material of the constituent particles is generally elastic. It seems that most of the plastic behaviour of agglomerates actually occurs not due to the plastic nature of the particle material, but due to weak bonds and high agglomerate porosity. For instance, the particles in Kendall and Weihs's (1992) agglomerates were held together only by van der Waals forces and the agglomerate porosity was about 60%. One of their 10-70 μm diameter zirconia agglomerates only failed at about 7% strain. Newitt and Conway-Jones (1958) reported 5% fracture strain for their sand and silt agglomerates (1-25 mm diameter), Rogowski et al (1968) between 4%-11% for their 2-8

mm diameter air-dry aggregates and Arbiter et al (1969) 1.2% for their sand-cement agglomerates. Compaction of the material near the agglomerate-platen interfaces generally produced two conical inverted zones at the poles (as for plastic solid samples) - see Newitt and Conway-Jones (1958), Kapur and Fuerstenau (1967) for 8-20 mm diameter limestone pellets, Arbiter et al (1969), Wynnyckyj (1985) for iron-ore agglomerates, Tanaka et al (1985) for sintered ferrite of 75-150 μm diameter agglomerates, Ghadiri et al (1990) for three ionic crystals specimens of 2 mm diameter, Salman et al (1994) for aluminium oxide samples of 5.15 mm diameter.

Apart from the plastic deformation represented by the local plastic flow at contacts (flattening), workers only rarely reported local cracking of samples before final failure. Arbiter et al (1969) noticed the development of minute, densely distributed cracks around the perimeter of agglomerate-platen contacts (before final failure). Testing a very large number of aluminium-oxide spheres, Salman et al (1984) observed several concentric ring cracks around the loading area and noted that they did not propagate far inside the material. In tests on hard samples of ionic crystals Ghadiri et al (1990) noted subsurface lateral cracks which produced local chipping in the form of flakes around the contact region. For their iron-ore pellets Meyers and Meyers (1984) describe local crushing at poles which only occurred if stiff-elastic platens were used. Breval et al (1987) also reported local crushing of material (into fines) at the contact with the platens for their proppants and sand specimens of 0.65-0.78 mm diameter.

Many workers reported that specimens behaved elastically before fracture, making reference to the shape of the load-displacement curve during the test - which was published by only a few. However, there is a disagreement between what shape would represent pure elastic deformation. Whereas Breval et al (1987) and Kendall and Weihs (1992) considered a concave curve to represent elastic behaviour, most other workers regarded a straight-line relationship to characterise the sample's elasticity.

Too many workers neglected the behaviour of specimens before fracture, this lead them to draw wrong conclusions about the character of failure. Disregarding the large initial plastic deformations (flattening and crushing at contacts) Rogowski et al (1967), Breval et al (1987), Wong et al (1987), Kendall and Weihs (1992) and many others classified failure of their samples as brittle.

3.6.3 Mode Of Failure

Although most of the agglomerates were reported to have fractured in diametrical compression tests, some specimens were crushed. For 15-30 mm diameter limestone pellets (5-10 μm particle size) Rumpf (1962) reported that the test usually produced a small primary

crack from which pellets crumbled. Cape's (1971, 1972) sand-salt agglomerates (49 - 28 μm particle size) also crushed, and so did some of Wynnyckyj's (1985) iron-ore agglomerates. Kendall and Weihs (1992) suggested that their agglomerates cracked and then fractured into many fragments, but only at high strains (so that they actually crushed). For spherical pharmaceutical tablets (lactose-providone of 1-1.8 mm diameter) Jarosz and Parrott (1983) explained that some samples fracture, others crush or only suffer local fracturing.

In diametrical compression tests, fracture was abrupt, along meridional plane/s and typically resulted in very few large fragments. Fracture into two hemispheres was reported by Newitt and Conway-Jones (1958), Meyers and Meyers (1984), Kapur and Fuerstenau (1967), Arbiter et al (1969), Wynnyckyj (1985), Tanaka et al (1985), Wong et al (1987) for 0.9 - 1.8 mm diameter ceramic (aluminosilicate clay) spheres, Salman et al (1994). Between 2 and 4 large fracture fragments were obtained by Meyers and Meyers (1984), Breval et al (1987), Ghadiri et al (1990) and Salman et al (1994). From tests on a very large number of samples, Salman et al (1994) found that catastrophic failure always occurred along meridional planes in one of the four "main" forms (presented in Fig. 6.60a,b,d,e in Chapter 6). Most frequently, the spheres fractured into one hemisphere and two quadrants (in 43% of all tests), or into four almost equal quadrants (in 39% of all tests). Salman et al (1994) believed that the two "deviations" from half-half fracture (that presented quadrants) were due to secondary fractures caused by further loading of one or both of the hemispherical fragments after the occurrence of the half-half fracture.

Apart from the large fragments, some workers also found evidence of the conical regions developed adjacent to the platens. The debris found at the end of a test by Meyers and Meyers (1984), Breval et al (1987), Ghadiri et al (1990) seems to have belonged to the conical sample-platen contact damage zones. Others detected cones which were compacted but unbroken - see Arbiter et al (1969), Salman et al (1994). Ghadiri et al (1990) actually found that the conical regions crush (transform into fines) only for the harder materials. Kapur and Fuerstenau (1967) and Wong et al (1987) seem to have found the contact compressed (densified) zones embedded in the large fragments.

As in diametrical compression tests on solid samples, many workers using brittle or semi-brittle agglomerates inferred that "fatal" fracture initiates close to the sample centre due to internal tensile stresses - see Meyers and Meyers (1984), Breval et al (1987), Wong et al (1987). Others did not specify the stress causing fracture but inferred that it initiated from an internal flaw - see Kendall and Weihs (1992).

Arbiter et al (1969), Tanaka et al (1985), Wynnyckyj (1985), Ghadiri et al (1990) and Salman et al (1994) reported that fracture initiated from the vicinity of the contact areas with the platens. Newitt and Conway-Jones (1958) inferred that cracks usually initiate inside the

agglomerates and propagate fast but observed that surface cracks first appeared in the zone between the poles and the equator and then rapidly spread across the whole meridian plane. Many workers described the inverted conical regions to be the cause of fracture, as these were pushed into the specimen and acted as wedges (stress concentrators) splitting the specimen in 2-4 large fragments - see Newitt and Conway-Jones (1958), Kapur and Fuerstenau (1967), Arbiter et al (1969), Tanaka et al (1985), Wynnyckyj (1985), Ghadiri et al (1990), Salman et al (1994).

Arbiter et al (1969) reported that failure started along the two (opposite) conical surfaces, the bases of the cones approximately corresponding to the areas of contact at the instant of failure. At the end of test, they found the cones covered (on their surface) by a layer of pulverised material. Arbiter et al (1969) suggested that this was due to a shearing mechanism. As the cones (having the base angle of $60°\pm5°$) were driven into the sample, hoop tensile stresses were induced - which finally split the specimen into two halves, due to running cracks starting from the periphery of the contact areas. Salman et al (1994) reported a very similar fracture mechanism. Ghadiri et al (1990) added that for their samples fracture was produced following a dislocation glide on 45° slip planes. Newitt and Conway-Jones (1958) explained that the peak angle of the cones depends on the internal friction coefficient, magnitude of the applied load and the platen roughness.

Although they also observed plastically deforming regions by the platens, Meyers and Meyers (1984) did not suggest that these had any role in fracturing. Instead, they reported that post-mortem microscopic observations of the fracture surfaces indicated a tensile cleavage-type fracture process.

In the case of agglomerates, fracture surfaces were generally described to be rough and non-planar and to reveal the constituent particles. Tanaka et al (1985) found that for ferrite spheres under diametrical compression fracture was mainly intragranular and that intergranular fracture predominated in samples of very low strengths. Others also found that some specimens have (interparticle) bonds stronger than constituent particles - e.g. Meyers and Meyers (1984) for iron-ore pellets. The results of Breval et al (1987) seem to indicate that bond strength and particle size, rather than sample porosity and density, determine the character of the fracture surface in diametrical compression.

A few workers realised that the more plastic the platen material, the less local crushing at sample-platen contacts occurs. Using rubber pads between sample and platens, Meyers and Meyers (1984) found that the formation of the crushed region adjacent to the platens was reduced or completely eliminated. The fracture load was 15% lower than in tests without pads, indicating that local crushing at the platens might have had an effect on fracture. This seems to demonstrate that either local crushing near the platens changes the stress

distribution or fracture does not initiate (as Meyers and Meyers, 1984 indicated) at the centre of the sample (due to attaining maximum tensile stresses), or both. Otherwise, their tests would show that local crushing near the platens strengthens the sphere.

3.6.4 Other Test Observations

Analysing the compressive strength of sand agglomerates, Newitt and Conway-Jones (1958) found that the breaking load was proportional to the square of the agglomerate diameter. Other workers obtained similar relationships for various spherical samples. Using iron-ore agglomerates, Wynnyckyj (1985) experimentally verified the strength factor introduced by Newitt and Conway-Jones (1958) which states that agglomerate strength is proportional to the failure load divided by agglomerate diameter. He concluded that this is valid only for strong agglomerates which exhibit very small contact deformation (flattening).

Capes (1971/72) carried out diametrical compression tests on 3.75-30 mm sand and graphite agglomerates made of particles (49 - 208 μm) held together by salt bridges. He obtained an empirical relationship for predicting the agglomerate strength

$$\sigma_f = kD^n \tag{3.20}$$

where D is the agglomerate diameter, n varies between 1 and 2 and is related to the distribution of solid bridges within the agglomerate and k is a strength factor which increases with increasing temperature (of drying the pellets) and decreasing bond strength (total quantity of solid bridges). The relationship (3.20) is interesting as it does not need the value of failure load, and therefore no diametrical compression test would be needed. However, due to the large variation of k and n, it has limited practical applicability.

From their diametrical compression experiments on limestone pellets, Kapur and Fuerstenau (1967) generated two equations correlating the pellet's mass with the fracture force and fracture deformation. The empirical equations were a result of their observation that, on a log-log scale, pellet weight varies linearly with load at fracture and with deformation at fracture. They obtained equivalent correlations using pellet diameter instead of pellet strength.

Capes (1971/1972) carried out several tests on spherical samples of different particle sizes and binder distribution. Cape's actual agglomerates were made of sand (of 49, 103 and 208 μm particle size), but were hardened over a certain thickness of the shell by the crystallisation of dissolved salt (NaCl) during a drying process. His experimental crushing strength was higher than the one obtained from his theoretical model (described in section 3.6.1). He justified this by observing that, on a closer inspection, the hardened shell was

actually thicker than initially measured. It is unfortunate that Capes did not describe in detail how the specimens failed. However, from his experimental work Capes concluded three main points: agglomerates fail if the bonds' tensile strength is exceeded; higher loads are needed to crush an agglomerate having smaller sized particles - this being directly due to the higher bonding strength (as the number of bonds per unit area increases); an agglomerate is stronger the smaller it is and the more uniformly its bonds are distributed over the volume. Wong et al (1987) confirmed Capes's findings that the strength increases as sample size decreases. Using Weibull's statistical analysis, they explained that this is due to a more uniform granulation process in forming the smaller aggregates. As the spherical aggregate size decreases, the Weibull moduli increases and the flaw size distribution is less wide.

Jarosz and Parrott (1983) tested 1-1.8 mm diameter pharmaceutical-powder (lactose, calcium phosphate) granules having increasing concentration of binder (providone or starch) in diametrical compression. They found that there is a normal distribution of agglomerate strength with increasing binder concentration.

For small ferrite agglomerates having the same composition but various sizes (75-150 μm), Tanaka et al (1985) found a large scatter in the fracture load but no dependence on agglomerate size. Using Hertzian theory, they calculated the diameter of the contact areas at fracture and found that they were comparable with the grain size of the constituent particles. They concluded that crack formation must be sensitive to the crystal orientation of grains and, therefore, this could be the reason for the large scatter in values of fracture load obtained for different but similar agglomerates.

3.6.5 Relevance Of The Tensile Strength Determined From Diametrical Compression Tests

Rumpf's (1962) work on limestone powder was probably the first to suggest that spherical samples (limestone pellets) do not fail solely due to tensile stresses in the diametrical compression test. He found that the tensile strength determined from direct tensile tests was larger and did not even vary linearly with the strength determined from diametrical compression. He believed that this was mainly due to the fact that the failure load in diametrical compression test is also influenced by the friction force between constituent particles.

The expression (3.14) was established by Hiramatsu and Oka (1966) for rocks and, although Wijk (1978) showed that even for rocks it underestimates the "tensile strength" for small contact areas at fracture, it has been extensively applied to other materials - e.g. Kschinka et al (1986) for glass, Sikong et al (1990) for brittle minerals (quartz, feldspar, limestone, marble and gypsum) and coal, Verall (1976) for glass-reinforced dental materials.

Lur'e (1964) actually found a similar expression, but for materials with values of Poisson ratio typical of most ceramics and glasses. Other workers used (3.14) but sometimes with different values of the parameter K - e.g. Rogowski (1964) and Dexter (1975) and Rogowski and Kirkham (1976) for dry soils *(K=0.573)*, Jaeger (1967) for rocks (marble - *K=0.55*, bowral trachyte - *K=0.29*, sandstone *K=0.32*, and limestone *K=0.5*), Breval et al (1987) for proppants and quartz sand *(K=0.81)*, Wong et al. (1987) and Kendall and Weihs (1992) for modelling clay and ceramic agglomerates, Haddas and Wolf (1984) for soil aggregates. Carrying out various direct and indirect tensile tests on rock specimens, Pandey and Singh (1986) concluded that the tensile strength is not a material but an experimental property - as it depends on the type of test performed.

Darvell (1990) was the first to openly criticise the use of the Hiramatsu and Oka relationship. He expressed serious doubts about even the possibility of a diametrical compression test (on a spherical sample) providing a reliable indication of the tensile strength. Using their numerical analysis, Shipway and Hutchings (1993b,c) finally demonstrated why the relationship (3.14) seemed to work and why it is wrong. One big mistake was that experimentalists employed Hiramatsu and Oka's (1966) relationship irrespective of the platens/padding materials used and, thus, irrespective of the size of the contact area with the platens. Furthermore, Shipway and Hutchings (1993) showed that, for brittle spherical samples, fracture initiates either due to internal shear stresses (for hard platens) or due to surface tensile stresses (for soft platens). Only for special cases - materials having significant bulk flaws - can failure be initiated by the internal tensile stress. Generally, they concluded that the internal tensile stress only contributes to the propagation of the already initiated cracks. Shipway and Hutchings (1993) did not provide an alternative to (3.14), but stressed that diametrical compression has very limited use in determining the tensile strength of spherical samples.

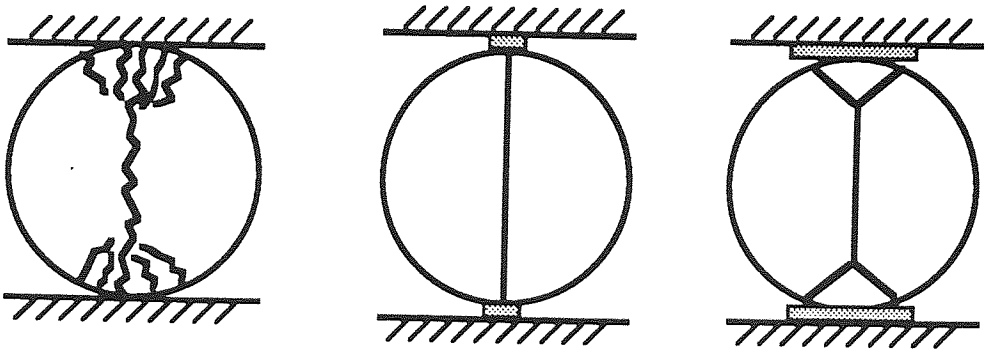

Fig. 3.1. Types of failure for cylindrical samples in diametrical compression (after Mitchell, 1961)

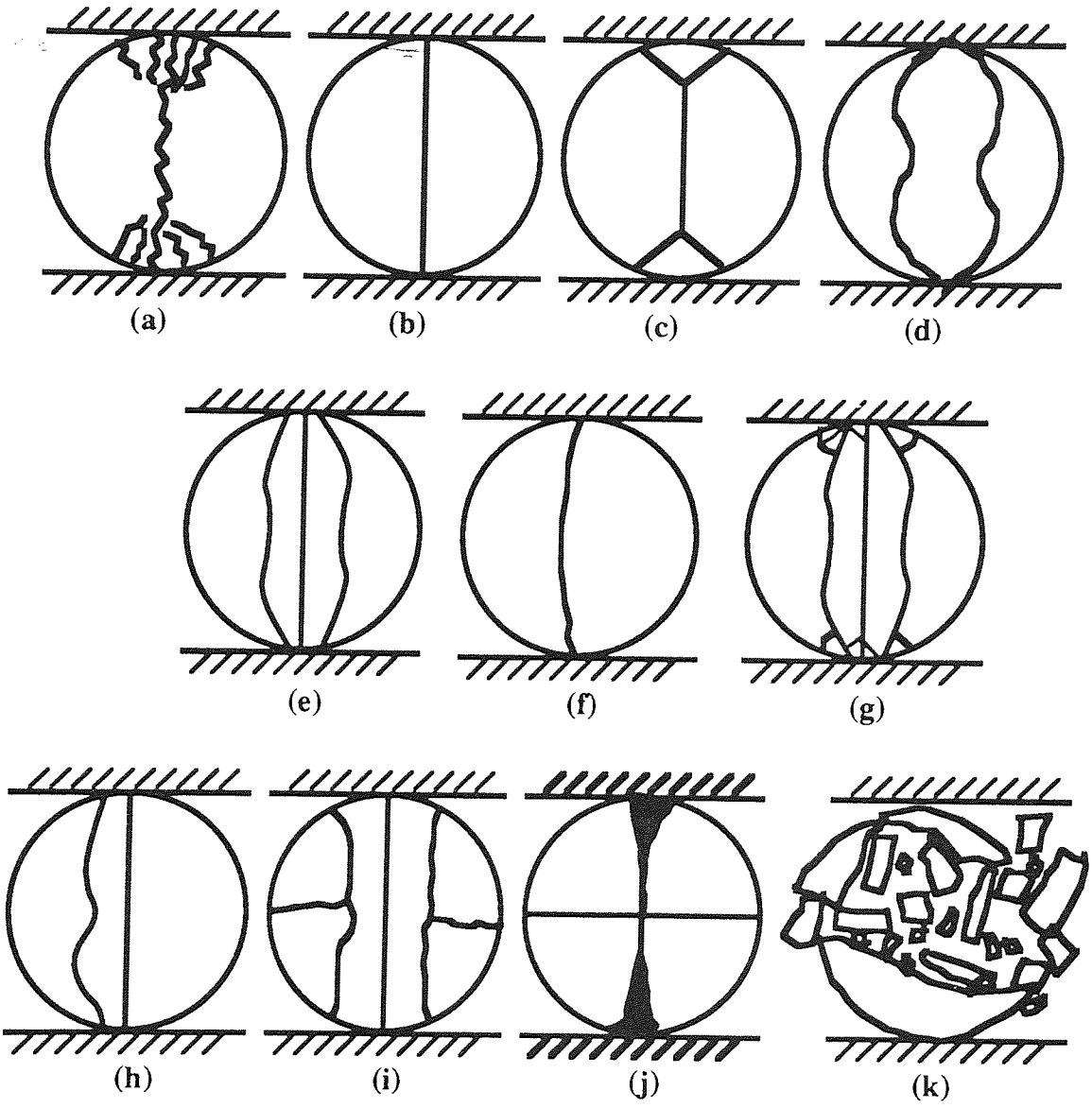

Fig. 3.2. Types of failure for disc-shaped samples in diametrical compression (after Ridgway, 1960, Fell and Newton, 1970, Marion and Johnstone, 1977, Colback, 1966, Rudnick et al, 1963, Mellor and Hawkes, 1971, Shotton and Ganderton, 1960)

CHAPTER 4

IMPACT TESTS

4.1 FREE-FALL IMPACT TESTS

In the "ad-literam" free-fall impact test, a sample is allowed to fall under gravity from a certain height onto a (usually rigid and fixed) target platen. If the platen is horizontal the impact is normal, if it is inclined the impact is called oblique. The impact velocity can easily be varied by varying the height of fall. Instead of increasing the height, the sample can be projected onto the platen, generally by using an eductor-gun. In this case the trajectory of the sample need not be vertical. Projecting samples constitutes an easy way of creating very high impact velocities. In general, free-fall impact tests refer to a single impact of a sample with a platen, the sample being free to move (rebound) after impact.

There are three main ways in which sample-platen impact tests have been carried out:
- impact of large numbers of "clone" samples to record how many survive (do not break) while different parameters (impact velocity, wall material, impact angle, etc.) are kept constant or varied;
- repeated impact of the same sample (for same conditions) and record the number of impacts needed before the sample fractures (number to be used as friability index);
- impact of one sample in order to analyse the breakage mechanism and/or the size distribution of the resulting products. (The tests simulated in this project relate to this last case).

Free-fall impact tests are often carried out using a number of samples at the same time. The multi-sample impact tests were devised to simulate, as close as possible, the way in which impact occurs in some real industrial processes. In these tests, many samples are simultaneously projected to impact a wall and, therefore, impacts occur at different angles - and not just between sample and wall, but also between samples themselves. It was shown that the first samples that arrive at the platen (and impact it) soften the fall of the other samples and thus reduce their breakage (British Materials Handling Board, 1987). These tests are very useful but have a very restricted application: a different test should be devised for each industrial process.

In free-fall impact tests, the force developed on the platen at fracture is difficult to measure; instead, for assessing a sample's impact strength, the input kinetic energy of the sample is generally used. For single samples, many experimentalists (British Materials Handling

Board, 1987, p. 59) used the minimum energy to cause damage as a measure of the sample's strength, others the number of necessary drops for breakage (from a fixed height) and others the minimum (necessary) free-fall height for causing sample breakage. Different standards/conventions were devised to aid better comparisons between different samples - for example, one of them imposed a fixed height of fall of 18 inches. The impact strength of agglomerates was defined by Pietsch (1991) as the maximum height from which the agglomerate (or a set of "clone" agglomerates) survives the drop without damage. Impacting many "clone" particles, other workers determined a kind of probability of breakage for specific conditions (percent of particles broken for a certain height of fall, impact velocity, target material, etc.). Other experimentalists carried out repeated experiments with different sizes of samples to (empirically) determine the minimum sample size for a given material and impact velocity (or just the minimum velocity for a given material) below which no fragmentation occurs (usually breakage into large fragments was allowed, but not the wear, chipping, or weakening of samples).

Impact testing is a main interest in comminution, as breakage is caused dynamically by impact in most size-reduction processes. The product from a comminution device is sorted according to fragment size. If the log-log plot of the cumulative weight of fraction finer than a given size versus that fraction's size is a straight line, the slope of the line is called the distribution modulus. Many theoreticians and experimentalists (e.g. Gaudin and Hukki, 1946, Charles, 1957, Gilvarry, 1961, Gaudin and Meloy, 1962) analysed the distribution modulus in impact and (slow) compression fracture of single specimens of different composition and shape. Crabtree et al (1964) explained that (in comminution or grinding machines) size reduction is composed of three mechanisms: impact, abrasion and chipping.

Unwanted breakage (attrition) also occurs in the comminution processes, mainly in the form of abrasion and chipping (Crabtree et al, 1964). Abrasion is the surface wear of a particle due mainly to friction when particles rub against each other or against other materials (mill walls, mill balls, etc.). Abrasion is unwanted as it generally produces two distinct size ranges of product: the coarse (parents) and the very fine, and thus have a high deficiency of sizes in between. Chipping is the breaking of small fragments from a particle, usually in the cases when complete particle fracture does not take place. Chipping can also occur after fracture, by breaking-off the corners or edges of fragments.

4.1.1 Solid Spheres

Many workers used elastic samples in free-fall impact tests. For perfect elastic spheres (thus unbreakable) impacting a perfect stiff-elastic platen the behaviour can be predicted by theory. Hertz (1895) developed the theoretical equations relating the maximum force developed on the target with impact velocity. Making several assumptions and approximations, Shipway

and Hutchings (1993) worked out a relationship to calculate the maximum force of impact for a plastic-deforming target - from the measured contact area and the impact velocity. For elastic targets, they established relationships for calculating the contact area - from the sample/target material properties and impact velocity. Dean et al (1952) theoretically analysed the case of an elastic sphere decelerated by a uniform pressure applied to one of its ends. Their solution is directly applicable to the free-fall (normal) impact case. Shipway and Hutchings (1993) truncated their relationships in order to numerically determine the stress distributions within an elastic sphere impacting a plastically-deforming target. The solutions assume that the contact pressure is uniform over the contact area. For a small contact area, both the maximum internal tensile stress and shear stress are reached close to the contact area. As the contact area increases, the positions of the maximum internal tensile stress and shear stress moves further into the sphere (and the peak stresses decrease).

Most experimentalists noted that final failure was preceded by plastic deformation in the sample-platen contact zone. The "plastic" deformation was usually considered to consist of local cracking, crushing and/or chipping - see Tilly and Wendy (1970) on glass spheres, Uuemois and Kleis (1975) for abrasive spheres, Kelly and Macmillan (1986) for glass and brittle single crystals, Cleaver and Ghadiri (1993) for sodium carbonate monohydrate samples, Shipway and Hutchings (1993) for glass and sapphire spheres. Uuemois and Kleis (1975) reported that the higher the impact velocity, the more fine dust is created at the impact zone in the initial stages of impact. In their experiments a part of the dust was radially ejected from the impact centre at velocities several times higher (up to 4 times) than the impact velocity of sample.

For different brittle spheres Kelly and Macmillan (1986) observed that, initially, the plastic deformation zone developed radially around the impact point. A relatively flat "fracture mirror" zone formed perpendicular to the applied load when the crack velocity was low. In glass (and rarely in ceramics) the mirror was bounded by "fracture mist" (a band of fine ridges and valleys parallel to the direction of wave propagation) which developed, as Kelly and Macmillan (1986) explained, because the accelerating cracks started to deviate from planarity.

For glass spheres impacting elastic platens Shipway and Hutchings (1993) reported that the plastic deformation zone at the impact point formed prior to fracture and was conical. Rumpf (1990) also stated that a conical region possessing the highest energy density almost always developed at the centre of impact. He also described cracks which initiated at the impact point and propagated like rays in directions perpendicular to the maximum tensile stresses.

A wide range of final failure modes were reported for elastic spheres in free-fall impacts, ranging from just extended local crushing/cracking, fracture, to breakage into small

fragments - see Chaudhri (1985) on glass and sapphire spheres as an example. The mode of failure was usually dictated by the impact velocity and the platen material. Tilly and Wendy (1970) and Rumpf (1990) concluded that "elastic" spheres only fracture at very high impact velocities. Below these velocities they only suffer contact plastic deformation (local crushing and cracking). For elastic samples Rumpf (1990) explained that, at failure, the high energy in the deformation zone is released, this resulting in the production of mainly fine material (from the contact zone). On the other end, Shipway and Hutchings (1993) reported that glass spheres impacted on plastic platens failed by suddenly breaking into small fragments (shattering). Following a detailed analysis similar to the one carried out for the diametrical compression tests, they concluded that fracture was initiated by surface tensile stresses in this case. Shattering and fragmentation of elastic specimens was noted by many experimentalists for very high impact velocities.

For elastic samples that fractured, some workers described that they broke roughly along meridional planes (see Chaudhri, 1985, Shipway and Hutchings, 1993), whereas others just reported breakage into elongated medium sized fragments (see Kelly and Macmillan, 1986). Most experimentalists inferred that failure initiated at the impact zone and that initiation and propagation of the "fatal" cracks was usually preceded by plastic deformation.

Chaudhri (1985) published photographs of the half-half fracturing of a glass sphere, in which it can be clearly observed how the breakage (the visual opening of the fracture surface) started from the pole opposite to the impact area. The fracture of Cleaver and Ghadiri's (1993) sodium carbonate monohydrate samples into large fragments occurred with much less debris, but the initial shape of the samples was only roughly spherical. Impacting glass spheres on elastic platens, Shipway and Hutchings (1993b,c) obtained fracture along meridional planes, into two hemispheres or into a number of orange-slice segments. Shipway and Hutchings (1993b,c) analysed their impact tests in detail. Apart from the large fragments, they also usually found a conical fragment representing a zone of densified material that was formed by the impact point in the initial stages of impact. They believed that fracture was produced by the cone pushing inside the specimen. This and their stress analysis made Shipway and Hutchings (1993b,c) conclude that failure was initiated by internal shear. As in diametrical compression tests they concluded that propagation of the fracture crack/s was also affected by the internal tensile stresses.

Kelly and Macmillan (1986) argued that glasses and brittle single-crystal spheres do not exhibit planar fracture surfaces. Instead, fracture produces multiple elongated medium-sized fragments (called hackle). Further acceleration of the cracks developed from the impacted area results in "velocity hackle" lines (a larger-scale pattern of ridges and valleys) which terminate when macroscopic crack branching occurs and the crack propagation reaches the surface of sphere. Observing Kelly and Macmillan's (1986) published figures would

suggest that fracture surfaces best approximated to oblique planes. Fracture along oblique planes was also reported by Salman et al (1988) in their high-velocity free-fall impacts of glass spheres. However, they did not mention any damaged zone at the impacted pole.

Many workers noted that wave propagation plays an important role in the failure of elastic spheres impacted on stiff-elastic platens. For perfect elastic materials, Rumpf (1990) concluded that, for very high impact velocities, fractures occur at wavefronts or where reflected waves converge. For lower velocities the stresses are not sufficiently high to produce fracture during the short transit time of wave propagation. For glass spheres that fractured, Chaudhri (1985) reported that breaking up started after rebound when the longitudinal stress wave had made at least 3 round trips of the sample.

For plastic samples the initial plastic deformation at the specimen-platen contact was described by Rumpf (1990) to be composed of locally compacted the material in a conical-shaped zone having the contact area as its base. He concluded that, in plastic spheres, a cone-shaped zone of material is pushed from the target into the centre of the sample forcing outwards the material to the side. It is, however, not clear (from his description) whether fracture of plastic samples occurs over meridional or oblique planes. Impacting (plastic) polystyrene samples on steel targets, Schönert (1973) found that, for diameters larger than 1 mm, the sphere flattened and meridional cracks were developed due to the pushing of the inverted cone (developed at the impact area) into sample. For larger samples and higher impact velocities, the number of meridional cracks increased. These cracks developed at a much lower speed than in elastic materials and often needed a second impact to propagate further. Higher velocities (or second impacts) usually generated additional cracks and often produced complete shattering of specimens.

4.1.2 Agglomerates

Agglomerates generally exhibit more local plastic deformation (at the zone of impact) than solid elastic specimens. A few workers noted local cracking but many others observed the formation of a conical compacted zone at the sample-platen contact area - see Arbiter et al (1969) for sand-cement spheres, Gildemeister and Schönert (1976), Santurbano and Fairhurst (1991) for 25 mm diameter limestone spheres, Salman et al (1994) for 5.15 mm diameter aluminium oxide spheres. From observations on their impact tests, Salman et al (1994) concluded that failure always starts with damaging of the conical region at the contact. Higher-velocity impacts transformed the entire cone into debris, whereas only a little material was lost at the contact area for low impact velocity tests. Salman et al (1994) indicated that the roughly conical boundaries of the contact zone correspond to the expected shear stress trajectories due to impact. Santurbano and Fairhurst (1991) also reported that, in their tests, the material in the cone was stressed by large (essentially compressive) deviatoric

stresses, which caused it to fail in shear. Other workers found that the conical region survived unbroken - see Arbiter et al (1969). As in the case of solid samples, failure of agglomerates was usually inferred to initiate from the impacted pole. For lower impact velocities Arbiter et al (1969), Gildemeister and Schönert (1976), Santurbano and Fairhurst (1991) and Salman et al (1994) reported that final failure always initiated due to the wedge-action of the inverted cone.

Fracture has been noted to occur over a certain range of low impact velocities. Only meridional fracture planes were obtained by Gildemeister and Schönert (1976), Ghadiri et al (1990), Santurbano and Fairhurst (1991) and Salman et al (1994). For limestone spheres at high velocities Salman et al (1988) observed mainly oblique fracture planes intersecting the point of impact, whereas Arbiter et al (1969) found both meridional and oblique fracture planes in their impacted specimens. Arbiter et al (1969) explained that fracture planes develop along the trajectories of maximum compression and that this was the reason why fracture surfaces can propagate both meridionally and obliquely. In their tests, breakage by oblique fracture planes was always preceded by at least one meridian fracture plane.

Impacting a very large number of samples, Salman et al (1994) found that fracture occurred suddenly, under the same 4 main patterns observed in their diametrical compression tests into 2, 3 or 4 large fragments. For higher velocities, they obtained more large fragments, but based on the secondary fragmentation of one of the 4 forms.

Apart from the orange segment-like slices and the cone of finely broken material originated from the contact zone, Gildemeister and Schönert (1976) and Santurbano and Fairhurst (1991) also found a larger intact cone originated from the pole opposite the platen in their tests. Santurbano and Fairhurst (1991) inferred that fracture occurred due to the dilation of material in the contact cone and that this acted as a wedge pushing into the sample, creating tensile stresses tangential to the interface. These tensile stresses created and propagated fractures to finally form the orange-slice shaped fragments. Due to bending stresses, they suggested that fractures linked in such a way that a conical fragment was also formed at the pole remote from the point of impact. As in their diametrical compression tests, Arbiter et al (1969) found the contact cone covered by a layer of pulverised material which indicates that the cone was pushed by shearing into the sample (similar to a conical indenter).

4.1.3 Energy Considerations

The total initial kinetic energy of the impacting sample is converted during impact into three main components: the energy transferred to the target, the kinetic energy of the rebounded sample (intact or in fragments), and the energy dissipated in breakage (plastic deformation, waves, thermal, etc.). Generally, the energy transferred to the target is very small, as stiff

elastic platens were usually used. Santurbano and Fairhurst (1991) recorded the evolution of the force developed on the target (see Fig. 6.62 in Chapter 6) and examined the redistribution of energy during impact. They found that almost all of a sample's initial kinetic energy was elastically stored within the sample and less than 0.5% was transferred to the metallic platen. They reported that about half of the stored energy was dissipated in fragmentation, the other half reappearing as kinetic energy of the flying-off fragments. Charles and DeBruyn (1956) stated that in the case of impact, apart from the kinetic energy of the fragments and debris, energy is also dissipated or transformed due to kinetic energy of vibration, potential energy as strain energy of residual stresses, heat from friction during plastic deformation, damping of elastic waves and new surface energy.

Using the same input energy levels, Charles (1957) found that high-velocity impact was more effective in fracturing and reducing size than low-velocity impact. He argued that this is due to the fact that, for high impact velocities, energy is more concentrated at the point of impact and fractures initiate earlier and propagate through the sample along with the travelling stress waves.

All impact tests have shown that the impact velocity is the main factor affecting the impact damage. Increasing the moisture content of samples usually led to less impact damage. From their impact tests on cotton seeds, Kirk and McLeod (1967) worked out the following relationship between the probability of seed rupture R and the seed impact velocity V

$$R = 4.77E^{-6}V^{4.38} \tag{2.26}$$

Varying the size of samples, many experimentalists found that smaller samples are more difficult to break under impact: higher impact velocities or initial input energies were needed.

Louvier and Calderwood (1967) demonstrated that stiffer walls produced more damage to seeds. Keller et al (1972) found similar results: polyurethane walls produced only 20% of the damage produced by concrete walls and only 17% of that caused by steel walls. Salman et al (1987) reported similar conclusions after impacting aluminium oxide spheres on steel, glass, aluminium and Plexiglas platens. They also showed that impacting on thicker walls results in an increased probability of particle breakage.

4.1.4 Oblique Impact

Keller et al (1972) carried out impact tests on corn seeds at different impact angles, using three different wall materials. They found that damage to the seeds was reduced by 23% by reducing the impact angle from 90° to 45°. For the same reduction of the impact angle, but

in the case of milled rice, Louvier and Calderwood (1967) found a 60% reduction of the damage.

In oblique impact tests on 5.15 mm diameter aluminium oxide spheres, Salman et al (1994) observed three types of behaviour. For impact angles from 90° (normal impact) to 20°, samples broke similar to the normal impacts forms: in two, three or four large fragments, having flat and smooth fracture surfaces. The difference (for oblique impacts) was that fracture planes were not exactly meridional, so that the resulting fragments were not symmetrical and equal sized. Impact at angles less than 20° produced no visual damage to the spherical samples. For angles of 90°-50°, the probability of sample failure was unexpectedly constant (for a given speed) but it decreased sharply at lower impact values. For impact angles in the range 70°-20° an additional, distinct form of failure was observed: a roughly circular chip of material was detached from the spherical particle; the fracture surface was concave, rough and uneven. Salmon et al (1994) explained that the distinct form of failure was caused by the tangential contact force, by diverting the propagating ring crack towards the nearest free surface. The fracture surface was characteristic of cracks propagating in non-uniform stress fields. It was inferred that crack initiation occurred due to the enhanced tension at the front end of the contact area. Salmon et al (1988) found similar results.

4.2 DOUBLE IMPACT TESTS

In double impact tests, samples are placed on a fixed platen and are impacted by a free-falling mass. Double impact tests are usually used in comminution studies, as they subject a sample to forces that are similar to those encountered during certain industrial processes. Experimentalists were generally not interested in the mechanism of breakage but in determining the optimum input energy for breakage. Some of the double impact tests were performed for comparison with free-fall impacts. The double impact test is also used by the pharmaceutical companies to measure the friability of tablets. A variable (increasing) weight is dropped from a fixed height on the tablet and the weight that breaks the sample is used as an index of tablet strength.

4.2.1 Solid Spheres

The detailed report of Arbiter et al (1969) on double impact tests of 25 mm diameter glass spheres best reveals the fracture mechanism. As in their diametrical compression tests, the sample deformed elastically until encircling spalling cracks (Hertzian cracks inclined at 70° to the loading axis) developed around the contact areas. Fine comminution of the material in conical zones by the sample-platen contacts followed shortly. Fracture was fast and resulted in large lune-shaped fragments and debris. The finer part of the debris belonged to the conical contact zones, whereas the other part originated from the sphere's core (the zone uniting the two cones along the loading axis). The material in the core was also disintegrated (though much coarser than in the cones) into elongated prismoidal and sphenoidal fragments, having their longest dimension parallel to the loading axis. Under a certain impact velocity, Arbiter et al (1969) concluded that the double impact test resulted in similar size distributions and shapes of fragments as the diametrical compression test.

Arbiter et al (1969) inferred that breakage started along conical surfaces with bases corresponding approximately to the areas of contact at fracture. The cones were pushed into the sample producing its failure. Arbiter et al (1969) explained in detail that local triaxial compression is the cause of the fine comminution of material in the conical zones from contacts, whereas very high compressive stresses along the loading axis and approximately uniform tension (normal to the loading axis) are responsible for disintegration of material in the sample's core. The hoop (uniaxial) tensile stresses were inferred to be the cause of the meridional fracture planes dividing the remaining of the material into large lune-shaped fragments.

4.2.2 Agglomerates

For agglomerates, Arbiter et al (1969) again provide the best description of the experimental behaviour. For double impact tests on 73.66-124.46 mm sand-cement spheres, Arbiter et al (1969) reported that initiation of failure was similar to that observed in the glass spheres: along the conical surfaces developed at the platens. However, apart from minute, densely distributed cracks lying along the periphery of the contact circles, the contact cones remained free from internal cracking.

The pattern of breakage was slightly different than that observed for the glass samples, but similar to that of sand-cement specimens in diametrical compression. The samples split into several spherical wedges (orange segments) along meridional planes. Straining of the sample before final failure was more extensive, 1.2 % strain compared to 0.1% failure strain for glass, and the size of fragments was larger than for glass. Very few fine-comminuted material was found except for a layer of pulverised material on the otherwise intact cones that formed at the contact.

For double impact tests on sand-cement spheres, Arbiter et al (1969) reported a similar general fracture mechanism as for the glass spheres. As the cones at the contacts were driven into the samples, the hoop tensile stresses broke the sample along several meridional planes. It seems that the plastic flow of the particulate material in the cones prevented them from internal cracking and comminution. In addition, the cones appear to have been larger for sand-cement than for glass spheres, so that the local compressive and shear stresses were not that localised, and thus not sufficiently high to cause internal cracking and comminution.

4.2.3 Energy Considerations And Discussion

For tests on 3-24 mm glass spheres, Bergstrom et al (1961) reported that higher impact velocities of the falling platen reduced the time to fracture, but also increased the amount of energy input required to fracture the sample. For 25 mm glass spheres Arbiter et al (1969) found that, compared to "slow" diametrical compression, double impact (at 11.2 ft/s) required about 80% more energy to initiate fracture, and 50% more energy to produce substantially similar fragment size distributions. They explained that the differences were due to the fact that in double impact tests there was more cracking inside the fragments, higher residual kinetic energy in the fragments and larger energy losses due to the experimental device used.

In fracture caused by dropped weight devices, Charles (1957) found that if the input energy is doubled, the energy useful to fracture is doubled. However, many workers also found that the input energy required for size reduction increases with the strain-rate of the moving

platen. As in slow diametrical compression tests, the input energy was found to be proportional to the third power of the particle size, to the square of the failure load, and inversely proportional to Young's modulus - see Oka and Majima (1970). On quartz, cement clinker and limestone spheres, Schönert (1972) showed that the energy utilisation (for comminution) decreases with increasing strain-rate. In addition, the smaller the particles, the better the energy-utilisation efficiency is. For quartz samples, Schönert (1972) concluded that 10 times more energy is required in ball milling (grinding) than in single-sample crushing for producing the same surface area. For impact crushing tests on Pyrex samples, Zeleny (1957) (see Bergstrom and Sollenberger, 1961) inferred that most of the energy input (84%) of the double impact test is finally dissipated into thermal energy. For sand-cement spheres, Arbiter et al (1969) reported that double impact consumed more energy for fracture and produced a larger amount of fine product compared to the samples in slow compression tests.

Pauw and Mare (1988) used 0.1, 0.3 and 1 kg falling iron masses to break different-shaped 3.35-12.7 mm iron-ore samples (agglomerates) placed on a steel platen. They criticised the traditional approach of determining the efficiency of breakage energy only from the amount of surface energy created in breakage and the input energy. They showed that efficient grinding needs more than simply the production of new surface area. It is also necessary that the final products are of the desired size. They proposed a new approach to efficient impact breakage, consisting of an optimal initial input energy and of the necessary number of impacts (as breakage steps). They assumed that the breakage efficiency is not significantly affected by the velocity of the drop-weight, but by the input energy alone. However, it is evident that in the case of large drop-masses (as the ones they used) relative to sample mass, the falling mass is still imparting energy after the first moment of impact. Pauw and Mare (1988) explained why it is inefficient to use too little or a too much input energy. If the input energy is insufficient, fracture does not occur and, they say, energy is "lost". Too much input energy produces too large a quantity of fines and (at the extreme) produces packed-bed conditions (compaction of particles after breakage). They found that different sample sizes required different values of optimum energy and, therefore, they proposed sorting particles before grinding. For a lower optimum energy they recommended hard platens and drop-masses.

The restricted impact configuration that Perry and Hall (1965) used for testing pea beans was somehow similar to the one in the double impact. Their rebound-restricting platen was actually a stationary block that was placed at the opposite pole to the striking platen, and was free to move after impact (as a result of the bean impacting it). They reported that the force on this rebound-restricting platen increased until the velocity of the bean and rebound-restricting platen reached that of the striking platen. They found that the temporary deformation was less for the beans that were not damaged (broken) during impact. Much of

the deformation during impact was elastic: temporary deformation averaged 21%, but permanent deformation averaged only 2.7%. Comparing restricted impact to the free-fall impact of the pea beans, Perry and Hall (1965) reported that the initial kinetic energies needed for obtaining same results were much larger when rebounding was restricted. As opposed to only 62% dissipated in the case of free-rebounding (free-fall) impact, 91% of the kinetic energy was dissipated in the restricted impact test.

4.3 SUMMARY

No published work was found on impact of small, coarse-grained agglomerates similar to the ones simulated in this project. In agglomerate impact experiments which have been reported, the agglomerates were either much larger than the simulated agglomerates or were composed of a much finer grain microstructure. Nevertheless, in the following chapters, comparisons will be made with the work of Arbiter et al (1969) and Salman et al (1988, 1994). Although the size of the sand-cement agglomerates tested by Arbiter et al (1969) was two orders of magnitude larger than the simulated agglomerates reported in this thesis, their detailed and comprehensive examination of agglomerate behaviour in free-fall impact tests, double punch impact tests and diametrical compression tests provides the best set of experimental results against which against simulations may be compared.

CHAPTER 5
SIMULATION GENERALITIES AND PRELIMINARY RESULTS

5.1 PRINCIPLES OF THE TRUBAL SOFTWARE

5.1.1 Background

TRUBAL is a software program that enables simulations of three-dimensional systems consisting of spherical particles. The program was developed in FORTRAN by Peter Cundall (see Strack and Cundall, 1978, and Cundall and Strack, 1979a,b) and is based on the Distinct Element Method (DEM). The BALL program - a two-dimensional version of TRUBAL (see Cundall and Strack, 1979a) - was, initially, more evolved and more used than TRUBAL. Both TRUBAL and BALL were developed from an earlier software program created by Cundall to model the behaviour of jointed rock masses (see Cundall, 1971). Since its development, the TRUBAL program has gone through many changes - each of them enhancing it by widening its range of applications and by making it more accurate.

The Aston research group started with Cundall's 1989 version of TRUBAL, but was already experienced in using the BALL software for several years. First enhancements to the TRUBAL software at Aston consisted in the implementation of more realistic interaction laws. The tangential contact forces were coded according to the theory of Mindlin and Deresiewicz (1953). Theories due to Johnson et al (1971) and Thornton (1991) were used to model adhesion at the contacts between particles (see Appendix A). Other improvements to TRUBAL include the possibilities of automatic generation of random and regular packings, of generating particles in defined spherical regions and of defining walls parallel to the work-space boundaries. An important enhancement to TRUBAL at Aston was the development of graphics routines for the two- and three-dimensional colour images of particles, clusters, velocities, contact forces and contacts.

Following the wider application of the program there are now, at Aston, three main versions of the TRUBAL code. The most used version is TRUBAL-DRY, which models the particles as elastic spheres with both interparticle friction and adhesion. When liquid bridges were incorporated at particle contacts (Lian, 1994, and Lian et al, 1993), for the simulation of moist particle agglomerates, a second version of the program evolved: TRUBAL-WET. The toroidal approximation (Fisher, 1926) was used to model the static forces of the liquid bridges; the viscous forces were modelled according to the theory of Adams and Perchard (1985). The third version is TRUBAL-PLASTIC (see Ning and Thornton, 1993, and Ning, 1995) which considers plastic deformation at the interparticle contacts.

At Aston University, TRUBAL has been applied to investigations of coalescence, attrition, fracture and fragmentation of agglomerates; involving simulations of agglomerate/wall impacts and agglomerate/agglomerate collisions - see Kafui and Thornton (1993), Lian (1994), Kafui and Thornton (1994) and Kafui (1996). Other recent applications of the program have included silo discharge, Kafui and Thornton (1995) and quasi-static shear deformation, Thornton and Sun (1994).

The Distinct Element Method (D.E.M) - as developed by Cundall (1971) - is itself the "engine" of the TRUBAL software program. The method simulates the system evolution using an explicit finite difference scheme. The transmission of forces between the system's particles and the particle displacements are modelled by cyclic calculations, in which the evolution of the system is advanced over a large series of time-steps. The time-step is chosen to be small enough to ensure that the movement of particles accurately satisfies Newton's second law of motion. From the resultant force acting on a particle (the out-of-balance force) at that particular moment, the translational and rotational accelerations are calculated; from these the new velocities and displacements of the particle are determined - by numerical integration over the small increment of time. Having the particles' displacements, their new coordinates are calculated and an efficient search (see Appendix A) for new contacts is carried out. Moving the particles to their new positions, new values of contact forces arise due to the new relative approaches between contacting particles. After determining and resolving the contact forces, new resultant forces for each particle are obtained which, in the next time-step, produce new accelerations of each particle. The time evolution of the system is achieved by repeatedly updating the contact forces and particle kinematics.

The diagram in Fig. 5.1 presents a general view of the way in which TRUBAL operates and helps a user to simulate tests and collect data. Each numbered box represents the work carried out by one or a group of software subroutines. Appendix A presents in detail the theoretical basis of the TRUBAL software at Aston University and the main laws incorporated into it.

5.1.2 Interaction With Users

TRUBAL is an interactive program from the point of view that it allows direct communication with its user. Although not very easy to use, TRUBAL possesses its own set of commands that enables the user to run, record data, monitor and control a simulation's progress. The user can interact directly with the TRUBAL program - by successively issuing a command, waiting for the program to execute it, analysing the results and then issuing a subsequent command, and so on. Alternatively, the user can interact indirectly

with TRUBAL (Fig. 5.1), by means of an input file - a list consisting of all the commands that are needed for a particulate system preparation, for a complete test simulation, or for plotting of images. The indirect interaction was used in this project; it allows the user to monitor the evolution of several simulation parameters and data but not to change anything during the running of the program.

Due to the D.E.M. (see the previous paragraph), a simulation with TRUBAL involves tens or hundreds of thousands of step-by-step calculations and thus a simulation is effectively performed as a sequence of cycles. Appendix B presents examples of command lists effectively utilised with TRUBAL in this project for creation/preparation of agglomerates, tests simulation and image plotting. Using a different TRUBAL command when starting a simulation, the user can either create a particulate system of certain specified characteristics, or they can employ TRUBAL to restore and use the state of a particulate system from an earlier problem (see Appendix B for more details). Issuing different commands, users can employ the software to execute a number of cycles, then to change some parameters and execute more calculation cycles. After any number of cycles the user can issue commands to output different parameters or to save the state of the program before continuing.

5.1.3 Additions To The TRUBAL Software

In the two-dimensional simulations of diametrical compression tests (see Yin, 1992 and Thornton et al, 1996) it was relatively easy to observe, at any moment of a simulation, where and when the maximum contact compressive forces occurred and also where and when the breaking of particle-particle contacts happened. It was found that the above aspects and many others were very difficult to distinguish in three-dimensional simulations. Enhancements to the program software were therefore needed to allow clearer observations of the agglomerate behaviour during the simulations.

The effective work in this project started with the tailoring of the TRUBAL-DRY software program for the specific simulations of diametrical compression and impact of particle agglomerates. Changes and additions to the software were carried out all through the three-year duration of this project whenever a need or new requirement arose. New software subroutines were created and existing ones were extended and enhanced. The final result (for simulating dry agglomerates) is the so-called TRUBAL-ACI software, whose main commands and capabilities are fully presented in Appendix B. Most of the additions were carried out with the aim of improving TRUBAL's output and graphical facilities; Figure 5.2 presents the main enhancements.

A software subroutine was created in the TRUBAL-ACI program (section 7 in Fig. 5.1.) to enable the writing, after each step, of a wide range of simulation data into 18 output files

(see Appendix B for details). By outputting selected data on the screen, the new subroutine also enables easy monitoring of the simulations. Each simulation was divided into 100-200 stages, each stage containing an equal number of cycles. After each step, the program displayed selected data on the screen and other information was saved in output files. At the end of a simulation, the data in the output files could be easily analysed either directly or by importing the files into Macintosh software packages (mainly Cricket Graph) where graphs could be produced. One of the newly-created arrays was employed to store, for each contact, its coordinates, the maximum (ever) normal contact force, the time and calculation cycle when this maximum force was attained, and the time and cycle when the contact was broken.

Another subroutine was added to plot images of particle displacements; other subroutines were expanded to distinguish easier where contacts are located and their evolution, to plot slices through the agglomerate and to follow the behaviour of the contacts and particles on the fracture surface. Colours were used to distinguish between different magnitudes and types of contact forces, between different-sized clusters, between directions of velocity vectors for would-be large fragments. A method of marking the large fragments immediately after fracture, but long before break-up was obvious, was also implemented in the new TRUBAL-ACI software. The new enhancements are achieved by the newly-added commands and options to commands which are presented underlined in Appendix B.

5.1.4 Types Of Tests Simulated In This Project

Three types of tests have been simulated during the project in order to examine agglomerate breakage processes: diametrical compression (DC), double (punch) impact (DI) and free-fall (or simple) normal impact (NI).

The diametrical compression tests (for both high and low strain-rates) were simulated by positioning the agglomerate between two parallel platens of infinite mass and moving either both platens or only the top platen (Chapters 6 - 9) with a constant velocity towards the agglomerate. The gravitational acceleration of 9.8 m/s^2 was always specified in the downward vertical direction.

Simulations of the double punch impact test are similar to the diametrical compression test simulations in which the bottom platen remains fixed in position except that the top platen represents a falling mass. Hence, the top platen is placed just above the agglomerate and is attributed with a finite mass (typically larger than that of agglomerate) and with an initial (vertically-downward) velocity corresponding to a notional height of fall in a gravity field. During the simulated evolution of the system, the top platen is further accelerated due to the gravitational acceleration, but at the same time also decelerated due to the resistance exhibited

by the agglomerate - whose movement is restricted by the bottom platen. As a result, the top platen may finally stop, crush the agglomerate, or/and rebound from the agglomerate.

To simulate free-fall impact tests, the agglomerate is positioned just above a fixed platen. All the primary particles are given the same initial (vertically-downward) velocity corresponding to a notional height of fall. Upon impact, due to the reaction forces generated at the platen, the agglomerate decelerates. At the end of the impact the agglomerate usually rebounds from the platen.

5.2 PREPARATION OF AGGLOMERATES

Most of the agglomerates created and used in the simulations reported in this thesis consisted of about 4000 primary particles with an average particle diameter of almost 60 μm. The mechanical properties of both the particles and the platens were specified as: solid density, $\rho = 2650\ kg/m^3$; Young's modulus, $E = 70\ GPa$; Poisson's ratio, $\nu = 0.35$ and the coefficient of interface friction μ, was generally taken to be 0.5. With these properties, both the particles and the platens may be considered to be composed of glass.

The first step when simulating the preparation stage is the creation of the primary particles within a specified spherical volume. The particles are then brought together to form an agglomerate of a certain particle density (solid fraction) and certain contact density (average coordination number). The final step in the preparation procedures is to create the platens and, usually, to move them very close to the agglomerate in order to save computer time. During the simulations of both the preparation stage and subsequent compression/impact the time evolution of the system was achieved using a time-step of the order of 1-10 nanoseconds (see Appendix A on how it is calculated).

5.2.1 Regular Packings

There are two ways of creating particles with a regular packing structure. One option creates regular packing within a defined spherical volume by a simple command, see Appendix B. The particles are generated with small gaps between them and it is necessary, therefore, to bring them together using a centripetal gravity field. However, the precision of the final regular packing was not considered to be good enough and this option was not employed in this project.

The alternative option, used in this project, is to use a separate command to create each individual primary particle in its approximate position within the prescribed regular structure. Using this option, the particles are created in contact with each other so that the

agglomerate is ready for simulation of the compression/impact stage. In all, nine body-centred cubic (BCC) and three face-centred cubic (FCC) agglomerates were created, with an average agglomerate diameter of approximately 1.1 mm. An arbitrary view of a typical BCC agglomerate is shown in Fig. 5.3; the agglomerate is already placed between two parallel platens. Figure 5.4 shows a view from front of a typical FCC agglomerate ready for simulation.

5.2.2 Random Packings

Systems of equal-sized spheres have a natural tendency to form clusters of regular packed zones. Therefore, in order to avoid this, it was decided to use seven slightly different particle sizes in the range 60 μm ± 5%. The particle size distribution chosen for the first random agglomerate created is shown in Fig. 5.5. To prepare random agglomerates, the primary particles were initially created at random locations within a designated spherical volume and then brought together in contact by applying a centripetal gravity field. An image of 4000 particles just after their creation is presented in Fig. 5.6. If it was intended to prepare a loose agglomerate then the interparticle friction and interface energy were specified prior to the application of the centripetal gravity field. In order to prepare dense agglomerates, the interface energy was introduced later, when the porosity was approaching a constant value. To obtain a very dense agglomerate, it was necessary to apply the centripetal gravity field to the system using zero interparticle friction and to introduce the desired values of interparticle friction and interface energy as late as possible in the preparation process.

Having obtained an agglomerate with the desired porosity, contact density, friction and interface energy, it was necessary to remove the centripetal gravity field gradually and carefully in order to preserve the agglomerate's equilibrium state. Therefore, it was necessary to ensure that, at the end of the preparation stage, the particle velocities and contact forces were very low - with the number of compressive contact forces approximately equal to the number of tensile contact forces. Following the above procedures, the preparation of random agglomerates would normally take over one month of computer time to complete. Figure 5.7 shows a 4000 particle random agglomerate, at the end of the preparation stage, in position between two parallel platens.

5.3 DIAMETRICAL COMPRESSION OF BCC AGGLOMERATES

At the time when this project started, the TRUBAL-DRY code was being used to simulate free-fall impact of FCC and BCC agglomerates consisting of approximately 8000 and 4000 primary particles respectively, Kafui and Thornton (1993). Varying the interface energy (at

the interparticle contacts) and impact velocity, it was found that the BCC agglomerates always exhibited ductile behaviour and could never be broken into large fragments by impacting them against a wall. It was decided to find out whether BCC agglomerates behave in a similar way in diametrical compression test simulations.

Six BCC agglomerates each consisting of about 4000 primary particles (60 μm diameter) were created with interface energies varying from 0.2 J/m^2 to 14.0 J/m^2. Each of these agglomerates had four particles in contact with each platen, as shown in Fig. 5.8. (In order to examine the significance of the number of particles initially in contact with the platens, a further three BCC agglomerates were created with slightly modified particle arrangements to provide 12, 16 or 20 particles in contact with a platen). Diametrical compression was simulated by moving both platens with equal and opposite constant velocities. Different platen velocities were used, from 0.05 m/s to 6.0 m/s, corresponding to a wide range of compressive strain rates.

Figure 5.9 shows the evolution of the platen force and damage ratio during a diametrical compression test on a BCC agglomerate with interface energy Γ=2 J/m^2 using a load-rate (platens relative velocity) of 0.05 m/s. The *damage ratio* is defined as the ratio of the number of contacts that have been broken to the initial number of contacts prior to the test. It can be seen that, for this test, the platen force increased to a maximum value at a nominal diametrical strain of about 0.1% and then reduced at a similar rate to a residual, and essentially constant, force at about 0.2% strain. As indicated by the damage ratio, only a few contacts were broken during the loading stage. Most of the contact breaking occurred during the unloading stage and, with further straining, there was a small but continuing increase in the number of contacts broken. In all the tests simulated on BCC agglomerates the platen force had fallen to a small residual value prior to 1% strain and, in a qualitative sense, Fig. 5.9 is typical of the observed behaviour. The final damage ratio was inversely proportional to the interface energy and increased at higher strain rates.

As the forces on platens dropped the agglomerate began to exhibit significant flattening at the contact with the platens and with further strain (sometimes to about 30% strain) the agglomerate deformed in a ductile manner. *Debris* formed adjacent to the platens was generally composed of singlets and doublets (*debris* in this project denotes fragments weighing less than 2.5% of the initial weight of the agglomerate - thus consisting of less than 11 particles for an agglomerate initially having 4000 particles). Medium-sized fragments were occasionally obtained but only at large strains (>5%) and after extensive damage. These fragments weighed (together) less than 60% of the initial agglomerate mass (consisted of less than 60% of the number of particles in the initial agglomerate) and were seriously weakened due to having more than 50% of their internal contacts broken.

It was found from the diametrical compression test simulations that none of the BCC agglomerates fractured into large fragments for any of the applied compressive strain rates. As in the impact simulations of Kafui and Thornton (1994) there was always a single large surviving cluster with debris created adjacent to the platens.

Figure 5.10a illustrates the internal structure of the BCC agglomerate shown in Fig. 5.8 by connecting the centres of contiguous particles to form an equivalent space lattice. A view from above of the space lattice, not showing the platens, is presented in Fig. 5.10b. The perfect regular structure is clearly seen. Figure 5.11 shows the (typical) contact force transmission paths during diametrical compression of the agglomerate in views from the front and above. In the figure each contact force is represented by a line of fixed length drawn at the same orientation as the resultant contact force and the thickness of the line represents the magnitude of the force scaled to the current maximum force in the system. It is noted that Fig. 5.11 clearly shows that the large forces are transmitted along lines of particles inclined at 45° to the applied loading direction, avoiding the central core of the agglomerate.

5.4 DIAMETRICAL COMPRESSION OF FCC AGGLOMERATES

Two FCC agglomerates were created with interface energies of 0.4 J/m^2 and 2.0 J/m^2 respectively. Diametrical compression was simulated by displacing the top platen at a constant velocity (in the range 0.01 m/s to 0.5 m/s) with the bottom platen fixed in position.

From the initial series of simulations of diametrical compression it was found that the FCC agglomerates behaved in a very similar manner to the BCC agglomerates in that fracture did not occur. The largest contact forces were transmitted along contiguous lines of particles inclined at $\leq 45°$ to the loading direction, as shown in Fig. 5.12. Figure 5.13 presents a typical view of the agglomerate from above showing the adjacent space lattice after the platen force had reduced to its residual value at a nominal diametrical strain of 2.66%. At this stage, 69% of the initial contacts (bonds) had been broken but, as is clear from Fig. 5.13, there is no evidence of fracture. The corresponding particle velocity field is illustrated in Fig. 5.14; each line represents the velocity vector of a particle, with the dot indicating the arrow (the vector's direction). The figure shows that there exists a conical region adjacent to the top (moving) platen which pushes other particles outwards.

Yin (1992) obtained clear evidence of fracture in his simulations of diametrical compression of random two-dimensional monodisperse agglomerates. Consequently, at this stage of the project, it was not clear why fracture did not occur during the three-dimensional simulations. However, further examination of Yin's (1992) data (see also Fig. 1a in Thornton et al,

1996) revealed that the force transmission was concentrated along a line of contiguous particles which were inclined almost orthogonal to the loading direction. Therefore, it was decided to re-orientate the FCC agglomerate so that the loading direction coincided with contiguous lines of particles, as shown in Fig. 5.15 (compare it with Fig. 5.4).

For this new orientation, it was found that the FCC agglomerates fractured into two, three or four large fragments as illustrated by the equivalent space lattice shown in Fig. 5.16, 5.17 and 5.18 (compare them with Fig. 5.13 from the test where the same FCC agglomerate did not fracture). On examination of the force transmission pattern it was found that, as shown in Fig. 5.19, the force transmission was concentrated along a single line of contiguous particles orthogonal to the loading direction. Fracture occurred at less than 0.4% strain and clearer examination of the simulation data revealed that this was due to buckling of the loaded column of particles shown in Fig. 5.19. It was concluded from the diametrical compression simulations on FCC agglomerates that fracture would occur if sufficient elastic stored energy could be achieved.

5.5 DIAMETRICAL COMPRESSION OF RANDOM AGGLOMERATES

A random agglomerate having 4000 particles and an interface energy $\Gamma = 0.4$ J/m^2 was prepared and diametrical compression test simulations were carried out using various platen velocities. In all cases, the agglomerate deformed in a ductile manner without fracturing. The behaviour was similar to that observed in diametrical compression tests on ductile spherical samples reported by Schönert (1973) and Rumpf (1990), see Section 3.5.3. As the areas in contact with the platens increased due to local compaction, two opposite cone-shaped zones of material formed adjacent to the platens which pushed the rest of the material outwards. However, the most unusual feature of the random agglomerate simulations was that the forces generated at the platens increased very slowly and remained very low, even at large strains. This clearly indicated that the input energy was not being stored in the agglomerate but, in some way, was easily dissipated.

When the detailed contact and particle information was examined, it was found that all the primary particles were rotating throughout the simulations, including the preparation stages. With this freedom to rotate, particle rotation increased continually during the diametrical compression stage. Consequently, the energy input via the platen movement tended to be converted into rotational kinetic energy leaving little energy available for stored elastic energy. Since the particle rotation prevented elastic energy from being stored within the agglomerate, it also appeared to be the reason for the inability to generate significant forces on the platens. In order to test this hypothesis, an "artificial" simulation was carried in which the rotation of all the primary particles was arbitrarily set to zero throughout the simulation.

As a result of preventing particle rotation, the forces on the platens increased and decreased in a manner similar to that shown in Fig. 5.9 and the agglomerate fractured into four large fragments at about 2% strain. It became clear, after the simulation, that there must be an error in the computer code.

In the TRUBAL code, the tangential contact interactions are prescribed by algorithms based on the theory presented by Thornton (1991). The theory assumes that initial tangential behaviour corresponds to the partial peeling process suggested by Savkoor and Briggs (1977) and that particle rotation cannot occur during this stage. When the contact has partially peeled due to the tangential interaction it is assumed that particle rotation is then possible. However, the rotational constraints were only considered in the context of situations which only involve a single contact such as the collision between two spheres or between a sphere and a wall. In a compact system of particles, most particles will be in contact with more than one other particle. In this case, due to the multiple contacts, a particle should only be free to rotate when all of its bonds have partially peeled.

It was discovered that if a simple contact had partially peeled the program calculated a moment contribution to the two particles in contact even though other contacts with these particles had not completed the partial peeling process. Consequently, when the particle motion was updated, particle rotations were calculated. Therefore, the code was modified to permit particle rotation only when all of a particle's contacts had completed the partial peeling process. In subsequent simulations of diametrical compression tests, using the modified TRUBAL program, the random agglomerates fractured.

For a random agglomerate (Γ = 0.4 J/m^2) diametrically compressed by moving the top platen at a constant velocity of 40 mm/s, Fig. 5.20a illustrates the spatial distribution of the largest compressive contact forces when the platen force was a maximum. It can be seen that the force transmission is much more concentrated along the loading direction using the modified code when compared with the corresponding force transmission pattern obtained with the unmodified code, which is shown in Fig. 5.20b. Consequently, significantly higher forces were generated on the platens and, as illustrated in Fig. 5.21 by the equivalent space lattice viewed from above, the agglomerate fractured into two large fragments.

Having corrected the coding error which permitted spurious rotational kinetic energy to be developed, progress on the project could continue by simulating diametrical compression, double punch impact and free-fall impact on random agglomerates. The results of these simulations will be presented and discussed in the remaining chapters of the thesis.

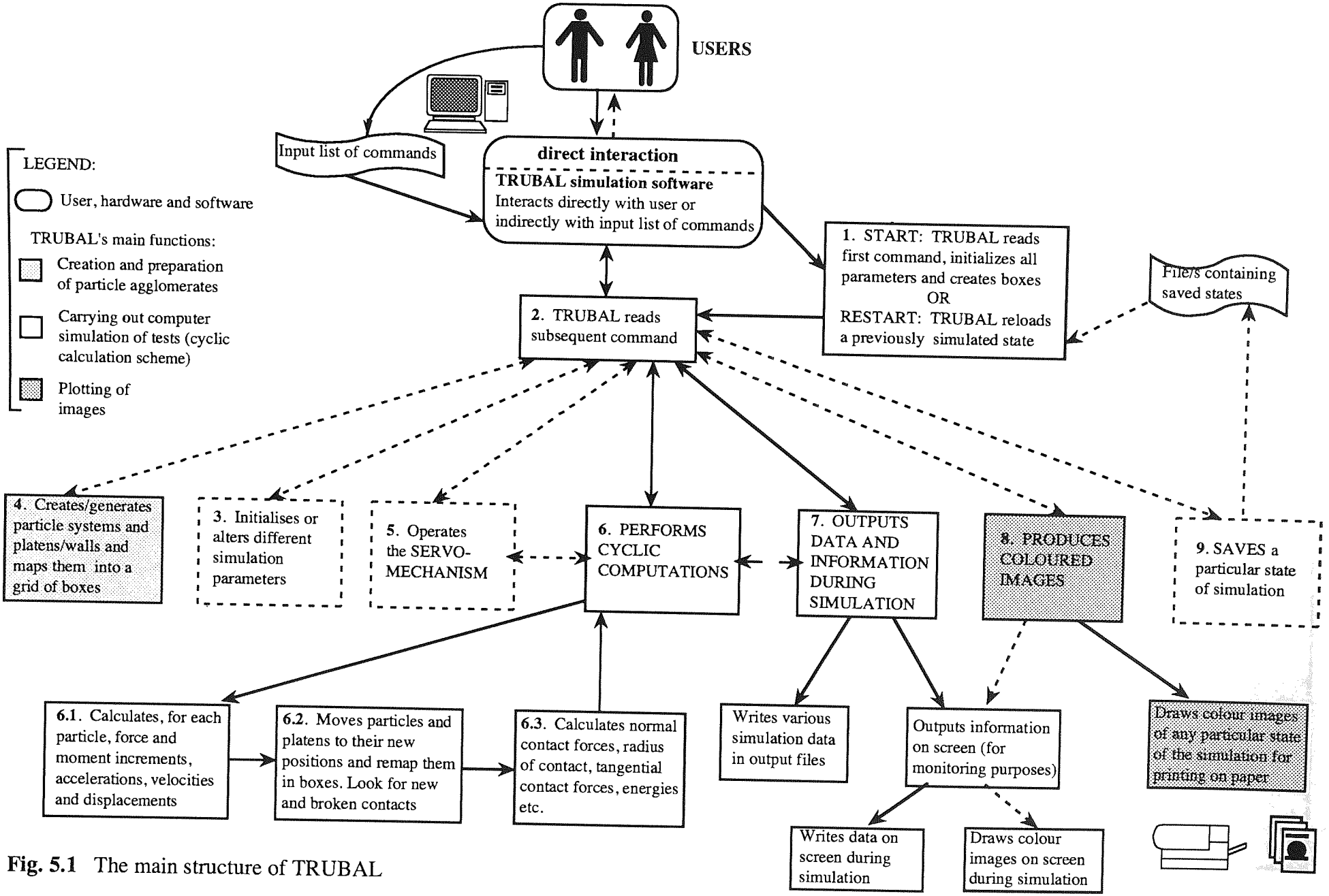

Fig. 5.1 The main structure of TRUBAL

PRINT ON-LINE INFORMATION

- Printing information on screen during the running of a simulation (advantage: can monitor long simulations and stop them if anything goes wrong)

OUTPUT OF DATA TO FILES

- Output a wide range of simulation data to files - readily-formatted to be transferred to graphics-producing packages (see Appendix B for details)

PLOT COLOUR IMAGES

- Made changes in order to print additional information on the graphics plot
- Created new plotting commands and new options to old commands:

• **plot displacements** - new command for plotting particle displacements
- option to colour-code displacement vectors according to magnitude

• **plot cforces/tforces** - new commands to only plot compressive/tensile forces
- option to plot only the largest forces: - above a certain magnitude, or
- only a certain number of the largest
- option to colour-code forces according to magnitude
- option to plot only contacts on the fracture surface

• **plot forces** - new options to it:
- option to plot only the largest forces: - above a certain magnitude, or
- only a certain number of the largest
- option to colour-code forces according to magnitude and type
- option to plot only contacts on the fracture surface and to colour-code them according to magnitude, or tangential to normal component ratio

• **plot velocities** - new options to it:
- option to colour-code velocity vectors belonging to different large fragments
- option to scale up or down the length of plotted vectors

• **plot clusters** - new options to it:
- option to automatically colour-code large clusters according to magnitude

• **plot ball** - new options to it:
- option to colour-code large fragments
- option to analyse, through colour-coding, the history of particles on fracture surface (e.g. when their contacts with fragments and/or debris are broken)

• **plot cnd** - new options to it:
- options to colour-code broken contacts according to position or magnitude
- option to plot contacts in different slices through agglomerate
- options to plot re-adhered and non-rigid contacts
- option to analyse (through colour-coding) the history of contacts on the fracture surface (e.g. their type, when they partially peel, when they break).

OTHER - Created other new commands, options and facilities for gathering information and monitoring behaviour during testing (see Appendix B for details)

Fig.5.2 Main additional features of the new TRUBAL-ACI simulation software

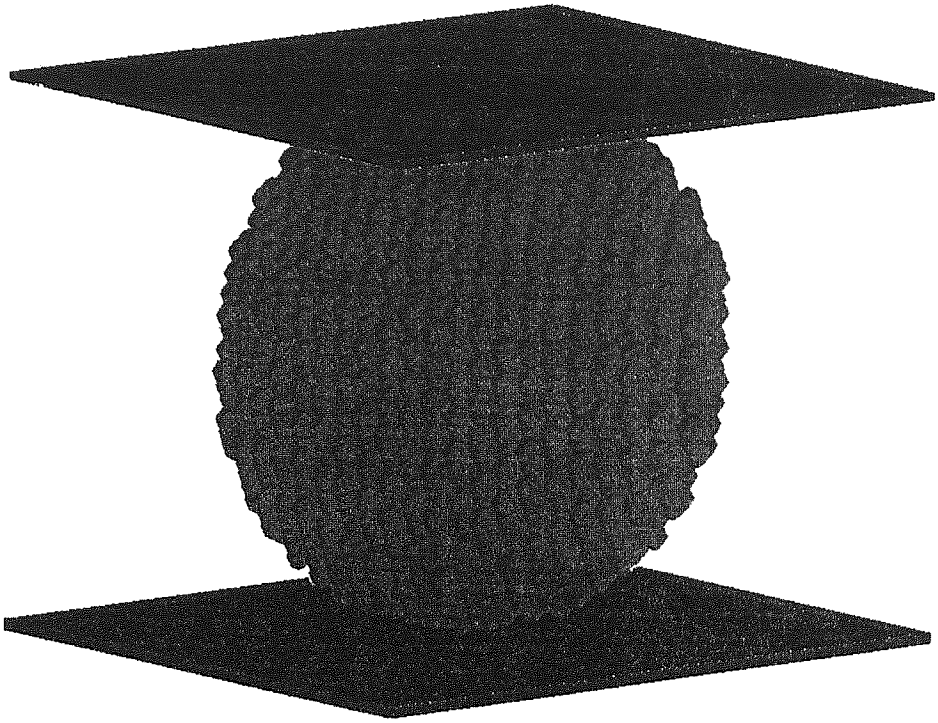

Fig. 5.3 One of the body-centred cubic agglomerates used (having 3897 constituent particles) at the end of the preparation process and already placed between the platens - arbitrary view

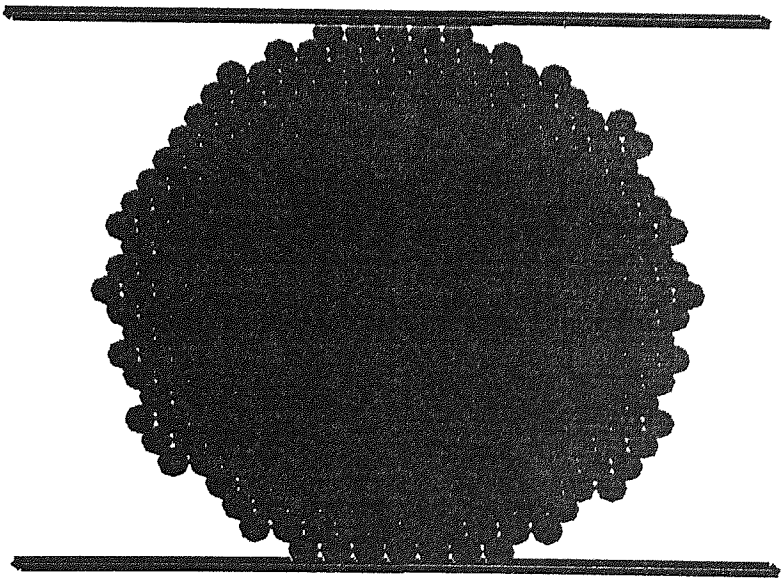

Fig. 5.4 A typical face-centred cubic agglomerate (having 4368 constituent particles) already placed between the platens - in a view from front

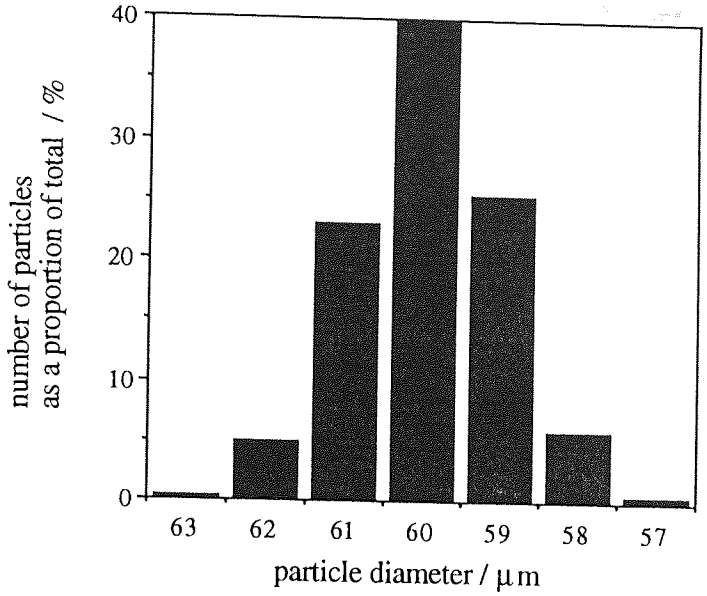

Fig. 5.5 The particle size distribution for the first 4000-particles random agglomerate

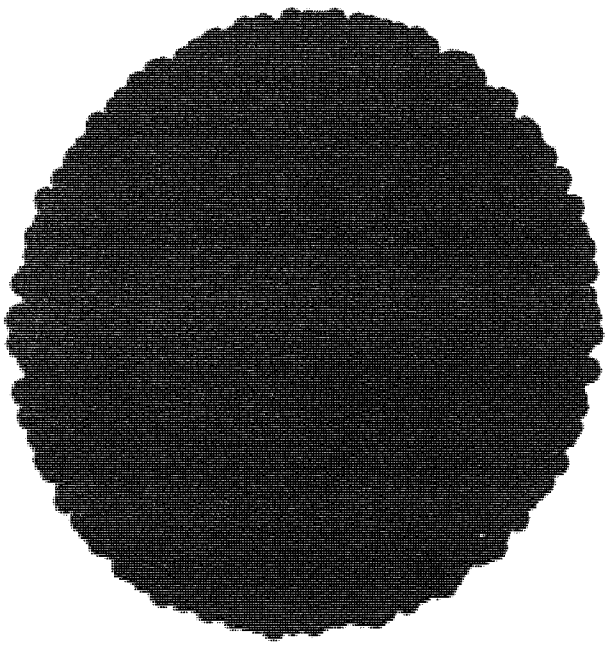

Fig. 5.6 Start of preparation stage: the 4000 particles after their creation at random within a specified spherical volume (coordination number = 0, porosity = 0.617)

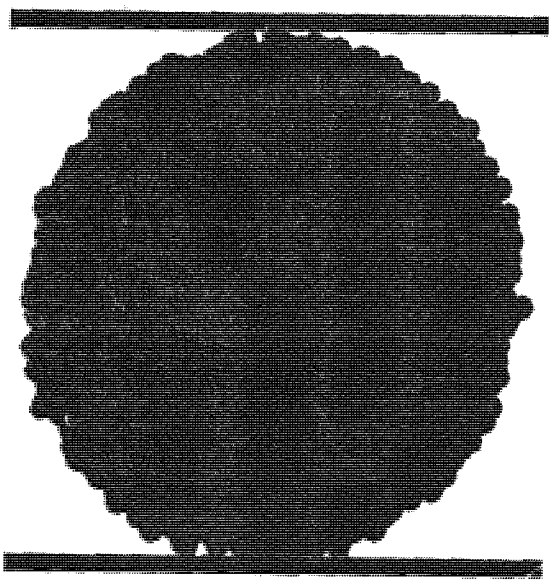

Fig. 5.7 End of preparation stage: the 4000-particles random agglomerate ready for testing. The top and bottom platens have also been created - in this view (from front) they are parallel to the viewpoint direction (coordination number = 5.45, porosity = 0.344)

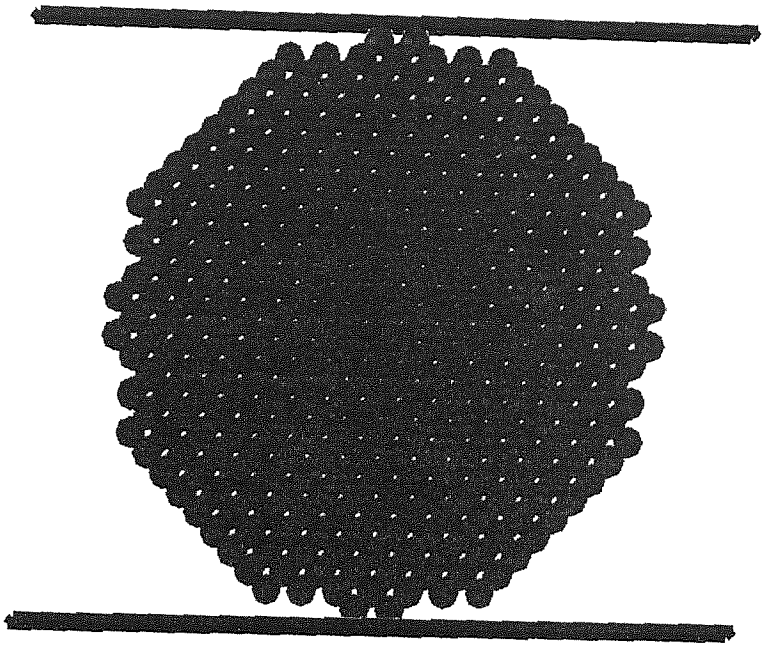

Fig. 5.8 View from front of the most used BCC agglomerate (having 3719 constituent particles and Γ=0.4 J/m^2) placed between platens and ready for testing (note that it has 4 particles in contact with each of the platens)

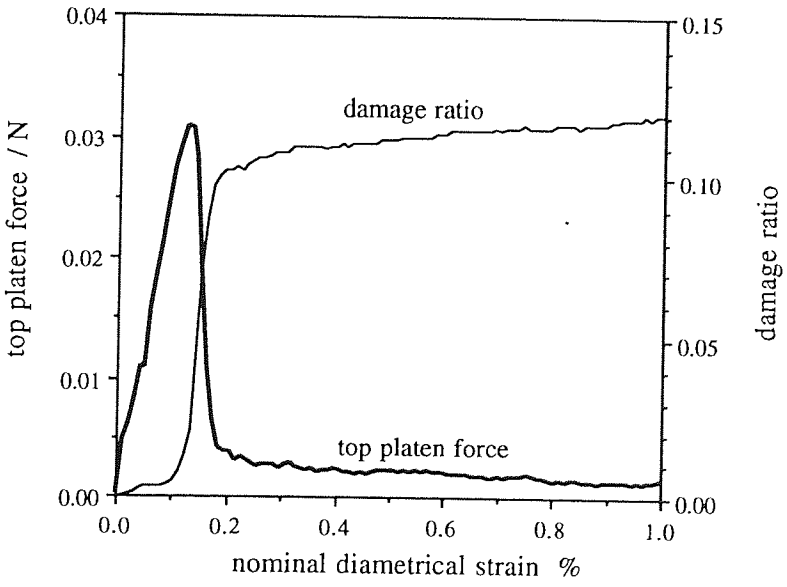

Fig. 5.9 Evolution of damage ratio and platen force, BCC agglomerate (Γ= 2 J/m^2, V = 0.05 m/s)

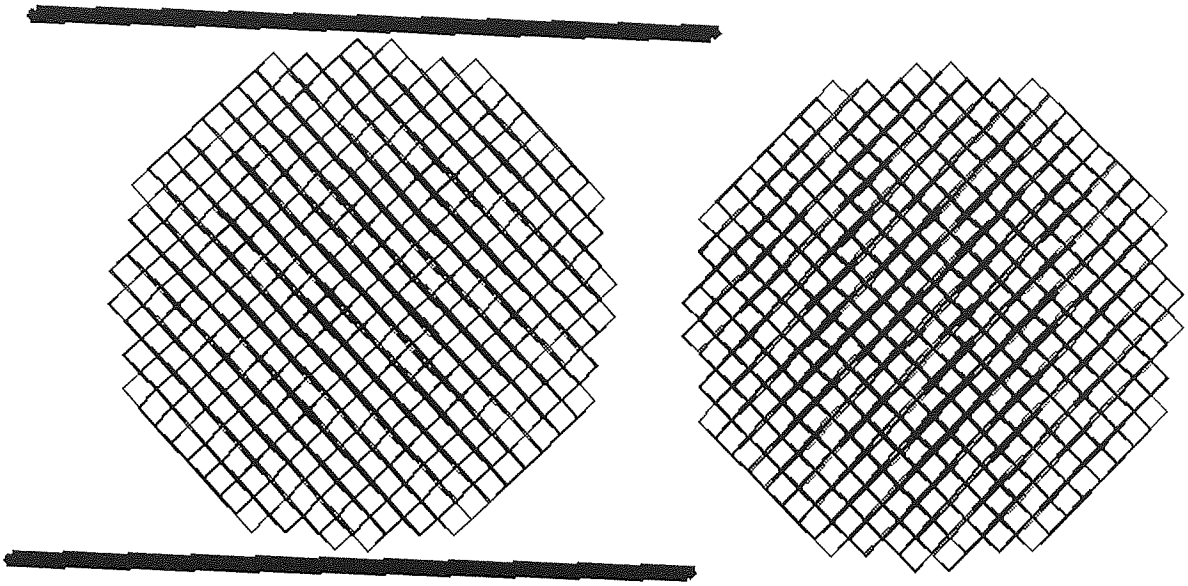

(a) view from front (b) view from above

Fig. 5.10 Equivalent space lattice at the start of tests, showing all existing bonds (as lines uniting the particles in contact), BCC agglomerate

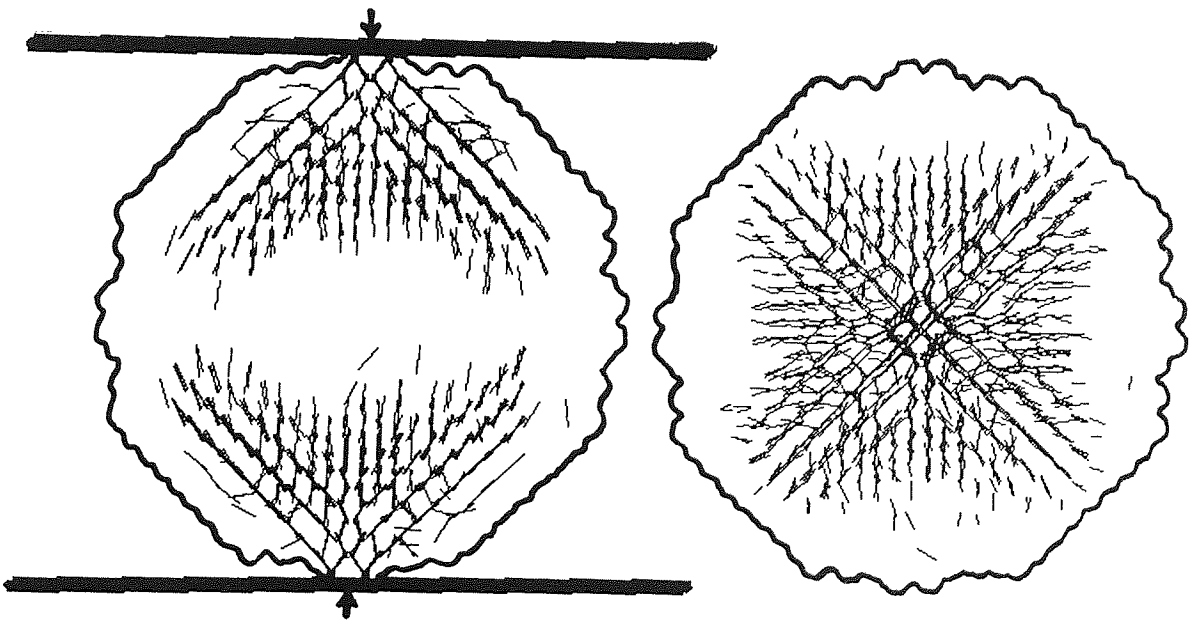

(a) view from front (b) view from above

Fig. 5.11 Typical location of the maximum compressive contact forces for a BCC agglomerate in diametrical compression tests (here the largest 22% of the compressive interparticle forces, $\Gamma = 2$ J/m^2, V = 0.05 m/s)

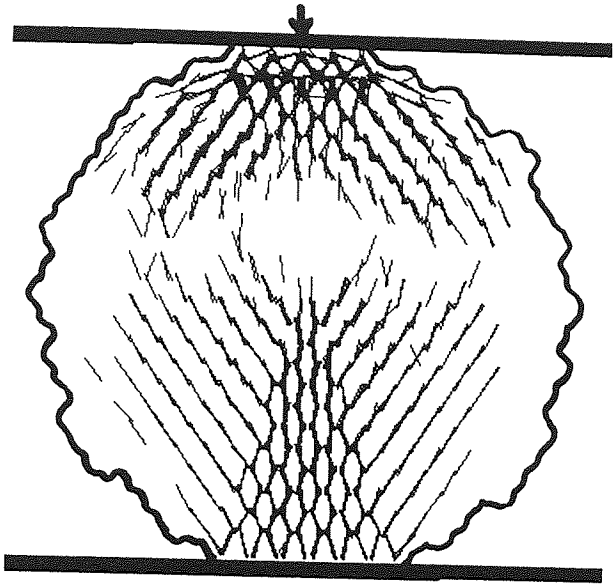

Fig. 5.12 Typical force transmission paths in tests where only the top platen was moved, FCC agglomerate, load direction was perpendicular on the close-packed planes (here $\Gamma = 0.4$ J/m^2, V = 0.1 m/s)

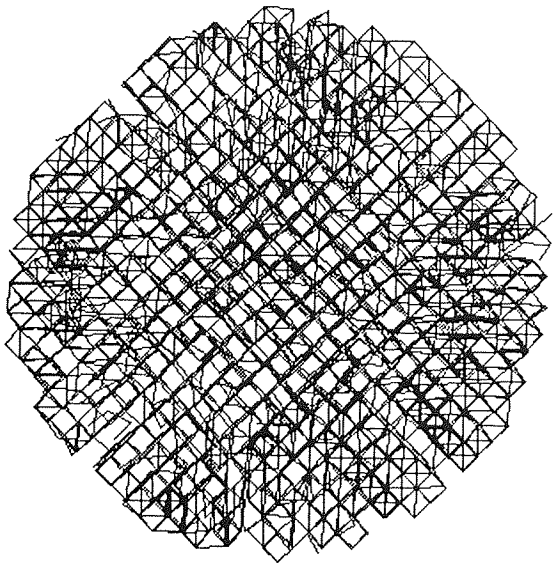

Fig. 5.13 Space lattice showing surviving bonds at 2.66% strain, long after the platen force dropped from its maximum attained value, FCC agglomerate ($\Gamma = 0.4$ J/m^2, V = 0.1 m/s)

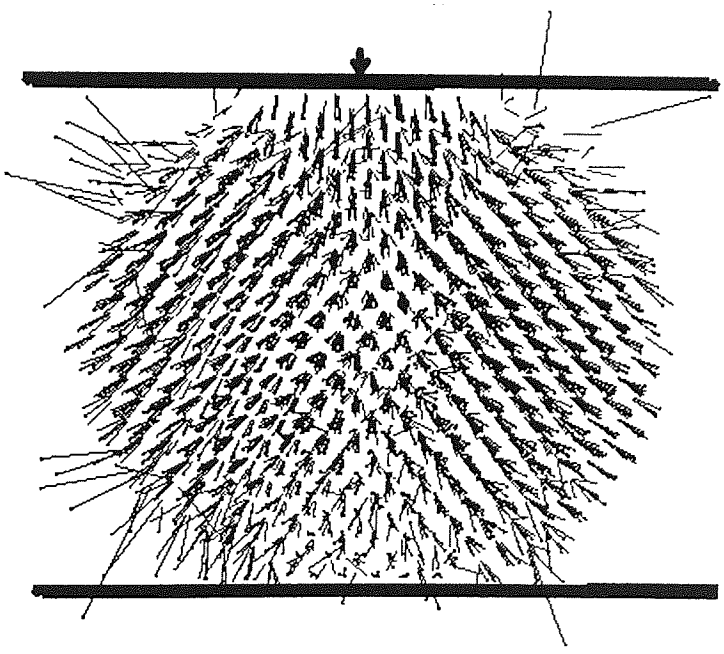

Fig. 5.14 Particle velocity field at 2.66% strain, FCC agglomerate ($\Gamma = 0.4$ J/m^2, V = 0.1 m/s)

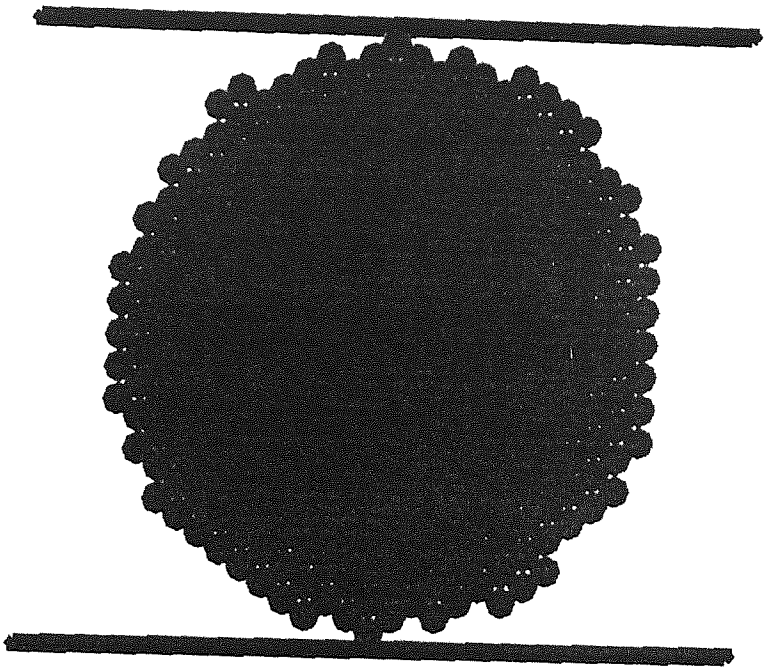

Fig. 5.15 The FCC agglomerate from Fig. 5.4 positioned under platens so that the loading direction is along contiguous lines of particles

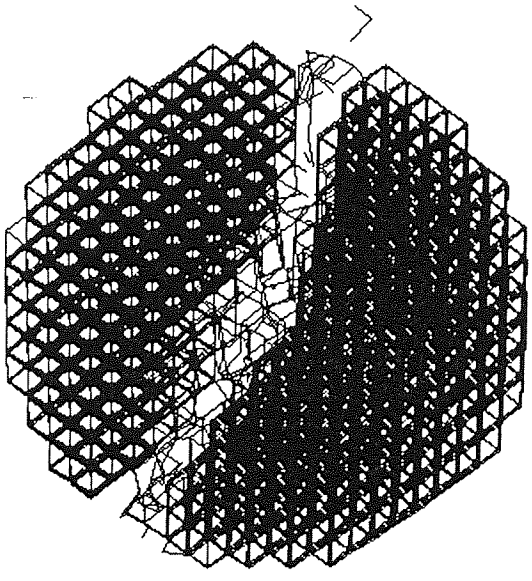

Fig. 5.16 Space lattice showing surviving bonds at 3.36% strain, view from above, FCC agglomerate, 14% of the initial bonds broke ($\Gamma = 0.4$ J/m^2, V = 0.005 m/s)

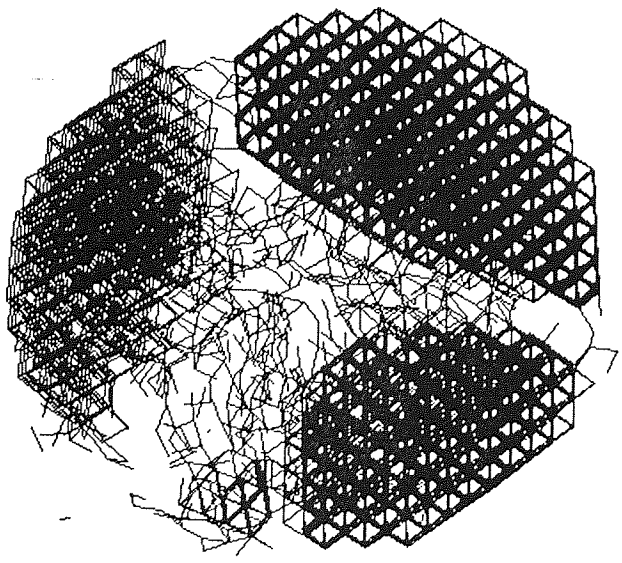

Fig. 5.17 Space lattice showing surviving bonds at 3.36% strain, view from above, FCC agglomerate, 32% of the initial bonds broke ($\Gamma = 2.0$ J/m^2, V = 0.1 m/s)

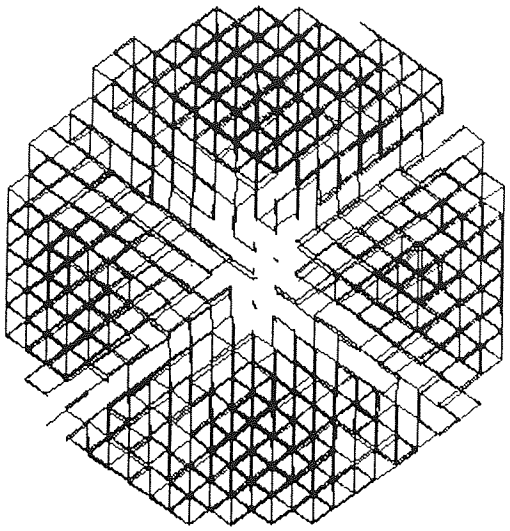

Fig. 5.18 Space lattice showing surviving bonds, view from above, FCC agglomerate, 75% of the initial bonds broke ($\Gamma = 0.4$ J/m^2, V = 0.1 m/s)

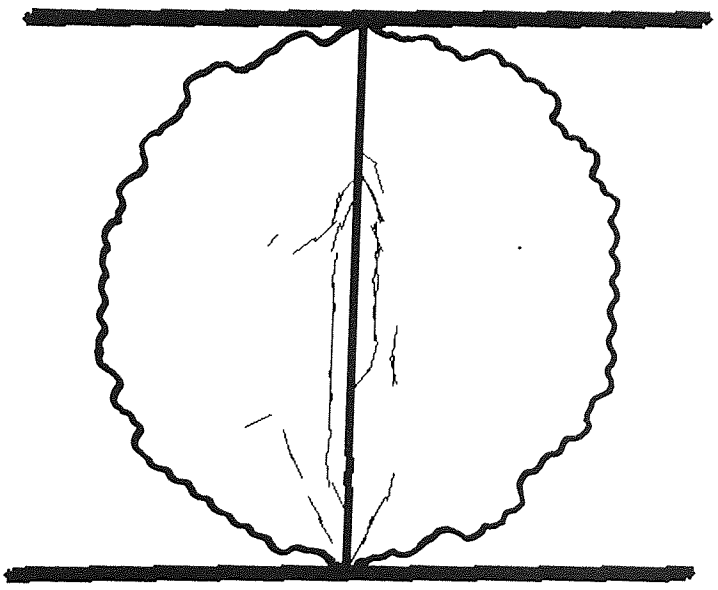

Fig 5.19 Typical force transmission path in tests where the FCC agglomerate fractured (load direction was along contiguous lines of particles) (here $\Gamma = 0.4$ J/m^2, V = 0.1 m/s)

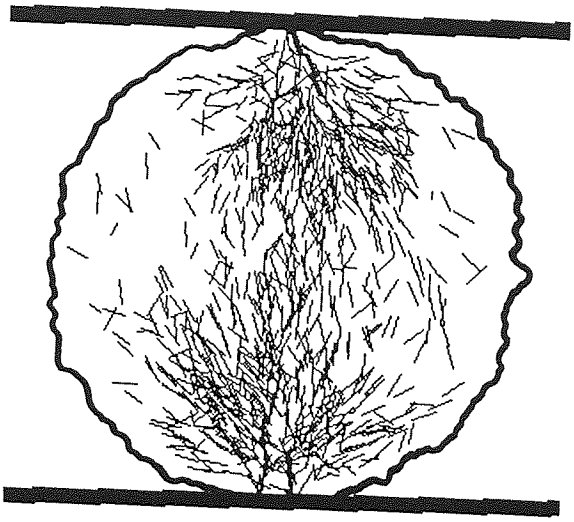

Fig. 5.20a Typical force transmission paths when the platen force was a maximum **(modified code)**, random agglomerate (here $\Gamma = 0.4$ J/m^2, V = 0.04 m/s)

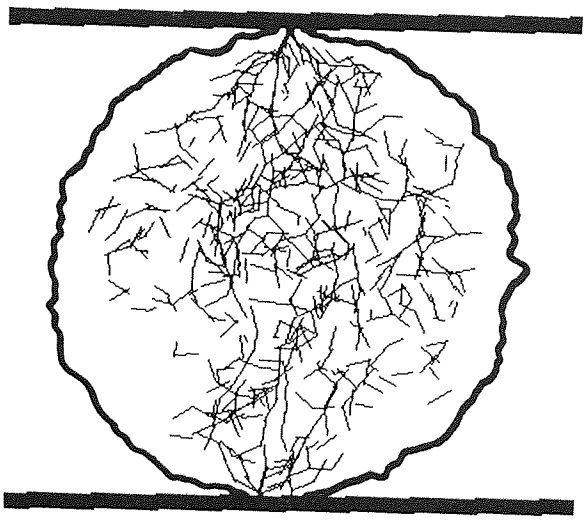

Fig. 5.20b Typical force transmission paths at 0.5 % agglomerate nominal diametrical straining **(unmodified code)**, random agglomerate (here $\Gamma = 0.4$ J/m^2, V = 0.005 m/s)

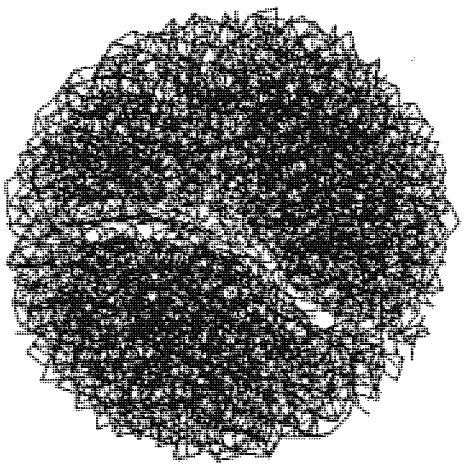

Fig. 5.21 Space lattice showing surviving bonds at 3.17% strain, view from top **(modified code)**, random agglomerate ($\Gamma = 0.4$ J/m^2, V = 0.04 m/s)

CHAPTER 6

SIMULATIONS OF FREE-FALL IMPACT TESTS

This chapter presents results of simulations of free-fall impact tests on dense and loose agglomerates. The simulation data are also compared with experimental data reported in the literature.

6.1 CHARACTERISTICS OF THE AGGLOMERATES USED

All the simulations reported in this chapter were performed on agglomerates composed of 4000 primary particles using the same elastic properties and friction coefficients for the particles and the platen as defined in Chapter 5. All the agglomerates used for free-fall impact simulations were attributed with an interface energy $\Gamma = 2\ J/m^2$. However, if a contact was broken during the impact and then reformed, or for new contacts created by the impact process, the interface energy was specified as $0.06\ J/m^2$.

Simulations were first carried out on a dense agglomerate having a solid fraction of 0.6530. A second agglomerate was prepared with essentially the same solid fraction but which had 15.73% more interparticle contacts. Results obtained from simulations using this second dense agglomerate will be reported in Section 6.2.5. Thirdly, free-fall impacts were simulated using a loose agglomerate having a solid fraction of 0.4364. The structural characteristics of the three agglomerate types are listed in Table 6.1. The *apparent coordination number,* Z_a, is the average number of contacts per particle and is calculated by taking into account all the agglomerate's particles and contacts. In contrast, *the mechanical coordination number,* Z_m, only takes into account the particles having more than one contact.

Figure 6.1 illustrates the three agglomerates prior to impact, showing the particle system on the left and the equivalent space lattice on the right of the figure. The particle size distributions are given in Fig. 6.2. Figure 6.3 additionally shows in comparison the exact way in which the coordination number was distributed within the three agglomerates prior to the impact tests.

6.2 BEHAVIOUR OF DENSE AGGLOMERATES

6.2.1 Impact Causing Only Local Damage (And Rebound)

For an impact velocity of 0.1 m/s, the dense[1] agglomerate rebounded. Only a small percentage of the initial bonds were broken, they were concentrated close to the impact zone, and resulted in a small amount of *fines* (very small fragments, see section 1.6) produced. Figure 6.4 illustrates the limited extent of the damage that occurred. In Fig. 6.4a the primary particles which constituted the surviving cluster are coloured grey. Particles which became detached from the main cluster and represent the debris are coloured black. The total number of debris particles was 36 which, in terms of mass, is slightly less than 1% of the initial agglomerate mass. Figure 6.4b shows the equivalent space lattice at the end of the impact in which the surviving bonds are shown in grey and the black lines indicate contacts which have been broken as a result of the collision. The total number of contacts broken was 223, corresponding to a damage ratio of 0.023.

Further data obtained from this simulation are shown in Figs. 6.5, 6.6 and 6.7. Figure 6.5 shows the evolution with time of the force generated on the platen and the translational kinetic energy of the agglomerate. It can be seen that the platen force increases to a maximum value at about 10 μs and then falls to zero at about 20 μs. As the platen force increases the kinetic energy of the agglomerate decreases until a minimum, almost zero, value is reached when the platen force is a maximum. The kinetic energy increases as the platen force decreases until a final constant kinetic energy is obtained when the platen force is reduced to zero. The final kinetic energy of the agglomerate when it rebounds from the platen is significantly less than the initial kinetic energy; and corresponds to a coefficient of restitution of approximately 0.55. The behaviour illustrated in Fig. 6.5 is similar to that of an elasto-plastic solid.

The evolution of the nominal straining of the agglomerate along the impact (vertical) direction is presented in Fig. 6.6. The figure indicates that the nominal straining reached a maximum of about 0.5% at the end of the loading stage. During unloading, partially due to the elastic recovery of agglomerate, but mainly due to the detachment of debris (from adjacent to the platen, Fig. 6.4.a) coupled with agglomerate rebound, the agglomerate expanded along the impact direction. Figure 6.6 also presents the evolution of the *average normal interparticle contact force* (the sum of all normal contact forces divided by the total number of contacts) - which gives a better (more precise) indication of the stored elastic energy's evolution than the platen force's evolution (Fig. 6.5). This is because the elastic energy is actually stored at the interparticle contacts within the agglomerate, mainly in the form of elastic deformation (straining) of the two particles in contact along the direction of the normal contact force. Larger elastic deformations of particles result in higher interparticle

contact forces and thus in a larger amount of elastic energy stored within the agglomerate. The evolution of the average normal contact force was not as smooth as the evolution of the platen force, but showed that almost the entire internal stored energy was used to produce the rebound of the agglomerate (that the internal stored energy was the driving engine for the rebound process).

Figure 6.7 presents the evolution of the damage ratio and debris ratio during the test. The *damage ratio* is the ratio of the broken bonds to the initial number of bonds, whereas the *debris ratio* is defined as the ratio of the mass of debris produced to the mass of the agglomerate at the start of the test. It can be observed that the number of bonds broken increased as the platen force increased. The maximum number of broken bonds was reached a little after the start of unloading. The subsequent drop in the damage ratio shows that several bonds re-adhered. The debris ratio increased throughout the loading and unloading stages, reaching a maximum value when the platen force had reduced to zero. This indicates that debris trapped between the agglomerate and the platen became detached from the agglomerate as the agglomerate rebounded off the platen. Both the damage ratio and the debris ratio remained essentially constant once rebound had occurred.

6.2.2 Impact Causing Fracture/Fragmentation

When impacted at a velocity of 0.2 m/s the dense agglomerate fractured into two large and one medium-sized fragments (at 13.3 μs and 22.2 μs). The images in Fig. 6.8, 6.9, 6.10, 6.11 and 6.16 present aspects observed at the end of test (311 μs). The simulated test was stopped long after the platen force dropped, when the total kinetic energy of particles, the damage and debris ratios levelled off (when the situation became stable in terms of bonds breakage and debris creation). Images in Fig. 6.8 show the agglomerate at the end of the simulation viewed from the front and from above. The particles belonging to the debris are represented in black, whereas the three larger fragments are indicated by three shades of grey - with the darkest shade of grey used for the medium-sized fragment. The figure shows that most of the debris was concentrated near the agglomerate-platen interface and only a small amount of debris formed in the top half of the agglomerate. Figure 6.9 presents the space lattice at the end of the test, as viewed from above. Fracture surfaces can be identified by the absence of lines. It can be seen that there appears to be a primary fracture surface which is almost perpendicular to the platen. The figure also suggests that there is a secondary fracture surface which has possibly propagated from the primary fracture surface. The existence of this second fracture surface is more clearly seen in Fig. 6.10 which presents a view from front of the space lattice showing both the existing bonds (grey) and broken bonds (black). The figure also demonstrates that almost all the bonds in a large zone adjacent to the platen had been broken. Almost 15% of the initial number of interparticle contacts were broken in this test. Only 24.4% of the total number of broken bonds were

situated in the top half of the agglomerate. In Fig. 6.11 only the broken bonds are shown, as viewed from front, almost along the primary fracture surface, and from above. The two images confirm that the fracture surfaces are perpendicular to the platen and indicate that the contact damage zone was roughly conical in shape. The two large fragments produced were approximately equal in volume and were almost free of internal damage. Ten times more debris was produced, compared to the impact at 0.1 m/s velocity.

Figure 6.13 shows the evolution of the platen force and the translational kinetic energy of the agglomerate during the period when fracture occurred. The kinetic energy continuously decreased during the collision but never reached a value of zero (or almost zero) prior to rebound because, in this case, fracture occurred before agglomerate had a chance to rebound. Because of the release of elastic stored energy in the fracture process, the remaining stored energy was not sufficient to produce enough kinetic energy for significant rebound of the agglomerate. The total kinetic energy of the resulting fragments, including debris, at the end of the test was about 24 times lower than the initial kinetic energy of the agglomerate. The fact that the kinetic energy dropped sharply to a low value which remained approximately constant until the end of the test (see Fig. 6.13) indicates that fracture was not explosive.

In order to identify the exact moment when fracture occurred, the evolution of the particle velocity field was monitored. Viewed from above, all the particle velocity vectors were directed radially outwards before fracture. Figure 6.12 shows the velocity vectors of the particles belonging to the two large fragments at 13.3 μs, just after the moment when primary fracture occurred. (In the figure the direction in which the vector points is indicated by a dot.) It can clearly be seen that a single primary fracture has occurred dividing the agglomerate into two hemispherical fragments. A little while after this fracture (at 22.2 μs) one of the large fragments was broken as a result of a secondary fracture. Figure 6.16 shows the particle velocity field, ignoring the debris, at the end of the test (311 μs). The figure clearly demonstrates the existence of the medium-sized fragment. There are three fragments which are moving in three different directions and in each fragment all the constituent particles have the same velocity. It can also be seen in Fig. 6.16a that the large fragment on the right hand side has already rebounded whereas the other two fragments are moving towards the platen.

The evolution of the force on the platen, Fig. 6.13, was not as smooth as in the test which resulted in the rebound of the agglomerate (Fig. 6.5). The primary fracture of the agglomerate into two large fragments occurred after the last peak on the force-time curve when the elapsed time was 13.3 μs. Secondary fracture occurred at 22.2 μs when the platen force had dropped to almost a tenth of its maximum value. Not much happened to the agglomerate after the secondary fracture had occurred. In Fig. 6.14 the evolution of

agglomerate nominal straining (along the direction of impact) is compared with the evolution of the average normal contact force in the agglomerate. The straining of the agglomerate was almost linear in time up to 8 μs (close to the moment of the primary fracture, see Fig. 6.14). The nominal straining of the large fragments continued, but at a slower rate, after the secondary fracture. The patterns of evolution are almost similar for the average normal contact force (Fig. 6.14) and the platen force (Fig. 6.13). However, the average normal contact force fluctuated about its maximum value until it (almost) suddenly dropped when primary fracture occurred. This demonstrates that the stored elastic energy was rapidly released at the moment of fracture.

Figure 6.15 shows the evolution of the damage and debris ratios. The damage ratio increased continuously until primary fracture occurred. No debris was produced until just before the platen force reached its maximum value, when the average normal contact force started to fluctuate. The debris ratio then increased until the force on the platen was zero. Strong fluctuations in the debris ratio - time curve can be observed after the primary fracture had occurred.

For a slightly lower impact velocity of 0.1785 m/s, the same dense agglomerate fractured into two large fragments but in a different way. Figure 6.17 shows all the particle velocity vectors at the end of the test (t=74 μs). Looking from above (Fig. 6.17b), the two fracture surfaces appear to be parallel to each other and possibly perpendicular to the platen. However, the view from front (Fig. 6.17a) reveals that the fracture surfaces are slightly inclined to the vertical, running almost radially from the damage zone formed adjacent to the platen. In this test, the large fragment on the right hand side was the first to separate from the agglomerate (at 11.3 μs), whereas the secondary fracture surface (the one on the left hand side in Fig. 6.17) concluded its propagation a little later, at about 13.8 μs. It can be observed that the large fragment on the right hand side is moving laterally, whereas the other two large fragments have already rebounded. The space lattice at the end of the test is illustrated in Fig. 6.18a. The figure shows that all the bonds around the impacted pole have been broken and that the fragments are almost free of internal damage. A front view of the agglomerate at the end of test is provided in Fig. 6.18b, where all the large fragments are indicated in grey. As in the previous test, debris (in black) mainly detached from around the impact zone. Since the total fracture surface was a little larger, slightly more interparticle contacts were broken than in the test at 0.2 m/s impact velocity but the quantity of debris was lower.

The graphs in Fig. 6.19-6.21 cover the interval in the simulation when the fractures occurred. Figure 6.19 presents the evolution of the platen force and the translational kinetic energy of the agglomerate. Although the patterns of evolution are similar to the ones obtained in the 0.2 m/s impact velocity test (see Fig 6.13), it was a little surprising that the

maximum attained platen force was a little higher. This aspect was actually reflected in the fact that the test of 0.1785 m/s impact velocity resulted in a very slightly larger amount of broken bonds (4%). In both tests primary fracture occurred just after the last clear peak in the platen force (see Fig. 6.13 and 6.19). However, the unloading before primary fracture was more abrupt in the test of 0.1785 m/s impact velocity. Also the kinetic energy of the agglomerate dropped to a value 41% lower than in the test of 0.2 m/s impact velocity (compare Fig. 6.13 to Fig. 6.19). The evolution of the average normal contact force, presented in Fig. 6.20, is roughly similar to the one of the platen force, Fig. 6.19. However, compared to the test of 0.2 m/s impact velocity, the overall unloading is much less sudden. At the moment of primary fracture both the platen force and the average contact force had a little lower values in the test of lower impact velocity (Fig. 6.19, 6.20 and 6.13, 6.14). This, correlated with the fact that primary and secondary fracture were much closer in time in the 0.1785 m/s impact velocity, reflect the different way in which the agglomerate fractured in each of the two tests. The less steep unloading after the primary fracture, Fig. 6.20, indicates that primary fracture did not consume much of the elastic stored energy. This and the fact that secondary fracture occurred shortly after the primary fracture suggests that the secondary fracture surface was well developed by the moment of primary fracture. Figure 6.20 also shows the evolution of the average velocity of the particles along the impact axis, which illustrates that the agglomerate can be considered to remain on the platen at the end of test.

Figure 6.21 presents the evolution of damage and debris ratios, which are very similar to the ones in Fig. 6.15, for the test of 0.2 m/s impact velocity. The slight difference is that the evolution of the debris ratios presented less fluctuation during its increase in the test of 0.1785 m/s impact velocity. The debris detached mainly from the zone adjacent to the platen, as indicated by Fig. 6.18b. Debris particles, after most of the bonds have been broken during the loading stage of the impact (see damage ratio in Fig 6.21), gradually detach (see the debris ratio in Fig. 6.21) from the large fragments. The figure 6.17b illustrates well the debris detachment process - the velocities of the debris particles are directed roughly towards the platen while the three large fragments rebounded.

When the dense agglomerate was impacted at a velocity of 0.3 m/s there were six surviving fragments at the end of the test (t=311 μs). Corresponding views of the space lattice and the particle configuration at the end of the simulation are illustrated in Fig. 6.22a and Fig. 6.22b respectively. Compared to the tests of lower impact velocity (0.2 m/s and 0.1785 m/s), much more bond breakage and debris detachment occurred in this test but again, mostly in the bottom half of the agglomerate. The surviving fragments were not just smaller but also weaker (due to more internal damage) than the fragments formed at lower impact velocities.

The evolution of the platen force and the kinetic energy of the agglomerate are presented in Fig. 6.23. In this test the platen force exhibited only one peak, compared to 2-3 peaks observed in the tests of lower impact velocities causing fracture (Fig. 6.13 and Fig. 6.19). The maximum platen force attained was a little larger than in the other tests and attained earlier; the unloading was more steep up to 15 μs (see Fig. 6.23 compared to Fig. 6.13 and Fig. 6.19). The evolution of the kinetic energy was similar to the one observed in the other two tests producing fracture, except that the "level-off" energy from after the fracture was much larger. Figure 6.24 presents the evolution of the average normal contact force and nominal straining of the agglomerate. The figure indicates that the elastic stored energy was kept approximately constant up to the moment of fracture (at 9.6 μs); the sharp unloading indicates the more sudden character of the fracture. The maximum elastic energy stored was only a little higher compared to the one obtained in the other tests, but the agglomerate nominal straining was much larger (over 2.5 times). Compared to the test of 0.2 m/s impact velocity (Fig. 6.14) the rate of strain did not alter much after fracture (see Fig. 6.24). The larger impact kinetic energy in this test did not produce a (proportionally) large increase in the platen force and the maximum stored energy. However, the more dynamic effect of the test was expressed in the larger amount of broken bonds, fragments and debris particles resulted after fracture. The evolution of the debris ratio and damage ratio, Fig. 6.25, was similar in trend to the one in the other tests causing fracture: they both levelled-off shortly after the fracture. The large kinetic energy remaining after the fracture (see Fig. 6.23 compared to 6.19 and Fig. 6.13) was mainly used to move all the fragments towards the platen, a fact reflected by the continuous increase in the nominal straining after (Fig. 6.24) and long after the fracture moment.

6.2.3 Impact Causing Shattering

The dense agglomerate shattered when impacted at a velocity of 0.9 m/s. The high impact velocity had first a tendency to break-up the agglomerate in many medium-sized fragments; this can be easily noted from Fig. 6.26 showing the space lattice (including broken bonds in black) at 9 μs, after the platen force dropped. Observing the groups of surviving bonds (in grey) one can notice that these medium-large fragments were elongated, with their longer dimension along the loading direction. However, the agglomerate did not break later in the test, as the medium-large fragments stayed grouped together (in contact with each other) within a large cluster of would-be large fragments. Almost all through the test the agglomerate consisted of this large surviving cluster; usually only debris managed to effectively detach from it. After 6.5 μs very weak medium-small clusters were sometimes detached from the large cluster, and then broke up fast (within 0.1-0.2 μs) into debris. The space lattice (including broken bonds in black) at the end of test (t=512 μs) is shown in Fig. 6.27 clearly indicating the extensive bond breakage. The largest fragment at the end of the test contained only 153 particles. Figure 6.28 shows the particle velocity field viewed from

both the front and above at the end of the simulation. The figures are illustrative of the shattering regime: most particles move independently (separately) rather than in groups and their displacements (relative to their initial location) are large. A characteristic of shattering was the extensive flattening of what was the agglomerate, as seen in Figs. 6.27b and 6.28a.

The evolution of the kinetic energy and the reaction force at the platen is presented in Fig. 6.29. Figure 6.30 shows the evolution of the average normal contact force and the average velocity of the particles towards the platen. The corresponding evolution of the damage ratio and debris ratio is provided in Fig. 6.31. The platen force increased to a maximum value of about 35 mN at 2.4 μs and then dropped rapidly to 3.5 mN at 16.5 μs (Fig. 6.29). This coincided with a rapid increase in the damage ratio to about 0.6, in the debris ratio to 0.63 and with a reduction in the number of particles in the largest cluster from 4000 to slightly more than 1000. After 15 μs, the platen force slowly reduced but with significant fluctuations (Fig. 6.29), whereas the damage ratio slowly increased at a decreasing rate (Fig. 6.31) to a final value (at the end of test) of 0.8. The debris ratio followed and then surpassed the damage ratio; at the end of the test it attained the value of 0.92. In the period of time represented in Fig. 6.30 the velocity of the particles towards the platen was very high compared to the tests in which the agglomerate fractured (see Fig. 6.20). Figure 6.30 indicates that the elastic strain energy, although attaining a maximum of over 2.5 times larger than in the tests causing fracture, was not maintained for a while (as in other tests, for instance see Fig. 6.14) at this maximum value. After a large rapid unloading it followed a less steep, fluctuating and very long unloading period (Fig. 6.30).

Bonds started to break almost randomly throughout the agglomerate almost from the very start of impact. The several slightly-more preferred directions of bond breakage (see Fig. 6.26) did not manage to result in fracture or fragmentation of the agglomerate. Instead, just before attaining the maximum platen force, debris started to detach from the agglomerate. Images in Fig. 6.32 show the particle system at 4.6 μs, 9 μs, 157 μs and 512 μs (end of test). The particles in the debris are black, the ones in the large surviving cluster are light grey, dark grey is used to indicate the particles belonging to the short-lived medium-small clusters. Particles were first detached from the external surface of the agglomerate, probably due to the large longitudinal wave (Fig. 6.32a). Debris was then detached mainly from the external surface of the bottom hemisphere of agglomerate, starting from the impacted pole upwards (see Fig. 6.32a and 6.32b). As flattening continued, debris became detached from the whole of the agglomerate apart from a (roughly-cylindrical) zone around the loading diameter. This can be easier observed by following the evolution of the largest surviving cluster during the test, presented in Fig. 6.33 (at 9 μs, 14.9 μs, 157 μs and 512 μs). From an oak tree-like appearance after the drop of the platen force (Fig. 6.33a, 2272 particles), the large cluster became smaller (1326 particles, Fig. 6.33b) but still remained almost intact in a large part of the agglomerate's top hemisphere. The cluster became progressively weaker

due to (extensive) internal bond breakage (the most damaging period was up to 8 μs, see Fig. 6.31). Due to its weakness and the relatively high remaining velocity (see particle velocity towards platen in Fig. 6.30) the large cluster suffered a gradual attrition. When it was reduced to 771 particles (Fig. 6.33c) the large cluster was very weak. At the end of the test, Fig. 6.33d presents the largest surviving cluster (of 153 particles) in light grey, the second largest cluster (150 particles) in dark grey and the next "large" clusters (of 55 and 54 particles) in black. The fact that at the end of the test there still was a force on the platen is because of the long column of particles belonging to the cluster in contact with the platen.

The velocity of the particles towards the platen (Fig. 6.30) decreased by only about 20% until 15 μs when the platen and average contact forces dropped to relatively low values. This high velocity of the particles continued to maintain (for a long duration in the test) a relatively high level of stored energy within the largest surviving cluster. This helped to increase further (although at a much slower rate) the damage and debris ratios. At 512 μs the nominal straining of the agglomerate attained was about 11%. The kinetic energy decreased at a decreasing rate throughout the test, Fig. 6.29, to a final value 5.2 times lower than the initial value. The residual kinetic energy at the end of the test was, nevertheless, much larger than in the tests causing fracture. This demonstrates the more "explosive" nature of the impact test causing shattering in which most of the resulting debris flew away on radial trajectories from the zone of impact (see Fig. 6.28b).

6.2.4 Effect Of Impact Velocity On Fracture/Fragmentation

Figure 6.34 provides a comparison of the fracture patterns produced by impact velocities of 0.2, 0.1785 and 0.3 m/s. The figures show the surviving space lattice (grey) and the broken bonds (black) as viewed from above at the end of the tests. Although there are some common features in the fracture patterns which suggests that there are inherent preferred internal planes of weakness this is not completely true. A comparison of Fig. 6.34b with Fig. 6.34c confirms that the two fracture surfaces created by an impact velocity of 0.1785 m/s are evident in the fracture pattern obtained for an impact velocity of 0.3 m/s. Comparing Fig. 6.34a and Fig.6.34c, the two forks of the fracture pattern obtained with an impact velocity of 0.2 m/s can also be seen as part of the complex fracture pattern produced by an impact velocity of 0.3 m/s. However, the other section of the fracture surface which separates the two large fragments produced by an impact velocity of 0.2 m/s, Fig. 6.34a, does not correspond to any fracture surface visible in either of the two other images in Fig. 6.34. This suggests that, although there may be inherent weak planes within an agglomerate, the statistical nature of the energy transmission may result in other planes being selected for fracture propagation. The figures viewed from front, roughly along the fracture surface (Fig. 6.10, 6.18a and 6.22b) also illustrate the few common and the distinct aspects of the fracture surface developed for the three different impact velocities causing fracture.

Analysing the evolution of different parameters in all the simulations causing fracture carried out on the dense agglomerates, it can be concluded that higher impact velocities lead to higher platen forces, average normal contact forces, local contact damage, agglomerate nominal straining, quantity of broken bonds, debris and dissipated energy prior to the fracture moment.

6.2.5 Effect Of Contact Density

A second dense agglomerate was prepared which, as indicated in Table 6.1, had 16% more initial bonds but the same solid fraction. When impacted at different velocities the general behaviour was found to be similar to that observed for the first dense agglomerate. However, some differences were noted.

When impacted at a velocity of 0.1 m/s the agglomerate rebounded with a coefficient of restitution of 0.71 compared to the value of 0.52 obtained for the first dense agglomerate at the same impact velocity. This indicates that less energy was dissipated although more debris (99 particles, most of them in the form of fines) was produced than in the corresponding test on the first dense agglomerate (which only produced 36 debris particles).

The second dense agglomerate fractured into two or more fragments for impact velocities above 0.1 m/s but the fragmentation patterns were different from these observed for the first dense agglomerate. Figures 6.35 (in views from above) and 6.36 (in views from lateral-right, along a main fracture surface) illustrate the fracture/fragmentation patterns obtained by showing the final space lattice (including broken bonds) for impact velocities of 0.12, 0.15, 0.2 and 0.3 m/s. Several preferred internal fracture surfaces can be identified. For example, the fracture surface obtained for an impact velocity of 0.12 m/s (Fig. 6.35a) can be easily identified in the more complex fracture patterns obtained with higher impact velocities. The views from the lateral-right, shown in Fig. 6.36, illustrate how the size of the damage zone, adjacent to the platen, increased with increasing impact velocity and extended over almost the whole of the bottom half of the agglomerate when the impact velocity was 0.3 m/s.

Figure 6.37 presents comparisons of the evolution of the platen force, damage ratio, debris ratio and average normal contact force for the two dense agglomerates impacted at a velocity of 0.3 m/s. The evolution of the platen force (Fig. 6.37a) was almost identical during loading and similar during unloading although the unloading was initially (slightly) more rapid for the second dense agglomerate. The damage ratio and debris ratio (see Fig. 6.37b) both levelled off at about the same time in both tests. However, 52% more bonds broke and 24% more debris was finally produced in the agglomerate with the higher initial contact density.

Fracture occurred a little earlier in the second dense agglomerate and the fragments flew-off with higher velocities after fracture than in the case of the first dense agglomerate. The behaviour of the second dense agglomerate was more brittle although the platen force evolution was similar to that of the first dense agglomerate. The differences in behaviour are best illustrated by the evolution of the average normal contact forces, Fig. 6.37c, which reflects the evolution of the stored elastic energy during the tests. The average contact force in the second dense agglomerate increased to a maximum value when the platen force was a maximum and reduced rapidly as the platen force dropped. Although the maximum platen force was the same for the two tests, the average normal contact force in the first agglomerate only increased to about 67% of that developed in the second dense agglomerate and fluctuated about the maximum before falling. The larger average normal contact forces in the second dense agglomerate during the loading phase (Fig. 6.37c) suggests that more energy is stored in this agglomerate.

6.3 BEHAVIOUR OF LOOSE AGGLOMERATES

The loose agglomerates behaved very different from the dense ones in the free-fall impact simulations. The main difference in behaviour was that the loose agglomerates did not fracture - for neither low, medium or high impact velocities.

6.3.1 Impact Causing Local Damage

For a 0.01 m/s impact velocity the loose agglomerate suffered only insignificant levels of damage and debris detachment. The test was halted at 5.8 ms, long after both the agglomerate's velocity towards the platen and the platen force became virtually zero. At the end of the test the agglomerate was resting on the platen (having only 3 particles in contact with it) due to the gravitational field. Most of the impact energy was dissipated locally at the agglomerate-platen contact. This was also indicated by the final 0.09% nominal agglomerate straining along the impact axis (and only 0.002% nominal straining along the axis perpendicular to the impact direction).

Figure 6.38 presents the evolution of platen force and kinetic energy up to 500 μs. It can be noted that, within the first 100 μs, the kinetic energy dropped to a value 4.6 times lower than the initial value and the platen force attained 3 larger peaks (at 11.1 μs, 33.2 μs and 96.9 μs). At 38.8 μs, just after the second peak, the platen force dropped to zero and, almost suddenly, 11 bonds broke and 197 particles detached from the vicinity of the agglomerate-platen contact. The bond breakage and debris detachment process "peaked" at around 49 μs when a total of 13 bonds were broken and 303 (7.58%) particles had detached

from the main cluster. Figure 6.39 shows the evolution of the average normal contact force and the velocity of agglomerate towards the platen up to 500 μs. The figure indicates that the evolution of the elastic stored energy was similar to the evolution of the platen force; the largest peaks were also attained at about 33.2 μs and 96.9 μs.

The particle configuration at 83.1 μs as viewed from the front and from below is illustrated in Fig. 6.40; the largest surviving cluster (3831 particles) is represented in light grey, a small-medium cluster (105 particles) in darker grey, whereas black denotes the 64 particles in the debris. The small-medium cluster can also be considered as debris, because it broke very soon afterwards (it proved to be a very weak and short-lived cluster). Only the first (before 50 μs, Fig. 6.39) amount of stored elastic energy contributed to the debris detachment. The last sharp increase in the platen force and average normal force (from about 50 to 100 μs) resulted in the creation of new interparticle contacts, probably due to the fact that the debris was compressed between the largest cluster and platen. This led to a process of re-adherence of debris to the large cluster.

Most debris had re-adhered by 249 μs - see Fig. 6.41 presenting the evolution of the number of particles in the largest cluster. The slow (debris) re-adherence process was completed only at 2.2 ms - and from this moment all the 4000 particles belonged to a single cluster. Fig. 6.41 also presents the evolution of agglomerate's nominal strain up to 1.5 ms. The sharper straining of up to about 150 μs was followed by a little expansion and then some more (but less fast) straining. The sharpest decrease in the agglomerate's velocity towards the platen occurred during the loading stages (see Fig. 6.39); the velocity zeroed and changed direction at 125 μs - soon after the second large peak in the average contact force. However, the agglomerate did not rebound off the platen; the nominal expansion of the agglomerate was only about 1/5 of the nominal straining up to 150 μs - see Fig. 6.41.

Figure 6.42 presents the evolution of the average normal contact force and the agglomerate's velocity towards the platen up to 1.5 ms. The figure illustrates the fact that the agglomerate oscillated several times on the platen before finally resting on it. The weak oscillations were a proof that the agglomerate exhibited elasto-plastic behaviour. The release of the second amount of stored energy (at 100 μs, Fig. 6.39) could not cause the rebound of the agglomerate, as the elastic energy was too low. However, the average velocity of the particles indicates that the agglomerate tried to move upwards. Very soon the gravity force generated by the agglomerate's mass caused it to reverse and press again on the platen, restoring some elastic energy again. It took a long time to achieve the complete damping of this oscillatory motion. From looking at Figs. 6.38, 6.39 and 6.42, one can conclude that in this test most of the impact energy was dissipated by 150 μs.

6.3.2 Impact Causing General Failure (Shattering)

Although the 0.2 m/s impact velocity caused fracture of the dense agglomerates, it produced shattering of the loose agglomerate - see Fig. 6.43 presenting all the particles at the end of the test. The 1532 particles belonging to the largest surviving cluster are represented in light grey, the 146 particles of a medium-small cluster in dark grey, and the 2322 particles belonging to the debris in black. The test was halted at 1.96 ms, long after the nominal agglomerate strain levelled off at around the 6.6% value, when the average velocity of the particles towards the platen became very small (36 times lower than the initial impact value). However, the process of bond breakage was not quite completely finished by the end of the simulation. The number of particles in contact with the platen was roughly constant (60) during the last 1 ms of the test.

The three images in Fig. 6.44 present the space lattice of the agglomerate at the end of the test. Figure 6.44a shows both the existing bonds (grey) and broken bonds (black). It can be observed that most bonds broke in the bottom half of the agglomerate. Figure 6.44b only presents the surviving bonds; the slight mushroom-like appearance is similar to the space lattice presented by dense agglomerates before shattering (in free-fall tests of higher impact velocities). The new (weak) bonds that were created during the test are presented in Fig. 6.44c. It can be observed that most of these bonds were formed in the contact zone (of the large cluster with the platen) due to the movement of the agglomerate's particles towards the platen (which caused a concentration of particles there). However, unexpectedly, many new bonds were created close to the external surface of the large cluster. This was in agreement with the observed behaviour of debris during the test - detached debris clusters often re-adhered to the largest surviving cluster.

Figure 6.45 presents the evolution of platen force and total kinetic energy of the particles. The platen force increased and then fluctuated around the 0.4 mN value up to about 550 μs when it suddenly dropped to a very low value. The figure is roughly similar to the one obtained for the dense[1] agglomerate for 0.1 m/s impact velocity (Fig. 6.5). As in that test, the kinetic energy dropped during loading and a part of it recovered afterwards. However, in the loose agglomerate the recovery of the kinetic energy only commenced a while after the platen force dropped (and not when it attained the maximum, as in the case of the dense agglomerate). Whereas the recovery of the kinetic energy in the dense agglomerate represented its rebound from the platen, the recovery of the kinetic energy in the loose agglomerate could only indicate that the increasing mass of debris was rebounding from the platen. This is because the average particle velocity towards the platen did not reverse, meaning that the largest cluster was still moving, but very slowly, towards the platen. Figure 6.46 shows the evolution of the particles' velocity towards the platen and of the average normal contact force. The figure indicates good agreement between the evolution of

the internally stored elastic energy and the platen force. The particles' velocity towards the platen was reduced considerably by the moment when the elastic stored energy was released.

Fig. 6.47 presents the evolution of the total number of particles in the largest cluster and of agglomerate nominal strain. The figure proves the absence of fracture: the final release of the elastic stored energy did not result in the breakage of the largest cluster, nor in a sudden detachment of a large mass of debris. Instead, one can observe that debris was detached from the agglomerate (largest cluster) at a roughly constant rate (Fig. 6.47) until the platen force dropped to a very low value (Fig. 6.45). The evolution of the nominal straining of the agglomerate was almost linear until the platen force dropped. From around 500 μs the number of particles in the largest surviving cluster fluctuated around the 1000 value.

Similar to the impact tests on dense agglomerates, bonds started to break from the agglomerate-platen contact area upwards. However, the zone of broken bonds did not progress as a conical volume - see Fig. 6.49 presenting the space lattice at 222 μs, when the platen force attained the high peak of 0.58 mN (Fig. 6.45). The black lines represent the broken bonds and the grey lines the surviving ones. The figure shows that bonds were broken only in the bottom half of the agglomerate up to 222 μs. Also the debris started detaching from the impacted pole upwards - see Fig. 6.50 presenting views from the front and from below of all the particles in debris (black and dark grey) and in the largest surviving cluster (in light grey) at 222 μs. It may be noted in Fig. 6.50b that particles situated in certain external areas of the bottom hemisphere were easier than others transformed into debris. The breakage of bonds extended over the whole volume of the agglomerate after the platen force dropped a little from its maximum value (Fig. 6.45). Figure 6.51 illustrates the space lattice at 388 μs, with broken bonds (721 in all) in black and surviving in grey. It is noted that the damage was not symmetric: more bonds broke on the right hand side of the agglomerate. This side was also the one experiencing more debris detachment - see Fig. 6.52 presenting the particles in the debris (black) in the two small-medium clusters (173 and 144 particles each, dark grey) and in the largest surviving cluster (light grey, 1802 particles). The zones inside the agglomerate with the largest concentration of broken bonds also contained newly-formed bonds - see Fig. 6.53 showing the newly created bonds at 388 μs.

All through the test the agglomerate consisted of a large surviving cluster and debris. Small-medium sized clusters (typically having 50-150 particles) were at times detached from the largest cluster (see Fig. 6.50, 6.52 and 6.43 in dark grey). These clusters had a very short life as they either broke further or re-adhered to the large cluster. The progressive shattering of the agglomerate can also be observed by monitoring the evolution of the largest cluster. The images in Fig. 6.54 show the particles in the surviving large cluster at 222 μs, 388 μs

and 1960 μs. Note the non-symmetry in the detachment of debris and small clusters and the weakness of the largest surviving cluster at the end of the test (Fig. 6.54c) even better reflected by the large amount of broken bonds (Fig. 6.44a) and new weak bonds (Fig. 6.44c) that it contained.

6.4 SUMMARY OF SIMULATION RESULTS

6.4.1 Dense Agglomerates

The dense[2] agglomerate behaved more brittle and elastic than the dense[1] one did. The higher contact density in the dense[2] agglomerate led to higher coefficients of restitution in free-fall impact tests compared to the dense[1] agglomerate. The dense[2] agglomerate fractured at lower impact velocities and at lower nominal strains than the dense[1] agglomerates; it also produced a higher number of large fragments for the same impact velocity. In the tests causing fracture, more of the input kinetic energy of the dense[2] agglomerate transformed into kinetic energy of the resulting fragments after fracture if compared to similar tests on the dense[1] agglomerate.

From tests at low impact velocities it was observed that the free-fall impact was able to produce a maximum of 0.05% nominal straining of both dense agglomerates without fracturing them. It seems that the platen force had to rise to about 15 mN for the fracture to occur. It also appears that a free-fall impact test can cause the fracture of a dense agglomerate only if the internally stored energy becomes larger than a certain critical amount (which seems to be specific for that agglomerate).

The platen force (loading) was transmitted approximately radially from the impact zone - see the two images in Fig. 6.55 presenting the largest compressive contact forces (i.e. the contacts carrying most of the load) in the dense[1], 0.1785 m/s impact velocity, and dense[2] agglomerate, 0.12 m/s impact velocity, at the moment close to when the platen force peaked. Observe that the load transmission paths were more dense and more clustered around the loaded diameter in the agglomerate having higher contact density.

For both dense agglomerates fracture generally occurred in the first half of the unloading phase, a short while after the platen force attained its maximum. When an agglomerate fractured into more than two large fragments, two-step fracture was usually observed: primary fracture surfaces completed a little while before further secondary fractures. Most of the agglomerate-platen contact damage zone (approximately conical-shaped) was transformed into debris after fracture (by the end of the test), although most bond breakage within it occurred before fracture, usually close to the start of the test.

From the breakage patterns obtained (Figs. 6.10, 6.18a, 6.22b, 6.34 for dense[1] and 6.35, 6.36 for dense[2] agglomerate) it can be inferred that the two agglomerates, as at the start of the test, were weaker along certain internal surfaces. However, the rate of loading seemed to significantly affect the location of the fracture surfaces. Most of the fracture surfaces were created along the impact direction or a little inclined from this direction, roughly starting from the impacted zone.

In all the simulations causing fracture into several large fragments, the debris at the end of the tests was mainly situated within a conical region above the contact area and along the fracture surfaces. A typical image of debris at the end of test is presented in Fig. 6.56 - which provides a front view roughly along the fracture surface showing the location of all the particles in the debris for the dense[1] agglomerate impacted at a velocity of 0.2 m/s.

Having 16% extra interparticle contacts, the dense[2] agglomerate behaved more like a solid brittle sample than the dense[1] agglomerate. The dense[2] agglomerate needed lower input energy to fracture, it was capable of storing more of the input energy internally, it "consumed" less energy in the fracturing process and it fractured at lower nominal strains.

Analysing the evolution of different parameters in all the simulations causing fracture carried out on the dense agglomerates, it can be concluded that higher impact velocities lead to higher platen forces, average normal contact forces, local contact damage, agglomerate nominal straining, quantity of broken bonds, debris and dissipated energy prior to the fracture moment.

6.4.2 Loose Agglomerates Compared To Dense Agglomerates

The main difference between the loose and dense agglomerates in the free-fall impact tests was that the loose agglomerate behaved more ductile - it was much weaker and it could not be fractured. On the other hand, both loose and dense agglomerates appeared to be "stronger" in the higher impact velocity tests - as they developed larger platen forces before failure. In fact, an increase in the impact velocity resulted also in higher (maximum attained) average normal contact forces, debris ratios, damage ratios, agglomerate nominal straining and flattening in all three tested agglomerates.

The behaviour of the three types of agglomerate at the beginning of the tests was very different. In the dense agglomerates the platen force and the amount of stored elastic energy increased sharply and continuously from the very start of the test, whereas debris started to detach only after the platen force reached about 1/6 (in tests causing rebound) - 1/2 (in tests causing shattering) of its maximum attained value. Conversely, the debris ratio usually

increased sharply from the very start of the test in the case of the loose agglomerate. The platen force and the average normal contact force increased more consistently after the debris ratio reached about 1/7 (in the test causing shattering) of its final value. Thus loading effectively started a little later in the tests on the loose agglomerate.

For sufficiently low impact velocities, both dense and loose agglomerates only suffered local damage at the impacted pole. However, dense agglomerates rebounded, whereas the loose agglomerates experienced irreversible flattening and remained on the platen. The differences in behaviour were mainly due to the large differences in contact density: breaking 13 bonds (of which only 9 were close to the contact zone) was sufficient for detaching 7.5% of the loose agglomerate's particles. Note that debris did not detach in the immediate neighbourhood of the agglomerate-platen contact area, as with the dense agglomerates (see Fig. 6.4), but from the surface adjacent to the contact area, Fig. 6.40. Almost all the nominal straining of the agglomerate due to impact, although low, remained as permanent deformation for the loose agglomerate - thus showing its highly ductile-plastic character. In contrast, a large part of the nominal straining in dense agglomerates was found to be reversible after rebound.

Both loose and dense agglomerates shattered for sufficiently high velocities; the minimum velocity to produce shattering in the loose agglomerate was about 4 times lower than in the dense agglomerate. Although the shattering of loose (Fig. 6.50, 6.52 and 6.54) and dense (Fig. 6.34) agglomerates appeared similar, many more bonds needed to be broken in the case of dense agglomerates (see Fig. 6.26 compared with 6.44a). In the case of the dense agglomerate the shattering was preceded by a tendency of the agglomerate to break into many medium-sized elongated fragments. In contrast, the loose agglomerate behaved as an agglomerate that already was heavily damaged inside from the very start of the test (as if it consisted from the beginning of a sum of small clusters held together only by very few bonds). The breakage of a very few bonds was, therefore, sufficient for the detachment of small fragments (debris) in the loose agglomerate.

For both types of agglomerate shattering was a gradual process since the agglomerate was not instantly transformed in debris. For a 4.5 times lower impact velocity, shattering of the loose agglomerate lasted about 4 times longer than that of the dense[1] agglomerate. The behaviour in the first part of test, up to about 1% nominal strain, was different for the two types of agglomerates. Whereas 60% of the bonds broke in the dense-strong agglomerate, only a mere 3% of bonds ruptured in the loose agglomerate. Subsequently, the two types of agglomerates seemed to experience similar processes: continuous bond breakage and debris detachment. Both loose and dense agglomerates became smaller and smaller due to a gradual debris detachment process.

Compared to the dense agglomerates, the loose one exhibited lower forces on the platen and stored much less energy internally. Shattering of the dense agglomerates needed large forces, so that the stored energy was large enough to break bonds all over the agglomerate's volume. In contrast, the shattering of the loose agglomerate was much easier, as bonds broke almost effortless due to the loose space lattice and the much higher freedom-of-movement of each of its constituent particles. In absolute numbers, the loose agglomerate had to break about 3.7 times less bonds for shattering than the dense agglomerates.

For both dense and loose agglomerates, shattering seemed to occur due to extensive volumetric damage (breakage of interparticle contacts). The breakage of contacts started close to the agglomerate-platen interface but spread rapidly throughout the agglomerate. Debris detached as a result of the continuously increasing damage ratio. The agglomerates slowly "eroded" by losing particles from the vicinity of platen first, then from their external surface, until only debris was left. As the volumetric-style damage was continuously advancing through the test, both the size and the internal "strength" of the largest surviving cluster decreased with time.

The fact that, for the same impact velocity of 0.2 m/s, the dense agglomerates attained about 6-7 times larger average normal contact forces (and a 22.5 times larger peak in the platen force) compared to the loose agglomerate indicates that the reason why the loose agglomerate could not fracture was that it could not store a sufficient amount of elastic energy internally. The main cause for the very low levels of elastic stored energy in the tests on the loose agglomerate must have been the low levels of contact density and solid fraction - as the interface energy, friction, particle and agglomerate size were the same as for the dense agglomerates. Firstly, the more sparse space lattice (Fig. 6.1) in the loose agglomerate forced the load to transmit along zig-zag trajectories that deviated more from the direction of loading. This led to particle sliding, displacements and rearrangements inside the agglomerate and a much more efficient dissipation mechanism for the input energy. The image in Fig. 6.57 presents the only the contacts carrying most of the load (the 108 contacts having the largest normal contact force) in the loose agglomerate at t = 388 μs (when the platen force was around its maximum attained value) for a 0.2 m/s impact velocity. It can be observed that the low contact density resulted in the load attempting to transmit along a single path, oriented roughly along the loading direction. In the dense agglomerates, the load transmitted along many paths oriented radially from the point of impact - see Fig. 6.55. Although the load (platen force) in Fig. 6.55 is much larger than the one in Fig. 6.57, comparing the two sets of figures strongly indicates that the load transmission is different for the dense and loose agglomerates, and that this must be a main reason for the large differences in the behaviour of loose and dense agglomerates.

At the beginning of the tests on dense agglomerates bonds broke mainly in the zones adjacent to the platens, where the compressive contact forces were the largest. Figure 6.58 presents a typical example - observe the broken bonds (in black) in the space lattice of the dense[1] agglomerate at the beginning (t = 3 μs) of the test of 0.2 m/s impact velocity. In contrast, bonds in the loose agglomerate did not break only where the compressive contact forces were the largest (see Fig. 6.49). This would mean that the bond breakage mechanism was slightly different than in the dense agglomerates in which bonds by the impacted pole always broke due to the particle displacements around the large contact forces generated by the applied load. For loose agglomerates most bond breakage seemed to have a different correlation with the transmission of load, probably because the maximum contact forces had much lower values. Instead it was the higher degree of freedom of particles (conferred by the lower contact density and solid fraction) that allowed them to displace much easier and thus to cause the breakage of the few bonds still connecting them. Also, the character of the debris formed during tests was different in the loose agglomerate. For the dense agglomerates, the debris detached at the beginning of the test consisted mainly of singlets and doublets - see Fig. 6.59 presenting the particles system at t = 8.9 μs (dense[1] agglomerate, 0.2 m/s impact velocity). In contrast, the debris consisted of slightly larger fragments in the case of the loose agglomerate - see Fig. 6.40.

In general terms, dense agglomerates behaved as a much more rigid and strong system of particles than the loose agglomerate - which could damage much easier, following the breakage of much fewer interparticle contacts.

6.5 COMPARISONS WITH EXPERIMENTAL DATA

Very good agreement was found between the results obtained in the simulations presented above and the laboratory tests reported in the literature. Depending on the impact velocity, dense agglomerates either survived with small local plastic deformations, fractured or shattered, as in laboratory experiments. The loose agglomerate could not be fractured for any of the impact velocities used. The simulation results obtained on dense agglomerates best agree with the results reported by Arbiter et al (1969) for sand-cement agglomerates, Salman et al (1994) for aluminium-oxide spheres and Santurbano and Fairhurst (1991) for limestone pellets.

6.5.1 Failure Initiation

As in most of the laboratory tests reported in Chapter 4, failure of dense agglomerates was initiated from the agglomerate-platen interface within a conical zone. Very shortly after the moment of impact, this zone started to deform inelastically: interparticle bonds started to

break there (Fig. 6.58) and the material in the cone was then compacted (through local re-arrangement of the particles). Later on, a few particles started to detach from the damaged region (Fig. 6.59) to form debris. The debris was actually detached from the surface of agglomerate in the immediate vicinity of the agglomerate-platen interface. Within the conical contact zone, bonds appeared to break at random, without following any pattern which could be clearly identified as a potential fracture surface. The location of the subsequently formed fracture surface could not be identified at this stage. The initial breakage of bonds in the simulated tests can be compared with the randomly distributed microcrack formation in the contact zone observed in indentation tests on alumina samples of similar grain size, Lawn et al (1994) and Guiberteau et al (1994). As in almost all the reported laboratory test results, the approximately conical damage zone was created due to the high local stresses. However, the simulations show that, for agglomerates, the damage zone coincides with the zone where the compressive interparticle contact forces are largest, demonstrating that the transmission of load is a determining factor in the formation of the cone.

Many workers have shown that fracture is initiated due to the conical zone's wedge-like action. The results of the dense agglomerate impacts indicate that although the cone-like damage zone plays the major role in failure, internal shear stresses cannot be solely responsible for the fracture of agglomerates. Arbiter et al (1969) argued that the hoop tensile stresses developed due to the tendency of pushing the cone into agglomerate appeared to have been the driving force for fracture in their free-fall impact tests. Chaudhri (1985) reported that, for impact tests on glass and sapphire spheres, fracture initiated at the pole opposite to the impacted area. In the free-fall impact simulations performed in this project, the fracture surface opened from the pole opposite to the impact zone.

As in many reported laboratory tests, a roughly-conical damage zone was observed adjacent to the platen in the dense agglomerates which fractured, see Fig. 6.58a. Being heavily stressed, the damage zone consisted mainly of debris at the end of the test (Fig. 6.56). The same observations, at the end of laboratory tests on limestone pellets which resulted in fracture, were made by Santurbano and Fairhurst (1991).

6.5.2 Fracture Patterns

For the dense agglomerates fracture into large fragments occurred at the start of unloading. For low impact velocities, the large fragments were accompanied only by debris; for slightly higher velocities medium-sized fragments were also formed. The range of impact velocities over which dense agglomerates fractured into two or three fragments and debris was relatively narrow. (The approximate range was 0.14 - 0.21 m/s for the dense[1] agglomerate, and even narrower for the dense agglomerate with the higher contact density: 0.12 - 0.13 m/s). The range of impact velocities for fracture in two or three large fragments

would appear to be wider in most laboratory experiments. The narrow band could, again, be due to the coarse-grained nature of the agglomerates simulated.

For velocities causing fracture into more than two large fragments, primary fracture into two large fragments occurred before secondary fractures produced more fragments. Salman et al (1994) also suggested that fracture first produces two near-hemispherical fragments which may then be further fragmented by the end of the test. The number of fragments obtained from dense agglomerates increased with increase in impact velocity. This was also observed in laboratory tests by Arbiter et al (1969) and Salman et al (1994).

The fracture patterns obtained from simulations of dense agglomerate impacts shown in Figs. 6.8, 6.10, 6.18, 6.23, 6.34, , 6.35 and 6.36 are very similar to the fracture patterns reported or described from experimental tests, as shown diagramatically in Fig. 6.60. Actual photographs of fractured agglomerates are presented in Fig. 6.61. It can be noted that the schematic figures reported for laboratory tests only roughly describe the real shape of the fragments obtained (compare, for example, Fig. 6.60a with Fig. 6.61b, or Fig. 6.60b with Figs. 6.61d, or Fig. 6.60d with Figs. 6.61c). The exact patterns illustrated in Fig. 6.60d,e,f were not obtained in the simulations performed in this project. It is possible that they could have been obtained if the point of impact on the dense agglomerate was changed. On the other hand, it might be the coarseness of the simulated agglomerates that prevented these types of fracture from occurring.

Most fracture surfaces that separated the large fragments were roughly meridional planes parallel to the impact direction (Fig. 6.8a, 6.10, 6.23 and 6.36), as were the fracture surfaces described by most experimentalists (Fig. 6.60g). Oblique fracture planes, as described in Arbiter et al's (1969) paper (Fig. 6.60h), were also obtained for dense agglomerates - see Fig. 6.18 and 6.23. The roughly conical-shaped fragment detached at the pole opposite the point of impact described by Gildemeister and Schönert (1976) and Santurbano and Fairhurst (1991) (see Fig. 6.60i) was also observed in the impact test of the very-dense agglomerates (Fig. 6.36b,c). For impact velocities greater than 0.9 m/s agglomerate shattering occurred in a manner similar to experimental reports of shattering.

Santurbano and Fairhurst (1991) recorded the evolution of the platen force during an impact. The example provided in their paper, see Fig. 6.62, is very similar to the platen force evolution obtained for the dense agglomerate impacted at 0.2 m/s (Fig. 6.13) and 0.1785 m/s (Fig. 6.20).

PROPERTY	Agglomerate type		
	dense[1]	dense[2]	loose
mean agglomerate diameter (mm)	1.113	1.046	1.170
average particle diameter (μm)	58.54	54.95	54.95
solid fraction Φ	.6530	.6525	.4364
number of initial bonds	9758	11293	4009
apparent coordination number Z_a	4.879	5.647	2.004
mechanical coordination number Z_m	4.927	5.647	2.590

Table 6.1 Structural characteristics of the agglomerates used

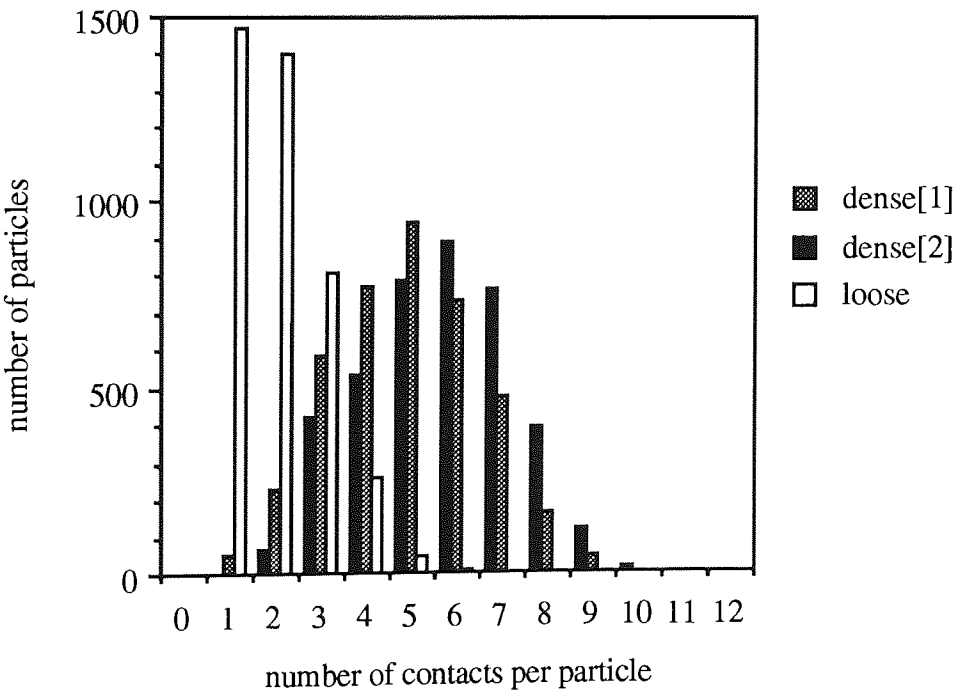

Fig. 6.3 Number of contacts per particle for each of the three types of agglomerate

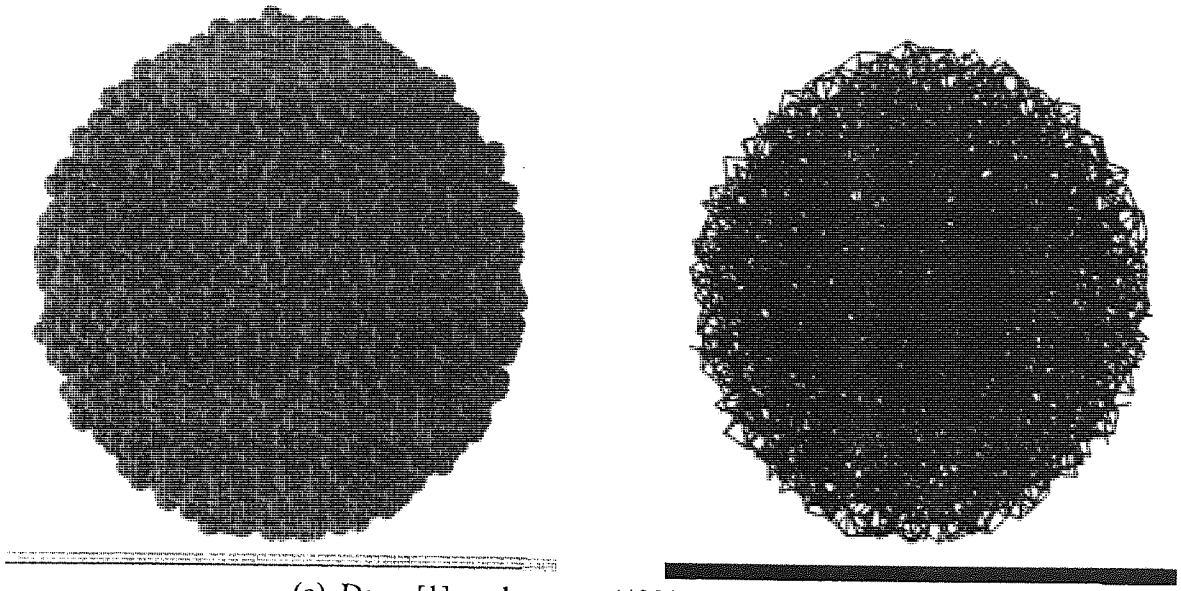

(a) Dense[1] agglomerate (4000 particles, 9758 bonds)

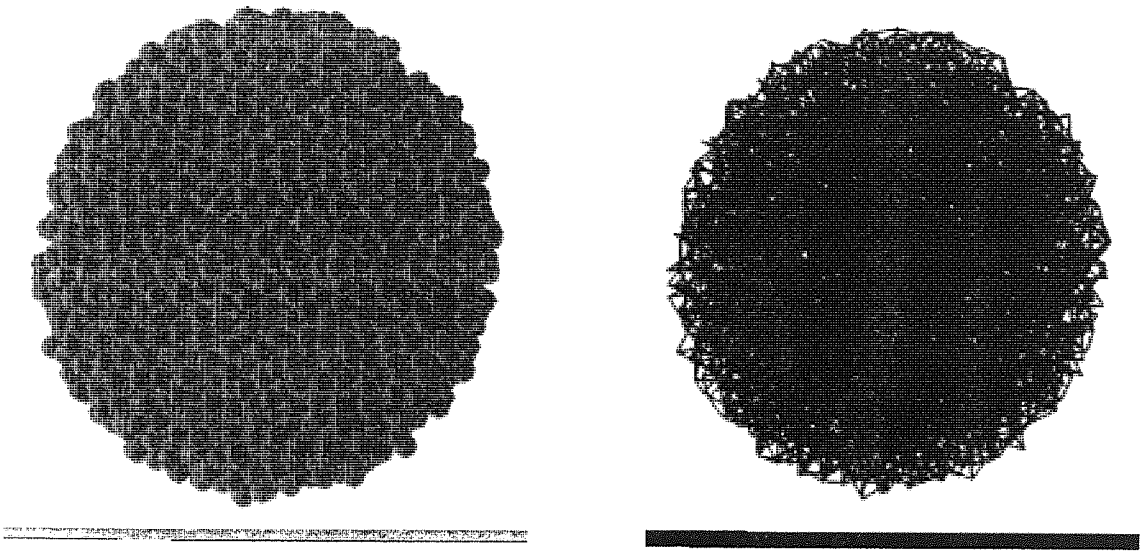

(b) Dense[2] agglomerate (4000 particles, 11293 bonds)

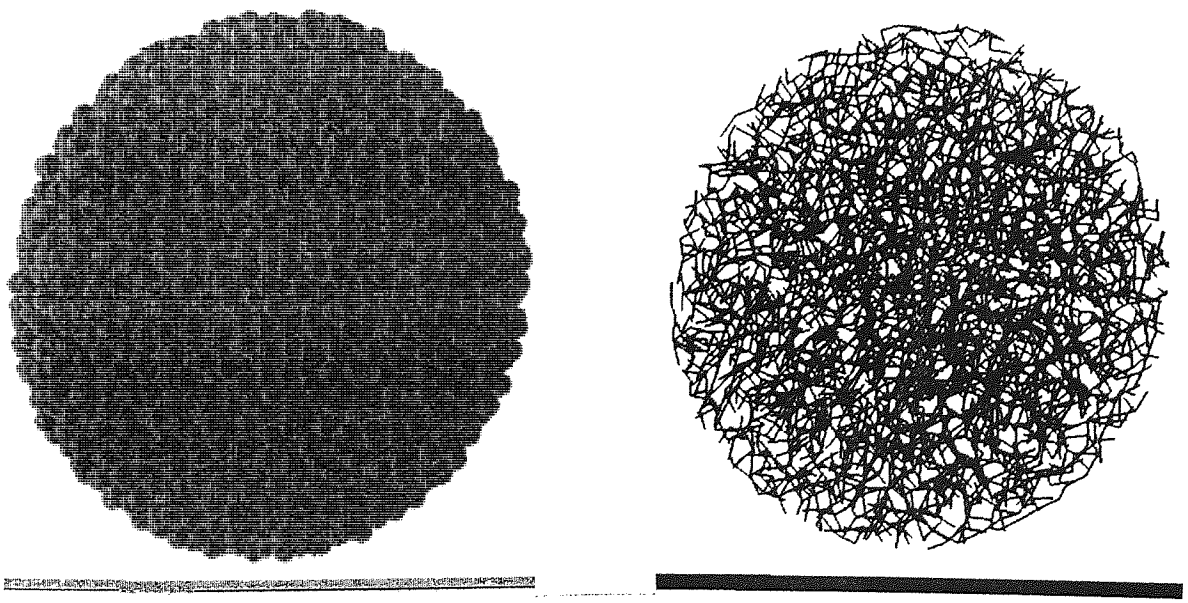

(c) Loose agglomerate (4000 particles, 4009 bonds)

Fig. 6.1 The three agglomerates prior to impact - particle system and equivalent space lattice (in views from side-right, $\Gamma = 2$ J/m^2)

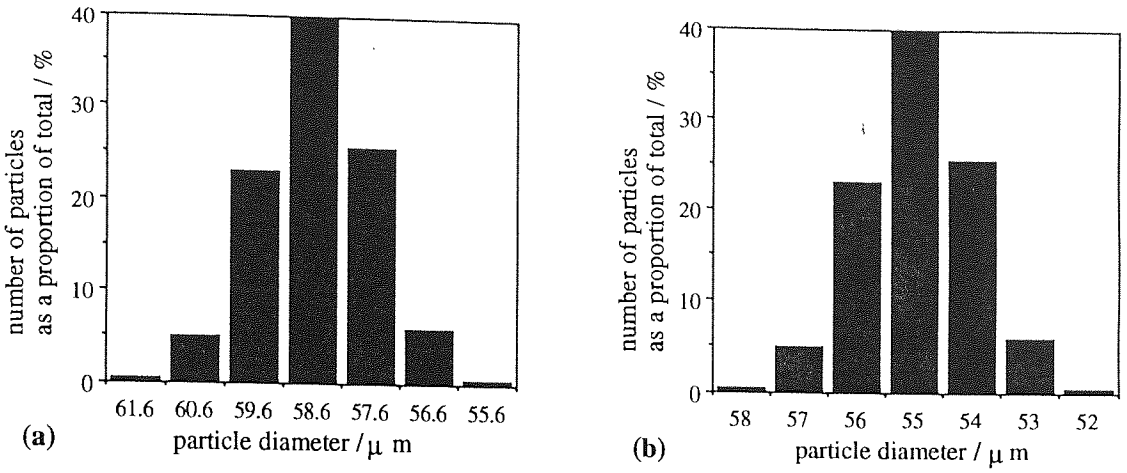

Fig. 6.2 Particle size distributions for:
(a) dense[1] agglomerate
(b) dense[2] agglomerate and loose agglomerate

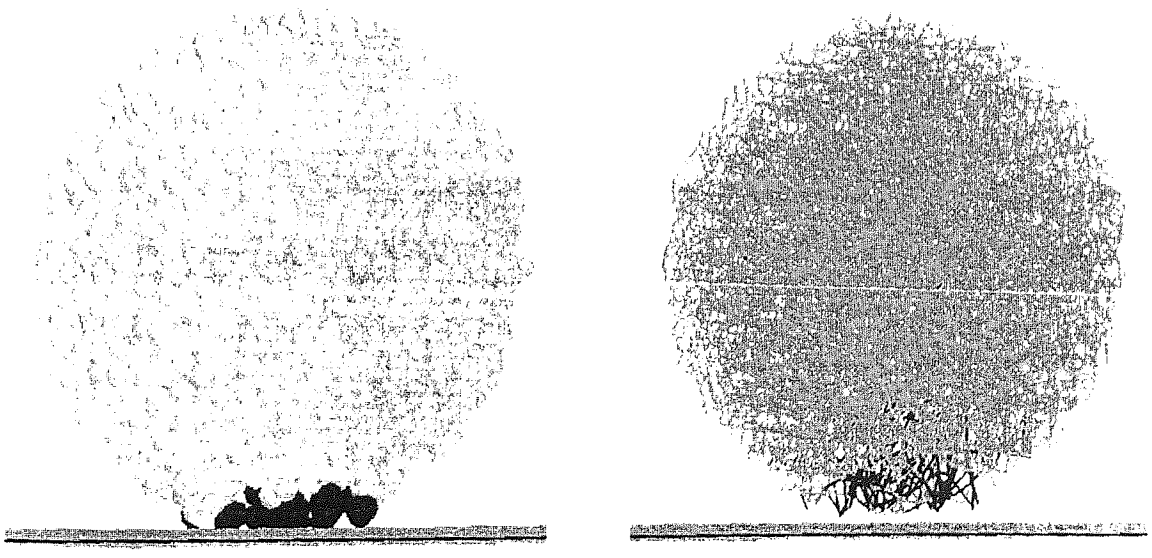

(a) particle configuration (surviving cluster particles shown in grey, particles detached from main cluster shown in black)

(b) equivalent space lattice (existing bonds shown in grey, broken bonds shown in black)

Fig. 6.4 Damage and debris produced by impacting the dense[1] agglomerate at a velocity of 0.1 m/s (views from front, $\Gamma = 2$ J/m^2)

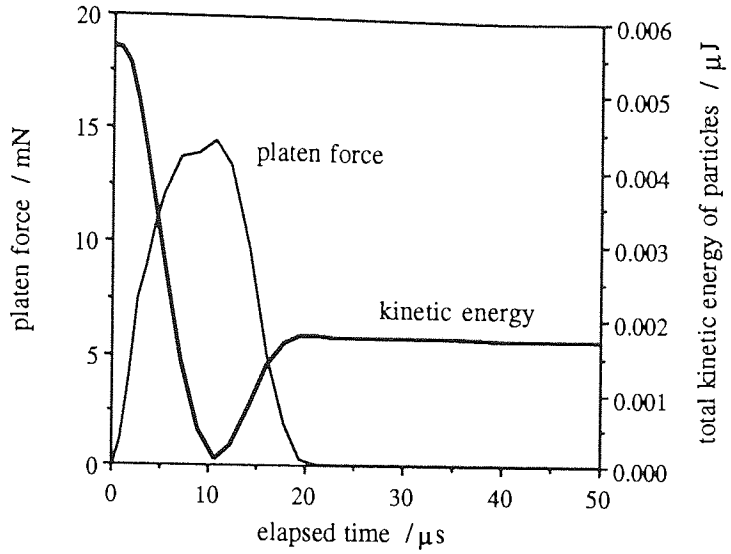

Fig. 6.5 Evolution of force on platen and kinetic energy, dense[1] agglomerate (Γ=2 J/m ^{2}, V=0.1m/s)

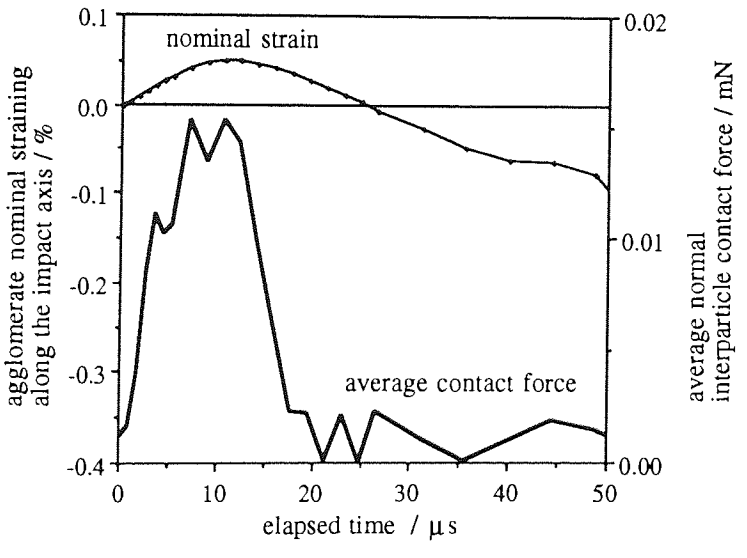

Fig. 6.6 Evolution of average normal contact force and of agglomerate nominal strain, dense[1] agglomerate (Γ=2 J/m^2, V=0.1 m/s)

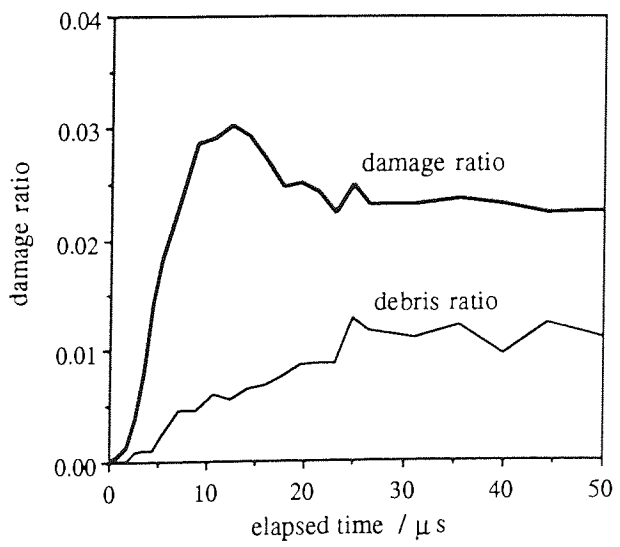

Fig. 6.7 Evolution of damage ratio and debris ratio, dense[1] agglomerate (Γ=2 J/m ^{2}, V=0.1 m/s)

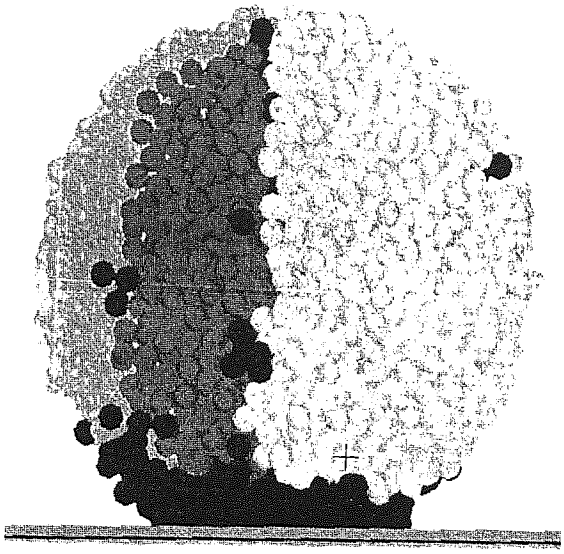

(a) view from front

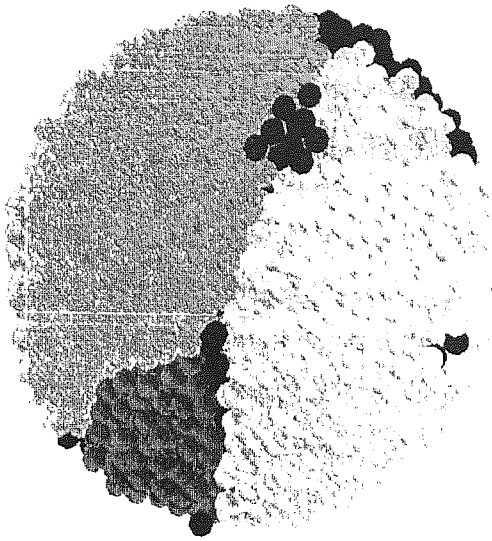

(b) view from above

Fig. 6.8 Dense[1] agglomerate (the particle system) at the end of the simulation showing the large fragments in 3 different shades of grey (lighter for larger fragments) and debris in black, t = 311 μs, dense[1] agglomerate (Γ = 2 J/m^2, V = 0.2 m/s)

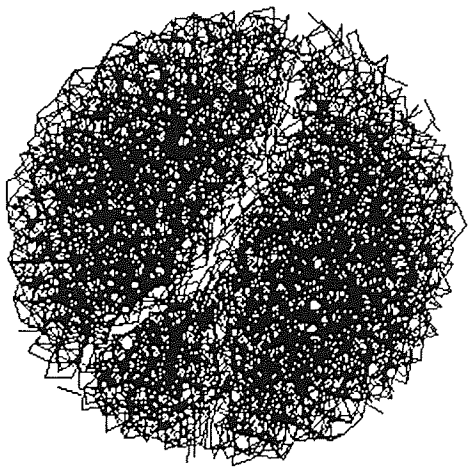

Fig. 6.9 Space lattice at the end of the test, viewed from above, showing only existing bonds, dense[1] agglomerate (Γ = 2 J/m^2, V = 0.2 m/s)

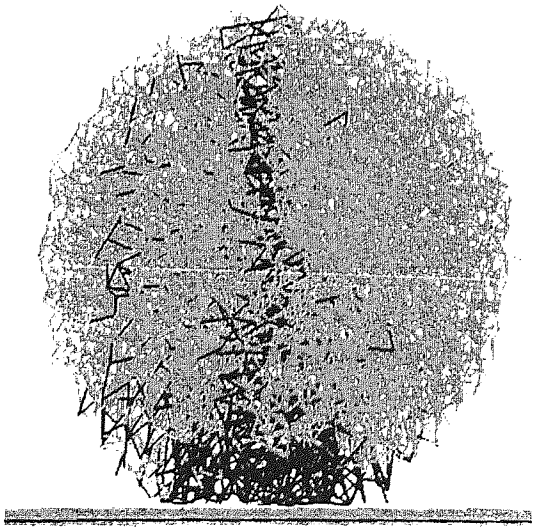

Fig. 6.10 Space lattice at the end of the test, viewed from front, showing existing bonds (grey) and broken bonds (black), dense [1] agglomerate (Γ = 2 J/m^2, V = 0.2 m/s)

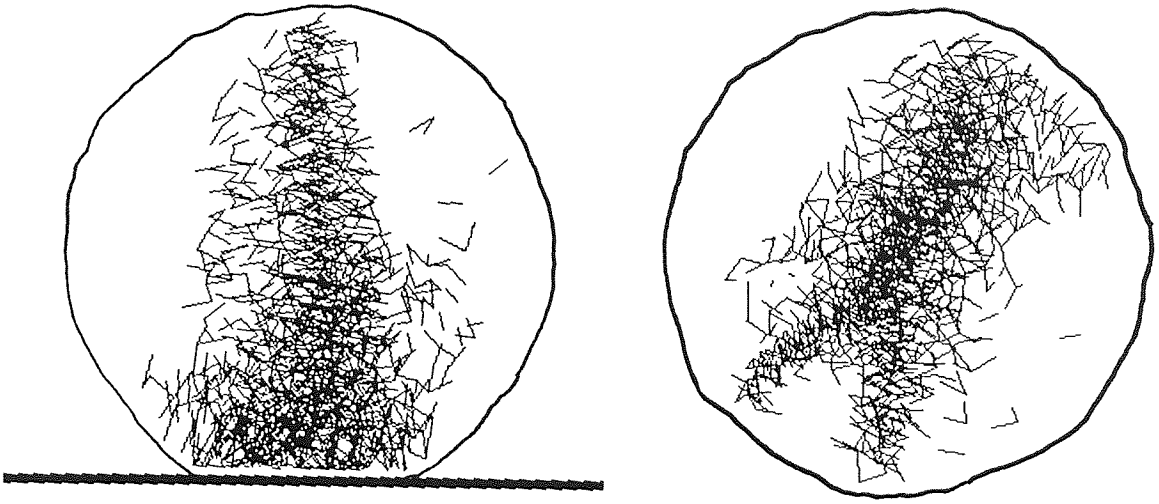

(a) view from front, roughly along the fracture surface

(b) view from above

Fig. 6.11 Space lattice at the end of the test showing broken bonds only, dense[1] agglomerate ($\Gamma = 2$ J/m^2, V = 0.2 m/s)

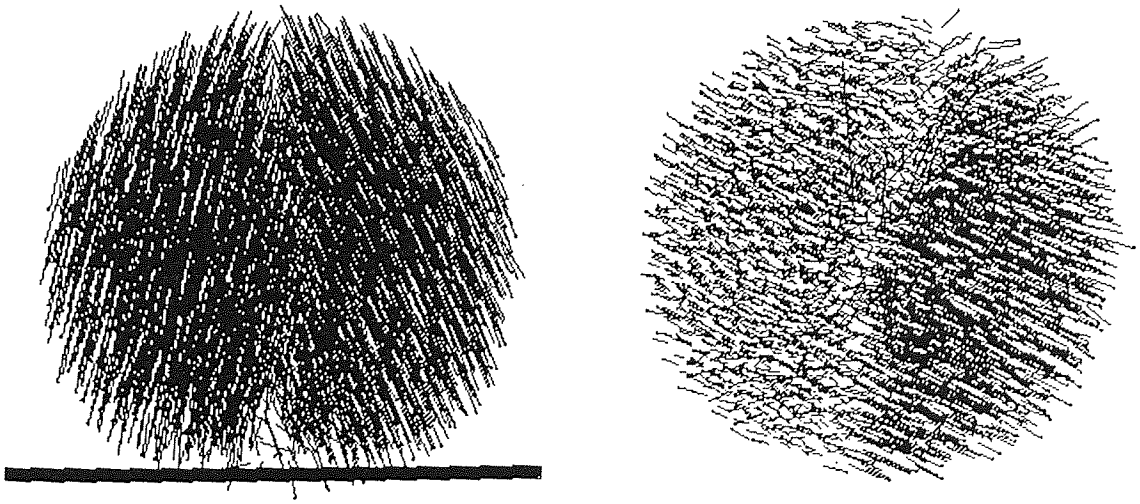

(a) view from front, approximately along the (primary) fracture surface

(b) view from above

Fig. 6.12 Particle velocity field (not showing debris) just after primary fracture, t = 13.3 μs, dense[1] agglomerate ($\Gamma = 2$ J/m^2, V = 0.2 m/s)

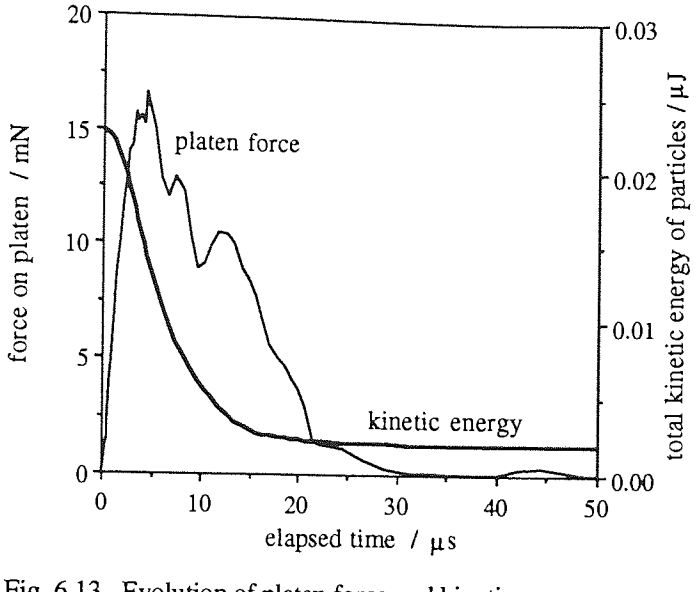

Fig. 6.13 Evolution of platen force and kinetic energy, dense[1] agglomerate (Γ=2 J/m^2, V=0.2 m/s)

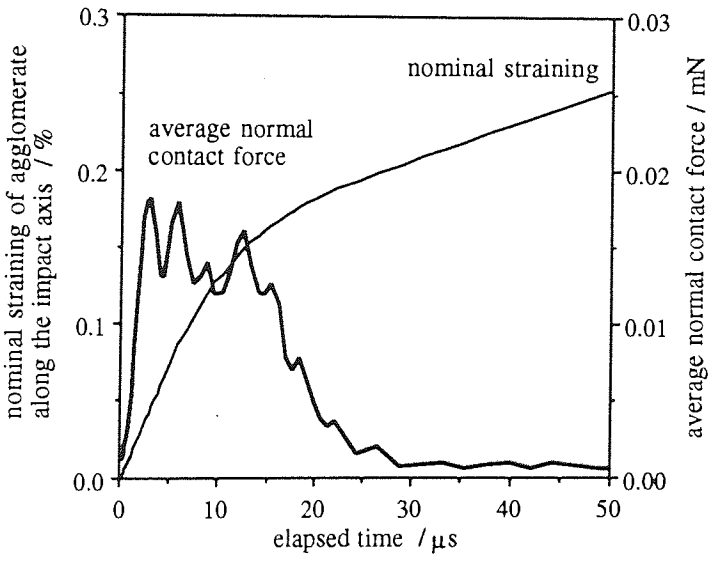

Fig. 6.14 Evolution of average normal contact force and of agglomerate nominal strain, dense[1] agglomerate (Γ=2 J/m^2, V=0.2 m/s)

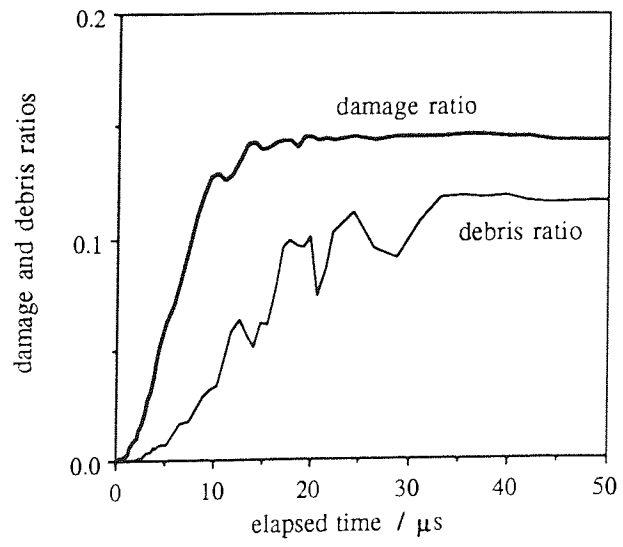

Fig. 6.15 Evolution of damage ratio and debris ratio, dense[1] agglomerate (Γ=2 J/m^2, V=0.2 m/s)

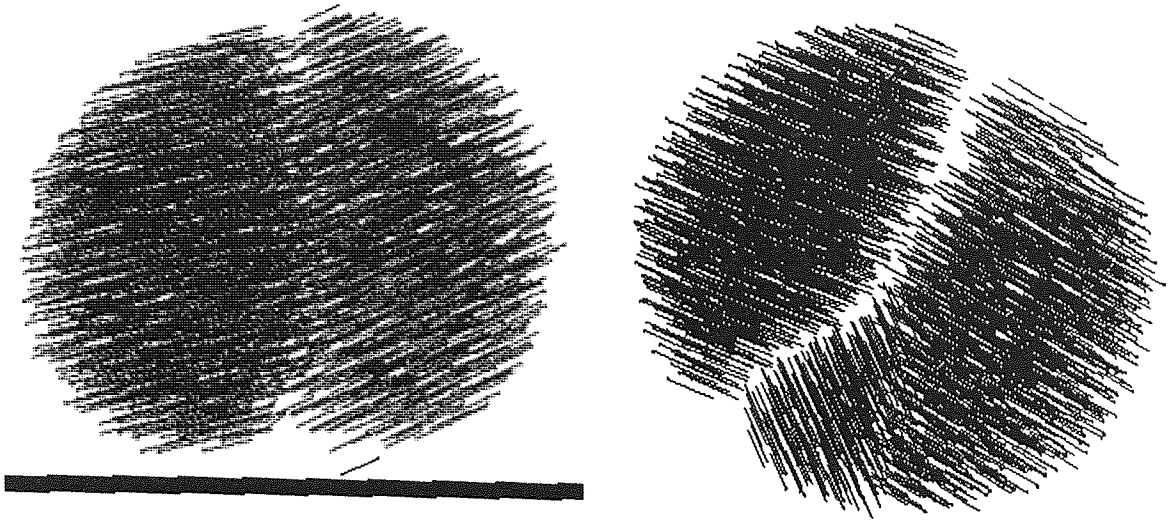

(a) view from front, roughly along the fracture surface

(b) view from above

Fig. 6.16 Particle velocity field at the end of the test (not showing debris), t = 311 μs, dense [1] agglomerate (Γ = 2 J/m^2, V = 0.2 m/s)

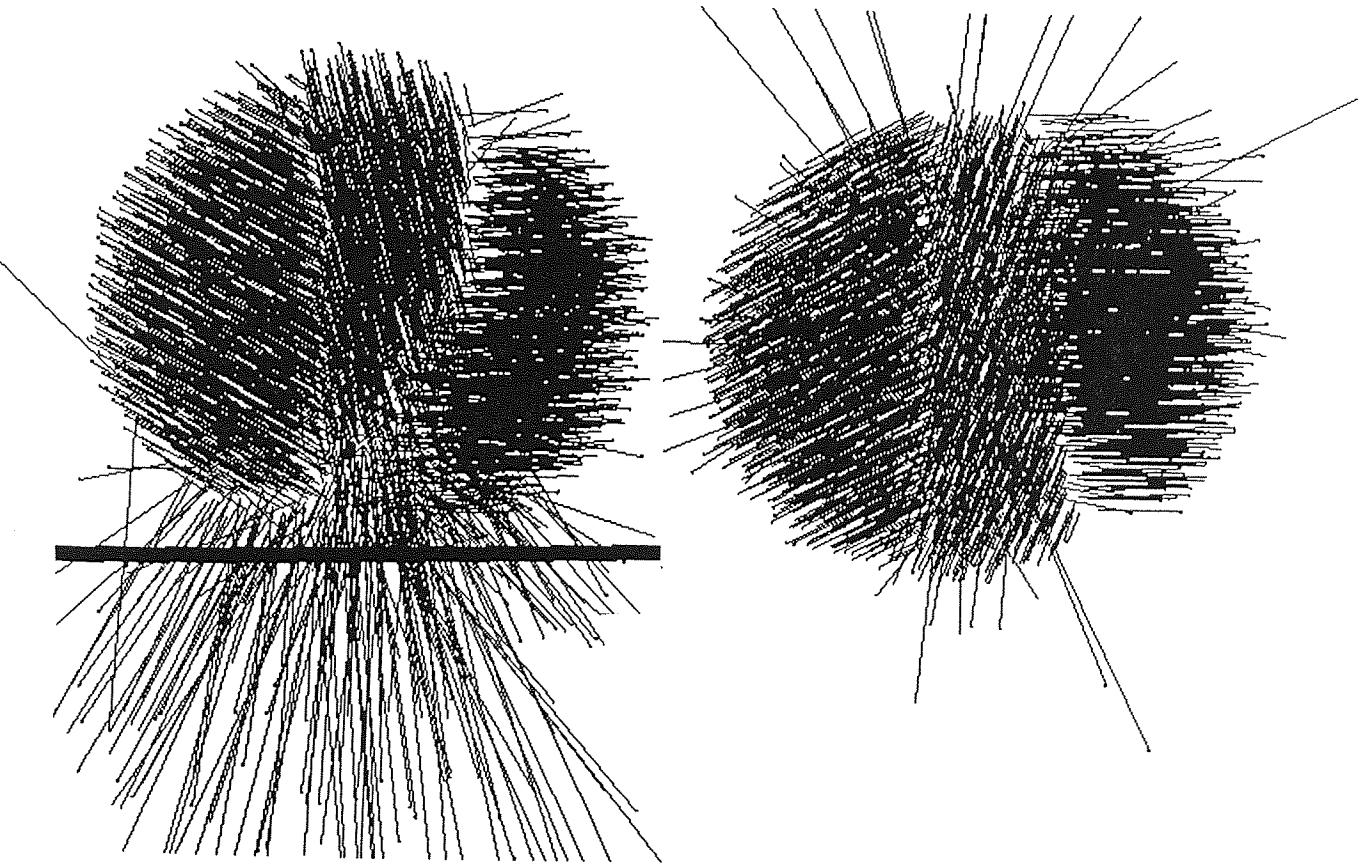

(a) view from front, roughly along the fracture surface

(b) view from above

Fig. 6.17 Particle velocity field (complete - also showing debris) at the end of the test, t = 74 μs, dense[1] agglomerate (Γ = 2 J/m^2, V = 0.1785 m/s)

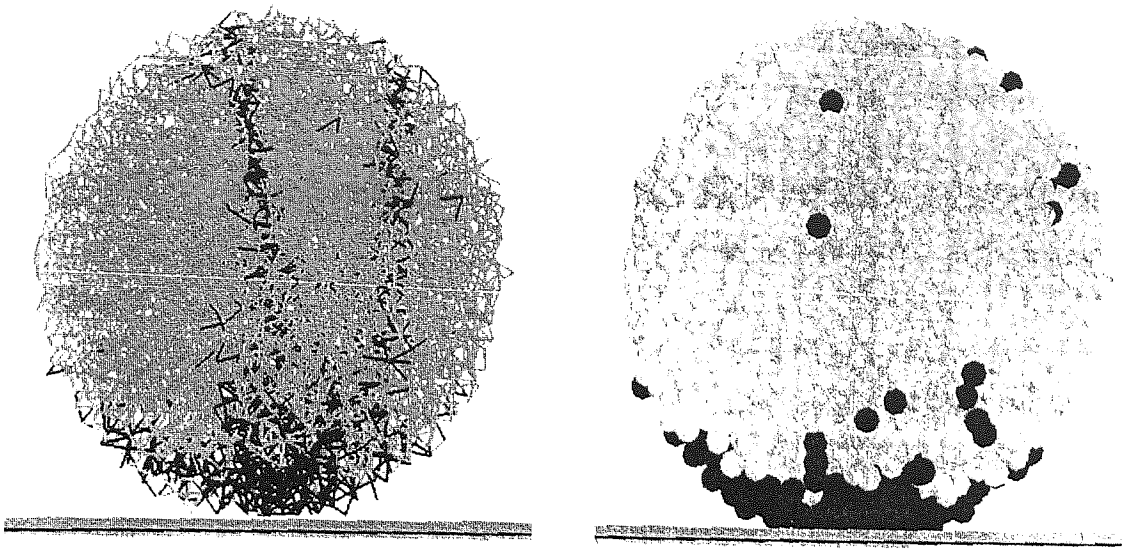

(a) space lattice showing existing bonds (grey) and broken bonds (black)

(b) particle configuration/system showing debris particles in black and the particles in the large surviving fragments in grey

Fig. 6.18 Damage and debris produced by the end of the test, t = 74 μs, dense[1] agglomerate (views from front, $\Gamma = 2$ J/m^2, V = 0.1785 m/s)

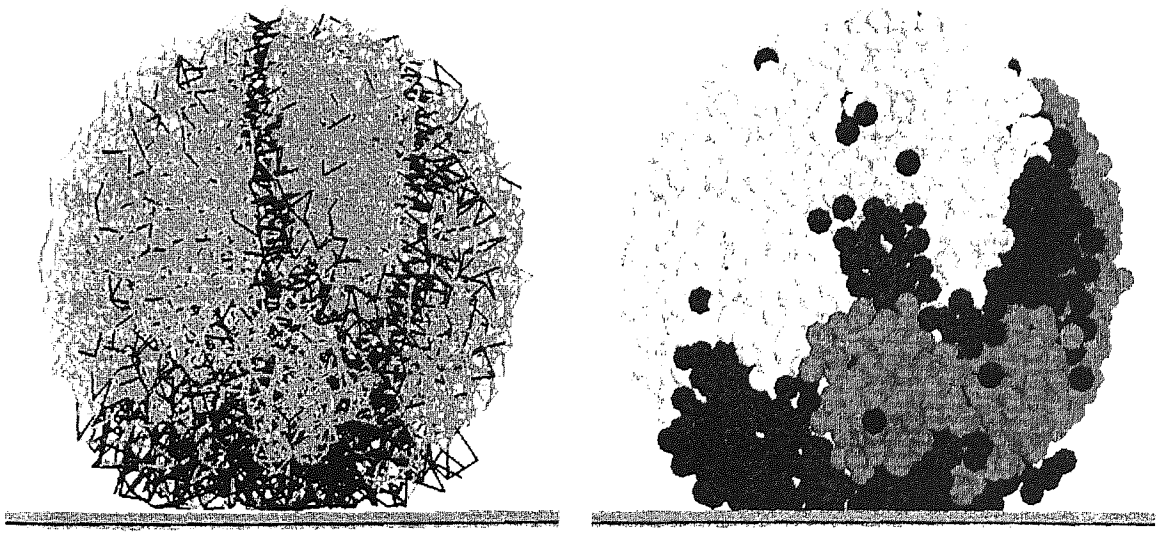

(a) space lattice showing existing bonds (grey) and broken bonds (black)

(b) particle system/configuration showing debris particles in black and the particles in the large surviving fragments in grey

Fig. 6.22 Damage and debris produced by the end of the test, t = 311 μs, dense[1] agglomerate (views from front, $\Gamma = 2$ J/m^2, V = 0.3 m/s)

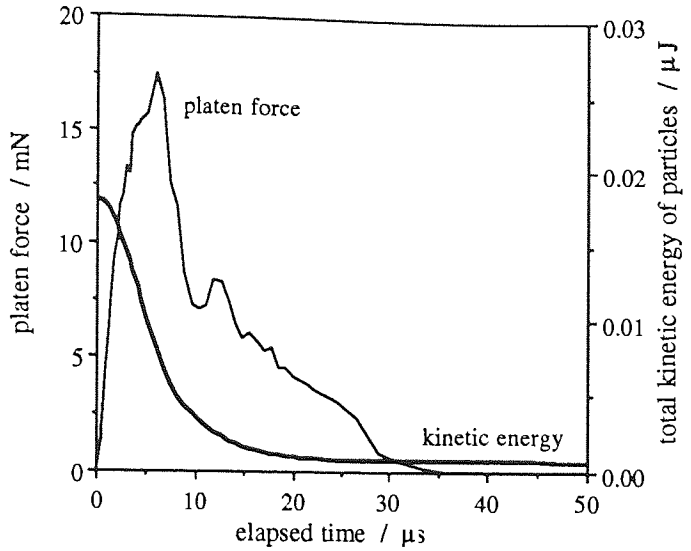

Fig. 6.19 Evolution of platen force and kinetic energy, dense[1] agglomerate (Γ=2 J/m^2, V=0.1785 m/s)

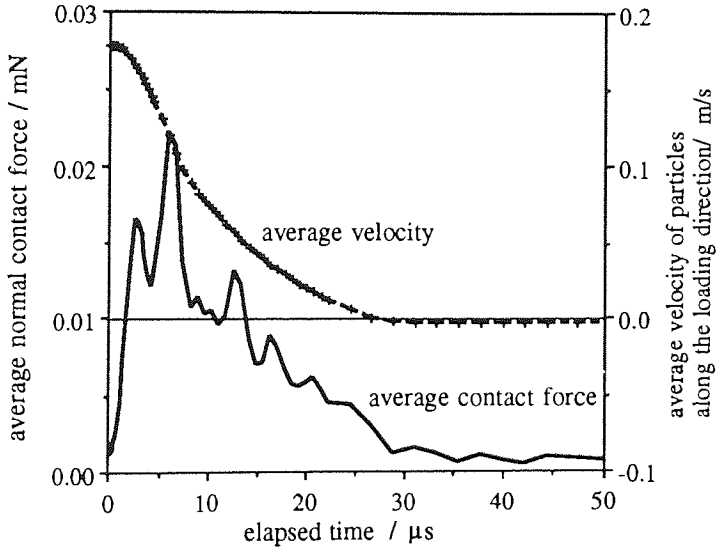

Fig. 6.20 Evolution of average normal contact force and average velocity of particles, dense[1] agglomerate (Γ =2 J/m^2, V=0.1785 m/s)

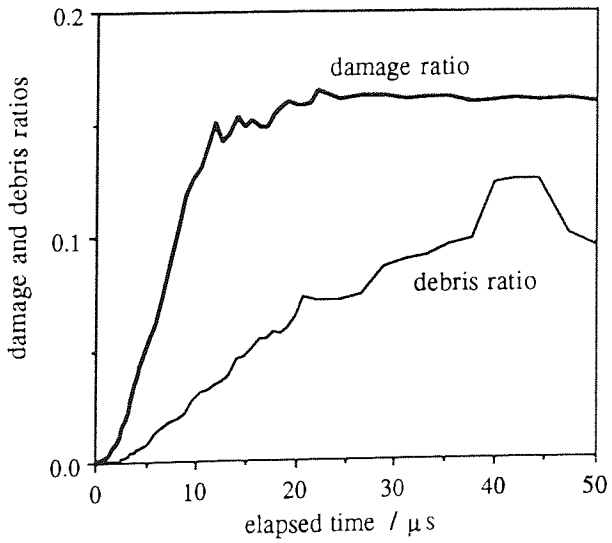

Fig. 6.21 Evolution of damage ratio and debris ratio, dense[1] agglomerate (Γ =2 J/m^2, V=0.1785 m/s)

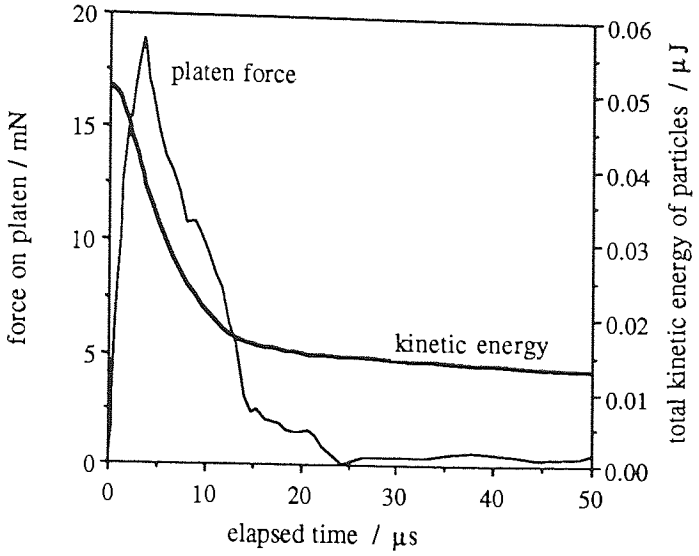

Fig. 6.23 Evolution of platen force and kinetic energy, dense[1] agglomerate (Γ =2 J/m^2, V=0.3 m/s)

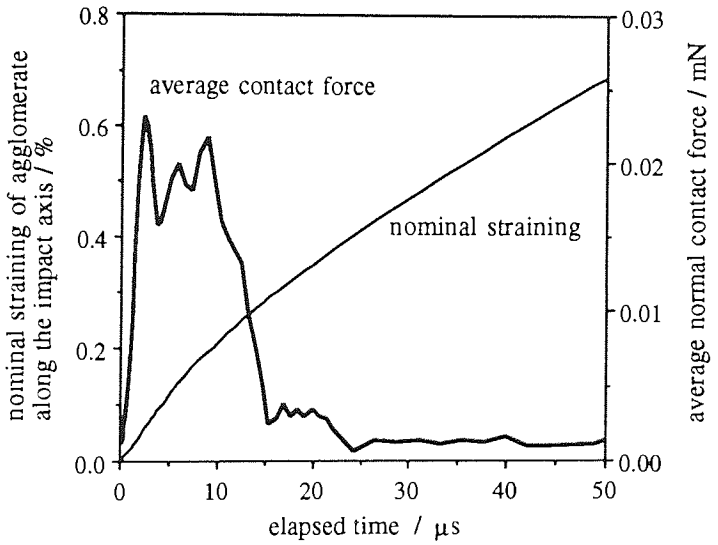

Fig. 6.24 Evolution of average normal contact force and of agglomerate nominal strain, dense[1] agglomerate (Γ =2 J/m^2, V=0.3 m/s)

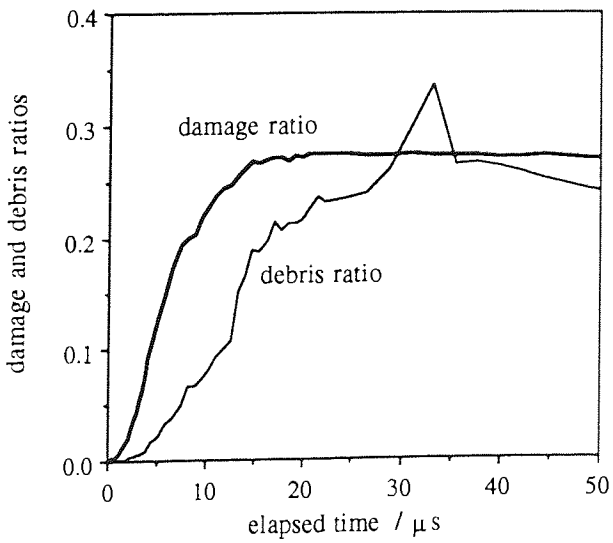

Fig. 6.25 Evolution of damage ratio and debris ratio, dense[1] agglomerate (Γ =2 J/m^2, V=0.3 m/s)

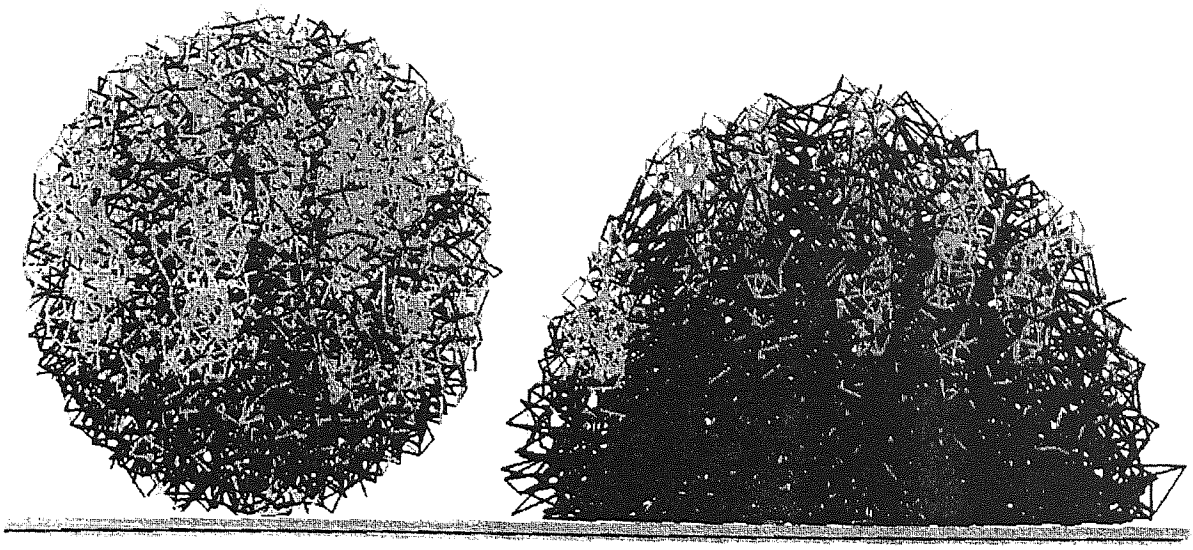

Fig. 6.26 Space lattice viewed from front, showing existing bonds (grey) and broken bonds (black), at t = 9 μs (after the platen force dropped, 4497 existing and 5261 broken bonds), dense[1] agglomerate (Γ = 2 J/m^2, V = 0.9 m/s)

Fig. 6.27 Space lattice viewed from front, showing existing bonds (grey) and broken bonds (black), at t = 512 μs (the end of the test, 1761 existing and 7997 broken bonds), dense[1] agglomerate (Γ = 2 J/m^2, V = 0.9 m/s)

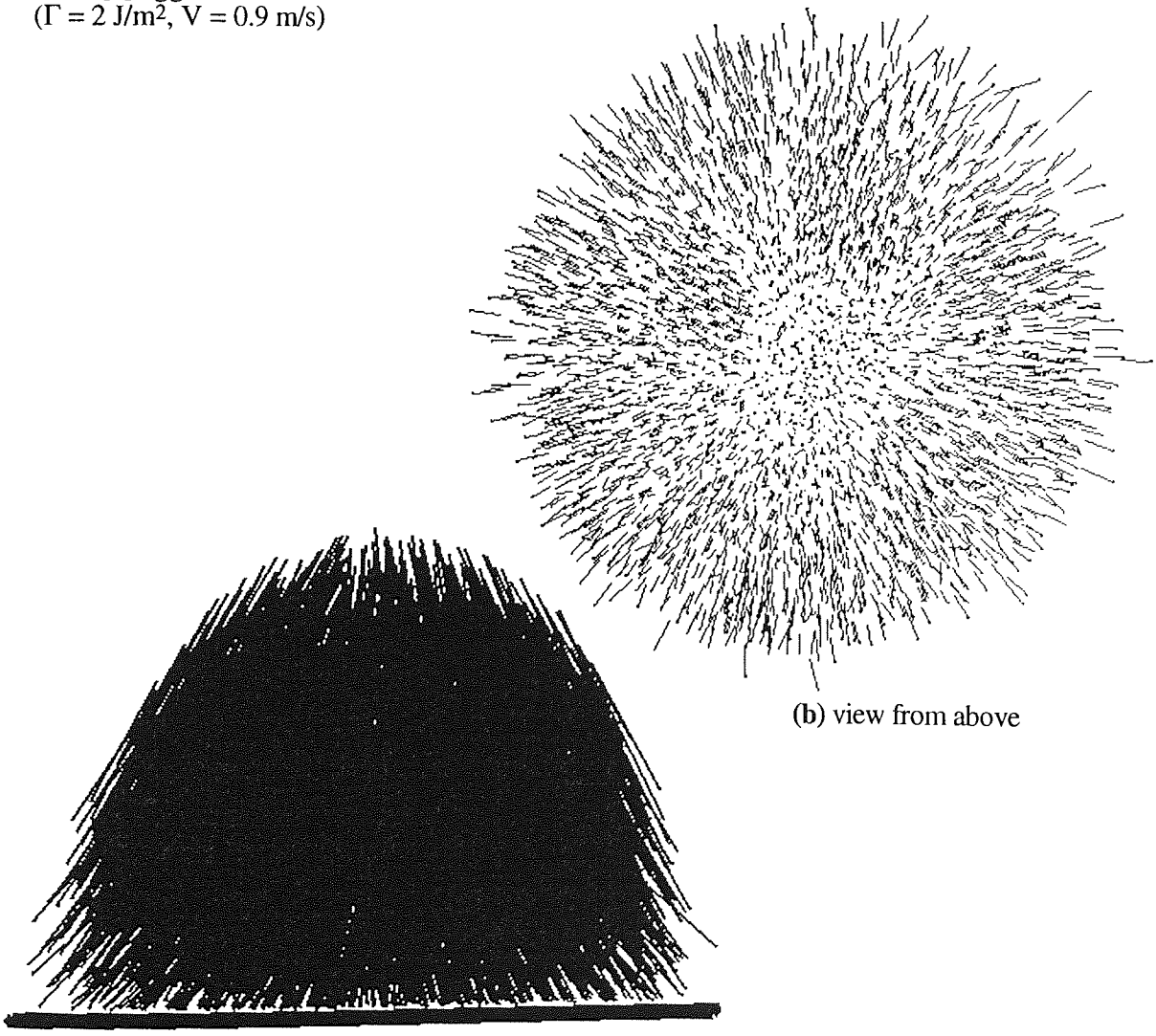

(**a**) view from front

(**b**) view from above

Fig. 6.28 Particle velocity field at the end of the test, t = 512 μs, dense[1] agglomerate (Γ = 2 J/m^2, V = 0.9 m/s)

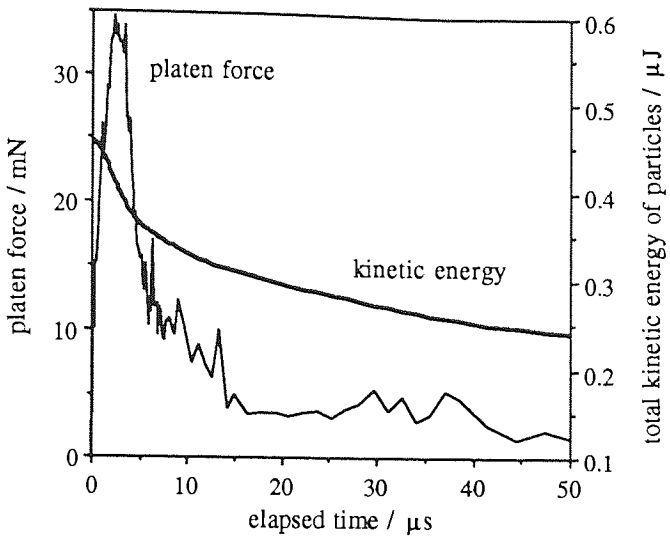

Fig. 6.29 Evolution of platen force and kinetic energy, dense[1] agglomerate (Γ=2 J/m^2, V=0.9 m/s)

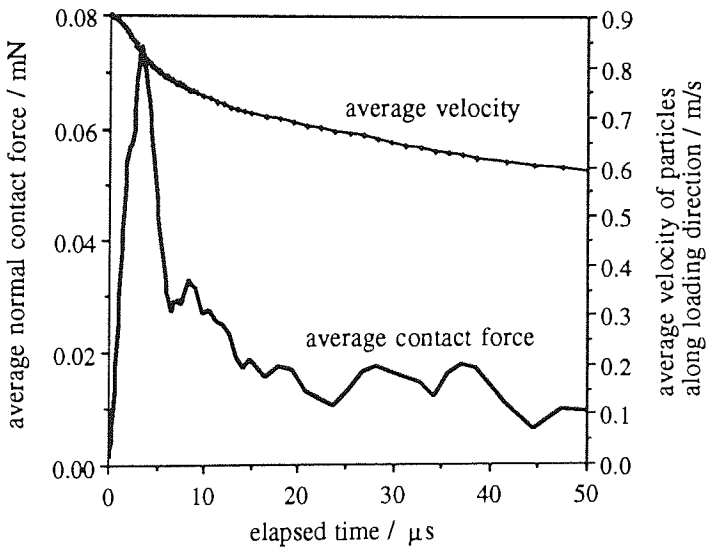

Fig. 6.30 Evolution of average normal contact force and average velocity of particles, dense[1] agglomerate (Γ=2 J/m^2, V=0.9 m/s)

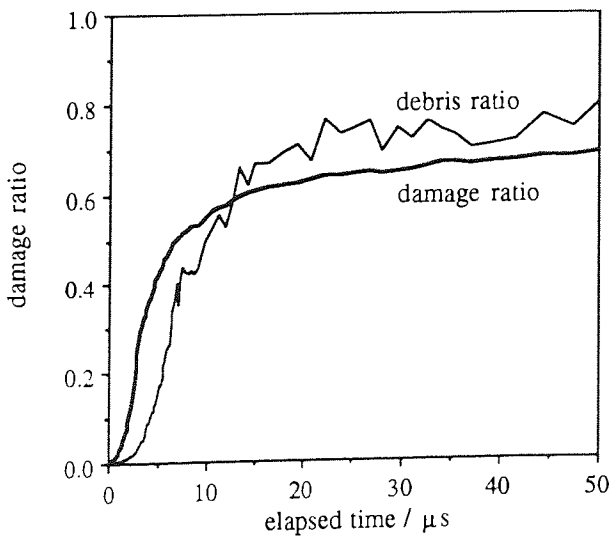

Fig. 6.31 Evolution of damage ratio and debris ratio, dense[1] agglomerate (Γ=2 J/m^2, V=0.9 m/s)

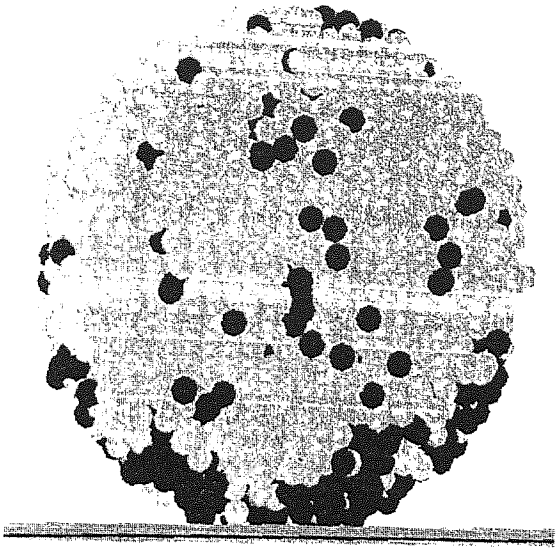

(a) t = 4.6 μs (the beginning of unloading), 286 particles are singlets

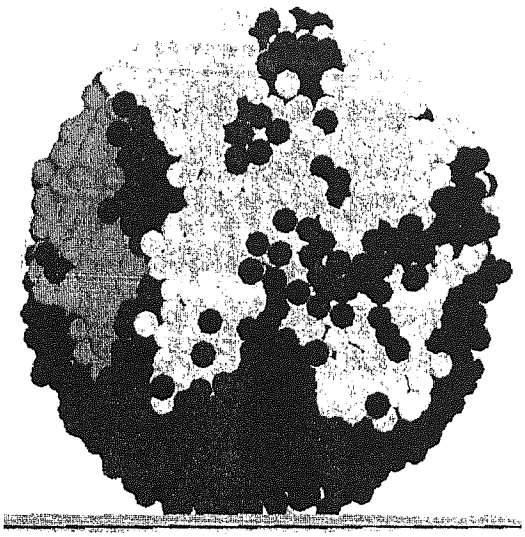

(b) t = 9 μs (after the platen force dropped), 656 particles are singlets

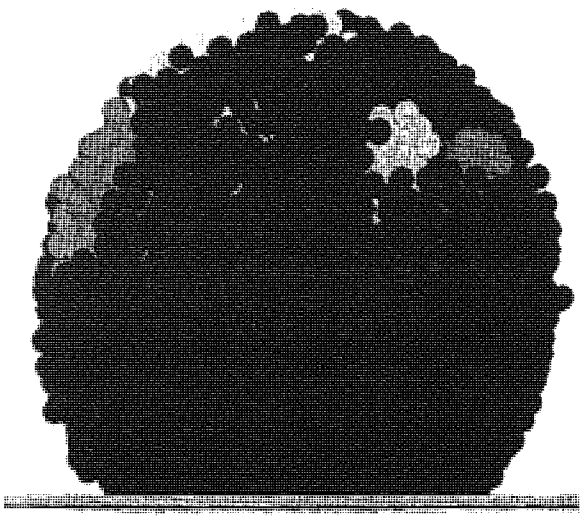

(c) t = 157 μs, 1763 particles are singlets

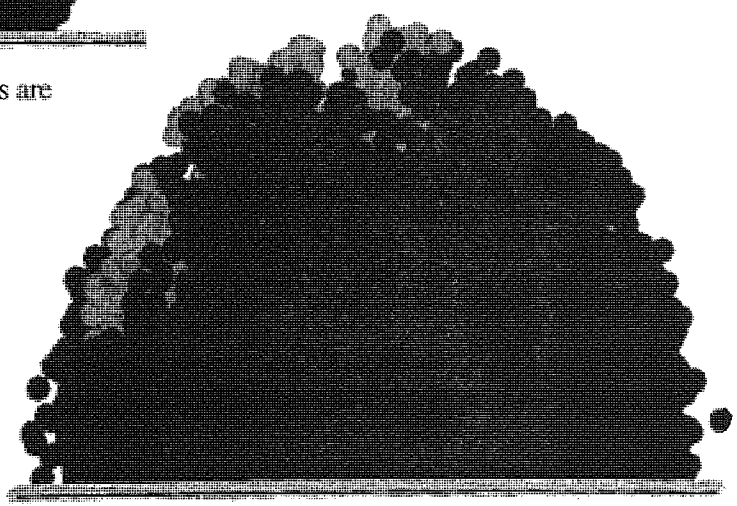

(d) t = 512 μs (the end of the test), 2351 particles are singlets

Fig. 6.32 Particle configuration/system showing debris particles in black and the particles in the large surviving clusters in shades of grey (the lightest shade of grey indicates the largest surviving cluster), dense[1] agglomerate (views from front, $\Gamma = 2$ J/m^2, V = 0.9 m/s)

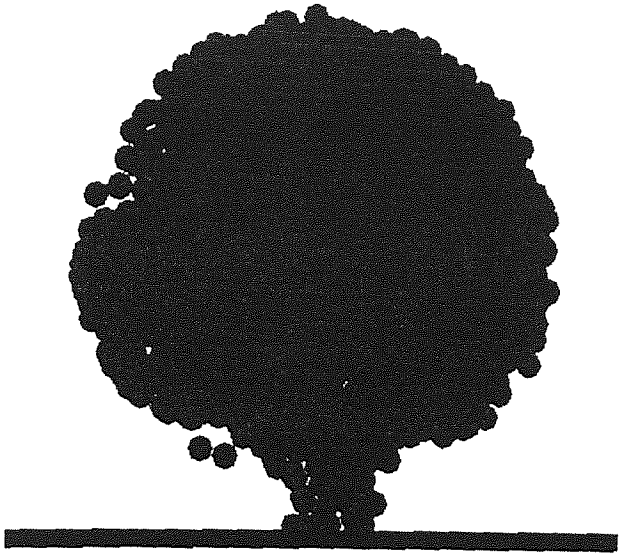

(a) t = 9 μs (after the platen force dropped), the cluster is in black and has 2272 particles

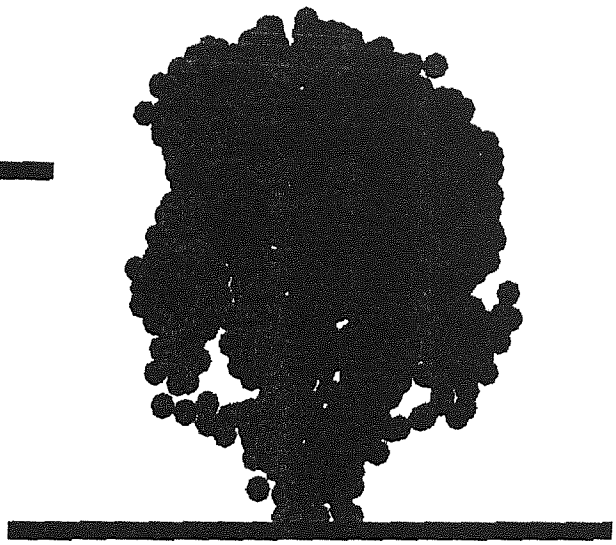

(b) t = 14.9 μs (when the debris ratio slowed down from increasing), the cluster is in black and has 1326 particles

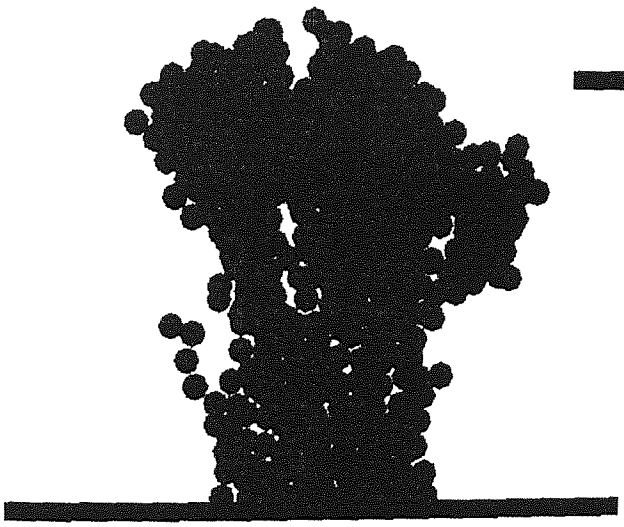

(c) t = 157 μs, the cluster is in black and has 771 particles

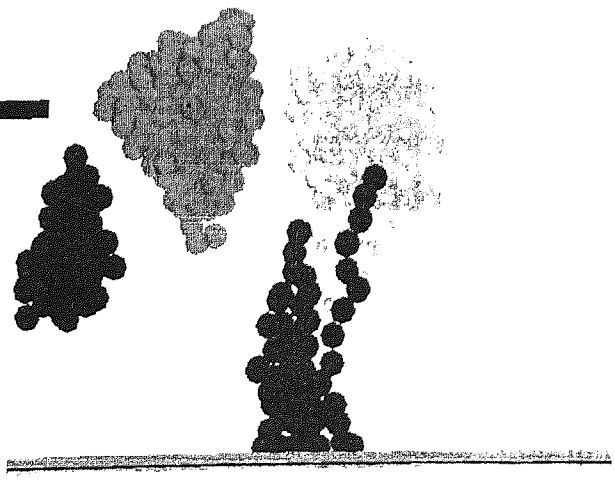

(d) t = 512 μs (the end of the test), the largest cluster is in lightest grey and has 155 particles, whereas the other three larger clusters (represented in darker shades of grey) had 150, 55 and 54 particles respectively

Fig. 6.33 Evolution of the largest surviving cluster during the test, dense[1] agglomerate (views from front, $\Gamma = 2$ J/m^2, V = 0.9 m/s)

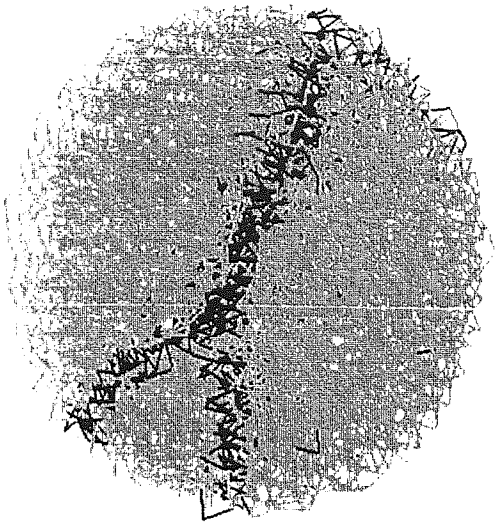

(a) impact velocity V = 0.2 m/s

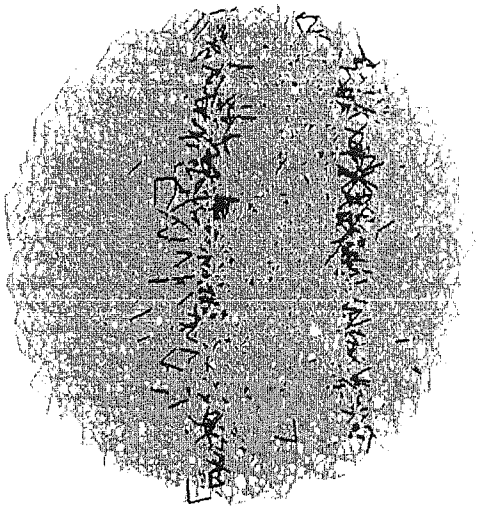

(b) impact velocity V = 0.1785 m/s

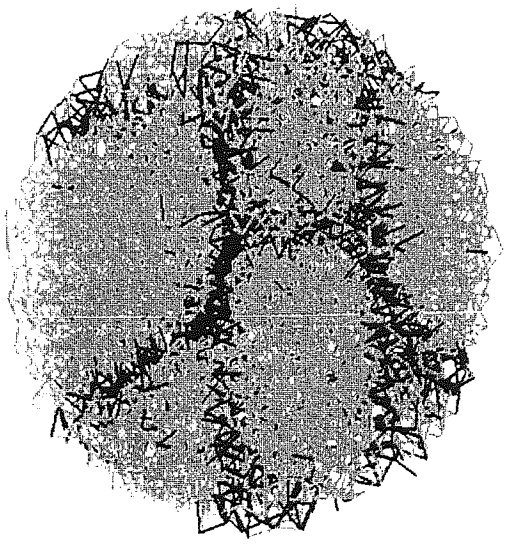

(c) impact velocity V = 0.3 m/s

Fig. 6.34 The space lattice viewed from above at the end of each of the three tests causing fracture, showing existing contacts (grey) and broken contacts (black), dense[1] agglomerate ($\Gamma = 2$ J/m^2)

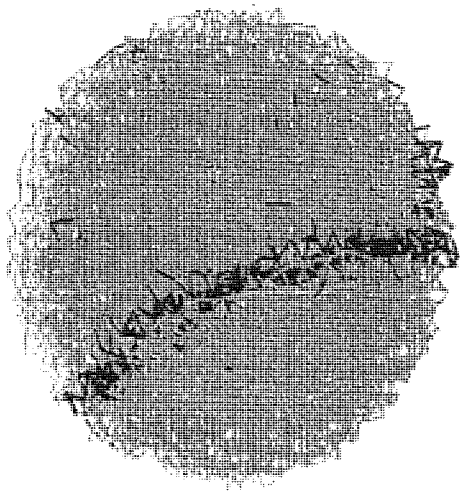

(a) impact velocity V = 0.12 m/s

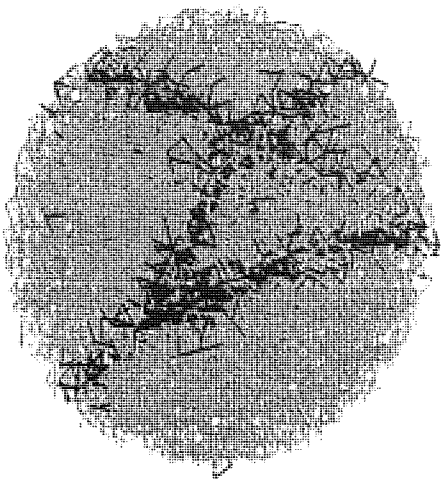

(b) impact velocity V = 0.15 m/s

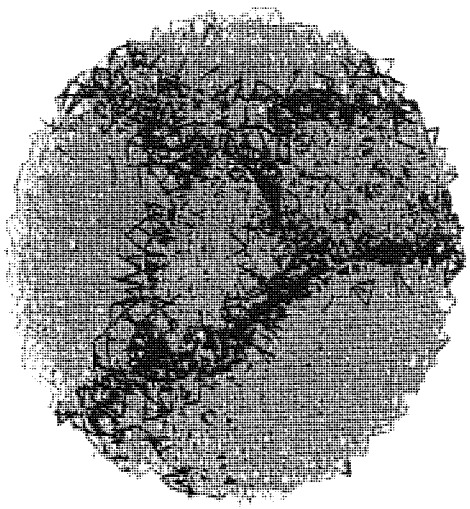

(c) impact velocity V = 0.2 m/s

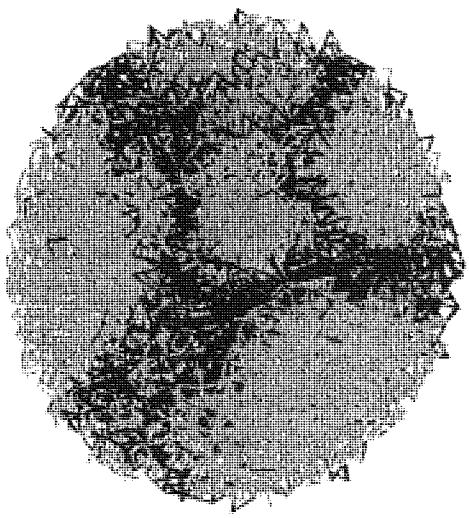

(d) impact velocity V = 0.3 m/s

Fig. 6.35 The space lattice viewed from above at the end of each of the four tests causing fracture, showing existing contacts (grey) and broken contacts (black), dense[2] agglomerate ($\Gamma = 2$ J/m^2)

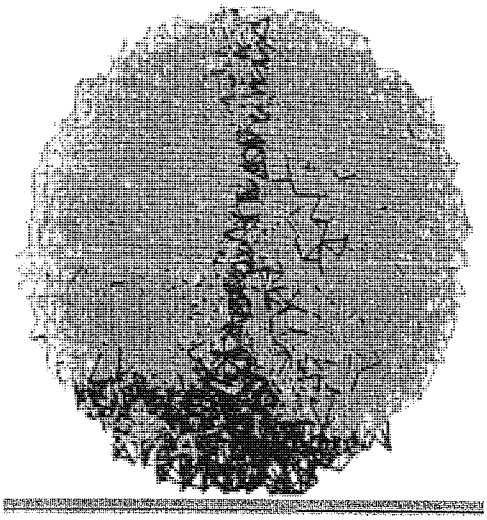

(a) impact velocity V = 0.12 m/s

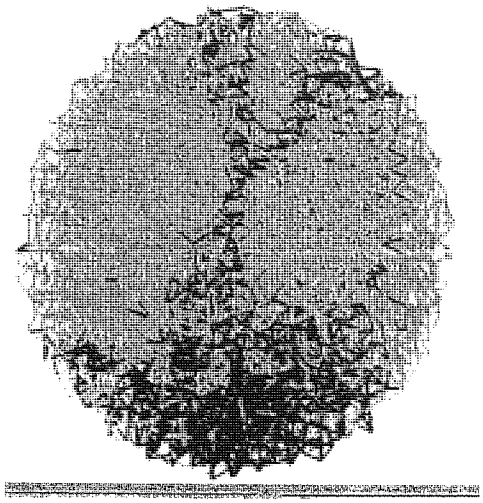

(b) impact velocity V = 0.15 m/s

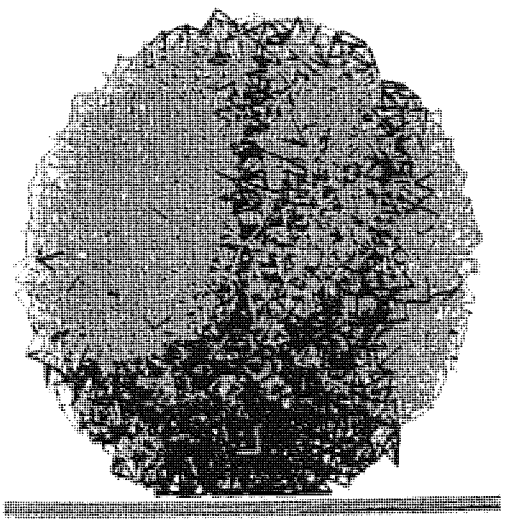

(c) impact velocity V = 0.2 m/s

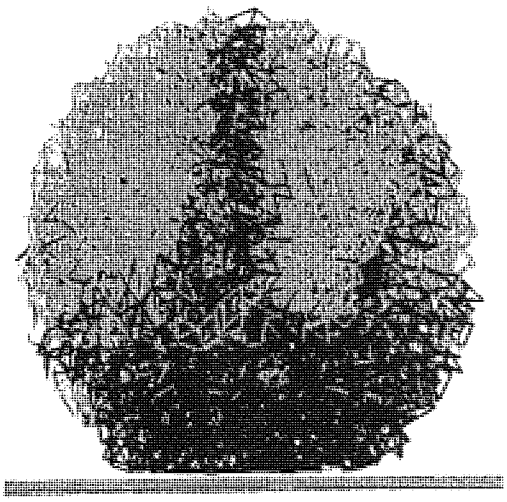

(d) impact velocity V = 0.3 m/s

Fig. 6.36 The space lattice viewed from side-right at the end of each of the four tests causing fracture, showing existing contacts (grey) and broken contacts (black), dense[2] agglomerate ($\Gamma = 2$ J/m^2)

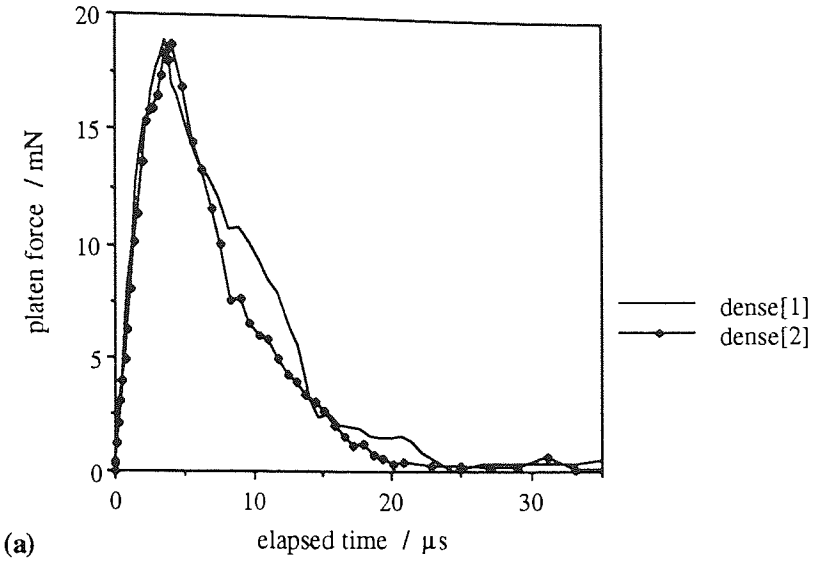

(a)

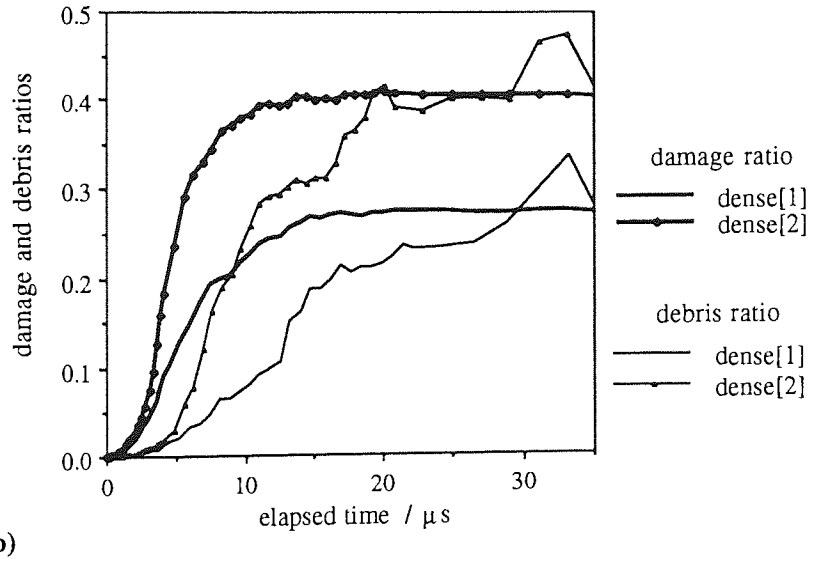

(b)

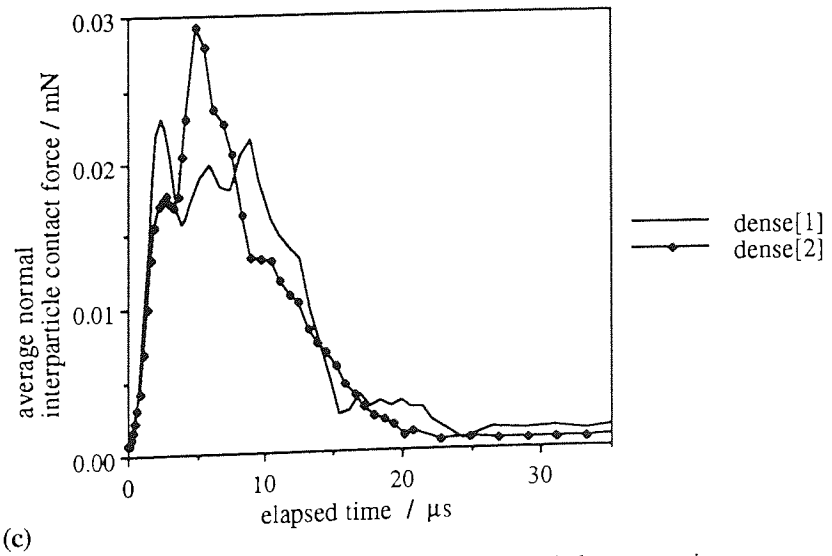

(c)

Fig. 6.37 Comparisons of a) platen force, b) damage ratio and debris ratio, and c) average normal contact force evolutions for the dense[1] and dense[2] agglomerates impacted at V=0.3 m/s

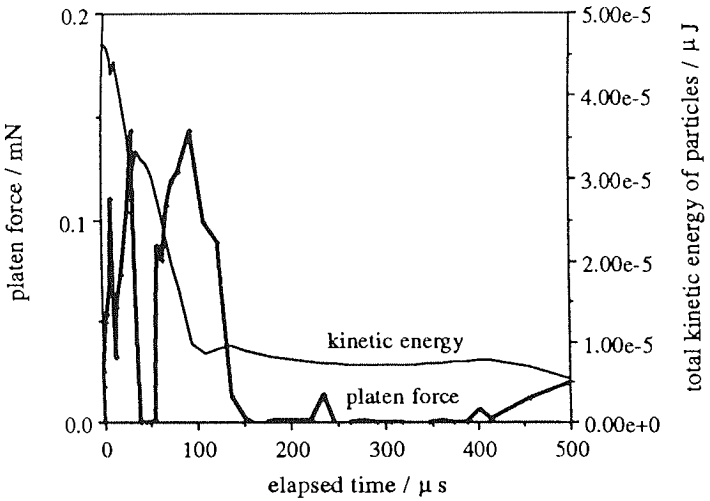

Fig. 6.38 Evolution of force on platen and kinetic energy, loose agglomerate (Γ =2 J/m^2 , V=0.01 m/s)

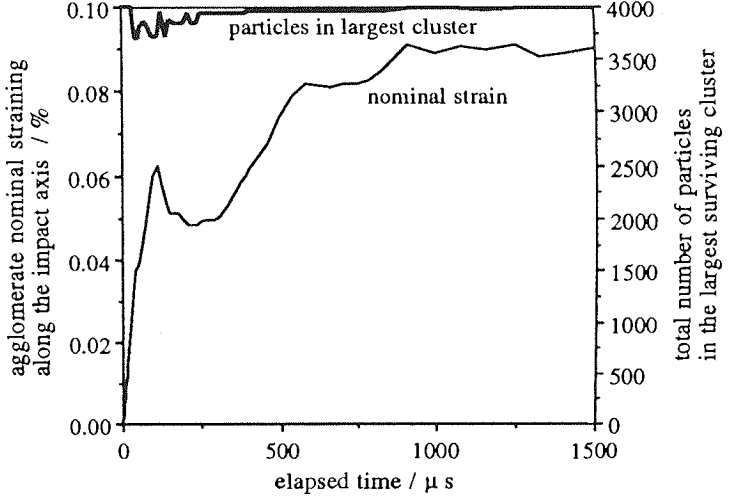

Fig. 6.41 Evolution of agglomerate nominal straining and number of particles in largest cluster, loose agglomerate (Γ=2 J/m^2 , V=0.01 m/s)

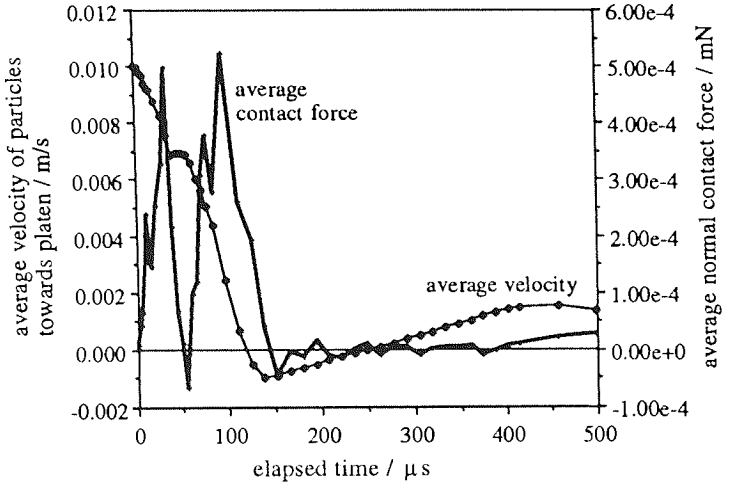

Fig. 6.39 Evolution of average normal contact force and of average velocity of particles, loose agglomerate (Γ =2 J/m^2 , V=0.01 m/s)

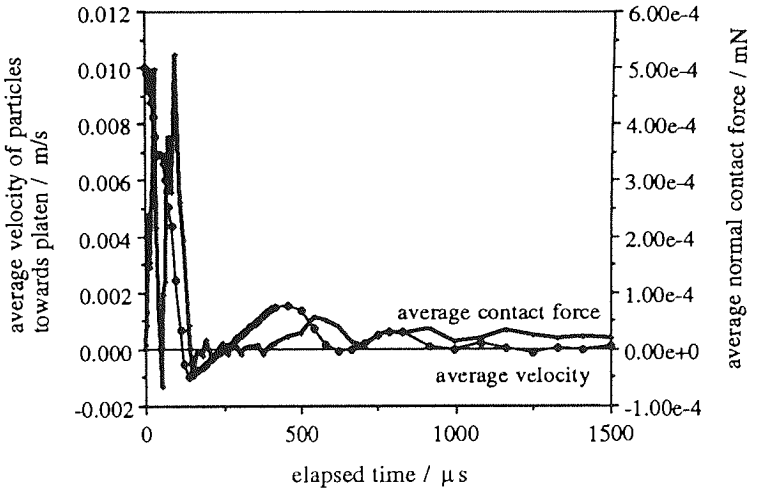

Fig. 6.42 Evolution of average normal contact force and average velocity of particles, loose agglomerate (Γ =2 J/m^2 , V=0.01 m/s)

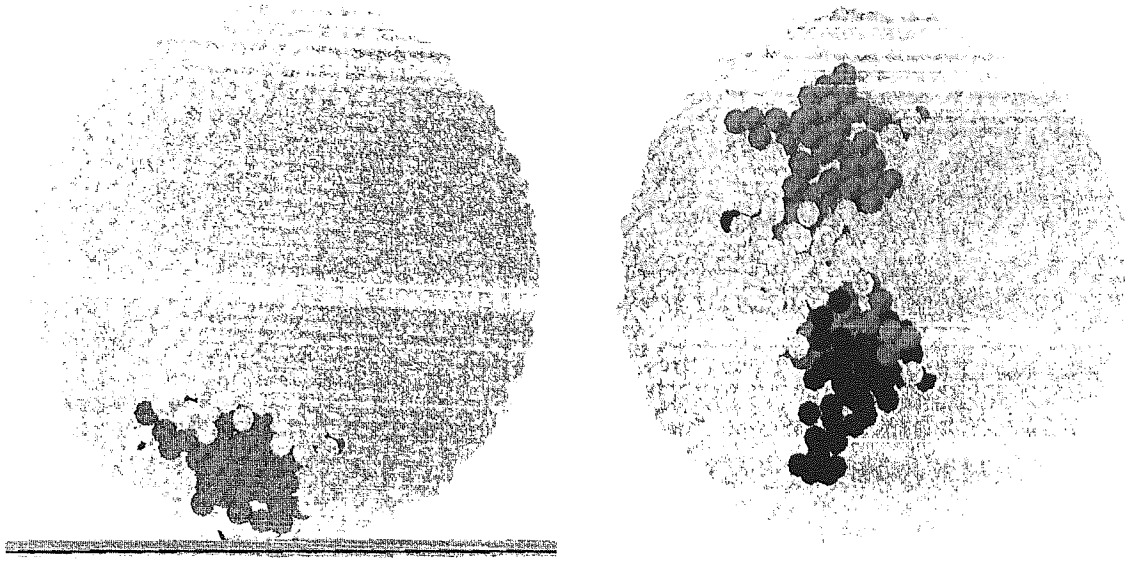

(a) view from front (b) view from below

Fig. 6.40 Particle configuration/system showing the 64 debris particles (black), the 105 particles in the medium-small fragment (dark grey) and the 3831 particles in the largest surviving cluster (light grey), t = 83.1 μs, loose agglomerate ($\Gamma = 2$ J/m^2, V = 0.01 m/s)

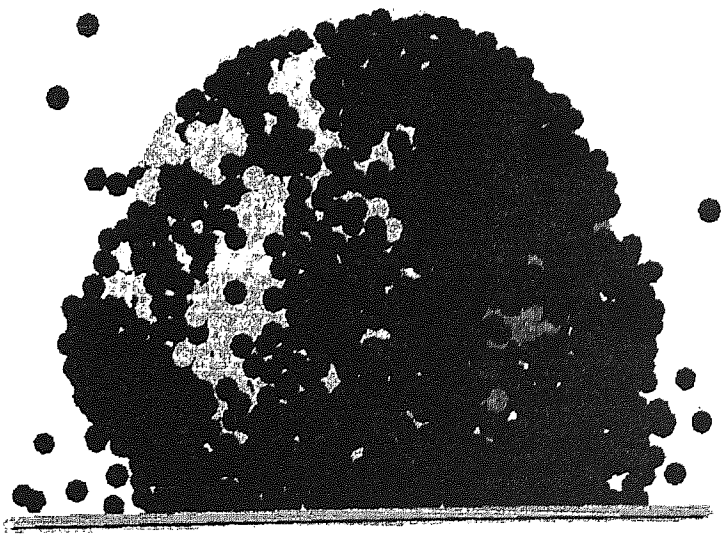

Fig. 6.43 Particle system/configuration showing debris particles in black and the particles in the large surviving clusters in shades of grey (the lightest shade of grey indicates the largest surviving cluster) at the end of the test, t = 1.96 ms, loose agglomerate (view from front, $\Gamma = 2$ J/m^2, V = 0.2 m/s)

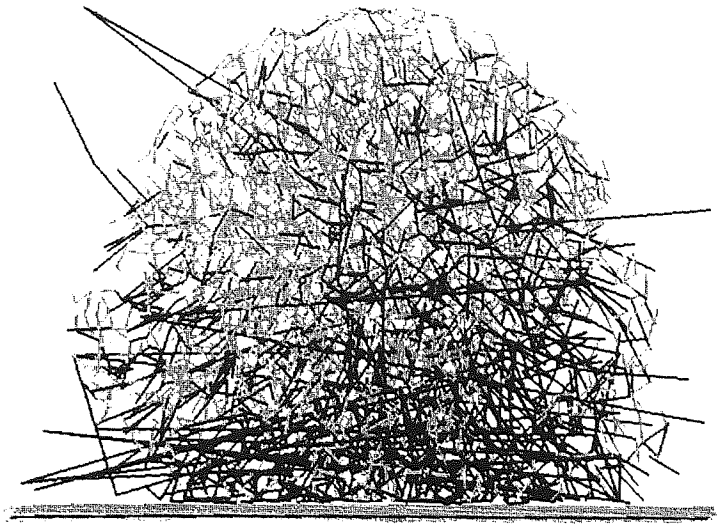

(a) the 2557 existing bonds (grey) and the 1452 broken bonds (black)

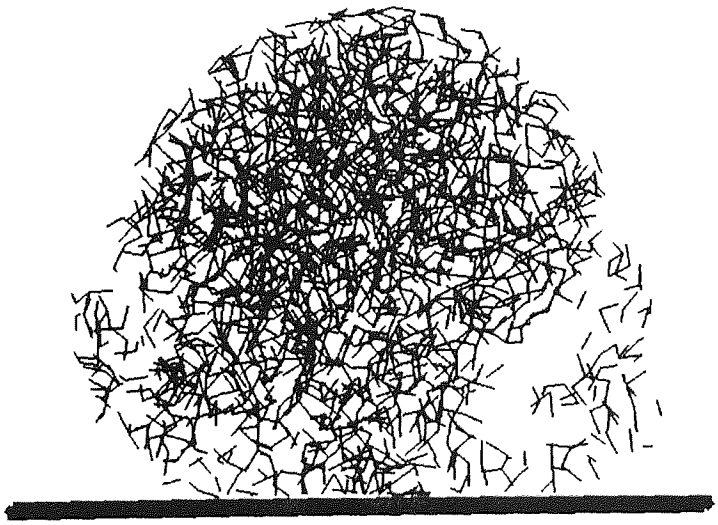

(b) only the 2557 existing bonds

(c) only the 287 newly created bonds (having $\Gamma = 0.06$ J/m^2)

Fig. 6.44 Space lattice at the end of the test, t = 1.96 ms, loose agglomerate (views from front, $\Gamma = 2$ J/m^2, V = 0.2 m/s)

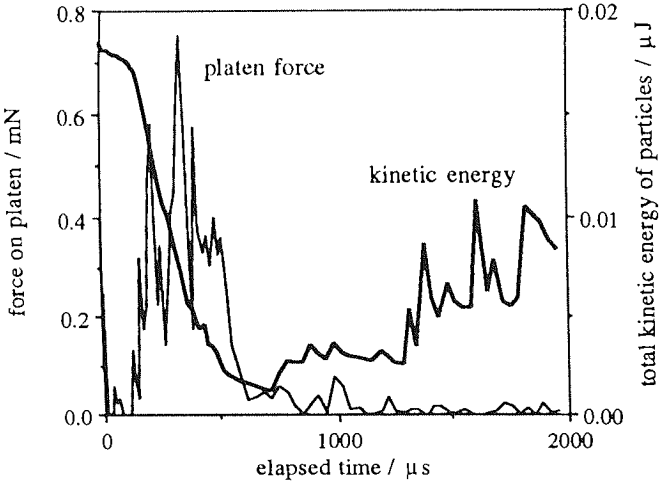

Fig. 6.45 Evolution of force on platen and kinetic energy, loose agglomerate (Γ=2 J/m^2 , V=0.2 m/s)

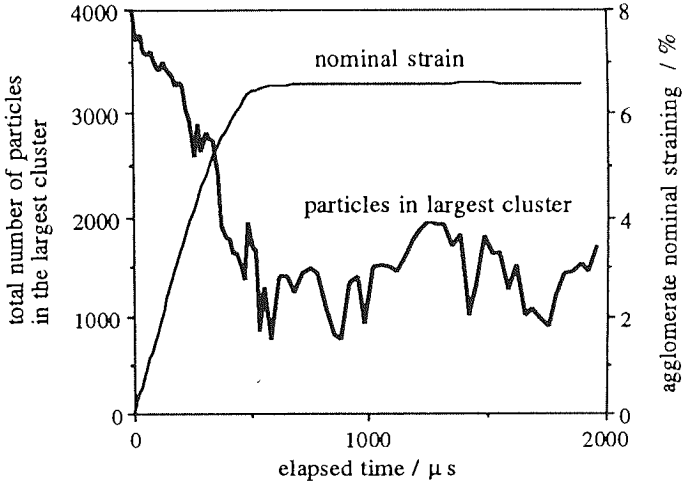

Fig. 6.47 Evolution of agglomerate nominal straining and number of particles in largest cluster, loose agglomerate (Γ=2 J/m^2 , V=0.2 m/s)

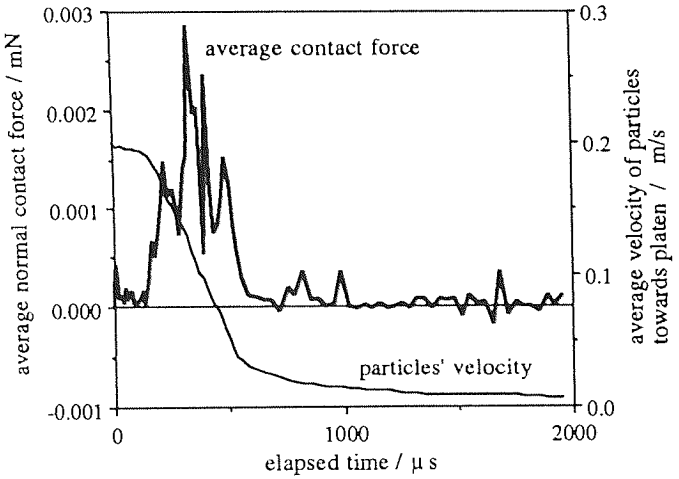

Fig. 6.46 Evolution of average normal contact force and of average velocity of particles, loose agglomerate (Γ=2 J/m^2 , V=0.2 m/s)

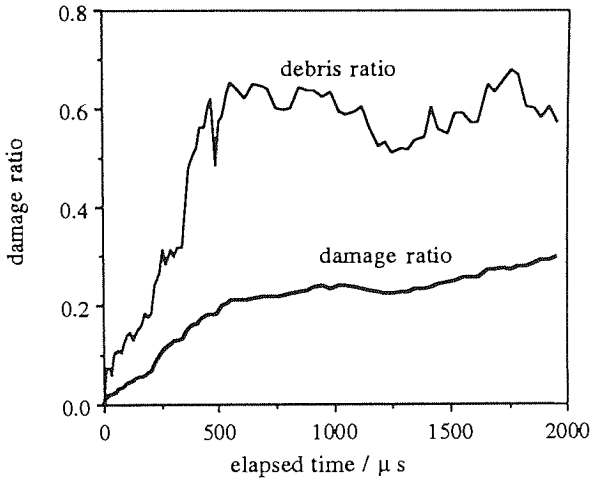

Fig. 6.48 Evolution of damage ratio and debris ratio, loose agglomerate (Γ=2 J/m^2 , V=0.2 m/s)

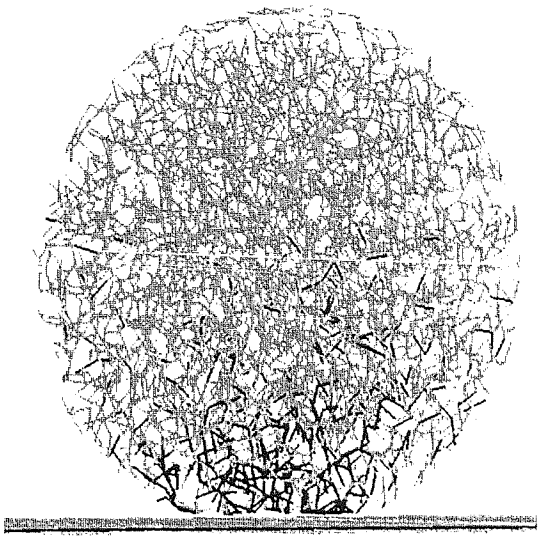

Fig. 6.49 Space lattice showing the broken bonds (in black) and the existing bonds (in grey) at t = 222 μs, loose agglomerate (view from front, $\Gamma = 2$ J/m^2, V = 0.2 m/s)

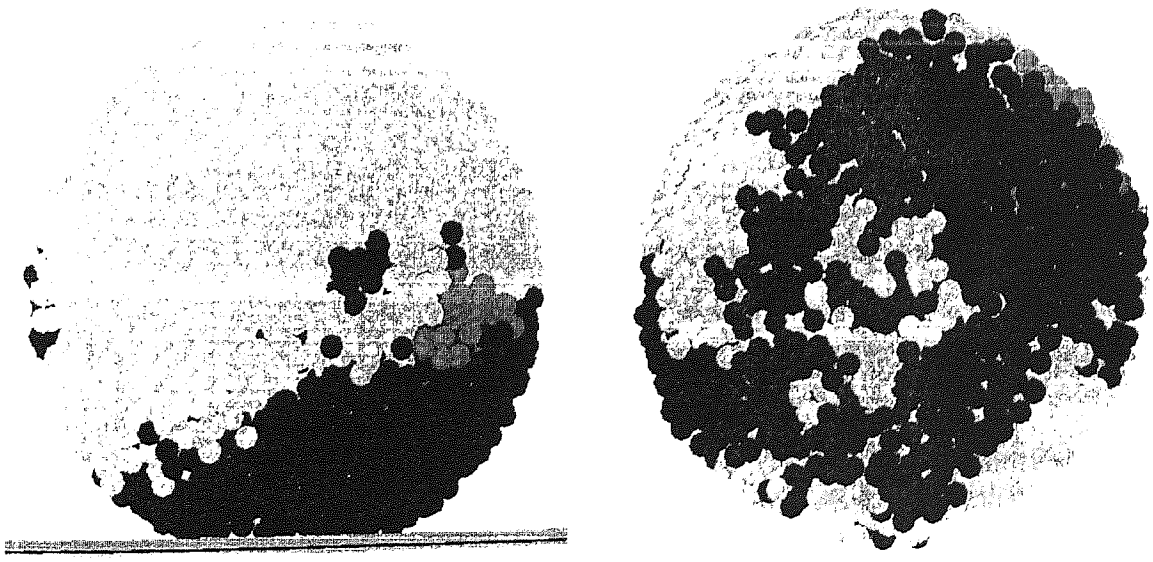

(a) view from front

(b) view from below

Fig. 6.50 Particle system/configuration showing debris particles in black and the particles in the large surviving clusters in shades of grey (the lightest shade of grey indicates the largest surviving cluster) at t = 222 μs, loose agglomerate ($\Gamma = 2$ J/m^2, V = 0.2 m/s)

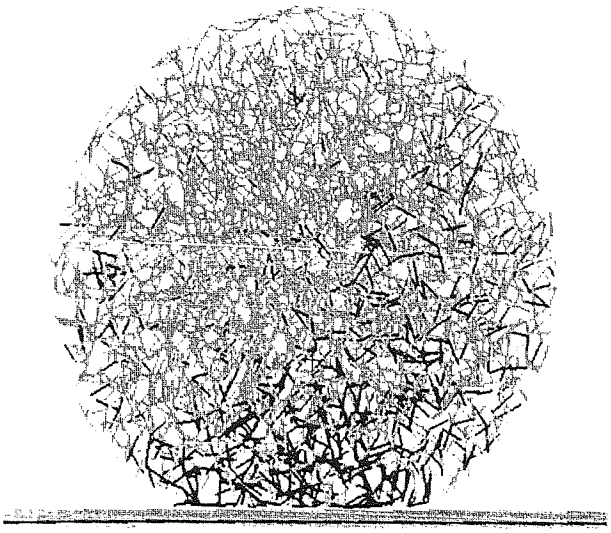

Fig. 6.51 Space lattice showing the broken bonds (in black) and the existing bonds (in grey) at t = 388 μs, loose agglomerate (view from front, $\Gamma = 2$ J/m^2, V = 0.2 m/s)

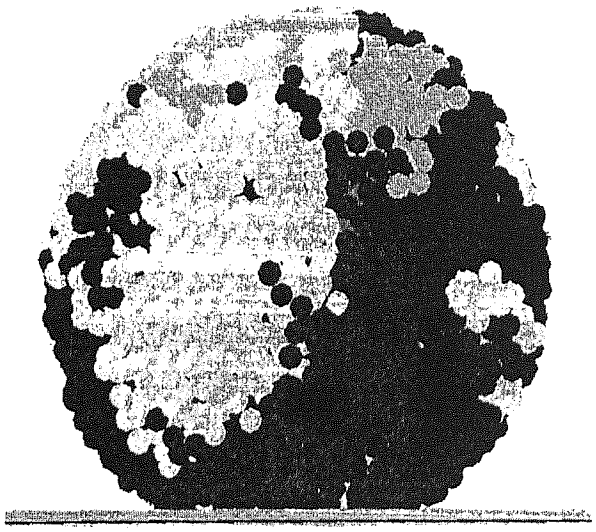

Fig. 6.52 Particle system/configuration showing debris particles in black and the particles in the large surviving clusters in shades of grey (the lightest shade of grey indicates the largest surviving cluster) at t = 388 μs, loose agglomerate (view from front, $\Gamma = 2$ J/m^2, V = 0.2 m/s)

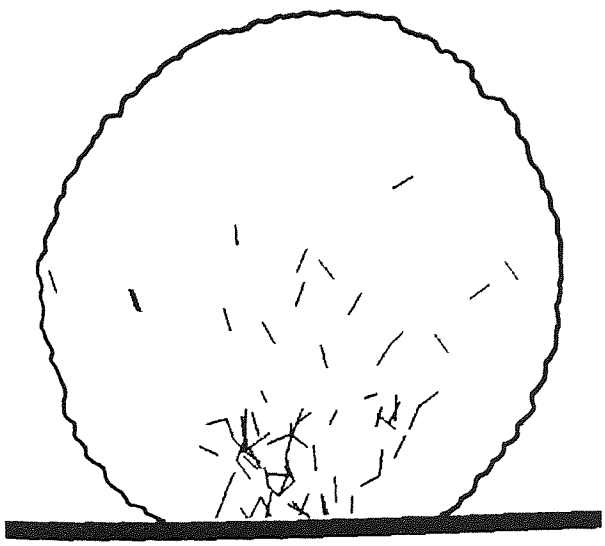

Fig. 6.53 Space lattice showing only the newly created bonds (having $\Gamma = 0.06$ J/m^2) at t = 388 μs, loose agglomerate (view from front, $\Gamma = 2$ J/m^2, V = 0.2 m/s)

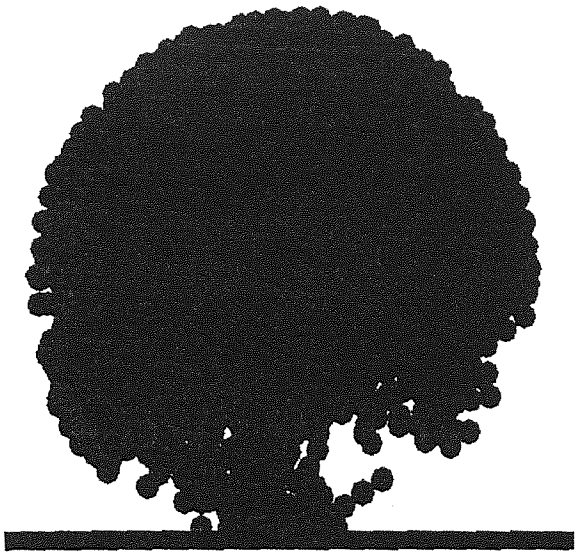

(a) t = 222 μs (during loading),
the cluster has 3039 particles

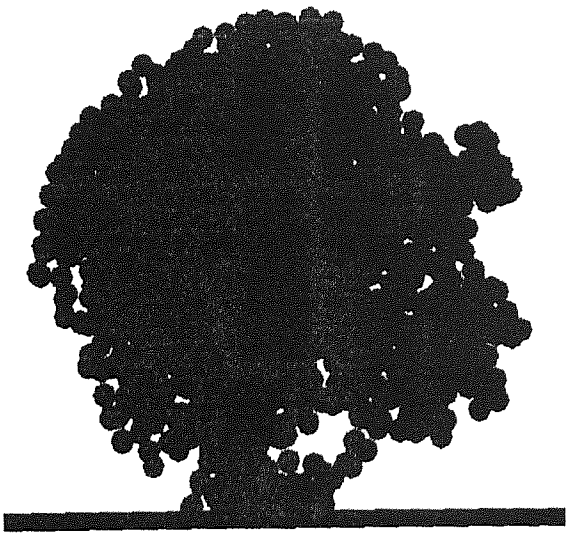

(b) t = 388 μs (end of loading),
the cluster has 1802 particles

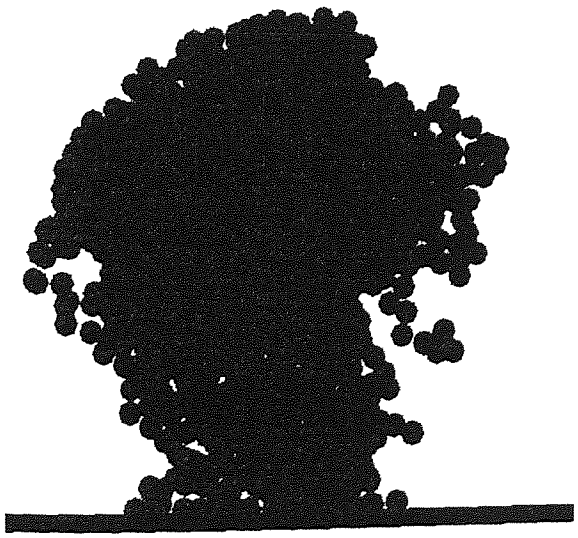

(c) t = 1960 μs (end of the test),
the cluster has 1532 particles

Fig. 6.54 Evolution of the largest surviving cluster during the test, loose agglomerate (views from front, $\Gamma = 2$ J/m^2, V = 0.2 m/s)

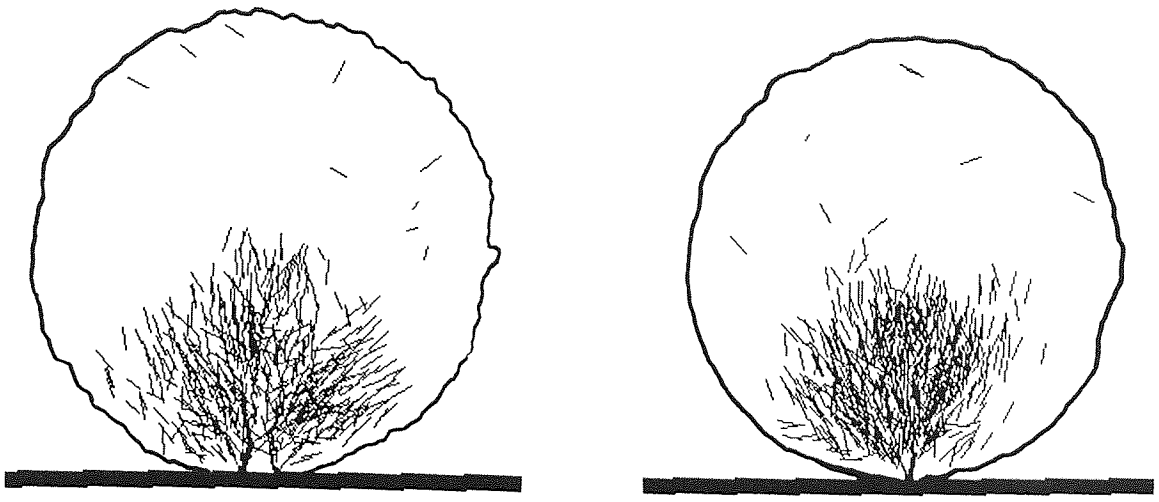

(a) dense[1] agglomerate, largest 558 compressive forces (V = 0.1785 m/s)

(b) dense[2] agglomerate, largest 606 compressive forces (V = 0.12 m/s)

Fig. 6.55 Largest compressive normal contact forces around the moment when platen force attained its maximum (views from front)

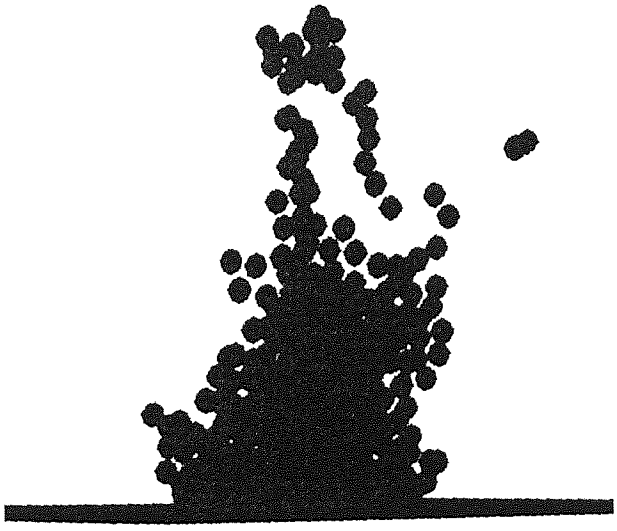

Fig. 6.56 Debris particles at the end of the test, dense[1] agglomerate (side view, $\Gamma = 2$ J/m^2, V = 0.2 m/s)

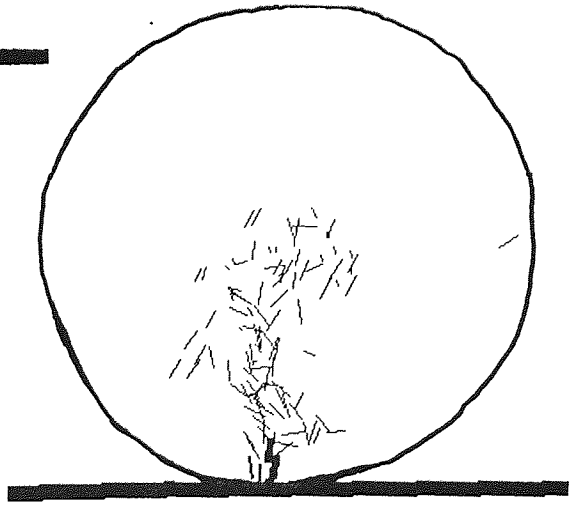

Fig. 6.57 Largest 108 compressive normal contact forces around the moment when platen force attained a maximum, loose agglomerate ($\Gamma = 2$ J/m^2, V = 0.2 m/s)

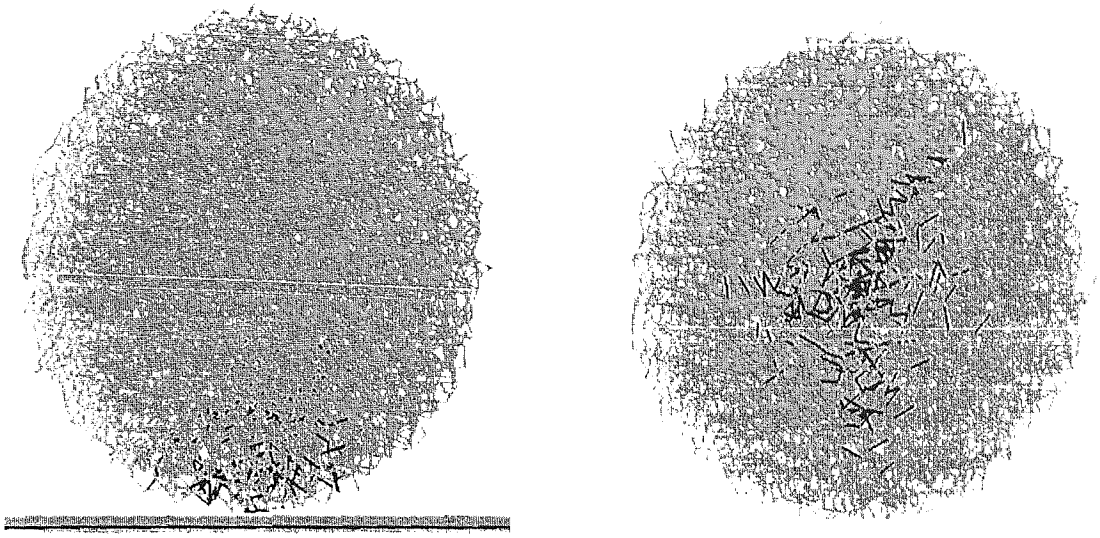

(a) view from front

(b) view from below

Fig. 6.58 Space lattice after 3 μs for dense[1] agglomerate impacted at 0.2 m/s showing existing bonds (grey) and broken bonds (black)

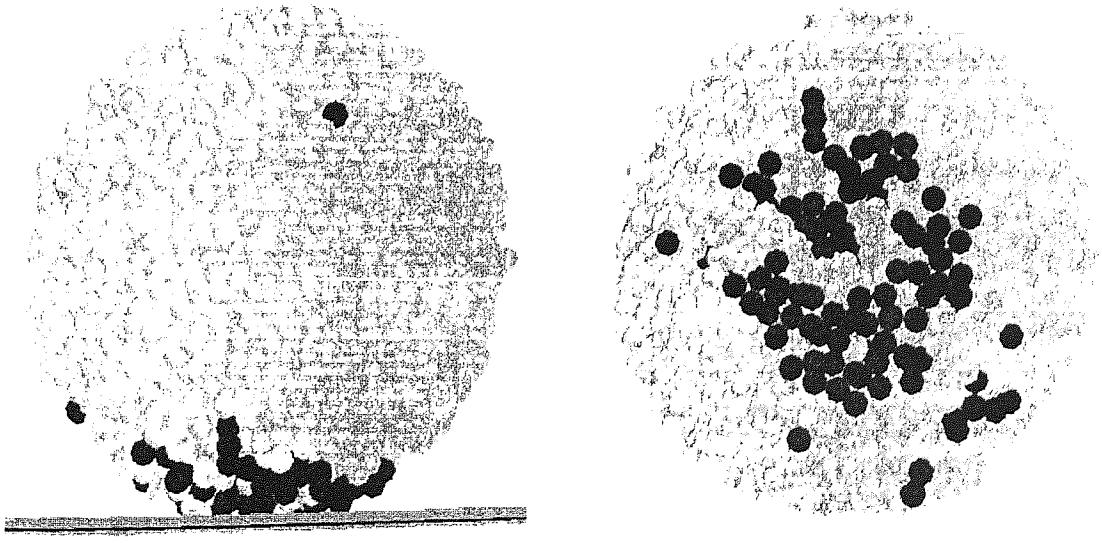

(a) view from front

(b) view from below

Fig. 6.59 Particle system after 8.9 μs for dense[1] agglomerate impacted at 0.2 m/s showing particles in debris (black) and agglomerate (grey)

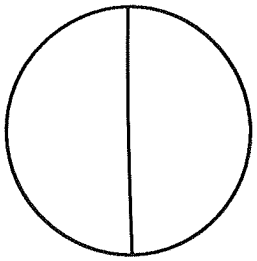

(a) fracture in two hemispheres - was reported by:
- Arbiter et al (1969)
- Salman et al (1994)
- Gildemeister and Schonert (1972)
- Santurbano and Fairhurst (1991)
- Ghadiri et al (1991)
- Shipway and Hutchings (1993)

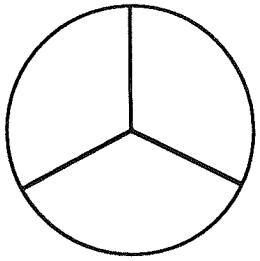

(b) fracture in three equal or nearly equal large fragments - was reporteded by:
- Arbiter et al (1969)
- Salman et al (1994)
- Ghadiri et al (1991)
- Shipway and Hutchings (1993)

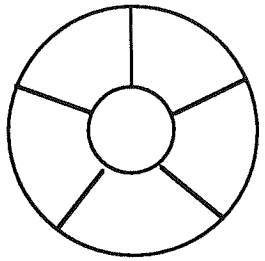

(c) fracture in "orange-slice" fragments with an additional conical fragment at the top pole - was reported by:
- Gildemeister and Schonert (1972)
- Santurbano and Fairhurst (1991)
- (Arbiter et al, 1969)

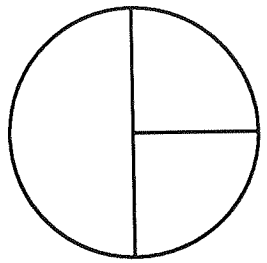

(d) fracture in one hemisphere and two quarters - was reported by:
- Salman et al (1994)
- Shipway and Hutchings (1993)

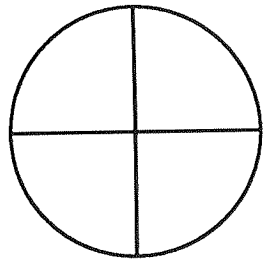

(e) fracture in four quarters - was reported by:
- Salman et al (1994)

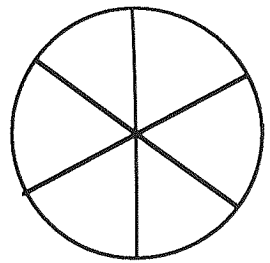

(f) fracture in "orange-slice" fragments - was reported by:
- Arbiter et al (1969)
- Shipway and Hutchings (1993)

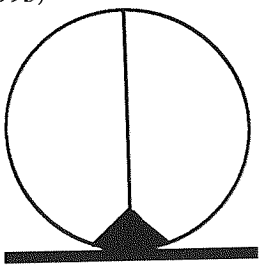

(g) fracture along meridional planes with a conical damage zone at the impacted pole - was reported by:
- Arbiter et al (1969)
- Salman et al (1994)
- Ghadiri et al (1991)
- Shipway and Hutchings (1993)

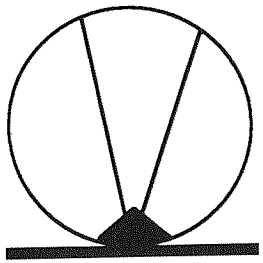

(h) fracture along radial/oblique fracture planes with a conical damage zone at the zone of impact - was reported by:
- Arbiter et al (1969)
- Salman et al (1988) did not mention a contact damage zone
- Kelly and Macmillan (1986) reported a larger and more flattened contact damage zone

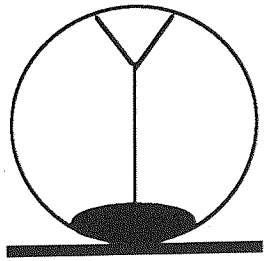

(i) fracture in "orange-slice" fragments, a conical fragment at the top pole and with a flattened damage zone at the impacted pole - was reported by:
- Gildemeister and Schonert (1972)
- Santurbano and Fairhurst (1991)

Fig. 6.60 Fracture modes reported from laboratory free-fall impact testing (presented schematically here) - in views from above (**a - f**) and from front, along the fracture plane (**g - i**)

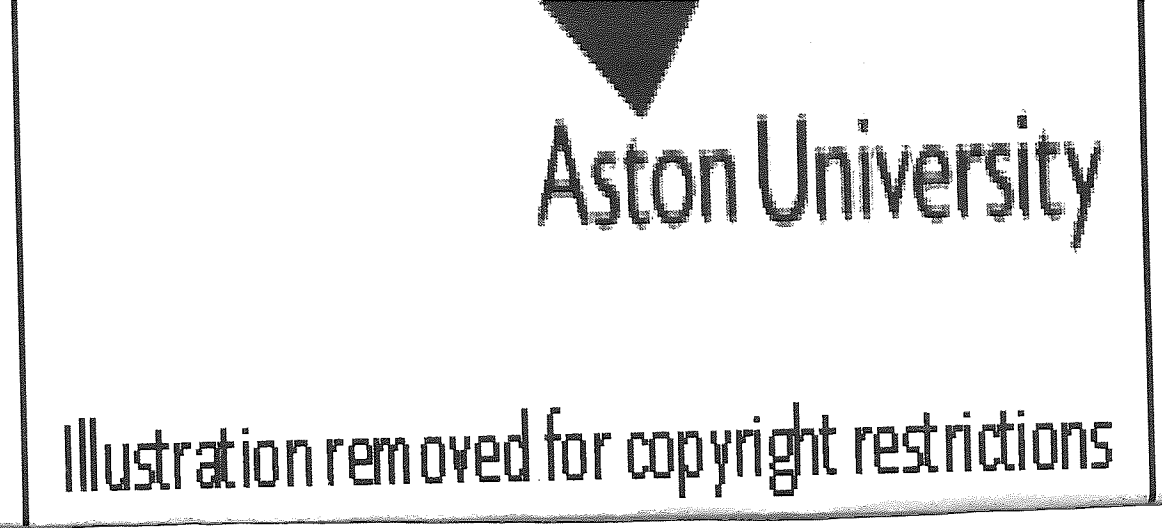

(**a, b, c**) Fractures in two and three large fragments of aluminium oxide agglomerates, Salman et al (1994), views from above and below

(**d,e**) Fractures in three and five large fragments of sand-cement agglomerates, Arbiter et al (1969), views from below

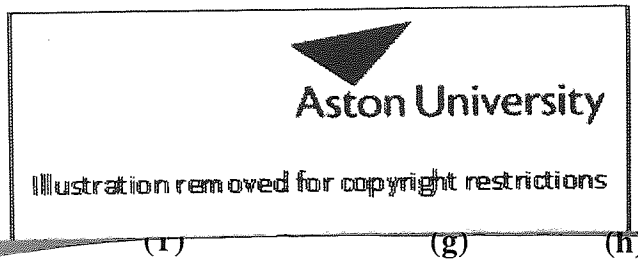

(f) (g) (h) (i) (j)

(**f, g, h, i, j**) Fractures along meridional and oblique fracture surfaces of sand-cement agglomerates, Arbiter et al (1969), views from front (roughly along the fracture surface)

Fig. 6.61 Photographs of fractured agglomerates reported from laboratory testing

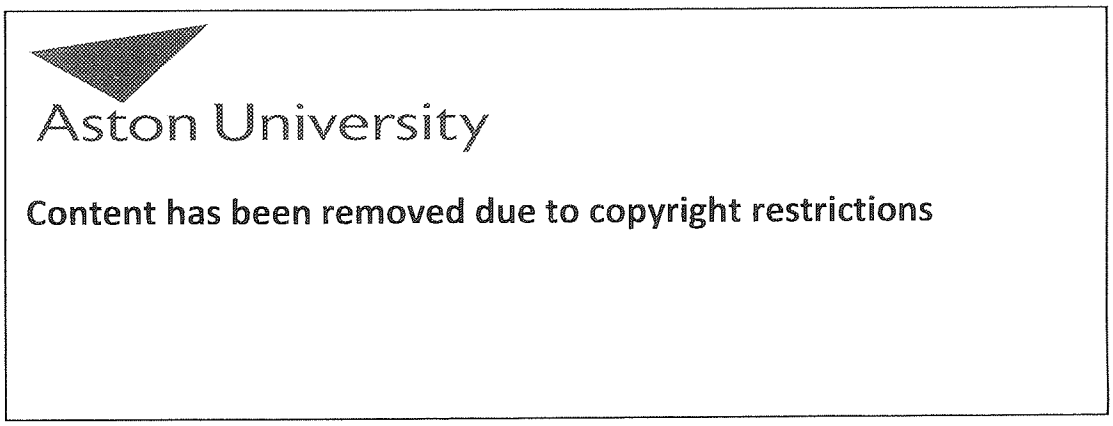

Fig. 6.62 Evolution of platen force during a laboratory free-fall impact test that resulted in the fracture of a limestone pellet, Santurbano and Fairhurst (1991)

CHAPTER 7

SIMULATIONS OF DOUBLE IMPACT TESTS AND OF DIAMETRICAL COMPRESSION TESTS

Both double impact and diametrical compression test simulations are presented in this chapter because the loading mechanism is very similar for the two test types: the sample is compressed between a descending top platen and a stationary bottom platen. The main difference between the two tests is the loading rate, given by the velocity of the top platen. The double impact test is dynamic; the velocity of the top platen varies during the test and the initial velocity is almost as high as the impact velocities used in free-fall impact test simulations. The diametrical compression test is a "quasi-static" test, as the top platen's velocity (and, hence, the nominal strain-rate) is very small and remains constant during the test.

7.1 CHARACTERISTICS OF THE AGGLOMERATES USED

The test results presented in this chapter refer to simulations carried out on agglomerates of 4000 particles each, which had the same elastic properties and friction coefficients as the ones described in Chapters 5 and 6.

A total of four agglomerates were used in the double impact tests: three dense and one loose. Table 7.1 presents the main structural characteristics of these agglomerates. A weaker dense (called weak-dense) agglomerate of 0.6530 solid fraction and 0.4 J/m^2 interface energy was the first one to be tested. The dense[1], dense[2] and loose agglomerates were identical to the ones tested in free-fall impact (see Chapter 6). All but the first (the weak-dense) agglomerate were also tested in DC. The other three agglomerates had 2.0 J/m^2 interface energy. The second agglomerate used (dense[1]) had the same solid fraction as the first one, but 1.2% more interparticle contacts. The third agglomerate (called dense[2]) had almost the same solid fraction as the first two, but 17.13% more interparticle contacts than the weaker dense agglomerate. Double impact tests were also simulated on a loose agglomerate of 0.4364 solid fraction. As in the free-fall impact test simulations, the interface energy attributed to new interparticle contacts that formed during the double impact and diametrical compression tests was 0.06 J/m^2.

7.2 GENERALITIES

As in the case of free-fall impact tests, the loading (impact or compression) axis is vertical also in both the double impact and diametrical compression tests. The strain of most interest is therefore the one along this vertical axis. In laboratory tests, the "agglomerate strain" refers to the nominal straining of the agglomerate but is always measured as the decrease in the distance between the platens. However, this is not always an accurate approximation of the agglomerate's nominal strain, as the vertical dimension of the agglomerate can sometimes be smaller than the distance between platens - especially in double impact tests (e.g. when the top platen rebounds from the agglomerate).

7.2.1 The Double Impact Test

Two main issues had to be initially decided in respect to this test: the mass of the impacting (falling) platen and the moment when the platen was to be arrested. It was decided that, for the purpose of this project (to obtain fracture, fragmentation or crushing of the agglomerate and not just local damage), the mass of the falling platen should be equal or larger than that of the agglomerate. For a very large platen mass, results would be expected to tend towards the results obtained in (fast) diametrical compression tests (as very low impact velocities would be used in these tests). On the other hand, a light impacting platen in the double impact test would necessitate higher impact velocities and would thus facilitate comparisons with the single (free-fall) impact tests.

Depending on the agglomerate's response, the impacting platen can simply rebound off the agglomerate after impact (producing just local damage of the agglomerate), or it can produce fracturing or even crushing/shattering of the agglomerate. For the case when the impacting platen produced agglomerate fracture, Arbiter et al (1969) and other workers arrested the falling platen just after the occurrence of fracture. In this way, they argued, what was obtained was "primary" fracture and was better comparable to the results of free-fall impact and diametrical compression tests. They argued that if the impacting platen was not stopped, it could produce secondary fractures and/or crushing of the agglomerate. The computer simulation allows a more complete and detailed analysis of the double impact test. Therefore, the falling platen could be arrested just after the primary fracture, but could also be left to rebound off the agglomerate or crush it.

7.2.2 The Diametrical Compression Test

The velocity of the moving platen in the diametrical compression test should be low enough for it to have an insignificant effect on the agglomerate's behaviour in order to model the so-called "quasi-static" regime. Only the top platen was moved in the diametrical compression

tests described in this chapter. The top platen velocity was taken from the "APPIE/G001" standard ("APPIE" stands for "The Association of Powder Process Industry and Engineering", Japan - see British Materials Handling Board, 1987) that recommends a constant platen velocity of 20 mm/min (0.000333 m/s). For the ≈1.11 mm diameter agglomerates used in this project, this would mean a strain-rate of about 0.3 s^{-1} which is well above the quasi-static regime. However, quasi-static simulations of a diametrical compression test would take in excess of six months to reach primary fracture. For this reason, only three diametrical compression test simulations were carried out using a top platen velocity of 10 mm/min.

7.3 BEHAVIOUR OF DENSE AGGLOMERATES IN DOUBLE IMPACT TESTS

The tests reported in sections 7.3.1 and 7.3.2 below were carried out on the weak-dense agglomerate (which had the lowest interface energy, 0.4 J/m^2). Both the effects of varying the falling platen's impact velocity and mass were analysed for this agglomerate.

7.3.1 Tests Using Same Platen Mass: Effect Of Varying Impact Velocity

A falling platen having a mass, M_p, 100 times larger than the mass, M_a, of the agglomerate was used to examine the effect of varying the platen's impact velocity between 0.01 and 1.0 m/s.

For an impact velocity of 0.01 m/s the weak-dense agglomerate did not break. The top platen did not rebound, but started moving up and down on the top of the agglomerate, without loosing contact with it. Insignificant flattening and no debris detachment occurred at the contacts with the platens. However, Fig. 7.1, presenting the broken bonds at the end of the test (t = 7.7 ms) shows that the agglomerate exhibited a fair amount of local damage: 307 (3.2%) of the initial bonds were ruptured in the local regions adjacent to the platens. Figure 7.2 presents the evolution of the force on the top (impacting) platen and the top platen velocity during nominal straining of the agglomerate (up to about 1.42 ms). After a steep loading phase, the platen force dropped to almost zero when the platen velocity reversed sign - see Fig. 7.2. The upward velocity attained a relatively small maximum, of only 12% of the impact velocity. As the platen force increased again to a value equal to almost 80% of the absolute maximum (peak) attained earlier (see Fig. 7.2), the impacting platen velocity became positive again for a while. This shows that the top platen performed an oscillatory motion on top of the agglomerate. The small amount of elastic energy stored internally in the agglomerate was not sufficient to cause rebound of the impacting platen from the agglomerate. Figure 7.3 shows the evolution of damage ratio and the kinetic energy of the

agglomerate. At the moment of impact the top platen caused a sudden increase in the kinetic energy of the agglomerate, as it induced some small (local) displacements of the particles situated near the platen regions. These sudden local displacements caused breakage of bonds which correlates well with the fact that the damage ratio started increasing from the very beginning of the test - see Fig. 7.3. Almost all the bond breakage (illustrated in Fig. 7.1) occurred during the initial loading of the agglomerate, which lasted up to about 0.12% nominal strain (see Fig. 7.2 and 7.3).

Although the release of the stored elastic energy caused the impacting platen to move upwards, the gravity force generated by the platen's large mass caused it to reverse and press again on the agglomerate, restoring some elastic energy again. The oscillatory motion of the impacting platen was only very lightly damped in time - see Fig. 7.4 which shows the evolution of the top platen velocity and the average normal contact force throughout the test. The oscillatory variation in the value of the average contact force proves that the elastic stored energy was the driving force for the oscillations. The test was halted when the damage ratio levelled off and the diametrical straining of the agglomerate ceased - after about 11 oscillations. Figure 7.5 presents the evolution of the agglomerate strain and the platen force up to the end of the test. It can be observed that most of the agglomerate nominal strain occurred prior to the first large unloading. However, the agglomerate continued to strain with another 0.015% during the next two oscillations. Both the average contact force (in Fig. 7.4) and total force on the platens (in Fig. 7.5) oscillated around a positive value - this showing that the agglomerate was continuously compressed between the heavy top platen and the bottom platen. The actual reversible deformation of the agglomerate was a little larger than the one suggested by the small recovery of strain after the first oscillation illustrated in Fig. 7.5. This was proved by the fact that further recovery of the diametrical strain occurred if the top platen was taken off the agglomerate.

Most of the irreversible deformation of the agglomerate was local, a fact reflected also by the observation that there was no expansion of the agglomerate in directions perpendicular to the loading direction. Debris did not detach from the local damage zones due to the fact that the impacting platen constrained the agglomerate by maintaining a continuous platen load.

During the many oscillations of the impacting platen on the agglomerate, the bonds acted similar to damped elastic springs. Figures 7.4 and 7.5 clearly show how the external load charged the agglomerate bonds with increasing compressive force and how the release of this energy stored at the contacts then produced upward movement of the platen leading to the oscillatory behaviour. Nevertheless, only the first larger amount of stored energy contributed to the breakage of interparticle contacts.

When impacted with a top platen having a velocity of 0.04 m/s the agglomerate fractured into two large fragments. Figure 7.6 presents the agglomerate just after the moment of primary fracture viewed in a direction almost along the fracture surface. The particles belonging to the debris are represented in black, whereas the fragments are coloured in grey. The figure indicates that most of the debris was concentrated under the impacting platen and close to the zone where the fracture surface met the external surface of the agglomerate. The corresponding space lattice, showing the surviving bonds in grey and the broken bonds in black just after the primary fracture is presented in Fig. 7.7. The fracture surface and the local contact damage zones can be easily identified by looking at the region dominated by the black lines. The fracture surface is vertical and it passes through the centre of the agglomerate. Figure 7.8 illustrates the agglomerate at 4.22% nominal strain. The image confirms that the fracture surface, identified by the absence of lines, passed through the agglomerate's centre. Additionally it can be observed that the fracture surface was perpendicular to the platens although it did not quite follow a diametral plane. The two large fragments obtained were not quite equal, corresponding to 55% and 38% of the initial mass of the agglomerate.

Figures 7.9 and 7.10 show the evolution of the forces on the platens and the damage and debris ratios up to 3.5% nominal strain. Monitoring the particle velocity field, it was found that primary fracture occurred at 2.06% nominal strain (t = 0.662 ms) when the platen forces dropped from their third large peak - see Fig. 7.9. Fracture was marked by a sudden increase in the damage ratio (Fig. 7.10), as a further 14% of the initial number of interparticle contacts were broken. Almost no debris was produced until each platen force reached its maximum value (the first peak in Fig. 7.9). The debris ratio increased in a little more continuous manner than the breakage of bonds - see Fig. 7.10 - until, shortly after primary fracture it represented 8% of the initial agglomerate mass. As in the free-fall impact simulations of dense agglomerates, the debris ratio levelled off a little while after the levelling off of the damage ratio, as the breaking up of the agglomerate into two fragments allowed the detachment of a few more particles.

Apart from their first (and largest) peak, the forces developed on each of the two platens evolved in a similar manner (Fig. 7.9). It can be observed in Fig. 7.10 that there was a rapid increase in bond breakage that corresponded to the development of the first and the drop immediately after the third peak in the force developed on the platens - see Fig. 7.9. The first increase corresponded to the breakage of bonds in the damage zone adjacent to the platens, whereas the second increase corresponded to the breakage of bonds along the fracture surface.

The evolution of the diametrical nominal straining and of the top platen's velocity up to t = 1.4 ms are presented in Fig. 7.11. It can be noted that the evolution of the straining was

almost linear with testing time even after the occurrence of fracture. The resistance of the agglomerate (towards the movement of the impacting platen) was stronger up to the moment of fracture (t = 0.622 ms), as it managed to reduce the velocity of the impacting platen from 0.04 to 0.034 m/s. After this, the resistance exercised by the two large fragments managed to keep the top platen's velocity roughly constant (Fig. 7.11).

For an impact velocity of 0.1 m/s the agglomerate broke in almost exactly the same way as in the 0.04 m/s velocity test, but at about 2.3% nominal strain (t = 0.265 ms) - see Fig. 7.12a presenting all the particle velocity vectors at primary fracture viewed from above. Figure 7.13 presents the space lattice of the agglomerate after primary fracture, indicating almost no difference from the test with 0.04 m/s impact velocity. However, if the impacting platen was not arrested after the primary fracture, the agglomerate exhibited secondary fracture at 6.6% nominal strain (t = 0.791 ms). Due to the continuous loading of the two large fragments, the larger of them broke up in two - see Fig. 7.12b presenting all the particle velocity vectors after secondary fracture. The test was halted at 8.72% nominal straining (t = 1.07 ms). Figure 7.14 shows the agglomerate at the end of the test viewed from the front, but not along the primary fracture surface. The particles in the debris are represented in black and the fragment that first broke off the agglomerate in a darker shade of grey. As the figure indicates, most of the debris was again situated under the impacting platen. Even for this relatively large nominal strain of 8.72% the debris did not fly-off.

The evolution of the forces on the platens is shown in Fig. 7.15, whereas the evolution of the damage and debris ratio can be found in Fig. 7.16 (represented with simple, uncrossed lines). One can observe that the general evolution of the force on the platens was similar to the one of the 0.04 m/s impact velocity test, except that primary fracture occurred after a fourth peak in the platen forces. Prior to primary fracture, the damage ratio increased in steps. Each step coincided with the development of a peak in the platen forces indicating bond breaking in the damage zones adjacent to the platen. A larger, rapid increase in the damage ratio occurred during propagation of the primary fracture, as the top platen force fell sharply from its fourth peak. After primary fracture, not much additional damage or debris was produced until about 6% nominal strain when the damage ratio increased due to the development of the secondary fracture. The rate at which the damage ratio increased at this stage (Fig. 7.16) would indicate that the secondary fracture was a slower process than that associated with the primary fracture.

For an impact velocity of 1.0 m/s, the agglomerate was entirely transformed into debris at about 9% nominal strain. This is demonstrated in Fig. 7.17 which presents the particle velocity vectors viewed from above and shows that all the particles flew off along outward radial directions from the loaded diameter. A notable feature of this test was the big

difference in the force evolution developed on the top and bottom platens, see Fig. 7.18. Due to the high impact velocity, the force on the top platen was much larger than the force on the bottom platen almost all through the test. At the beginning of the test the evolution of the force on the top platen was similar to the platen force evolution in a free-fall impact test, as it increased rapidly (see Fig. 7.18) and attained its maximum value while the force on the bottom platen was still zero. This implies that up to this moment the test was effectively a single impact test, as the bottom platen seemed not to "know" that an impact had occurred. The rates of bond breakage and debris detachment were much higher than the rates observed for the tests of lower impact velocity - see Fig. 7.16 presenting the damage and debris ratios (with crossed lines, up to 4.3% strain only) in comparison to the ones observed for the test of 0.1 m/s impact velocity. To the first and largest increase in top platen force (Fig. 7.18) corresponded the first and most sharp increase in damage ratio (Fig. 7.16).

Figure 7.19 presents all the particles at an early stage of crushing (at 4.3% nominal strain), with the debris particles represented in black and the surviving cluster in grey. It can be noted how much more debris was formed in the top (impacted) half of the agglomerate compared to the bottom half. Presenting only the largest surviving cluster at 4.3% nominal strain, Fig. 7.20 shows that the debris was more than just a layer at the surface of the agglomerate (as it was in the case of the 0.04 m/s impact velocity test). While the agglomerate's top half was being crushed, the bottom half remained almost intact. Bonds breakage and debris detachment started from the agglomerate's top pole, although the region along the loaded (vertical) diameter was the last to be crushed.

If the falling platen was arrested, the agglomerate behaved differently depending on when exactly during the test this was carried out. In the case when the top impacting platen was arrested just after the platen force started decreasing from its maximum value (at 0.27% nominal strain, see Fig. 7.18), the agglomerate broke up into two large fragments - see Fig. 7.21 presenting the velocity vectors of all the particles in the large fragments at fracture. The fracture pattern was not exactly the same as obtained in the 0.04 and 0.1 m/s impact velocity tests already described (Figs. 7.8 and 7.13). Furthermore, the two large fragments were weaker and smaller due to bonds having been broken all over the agglomerate. This was reflected by the fact that the damage and debris ratios at primary fracture were about twice what they were in the other tests. Figure 7.22 presents all the particles belonging to the two large fragments (representing 89% of the initial agglomerate mass) a little while after the top platen was halted. In addition to the primary fracture, the impact clearly produced local failure of the agglomerate's impacted pole region. Due to the extensive internal damage to the fragments (and the fact that in this test the two large fragments did not displace much relative to each other) it was difficult to identify the fracture surface - see Fig. 7.23 presenting the space lattice viewed from above a while after the platen was arrested.

When the impacting platen was arrested only after the force on both platens had dropped (at 1.59% nominal strain, see Fig. 7.18), the agglomerate broke up into 8 medium-sized fragments. Figure 7.24 presents the particle velocity vectors in the largest fragments after the break-up. The main fracture surface corresponds to the one obtained when the impacting platen was arrested at 0.27% strain - see Fig. 7.21. The space lattice viewed from above, a while after the platen was arrested, is illustrated in Fig. 7.25 - indicating a few of the internal irregular surfaces along which bonds were broken. Although not planar, the fracture surfaces tended to be perpendicular to the platens and some of them passed through the agglomerate's loaded (vertical) diameter. The medium-sized fragments were very weak as many of the internal bonds were broken. Figure 7.26 shows the particles in the larger fragments at the end of the test, clearly indicating that, in this case, the entire top (impacted) half of the agglomerate was transformed into debris.

Comparing the results of the tests using same platen mass it can be concluded that, depending on the impact velocity, the weak-dense agglomerate can either be just locally damaged, can be fractured into two or three large fragments, can experience multiple fractures, or it can be completely reduced to debris at significantly high platen velocities. All four types of behaviour were observed by arresting the impacting platen at different moments during the test in which the impact velocity was 1.0 m/s.

For the chosen falling mass, the platen velocity after the impact moment decreased in all the four tests simulated. However, the relative degree of deceleration was lower for tests of higher impact velocity. Only for the impact velocity of 0.01 m/s was the agglomerate capable of stopping the mass-platen and of reversing its velocity. In all four tests the first and largest peak of the average normal contact forces and in the platen forces was attained prior to achieving 0.2% agglomerate nominal strain. Only during the loading to this first peak was the evolution of the damage and debris ratios the same in all four tests.

No signs of fracture could be found in the test with 0.01 m/s impact velocity. For the tests with 0.04 m/s and 0.1 m/s impact velocities the primary fracture occurred along the same fracture surface, forming two large fragments (Figs. 7.8 and 7.13). It would, therefore, appear that the fracture surface is pre-destined, that there were some pre-existing weak planes (internal surfaces) in the weak-dense agglomerate. It seems that, for these two tests producing fracture, there is a range of strain (2.0 - 2.4%) up to which the weak-dense agglomerate can deform without fracturing. However, the agglomerate broke up at a much lower strain (0.3%) in the test with 1.0 m/s impact velocity. Additionally, the fracture surfaces in the simulations where the platen was arrested early in the failure process were slightly differently located (see Figs. 7.21, 7.23, 7.24 and 7.25). Comparing the four tests, the quantity of debris and of broken interparticle contacts (damage) at the moment of primary fracture was larger for the tests with higher impact velocities.

7.3.2 Tests Using The Same Impact Velocity: Effect Of Varying The Mass Of The Impacting Platen

Another set of simulations was carried out on the weaker dense agglomerate using the same platen impact velocity of 0.04 m/s, but varying the mass of the impacting platen.

When a falling platen having a mass of only 20 times larger ($M_p = 20\ M_a$) than that of the agglomerate was used, the agglomerate suffered no fracture. The impacting platen was arrested by the agglomerate's reaction and the platen velocity reversed at only 0.77% nominal strain. At this point 5.9% of the agglomerate's bonds were broken and a small amount of debris (2.4%), almost entirely in the form of fines, was detached close to the area where the top platen impacted the agglomerate. The results obtained were similar to the results of the 0.01 m/s impact velocity test with $M_p = 100\ M_a$ which was described in section 7.3.1. Although the maximum platen force attained was almost the same in both tests, the 0.04 m/s impact velocity test with the lighter platen developed a slightly larger average normal force. This resulted in twice the number of broken bonds (0.06 damage ratio) and the creation of some debris by the impacted pole.

A very heavy platen ($M_p = 672.6\ M_a$) produced fracture of the agglomerate directly into three large fragments (38.6%, 36.2% and 17.4% mass) at 1.68% nominal strain - as shown in Fig. 7.27 presenting the space lattice a while after fracture.

In order to simulate an impacting platen of "infinite mass" the top platen velocity was artificially maintained constant at the value of 0.04 m/s during the whole test, as in a fast diametrical compression test. In this way, therefore, the movement of the platen was not free any more, as the gravitational force and the reaction force (due to the agglomerate) could not control it. Primary fracture, consisting of the breakage of the agglomerate into two large fragments occurred at 1.9% nominal strain - see Fig. 7.28a presenting the velocity vectors of all the particles in the agglomerate just after primary fracture. If the moving (top) platen was stopped immediately after primary fracture, only a small amount of additional debris was produced and no secondary fractures occurred. If the top platen was stopped a while earlier, exactly when the platen force was a maximum, fracture did not occur.

If loading was continued, at 3.18% strain the largest fragment itself broke up into two large fragments - see Fig. 7.28b presenting the particle velocity vectors just after secondary fracture. The final product at this stage in the test was similar to the final product obtained in the test using the very heavy platen mass (Fig. 7.27). However, Fig. 7.29 presenting the space lattice at 4.76% strain indicates that the fracture planes were slightly differently located, one of them being inclined to the direction of loading.

A similar test, but with a larger constant platen velocity, of 0.1 m/s, was also carried out. It resulted in the breakage of the agglomerate into three large fragments - see Fig. 7.30 presenting the space lattice at 4.76% nominal strain. A closer examination of the figure, however, revealed that the exact locations and inclinations of the fracture surfaces were slightly different compared to the other tests.

Figure 7.31 presents the evolution of the top platen velocity during the different tests with the same 0.04 m/s impact velocity. The agglomerate managed to stop the lightest platen, but only to slow down a little the platen of mass $M_p = 100\ M_a$. The heaviest impacting platen ($M_p = 672.6\ M_a$) accelerated during the test due to the large gravitational force generated by its larger mass. Having the fastest rate of loading, primary fracture occurred the earliest in this test (with the least nominal straining prior to fracture).

In terms of fracture patterns, the effect of using a top platen of larger mass was similar to the effect of increasing the impact velocity, as described in section 7.3.1. The agglomerate either suffered only local failure at the poles for the lowest platen mass, or broke into two or three fragments for the higher platen masses. A five times increase in the mass of the platen (and thus in the impact kinetic energy) was sufficient to fracture the agglomerate in two. A further 6.7-fold increase in platen mass produced fracturing of the agglomerate directly into three large fragments. In the test in which the velocity of the top platen was maintained constant (and thus it was not influenced by the agglomerate's reaction) the fracture patterns were very similar to the ones obtained in tests with the same impact velocity and a finite platen mass in which little variation in the evolution of the platen velocity occurred during the test.

Figures 7.32 - 7.36 present the evolution of the force developed on the impacting platen, the average normal contact force, the damage and debris ratios and the total work input for the four test simulations using a top platen impact velocity of 0.04 m/s. All the figures show no significant effect on the evolution of the different parameters as a result of changing the impact kinetic energy by varying the mass of the top platen. As shown in Fig. 7.36, the evolution of the work input was very similar for each test up to the moment of primary fracture. However, in the test with $M_p = 672.6\ M_a$, the work input was lower after fracture had occurred.

7.3.3 Effect Of Interface Energy

The strong dense agglomerate "dense[1]" (see Table 7.1) was also subjected to double punch impact. It had the same solid fraction and almost the same contact density (as the

weak-dense), but a larger interface energy, of 2.0 J/m^2. Two tests were simulated with $M_p = 100\ M_a$ using impact velocities of 0.02 m/s and 0.1 m/s.

In the 0.02 m/s impact velocity test, the agglomerate fractured into two large fragments at only 0.174% agglomerate strain. The fracture surface was very close to a diametral plane - as shown in Fig. 7.37a presenting the space lattice at 1.07% strain. Figure 7.38 shows the evolution of the platen force and the top platen velocity until 1.92% strain when the test was stopped. Fracture occurred immediately after the platen force started to fall from its maximum value. If the falling platen was not stopped at fracture, the agglomerate continued to be strained until 1.92% when the impacting platen rapidly decelerated as it came to rest on the agglomerate. The continuous line in Figs. 7.39 - 7.41 illustrate the evolution of the platen force, average normal contact force, damage ratio and debris ratio. After the rapid loading period during the first 0.1% strain, the platen force (Fig. 7.39) fluctuated around 20 mN until fracture occurred when the platen force suddenly dropped to about 2 mN. The evolution of the average normal contact force, which reflects the amount of elastic energy stored, evolved in a very similar manner, as can be seen in Fig. 7.40. Figure 7.41 demonstrates that negligible amounts of damage (bond breakage) and debris were produced after fracture occurred at 0.174% strain.

For a higher impact velocity of 0.1 m/s the agglomerate fractured in a similar way as in the 0.02 m/s test (Fig. 7.37a), but at a slightly lower strain (0.146%). However, if the platen was not stopped at the primary fracture, the larger fragment subsequently broke up (at 0.173% strain) into two large fragments - see Fig. 7.37b presenting the space lattice viewed from above at 2.41% strain. Later in the test, the other fragment also fractured twice, at 3.48% strain and at 7.45% nominal strain, so that five large fragments were finally obtained (see Fig. 7.37c presenting the space lattice at 7.50% nominal straining).

A test was carried out with an impacting platen having the same mass as that of agglomerate. The impact velocity in this case was 0.2 m/s. Again the dense agglomerate broke first into two large fragments (similar to the ones in Fig. 7.37a) at 0.183% nominal strain. Secondary fracture occurred very soon after 0.191% nominal strain and was similar to the one in Fig. 7.37b. The top platen then rebounded off the agglomerate at about 0.5% strain.

It can be noted that the dense[1] agglomerate, compared to the weak-dense agglomerate, fractured at nominal strains of about ten times lower (in the range 0.14% - 0.19%). For various platen masses and impact velocities the dense[1] agglomerate initially fractured into two approximate hemispheres along almost the same fracture surface (see Fig. 7.37a). Fracturing of the dense[1] agglomerate was also cleaner, as it produced about five times less debris and about 40% less bond breakage than in the case of the weak-dense agglomerate.

Consequently, it can be concluded that increasing the interface energy increases the tendency towards brittle-elastic behaviour of dense agglomerates.

7.3.4 Effect Of Contact Density

Only one double punch impact test was carried out on the strong dense[2] agglomerate which had a significantly higher contact density (Table 7.1) than the other two dense agglomerates. For a top platen 100 times heavier than the agglomerate and an impact velocity of 0.02 m/s, primary fracture occurred directly into three approximately equal-sized large fragments at 0.098% strain - see Fig. 7.37d presenting the space lattice at 0.79% straining. Figures 7.39 - 7.41 (with dotted lines) present the evolution of platen force, average normal contact force, damage and debris ratios so that they may be compared with the results of the test on the dense[1] agglomerate with a lower contact density (shown by continuous lines). Figure 7.39 illustrates that although the loading phase was similar for both agglomerates, in the test on the agglomerate with a higher contact density unloading occurred almost immediately after loading, at about 0.1% strain. For both agglomerates, the evolution of the average normal contact force was similar to that of the platen force, Fig. 7.40. Figure 7.41 shows that the evolution of both the damage and debris ratios changed abruptly when fracture occurred for both agglomerates. In the agglomerate with the higher contact density almost twice the number of bonds had been broken and six times the amount of debris had been created by the time that fracture had occurred. The agglomerate with the more initial contacts was therefore behaving more brittle since it broke sooner and easier (with less work input) than the other agglomerate, for the same test conditions. The fact that the agglomerate with the higher contact density produced more bond breakage and generated more debris prior to primary fracture was probably mainly due to the fact that its fracture surface was 50% larger (approximately one and a half diametral planes, instead of just one).

At about 0.5% strain the damage and debris ratios for the agglomerate with the higher contact density started to increase again if the impacted platen was not arrested after fracture - see Fig. 7.41. This was partly due to the fact that the top (impacting) platen velocity in this test increased after fracture. The platen, in fact, accelerated as the three large fragments offered less resistance than the two fragments produced in the other dense agglomerate.

The three large fragments exhibited less internal damage (bond breakage) than the two large fragments obtained from the other dense agglomerate. Although the three large fragments were loaded continuously after their formation, they could not be broken even after an additional 5% strain. After the primary fracture the breaking of bonds and the debris formation occurred at the (fragments') sharp corners and at the external surface of the three fragments, along the primary fracture surfaces.

7.4 BEHAVIOUR OF THE LOOSE AGGLOMERATE IN DOUBLE IMPACT TESTS

When the loose agglomerate was impacted at 0.02 m/s velocity with a platen having a mass 100 times heavier than the agglomerate, it was found that the loose agglomerate's behaviour was very different from that obtained for the dense agglomerates. Fig. 7.42 presents the evolution of forces on the top and bottom platens. It can be observed that the forces on the platens were slowly but constantly increasing until 7.71% nominal strain when they started to level off. The maximum value attained was more than 10 times lower than the maximum platen force developed in the double impact tests on dense agglomerates (for the same impact velocity). Figure 7.43 shows the evolution of the average normal contact force and the work input, demonstrating that the amount of internally stored energy attained a maximum value which was much smaller than that obtained for the dense agglomerates impacted at the same velocity. Compared to the dense agglomerates, the loose agglomerate exhibited a plastic-ductile type of behaviour due to the fact that it could not store a notable amount of elastic energy internally. Figure 7.44 shows, in comparison, the evolution of the total number of particles in contact with the platens and the total platen force. It appears that the platen forces only increased due to the flattening of the agglomerate. Hence, the average pressure at the agglomerate-platen interfaces remained approximately constant - see Fig. 7.45 presenting the evolution of the total platen force divided by the total number of particle-platen contacts. The rate of the increase of the work inputted by the top platen (Fig. 7.43) also increased with agglomerate straining and flattening.

Figure 7.46 presents the evolution of the damage ratio and the total number of particles contained in the largest surviving cluster. Since the loose agglomerate possessed much fewer interparticle contacts from the very start, breaking a few bonds at the beginning of the test was sufficient to initiate and continue the detachment of debris from the agglomerate (Fig. 7.46). Most of the agglomerate's degradation had occurred up to 4% strain. The test was actually halted shortly after 10% strain, as the size of the largest surviving cluster tended towards an asymptotic value at this point. Up to 50% more bonds broke in the top half of the agglomerate than in the bottom half. However, breakage of bonds occurred at relatively random locations, without any concentration in the immediate vicinity of the platens.

A small amount of debris was detached from the zones adjacent to the platens at the beginning of the test. At 1.22% strain one large and three medium-sized clusters detached from the zone close to the surface of the agglomerate - see Fig. 7.47 presenting all the particles at 1.22% strain. The particles belonging to the debris are represented in black, the largest surviving cluster is coloured light grey and the three clusters that became detached are

represented in darker shades of grey. The "fracture" was a short-lived process since, after an additional 0.05% strain, the detached clusters became re-adhered to the agglomerate.

All through the test the bonds broke all over the agglomerate's volume, instead of preferring the zones adjacent to the platens, as was the case with the dense agglomerates. However, the debris could not detach randomly from all over the agglomerate's volume but, instead, it detached gradually, starting with the agglomerate's external surfaces. As in the case of the free-fall impact, the debris detachment looked like a wearing process which started from the outer shell of the agglomerate inwards, but not in an orderly manner. Fig. 7.48 presents the particles belonging to the largest surviving cluster at 9.7% nominal strain.

Until 1.22% strain the flattening of the agglomerate was not accompanied by expansion in directions perpendicular to the load, this showing that the nominal strain from the beginning of test was mainly due to the local compaction of the material adjacent to the platens. Further straining of the agglomerate produced particle rearrangements and compaction within the whole volume of the agglomerate.

7.5 DISCUSSION OF DOUBLE IMPACT TESTS

7.5.1 Dense Agglomerates

Depending on the impact kinetic energy of the top platen, the dense agglomerates were either found to survive the impact, to fracture, or to crush. The mass of the impacting platen was found to have little effect on the agglomerate failure behaviour, although it seemed to influence the way in which dense agglomerates fractured (the fracture pattern). It was actually the evolution of the platen velocity during the test (which was induced by the mass of the impacting platen, see Fig. 7.31) that produced variations in the fracture patterns (in the tests of same impact velocity).

In all the tests on dense agglomerates the top platen force increased sharply from the very beginning of the test and attained a maximum value at less than 0.2% strain. The weak-dense agglomerate generated a platen force three times lower and fractured at about 2% strain compared to the two strong dense agglomerates. For higher impact velocities which resulted in crushing, the force on the impacting platen and the average normal contact force were much higher than those induced in tests which produced fracture. Dense agglomerates were thus capable of storing more elastic energy internally for the higher impact velocities.

It is interesting that, overall, the dense[1] agglomerate suffered the lowest amount of bond breakage and debris detachment by the fracture moment. The dense[2] agglomerate had

higher debris and damage ratios by the moment of fracture because it behaved more brittle than the dense[1] agglomerate. On the other hand, the weak-dense agglomerate showed higher damage and debris ratios because they took longer to fracture (they could only fracture at 10 times larger nominal strains) than the dense[1] agglomerate.

7.5.2 Loose Agglomerates Compared To Dense Agglomerates

The loose agglomerate behaved differently under double impact tests than the dense agglomerates. The loose agglomerate did not fracture, but instead suffered a long and continuous process of crushing, up to very high nominal strains of over 10%.

The loose agglomerate presented a very slow increase in platen force in contrast with the dense agglomerates. At 0.2% nominal strain, when the top platen force was generally a maximum in the tests on dense agglomerates, the top platen force in the test on the loose agglomerate was almost zero. The platen force values started to be roughly equal for all tested (four) agglomerates only after 2% nominal strain (after the failure of the dense agglomerates).

The smallest number of broken bonds occurred in the tests on the loose agglomerate. The largest amount of bond breakage was suffered by the dense agglomerate having the largest contact density. Interparticle contacts started breaking by the platens in the dense agglomerates, whereas in the loose agglomerate bonds broke at random locations within the agglomerate from the very beginning of the test.

The transmission of load in the dense agglomerates was radial from the two loading areas - see Fig. 7.49 illustrating only the largest 16% of the compressive contact forces for the 0.02 m/s impact velocity tests on the dense[1] and dense[2] agglomerates close to the moment when the platens force attained its maximum value. Each line represents the location of a contact force and its direction. It can be observed that the load shows a tendency to be transmitted along the loaded diameter.

Since the loose agglomerate had a much lower contact density, the load was transmitted along fewer pathways. Fig. 7.50 shows the largest 10% of the compressive forces in the loose agglomerate (0.02 m/s impact velocity) at 1.22% and 7.7% nominal strain. The thickest lines represent the largest 3% of the compressive forces. At the beginning (up to about 4% nominal strain) the load was almost entirely dissipated within the loose agglomerate, as the loose agglomerate was unable to store a significant amount of elastic energy. It can be observed in Fig. 7.50a that there appears to be one zig-zag transmission path from the top to the bottom platen. As the agglomerate-platen contact areas increased with increasing strain, a few more transmission paths from the top to the bottom platen

developed. At the moment when the platen force attained its maximum value - at about 7.7% strain, see Fig. 7.50b - four almost vertical transmission paths could be observed. With further strain, more vertical transmission paths developed as the agglomerate became flattened, as might be expected in a crushing test on a cubical sample. This load transmission through several parallel paths alone suggests that the agglomerate experiences a crushing process and that fracturing of the loose agglomerate is not possible.

Crushing of both dense and loose agglomerates was a long process (requiring over 8% nominal strain) and was based on a degradation process that broke bonds all over the agglomerate. In the loose agglomerate debris was gradually detached starting from the agglomerate's external surface until the agglomerate was itself reduced to debris. For the weak-dense agglomerate, high impact velocities induced the production of debris starting from the agglomerate's impacted pole.

The results obtained in the double impact tests carried out in this project indicate that an agglomerate behaves in a more brittle manner the higher the density of its interparticle contacts, the higher the contact interface energy and the higher its solid fraction is. Increasing the impact velocity also increased the tendency towards brittle behaviour. The dense agglomerate having the largest contact density (dense[2]) fractured most rapidly and at the lowest nominal strains; it required the lowest input energy for breakage and the resulting fragments exhibited the least internal damage. On the other hand, the other dense agglomerate of 2.0 J/m^2 interface energy (dense[1]) seemed to be the "strongest", as it managed to hold the internal stored energy for longer being thus more efficient in "resisting" the applied load (in stopping the impacting platen). As in the case of the free-fall impact tests, the loose agglomerate behaved more inelastic and ductile because it could only store very low quantities of elastic energy internally.

7.6 BEHAVIOUR OF DENSE AGGLOMERATES IN DIAMETRICAL COMPRESSION TESTS

Diametrical compression tests were carried out on each of the two dense agglomerates with 2.0 J/m^2 interface energy. Half the velocity recommended in the "APPIE/G001" standard was used: 10 mm/min.

The dense agglomerate having the largest contact density (dense[2]) initially fractured into two large fragments at 0.1279% strain, while the force on the platens was suddenly dropping. Figure 7.51 presents the space lattice immediately after primary fracture, as viewed along the fracture surface and from above. The surviving bonds are represented in grey, whereas black was used for the broken bonds. The fracture surface appears to be a little inclined to the vertical direction of loading - see Fig. 7.51a. Figure 7.51b indicates that the fracture surface could be approximated as being formed of two half diametral planes. There was a 30% difference in the mass of the large fragments. Figure 7.52 only presents the broken bonds immediately after primary fracture. The figure indicates that, of all the bonds broken, most of them broke along the fracture surface; only a few were broken adjacent to the platens and almost none broke inside the large fragments formed by the primary fracture. An almost equal number of contacts broke in the agglomerate's top half as in its bottom half. Figure 7.53 presents all the particles just after the primary fracture, black being used for the particles belonging to the debris. It can be seen that only a small amount of debris was formed and that half of it was detached from along the fracture surface. All the particle velocity vectors viewed from above at the moment of primary fracture are shown in Fig. 7.54 from which the two large fragments are easily distinguished.

If the test was not halted immediately after the forces on the platens had reached their maximum value a secondary fracture occurred. Very shortly after the primary fracture a medium-sized fragment broke off the largest fragment at 0.1282% strain - see Fig. 7.55 presenting all the particle velocity vectors at the moment of secondary fracture. It is most probable that, in a laboratory test, the secondary fracture would have been considered as part of the primary fracture, as it would be very difficult to distinguish the secondary fracture from the primary one.

The force on each of the two platens evolved in an almost identical manner - see Fig. 7.56 showing the evolution of the force on the top and bottom platens. Figure 7.57 illustrates the evolution of the total force on the platens and the damage ratio. The platen force increased almost linearly with strain up to a maximum value from which it dropped almost instantly. As the platen force dropped there was a sudden increase in the damage ratio. In terms of damage ratio, primary fracture occurred before it attained its maximum value of 0.135, at a

value of about 0.09. The form of the platen force evolution (presenting the sudden drop at fracture) and the fact that the fracture strain was relatively low suggests brittle behaviour characteristics. The sudden jump in the damage ratio evolution indicates that fracture was rapid.

Figure 7.58 illustrates the evolution of the debris ratio and the kinetic energy of the agglomerate. Immediately after the moment of primary fracture the debris ratio attained a maximum of 4%. However, over half of this very small quantity of debris (which was produced suddenly at primary fracture) re-adhered to the large fragments within a further 0.01% strain. The agglomerate kinetic energy was very low during the test but suddenly increased by an order of magnitude when fracture occurred. This indicates that fracture in the diametrical compression test was dynamic. Figure 7.58 also shows that the sudden peak in the kinetic energy was associated with the sudden development of debris. The remaining debris immediately after the primary fracture represented a mere 1.4% of the initial mass of the agglomerate. The very small fracture strain, and the low levels of damage (breaking 9% of the initial number of bonds was sufficient to induce fracture) and the debris produced suggest brittle elastic behaviour.

The fact that two thirds of the debris detached at fracture re-adhered was also reflected by the fact that 3% of the broken bonds reformed. One of the two causes for re-adhering was that most of the debris produced at fracture was not ejected at very high velocities from the fractured agglomerate. Instead, most of the debris was located along the fracture surface, between the large fragments formed - this making their re-adhering to the two large fragments almost inevitable. On the other hand, a proportion of the debris detached at the agglomerate-platen interfaces re-adhered due to the continued straining of the sample. A more detailed analysis of the fracture process in this diametrical compression test is reported in Chapter 8.

The dense agglomerate having a lower contact density but same interface energy and porosity (dense[1]) was also tested in diametrical compression. Its behaviour during the test was found to be more or less similar to that described above. Several differences were, however, noted. The two images in Fig. 7.59 present the space lattice just after the primary fracture, as viewed along the fracture surface and from above. Grey is used for the surviving bonds, whereas the broken bonds are represented in black. Figure 7.59a is roughly similar to Fig. 7.51a, except that the fracture surface is orthogonal to the platens. The agglomerate broke up into approximately two hemispheres. The fracture surface's location was very similar to the primary fracture surface obtained in the double impact test on the same agglomerate - see Fig. 7.37a. Compared to the agglomerate of higher contact density, 20% less bonds were broken in this test and 12% less mass of debris was formed.

Primary fracture occurred at a larger strain, of 0.298%, which was 2.33 times larger than in the other diametrical compression test. This agglomerate therefore appears to be "stronger" than the one with the higher contact density since it was capable of storing elastic energy internally for longer. If the top platen was not arrested after fracture and the straining was continued to 0.38%, no secondary fracture occurred but the damage of the two large fragments continued. More details of this test are presented in Chapter 9, where the behaviour is presented in comparison to the behaviour of the same agglomerate subjected to free-fall impact and double punch impact.

7.7 BEHAVIOUR OF THE LOOSE AGGLOMERATE IN DIAMETRICAL COMPRESSION TESTS

A diametrical compression simulation up to 0.5% strain was carried out on the loose agglomerate using a top platen velocity of 20 mm/min. Apart for the slight flattening under the platens, the test induced almost no change in the agglomerate's initial state. The agglomerate only deformed locally adjacent to the platens. Very little damage (bond breakage) occurred and, moreover, this took place at random locations within agglomerate. Very few debris particles were detached - adjacent to the agglomerate-platen interface. Compared to the dense agglomerates, an interesting phenomenon was observed with the loose agglomerate: the amount of bond breakage was almost compensated for by the amount of newly-formed bonds.

From the results of the first diametrical compression test on the loose agglomerate it was realised that much larger strains than 0.5% were required for producing the general failure of this agglomerate. The problem was that a simulation up to, for example, 5% strain would take about a year to perform with the same platen velocity (strain-rate) as used for the dense agglomerate. To reduce the simulation time, a velocity of 180 mm/min had to be used.

Although the test was carried out up to 7.3% nominal strain, the loose agglomerate could not be fractured. The image in Fig. 7.60 shows the agglomerate at the end of the simulation, viewed from the front. The particles belonging to the fines are represented in black, whereas the clusters are indicated by two shades of grey: the darker one for the small clusters (other than fines) and the lighter one for the largest surviving cluster. The largest surviving cluster is also presented in Fig. 7.61. Debris was detached at apparently random locations from the surface of the agglomerate. This corresponds to the dispersed nature of bond breakage, reflected by the image in Fig. 7.62 representing the space lattice at the end of the simulation (black indicating the broken bonds). After about 3% strain the newly-formed bonds outnumbered the number of broken bonds. The formation of new bonds appeared to occur

at random locations within the agglomerate. By the end of the test the number of bonds broken was almost half the number of newly-formed bonds.

Figure 7.63 presents the evolution of the force developed on the top and bottom platens. It is noted that, although the forces fluctuated, the force evolution on both the top and bottom platens was almost identical - this indicating that the test could be considered to be "quasi-static". Figure 7.64 illustrates that the evolution of the platen force correlates with the number of particles in contact with the platens in a manner similar to that observed in the double impact test on the loose agglomerate using an impact velocity of 0.02 m/s (Fig. 7.44). This indicates that the behaviour of the loose agglomerate is almost insensitive to the top platen velocity (strain-rate). Figure 7.65 presents the evolution of the average normal contact force and average pressure on the platens. As in the case of the double impact test, the evolution of the elastic stored energy followed the evolution of the platen force. However, the maximum attained average normal contact force was about 10.5 μN (attained at about 6.7% strain, Fig. 7.65), which was 34.6% larger than the maximum attained average normal contact force obtained in the double impact test (7.8 mN, attained at about 7.6% strain, Fig. 7.43). It can, therefore, be concluded that the loose agglomerate was capable of storing almost 34.6% more energy in the diametrical compression test. After 3% strain the average pressure on the platens started to fluctuate around a constant value, which was about twice as large compared to the one developed in the double impact test (Fig. 7.45). The evolution of the number of particles in the largest surviving cluster and of the work input are shown in Fig. 7.66. At the beginning of the test (up to 0.7%) the agglomerate flattened with very little damage and debris. The diametrical compression tests produced less debris but required more work input for the same strain than the double impact test (compare Fig. 7.66 with Figs 7.43 and 7.46).

The location of the largest 13.8% compressive contact forces when the platen force was a maximum value (at 6.8% nominal strain) is illustrated in Fig. 7.67. The figure is similar to the one obtained in the double impact test on the loose agglomerate (Fig. 7.50b) in that it shows that there are a few continuous load transmission paths between one platen and the other. The load transmission patterns shown correspond to a stage when the agglomerate is significantly flattened and indicates that the loose agglomerate would not fracture, even at large strains but, instead, it would slowly be crushed.

7.8 DISCUSSION FOR DIAMETRICAL COMPRESSION TESTS

7.8.1 Dense Agglomerates

Both dense agglomerates initially fractured into two large fragments and exhibited brittle-elastic behaviour (they fractured at less than 0.3% strain with very low levels of damage and debris ratios). The values of the maximum attained platen force and the maximum attained average normal contact force were almost the same for both dense agglomerates. Having higher contact density, the dense[2] agglomerate behaved more brittle and elastic than the dense[1] agglomerate also in diametrical compression tests. The almost linear increase of the platen force and its subsequent sudden drop at primary fracture (Fig. 7.56) reflected a unique behaviour among all the diametrical compression and impact simulations carried out. Although fracture in the dense[2] agglomerate necessitated a 33% larger damage ratio than dense [1] agglomerate, it occurred at a much lower (2.3 times lower) nominal strain and it consumed much less (almost 3 times less) work input.

7.8.2 Loose Agglomerates Compared To Dense Agglomerates

Not surprisingly, similar as in the impact tests, the loose agglomerates exhibited highly ductile-plastic behaviour also in the diametrical compression test. Loose agglomerates were again very efficient in dissipating energy - resulting in irreversible displacements of particles (and thus plastic deformation of agglomerate) - and very ineffective in storing elastic energy. While the dense agglomerates fractured, the loose agglomerate experienced a very long process of crushing. Strains well over 7.3% would, however, have been needed for complete crushing of the loose agglomerate.

Although the platen force and the average normal contact forces exhibited much lower values than the ones found in dense agglomerates, they varied more with the rate of loading. For a nine times decrease in the top platen velocity, the loose agglomerate exhibited twice the value of platen force and average normal contact force at the same strain level of 0.5%. Common to the behaviour of both loose and dense agglomerates under diametrical compression were the low levels of bond breakage and debris detachment - compared to free-fall impact and double impact tests. However, whereas debris was detached mainly adjacent to the platens and along the fracture surface in the tests on the dense agglomerates, for the loose agglomerates debris was detached in an almost random manner from the external surface of the agglomerate.

7.9 COMPARISONS BETWEEN THE RESULTS OBTAINED IN SIMULATIONS AND LABORATORY TESTING

As with the free-fall impact tests, very good agreement with the laboratory tests reported in the literature was also found for diametrical compression and double impact test simulations. Similar to the experiments, the dense agglomerates fractured almost along meridional planes, whereas the loose agglomerates did not fracture but crushed at very high nominal strains (and exhibited highly ductile-plastic behaviour).

7.9.1 Double Impact Tests

The simulation results of agglomerate fracture in double impact tests on dense agglomerates agree well with the results obtained by Arbiter et al (1969) in their tests on sand-cement agglomerates. As in their published paper, the failure of dense agglomerates in double impact test simulations initiated at the agglomerate-platen interfaces, where shear and compressive stresses broke bonds and compacted the material - see Fig. 7.68 presenting a typical space lattice of a dense agglomerate a while before fracture (in black are represented the broken bonds). As pointed out by Arbiter et al (1969), the plastic zones formed by the platens in the double impact test were very similar to the plastic zone created in the free-fall impact test at the impacted pole and were roughly conical in shape. Arbiter et al (1969) did not, however, mention that, above a certain impact velocity, more damage and debris was produced at the top impacting platen than at the bottom stationary platen - see section 7.3. This was due to the local effect of dynamic loading: local plastic (irreversible) deformation was higher by the impacted pole, as some of this deformation developed before the load had time to transmit to the other (stationary) platen.

Considering primary fractures, dense agglomerates broke up into large fragments only along approximately meridional planes - same as the agglomerates tested by Arbiter et al (1969). The two or three large fragments observed in the simulations also had the appearance of spherical wedges (orange segments) - as did the fragments obtained by Arbiter et al (1969) from double impact tests.

Apart from the work of Arbiter et al (1969), no other detailed reports of laboratory double impact tests were found in the literature. However, Arbiter et al (1969) also postulated that double impact tests induced similar stress fields as diametrical compression tests and, therefore, both produced very similar end results. Their suggestion is supported by the results of this project. Firstly, comparing diametrical compression tests with double impact tests of similar impact velocity it was found that the end results are roughly similar - see section 7.3. Secondly, all the fracture patterns obtained in the simulated double impact tests

agree well with the ones obtained in laboratory diametrical compression tests on spherical samples of different material compositions.

7.7.2 Diametrical Compression Tests

The diametrical compression test simulation results agree best with the results and comments published by Arbiter et al (1969), Salman et al (1994), Kapur and Fuerstenau (1967), Wynnyckyj (1985) and Newitt and Conway-Jones (1958), and with the results obtained by Meyers and Meyers (1984), Breval et al (1987) and Tanaka et al (1985) in their laboratory tests.

Figure 7.69 presents three schematic mechanisms of fracture in diametrical compression tests inferred from laboratory testing of agglomerates. The results of the diametrical compression test simulations indicate that, in dense agglomerates, failure is initiated from the agglomerate-platen interfaces, as in both types of impact tests. The local plastic deformation adjacent to the platens is the first phase of the general failure process of agglomerates. Almost all laboratory test reports on spherical samples subjected to diametrical compression noted at least a little plastic deformation at the platen-sample interfaces before failure (see Chapter 3). However, even for agglomerates, most of the workers believed that, in diametrical compression tests, failure initiates at the centre of the sample where tensile stresses are expected (from theoretical analysis) to have the largest values - see, for example, the mechanism inferred by Meyers and Meyers (1984) for iron-ore pellets, presented in Fig. 7.69c. Consequently these many workers carried out diametrical compression tests in order to use the fracture strain for determining the agglomerate's *tensile* strength.

Compared to the dynamic tests, in slow diametrical compression tests the load had sufficient time to transmit into the agglomerate from the loaded areas. However, this did not prevent fracture from initiating from the platen regions in the tests simulated in this project - as also inferred by Newitt and Conway-Jones (1958), Arbiter et al (1969), Salman et al (1994), Kapur and Fuerstenau (1967), Wynnyckyj (1985), Ghadiri et al (1990) and Tanaka et al (1985) from their laboratory tests. The two plastic deformation zones created near the platens in the simulated tests were similar to the ones formed in double impact simulations, but smaller (see Figs. 5.51a and 7.59a). As in most laboratory tests, their shape was almost conical. Pushing the local deformation zones into the agglomerate seemed to be the "driving force" of fracture - as also inferred by several workers, including Kapur and Fuerstenau (1967) and Wynnyckyj (1985), see schemes in Figs. 7.69a and 7.69b.

As in the double impact and free-fall impact test simulations, the fracture of the dense agglomerates in the simulated diametrical compression tests was initiated at the start of unloading. The dense agglomerates simulated in this thesis behaved as most spherical

samples tested in the laboratory, in that they usually fractured into two or three large fragments. Primary fracture occurred in approximately two hemispheres for both dense agglomerates, same as was described in the majority of reports on diametrical compression of spherical samples. The photographs in Fig. 7.70 present actual fractures of agglomerates obtained in laboratory tests by Newitt and Conway-Jones (1958) on sand and silt agglomerates, Kapur and Fuerstenau (1967) on limestone pellets, Meyers and Meyers (1984) on iron-ore pellets, and Wynnyckyj (1985) on magnetite and hematite pellets. Very soon after the primary fracture, the dense agglomerate having the largest contact density exhibited secondary fracture, and therefore finally resulted in three large fragments. This is consistent with the presumption of Salman et al (1994) who concluded that fracture in over two large fragments could be a sign of secondary fracture occurring due to the continuation of loading the two large fragments produced by the primary fracture.

Similar fracture patterns with the ones obtained in the simulations were also described by Arbiter et al (1969) on sand-cement agglomerates, Salman et al (1994) on aluminium-oxide agglomerates, Breval et al (1987) on proppants and sand spheres, Rogowski et al (1968) on air-dry soil spheres, Wong et al (1987) on ceramic spheres, Verall (1976) on glass-reinforced spheres, Ghadiri et al (1990) on ionic KCl, NaCl and MgO samples and Shipway and Hutchings on glass spheres.

Compared to the dynamic (impact) tests simulated, fracture of the dense[2] agglomerate occurred the most suddenly, after a steep and almost steady (linear) loading stage (Fig. 7.56), very similar to the corresponding data published for agglomerates and other spherical samples by Breval et al (1987), Kapur and Fuerstenau (1967), Arbiter et al (1969), Wong et al (1987) - shown in Fig. 7.71 - and also by Rogowski et al (1968), Kendall and Weihs (1992), Brecker (1974) and other workers. A few of the published load evolution curves (see for example the one for green pellets in Fig. 7.71d) are similar to the evolution of the platen force in the diametrical compression of the dense[1] agglomerate (shown in Chapter 9) and in the double impact simulations of all the dense agglomerates.

The nominal strain at fracture for the dense agglomerates tested in this project - under 0.3% - best agree with the fracture strain of 0.5% reported by Kapur and Fuerstenau (1967) for one of their 20 mm diameter limestone pellets (having a mean constituent particle size of 30 μm). Other reported experimental fracture strains of agglomerates - 1.2% Arbiter et al (1969), 4-15% Wynnyckyj (1985) and Rogowski et al (1968), 5% Newitt and Conway-Jones (1958), 7.1% Kendall and Weihs (1992) - were higher than the ones obtained for the dense agglomerates. This was mainly a consequence of the higher solid fraction (0.653) and bond strength (2.0 J/m2 interface energy) of the dense agglomerates simulated in this project.

PROPERTY	Agglomerate type			
	dense			loose
	weak-dense	dense[1]	dense[2]	
mean agglomerate diameter (mm)	1.113	1.113	1.046	1.170
average particle diameter (μm)	58.54	58.54	54.95	54.95
solid fraction Φ	0.6530	0.6530	0.6525	0.4364
number of initial bonds	9641	9758	11293	4009
apparent coordination number Z_a	4.892	4.879	5.647	2.004
mechanical coordination number Z_m	4.877	4.927	5.647	2.590

Table 7.1 Structural characteristics of the agglomerates used

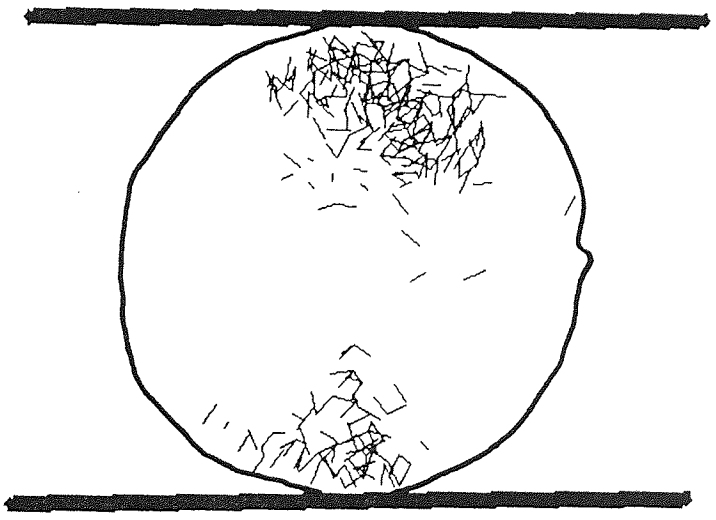

Fig. 7.1 Space lattice at the end of the double impact test, view from front showing broken bonds only, weak-dense agglomerate (Γ=0.4 J/m^2, V=0.01 m/s, M_p = 100 M_a)

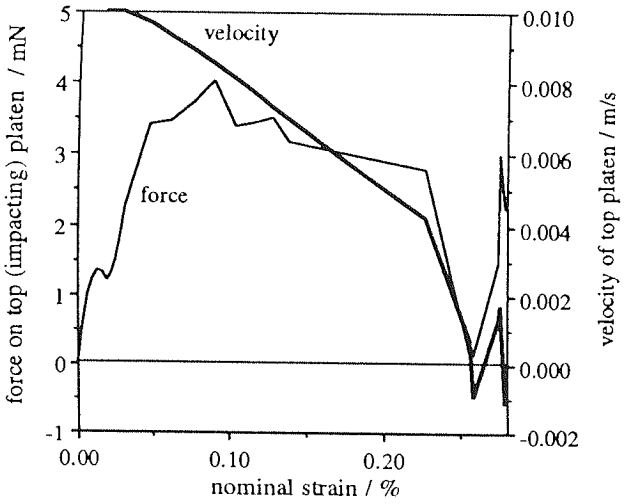

Fig. 7.2 Evolution of top platen velocity and force on top (impacting) platen, weak-dense agglomerates (Γ=0.4 J/m ^{2}, V=0.01 m/s, M_p=100 M_a)

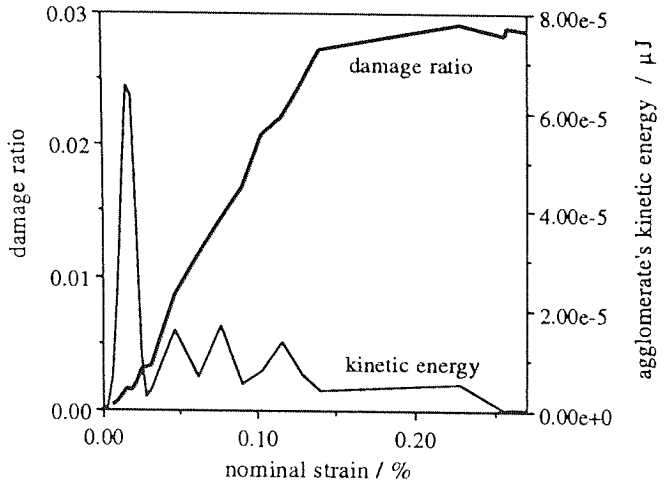

Fig. 7.3 Evolution of damage ratio and agglomerate's kinetic energy, weak-dense agglomerate (Γ=0.4 J/m ^{2}, V=0.01 m/s, M_p=100 M_a)

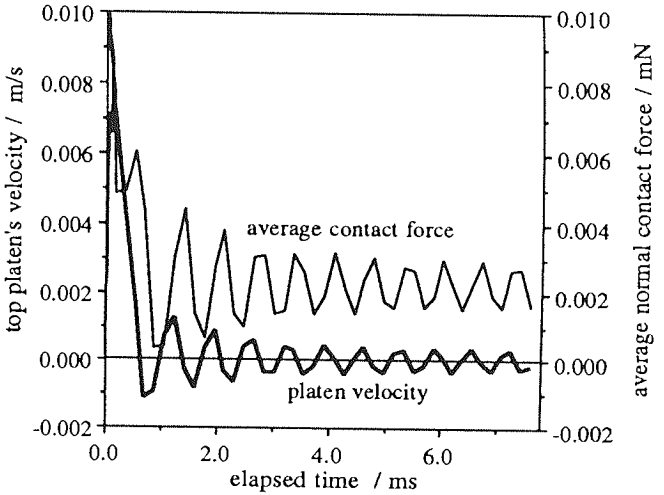

Fig. 7.4 Evolution of platen velocity and average normal contact force, weak-dense agglomerate (Γ=0.4 J/m ^{2}, V=0.01 m/s, M_p=100 M_a)

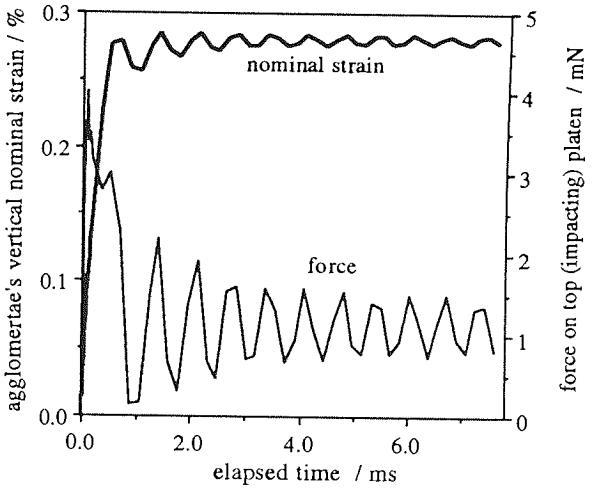

Fig. 7.5 Evolution of nominal strain and force on top (impacting) platen, weak-dense agglomerate (Γ=0.4 J/m ^{2}, V=0.01 m/s, M_p= 100 M_a)

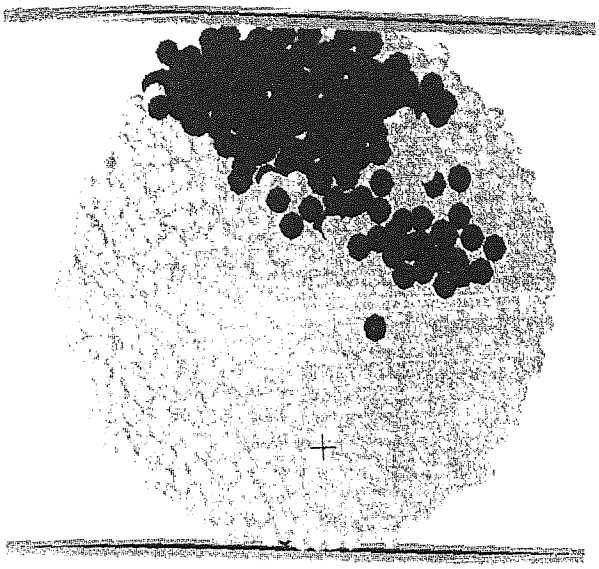

Fig. 7.6 Particle configuration at primary fracture in a view approximately along the fracture surface (surviving cluster particles are shown in grey, particles in debris are shown in black), weak-dense agglomerate (Γ=0.4 J/m^2, V=0.04 m/s, M_p = 100 M_a)

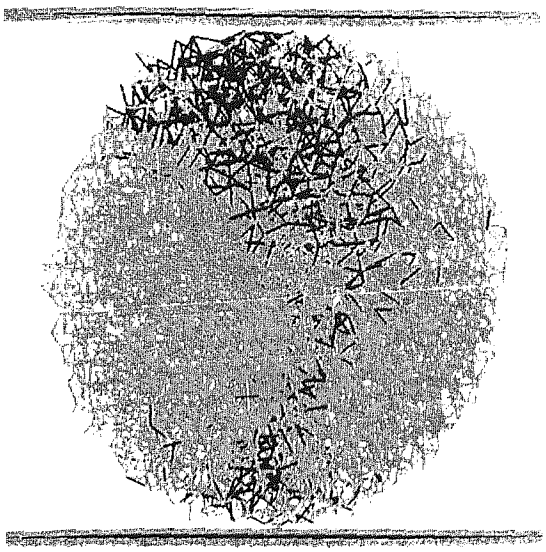

Fig. 7.7 Space lattice at primary fracture in a view approximately along the fracture surface (existing bonds are shown in grey, broken bonds are shown in black), weak-dense agglomerate (Γ=0.4 J/m^2, V=0.04 m/s, M_p = 100 M_a)

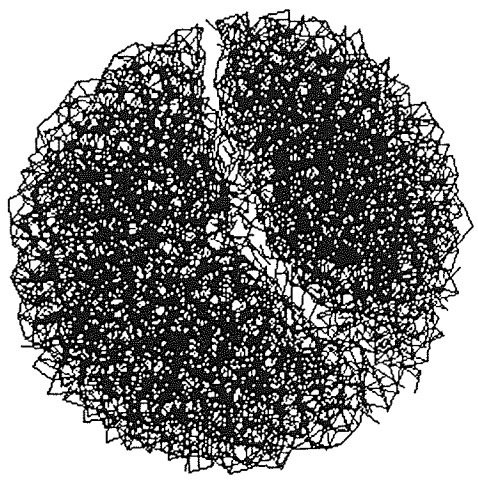

Fig. 7.8 Space lattice at 4.22% strain showing the existing bonds only, view from above, weak-dense agglomerate (Γ=0.4 J/m^2, V=0.04 m/s, M_p = 100 M_a)

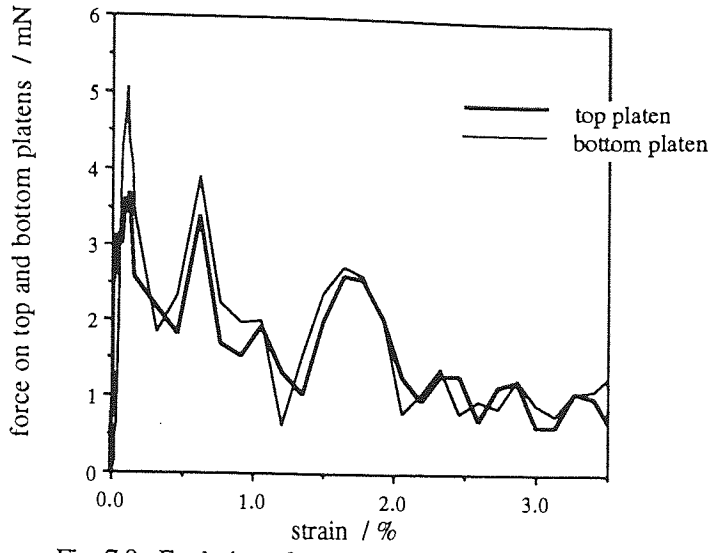

Fig. 7.9 Evolution of platen forces, weak-dense agglomerate (Γ=0.4 J/m^2, V=0.04 m/s, M_p =100 M_a)

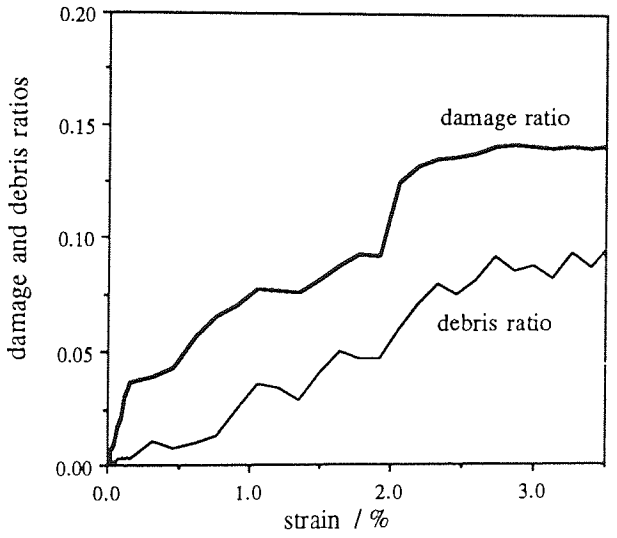

Fig. 7.10 Evolution of damage and debris ratios, weak-dense agglomerate (Γ=0.4 J/m^2 , V=0.04 m/s, M_p =100 M_a)

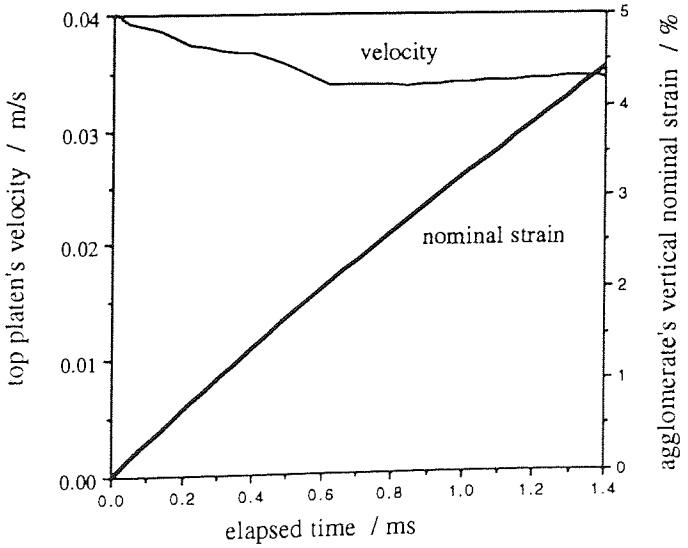

Fig. 7.11 Evolution of diametrical nominal strain and platen velocity, weak-dense agglomerate (Γ=0.4 J/m^2 , V=0.04 m/s, M_p =100 M_a)

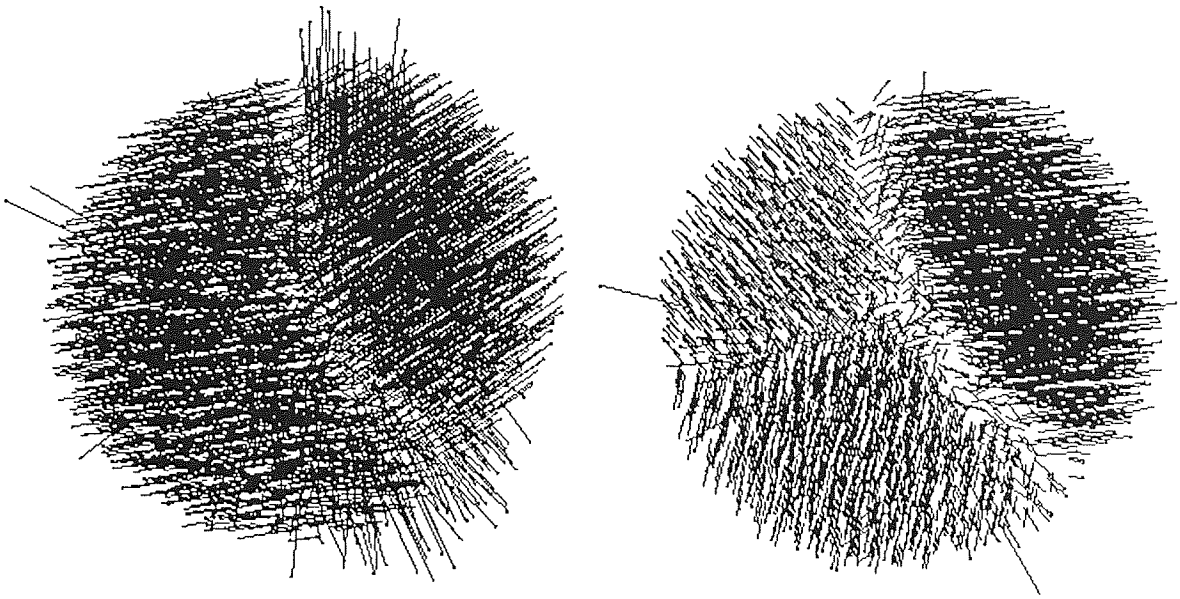

(a) at the moment of primary fracture (2.3% nominal strain)

(b) at the moment of secondary fracture (6.6% nominal strain)

Fig. 7.12 Particle velocity field viewed from above, weak-dense agglomerate (Γ=0.4 J/m^2, V=0.1 m/s, M_p = 100 M_a)

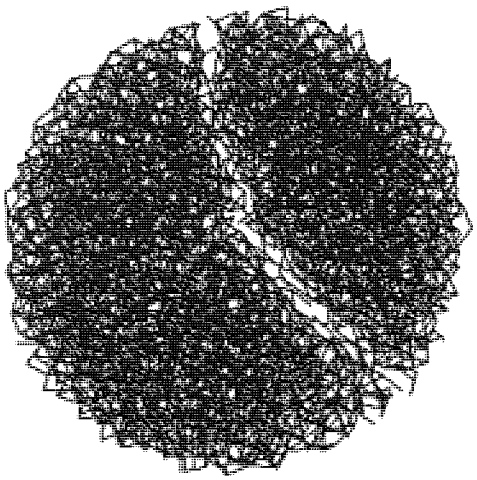

Fig. 7.13 Space lattice at 4.53% strain showing the existing bonds only, view from above, weak-dense agglomerate (Γ=0.4 J/m^2, V=0.1 m/s, M_p = 100 M_a)

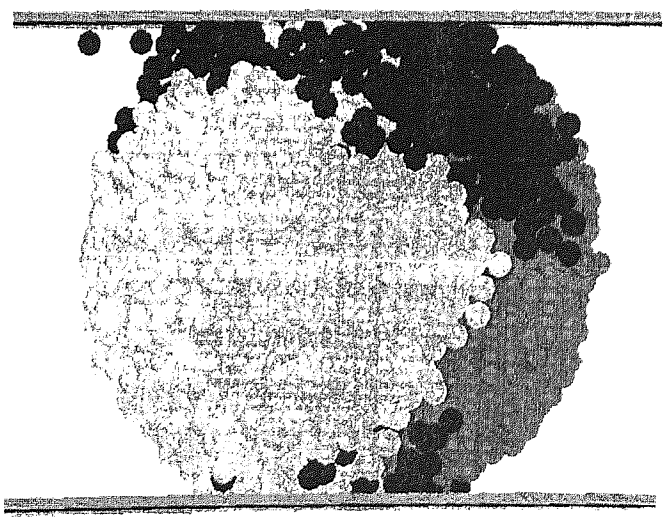

Fig. 7.14 Particle configuration at the end of test, 8.72% strain (surviving cluster particles shown in shades of grey, particles in debris shown in black), weak-dense agglomerate (Γ=0.4 J/m^2, V=0.1 m/s, M_p = 100 M_a)

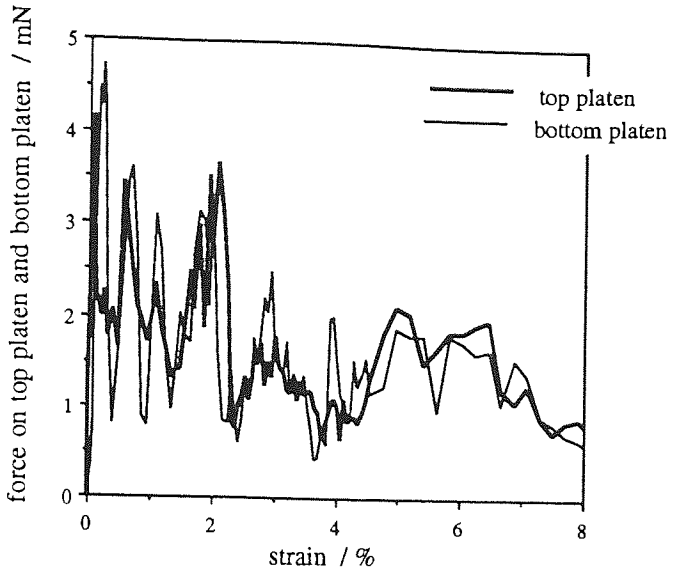

Fig. 7.15 Evolution of platen forces, weak-dense agglomerate, (Γ=0.4 J/m^2 , V=0.1 m/s, M_p =100 M_a)

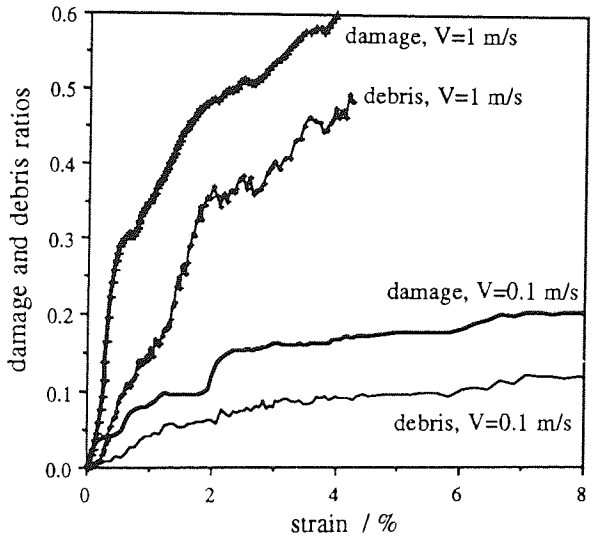

Fig. 7.16 Evolution of debris and damage ratios, V=0.1 m/s and V=1 m/s, weak-dense agglomerate (Γ=0.4 J/m^2 , M_p =100 M_a)

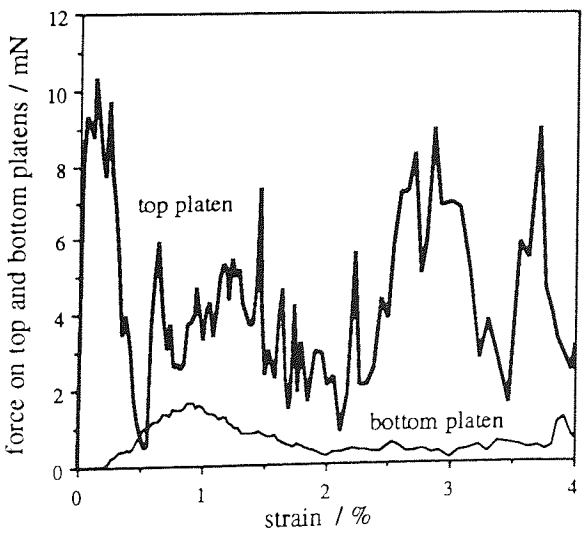

Fig. 7.18 Evolution of forces on top and bottom platens, weak-dense agglomerate (Γ=0.4 J/m^2 , V=1.0 m/s, M_p =100 M_a)

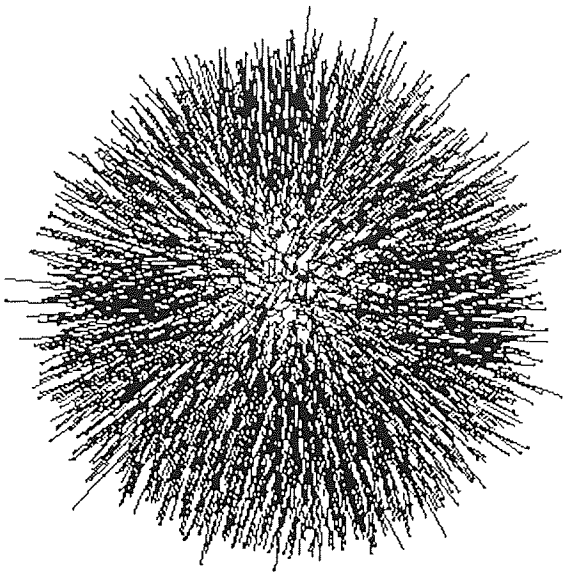

Fig. 7.17 Particle velocity field viewed from above, end of the test (9% strain), weak-dense agglomerate (Γ=0.4 J/m^2, V=1 m/s, M_p = 100 M_a)

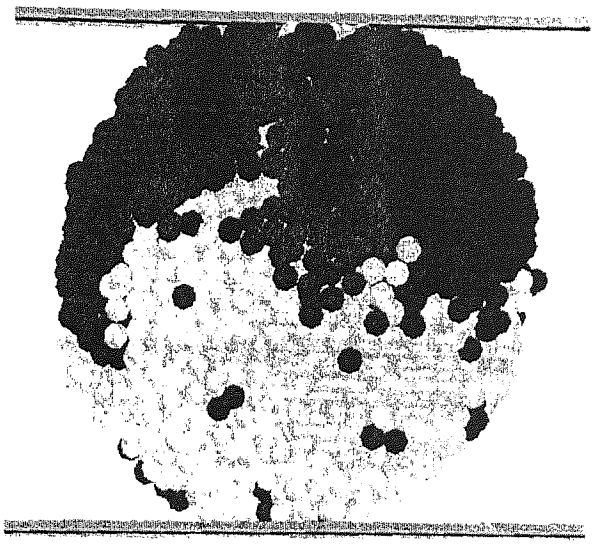

Fig. 7.19 Particle configuration at 4.3% strain (surviving cluster particles shown in grey, particles in debris shown in black), weak-dense agglomerate (Γ=0.4 J/m^2, V=1 m/s, M_p = 100 M_a)

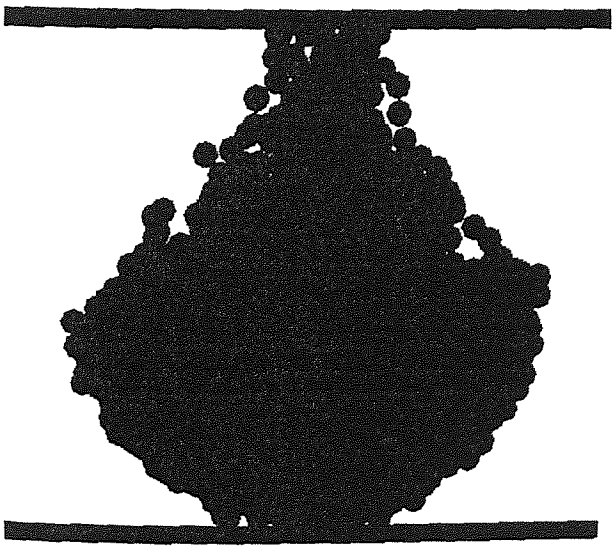

Fig. 7.20 The largest surviving cluster at 4.3% strain, weak-dense agglomerate (Γ=0.4 J/m^2, V=1 m/s, M_p = 100 M_a)

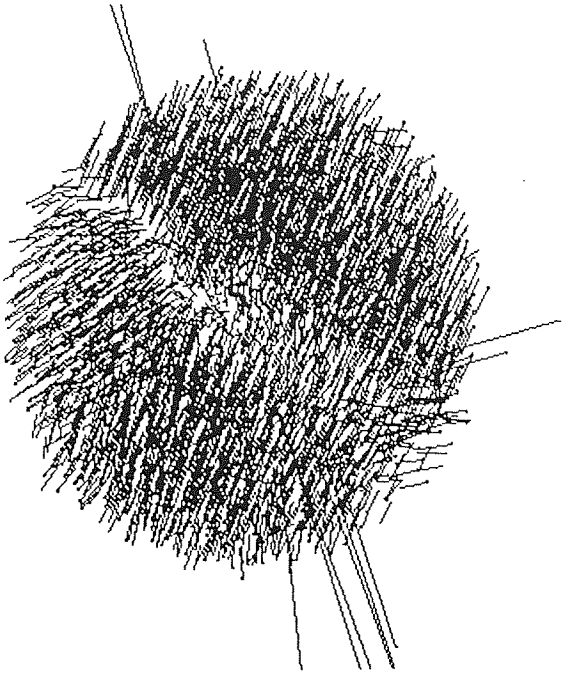

Fig. 7.21 Particle velocity field (not showing most of the debris) viewed from above, a while after the platen was arrested at 0.27% strain, weak-dense agglomerate (Γ=0.4 J/m^2, V=1 m/s, M_p = 100 M_a)

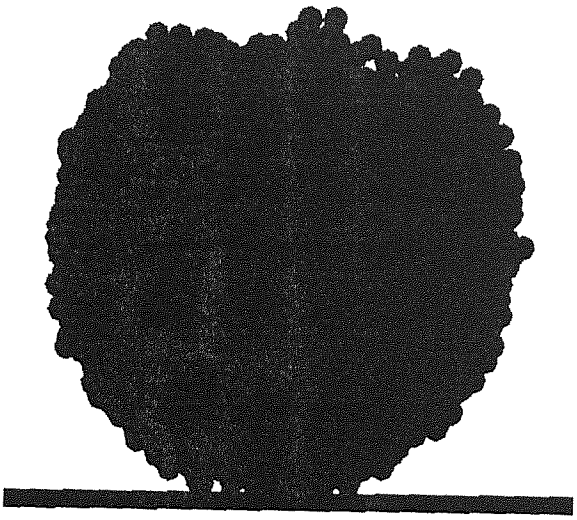

Fig. 7.22 The particles in the largest surviving cluster a while after the platen was arrested at 0.27% strain, weak-dense agglomerate (Γ=0.4 J/m^2, V=1 m/s, M_p = 100 M_a)

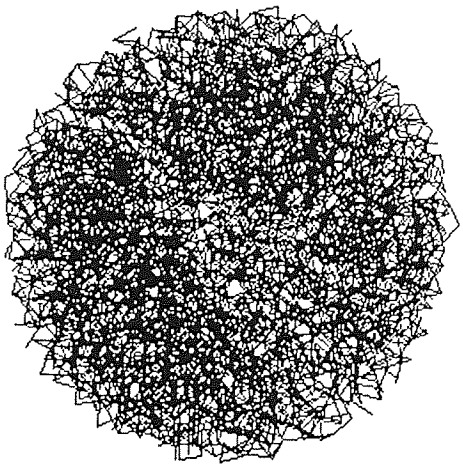

Fig. 7.23 Space lattice (showing the existing bonds only) a while after top platen was arrested at 0.27% strain, view from above, weak-dense agglomerate (Γ=0.4 J/m^2, V=1 m/s, M_p = 100 M_a)

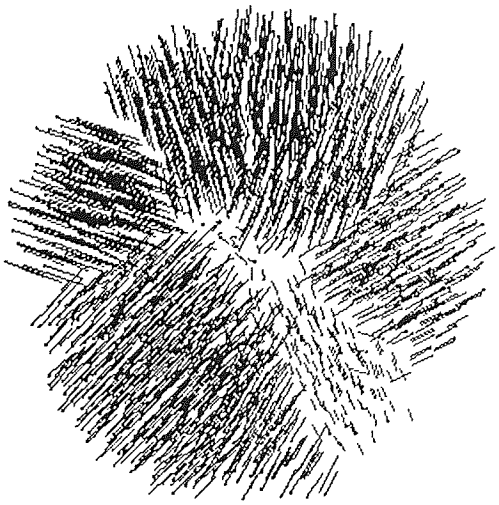

Fig. 7.24 Particle velocity field (not showing debris) viewed from above, a while after the platen was arrested at 1.59% strain, weak-dense agglomerate (Γ=0.4 J/m^2, V=1 m/s, M_p = 100 M_a)

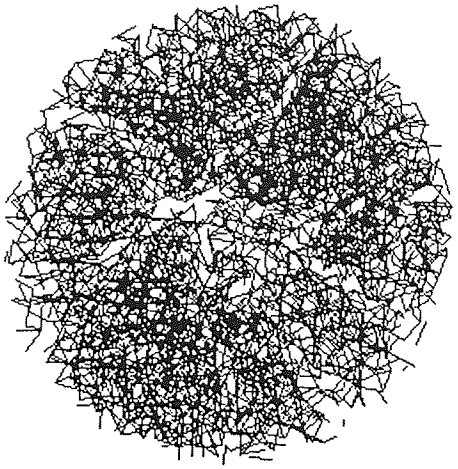

Fig. 7.25 Space lattice (showing the existing bonds only) a while after top platen was arrested at 1.59% strain, view from above, weak-dense agglomerate (Γ=0.4 J/m^2, V=1 m/s, M_p=100 M_a)

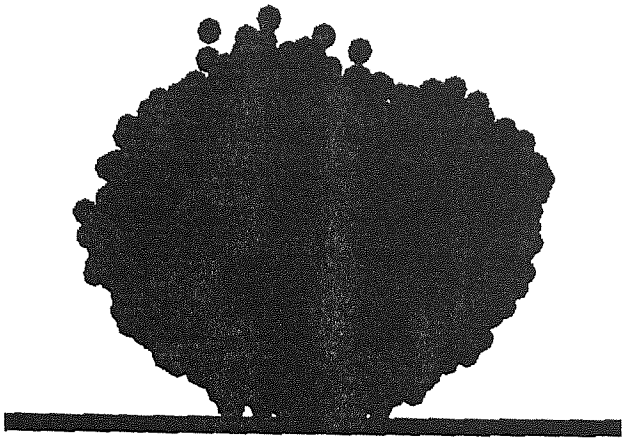

Fig. 7.26 The particles in the largest surviving cluster a while after the platen was arrested at 1.59% strain, weak-dense agglomerate (Γ=0.4 J/m^2, V=1 m/s, M_p=100 M_a)

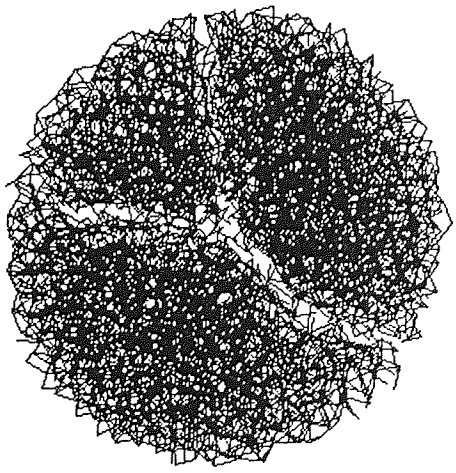

Fig. 7.27 Space lattice at 3.43% strain showing the existing bonds only, view from above, weak-dense agglomerate (Γ=0.4 J/m^2, V=0.04 m/s, M_p=672.6 M_a)

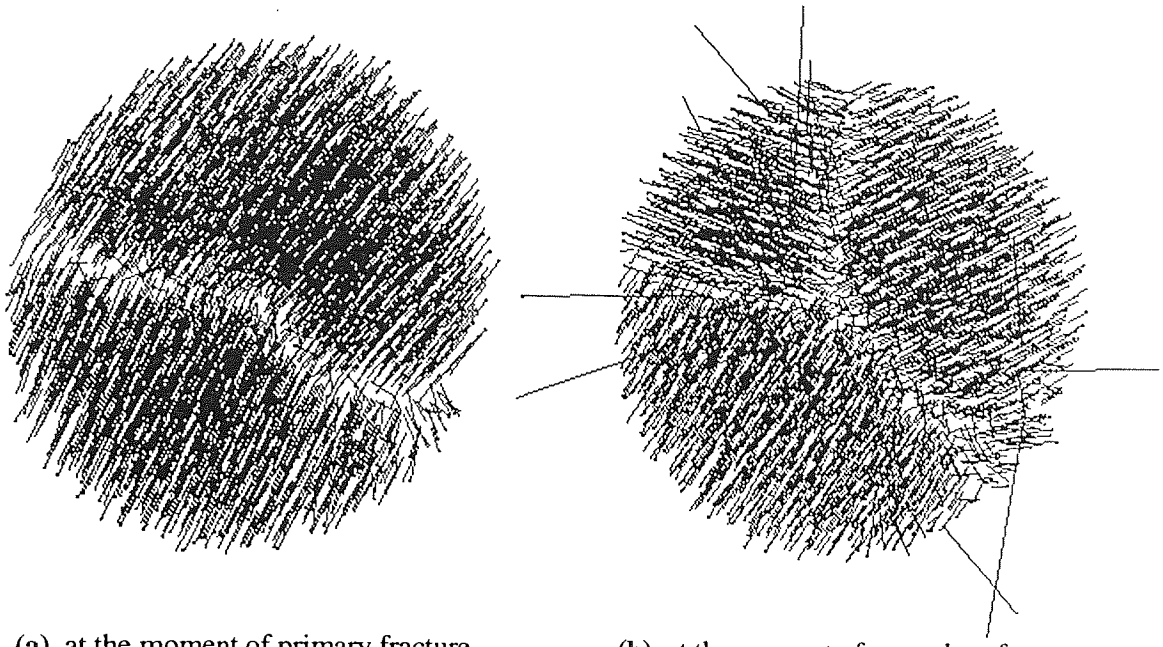

(a) at the moment of primary fracture, not showing debris (1.9% strain)

(b) at the moment of secondary fracture (3.18% strain)

Fig. 7.28 Particle velocity field viewed from above in the test where the velocity of the top platen was maintained constant at V=0.04 m/s, weak-dense agglomerate (Γ=0.4 J/m^2, "infinite" platen mass)

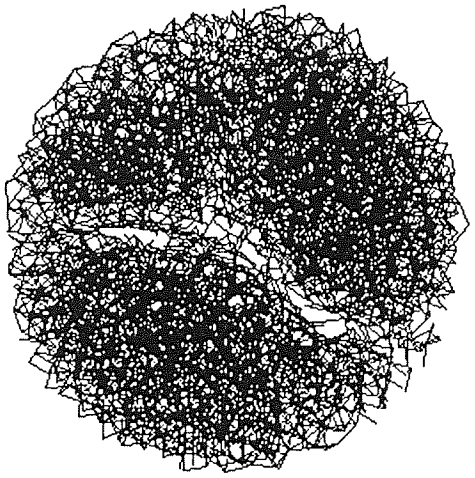

Fig. 7.29 Space lattice at 4.76% strain showing only the existing bonds in the test where the velocity of the top platen was maintained constant at 0.04 m/s, view from above, weak-dense agglomerate (Γ=0.4 J/m^2, "infinite" platen mass)

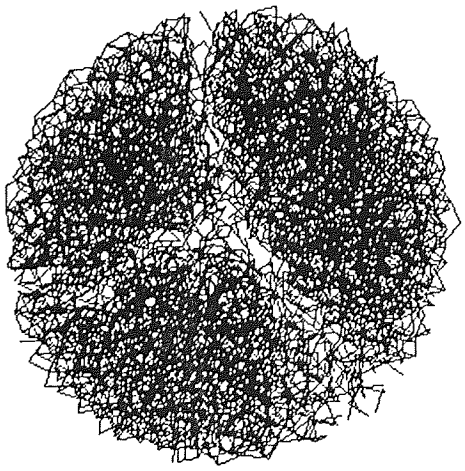

Fig. 7.30 Space lattice at 4.76% strain showing only the existing bonds in the test where the velocity of the top platen was maintained constant at 0.1 m/s, view from above, weak-dense agglomerate (Γ=0.4 J/m^2, "infinite" platen mass)

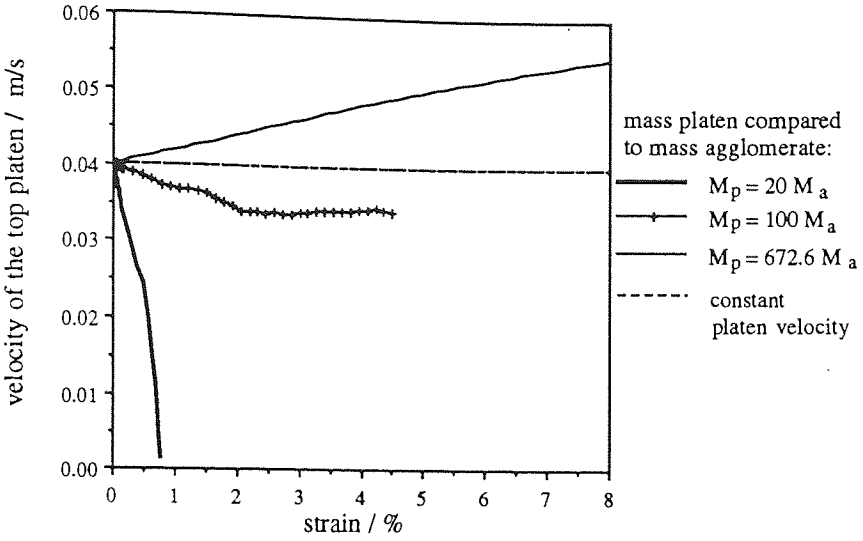

Fig. 7.31 Evolution of top platen velocity in four different tests (Γ=0.4 J/m^2 , V=0.04 m/s)

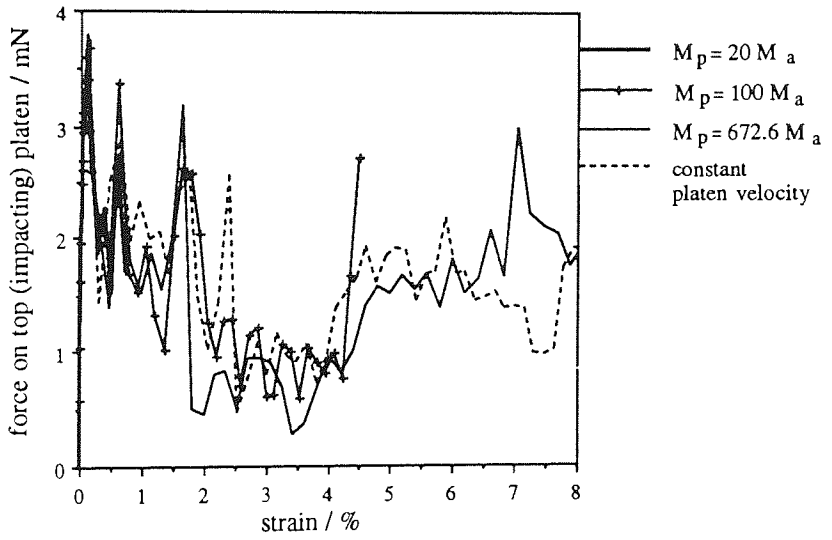

Fig. 7.32 Evolution of force on top platen in four different tests (Γ=0.04 J/m^2, V=0.04 m/s)

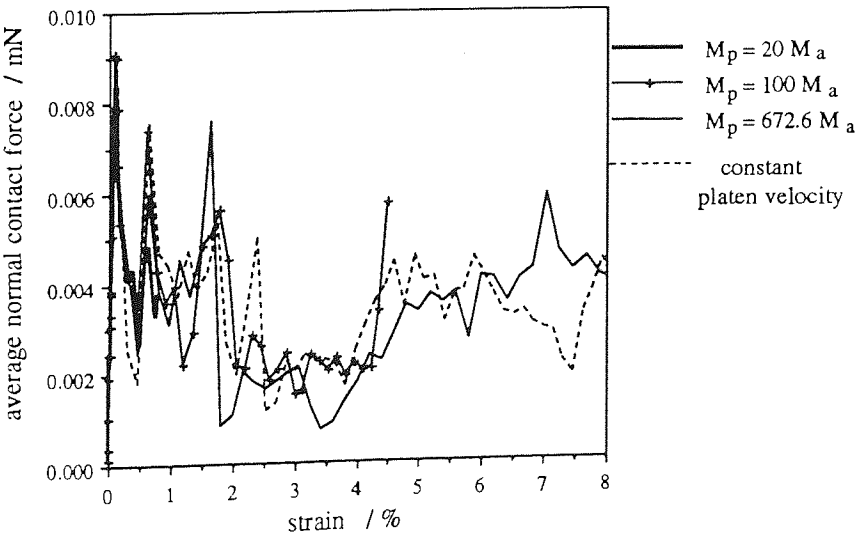

Fig. 7.33 Evolution of average normal contact force in four different tests (Γ=0.4 J/m^2 , V=0.04 m/s)

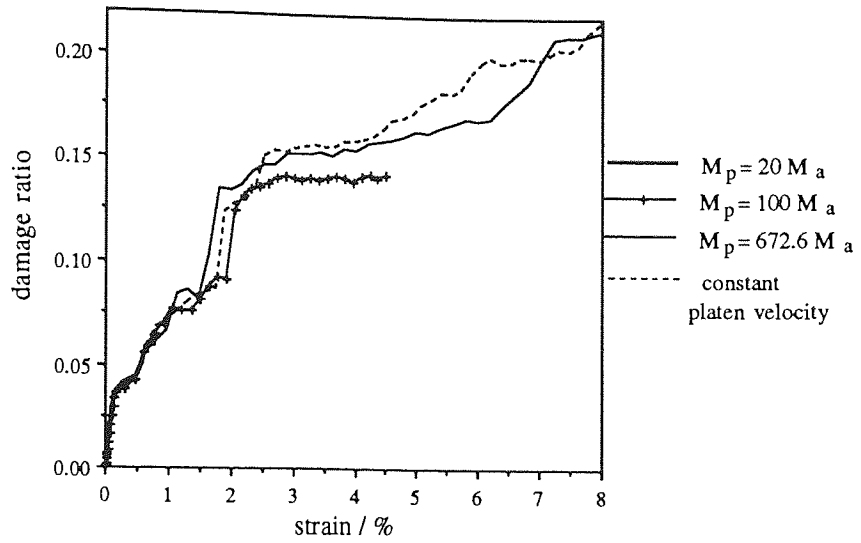

Fig. 7.34 Evolution of damage ratio in four different tests (Γ=0.4 J/m^2, V=0.04 m/s)

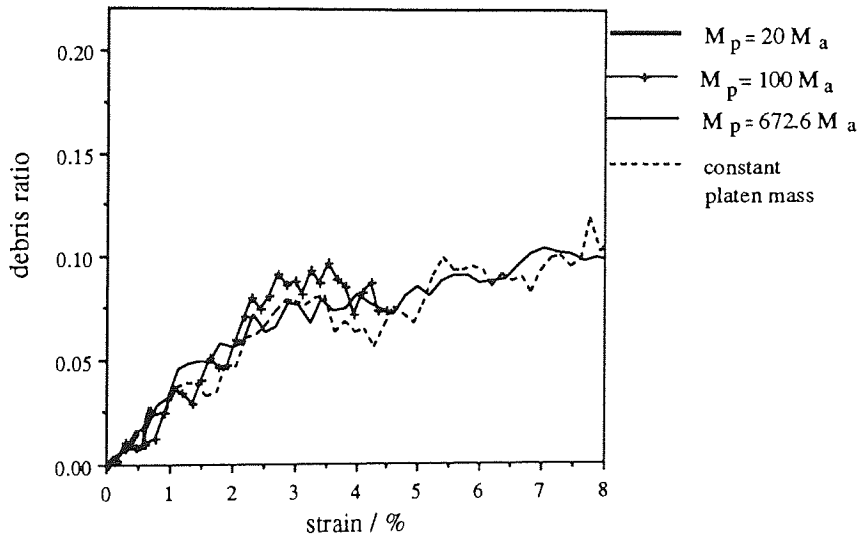

Fig. 7.35 Evolution of debris ratio in four different tests (Γ =0.4 J/m^2, V=0.04 m/s)

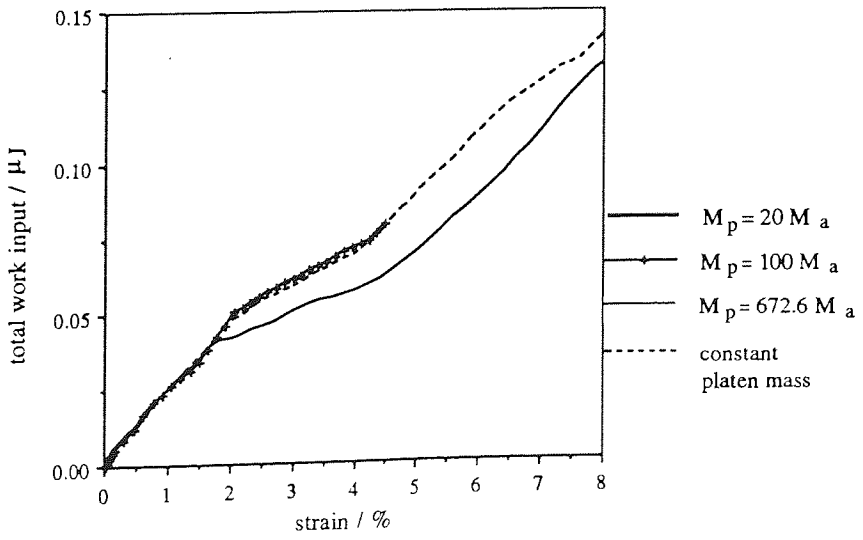

Fig. 7.36 Evolution of total work input in four different tests (Γ=0.4 J/m^2, V=0.04 m/s)

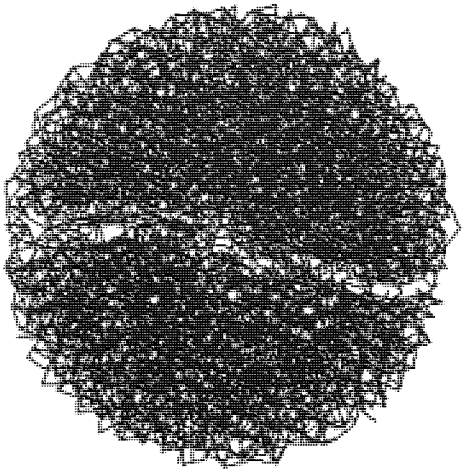

(a) at 1.07% strain (V=0.02 m/s, dense[1] agglomerate)

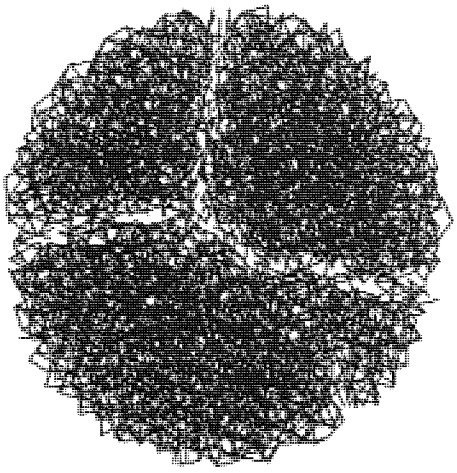

(b) at 2.41% strain (V=0.1 m/s, dense[1] agglomerate)

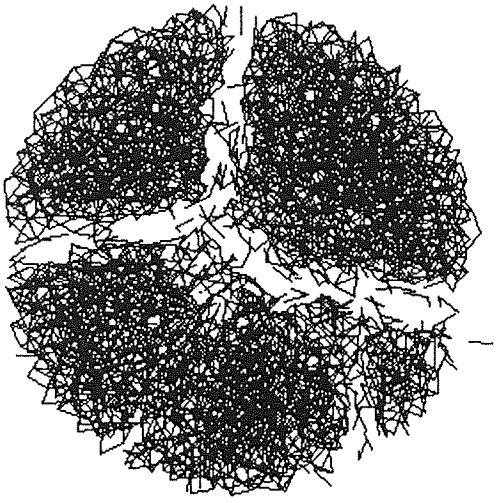

(c) at 7.50% strain (V=0.1 m/s, dense[1] agglomerate)

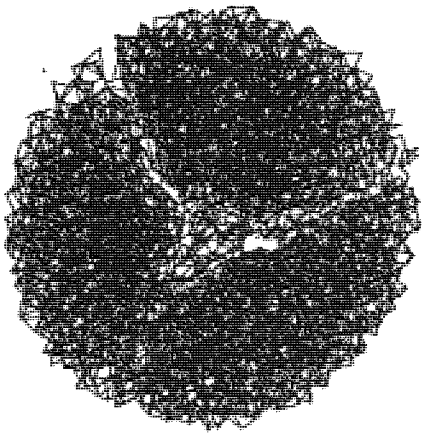

(d) at 0.79% strain (V=0.02 m/s), dense[2] agglomerate (dense of higher initial contact density)

Fig. 7.37 Space lattice after fracture in double impact tests on the strong dense agglomerates, view from above (Γ=2.0 J/m^2, M_p=100 M_a)

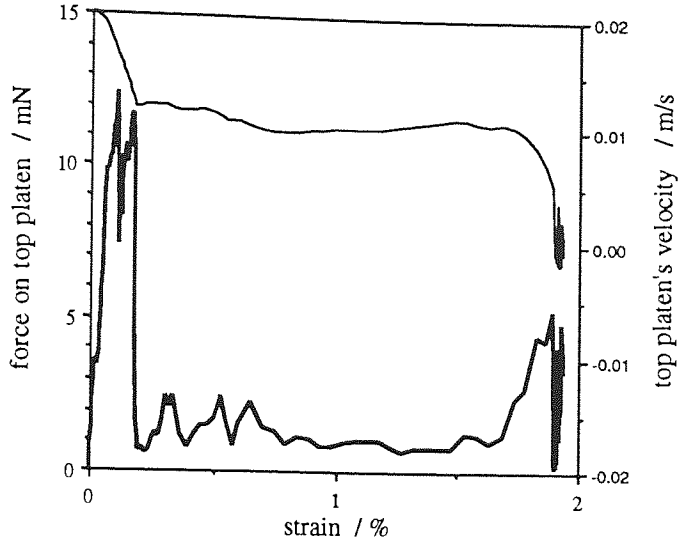

Fig. 7.38 Evolution of top platen velocity and top platen force, dense[1] agglomerate (Γ=2.0 J/m^2, V=0.02 m/s, $M_p = 100\ M_a$)

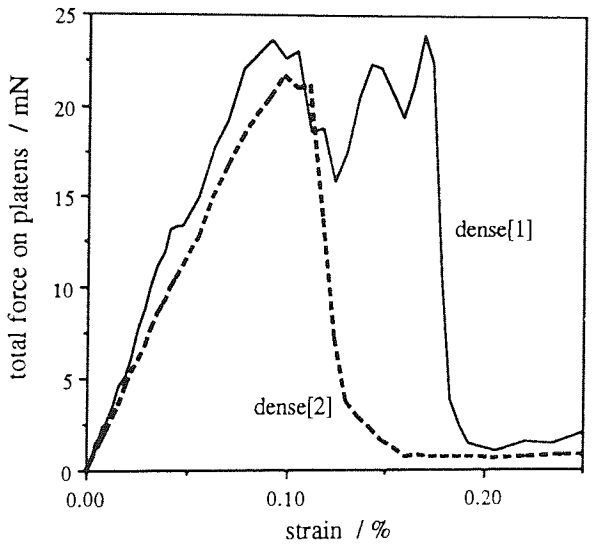

Fig. 7.39 Evolution of total force on platens, dense[1] and dense[2] agglomerates (Γ=2.0 J/m^2, V=0.02 m/s, $M_p = 100\ M_a$)

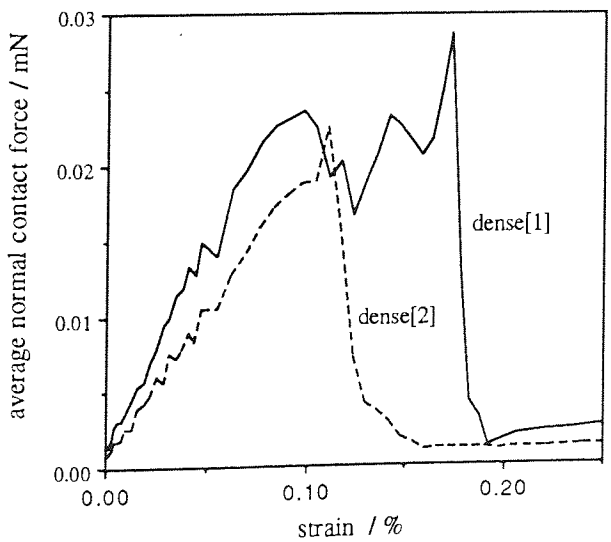

Fig. 7.40 Evolution of average normal contact force, dense[1] and dense [2] agglomerates (Γ=2.0 J/m^2, V=0.02 m/s, $M_p = 100\ M_a$)

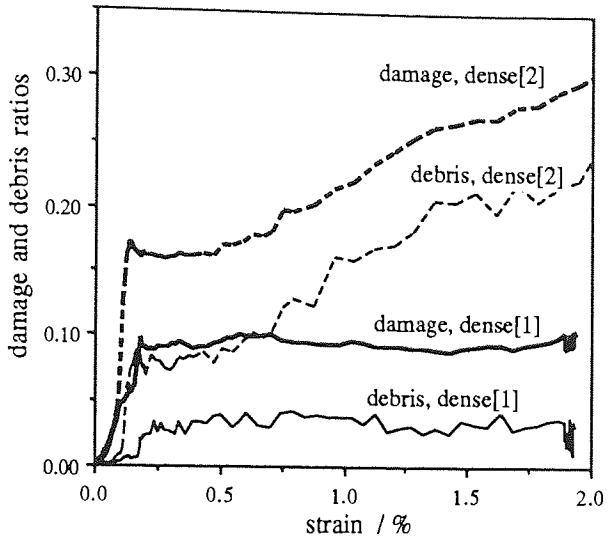

Fig. 7.41 Evolution of damage and debris ratios, dense[1] and dense[2] agglomerates (Γ=2.0 J/m^2, V=0.02 m/s, M_p= 100 M_a)

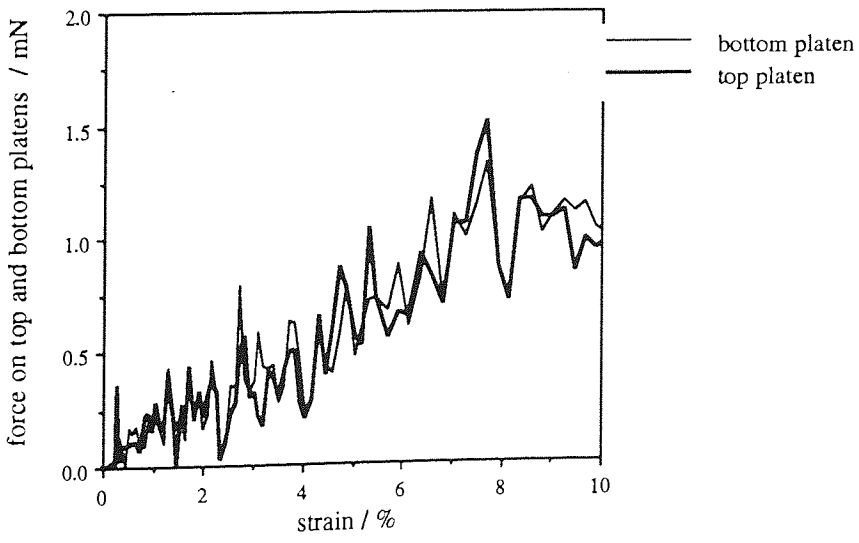

Fig. 7.42 Evolution of force on platens, loose agglomerate (Γ=2.0 J/m^2, V=0.02 m/s, M_p= 100 M_a)

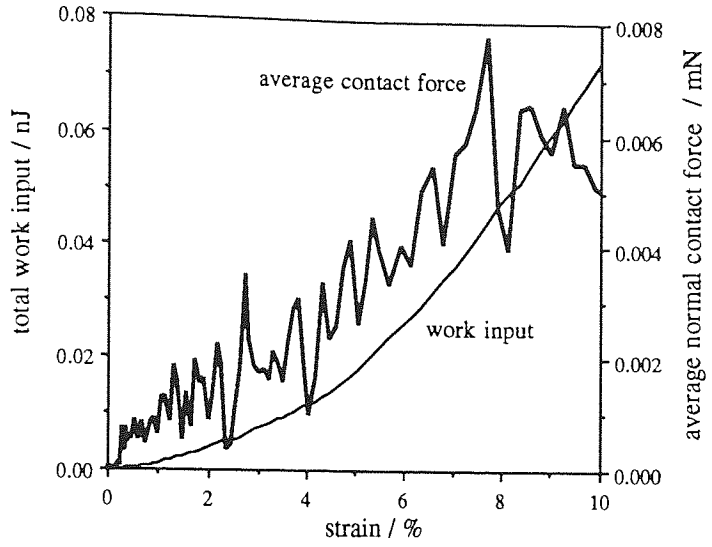

Fig. 7.43 Evolution of work input and average normal contact force, loose agglomerate (Γ=2.0 J/m^2 , V=0.02 m/s, M_p =100 M_a)

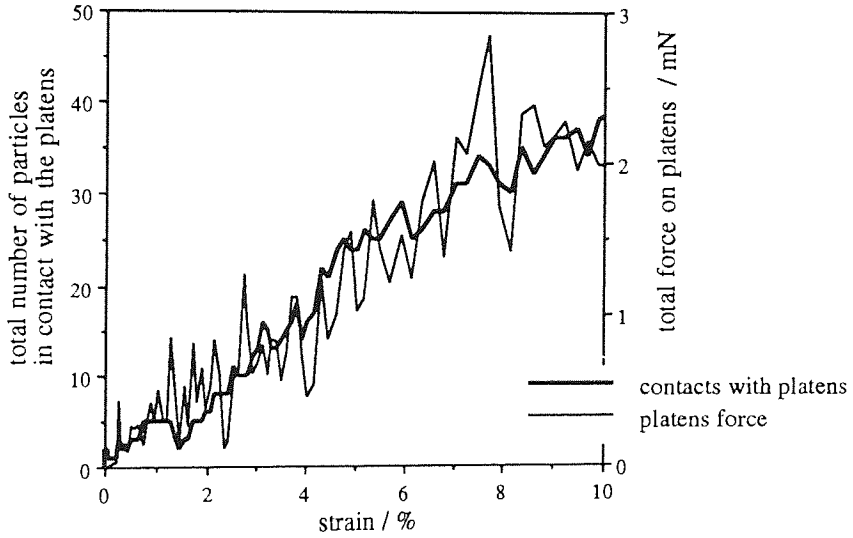

Fig. 7.44 Evolution of number of particles in contact with platens and of platens force, loose agglomerate (Γ=2.0 J/m^2 , V=0.02 m/s, M_p =100 M_a)

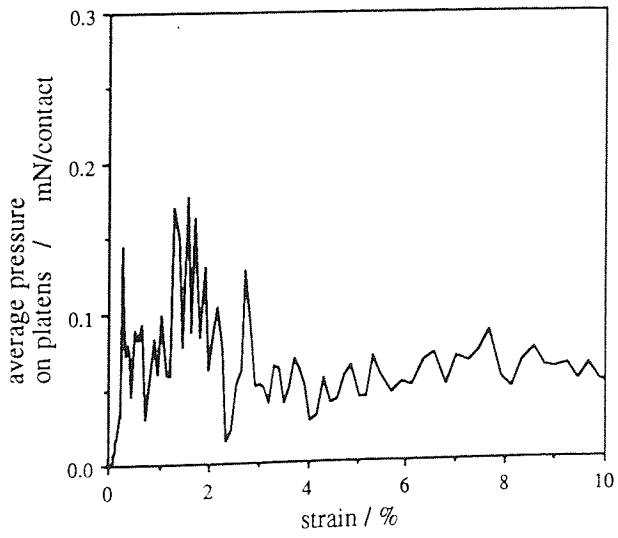

Fig. 7.45 Evolution of average pressure on platens, loose agglomerate (Γ=2.0 J/m^2 , V=0.02 m/s, M_p =100 M_a)

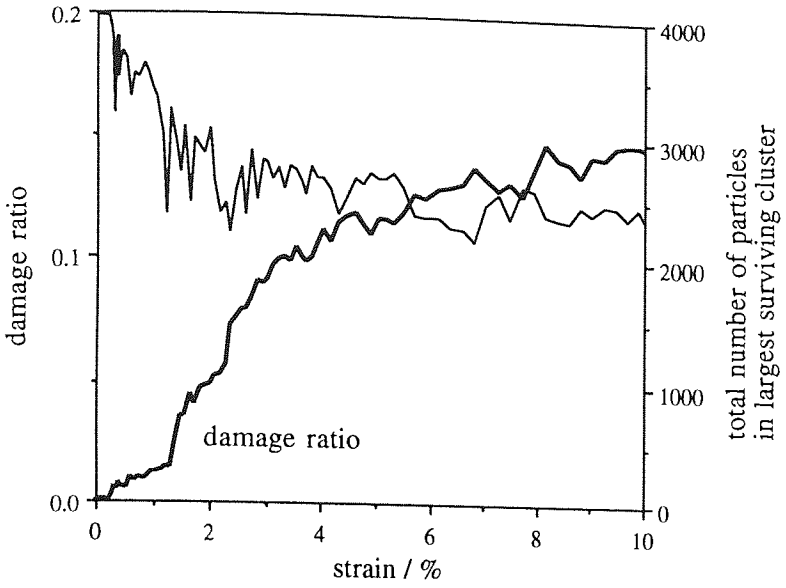

Fig. 7.46 Evolution of damage ratio and of number of particles in largest cluster, loose agglomerate (Γ=2.0 J/m^2 , V=0.02 m/s, M_p =100 M_a)

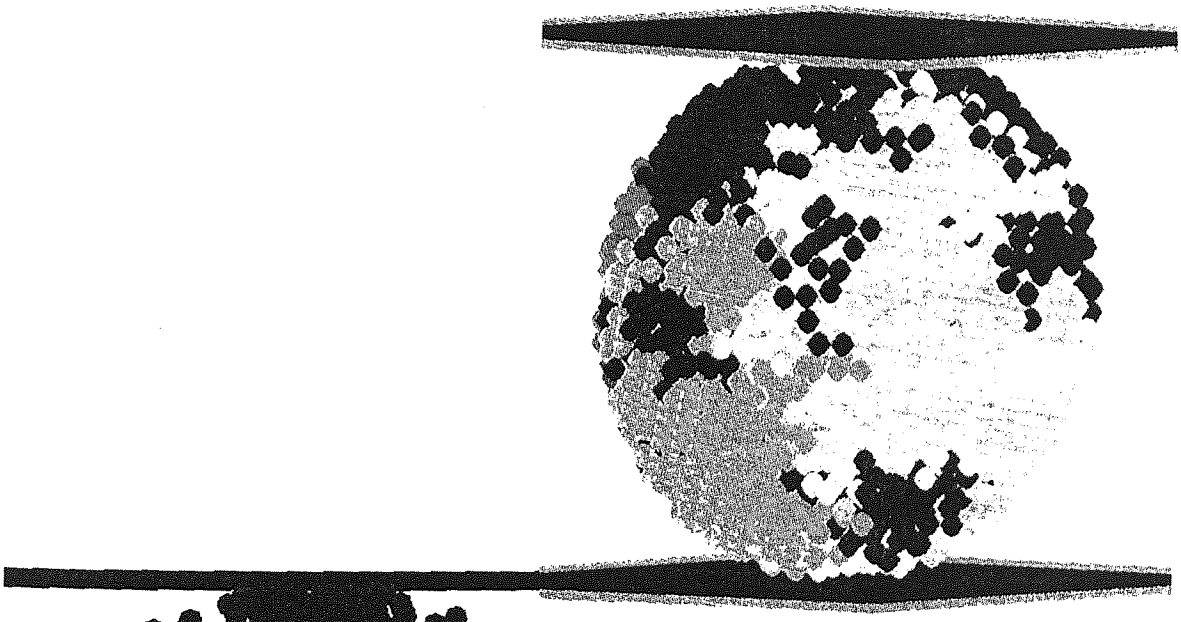

Fig. 7.47 The particle configuration at 1.22% strain, double impact test (surviving cluster particles shown in shades of grey, particles in debris shown in black), view from side, loose agglomerate (Γ=2.0 J/m^2, V=0.02 m/s, M_p=100 M_a)

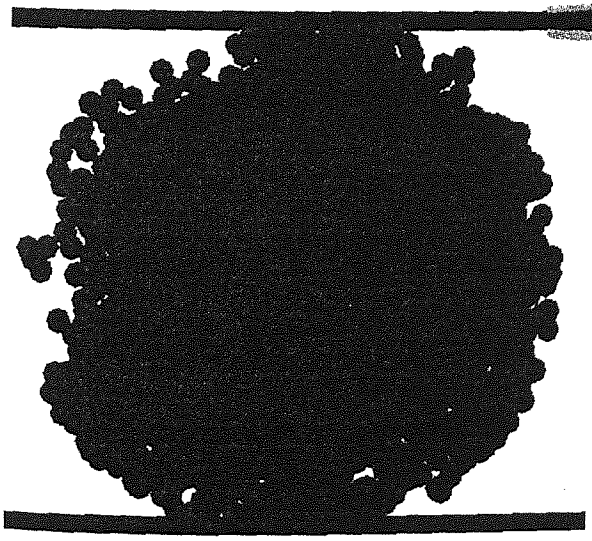

Fig. 7.48 The particles in the largest surviving cluster at the end of the double impact test (9.9% strain), view from front, loose agglomerate (Γ=2.0 J/m^2, V=0.02 m/s, M_p=100 M_a)

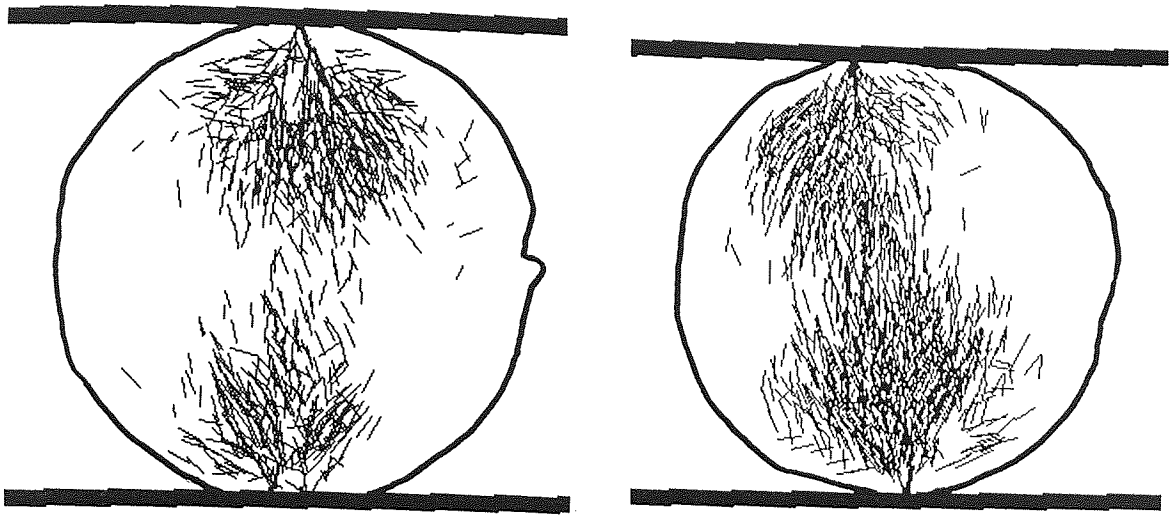

(a) largest 817 compressive forces at 0.16% strain, dense[1] agglomerate

(b) largest 1199 compressive forces at 0.11% strain, dense[2] agglomerate

Fig. 7.49 The largest ≈16% of the compressive interparticle contact forces close to the moment when platen forces attained a maximum, views from front, double impact test, strong dense agglomerates (Γ=2.0 J/m^2, V=0.02 m/s, M_p=100 M_a)

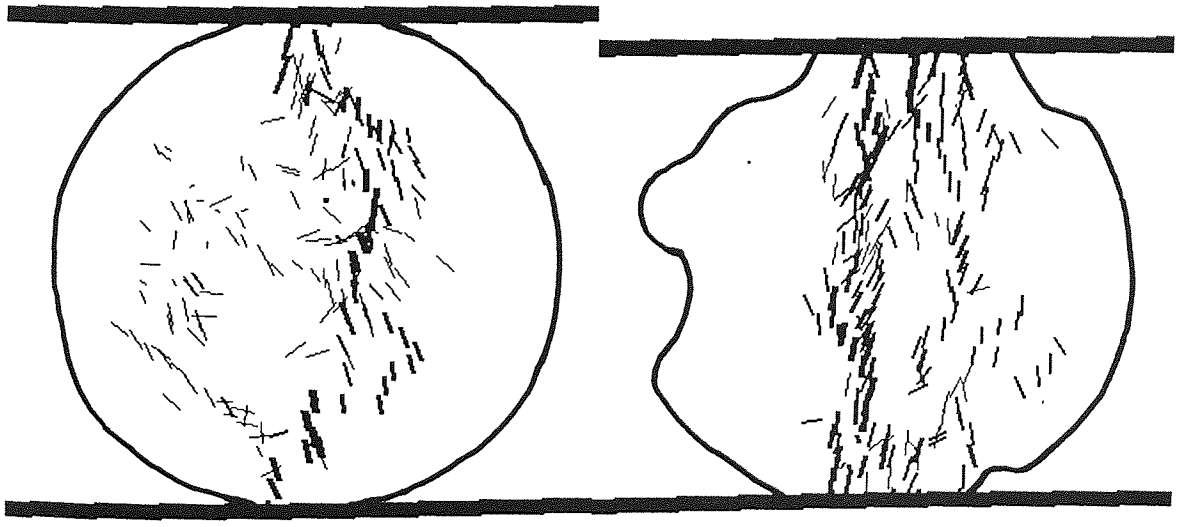

(a) view from front at 1.22% strain

(b) view from front at 7.7% strain

Fig. 7.50 The largest 10% of the compressive interparticle contact forces when platen force was a maximum, view from front, double impact test, loose agglomerate (Γ=2.0 J/m^2, V=0.02 m/s, M_p=100 M_a)

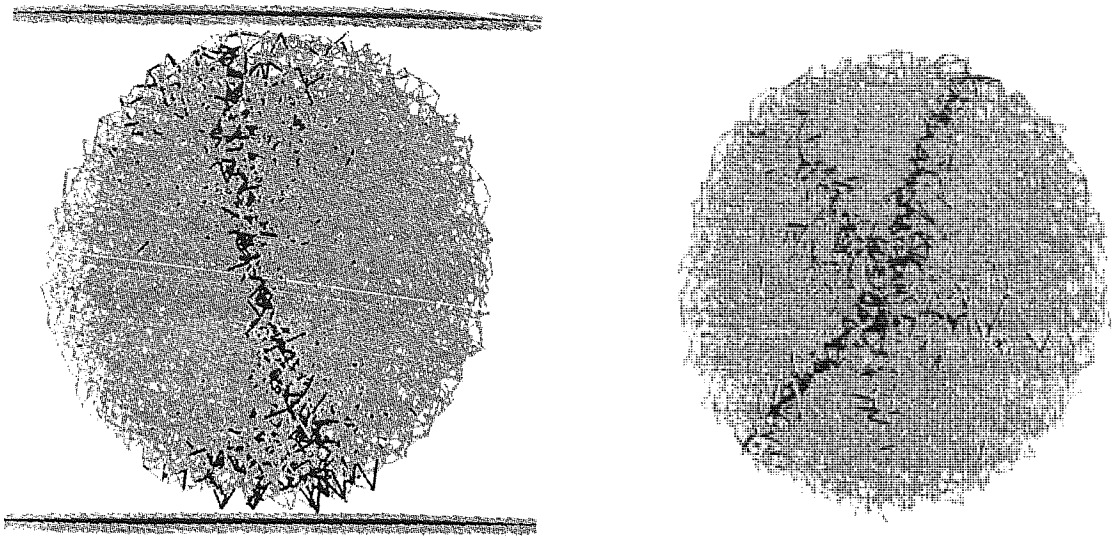

(a) view along the fracture surface

(b) view from above

Fig. 7.51 Space lattice at primary fracture, diametrical compression test (existing bonds shown in grey, broken bonds shown in black) dense[2] agglomerate (Γ=2.0 J/m^2, V=10 mm/min)

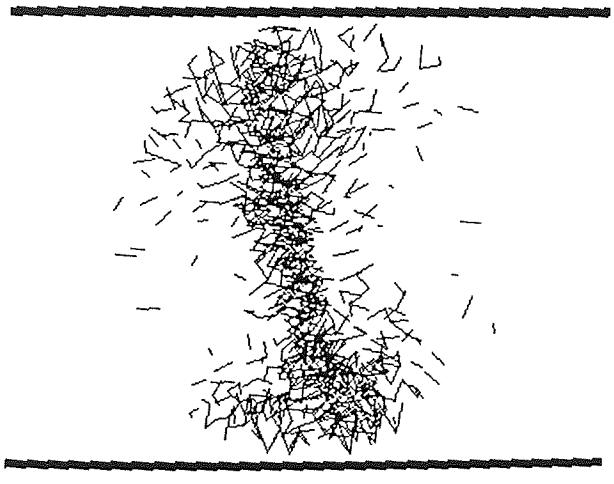

Fig. 7.52 Space lattice (showing broken bonds only) at primary fracture viewed along the fracture surface, dense[2] agglomerate (Γ=2.0 J/m^2, V=10 mm/min)

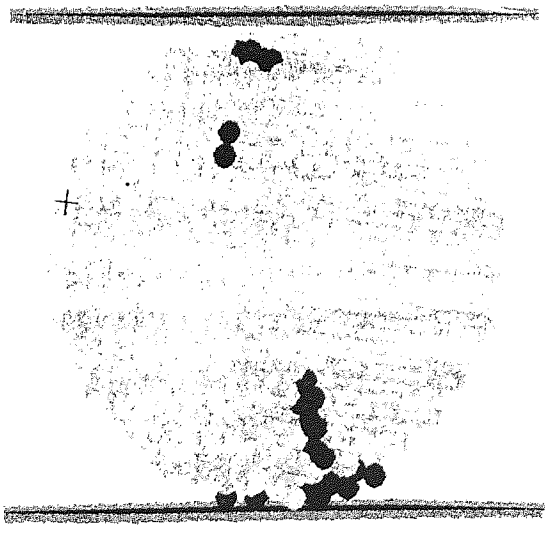

Fig. 7.53 Particle configuration at primary fracture (particles in the two large fragments shown in grey, particles in debris shown in black), viewed roughly along the fracture surface, dense[2] agglomerate (Γ=2.0 J/m^2, V=10 mm/min)

Fig. 7.54 Particle velocity field (not showing debris) viewed from above at primary fracture (0.1279% strain), dense[2] agglomerate (Γ=2.0 J/m^2, V=10 mm/min)

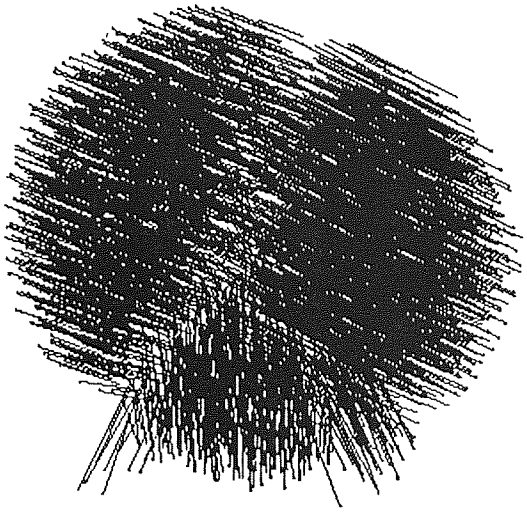

Fig. 7.55 Particle velocity field (not showing most of the debris) viewed from above at secondary fracture (0.1282% strain), dense[2] agglomerate (Γ=2.0 J/m^2, V=10 mm/min)

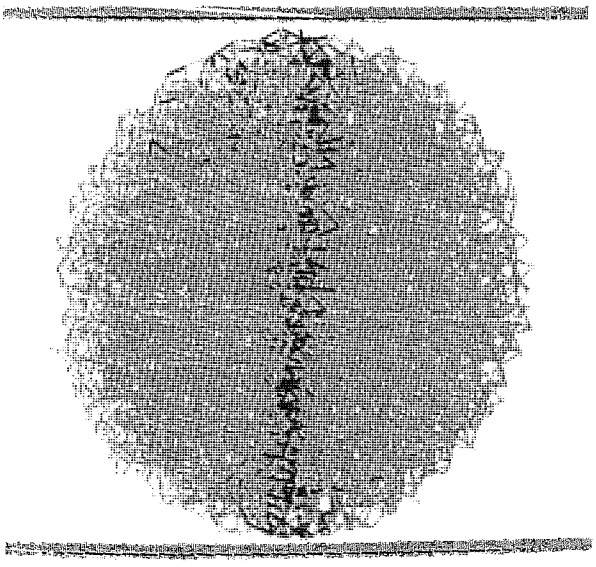

(a) view along the fracture surface

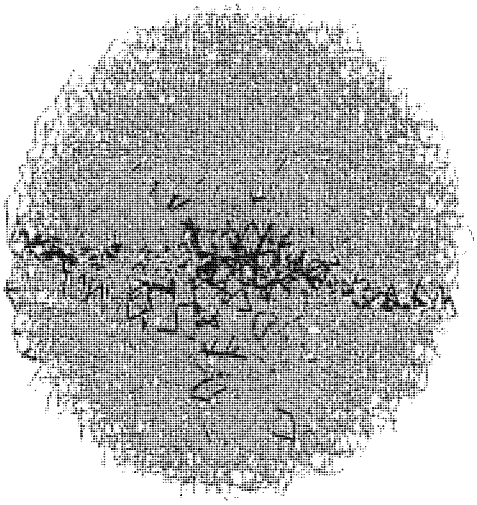

(b) view from above

Fig. 7.59 Space lattice at primary fracture (0.1279% strain), surviving bonds are shown in grey, broken bonds are shown in black, dense[1] agglomerate (Γ=2.0 J/m^2, V=10 mm/min)

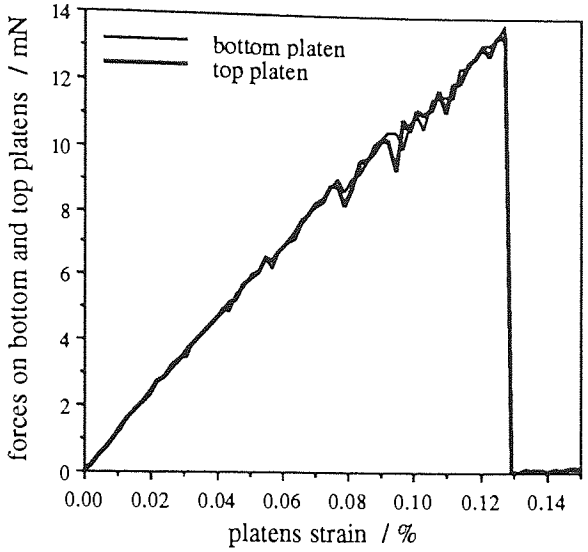

Fig. 7.56 Evolution of forces on top and bottom platens, diametrical compression test, dense[2] agglomerate (Γ=2.0 J/m^2 , V=10 mm/min)

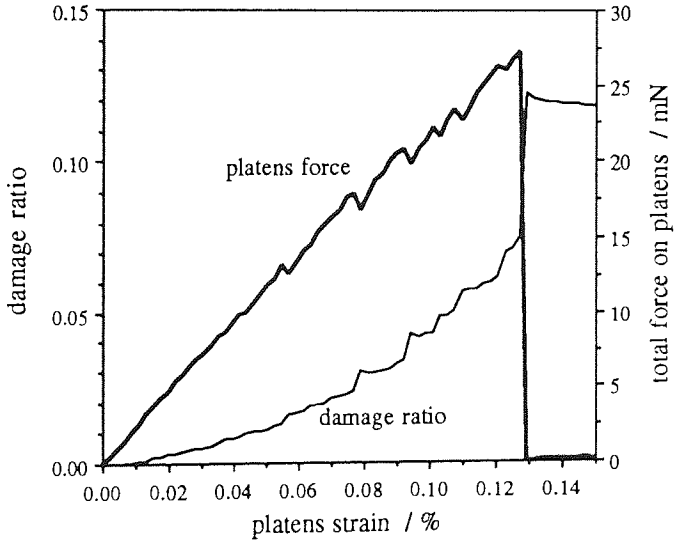

Fig. 7.57 Evolution of damage ratio and total force on platens, dense[2] agglomerate (Γ=2.0 J/m^2, V=10 mm/min)

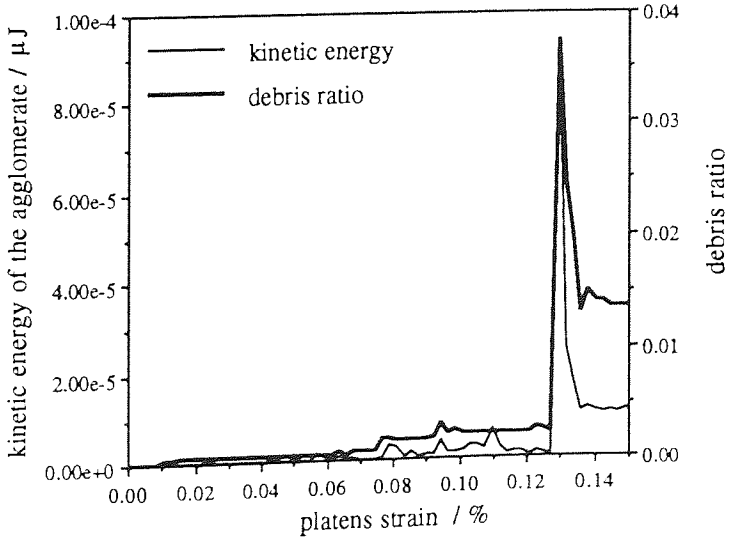

Fig. 7.58 Evolution of debris ratio and kinetic energy of the agglomerate, dense[2] agglomerate (Γ=2.0 J/m^2 , V=10 mm/min)

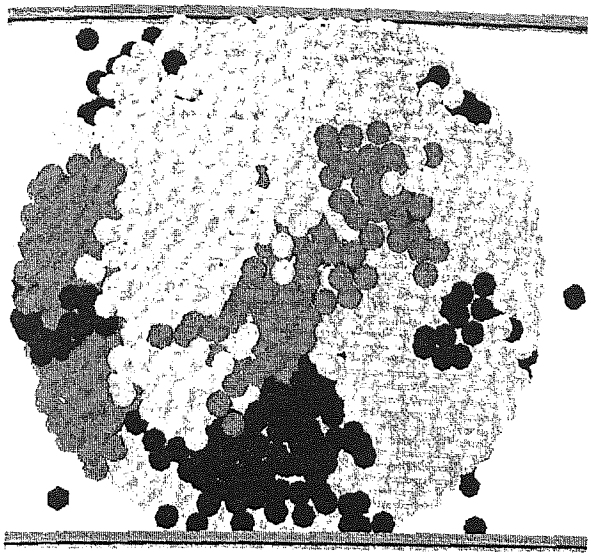

Fig. 7.60 Particle configuration at the end of the diametrical compression test (7.3% strain), surviving cluster particles are shown in light grey, particles in debris are shown in black and particles in the other small clusters are shown in dark grey, loose agglomerate (Γ=2.0 J/m^2, V=180 mm/min)

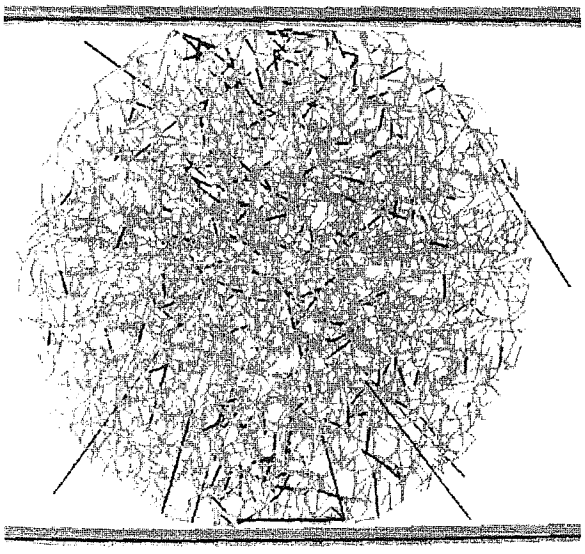

Fig. 7.62 Space lattice at the end of the test (7.3% strain), surviving bonds are shown in grey and broken bonds are shown in black, loose agglomerate (Γ=2.0 J/m^2, V=180 mm/min)

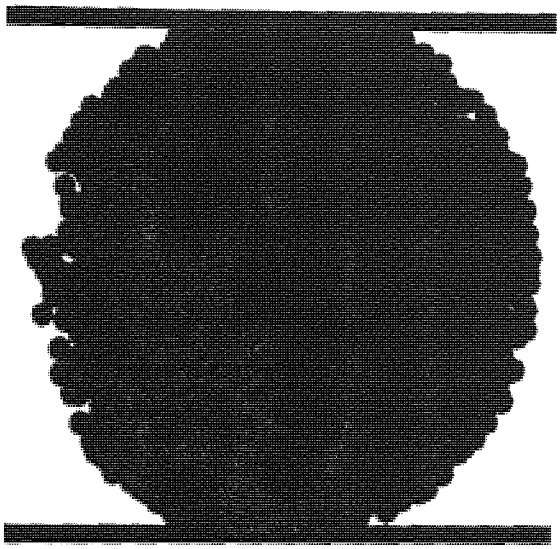

Fig. 7.61 Particles in the largest surviving cluster at the end of the test (7.3% strain), loose agglomerate (Γ=2.0 J/m^2, V=180 mm/min)

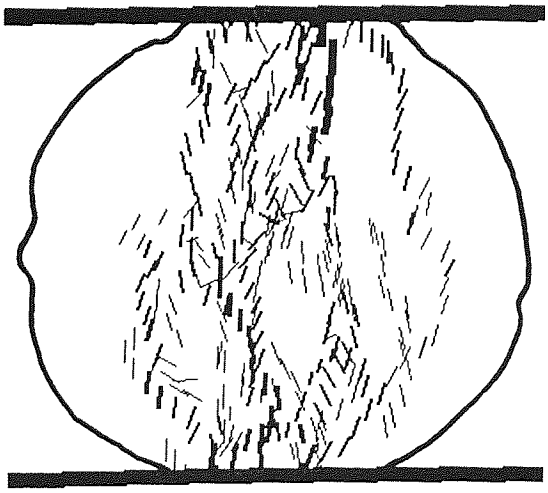

Fig. 7.67 The largest 13.7% of the compressive interparticle contact forces at 6.8% strain, diametrical compression test, loose agglomerate (Γ=2.0 J/m^2, V=180 mm/min)

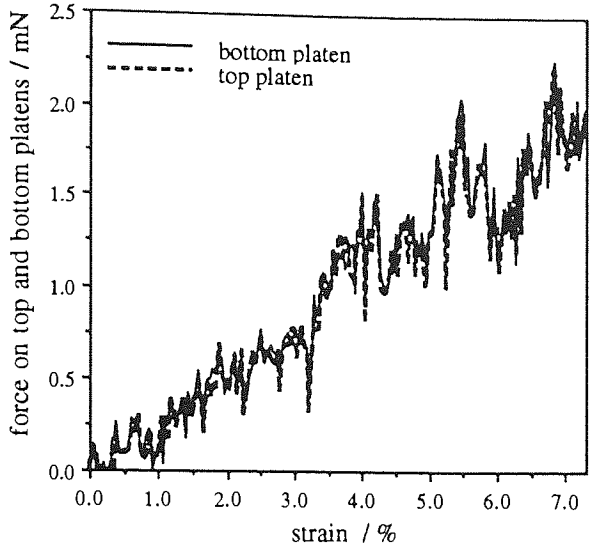

Fig. 7.63 Evolution of force on top and bottom platens, diametrical compression test, loose agglomerate (Γ=2.0 J/m^2 , V=180 mm/min)

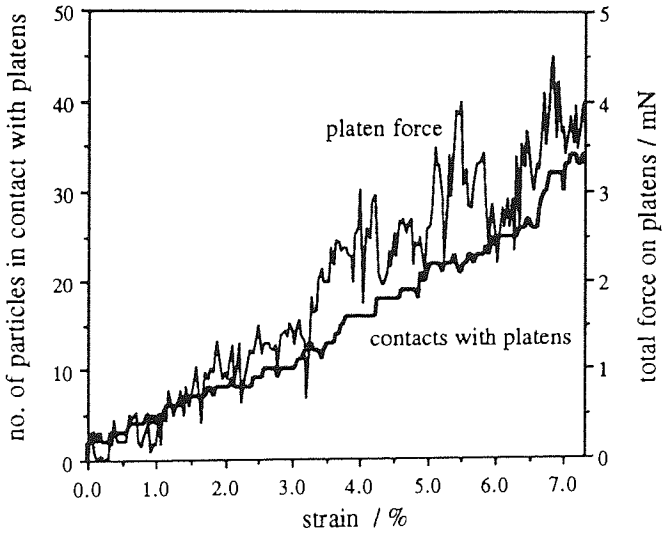

Fig. 7.64 Evolution of platen force and number of particles in contact with platens, loose agglomerate (Γ=2.0 J/m^2 , V=180 mm/min)

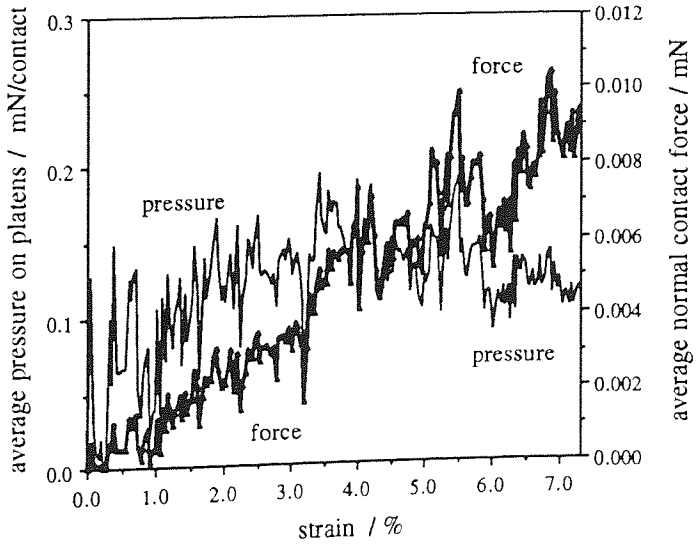

Fig. 7.65 Evolution of average pressure on platens and average normal contact force, loose agglomerate (Γ=2.0 J/m^2 , V=180 mm/min)

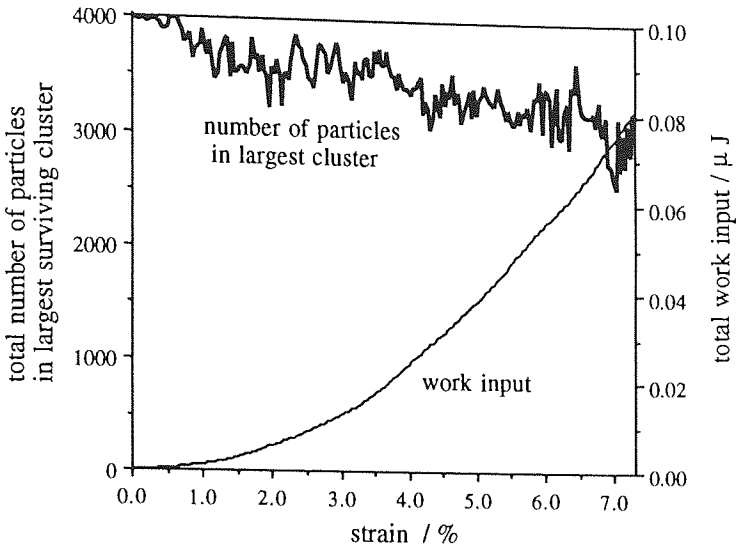

Fig. 7.66 Evolution of work input and number of particles in largest cluster, loose agglomerate (Γ=2.0 J/m^2, V=180 mm/min)

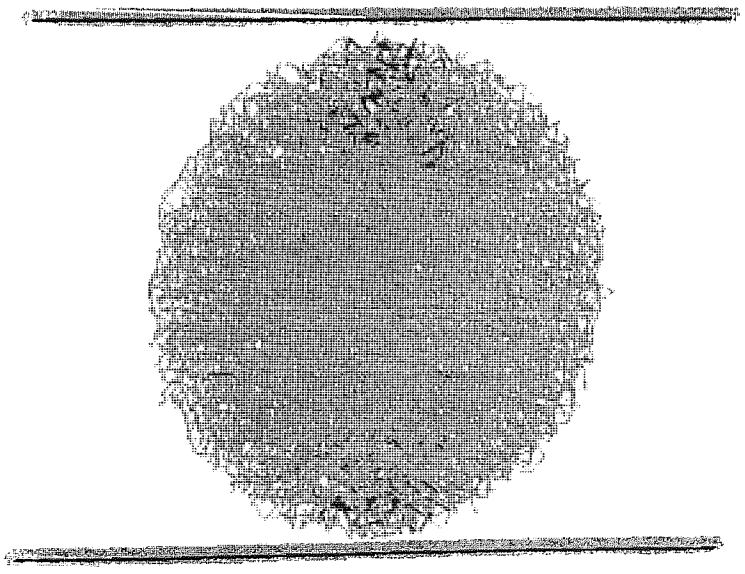

Fig. 7.68 Space lattice at 0.1% strain, view from front, double impact test, surviving bonds are shown in grey, broken bonds are shown in black, dense[1] agglomerate (Γ=2.0 J/m^2, V=0.02 m/s, M_p=100 M_a)

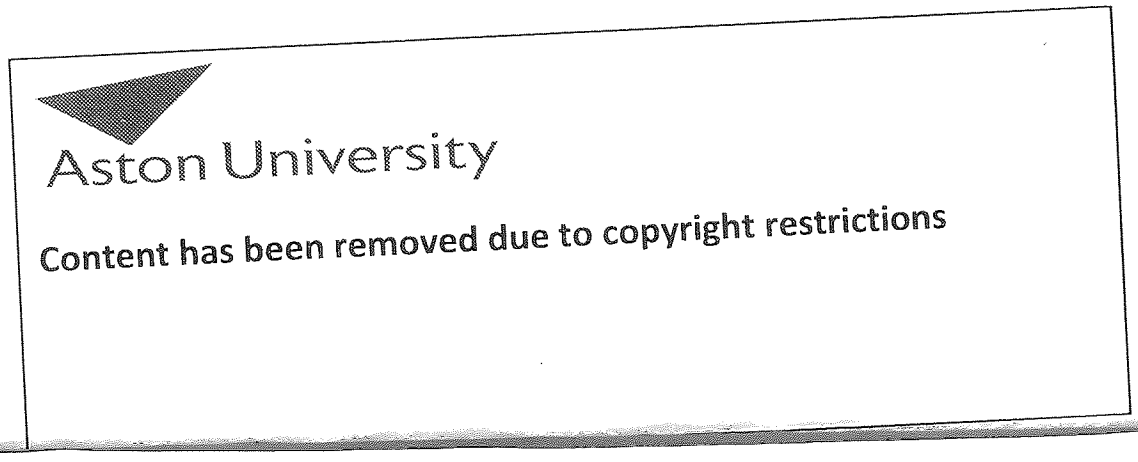

(a) (b) (c)

ig. 7.69 Schematic mechanisms of fracture in diametrical compression tests on gglomerates inferred from laboratoty tests:
a) Kapur and Fuerstenau (1967) on 8-20 mm diameter limestone pellets
b) Wynnyckyj (1985) on 15 mm diameter magnetite and hemetite pellets
c) Meyers and Meyers (1984) on 9-16 mm iron-ore pellets.

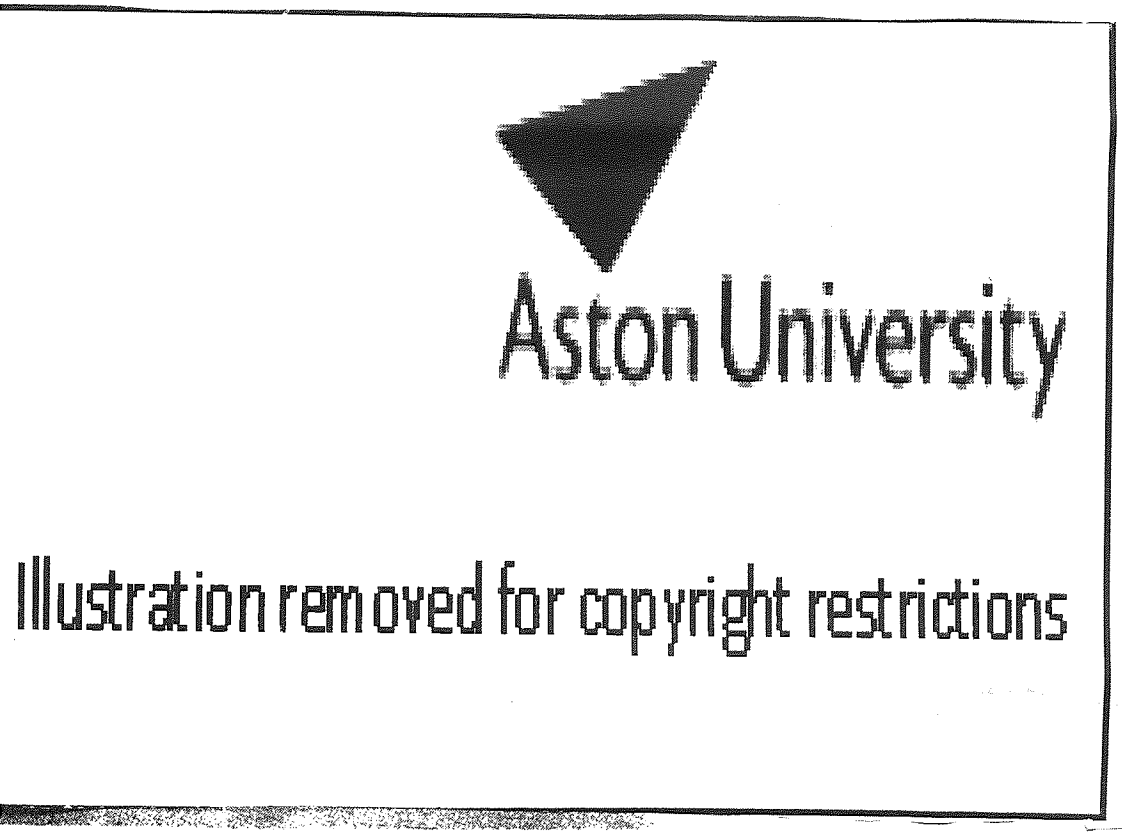

(c) (d) (e)

ig. 7.70 Photographs of actual fractures of agglomerates in laboratory diametrical ompression tests:
) largest fragment, Newitt and Conway-Jones (1958), sand and silt agglomerates
) two large fragments, view from above, Kapur and Fuerstenau (1967)
) three large fragments and **(d)** two large fragments, views from above, eyers and Meyers (1984)
) two large fragments, view from below, Wynnyckyj (1985).

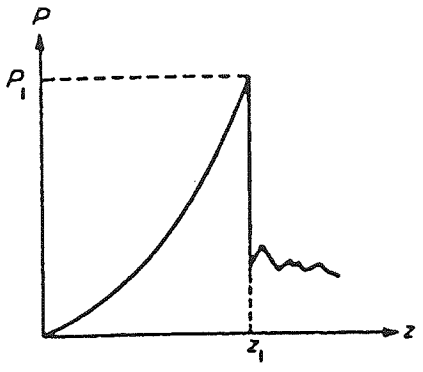

(a)

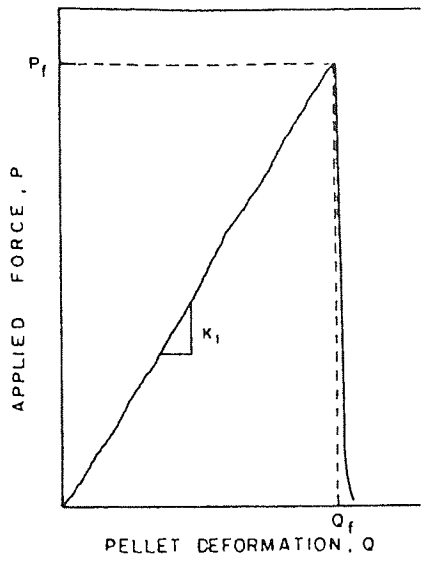

(b)

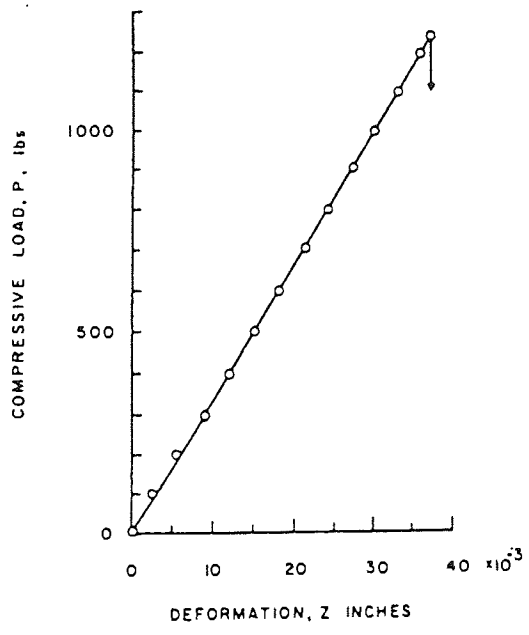

(c)

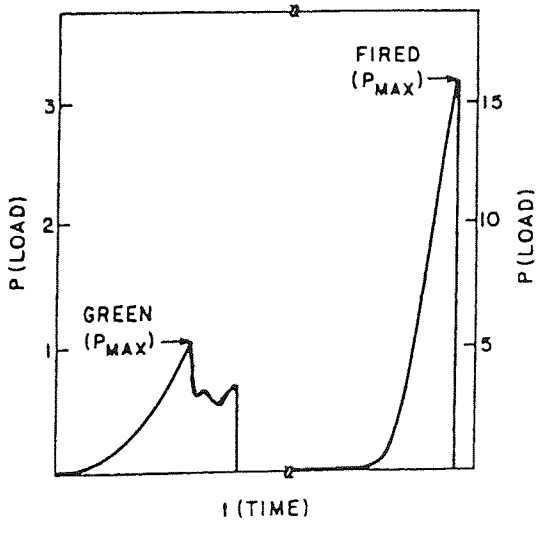

(d)

Fig. 7.71 Evolution of load measured in laboratory diametrical compression tests
(a) from Breval et al (1987), proppants and sand spheres
(b) from Kapur and Fuerstenau (1967), limestone pellets
(c) from Arbiter et al (1969), sand-cement agglomerates
(d) from Wong et al (1987), ceramic spheres.

CHAPTER 8

EVOLUTION OF DAMAGE/FRACTURE PROCESSES

8.1 INTRODUCTION

This chapter is concerned with the micromechanical processes of agglomerate fracture in each of the three types of tests simulated in this project. The tests resulting in other forms of agglomerate failure (fragmentation, crushing, shattering) or just local damage are not considered. Details of the fracture evolution, from initiation to completion, were examined by means of computer graphics. The information obtained in this way is novel as it would be impossible to obtain from laboratory tests - due to the small size of agglomerates (about 1 mm in diameter), to the inability of closely monitoring the complex behaviour of particulate material and to the impossibility of carrying out any number of tests on the same agglomerate.

Fracture of the agglomerates was 100% intergranular. The fracture behaviour of agglomerates can be considered, similar to that of solids, as a process of crack initiation and propagation. If one interparticle bond breaks, this can be interpreted as the formation of a microcrack. If a group of microcracks form, this can either be viewed as crack propagation or as local damage. Successive breakage of bonds along a certain direction inside the agglomerate can be considered as a crack propagation process. Microcracks can also form adjacent to existing cracks. A concentrated random distribution of broken bonds in which there is no preferred orientation can also occur due to plastic deformation of the agglomerate. This will be termed "damage". When broken bonds re-adhere, this can be considered as "healing" of microcracks or cracks. However, re-adhered bonds are much weaker than bonds that never broke, as their interface energy is only 0.06 J/m^2 (compared to 0.4 or 2.0 J/m^2 for the unbroken bonds).

It was shown in the previous two chapters that the dense agglomerates can fracture in all three types of test. In the diametrical compression tests the dense agglomerates always fractured. In the free-fall and double impact tests the dense agglomerates only fractured if the value of the impact velocity was in a certain narrow range - which depended on the interface energy, density of interparticle bonds (and mass of the impacting platen in double impact tests).

It is much easier to pin-point the exact moment of fracture in simulations than in laboratory tests. The moment of fracture is considered to be when the particle velocity vectors viewed from above are no longer directed radially outwards from the agglomerate's centre but, in

each large fragment, are all parallel (indicating that all the particles belonging to each fragment move in unison).

The fracture mode and the typical shape of fragments obtained from the simulations agreed well with most of the results obtained in laboratory tests. Fracture was tensile and generally occurred along planes perpendicular to the platens and the fragment shape was either hemispherical or wedge-like (sphere segments). In all three types of test, agglomerate fracture was found to initiate from the agglomerate-platen interface and not from the centre of the agglomerate, as many workers have inferred from laboratory testing, especially in diametrical compression. Additionally, the fracture process seemed to have started while the force was increasing on the platen/s, and to complete shortly after the platen force started its final drop. A more detailed analysis was needed to verify the conclusions and deductions made so far and to find exactly how the fracturing process evolved.

8.2 EVOLUTION OF DAMAGE

For simplicity, the three tests closely scrutinised in this chapter are the ones in which primary fracture produced only two large fragments. Interesting details of the fracturing process were observed by analysing images of the evolution of bond breakage at different stages during the three types of tests.

8.2.1 Free-Fall Impact

The evolution of the platen force, kinetic energy of the agglomerate, the damage ratio and the debris ratio is shown in Fig. 8.1 for the dense[1] agglomerate during free-fall impact with an impact velocity of 0.2 m/s. Superimposed on the curves are small circles which are numbered to identify the six different states which will be illustrated in Figs 8.2 and 8.3.

Figure 8.2 presents images of all broken contacts for the six states indicated in Fig. 8.1. The broken bonds are represented as lines tangent to the former contact; the length of each line is equal to the distance between the centres of particles that were in contact. The boundary of the roughly spherical agglomerate is represented by a thick yellow line. For each state in Fig. 8.2 there are two images: a view from above (perpendicular to the platen) and a side view (observed from the right) perpendicular to the fracture surface. Red is used to identify the broken bonds in the top half of the agglomerate, black is used for the broken bonds in the bottom half. Figure 8.3 presents exactly the same broken bonds as shown in Fig. 8.2 but viewed from the front, along the fracture surface.

Immediately after the moment of primary fracture the side view (Fig. 8.2 - state {5}, right) displays the fracture surface as an approximately circular area "filled" by lines representing the broken bonds. The figure also shows the other bonds that broke inside the agglomerate (mostly near the platen). The sequence of side views in Fig. 8.2 show how bond breakage evolved during the test. It can be observed that, generally, the bonds farther from the platen were broken later. The sequence of side views also gives an approximate indication of when and where bonds were broken on the fracture surface. The views along the fracture surface in Fig. 8.3 reveal how rough and non-planar the fracture surface was and how cracks ascended through the agglomerate.

In the views from above (Fig. 8.2, left), the primary fracture moment coincides with the image in which broken bonds manage to form a concentrated band across the agglomerate (see Fig. 8.2, state 5, left). One can observe that cracks tended to propagate from the loaded (vertical) diameter radially outwards, along surfaces approximately equal to half the agglomerate's diametral plane. For simplicity, these cracks can be called *"HDP"* (half diametral plane) cracks. HDP cracks can be easily differentiated by the cardinal point direction (N, S, W or E) they propagate towards in the views from above. Cracks that tend to propagate along an approximately full-diametral plane can be named *"FDP"* (full diametral plane) cracks.

In the first part of the test before state {1}, bonds broke in a random manner without clearly indicating initiation of any cracks. In both Fig. 8.2 and 8.3, images of state {1} clearly illustrate that failure started with the formation of a roughly conical damage zone by the impacted platen - see the concentration of broken bonds in the side views. However, the base of the cone was much larger than the area of contact with the platen. In fact the contact area increased very little prior to fracture, as there was no increase in the number of particles in contact with the platen.

The view from above of state {1} suggests that HDP cracks were already initiated here, as three favoured directions for bond breakage can be easily identified: from the agglomerate's centre towards the cardinal points N, W and SE. One can observe in Fig. 8.1a that the point representing state {1} is in the last part of loading stage. However, the average interparticle contact force had attained its maximum value already, indicating that the stored elastic energy started to be utilised in the fracture process from state {1} onwards.

State {2} images show a little radial-like enlargement of the initial conical damage zone; the darkest area in the side view of Fig. 8.2 indicates that almost all the bonds situated in the contact damage zone had broken by state {2}. A few debris particles even started to detach off the agglomerate at the interface with the platen. The three cracks observed in state {1} had propagated a little further. Additionally, the HDP cracks heading N and SE merged into

a curved FDP crack approximately oriented N-SE; several microcracks also developed along this longer crack. A HDP crack towards the S direction was also initiated just before state {2}. Side views reveal that bond breakage inside the agglomerate had spread to the agglomerate's centre. At this point the platen force attained its maximum value (Fig. 8.1a).

The lateral views of state {3} indicate that there was at least a crack propagating towards the top pole of the agglomerate. The view from above reveals that a number of new bonds have been broken in the SW quadrant. Half of the bonds that were broken in the impact test had already been broken by state {3} - see Fig. 8.1b.

In state {4} the agglomerate was very close to fracture, as a FDP crack (directed N-S) - had now almost reached the agglomerate's top pole (see the side views in Fig. 8.2). The old trajectory of the FDP crack towards SE was not just abandoned, but even healed almost completely - as most of the broken bonds re-adhered (see the view from above). Whereas some microcracks formed along the fracture crack, others disappeared. Apart from propagating the FDP crack upwards through the top half of the agglomerate, two HDP cracks were also propagated a little further - but only in the bottom half of the agglomerate (towards SW and W).

Between state {4} and {5} the fracture crack (directed N-S) advanced to the top of the agglomerate. As it propagated, the views from above indicate that it also "adjusted" its upper curved surface - observe how the red curve (representing the portion of the fracture crack situated in the agglomerate's top half) straightened up from state {4} to {5}. The fact that the FDP fracture crack became more straight can also be noted from its narrowing in the view from the front images in Fig. 8.3. By state {5} the HDP crack towards SW had propagated well into the agglomerate's top half.

Primary fracture occurred just before state {5}. The crack trajectory (approximately directed N-S) became the fracture surface. Fracture seemed to occur approximately when the platen force dropped to the value of the average interparticle contact force. Some debris was detached immediately after fracture, a fact demonstrated by the steep increase in the debris ratio - Fig. 8.1b.

Agglomerate damage did not cease with the primary fracture: a secondary fracture occurred just before state {6}, as a result of continuing the propagation of the HDP crack towards SW. There are two main reasons why there was a secondary fracture. One was that at the moment of primary fracture there was still a significant amount of elastic energy stored inside the agglomerate (as indicated by the relatively high values of average interparticle contact force and platen force). Secondly, the HDP crack towards SW was well developed even within the top half of the agglomerate at the moment of primary fracture, so that only a

little additional energy was needed to complete the propagation to the top surface. The levelling-off in the damage ratio's evolution between states {5} and {6} (see Fig. 8.1.b.) denotes that about the same quantity of bonds broke and re-adhered between primary and secondary fracture.

8.2.2 Double Impact Tests

The test selected for analysis is the 0.02 m/s impact velocity double impact test of the dense[1] agglomerate, as it resulted in a half-half fracture. The top platen mass was 100 times heavier than the agglomerate. The initial kinetic energy was the same as in the free-fall impact test analysed in Section 8.2.1. However, the impact velocity was ten-fold lower and, along the loading direction, the agglomerate was constrained by the two platens. The evolution of the force on the top platen, of the work input and of the kinetic energy of both the top platen and the agglomerate is shown in Fig. 8.4 with six points indicated on the curves. Fig. 8.5 presents the images of all broken bonds at the six different states during the test. Both views from above (perpendicular to the platens) and side views (perpendicular to the fracture surface) are shown. The bonds broken in the top half of the agglomerate are shown in red. The states {1}, {2}, {3}, {5} and {6} are the same ones that also appeared in Fig. 8.4.

Before state {1} bonds broke (microcracks were formed) within two opposite roughly-conical zones adjacent to the platens, in an almost symmetrical manner. The initial velocity of the top platen seems to have been low enough for the damage to occur in a similar way at both platens (see the side view of state {1}). Not only did damage originate from both platens, but cracks also initiated and started to propagate from each platen (see view from above). In the top half of the agglomerate five different HDP cracks could easily be distinguished: two towards S and one each towards the NE, SW and W cardinal points. The agglomerate's bottom half developed three larger HDP cracks, towards SE, NW and N. It is noted that there was no crack propagating from the top pole with the same orientation as any crack propagating from the bottom pole. The platen force attained its first maximum value at state {1}, when over a third of the work to fracture had already been done (Fig. 8.4a). Over half (0.09%) of the strain to fracture had taken place and about 45% of the bond breakage to fracture had already occurred by state {1}, but almost no debris had been detached from the agglomerate (Fig. 8.4b).

Although state {2} was much closer to the fracture moment, the propagation of cracks between states {1} and {2} reveals that the two halves of the agglomerate still acted somewhat independently (at least in respect to the fracture behaviour). All the cracks that could be observed at state {1} were found to have propagated further in state {2}. Two new extra HDP cracks had started to propagate: one towards E in the top half and one towards W

in the bottom half. The conical damage zone remained roughly the same in size but suffered additional damage as some more bonds were broken within it.

State {2} was also the moment when cracks propagating from the two poles reached the agglomerate's centre and met (see the side view). From this moment it seems that the two halves started to act together (see the views from above of states {2} and {3}). The HDP crack towards E from the top half propagated further and, to adjust to this, an HDP crack having the same direction (towards E) had also propagated in the bottom half. Additionally, the crack towards W in the bottom half, which had the same direction as the one in the top half, propagated a little further. None of the other cracks propagated further between states {2} and {3} (see views from above). From a closer look at the view from above of the state {3} it can be observed that the two HDP cracks that have the same direction in both halves (E and W) tended to merge in an attempt to form a FDP crack. The platen force was at its highest peak at state {3} - see Fig. 8.4a. The just-after-fracture state {5} confirms the successful formation of an FDP crack directed W-E (see the view from above) which propagated to the surface of the agglomerate producing fracture in two halves (see the side view). At fracture the platen force dropped abruptly (Fig. 8.4a).

Very shortly after fracture many microcracks formed along the fracture surface - see the increase in damage ratio after state {5} in Fig. 8.4b and the view from above of state {6}. This produced a sudden increase in the debris ratio, as some debris particles detached from the faces of the fracture surface (from the two large fragments). The drop in damage ratio just before state {6} indicates that a number of bonds re-adhered: observe in the view from above that all the non-fracture cracks but one (towards N) healed almost completely. The view from above of state {7} reveals that, a long while after fracture, continuation of loading resulted in the formation of more microcracks along the fracture surface and the complete healing of all the non-fracture cracks.

8.2.3 Diametrical Compression Tests

Although the test conditions were different, many similarities were found in the fracturing of the agglomerates in diametrical compression and low-velocity double impact tests. The fact that, in both tests, the agglomerate was actually compressed between two platens appeared to be the most determining factor in the fracture behaviour.

The evolution of the force on the top platen, of the work input, damage ratio and debris ratio is shown in Fig. 8.6 for the dense[2] agglomerate subjected to diametrical compression using a top platen velocity of 10 mm/min. The images of the six main states indicated in Fig. 8.6 during the fracturing of the dense[2] agglomerate are shown in Fig. 8.7. As in the other

two tests analysed in the previous two subsections, the bonds broken in the top half of the agglomerate are coloured red in both the top and side views.

As in the double impact tests, initial bond breakage (local microcrack formation) created two opposite conical-shaped damage zones at the agglomerate-platen interfaces. The plastic-deformation zones were, as expected, roughly equal due to the low strain-rate used. The crack initiation from these contact zones started at relatively low strain. At state {1} (see view from above in Fig. 8.7) HDP cracks towards SW, NW and E formed near the top platen, whereas HDP cracks towards SW, NW, NE and SE initiated near the bottom platen. Two-thirds of the strain to fracture already occurred by state {1}, whereas the damage (in terms of bonds broken) was only one quarter of the damage at fracture (see Fig. 8.6). This shows that the very low strain-rates allowed the agglomerate to deform, to "adjust" the position of its particles, without much bond breakage.

Despite the "quasi-static" nature of the applied loading, state {2} still did not show any sign that crack propagation in the agglomerate's top half was at all influenced by the crack propagation in the bottom half of the agglomerate (and vice versa). The cracks observed in the view from above of state {1} had propagated further by state {2}. Only at state {2} had some cracks managed to reach the agglomerate's centre. No noticeable expansion of the conical plastic deformation zones adjacent to the platens occurred between states {1} and {2} but more microcracking occurred inside these zones.

Between states {2} and {3} there was an increase in the propagation of cracks oriented in both halves towards the SW cardinal point (see view from above). An HDP crack towards NE was initiated in the agglomerate's top half, either to correspond with the propagation of the HDP crack towards NE in the bottom half or as a transformation of the top half's HDP crack towards SW into an FDP crack SW-NE. It seems almost certain from state {3} that the agglomerate is "preparing" to fracture along an internal surface given by the fracture crack direction SW-NE (see both views from above and the side). State {3} was the moment when the force on the platens attained its maximum value and, after an almost continuous increase, commenced to fall suddenly (Fig. 8.6a). Until state {3} elastic energy was continuously stored in the agglomerate and was only now starting to be used in the fracture process.

Most bonds broken between states {3} and {4} actually represented the propagation of the fracture (SW-NE) crack to the equatorial surface of the agglomerate. From state {4} to state {5} the NE part of the crack situated in the bottom half adjusted a little to the left (see views from above), to conform better to the part of the crack located in the top half. The crack adjustment actually meant that a few bonds broke and others re-adhered, without changing the apparent damage ratio (Fig. 8.6b). This made the FDP crack straighter and more like a

meridional crack, preparing the fracture of the agglomerate into two fragments along an almost meridional SW-NE plane - at state {5}. Fracture was the moment when most of the debris was detached from the agglomerate (see Fig. 8.6b), demonstrating the sudden character of breakage.

Compared to the view from above of the fracture surface in the double impact test analysed in the previous sub-section (Fig. 8.5), the fracture surface in the diametrical compression test appeared to be less narrow when viewed from above. However, this was because the fracture surface was not quite perpendicular to the platens. The dense agglomerates were not perfect spheres. At the start of the diametrical compression test the two contacts of the dense[2] agglomerate with the platens were not situated along the vertical diameter of the agglomerate. Consequently, the top damage zone was not located exactly above the bottom damage zone (Fig. 8.7) and the fracture surface was not (quite) vertical. Therefore, in diametrical compression tests conducted at low strain-rates, the fracture orientation is sensitive to the exact agglomerate shape and the positioning of the agglomerate between the platens.

As the platen force dropped to almost zero (Fig. 8.6a) the agglomerate developed a secondary fracture that occurred at state {6}: one of the two large fragments broke up along an almost half diametral plane. Whereas the direction of the primary fracture surface was predictable even from state {2}, the direction of secondary fracture surface could not have been anticipated. Even from the view from above of state {2} one would have expected that the most likely crack to cause secondary fracture was the half-propagated HDP crack directed towards NW. However, it appeared to have been easier to initiate and propagate an almost new HDP crack towards SE - maybe simply because, after primary fracture, most of the load was carried by the fragment on the right hand side of the view from above. A few broken bonds re-adhered immediately after state {6} (see the view from above) - this agrees with the evidence that half of the debris rejoined the three large fragments (see Fig. 8.6b).

8.3 EVOLUTION OF THE FRACTURE SURFACE

In the fracturing in two of agglomerates, the fracture surface is considered to consist of all the interparticle bonds that had to break in order to separate the two large fragments. For a more accurate analysis of fracture, new software subroutines were developed to locate the bonds along the future fracture surface and to monitor their evolution throughout a test. The best method was found by considering only the particles belonging to the future largest fragment and examining when bonds broke between it and the rest of the agglomerate, to produce the primary fracture surface.

8.3.1 Free-Fall Impact

As in other free-fall impact tests, fracture of the dense[1] agglomerate, impacted at 0.2 m/s velocity, was accompanied by the detachment of debris from the impacted zone. However, in this test many debris particles were also found to have detached from along the fracture surface prior to fracture. For this reason the breakage of bonds between the largest fragment and debris was also monitored during the test.

In Fig. 8.8a,b,c green was used to indicate the bonds that connected the particles in the largest fragment with the ones in the second largest fragment (these were the bonds that had to break in order to completely separate the future two large fragments) at the start of the test, i.e. state {0}. The fracture surface also included bonds which broke between the largest fragment and debris particles prior to fracture. All the bonds that needed to break between the largest fragment and debris prior to the moment of primary fracture are coloured light blue in Fig. 8.8a,b,c. However, only a fraction of these light blue bonds are situated on the fracture surface, which is almost a diametral plane perpendicular to the platens (see Fig. 8.8a,c). A view perpendicular to the fracture surface, Fig. 8.8b, reveals that this surface is a nearly circular area and that bonds with future debris particles were mainly situated towards the bottom-right. Fig. 8.8d shows the state of the contacts along the fracture surface at the moment of primary fracture, i.e. state {5}. The black lines represent the bonds broken between the largest and second largest fragments; the dark blue lines denote the bonds lost between the largest fragment and the debris. It is interesting that not all the green bonds at the initial state in Fig. 8.8b turned black (had broken) at the time of fracture. Figure 8.8d shows that a few bonds still bridged across the two large fragments at the moment of primary fracture. This is however understandable as, due to the irregularities (roughness) of the faces of the fracture surface, a few particles belonging to one large fragment were trapped between other particles belonging to the other large fragment.

The particle system immediately after the moment of primary fracture is presented in Fig. 8.9. In order to clearly distinguish the shape of fragments and the location of debris, the two large fragments have been "artificially" displaced horizontally. Figure 8.10 shows only the largest fragment immediately after the moment of primary fracture. The particles coloured green are the ones that were in contact with the second largest fragment at the start of the test. In Fig. 8.10a,b several particles that were prone to be trapped between the second largest fragment's particles can be easily distinguished, as they "stick out" from between the other particles by the fracture surface. These particles can also be observed in Fig. 8.9. Note that these figures include the largest fragment's particles connecting it with the impacted platen: these particles seem to belong to debris rather than to the largest fragment. However, these particles have at least one bond with each other and three of them were still transmitting load between the platen and the largest fragment at the moment of fracture (this being proved

by Fig. 8.1a showing that at the primary fracture moment, state {5}), the platen force was still relatively large, about 40% of its maximum value. All of these particles connecting the largest fragment with the platen transformed into debris after fracture, as soon as there was no load transmitted between the largest fragment and the platen.

Images similar to the one in Fig. 8.10c were plotted, Fig. 8.11, to monitor the evolution of the fracture surface. The states {1}-{5} are the same ones that also appeared in Fig. 8.1 and Fig. 8.3. State {0} illustrates the fracture surface at the start of the test: green particles were in contact with the future second largest fragment and light blue particles were in contact with future debris particles. The convention is that when a green particle looses all its contacts with the future second largest fragment it turns black. In a similar way, a light blue particle turns dark blue when it looses all bonds with the debris. Using the above colour-coding for the particles situated in the part of the agglomerate that will become the largest fragment at primary fracture proved to be a good method of observing the fracture initiation and propagation.

State {1} in Fig. 8.11 clearly indicates that the fracture crack initiated from the platens and propagated radially and upwards. From the images of states {1} and {2} one can already observe that there was no perfect crack front during fracture propagation. Although state {2} indicates that the crack propagated along almost a triangular surface (observe that the black and dark blue particles roughly form a triangle with the bottom platen), there are still contacts inside the triangle which have not broken. State {2} is the moment when the fracture had propagated to reach the agglomerate's centre and when the platen force reached its maximum value (Fig. 8.1b). Comparing state {2} in Figs. 8.11 and 8.2, it can be noted that the "fracture crack propagation" seen as bond breakage on the fracture surface is a little in advance of the "fracture crack propagation" considered by complete separation of particles along the fracture surface. These two terms were a little different because, for example, a particle in the largest fragment could have more than one bond with particles in the second largest fragment.

State {3} in Fig. 8.11 correlates well with the one in Fig. 8.2. The fracture crack had propagated above the equatorial plane of the agglomerate. However, Fig. 8.11 also indicates that some particles situated approximately along the loaded diameter continued to maintain contact with the future second largest fragment. This appears to be mainly due to the fact that these particles belonged to the damage zone adjacent to the platen (and these "stubborn" contacts were actually transmitting/carrying load from the platen into the agglomerate, as seen in Fig. 6.55).

The fracture crack continued to propagate through the top half of the agglomerate, state {4} in Fig. 8.11, and reached the upper top of the agglomerate at state {5} producing fracture.

Although fracture meant that all particles in the largest fragment started moving in an opposite way from the particles in the second largest fragment, some particles (mainly situated in the zone of high compressive stresses close to the platen) in the largest fragment still maintained contact with the second largest fragment. The two large fragments were completely separated from each other only later; as soon as the platen force had dropped completely. The entire evolution of the fracture surface is presented schematically in Fig. 8.23, where shaded areas indicate the extent of crack propagation.

8.3.2 Double Impact

The fracture surface of the dense[1] agglomerate in the double impact test, for 0.02 m/s impact velocity (M_p=100 M_a), was more planar and meridional than in the free-fall impact test with 0.2 m/s impact velocity (see Fig. 8.12 compared to Fig. 8.9). Additionally, much less debris had been detached at the moment of fracture. It is interesting that the fracture surface in the double impact test was so differently located, being oriented almost perpendicular to the one in the free-fall impact test - see Fig. 8.12a compared to Fig. 8.9a.

In the same way as for the free-fall impact test discussed in Section 8.3.1, the evolution of fracture along the fracture surface was examined by monitoring the state of particles in the largest fragment, in a view perpendicular to the fracture surface. Six states, from {1} to {6}, are presented in Fig. 8.13; they are the same as the ones appearing in Fig. 8.4 and 8.5. Green particles are the ones still in contact with the second largest fragment; when a green particle looses all its contacts with the second largest fragment it turns black.

At half the strain to fracture (see Fig. 8.4), state {1} in Fig. 8.13 demonstrates that fracture initiated from both platens as two almost symmetric cracks. The fracture cracks propagated first over two roughly triangular areas starting from the agglomerate-platen interfaces. At state {2}, the two fracture cracks met at the agglomerate's centre as the triangular areas of propagation enlarged.

The propagation of the fracture cracks was even less uniform than in the free-fall impact test, especially after state {2}. One of the main reasons is that, in double impact tests, there are two loading points compared to only one in free-fall impact tests. The few (green) particles, mainly located along the loaded diameter, that persisted in maintaining contacts with the second largest fragment, made it very difficult to follow the fracture propagation.

Carefully comparing state {3} with state {2} one can observe that the two cracks propagated from the poles inwards and from the loaded diameter outwards. The same can be noted by comparing state {4} with state {3}. The last areas reached by the propagating cracks prior to fracture, state {5}, are the ones situated close to the agglomerate's equator. As soon as the

compressive forces close to the platens along the loaded diameter dropped, the "trapped" particles started to lose contact with the second largest fragment - see state {6} in Fig. 8.13. The decrease in the compressive forces is confirmed by the large drop in platen force between states {5} and {6} in Fig. 8.4a. The evolution of the fracture surface is presented schematically in Fig. 8.24, where shading is used to indicate the areas over which the crack had already propagated.

8.3.3 Diametrical Compression

The dense[2] agglomerate with the higher contact density fractured into two large fragments in the diametrical compression test (platen velocity = 10 mm/min) - see Fig. 8.14. Compared to the half-half fracturing of the dense[1] agglomerate, the fracture surface was not quite parallel to the applied loading direction (Fig. 8.14b). This was due to the eccentric location of the two agglomerate-platen contacts. As in the case of the double impact test described above, fracturing occurred with very little debris detachment and the fracture faces exhibited several irregularities (Fig. 8.14).

The evolution of the fracture surface was examined using the second largest fragment (the left-hand-side fragment in Fig. 8.14b). As in the previous analyses six milestone states in the fracture process are presented in Fig. 8.15, corresponding to the states shown in Figs. 8.6 and 8.7. Black is again used to mark the particles along the fracture surface which lost all contacts with the largest fragment.

As in the double impact test, fracture cracks initiated from both platens (see state {1} in Fig. 8.15) towards the agglomerate's centre. However, the fracture cracks appear to have propagated in an even more disorderly way than in the double impact test of the dense[1] agglomerate. From the area close to the platens, see state {1}, the two fracture cracks propagated and met at the agglomerate's centre at state {2}. Between state {2} to state {5} the merged fracture crack propagated towards the equatorial surface. From states {4} and {5} it can clearly be seen that complete fracture had been established also over the whole right hand side of the fracture surface.

The last bonds to break between the two large fragments were again situated on the vertical diameter and broke a while after primary fracture, state {5}, when the platen force dropped almost to zero. State {6} in Fig. 8.15 reveals that these was still a few particle bonds connecting the large fragments. The evolution of the fracture surface was very similar to the one in the dense[1] agglomerate subjected to double impact, presented schematically in Fig. 8.24.

8.3.4 Discussion

Because of irregularities in the propagation of the fracture crack, the fracture propagation illustrated in Fig. 8.11, 8.13 and 8.15 was not as smooth as the schematic diagrams Fig. 8.23 and 8.24. The explanations presented below must be considered having in mind that only in idealistic homogeneous solids would a fracture crack be expected to propagate behind a "perfect" (smooth) crack front.

The coarseness of the agglomerate is the reason for most irregularities in behaviour. The several particles, situated around the vertical diameter (generally) close to the platen/s, which maintained bonds until the very end of the fracture process were observed in all types of test. These particles were located in regions of high compressive stress and, consequently, they only lost these bonds when the platen forces dropped to near zero. This demonstrates that the particles were a part of a "trapping" mechanism: one particle that belongs to a future large fragment is "trapped" between particles belonging to another future large fragment. This phenomenon was recently also observed experimentally in indentation tests on heterogeneous materials, and was called "bridging (frictional) grain pullout" - see Swanson et al (1987), Chantikul et al (1990), Lawn (1993). It is said to be a characteristic of intergranular crack propagation and is more pronounced for a certain range of grain (constituent particle) size. A simplified two-dimensional scheme of the mechanism is presented in Fig. 8.16 (see page 263).

The coarseness of the agglomerates also made it difficult for a clean fracture to propagate. This was because, as the fracture was 100% intergranular, the fracture crack had to follow a small-scale zig-zag trajectory. Also, having a random distribution of particles in the agglomerate and the fact that some interparticle elastic overlaps (at bonds) were much larger than others, some bonds in the fracture trajectory were much more difficult to break than others.

A few of the particles which still maintained contact between the two large fragments at the moment of fracture (and a while after that) were actually debris particles detached from the fracture surface. This is only one of the ways in which the "straightening-up" processes of the fracture crack observed in the simulations contributed to the "irregularities" observed in the evolution of cracks along the fracture surface.

8.4 "SELECTION" OF THE FUTURE FRACTURE SURFACE

At the start of any of the three types of test there was an infinite number of directions in which agglomerate fracture could occur. However, as a result of a complex selection process, only one direction became the one along which the agglomerate fractured into two fragments. The selection process takes into account, as many researchers would assert, the pre-existing "flaw population" of the agglomerate along the loading direction. However, the exact test conditions and the rate of the applied load were found to be at least as significant in the selection process.

8.4.1 Analysis Of The End-Products

In Chapters 6 and 7 it has been shown that the dense agglomerates can fracture in each of the three types of test considered. For all these types of test the load is compressive and is acting along exactly the same agglomerate diameter (as the position of the agglomerates relative to the platen/s was the same for each test). If exactly the same agglomerate is tested under the same (compressive) load orientation, one might infer that, for tests producing fracture of the agglomerate, the primary fracture surface will be the same not just for slightly different loading rates, but will be the same for all three types of test configurations. The basis of this presumption is that the agglomerate would always fracture along its weakest internal plane, and that this weak plane is "inherent" at the start of test due to the distribution of pre-existing flaws. If a sphere fractures along a plane in one test, one would believe that plane was the weakest from the very beginning and that is why it was "selected" for fracture; and that for similar loading conditions the sphere would fracture along the same plane (at least the primary fracture) even for different loading rates.

This project's results indicate that fracture surface "selection" is a very complicated process, at least for coarse agglomerates. The fracture surfaces over which the three dense agglomerates fractured in the three types of test are presented schematically in Figs. 8.17 - 8.20. The thicker lines denote the primary fracture surface, the thinner ones indicate the location of the secondary fracture surfaces.

A first glance at the results of the double impact and fast diametrical compression tests on the weak-dense agglomerate, presented schematically in Fig. 8.17, would suggest that there are three approximately half-diameter planes (HDP) over which fracture is most likely to occur in this agglomerate. The approximate directions of the HDPs are from the agglomerate centre towards the cardinal points N, SE and W. However, it can be observed that the exact direction of the fracture surfaces varied slightly with the loading rate, mass of platen and type of test. In the case of a heavier platen the weak-dense agglomerate fractured directly in three; two of the HDPs (the ones approximately directed W and SE) had slightly different

locations than in tests when a lower striking-platen mass was used. For the same initial platen velocity, the fast diametrical compression test produced primary fracture along a different direction than in the double impact test (see Fig. 8.17d compared to 8.17a). Both fast diametrical compression tests resulted in slightly different locations of the three fracture HDPs compared to the double impact tests (see Fig. 8.17d,e compared to 8.17a,b,c).

In the case of the dense[1] agglomerate, the surface along which primary fracture occurred was almost the same for the diametrical compression and double impact tests (for the very few strain-rates and platen masses considered - see Fig. 8.18d,e,f). However, in the case of the free-fall impact test the location of fracture surfaces was very sensitive to the impact velocity. First of all, a bit surprisingly, the free-fall impact tests resulted in primary fracture along directions that were almost perpendicular to the primary fractures obtained in the diametrical compression and double impact tests (see Fig. 8.18a,b,c compared to 8.18d,e,f). Primary and secondary fracture for an 0.1785 m/s impact velocity occurred along fracture surfaces that had quite different locations from the primary fracture surface obtained for 0.2 m/s impact velocity (see Fig. 8.18a and 8.18b). Observe that the main fracture pattern from the 0.1785 m/s test "reappeared" in the test using an impact velocity of 0.3 m/s (Fig. 8.18c). Not only was the location of the fracture surfaces sensitive to the impact velocity, but also the inclinations of these surfaces relative to the loading direction. Whereas the primary fracture surface for the 0.2 m/s impact velocity test can be approximately considered to be a meridional plane, the fracture surfaces for the 0.1785 m/s and 0.3 m/s impact velocity tests are oblique planes (see Fig. 8.20).

Slightly different locations for the secondary fracture surfaces were found in the free-fall impact tests on the dense[2] agglomerate (with the higher contact density, see Fig. 8.19b,c and 8.20c,d). An increase in the impact velocity produced an increasingly large fragment at the pole opposite the point of impact. However, the location of the primary fracture surface was almost the same for impact velocities between 0.12-0.2 m/s. The dense[2] agglomerate proved to be very sensitive to the exact configuration of each type of test. The fracture surfaces obtained (Fig. 8.19) are so different for each type of test that they seem to have been obtained using three different agglomerates.

For both dense[1] and dense[2] agglomerates it was found that the fracture plane was slightly inclined to the direction of loading in the case of diametrical compression tests. In the impact tests - especially for higher impact velocity - the primary fracture plane was, with one exception, along the loading direction. It thus appears that higher loading rates tend to produce primary fractures along the loading direction.

8.4.2 Crack Initiation And Propagation

Having observed that the location of the fracture surface in an agglomerate varies with loading rate and the exact test configuration, it is interesting to analyse in more detail how and why this phenomenon occurs. The answer must lie in the initiation and propagation of cracks since they produce the fracture.

As observed in section 8.2, agglomerate damage starts with the development of plastic deformation zones (roughly conical in shape) adjacent to the agglomerate-platen interfaces. The initial plastic deformation consists mainly of bond breakage (forming of microcracks) and local rearrangement of the particles due to sliding. From each damage zone more HDP cracks are initiated and start to propagate into the agglomerate. However, not all these cracks develop at the same speed and only a few of them (usually two, but sometimes none) will contribute to producing the primary fracture. It is important to know if, for the same agglomerate, different loading rates or even slightly different test conditions will initiate exactly the same cracks and also to identify what causes some cracks to propagate almost continuously and others to stop.

Generally, it was observed that 100-150 bonds broke near each platen during the initial damage zone formation. Figure 8.21 presents views from above of the bonds that broke in various tests on the dense[1] agglomerate roughly until the moment when the bond breakage reached the centre of the agglomerate. Figure 8.22 presents similar views of the bonds that broke in various tests but on the dense[2] agglomerate, this time until a little (while) before the moment when the bond breakage reached the centre (equatorial plane) of the agglomerate. The initiation and initial propagation of the first-created cracks in exactly the same agglomerate can, therefore, be easily compared for different tests.

First of all, it is interesting to note that some cracks initiated near the top and bottom platens were similar for different loading rates and even for different test types. However, the propagation of cracks exhibited some differences, even for tests resulting in almost the same fragmentation. The first case to be analysed was the dense[1] agglomerate (Fig. 8.21a,b,c and Fig. 8.5 state {2}), as in all four tests the primary fracture finally occurred along roughly the same W-E surface (see Fig. 8.18d,e,f). Although occurring at slightly different times in the test, the total number (five at the top and three at the bottom) and direction of HDP cracks initiated was approximately the same for all four tests. However, in some tests several cracks developed more than others, or in slightly different directions. For example, the top cracks towards W and E were more focused in the diametrical compression test than they were in the double impact tests. The bottom cracks were more focused towards the three main directions (N, W and SE) in tests at lower loading rates (Fig. 8.21c and Fig. 8.5

state {2}) and in free-fall impact tests (Fig. 8.21d and Fig. 8.2 state {2}); they also propagated more in these tests.

An important aspect to observe in Figs. 8.21, 8.22 and state {2} in Figs. 8.2, 8.5 and 8.7 is that, although at the start more or less the same cracks initiated for the same agglomerate they initiated and propagated at different times during different tests. Moreover, only about 50% of the actual bonds that broke to form the initial crack propagation were the same ones for each of the tests. In the free-fall impact tests the most likely direction for the future primary fracture can usually be anticipated from the initial stages of crack propagation (as cracks propagate from one platen only). It is, however, more difficult for double impact and diametrical compression tests, where one must observe separately the cracks developed at both the top and bottom platens.

In the free-fall impact test on the dense[1] agglomerate (V=0.2 m/s) it was relatively easy to anticipate the approximate direction of the future fracture surface from a very early stage (Fig. 8.2), as two HDP cracks developed more than others and tended to merge to form an FDP crack. In other free-fall impact tests (see Fig. 8.21d and 8.22c,d) the direction of the primary fracture surface could only be inferred at a later stage in the test. In the double impact test with the highest impact velocity causing fracture (0.2 m/s, see Fig. 8.22b) the fracture surface was dictated by the intervention with the top platen, as the cracks in the bottom half of the agglomerate only developed at a much later stage when they were already influenced by the direction and propagation of the cracks in the top half.

In slow-velocity double impact and diametrical compression tests one has to find at least two HDP cracks developed towards almost the same direction in both at the top and bottom halves. In order to be the best candidates for the future fracture surface these cracks have to tend to form an FDP crack. The W-E direction of primary fracture can be identified early in tests from Fig. 8.21a,b,c and 8.5, and the NE-SW direction can already be inferred from state {2} in Fig. 8.7. Approximate directions for fracture (towards NW, SW and NE) could also be anticipated early from Fig. 8.22a.

The higher the impact velocity, the larger was the damage zone developed by the platens. This usually resulted in more cracks initiating and propagating from the damage zone and in more extensive propagation (see Fig. 8.22c,d). Tests at higher impact velocities, therefore, resulted in fracture of the agglomerates into more fragments. In tests resulting in agglomerate fragmentation (e.g. very high velocity impacts) cracks were usually initiated at later stages in the test and were more difficult to distinguish.

8.5 CRACK VELOCITY

The rate of advancement of broken bonds into an agglomerate can provide useful information about the damage behaviour. The average propagation velocity of broken bonds along the fracture surface was calculated for the four successive steps ending in primary fracture (Fig. 8.23 and 8.24). Calculations were performed for tests resulting in fracture for all three dense agglomerates - see Table 8.1.

8.5.1 Free-Fall Impact

For free-fall impact tests the progress of bond breakage was measured vertically upwards, along the loaded diameter, in steps corresponding to half the radius of the agglomerate, as presented in Fig. 8.23.

The average velocities displayed in column (9) of Table 8.1 are simply the diameters of the agglomerate divided by the time to primary fracture. The test exhibiting the fastest fracture was the free-fall impact test on the strong dense agglomerate with the higher contact density (dense[2]), for 0.2 m/s impact velocity. This test will be discussed first as the average velocities vary very differently from the other five free-fall impact tests presented in Table 8.1. The velocity of the damage zone formation, column (5), is not much larger than for the other two free-fall impact tests on the same agglomerate. However, the average fracture crack propagation velocity (column (10)) is much higher than in the other tests. From columns (6)-(8) it can also be observed that the fracture crack accelerates throughout the fracture propagation process. This test in fact marks the transition from agglomerate fracturing to agglomerate fragmentation (as three large fragments and five medium-sized fragments were eventually produced).

Results of the other two free-fall impact tests on the same agglomerates, columns (6)-(8), show that fracture crack propagation accelerates and then decelerates (quite sharply) during the final stage of propagation. It is interesting that in the case of the other strong agglomerate (dense[1]), the fracture crack starts to decelerate earlier - approximately at the moment when it reaches the agglomerate's centre.

8.5.2 Double Impact

The results of the higher-velocity (0.2 m/s) double impact test on the dense[1] agglomerate are best compared to the free-fall impact test of the same agglomerate with the same impact velocity. The velocity of the damage zone creation , column (5), was 40% of that in the free-fall impact test, presumably due to the fact that two zones had to be created instead of one. The overall average fracture crack velocity, column (10), was 70% higher in the double impact test, indicating that it is easier (and faster) to fracture an agglomerate when it is

confined between two platens than when it is free to rebound or displace from the point of impact. Another difference between the two tests is that the fracture crack does not decelerate towards the end of the fracture process (see column (8) compared (7)), as was the case in the free-fall impact test. For a lower-velocity impact (0.02 m/s) the average fracture crack propagation velocities are lower during each step. However, in this test, from initiation to fracture the crack is almost constantly accelerating up to a final value.

The measurements for the 0.04 m/s impact velocity test on the weak-dense agglomerate are also interesting. For double the impact velocity (M_p=100 M_a) approximately the same final velocity of fracture crack propagation, column (8), was reached as in the dense[1] agglomerate (V=0.02 m/s, M_p=100 M_a). However, the overall average fracture crack propagation velocity was more than seven times lower, column (10), this suggesting that it was much more difficult to fracture the weak-dense agglomerate than the dense[1] one.

8.5.3 Diametrical Compression

The fracture crack propagation velocity followed a similar trend in diametrical compression tests as in double impact tests of low impact velocity in that it was continually increasing from initiation to fracture, see columns (6)-(8). For the dense[1] agglomerate, although there was not much difference in the fragments produced by the diametrical compression and the 0.02 m/s double impact test, the average fracture crack velocity was almost 200 times lower (column (10)). Even at the end of the fracture process, column (8), the crack velocity was only about 5% of that at the end of the double impact test.

In the diametrical compression test on the dense[2] agglomerate (with the higher contact density), the overall average fracture crack velocity (see column (10)) was almost four times higher than for the other, dense[1] agglomerate. Close to the fracture moment the fracture crack accelerated rapidly and reached half the velocity obtained in the free-fall impact test (0.12 m/s impact velocity) for the same final stage of propagation, column (8).

8.6 MAIN PHASES OF FRACTURE

From the results obtained from all three types of test on the two strong-dense agglomerates exhibiting primary fracture in two or three large fragments, it is concluded that there are 8 distinct phases in the fracturing of coarse agglomerates.

Phase 1: Elastic deformation. In each test simulation there was, at the start, a very short phase during which no damage (bond breakage) at all occurred. The agglomerate's response

was elastic and the work input was transformed into internally-stored energy. This elastic deformation phase usually lasted until the platen force/s reached 1-2 mN.

Phase 2: Development of plastic deformation (damage) zone/s. Microcracks started to form first just by the agglomerate-platen interfaces, and then almost randomly within an approximately conical region adjacent to the platen/s. This region approximately corresponded to the zone in which the interparticle forces were the largest (compressive), due to the load transmission into the agglomerate. Ideally, load transmission would be directed along the agglomerate's vertical diameter but, due to the randomly-distributed interparticle contact network, branching occurred within a conical region. The larger compressive interparticle contact forces resulted in larger overlaps at interparticle bonds and thus unequal small displacements of particles within the agglomerate. The randomly-distributed orientation of bonds and the unequal particle overlaps allowed displacements of some particles relative to each other, which finally resulted in sliding at interparticle contacts and breakage of bonds, in a random-like manner within the conical zones. Not just the location, but also the orientation of broken bonds (microcracks) in the damage zone/s was roughly random. Under the applied load some particles in the cones were, therefore, able to rearrange in order to accommodate the load. Plastic straining of the agglomerate commenced in phase 2 due to the irreversible displacements (rearrangements) of the particles in the damage zones.

Column (5) in Table 8.1 suggests that the extreme velocities in the development of the plastic zone/s occurred with the dense[1] agglomerate: the maximum was noted for the free-fall impact test of 0.3 m/s impact velocity, and the minimum for the diametrical compression test (about 2300 times lower than the maximum). It is also noted that varying the impact velocity in free-fall impact tests did not bring much variation in the velocity of the damage zone creation/development. The increasing compressive load at the agglomerate's pole/s developed the inverted conical plastic deformation zones which induced increasing hoop tensile stresses inside the agglomerate. These stresses "encouraged" the initiation and propagation of vertical cracks. Phase 2 usually corresponded to the interval of time between stage 0 and stage I in Figs. 8.23 and 8.24.

Phase 3: Initiation of cracks. Even the damage zone formation can be seen as a process of crack initiation, as the initiation of a very large number of micro-cracks. However, the initiation of the cracks which were to propagate farther into the agglomerate started to occur only shortly before the creation of the damage zone was accomplished (usually a little before stage I in Figs. 8.23 and 8.24). Not all cracks initiated at once, and some propagated more than others. Usually 3-5 larger cracks plus 3-5 smaller cracks initiated from the periphery of each damage zone. Due to the shape of the damage zone pushing into the agglomerate as a

result of the compressive load, each crack developed from the damage zone along an approximately half-diametral plane (HDP).

Phase 4: Initial propagation of cracks. This phase actually overlapped with the crack initiation phase and continued until some cracks had reached the agglomerate's centre (stage II in Fig. 8.23 and 8.24). From each platen typically 3-5 cracks propagated more than others, of which only one or two reached the agglomerate's centre. Although the agglomerate was confined between two platens in diametrical compression and double impact tests, the propagation of cracks in this phase was no different from that in free-fall impact tests. Cracks originating from one pole were not influenced by the propagation of cracks from the other pole. (During this phase, cracks propagated much faster in the free-fall impact and high-velocity double impact tests than in the diametrical compression and low-velocity double impact tests, see column (6) in Table 8.1.) In free-fall impact tests this phase lasted until the platen force attained its maximum value whereas in double impact tests it corresponded to the last peak of the platen force. This means that, from this moment, the internal stored energy started to be used in the fracture process of the impact tests.

In phase 4 development of the conical damage zone/s continued. The zones did not enlarge in the diametrical compression and low-velocity double impact tests but more microcracks formed inside the cones due to increased local plastic deformation. In high-velocity impact tests the damage zone even expanded a little radially, forming a slightly larger conical zone.

Phase 5: Fracture crack selection. This phase lasted approximately until cracks had about a quarter of the diameter left to propagate (stage III in Fig. 8.23. and 8.24.). Compared to the previous phase, phase 5 was when the selection of the fracture crack was finally established. Generally, only the fracture crack continued to propagate once the selection had been made.

In free-fall impact and high-velocity double impact tests, the fracture crack was decided by the agglomerate's impacted half only. The fracture crack was usually created from two similarly oriented HDP cracks propagating in opposite directions. In other words, two HDP cracks merged to form an FDP crack.

In diametrical compression and slow double impact tests, cracks propagated from both poles and the moment when they reached the agglomerate's centre was also the moment when cracks from one pole met the cracks from the other pole. The orientation of cracks in the two halves of the agglomerate did not necessarily correspond with each other. During phase 5 the two halves of the agglomerate adjusted to produce compatible sets of cracks in both hemispheres from which the fracture crack was selected. The ideal "easy" situation was when there were four HDP cracks similarly oriented (two propagating from each pole). However, it was usually the case that at most three cracks (two propagating from one pole

and one from the other) had similar orientation. In this case the fourth ("missing") crack was quickly (during this phase) initiated and propagated in order to establish the crack selected for fracture. There was almost no additional microcracks formed in the damage zone/s during this phase although plastic deformation continued to occur. Some non-fracturing cracks and microcracks started to heal.

Usually, only by the end of phase 5 did the platen force in the diametrical compression test attain its maximum value. In the impact tests the average interparticle contact force and the platens force had already dropped a little indicating that, during this phase, some of the internally stored energy was already used in the fracture process.

Phase 6: Final phase of crack propagation. During this phase the fracture crack propagated over the last remaining area of the future fracture surface (between stage III and stage IV in Figs. 8.23 and 8.24). Unlike the other two crack propagation phases, bond breakage was exclusively related to the propagation of the well-established fracture crack.

Crack propagation velocity in phase 6 dropped considerably in the free-fall impact tests (sometimes to under half compared to the previous phase - see column (8) compared to (7) in Table 8.1). This was probably as a result of the large drop in the agglomerate's kinetic energy and of the fact that this part of the fracture surface was the farthest from the agglomerate-platen interface (impact point) - see stage {1} in Fig. 8.23. Inversely, the fracture crack's propagation velocity increased considerably (about 150 times for the dense[2] agglomerate) in the case of diametrical compression and slow double impact tests - this was certainly as a result of the agglomerate being confined between platens and of the stored energy's larger and more sudden contribution to the fracture process (than in the case of the free-fall impact tests).

In some tests it was observed that the fracture crack also went through a process of "straightening-up" during this phase (sometimes this process starts in phase 5). As the fracture crack adjusted, some bonds re-adhered while others broke along the crack's "improved" direction (see Fig. 8.2 state {2}-{5}, for example). Often the fracture crack "improved" its orientation even for the surfaces created earlier, during the previous two phases. For instance, this phenomenon can be observed in the free-fall impact test of the dense[1] agglomerate (0.02 m/s impact velocity, Fig. 8.2) in which the fracture crack changed its direction from N-SE to a surface closer to a N-S plane. In tests in which agglomerates were confined between platens the fracture crack also displayed a tendency to propagate as close as possible along a plane passing through the agglomerate's centre.

Apart from the propagation and the "straightening-up" of the fracture crack, many cracks and microcracks re-adhered during this phase. The amount of crack healing that occurred in the

agglomerates prior to fracture was significant: the re-adhered bonds at the moment of fracture were typically half as many as the broken bonds. This is confirmed by Fig. 8.25, presenting the re-adhered and sliding contacts immediately after primary fracture in the dense[1] agglomerate (0.2 m/s impact velocity).

Phase 7: Primary fracture. This phase was very short, almost instantaneous. The large fragments separated by the freshly-completed fracture surface started to displace independently, in almost opposite directions. Because the platen force was still large and the fracture surface was rough, some bonds still maintained contacts between the new large fragments. Several particles belonging to a fragment were "trapped" between particles in the other fragment. Additionally, some contacts between the two fragments were maintained by would-be debris particles from along the fracture surface. Although connecting the two large fragments at fracture, these "odd" bonds did not prevent the large fragments from moving apart.

Phase 8: Post primary fracture. Assisted by the fact that the (usually two) large fragments were moving apart from each other (and thus the fracture surface started to "open up"), a few more bonds started to break from the large fragments, along the fracture surface. This resulted in the detachment of many debris particles from along the fracture surface (see the sudden increase in debris ratio in all tests where agglomerates fractured, for example Fig. 8.1, 8.4 and 8.6). If the platen force had almost completely dropped by primary fracture, debris particles from the contact damage zones also started to detach from the agglomerate. This debris was actually formed earlier in the test but remained "trapped" between the agglomerate and the platen/s. The relatively long healing process of non-fracture cracks continued during this phase.

More crack propagation and secondary fractures occurred in free-fall impact tests in which there was still a significant amount of elastic energy stored in the agglomerate after the primary fracture, and in double impact and diametrical compression when the tests were not stopped at primary fracture.

Generally, due to the high platen forces at primary fracture, the large fragments produced (at the primary fracture) continued to be loaded - this time separately. The elastic stored energy helped cracks (usually existing ones) to propagate and thus produce secondary fractures. There were a few tests where a secondary fracture crack propagated almost at the same time as the primary fracture crack. In these cases the secondary fracture occurred very shortly after the primary fracture. Debris particles trapped between the agglomerate and the platen/s detached very soon after the force on the platen/s dropped.

8.7 DISCUSSION AND CONCLUSIONS

This chapter's findings support the general observations and conclusions reported in the previous two chapters. Furthermore, as a result of the more detailed examination, a clearer understanding of the fracture process has been obtained. An important finding of this chapter is the precise evolution of the fracture crack along the fracture surface, which was schematically represented in Fig. 8.23 and 8.24.

Compared to brittle solids which are described as elastic until the fracture moment, the dense agglomerates in the tests analysed in this chapter exhibited a very short phase of pure elastic behaviour at the very start of each test. Fracture of the dense agglomerates was semi-brittle and was the result of a process of cracks initiation and propagation. However, this process was not as simple as is often assumed for homogeneous solids, where the crack propagates along a precise, clear crack front. In the agglomerates, cracks propagated from the damage zone behind a crack front whose shape was not so neat (and was unique for each test). Microcracks often formed ahead of this crack front, along the future trajectory of the crack. From the multiple cracks initiated and propagated from the damage zones the fracture crack emerged following a "selection" process. The fracture crack tended to propagate along the loading direction. To complicate matters even more, the fracture crack also had a tendency to adjust and realign itself to produce a more planar surface.

The pre-existing flaw population in an agglomerate was found to determine the initiation of the first cracks from the damage zone/s and the initial propagation of these cracks. However, it did not always determine the direction of the fracture surface. The exact test conditions and the loading rate were significant in selecting the fracture crack from the initial cracks and other cracks formed at later stages. In the free-fall impact and high-velocity double impact tests, only the flaw population in the impacted hemisphere can affect the direction of the future fracture surface, as the fracture crack was usually selected from the cracks developed from the impacted agglomerate-platen interface. In diametrical compression and low-velocity double impact tests, the flaw population in the whole agglomerate contributes to the selection of the fracture crack since all the initial cracks (developed from both agglomerate-platen interfaces) were considered in the fracture crack's selection process. In free-fall impact tests the primary fracture crack will tend to create a fracture surface along the loading direction whereas in diametrical compression and double impact tests the primary fracture crack/s will attempt to create a fracture surface along planes passing through the agglomerate's centre and the agglomerate-platen contacts.

In some cases the fracture crack was not selected from the initial cracks developed due to the agglomerate's initial flaw population. It was found that the loading rate of a particular type of test can change the exact location and direction of the fracture surfaces (see Fig. 8.17b,c,d,e

and Fig. 8.18a,b,c). Moreover, the loading rate can sometimes change the number and even the direction of some of the initially-formed cracks (see Fig. 8.2 and 8.21d). The loading rate actually determines which flaws will first be "activated" and therefore which cracks will be initiated and propagated first. A higher loading rate can therefore lead to the selection of a different fracture crack.

The initial flaw population in the simulated agglomerates is only represented by the positions of the constituent particles relative to the applied load. For instance, in the free-fall impact tests on the dense[1] agglomerate, the positions of the particles in the agglomerate's impacted half relative to the vertical compressive load determines three "weaker" planes along which the initial cracks will develop (see Fig. 8.2 for example). In the agglomerates simulated there are no flaws in the bonding forces as the interface energy is the same at all contacts. The small differences in the initial values of the interparticle contact forces cannot be considered as flaws as these differences are negligible. In Fig. 8.26 and 8.27 are plotted only the tensile interparticle contact forces in the two strong-dense agglomerates before testing. No particular "weaker" planes can be distinguished, even if the top and bottom halves of the agglomerates are considered separately.

The observed fracture mode was tensile (mode I) and occurred due to tensile hoop stresses. However, the complete fracture process was not entirely tensile since the damage zones did not fail in tension. The tensile character of fracture is clearly indicated by the rough aspect of the fracture faces: they could not have been created by shear. Shearing did not even occur between the conical-shaped damage zones and the rest of the agglomerate. The damage zones adjacent to the platens did not, therefore, produce the fracturing of the agglomerate in shear, as some experimentalists have inferred. The tensile rather than shear character of fracture was most clearly indicated by the particle velocity fields observed.

It is now certain that fracture of the agglomerates, in all three types of tests initiated from near the platen/s, as a few published results on tests of spherical samples have indicated. In diametrical compression tests most experimentalists have inferred that the fracture crack initiates at the agglomerate's centre and propagates towards the platens. Similar to most laboratory results, fracture of the dense agglomerates resulted in hemispherical or wedge-like large fragments and the primary fracture generally occurred along a meridional plane (approximately). Higher loading rates produced more fragments, because higher loading rates resulted in larger damage zones and the initiation of more cracks. Lower loading rates, as the ones producing half-half fracture for example, developed a lower number of initial cracks and allowed more time for the fracture crack selection process.

Although the shape of the agglomerate-platen contact zone was the same (approximately conical) as the one inferred in most published tests, its base did not correspond with the

agglomerate-platen contact area. In fact the contact flattening of the agglomerate up to the fracture moment (seen as an increase in the agglomerate-platen interface area) was very low in diametrical compression tests and almost insignificant in the impact tests. The area of the "base" of the "cone" was thus much larger than the agglomerate-platen interface area. The coarseness of the simulated agglomerates seems to have been the main cause of this phenomenon.

Fracture in the dense agglomerates was not sudden, as described by many experimentalists testing spherical samples. Fracture was actually a process that, from the first moment of crack initiation, lasted between two thirds and three quarters of the entire failure process (considered from the start of the test to primary fracture) see Table 8.1. What was sudden (and was called the "moment of fracture" in this project) was the actual break-up of the agglomerate at primary fracture, the separation of the resulting large fragments and the detachment of some debris. Most of the "fracture" debris detached from the large fragments a little while after the moment of fracture.

The fracture crack propagation occurred at the same time as other processes of agglomerate damage - mainly plastic deformation of the damage zone/s but also microcrack formation around the fracture crack and the propagation of other cracks in the agglomerate. Only between stages 3-4 (Fig. 8.23 and 8.24) was fracture crack propagation the main damage process going on.

An interesting feature observed in the simulations is the "hidden damage" represented by the re-adhered bonds. The fragments resulting from fracture were found to have a large amount of "hidden damage" even at the moment of fracture. This certainly made them weaker than might be expected. Experimentalists would expect crack healing to occur in the unloading phase after the fracture moment. However, the results of this project reveal that a significant amount of crack healing can occur before the fracture moment, sometimes even before the drop in the platen force (before unloading commences).

Many small fluctuations were noticed in the evolution of the platen force (Fig. 8.1a, 8.4a and 8.6a) which often correlated with fluctuations in the damage ratio evolution. The cause was the sudden breakage of groups of bonds - due to the sudden advance of a particular crack, or the sudden forming of a group of microcracks. In the other cases, the force fluctuations appeared to be due to local rearrangements (due to the local compaction process) of the particles in the damage zones adjacent to the platens.

Type of test	Agglo-merate type (see Table 7.1)	Ratio of platen mass to agglomerate mass (for double impact tests)	Impact velocity or top platen velocity [m/s]	Average crack propagation velocity along primary fracture surface [m/s]				overall average crack propagation velocity [m/s]		
				stage 0-1	stage 1-2	stage 2-3	stage 3-4	stage 0-4	stage 1-4	
(1)	(2)	(3)	(4)	(5)	(6)	(7)	(8)	(9)	(10)	
FREE-FALL IMPACT	dense[1]		0.2	106.1	156.2	85.2	32.3	68.2	61.1	high loading rate
			0.3	111.5	210.6	135.4	94.8	126.4	132.2	
	dense[2]		0.12	63.2	105.3	111.5	75.8	84.2	94.8	
			0.15	72.9	135.4	236.9	157.9	126.3	167.2	
			0.2	78.9	210.6	270.8	379.1	168.5	270.8	
DOUBLE IMPACT	dense[1]	1	0.2	41.7	125.0	94.8	98.7	75.8	104.2	low loading rate
		100	0.02	7.04	5.53	13.76	41.29	9.53	10.8	
	dense-weak	100	0.04	6.88	0.68	1.76	38.71	1.81	1.45	
DIAMETRICAL COMPRESSION	dense[1]		0.0001667	0.045	0.033	0.055	1.88	0.056	0.061	very low loading rate
	dense[2]		0.0001667	0.056	0.126	0.206	31.59	0.130	0.234	

Table 8.1 Average crack propagation velocity along the primary fracture surface for various tests

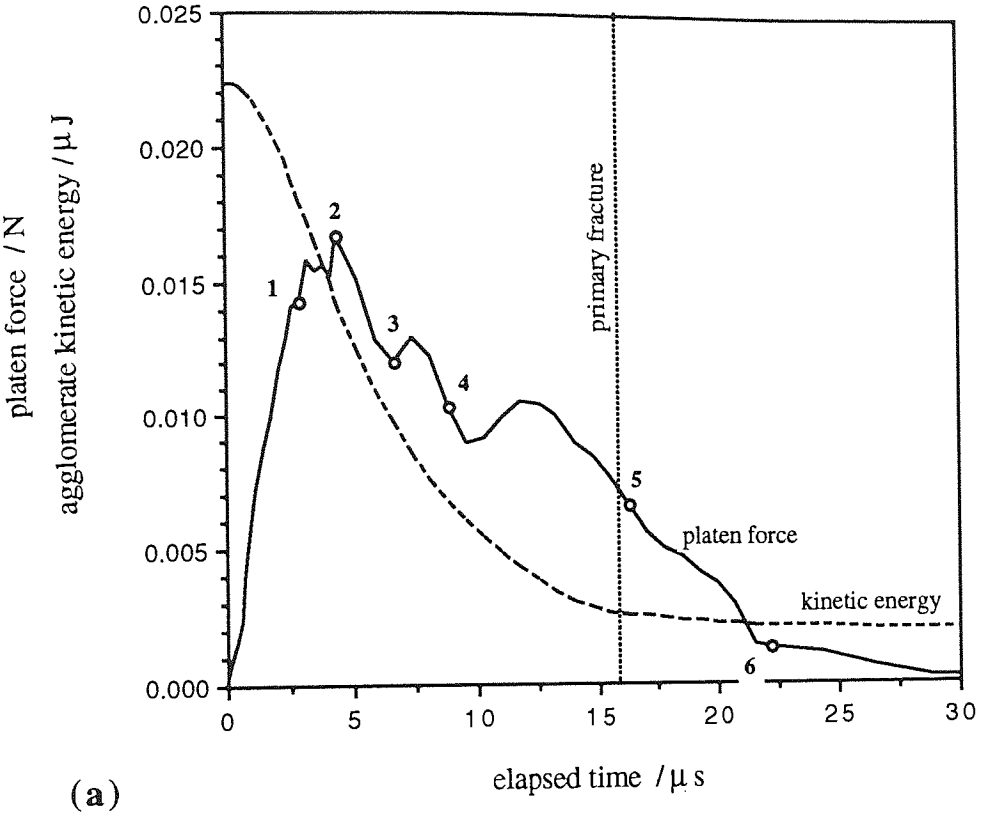

(a)

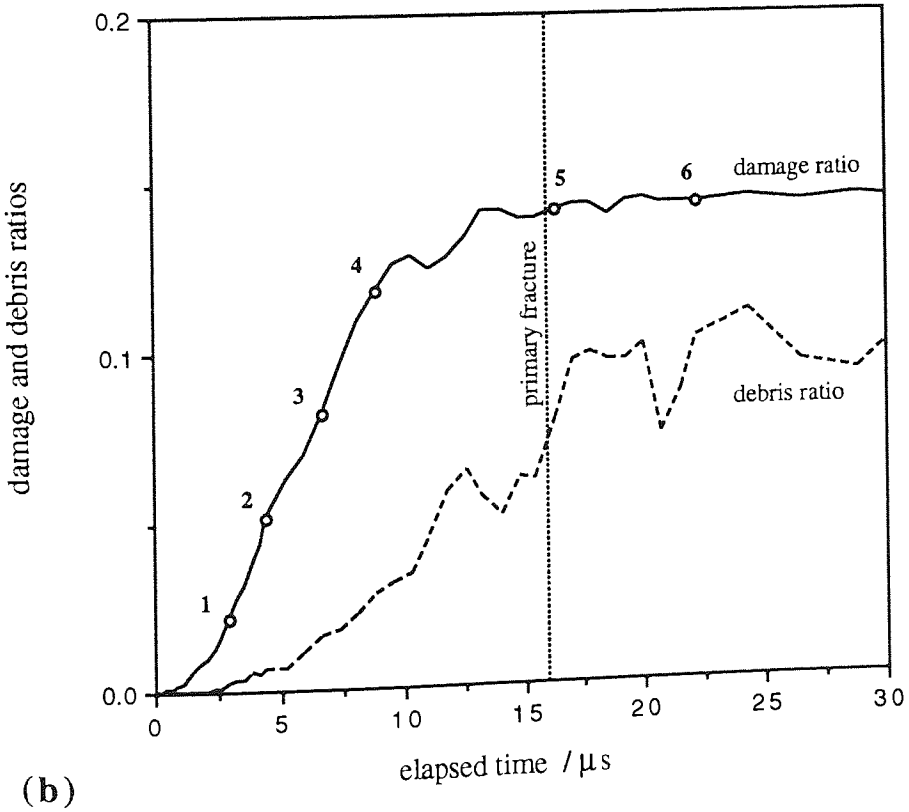

(b)

Fig. 8.1 Evolution of (**a**) platen force and kinetic energy of the agglomerate, (**b**) damage ratio and debris ratio, free-fall impact, dense[1] agglomerate (V=0.2 m/s) The states marked by the dots **1-6** are presented in Figs. 8.2 and 8.3.

State {**1**}: t = 3.0 μs (agglomerate strain = 0.04%, broken bonds: 2.24% in bottom half + 0% in top half of the agglomerate)

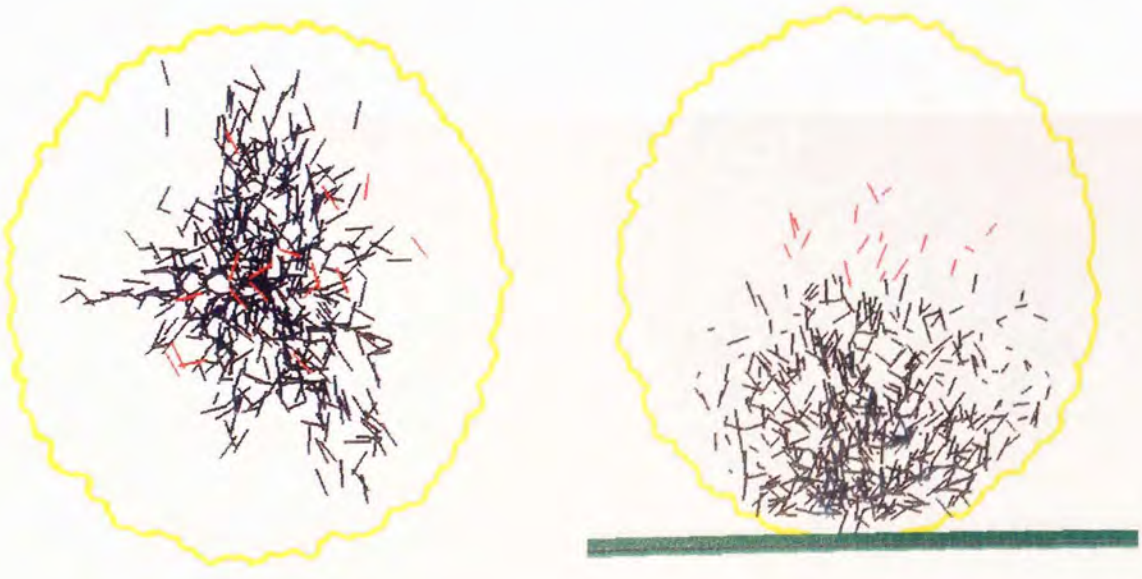

State {**2**}: t = 4.4 μs - maximum platen force (agglomerate strain = 0.06%, broken bonds: 5.01% in bottom half + 0.17% in top half of the agglomerate)

Fig. 8.2 Evolution of the distribution of bonds broken in the dense[1] agglomerate, free-fall impact (V=0.2 m/s). A view from above and one from the side (perpendicular to the fracture plane) are presented for each of the states {**1**} - {**6**}. Red is used for the top half and black for the bottom half of the agglomerate. Bonds are represented as lines tangent to the former contact; the length of each line is equal to the distance between the centres of the particles that formed the broken bond. The agglomerate is situated inside the yellow outline.

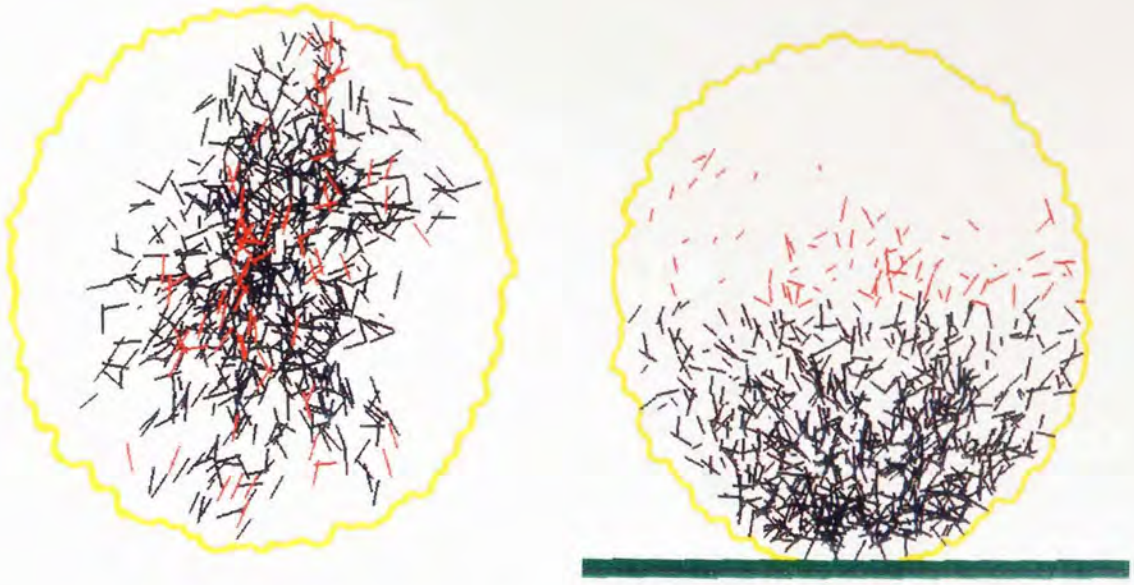

State {**3**}: t = 6.7 μs (agglomerate strain = 0.09%, broken bonds: 7.41% in bottom half + 0.81% in top half of the agglomerate)

State {**4**}: t = 8.9 μs (agglomerate strain = 0.12%, broken bonds: 9.18% in bottom half + 2.78% in top half of the agglomerate)

Fig. 8.2 Evolution of the distributions of bonds broken in the dense[1] agglomerate, free-fall impact test, V=0.2 m/s (continued).

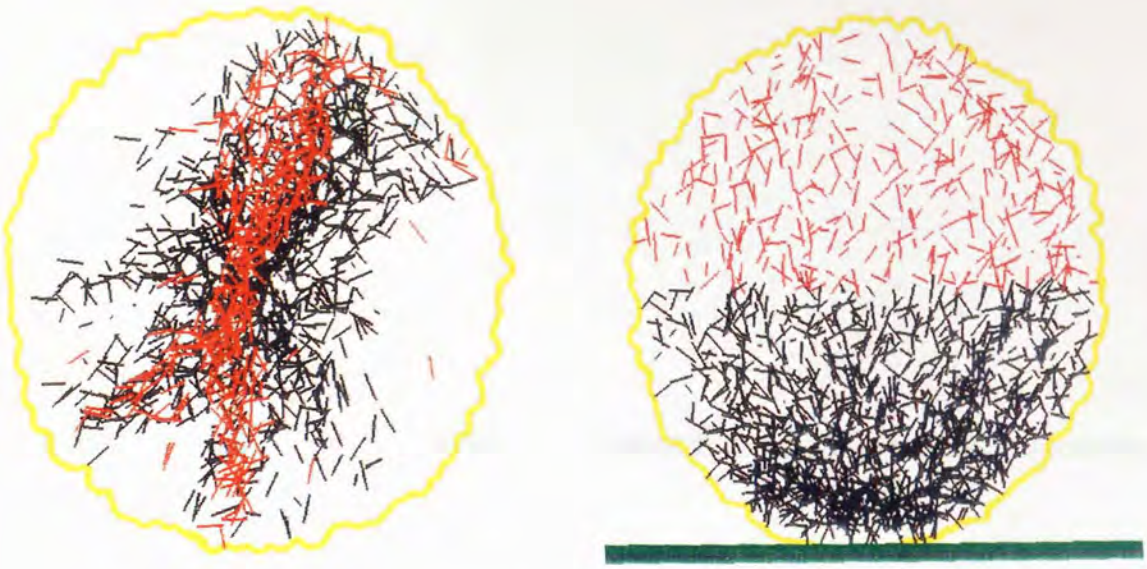

State {**5**}: t = 16.3 μs - immediately after primary fracture (agglomerate strain = 0.14%, broken bonds: 10.92% in bottom half + 3.42% in top half of the agglomerate)

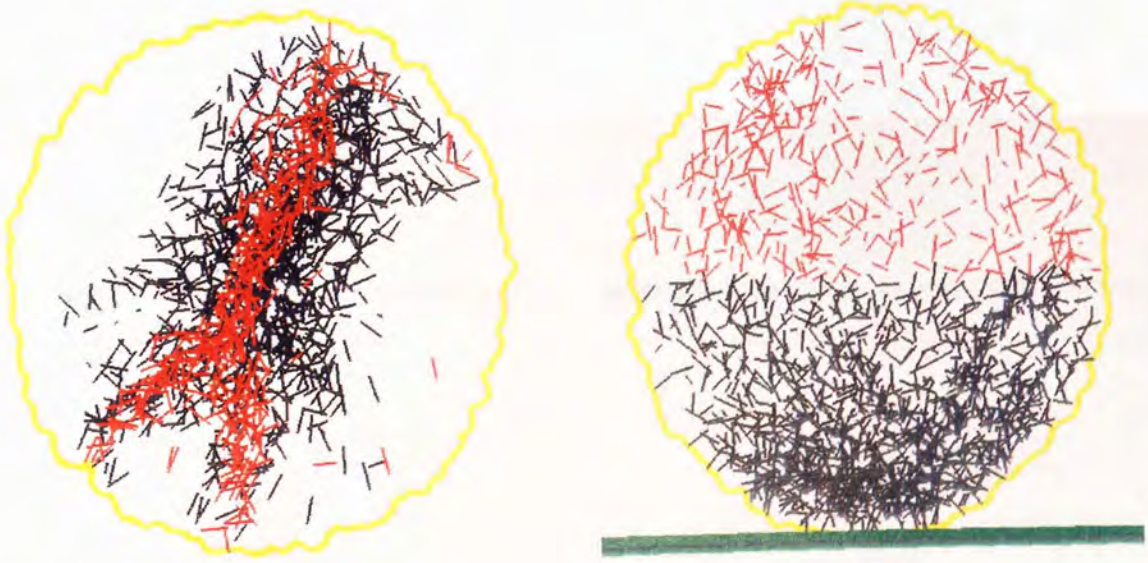

State {**6**}: t = 22.2 μs - immediately after secondary fracture (agglomerate strain = 0.19%, broken bonds: 10.88% in bottom half + 3.57% in top half of the agglomerate)

Fig. 8.2 Evolution of the distributions of bonds broken in the dense[1] agglomerate, free-fall impact test, V=0.2 m/s (continued).

State {**1**}: t = 3.0 μs

State {**2**}: t = 4.4 μs
(maximum platen force)

State {**3**}: t = 6.7 μs

State {**4**}: t = 8.9 μs

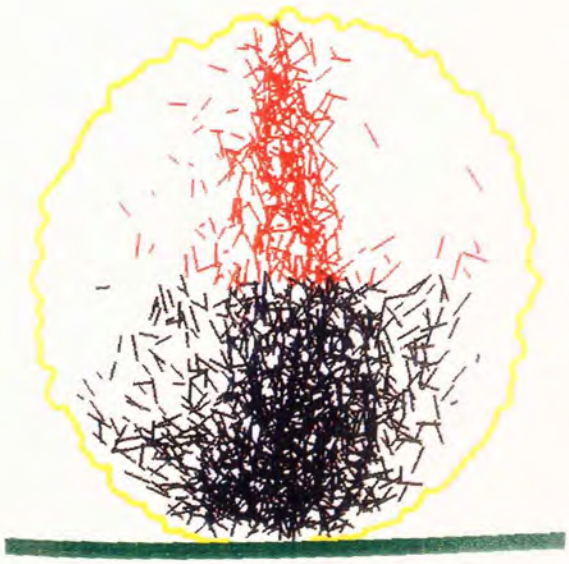

State {**5**}: t = 16.3 μs
(immediately after primary fracture)

State {**6**}: t = 22.2 μs
(immediately after secondary fracture)

Fig. 8.3 Evolution of the distribution of bonds broken in the dense[1] agglomerate, free-fall impact test (V=0.2 m/s). Same as in Fig. 8.2, but here the agglomerate is viewed from the front, along the fracture surface.

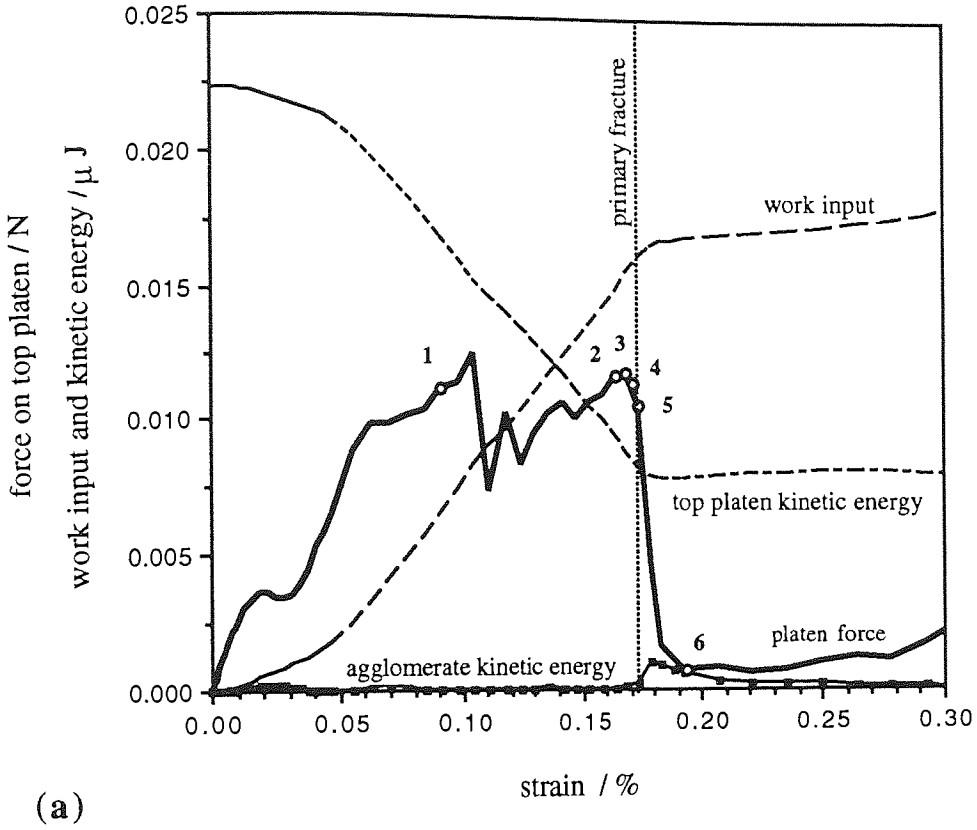

(a)

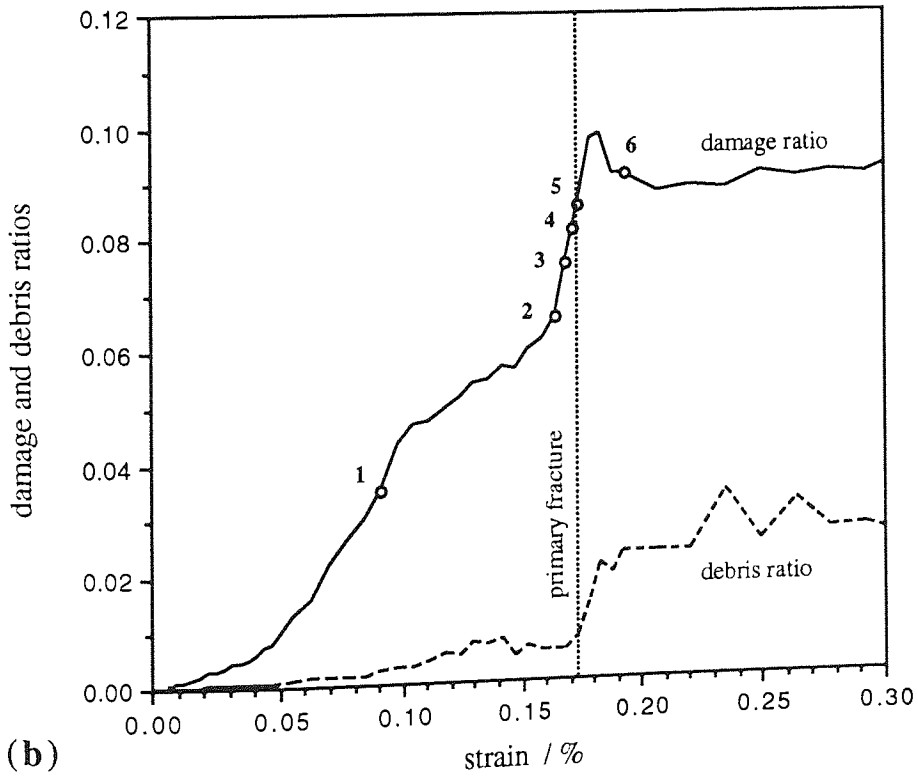

(b)

Fig. 8.4 Evolution of (**a**) platen force, work input, top platen's kinetic energy and kinetic energy of the agglomerate, (**b**) damage ratio and debris ratio, double impact, dense[1] agglomerate, (V=0.02 m/s, $M_p = 100\ M_a$). The states marked by the dots **1,2,3,5,6** are presented in Fig. 8.5.

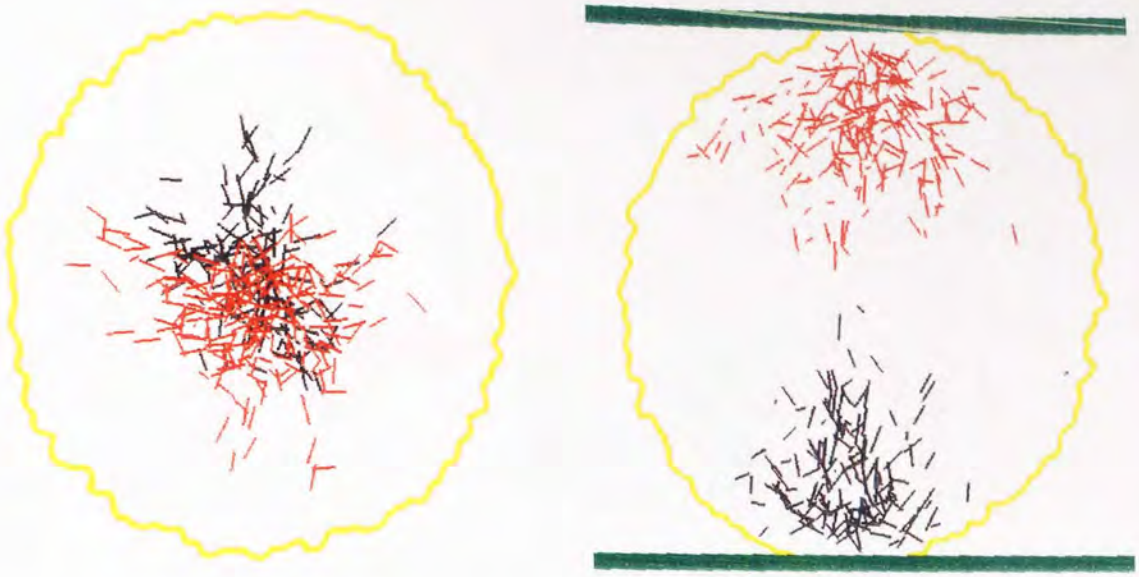

State {**1**}: t = 0.053 ms (strain = 0.091%, broken bonds: 1.53% in bottom half + 2.06% in top half of the agglomerate)

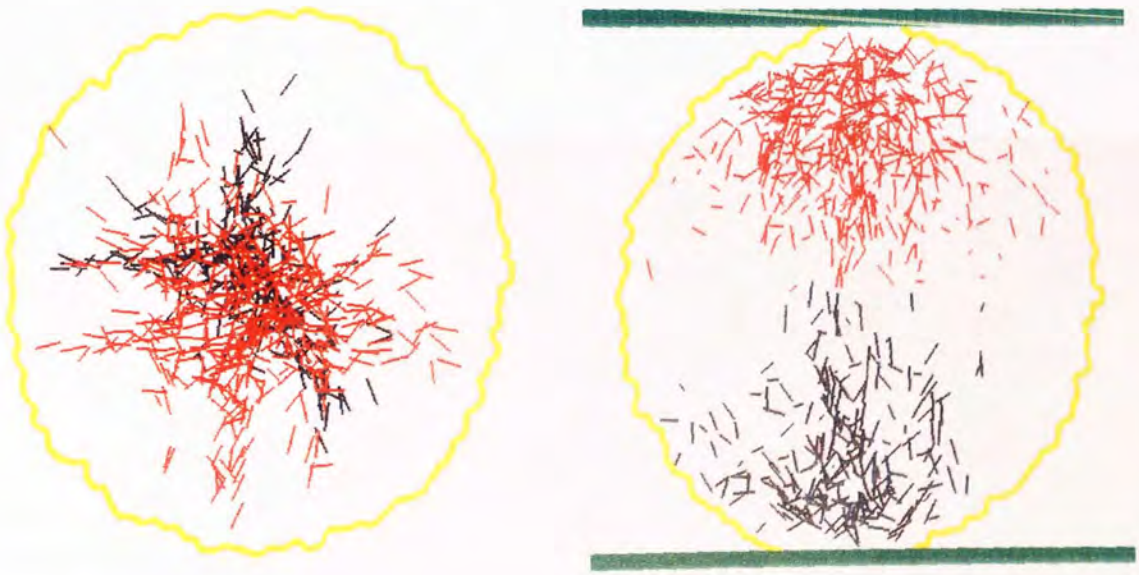

State {**2**}: t = 0.107 ms (strain = 0.164%, broken bonds: 2.40% in bottom half + 4.26% in top half of the agglomerate)

Fig. 8.5 Evolution of the distribution of bonds broken in the dense[1] agglomerate, double impact test (V=0.02 m/s, M_p=100 M_a). A view from above and one from the front (perpendicular to the fracture plane) are presented for each of the states {**1-3**} and {**5-7**}. Bonds are represented as lines tangent to the former contact; the length of each line is equal to the distance between the centre of particles that formed the broken bond. Red is used for the top half and black for the bottom half of the agglomerate. The agglomerate is situated inside the yellow outline.

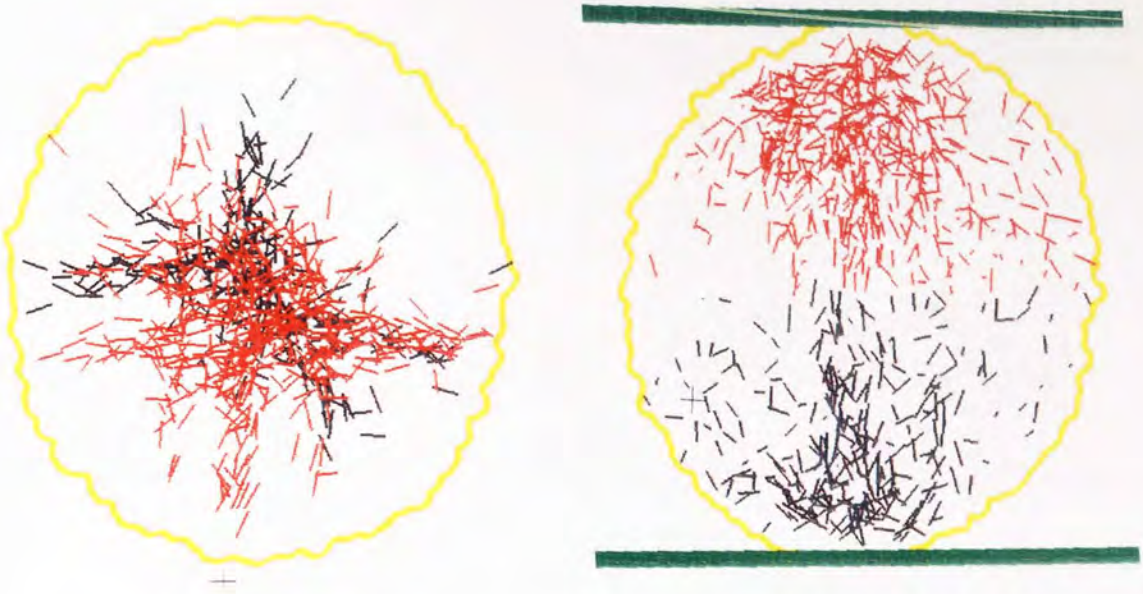

State {**3**}: t =0.111 ms - maximum platen force (strain = 0.169%, broken bonds: 2.89% in bottom half + 4.75% in top half of the the agglomerate)

State {**5**}: t = 0.115 ms - immediately after primary fracture (strain = 0.174%, broken bonds: 3.68% in bottom half + 5.05% in top half of the agglomerate)

Fig. 8.5 Evolution of the distribution of bonds broken in the dense[1] agglomerate, double impact test, V=0.02 m/s (continued).

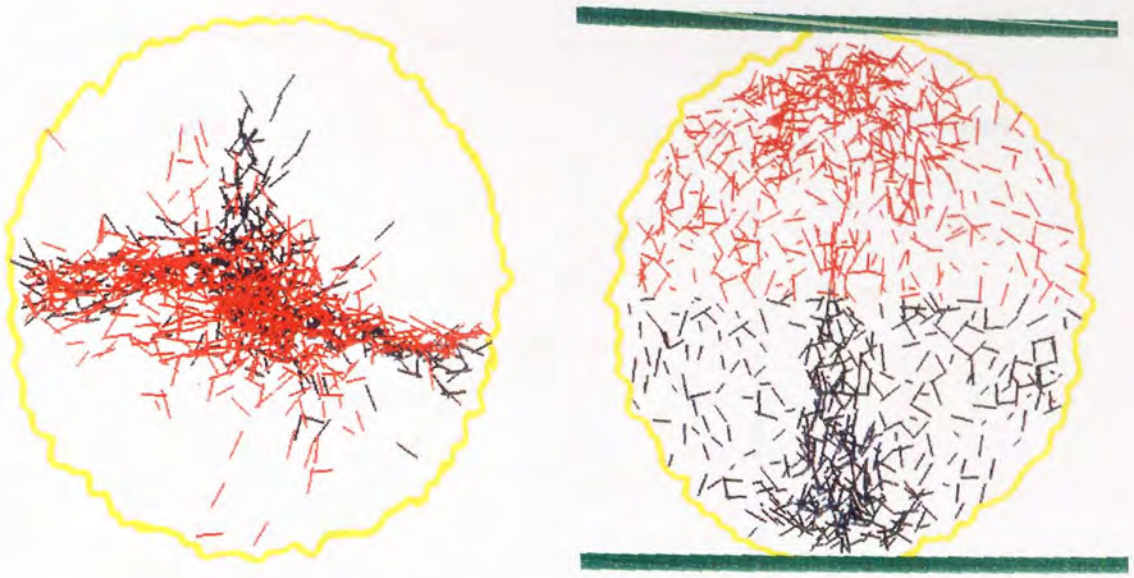

State {**6**}: t = 0.133 ms (strain = 0.193%, broken bonds: 4.14% in bottom half + 5.11% in top half of the agglomerate)

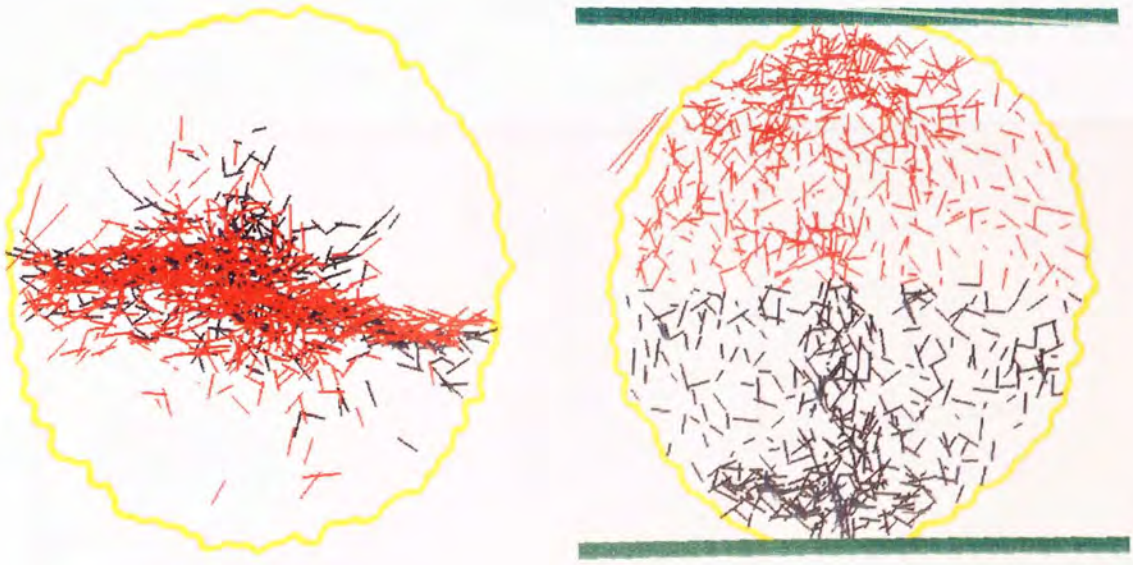

State {**7**}: t = 2.66 ms (strain = 1.903%, broken bonds: 4.37% in bottom half + 5.20% in top half of the agglomerate)

Fig. 8.5 Evolution of the distribution of bonds broken in the dense[1] agglomerate, double impact test, V=0.02 m/s (continued).

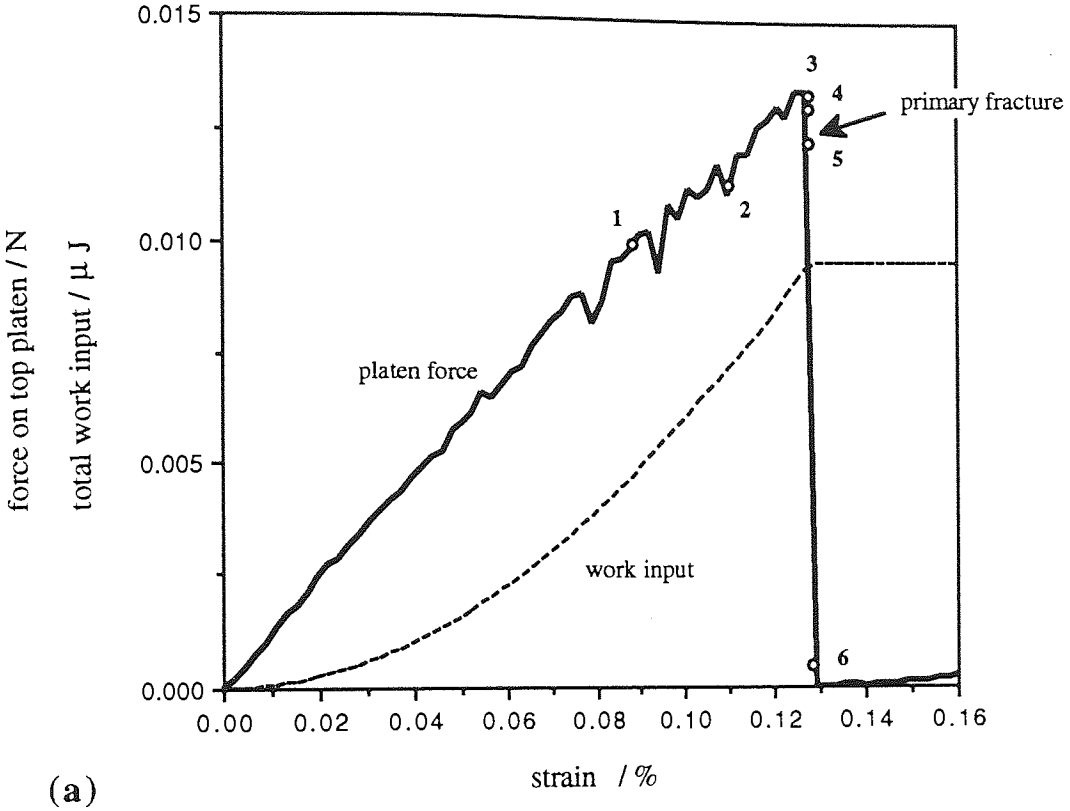

(a)

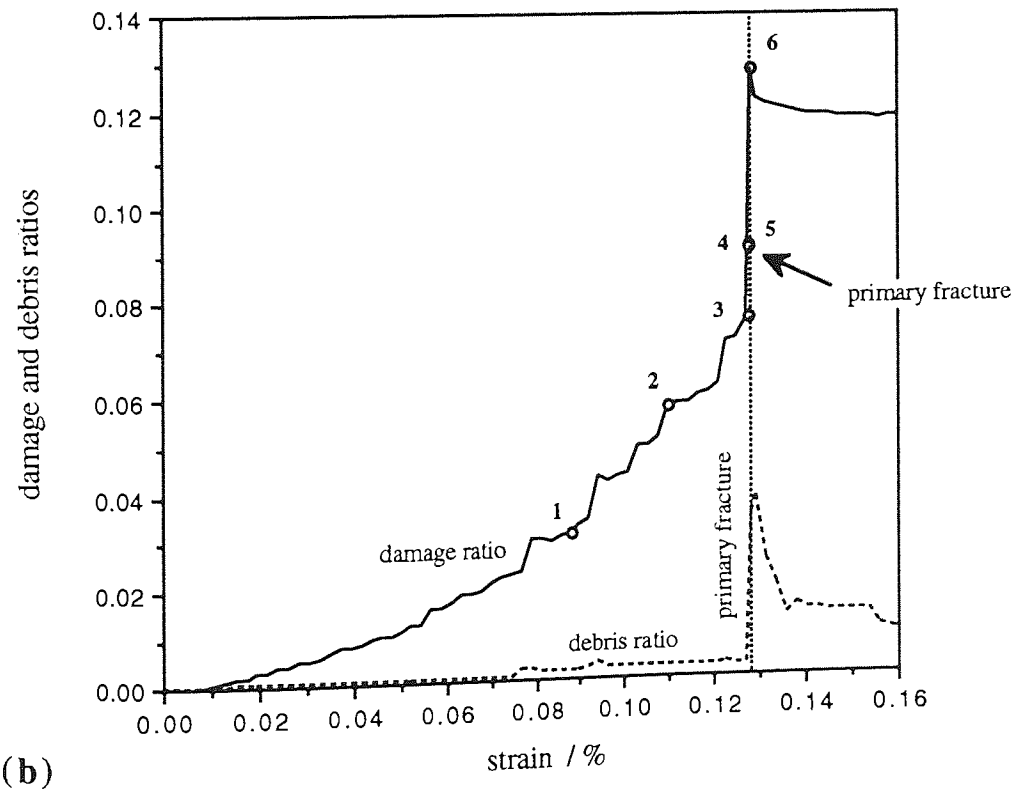

(b)

Fig. 8.6 Evolution of (**a**) platen force and work input, (**b**) damage ratio and debris ratio, diametrical compression, dense[2] agglomerate (V=10 mm/min)
The states marked by the dots **1-6** are presented in Fig. 8.7.

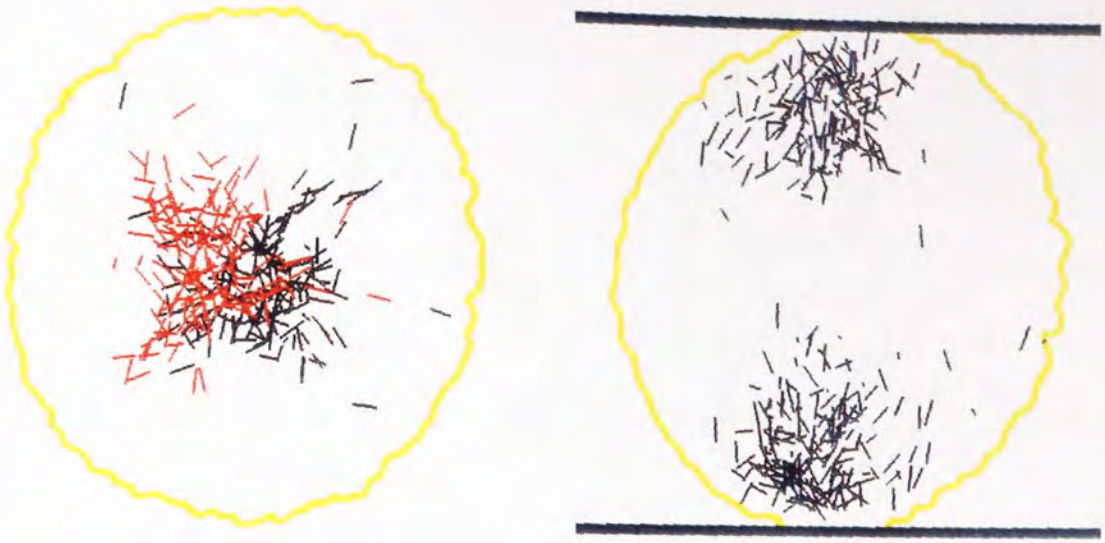

State {**1**}: t = 5.53 ms (strain = 0.088%, broken bonds: 1.62% in bottom half + 1.47% in top half of the agglomerate)

State {**2**}: t = 6.9 ms (strain = 0.11%, broken bonds: 2.65% in bottom half + 3.09% in top half of the agglomerate)

Fig. 8.7 Evolution of the distribution of bonds broken in the dense[2] agglomerate, diametrical compression test (V=10 mm/min). A view from above and one from the side (perpendicular to the fracture plane) are presented for each of the states {**1**} - {**6**}. In the views from above red is used for the top half and black for the bottom half of the agglomerate. Bonds are represented as lines tangent to the former contact; the length of each line is equal to the distance between the centres of the particles that formed the broken bond. The agglomerate was initially situated inside the yellow outline.

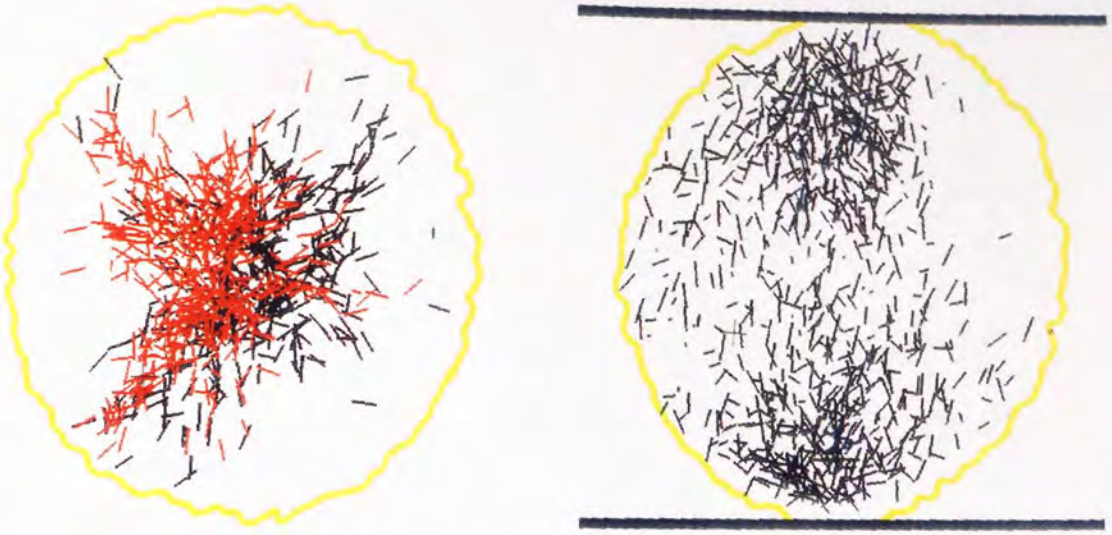

State {**3**}: t = 8.041 ms - maximum platen force (strain = 0.1278%, broken bonds: 3.68% in bottom half + 3.90% in top half of the agglomerate)

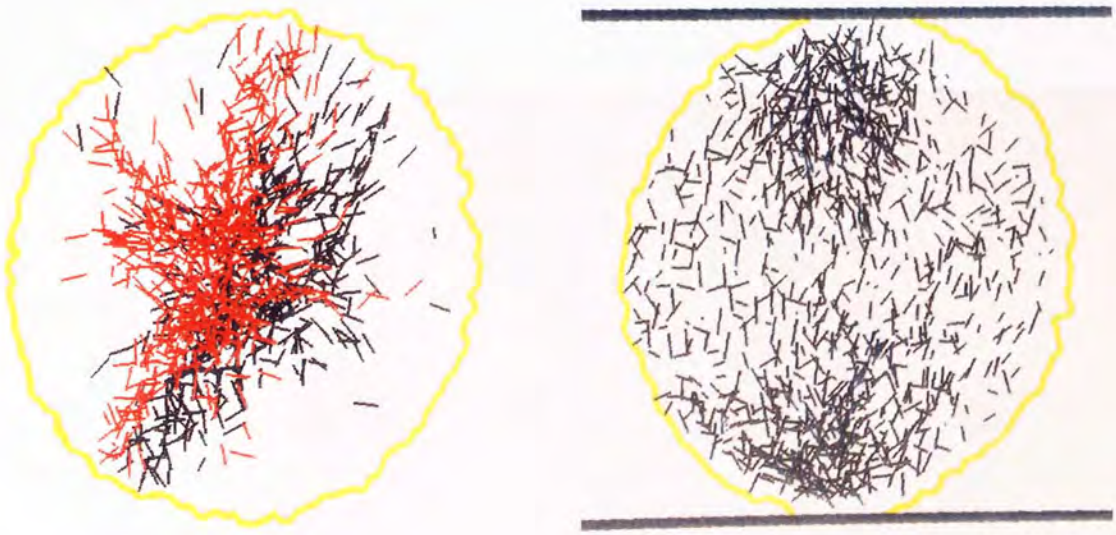

State {**4**}: t = 8.048 ms (strain = 0.1279%, broken bonds: 4.52% in bottom half + 4.59% in top half of the agglomerate)

Fig. 8.7 Evolution of distributions of bonds broken in the dense[2] agglomerate, diametrical compression test, V=10 mm/min (continued).

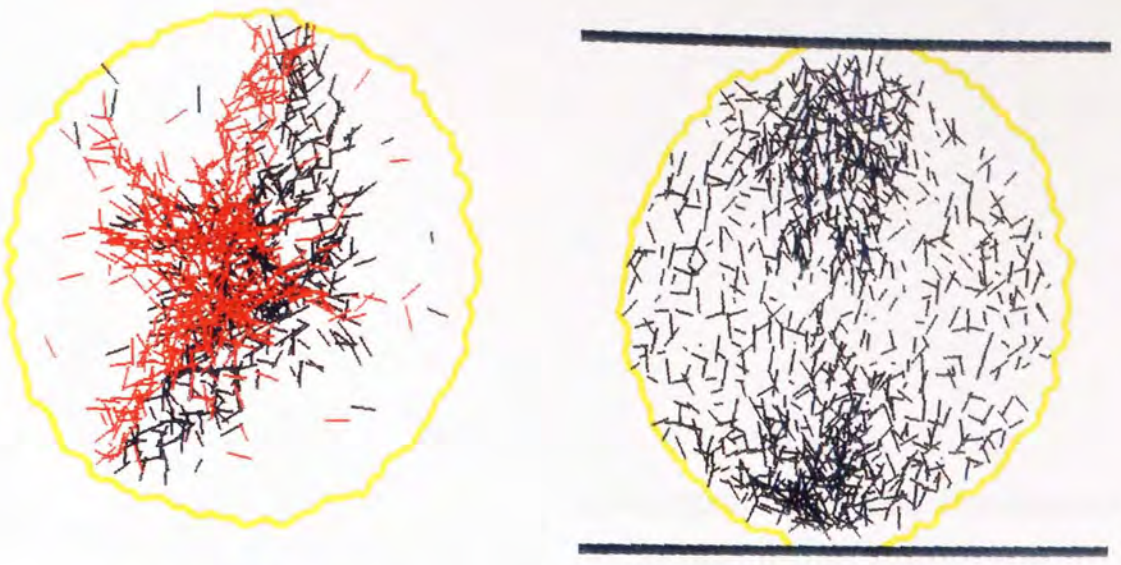

State {**5**}: t = 8.049 ms - immediately after primary fracture (strain = 0.1279%, broken bonds: 4.45% in bottom half + 4.62% in top half of the agglomerate)

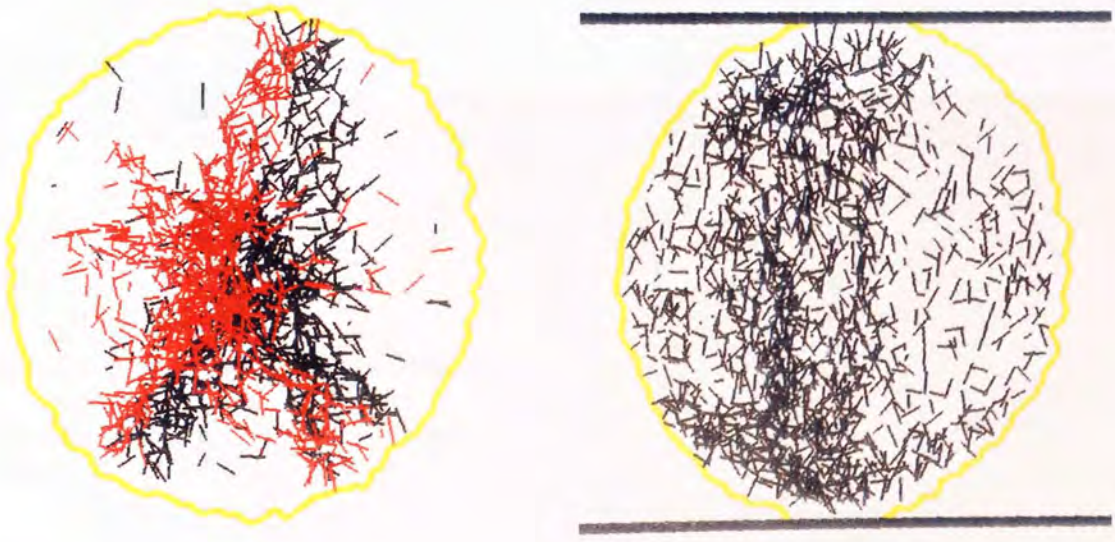

State {**6**}: t =8.07 ms (strain = 0.1284%, broken bonds: 7.01% in bottom half + 5.80% in top half of the agglomerate)

Fig. 8.7 Evolution of distributions of bonds broken in the dense[2] agglomerate, diametrical compression test, V=10 mm/min (continued).

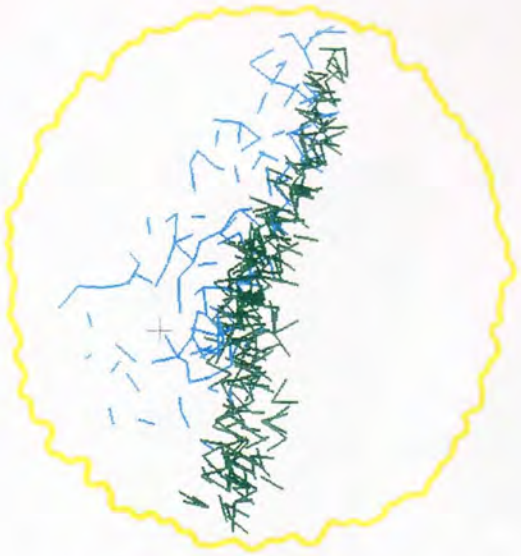

(a) State {**0**}: t = 0, view from above

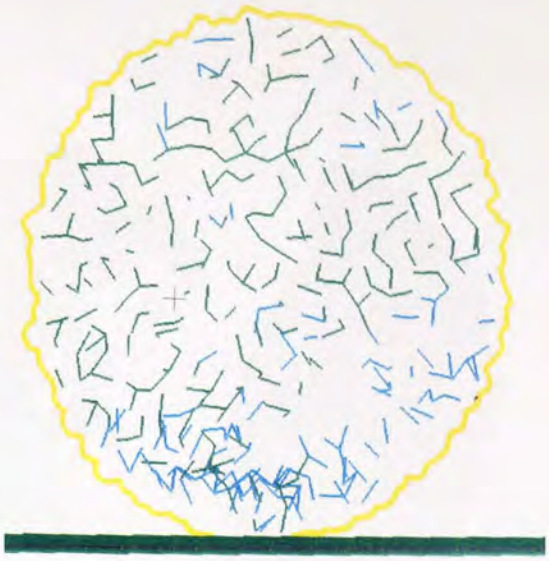

(b) State {**0**}: t = 0, view from side, perpendicular to the fracture surface

(c) State {**0**}: t = 0, view from the front, along the fracture surface

(d) State {**5**}: t = 16.3 μs, side view, perpendicular to the fracture surface

Fig. 8.8 Location of the 392 bonds between the largest fragment and the rest of the agglomerate. Each bond is represented as a line joining the centres of the two particles that were initially in contact. Figures (**a**), (**b**) and (**c**) show the large fragment's 267 bonds with the second largest fragment (coloured in green) and its 125 bonds with the particles that will belong to the debris at the moment of the primary fracture (light blue). Figure (**d**) represents moment of the primary fracture. Apart from the 16 bonds still connecting the two large clusters (green), the immage presents the 251 bonds broken between the the two large fragments (black), the one bond newly-formed between the two large fragments (yellow) and the 125 bonds broken between the largest fragment and the debris (dark blue).

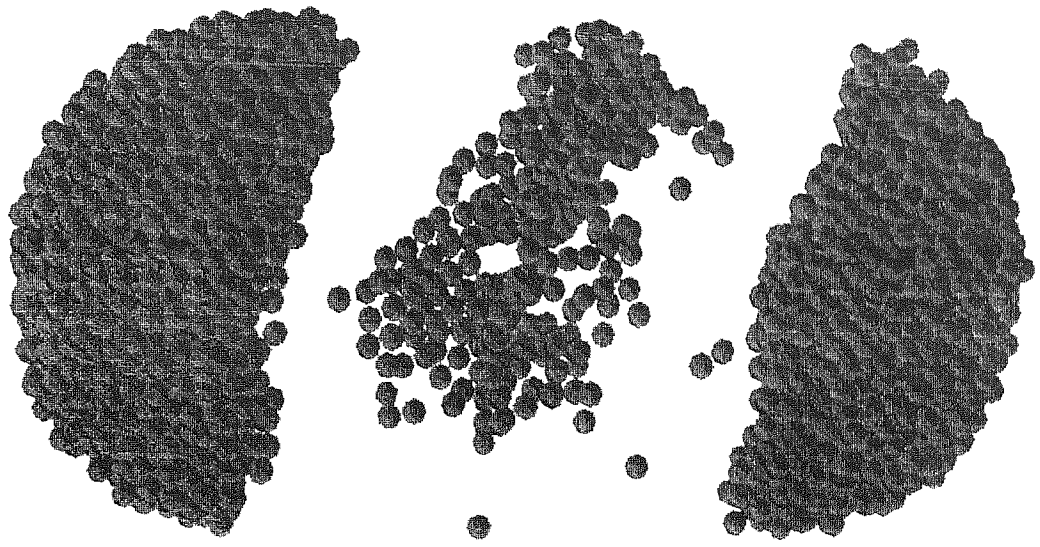

(a) view from above

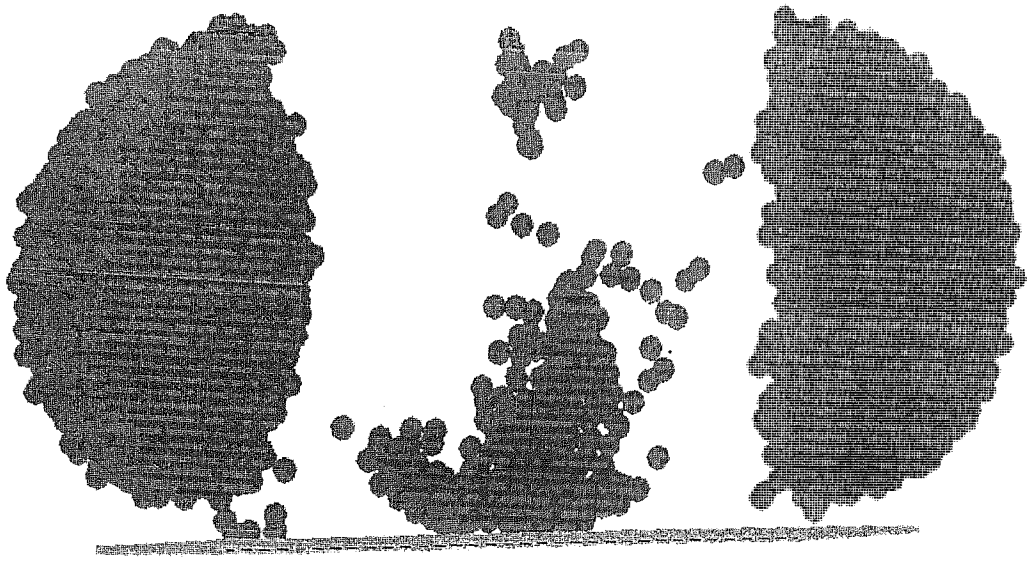

(b) view from the front, along the fracture surface

Fig. 8.9 The results of primary fracture (t=16.3 μs): two large fragments plus debris (dense[1] agglomerate, free-fall impact test, 0.2 m/s impact velocity). The two large fragments have been "artificially" displaced horizontally.

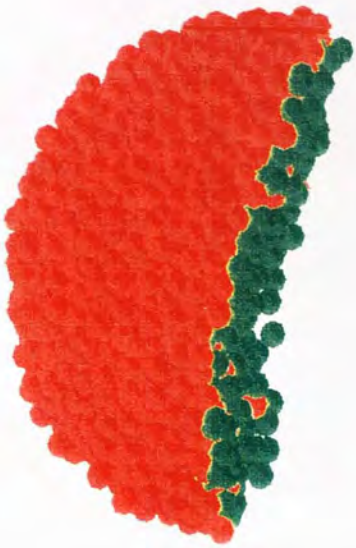

(a) view from above

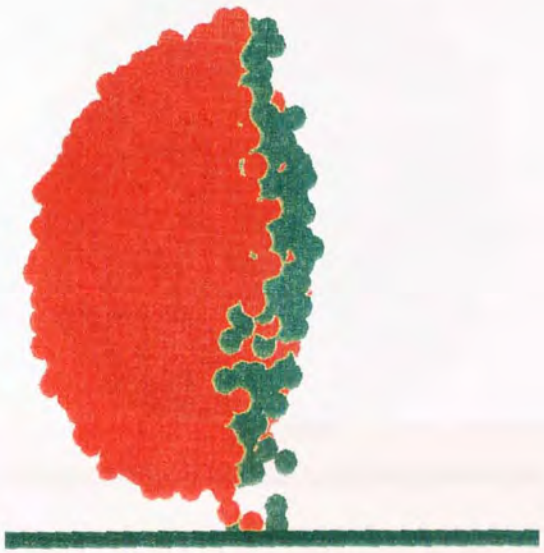

(b) view from the front,
along the fracture surface

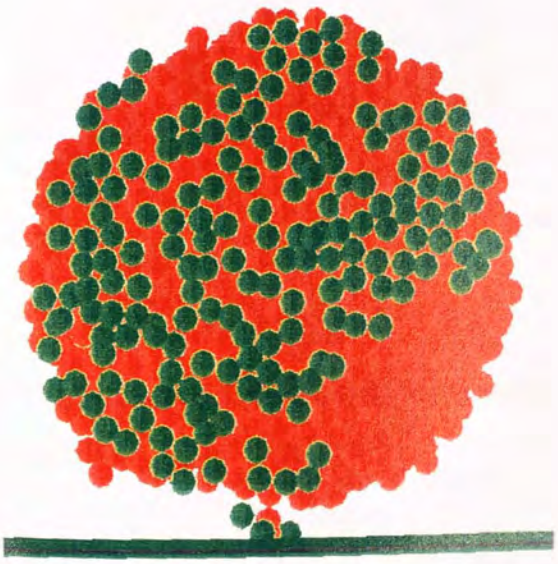

(c) view from side,
perpendicular to the fracture surface

Fig. 8.10 The largest fragment immediately after primary fracture (t=16.3 μs). The particles coloured green are the ones along the fracture surface which broke bonds with the particles in the second largest fragment.

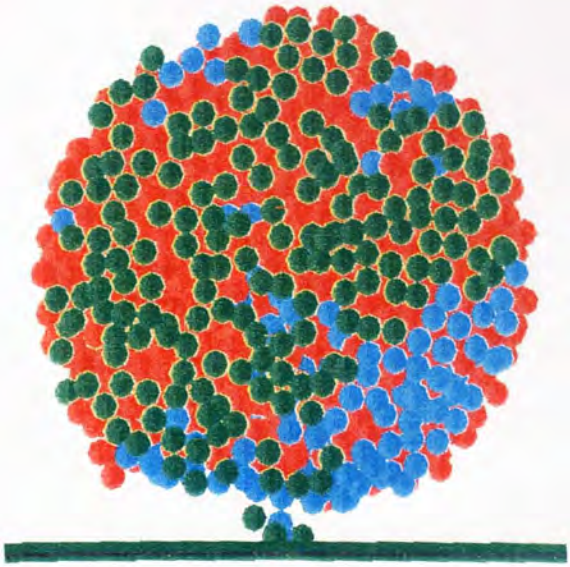

State **{0}**: t = 0 - start of test. There are a total of 316 particles on the fracture surface: 181 have bonds connecting the future two large fragments, whereas 135 are in contact with the future debris particles.

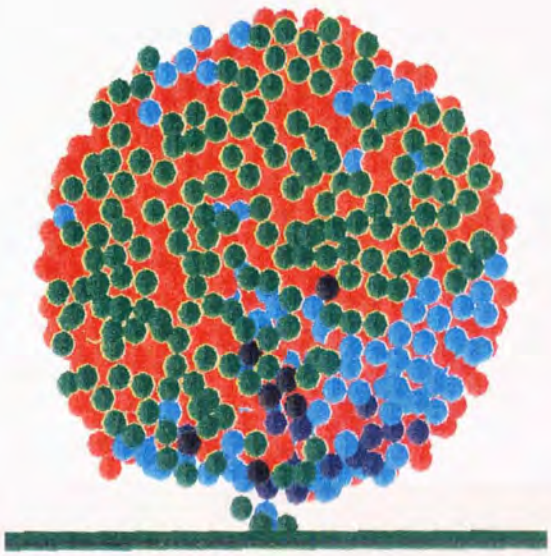

State **{1}:** t = 3.0 μs. Number of particles that have lost contacts - 24 (7.6%): 7 with the future second largest fragment and 17 with debris particles.

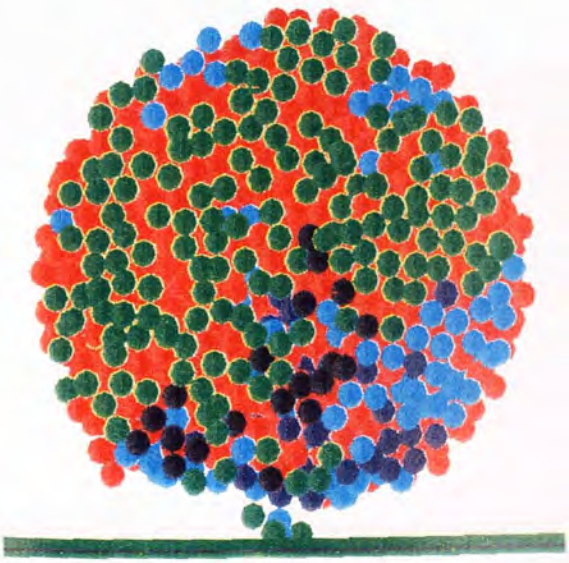

State **{2}:** t = 4.4 μs. Number of particles that have lost contacts - 52 (16.5%): 20 with the future second largest fragment and 32 with debris particles.

Fig. 8.11 Evolution of the state of particles on the fracture surface in the dense[1] agglomerate, free-fall impact test (V=0.2 m/s). Only the 1962 particles which, at primary fracture, will be in the largest fragment are plotted in a view perpendicular to the fracture surface. All but the red particles are situated on the fracture surface. The green particles are the ones still in contact with what will later be the second largest fragment. Particles which have broken contact with the would-be second largest fragment are represented in black. The light blue particles are the ones still in contact with particles that will later detach to form debris. Particles from which debris has detached are represented in dark blue.

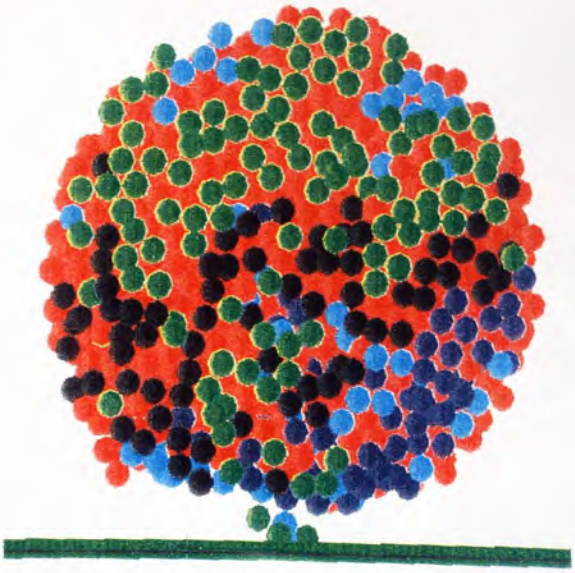

State **{3}:** t = 6.7 μs. Number of particles that have lost contacts - 133 (42.1%): 71 with the future second largest fragment and 62 with debris particles.

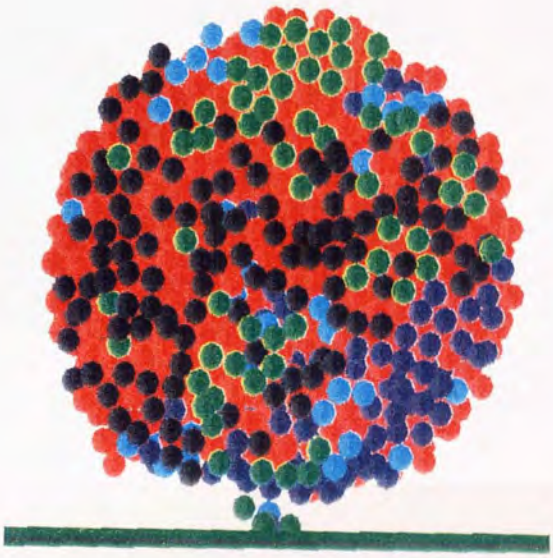

State **{4}:** t = 8.9 μs. Number of particles that have lost contacts - 213 (67.4%): 119 with the future second largest fragment and 94 with debris particles.

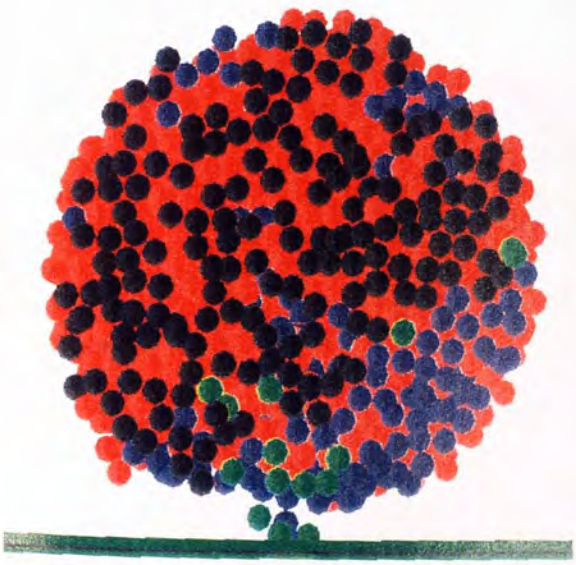

State **{5}:** t = 16.3 μs (just after primary fracture). Number of particles that have lost contacts - 301 (95.3%): 166 with the future second largest fragment and 135 with debris particles.

Fig. 8.11 Evolution of the state of particles on the fracture surface in the dense[1] agglomerate, free-fall impact, V=0.2 m/s (continued).

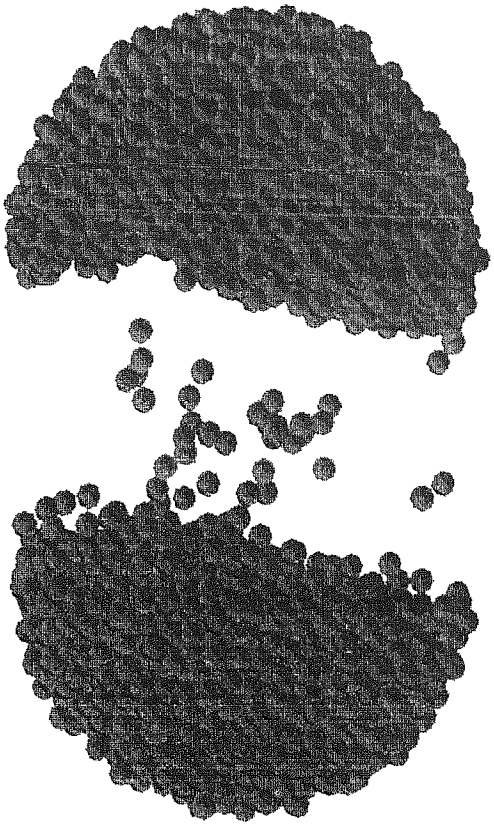

(a) view from above

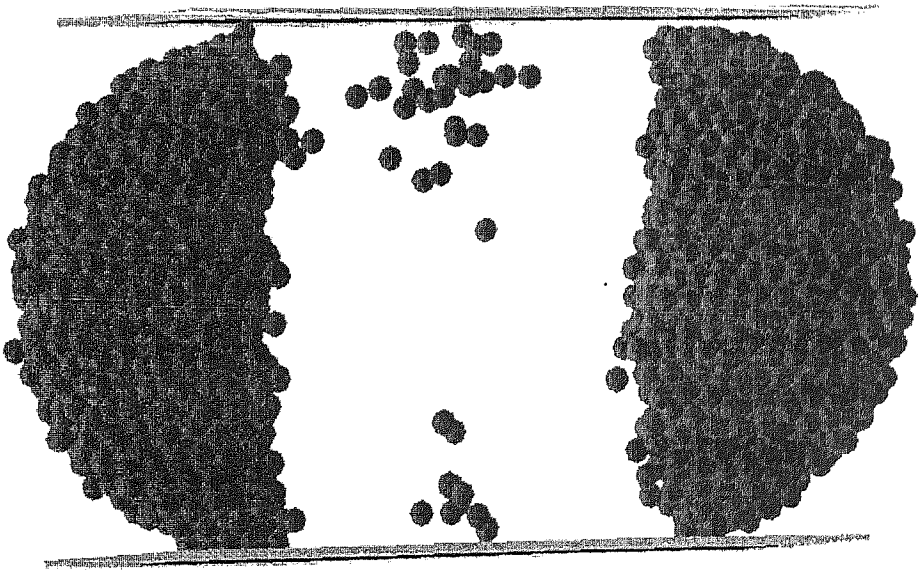

(b) view from side, along the fracture surface

Fig. 8.12 The results of primary fracture (t=115 μs): two large fragments plus debris (dense[1] agglomerate, double impact test, V=0.02 m/s, M_p=100 M_a) The two large fragments have been "artificially" displaced horizontally.

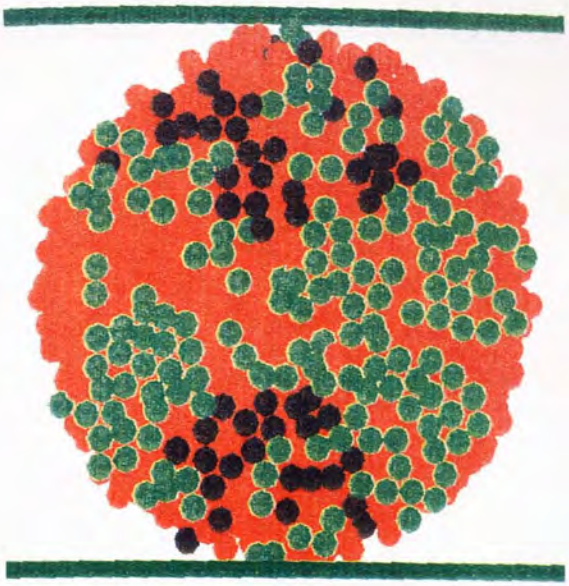

State **{1}:** t = 53.3 μs. Number of particles that have lost contact with the second largest fragment: 52 (24.1%).

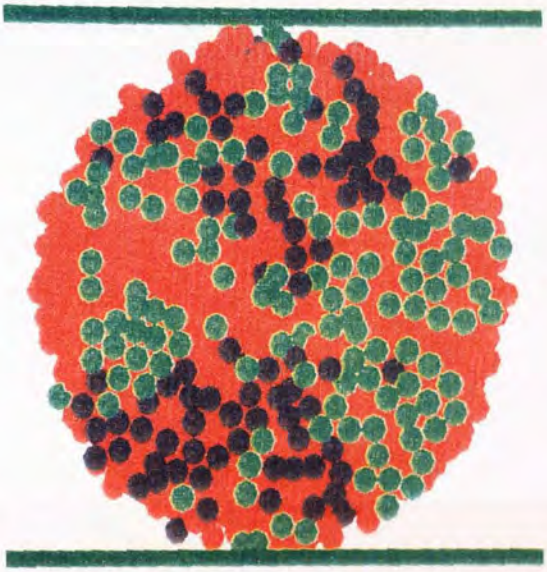

State **{2}:** t = 107 μs. Number of particles that have lost contact with the second largest fragment: 85 (39.35%).

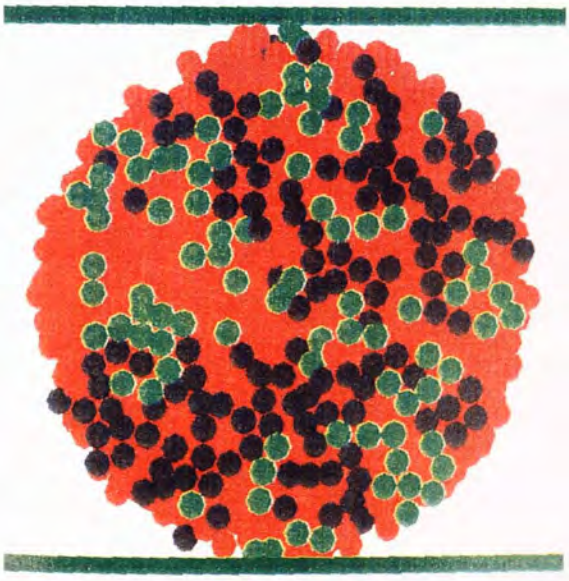

State **{3}:** t = 111 μs. Number of particles that have lost contact with the second largest fragment: 128 (59.26%).

Fig. 8.13 Evolution of the state of particles on the fracture surface in the dense[2] agglomerate, double impact test (V=0.02 m/s, M_p=100 M_a). Only the 2126 particles which, at primary fracture, will be in the largest fragment are plotted, in a view perpendicular to the fracture surface. All but the red particles are situated on the fracture surface. The largest fragment had 216 particles in contact with the second largest fragment. The green particles are the ones still in contact with what will later be the second largest fragment. Particles which have broken contact with the would-be second largest fragment are represented in black.

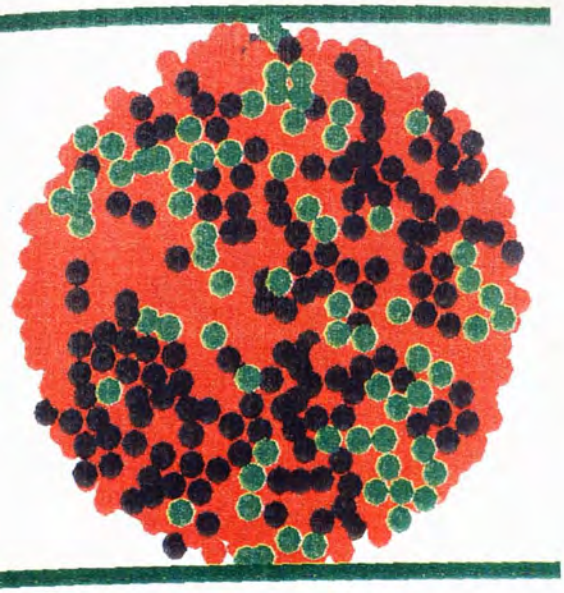

State **{4}:** t = 113.8 μs. Number of particles that have lost contacts with the second largest fragment: 145 (67.13%).

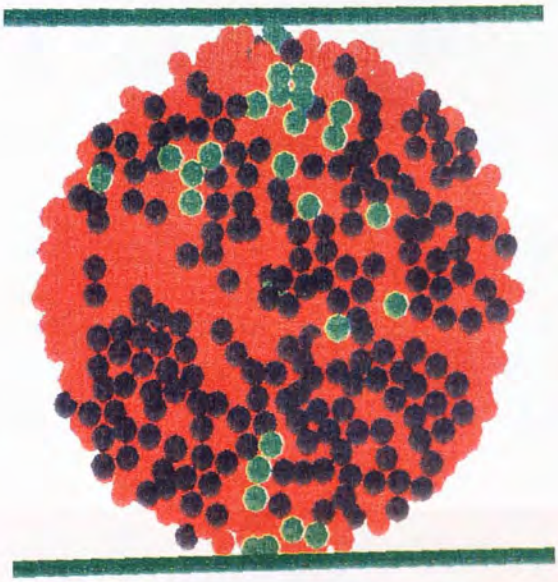

State **{5}:** t = 115 μs (immediately after primary fracture). Number of particles that have lost contacts with the second largest fragment: 187 (86.57%).

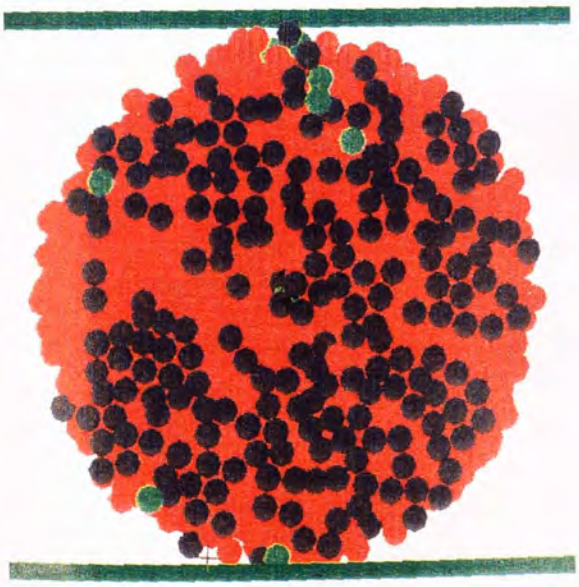

State **{6}:** t = 133 μs. Number of particles that have lost contacts with the second largest fragment: 207 (95.83%).

Fig. 8.13 Evolution of the state of particles on the fracture surface in the dense[1] agglomerate, double impact test, V=0.02 m/s, M_p=100 M_a (continued).

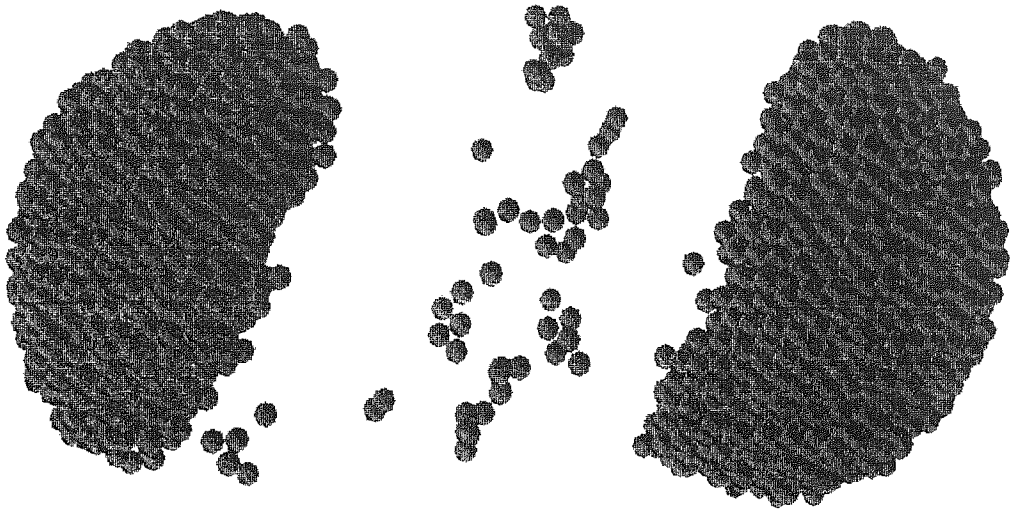

(a) view from above

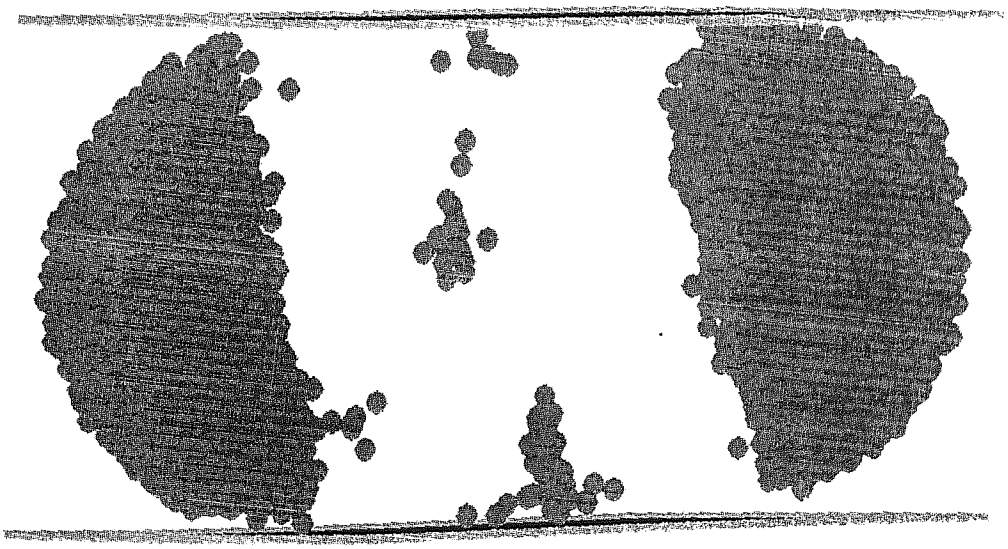

(b) view from the front, along the fracture surface

Fig. 8.14 The results of primary fracture (t=8049 μs): two large fragments plus debris (dense[2] agglomerate, diametrical compression, platen velocity = 10 mm/min). The two large fragments have been "artificially" displaced horizontally.

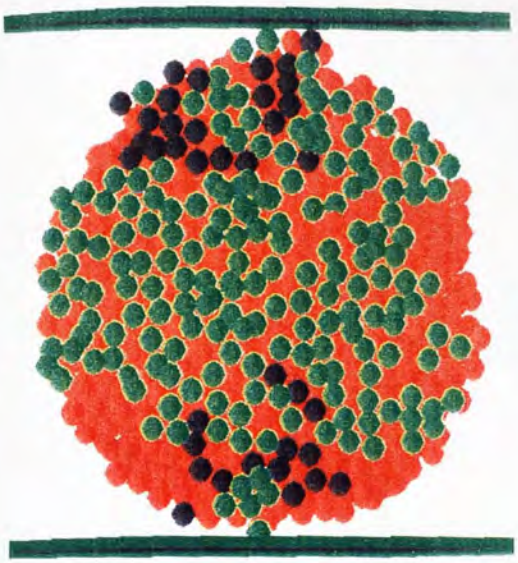

State **{1}:** t = 5.53 ms. Number of particles that have lost contact with the largest fragment: 37 (16.7%).

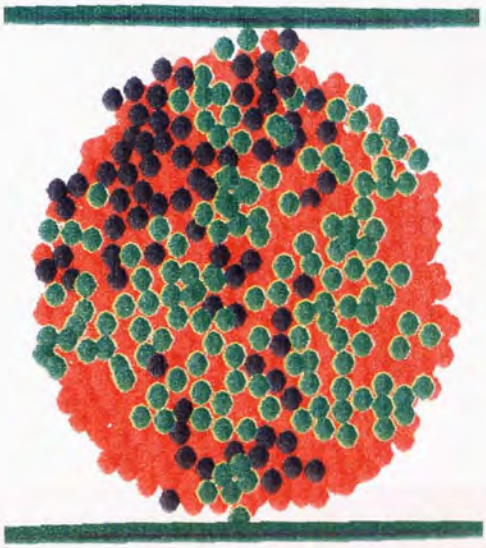

State **{2}:** t = 6.9 ms. Number of particles that have lost contact with the largest fragment: 76 (34.4%).

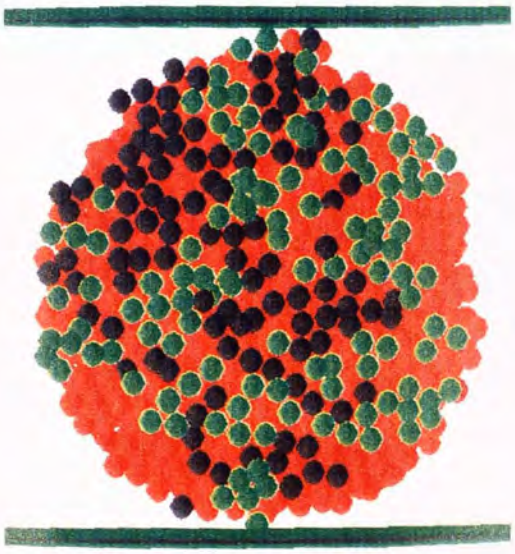

State **{3}:** t = 8.041 ms. Number of particles that have lost contact with the largest fragment: 103 (46.6%).

Fig. 8.15 Evolution of the state of particles on the fracture surface in the dense[2] agglomerate, diametrical compression test (platen velocity = 10 mm/min). Only the 1639 particles which, at primary fracture, will be in the second largest fragment are plotted, in a view perpendicular on the fracture surface. The second largest fragment had 216 particles in contact with the largest fragment. All but the red particles are situated on the fracture surface. The green particles are the ones still in contact with what will later be the largest fragment. Particles which have broken contact with the would-be largest fragment are represented in black.

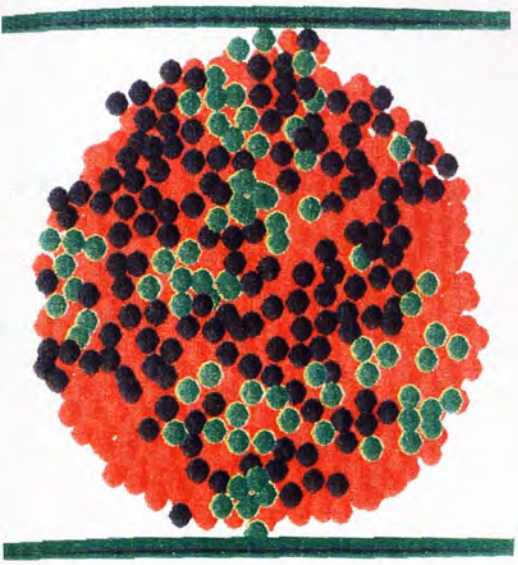

State **{4}:** t = 8.048 ms. Number of particles that have lost contacts with the largest fragment: 144 (65.2%).

State **{5}:** t = 8.049 ms (just after primary fracture). Number of particles that have lost contacts with the largest fragment: 172 (77.83%).

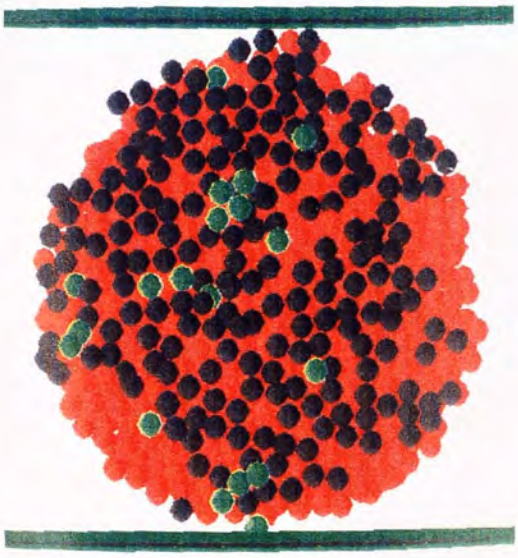

State **{6}:** t = 8.07 ms (just after secondary fracture). Number of particles that have lost contacts with the largest fragment: 202 (91.4%).

Fig. 8.15 Evolution of the state of particles on the fracture surface in the dense[2] agglomerate, diametrical compression test, V = 10 mm/min (continued).

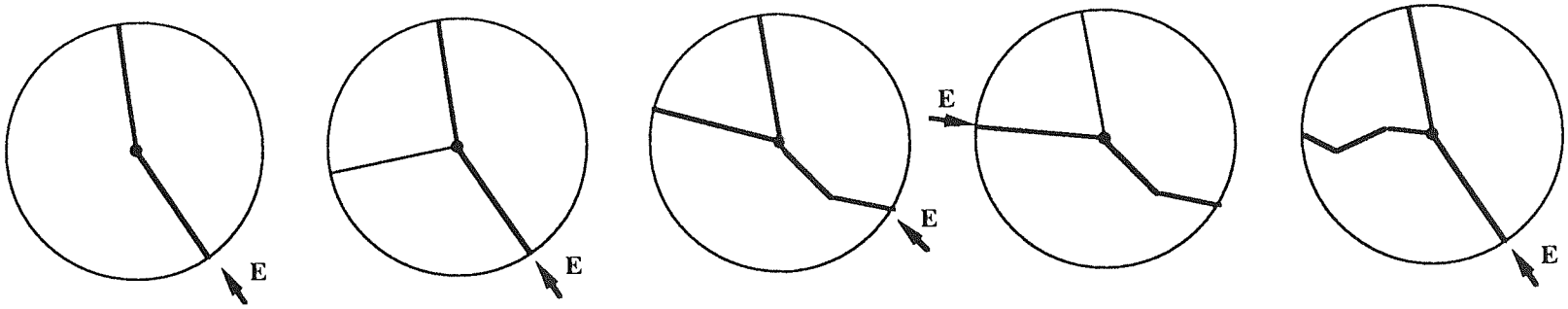

(a) DI, V=0.04 m/s, M_p=100 M_a **(b)** DI, V=0.1 m/s, M_p=100 M_a **(c)** DI, V=0.1 m/s, M_p=672.6 M_a **(d)** fast DC, V=0.04 m/s **(e)** fast DC, V=0.1 m/s

Fig. 8.17 Schematic views from above of the fracturing of the weak-dense agglomerate

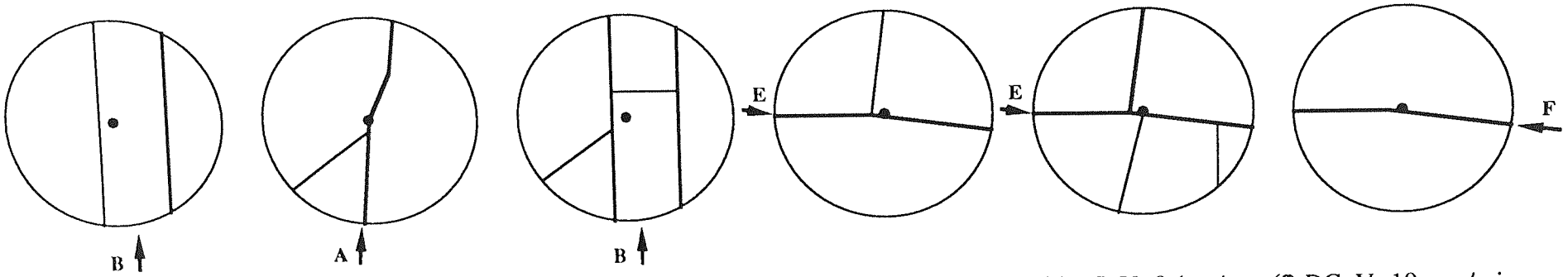

(a) FFI, V=0.1785 m/s **(b)** FFI, V=0.2 m/s **(c)** FFI, V=0.3 m/s **(d)** DI, V=0.2 m/s, M_p=100 M_a **(e)** DI, V=0.1 m/s, M_p=100 M_a **(f)** DC, V=10 mm/min and DI, V=0.02 m/s, M_p=100 M_a

Fig. 8.18 Schematic views from above of the fracturing of the dense[1] agglomerate

Legend: **FFI** - free-fall impact test, **DI** - double impact test, **DC** - diametrical compression test

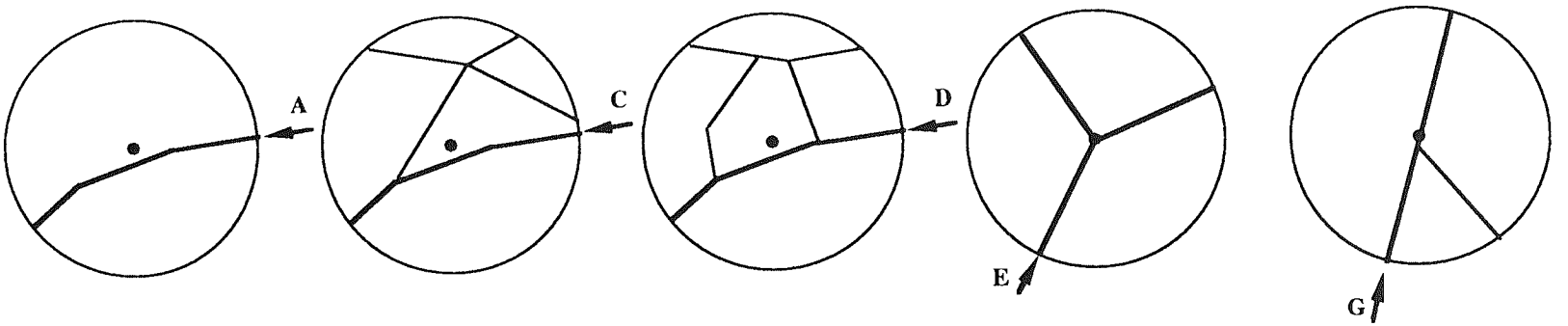

(a) FFI, V=0.12 m/s

(b) FFI, V=0.15 m/s

(c) FFI, V=0.2 m/s

(d) DI, V=0.02 m/s M_p=100 M_a

(e) DC, V=10 mm/min

Fig. 8.19 Schematic views from above of the fracturing of the dense[2] agglomerate (the dense with the higher contact density)

Legend: FFI - free-fall impact test, **DI** - double impact test, **DC** - diametrical compression test

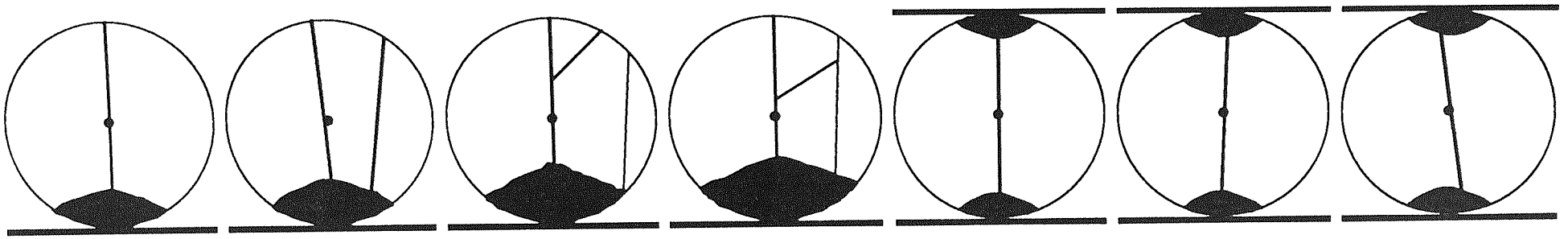

view A

view B

view C

view D

view E

view F

view G

Fig. 8.20 Schematic views along the primary fracture surface, dense agglomerates (cf. Figs. 8.17 - 8.19)

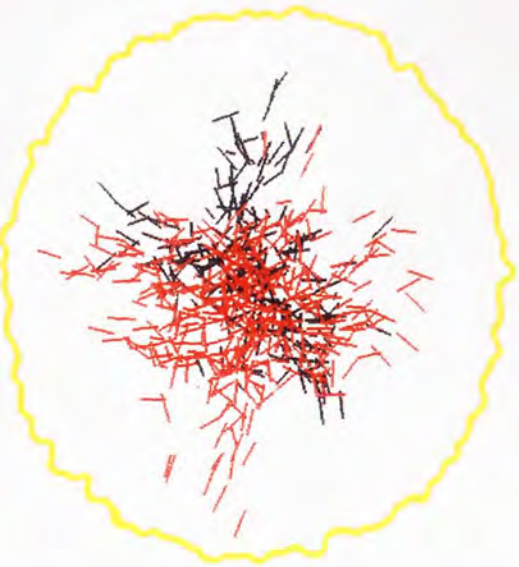

(a) double impact test, 0.1 m/s impact velocity, M_p=100 M_a: the first 343 bonds broken in the top half and 213 in the bottom half of the agglomerate.

(b) double impact test, 0.2 m/s impact velocity, M_p=M_a: the first 417 bonds broken in the top half and 106 in the bottom half of the agglomerate.

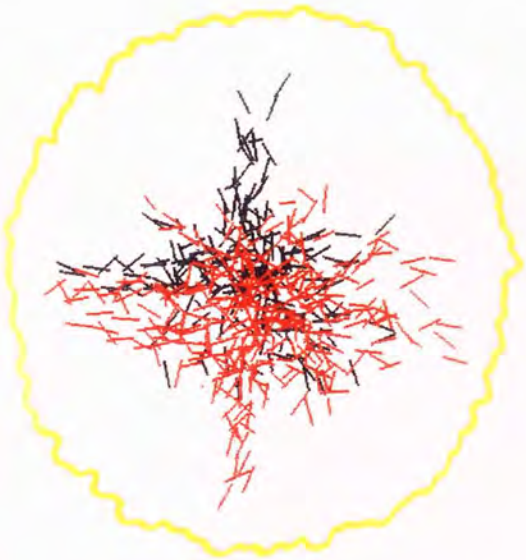

(c) diametrical compression test, 10 mm/min top platen velocity: the first 296 bonds broken in the top half and 195 in the bottom half of the agglomerate.

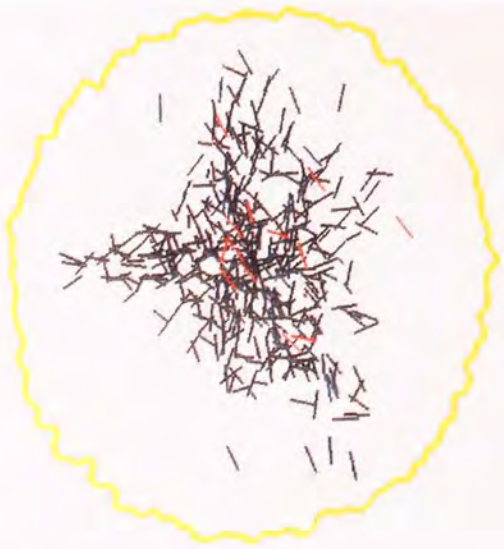

(d) free-fall impact test, 0.1785 impact velocity: the first 420 bonds broken in the bottom half (and 7 in the top half) of the agglomerate.

Fig. 8.21 Location of the bonds broken in the dense[1] agglomerate in the initial stages of various tests: double impact in **(a)**, **(b)**, diametrical compression in **(c)**, and free-fall impact in **(d)**. Bonds are represented as lines tangent to the former contact; the length of each line is equal to the distance between the centre of particles that formed the broken bond. Red is used for the top half and black for the bottom half of the agglomerate.

(a) double impact test, 0.02 m/s impact velocity, M_p=100 M_a: the first 197 bonds broken in the top half and 299 in the bottom half of the agglomerate.

(b) double impact test, 0.2 m/s impact velocity, M_p=M_a: the first 339 bonds broken in the top half and 306 in the bottom half of the agglomerate.

(c) free-fall impact test, 0.12 m/s impact velocity: the first 263 bonds broken in the bottom half of the agglomerate.

(d) free-fall impact test, 0.3 m/s impact velocity: the first 282 bonds broken in the bottom half of the agglomerate.

Fig. 8.22 The start of the propagation of cracks in the strong dense agglomerate with the higher contact density (dense[2]) for various tests: double impact in **(a)**, **(b)**, and free-fall impact in **(c)**, **(d)**. Bonds are represented as lines tangent to the former contact; the length of each line is equal to the distance between the centre of particles that formed the broken bond. Red is used for the top half and black for the bottom half of the agglomerate.

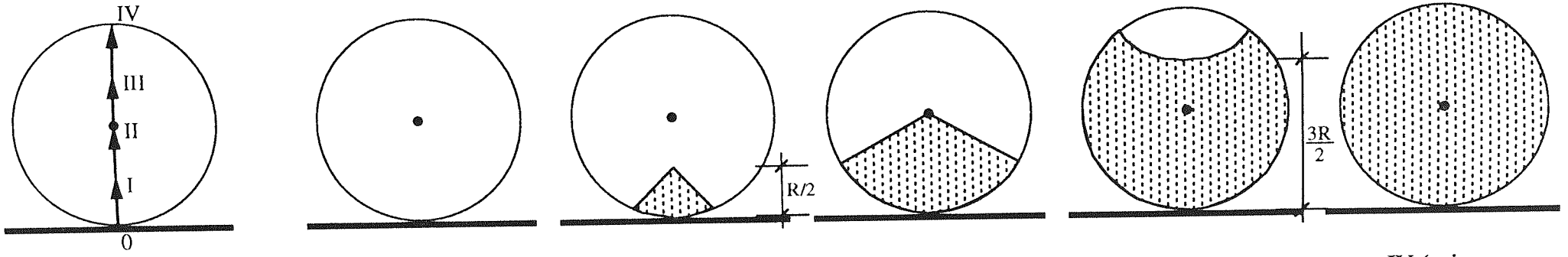

Fig. 8.23 Schematic evolution of fracture in free-fall impact tests

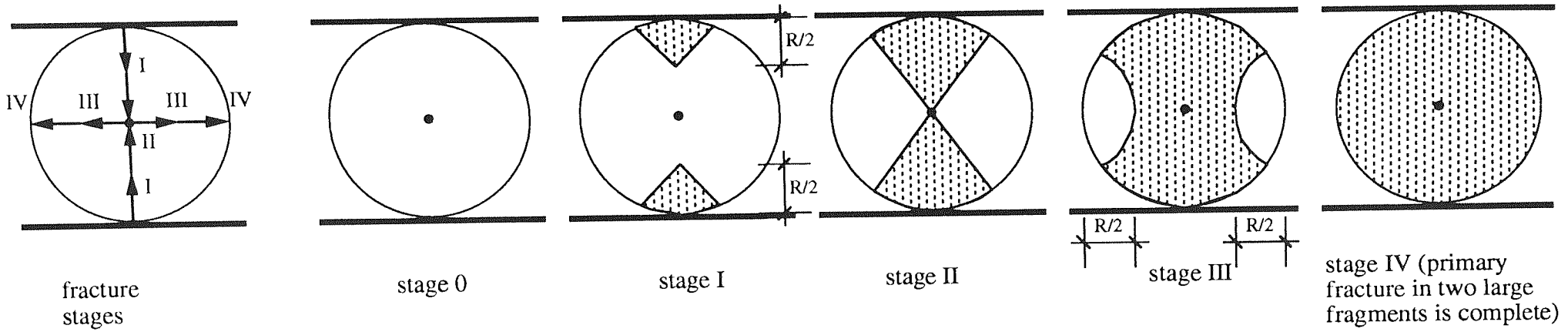

Fig. 8.24 Schematic evolution of fracture in diametrical compression and low-velocity double impact tests

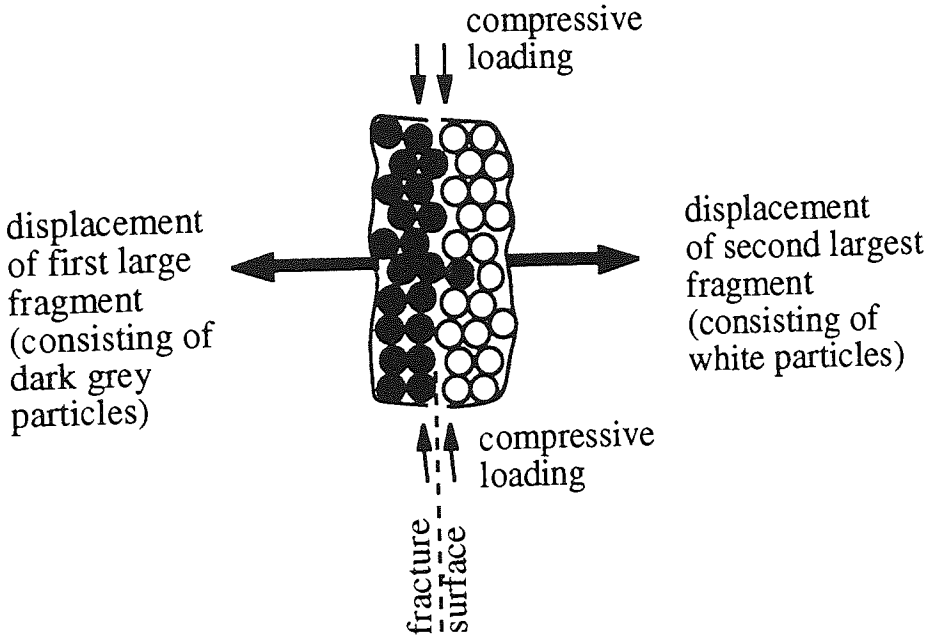

Fig. 8.16 A two-dimensional schematic representation of the "bridging" (frictional) grain pullout" mechanism

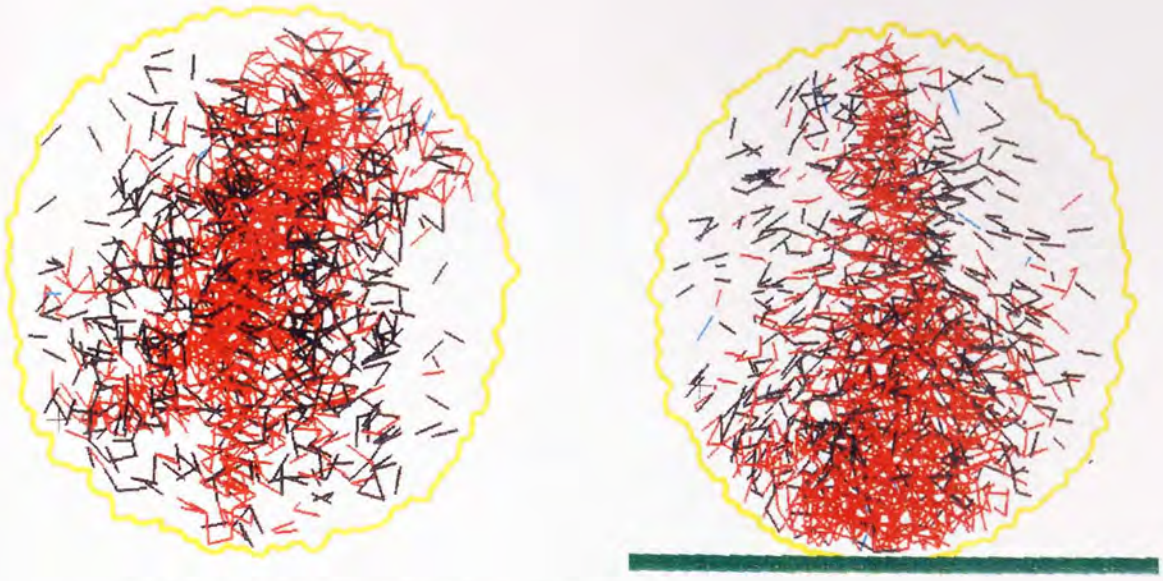

Fig. 8.25 Distribution of re-adhered and sliding contacts just after primary fracture in the dense[1] agglomerate, 0.2 m/s impact velocity. A view from above and one from the front (along the fracture plane) are presented. Bonds are represented as lines joining the centre of particles that form (or formed) the contact. The 11 sliding bonds are represented in light blue, whereas the 706 re-adhered bonds are drawn in black. Red is used to mark the 1399 broken bonds. The agglomerate is situated inside the yellow outline.

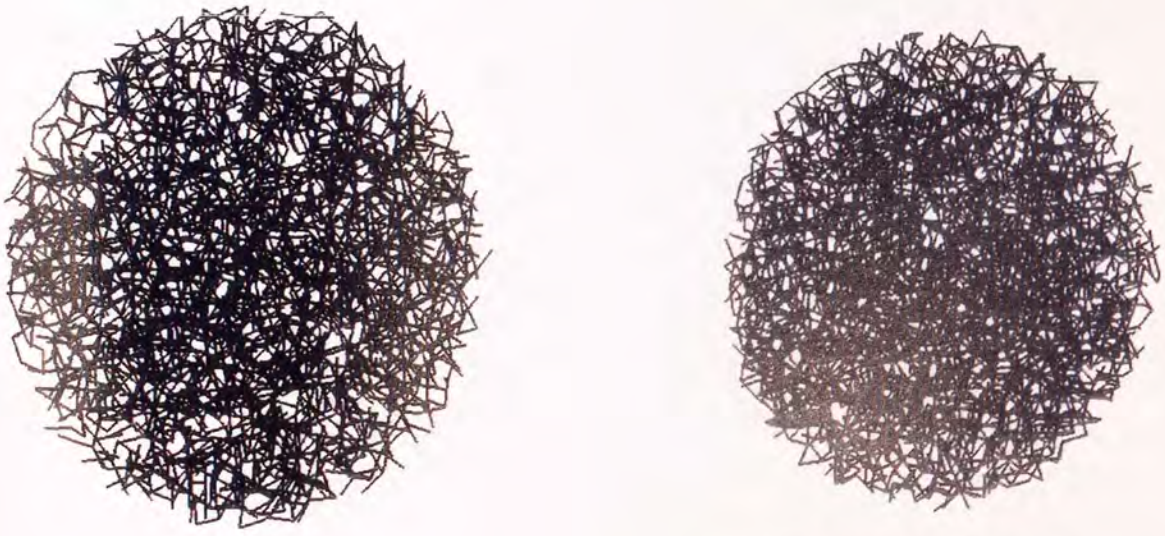

(a) The 3813 (39.1%) tensile bonds in the dense[1] agglomerate.

(b) The 4644 (41.1%) tensile bonds in the dense[2] agglomerate (with the higher contact density).

Fig. 8.26 Top views of the tensile bonds in **(a)** the dense[1] agglomerate and **(b)** the dense[2] agglomerate (with the higher contact density) before testing. In the dense[1] agglomerate 3813 (39.1%) bonds were tensile, whereas 4644 (41.1%) bonds were tensile in the other strong dense agglomerate. Each tensile bond is represented as a line joining centres of the two particles forming the bond.

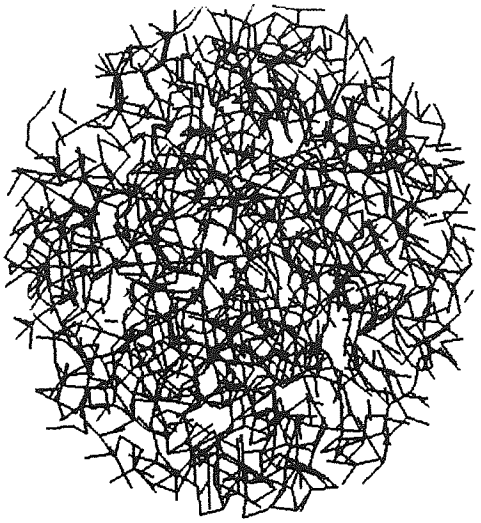

(a) The 1853 tensile bonds in the top hemisphere, dense[1] agglomerate.

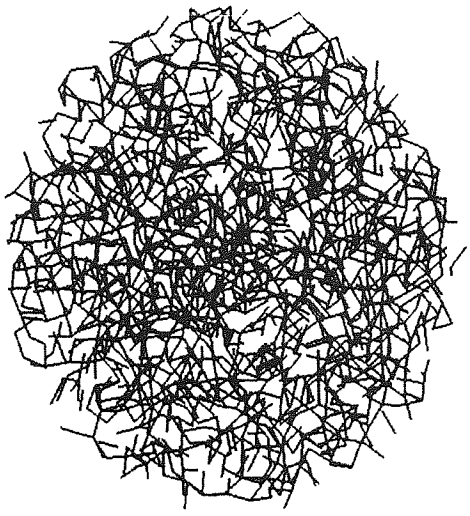

(b) The 1960 tensile bonds in the bottom hemisphere, dense[1] agglomerate.

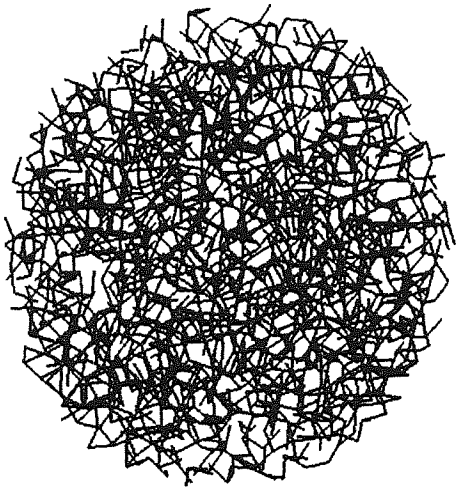

(c) The 2329 tensile bonds in the top hemisphere, dense[2] agglomerate.

(d) The 2315 tensile bonds in the bottom hemisphere, dense[2] agglomerate.

Fig. 8.27 Top views of the tensile bonds in **(a)**, **(b)** the dense[1] agglomerate and **(c)**, **(d)** the dense[2] agglomerate (with the higher contact density) before testing. Each tensile bond is represented as a line joining the centres of the two particles in contact.

CHAPTER 9

OTHER OBSERVATIONS

9.1 COMPARISON BETWEEN FREE-FALL AND DOUBLE IMPACT TESTS OF SAME IMPACT VELOCITY AND SAME INITIAL KINETIC ENERGY

For an impact velocity of 0.2 m/s the dense[1] agglomerate broke into two roughly hemispherical fragments at primary fracture for both the free-fall impact and double impact tests - see sections 6.2.2 and 7.3.3. The "high"-velocity double impact test presented here is the one in which the mass of the impacting (top) platen was equal to that of the agglomerate and the top platen was not arrested after fracture. As the impacting platen in the double impact test has the same mass as the agglomerate, the two impact tests had not just the same impact velocity but also the same impact kinetic energy. In Figs. 9.1 - 9.6 the evolution of various parameters of interest during the two tests are compared.

In both tests, the agglomerate had suffered primary and secondary fracture at around 0.2% nominal strain: in the free-fall impact test primary fracture occurred at 0.0133 ms and secondary at 0.0222 ms, whereas in the double impact test primary fracture occurred at 0.0148 ms and secondary at 0.0163 ms. Although the test configurations were different for the two tests it is noted that the evolution of the nominal (diametral) strain of the agglomerate - presented in Fig. 9.1 - was identical prior to the moment of primary fracture. This suggests that similarities must exist in the behaviour of the dense[1] agglomerate up to the fracture moment in the two impact tests. The fact that under double impact the agglomerate experienced more nominal straining than under free-fall impact after primary fracture is mainly due to the fact that the top platen was not arrested at primary fracture in the double impact test (and thus continued to force the large fragments to strain).

Figure 9.2 presents the evolution of the forces developed on the platens in the two tests. At the very beginning of the tests, in the initial almost elastic loading stage (up to about 0.8 μs in Fig. 9.2), the evolution of the platen force in the free-fall impact test was identical to the evolution of the force on the impacting platen in the double impact test. After this very short stage the platen force in the free-fall impact test increased faster - almost until attaining its maximum value. Up to about 3 μs the double impact test behaved as a free-fall impact test, as it developed force on one platen only (the top, impacted one). However, the value of the platen force attained at 3 μs was lower than the one obtained in the free-fall impact test. This may be because a different (diametrically opposite) pole suffered impact in each of the two tests. The evolution of the force on the impacted platen at the beginning of the two 0.2 m/s impact velocity tests reflects the local behaviour of the agglomerate in the zone close to the

platen. The similar trends in the evolution of the force, Fig. 9.2, indicate that the material adjacent to the agglomerate-platen interfaces behaves similar in both types of impact test, irrespective of the point of impact. In the double impact test the top platen produced a nominal strain of 0.05% before the force on the bottom platen started to build up. Figure 9.2 indicates that as soon as loading started to develop on the bottom platen the force on the top platen began to fluctuate around its maximum value.

Figure 9.3 shows the evolution of the agglomerate's kinetic energy in the free-fall impact test compared to the evolution of the work input in the double impact test. The kinetic energy in the free-fall impact test decreased continuously during both loading and unloading. The decrease in agglomerate's kinetic energy corresponds to the work input into the agglomerate during the free-fall impact test. The change in the gravity-potential energy was negligible for both impact tests (as the displacement of the agglomerate until the fracture moment was insignificant). Figure 9.3 illustrates that, although having different test configurations, the work input is similar and levels off at almost the same value in both the free-fall impact and double impact tests.

The comparison in the evolution of the damage ratio and debris ratio for the two impact tests is presented in Fig. 9.4. The evolution of both the damage and debris ratios was almost identical for both tests at the beginning, during the first 3 μs. Also, the final amount of broken bonds was essentially the same for the two tests. Figure 9.4 indicates that the free-fall impact test produced a little more debris. Having the same number of bonds broken, this would indicate that the large fragments produced in the free-fall impact test were stronger, more intact, than the large fragments obtained in the double impact test. Further details of the comparison between these tests in terms of the debris produced will be discussed in section 9.4.3.

Figure 9.5 shows that the evolution of the average normal particle-particle contact force is similar to the evolution of the total platen force (sum of the forces on top and bottom platens for double impact) during each of the two impact tests. However, a closer look at the four curves in Fig. 9.5 reveals that some differences can be noted. For the double impact test the evolution of the average normal force presented several more fluctuations compared to the evolution of the total force on the platens; its maximum was attained a little later, almost exactly at the moment of primary fracture. Basically (overall), in the free-fall impact test the agglomerate presented a short loading and a longer (fluctuating/stepped) unloading, whereas, in contrast, in the double impact test it presented a longer (and less steep) loading phase, a larger maximum, and a more steep (and continuous) unloading. Figure 9.5 also indicates that the elastic stored energy was maintained around the maximum attained value until the primary fracture moment in the free-fall impact test and that the amount of elastic stored energy just before the primary fracture moment was only half that in the double

impact test. It can therefore be implied that the fracture process was more gradual in the free-fall impact test and that the last part of the fracture process was more explosive in the case of the double impact test. This agrees with the comparison of fracture speeds for the two types of impact tests (see section 8.5): the fracture crack velocity was generally decreasing during free-fall impact test and increasing during double impact tests.

The fact that the double impact test behaved like a free-fall impact test until 3 μs (since the load only affected the local impact zone during this period) is also reflected in Fig. 9.6, presenting the evolution of the total number of compressive and tensile forces in the two tests. The evolution up to 4 μs was identical for the two tests. At the very start (up to about 2 μs) the number of compressive forces increased as the number of tensile forces decreased. This indicates that the load transmission converted a large number (38%) of contacts from tensile to compressive, as it transmitted radially (from the impact point) through a large number of particle chains. The paths branched as the load transmitted farther into the agglomerate converting more and more contacts from tensile to compressive. From 2 μs the reduction in the number of compressive forces and increase in the number of tensile forces (Fig. 9.6) suggests that the load, although larger (Figs. 9.2 and 9.5), propagated along fewer transmission paths so that many contacts were converted back to tensile. The reflected longitudinal wave may have affected this process (this will be discussed in section 9.6.2). The fact that, between 4 μs and the primary fracture moment, there were more compressive contact forces in the double impact tests compared to the free-fall impact test is as expected, since the double impact test had two loading points which continued to confine the agglomerate under compressive loading for longer. Despite the differences in the evolution of the average normal contact force between 1.5 μs and 4 μs (see Fig. 9.5), it is interesting that different quantities of elastic energy was stored in the same number of interparticle contacts up to about 4 μs - see Fig. 9.6. It appears that the exact point of loading can slightly change the elastic strain energy an agglomerate can store, but not the number of interparticle contacts that transmit most of the load.

The results presented above show that two different types of impact test on the same dense agglomerate present many similarities if the impact velocity and the impact kinetic energy are the same. It thus seems that one of the reasons why the same dense agglomerate presented such different fracture patterns in free-fall and double impact was that the impacted pole was not the same one.

9.2 DENSE AGGLOMERATES - COMPARISON BETWEEN FREE-FALL, DOUBLE IMPACT AND DIAMETRICAL COMPRESSION TESTS

Most of the free-fall impact tests presented in this thesis were very short in duration, as the impact velocities were relatively high and most processes (e.g. breakage of bonds, detachment of debris) usually terminated within 50 μs. The double impact tests generally lasted about 50 times longer (e.g. 2-3 ms) than the free-fall impact tests due to the (usually) lower impact velocities used. The diametrical compression test was the longest type of test (over 8 ms usually) as the loading rates were very low. It would thus be very difficult to carry out a comparison between the three types of test by looking at the evolution of different parameters with elapsed time. From Chapters 6 and 7 it can be observed that, for the same agglomerate, the fracture strains are almost the same irrespective of the type of test carried out. In section 9.1. it was shown that, for tests causing fracture in 2-3 large fragments, the nominal straining of the strong-dense agglomerate was identical in both the free-fall impact and double impact tests up to the moment of fracture. It is, therefore, more appropriate to present the comparisons between the three types of tests in terms of the evolution of agglomerate strain.

9.2.1 Dense[1] Agglomerate

The tests considered for comparison were the ones that produced an almost half-half primary fracture of the dense[1] agglomerate: the free-fall impact test of 0.2 m/s impact velocity (see section 6.2.2), the double impact test of 0.02 m/s impact velocity (having the falling mass 100 times heavier than the agglomerate - see section 7.3.3) and the diametrical compression test (see section 7.6). The impact kinetic energies for the two impact tests were the same. Primary fracture occurred at 0.15% nominal strain in the free-fall impact test, at 0.16% strain in the double impact test and at 0.29% strain in the diametrical compression test.

A comparison of the force developed on each platen for the three tests is provided in Fig. 9.7. It is noted that the largest drop in the platen forces occurred around 0.17% nominal strain for both impact tests, but only at around 0.29% strain in the diametrical compression test. However, until its largest drop, the evolution of the platen forces in the double impact test was much more similar to the one in the diametrical compression test, than to the one in the free-fall impact test. At the beginning (up to 0.5% strain), the force on the impacted (bottom) platen in the free-fall impact test increased more rapidly with strain than the force developed on any single platen in the other two tests. This proves that the largest (and more dynamic) local load occurred in the free-fall impact test at the contact with the platen. One might therefore expect that this test would suffer the most local contact damage.

The evolution of the work input in the three tests is presented in Fig. 9.8. For the free-fall impact test the work input is represented as the decrease in the kinetic energy of the agglomerate. Only at the very beginning up to about (0.02% strain) was the evolution of the work input similar for the three tests. Subsequently, a little more work input was required in the free-fall impact test to produce the same nominal strain (see Fig. 9.8). The evolution of the work input was identical for the double impact and diametrical compression tests until the moment of fracture in the impact test. Requiring one third more straining to fracture the agglomerate, the diametrical compression test consumed the most work input.

The evolution of the damage and debris ratios are presented in Fig. 9.9 and 9.10 respectively. Although the agglomerate suffered the largest nominal strain before fracture in the diametrical compression test, it also produced the lowest levels of bond breakage and mass of debris. This is certainly due to the less dynamic effect of loading in the diametrical compression test. When comparing the diametrical compression with the two impact tests, Arbiter et al (1969) reported similar findings (regarding debris) from results of experiments on sand-cement agglomerates. Figure 9.7 suggests that the higher loading rates in the free-fall impact test produced larger stresses in the single local zone of impact, thus producing more bond breakage (Fig. 9.9) and a much larger total mass of debris in that polar region (Fig. 9.10).

Although attaining approximately the same maximum for all three tests, the evolution of the total number of compressive interparticle forces (Fig. 9.11) was not the same in the three tests. In the low impact velocity (0.02 m/s) of the double impact test the evolution was reasonably smooth and similar to that in the diametrical compression test (compare this to Fig. 9.6 in which the evolution in the double impact test of 0.2 m/s impact velocity was similar to the one in the free-fall impact test at the beginning of simulation). This clearly indicates the main difference in internal behaviour induced by high and low loading rates. During the loading phase in the high loading rate (free-fall or double impact) tests there is only a very short period during which the compressive load is transmitted through a large number of interparticle contacts as, in these tests, the load becomes more rapidly "focused" (transmitted through a lower number of transmission paths). At low and very low loading rates (double impact and diametrical compression tests) the "focusing" of the load transmission also takes place but is a more gradual process (see Fig. 9.11). It appears that the faster "focusing" of the load transmission in the higher loading rate tests (see the interval between 0.03% and 0.07% strain in Fig. 9.11) contributes to the higher amount of broken bonds and debris in these tests. "Focusing" of the load transmission means larger contact forces along fewer transmission paths within the agglomerate, which means larger stresses, resulting in more breakage of bonds. What remains constant for any loading rate and any test type is the maximum number of interparticle contacts through which the load can be transmitted.

The evolution of the average normal contact force, Fig. 9.12, was similar to the evolution of the total platen forces (sum of the top and bottom platen forces for double impact and diametrical compression tests - the graph is not shown in the thesis). Figure 9.12 clearly shows that the dense[1] agglomerate needed to maintain the maximum attained stored elastic energy until the fracture moment in all three types of test. Returning to Fig. 9.5 it can be seen that this was not exactly the case for the double impact test with a higher (0.2 m/s) impact velocity, in which the force evolution on the top and bottom platens was different. From Fig. 9.12 three phases can be identified in all three tests: loading during which elastic energy was stored, a "plateau" phase when the elastic stored energy was maintained at its maximum value, and a steep unloading phase with the release of energy around the moment of fracture. The maximum value of the elastic stored energy was higher for the double impact and diametrical compression tests (see Fig. 9.5 and 9.12) because in these tests the agglomerate was confined between the two platens.

9.2.2 The Dense[2] Agglomerate

As described earlier the dense[2] agglomerate had an initial contact density 16% higher than the dense[1] agglomerate. The dense[2] agglomerate tests selected for comparison were the ones in which primary fracture occurred in 2 or 3 large fragments: the free-fall impact test of 0.12 m/s impact velocity (see section 6.2.5), the double impact test of 0.02 m/s impact velocity (mass of top platen was 100 times larger than that of the agglomerate, see section 7.3.4) and the diametrical compression test (see section 7.6). Primary fracture occurred at 0.063% strain in the free-fall impact test, at 0.098% strain in the double impact test and at 0.128% strain in the diametrical compression test. The first point to note is that the smallest strain to fracture occurred in the free-fall impact test.

For the three different tests, Fig. 9.13 presents the evolution of the platen force in the free-fall impact and of the force on the top platen in the double impact and diametrical compression tests. As for the dense[1] agglomerate (Fig. 9.7), the platen force in the free-fall impact test exhibited the fastest increase and the largest maximum. What clearly distinguished the dense[2] agglomerate from the dense[1] agglomerate was that the evolution of the total force on platens did not exhibit a "plateau" zone (see Fig. 9.13 compared to 9.7). Instead, unloading commenced immediately after the attainment of the maximum platen force in all three tests.

The evolution of the work input (Fig. 9.14) in the three types of test indicates that the free-fall impact test is the most efficient in producing fracture as it required the least work input. Fracture occurred at almost 50% lower nominal strains than in the dense[1] agglomerate and only required about half the work compared to the dense[1] agglomerates for all three types

of test (see Fig. 9.14 compared to Fig. 9.6). Despite the similarities in the evolution of the platen force and the work input in the double impact and diametrical compression tests (Fig. 9.13 and Fig. 9.14), one can note the more brittle-elastic character of the end of the fracture process for very low loading rates (the diametrical compression test). Although fracture occurred at a slightly higher nominal strain in the diametrical compression test, the fracture moment was marked by a slightly more sudden unloading (see in Fig. 9.14 how at fracture the agglomerate starts suddenly to strain without the need of additional work input).

Figure 9.15 presents the evolution of the average normal contact force in the three tests, which is very similar to the evolution of the total platen force for the three tests (not shown here). As in the case of the dense[1] agglomerate (Fig. 9.8), the diametrical compression test required the most work input to produce fracture, but not much more than the double impact test (see Fig. 9.14 compared to Fig. 9.8). However, the dense[2] agglomerate was also able to store the most elastic energy in the diametrical compression test compared to the other two tests (see Fig. 9.15). The maximum average contact force attained in the free-fall impact test was only approximately half that attained in the diametrical compression test. Figure 9.15 suggests that, for higher loading rates, the dense[2] agglomerate fractures with less agglomerate strain. The figure also reveals that the dense[2], when compared to the dense[1] agglomerate, exhibits only two phases in the evolution of the internal elastic stored energy, as the "plateau" phase is missing (see Fig. 9.15 compared to Fig. 9.12).

Figure 9.16 presents the evolution of the damage ratio in the three tests. As in the case of the dense[1] agglomerate, the test at the highest loading rate (the free-fall impact test) broke bonds fast, with the least amount of strain required (Fig. 9.16), and produced the largest quantity of debris.

9.2.3 Overall Comparison For Tests Causing Fracture

Elastic deformation of the agglomerates occurred at the very start of the tests and was found to be very small. This was followed by a relatively long stage of elasto-plastic deformation. The material from an approximate conical zone at the contact with the platen/s was under high stresses, due to the high compressive interparticle forces created locally by the applied load's transmission into the sample. As a result, particles in the cones were displaced relative to each other, which caused many interparticle contacts/bonds to break. The conical regions thus became a little denser but much weaker than the rest of the material in the agglomerate; some debris started to be detached from there. Elastic energy was stored in the agglomerates (at the interparticle contacts) in a way almost mirroring the rise in total platen force. Mainly due to the hoop tensile stresses created by the contact damage zone/s pushing into the agglomerate, bonds started to break along certain planes - starting from the damage zone/s to inside the agglomerate, into the "virgin" material of the agglomerate. The agglomerate finally

experienced primary fracture usually along one of the internal planes of broken bonds, while the platens force and the elastic strain energy (represented by the average interparticle contact force) were engaged in their final drop.

"Fracture was not a "clean" process, as the simulation results showed that relatively large local plastic deformation occurred adjacent to the agglomerate-platen interfaces before fracture. Generally, the lower the loading-rate or impact velocity used to cause fracture, the smaller was the agglomerate's vertical strain at fracture and the amount of local damage produced before fracture. In the double impact test, although the largest agglomerate strain at fracture was experienced by the weak-dense agglomerate (over 10 times larger than the fracture strain of the strong dense agglomerates), the damage and debris ratios at fracture were very similar for all three dense agglomerates. The dense[1] agglomerate had less or slightly less broken contacts and debris particles at the fracture moment than the other two dense agglomerates. Flattening of the strong dense agglomerates to fracture was found to be small in the diametrical compression tests and insignificant in impact tests. The most flattening prior to fracture was experienced by the weak-dense agglomerate.

The values of the maximum platen force and stored (strain) energy were lowest for free-fall impact tests, where agglomerate was not confined (trapped) between two platens. For the same agglomerate, nominal strains at fracture were found to be very close in value for all the three types of test simulated. Agglomerate flattening at fracture was found to be highest in the case of the diametrical compression test on the dense[1] agglomerate and of the double impact test on the dense[2] agglomerates. The "quasi-static" loading regime was found to produce less damage and debris, but also to "encourage" plastic flow.

9.3 THE LOOSE AGGLOMERATE - COMPARISON BETWEEN FREE-FALL, DOUBLE IMPACT AND DIAMETRICAL COMPRESSION TESTS

The same type of comparison was carried out for the loose agglomerate, up to a nominal strain of 7.3%. The tests selected was the free-fall impact with 0.2 m/s impact velocity (see section 6.3.2), the double impact with 0.02 m/s impact velocity (platen 100 times heavier than the agglomerate, see section 7.4) and the diametrical compression test using a platen velocity of 0.003 m/s (see section 7.7).

Figure 9.17 illustrates the evolution of the platen force in the free-fall impact and of the force on the top platen in the double impact and diametrical compression tests. It can be observed that the lower the loading rate, the faster was the overall increase in the force on the platens. The free-fall impact test was the only one that experienced complete loading and unloading before 7% strain. When the agglomerate attained its maximum nominal strain (of about

6.55%) the platen force dropped to almost zero as the agglomerate's velocity almost reduced to zero - indicating that the flattened agglomerate remained adhered to the platen. For the double impact and diametrical compression tests the platen force increased slowly but continuously. However, after attaining 8% strain the platen force began to fluctuate about a constant value. The top platen force never reached 1.5 mN in the double impact test or 2.5 mN in the diametrical compression test even at large strains of 13% (not shown in Fig. 9.17).

The evolution of the average normal contact force, shown in Fig. 9.18, is again very similar to the evolution of the total force on platens (not shown in this thesis). The maximum average contact force attained in the free-fall impact test (0.0024 mN) was about 7.5 times lower than that attained in the free-fall impact test of the dense[1] agglomerate (for the same impact velocity). Furthermore, this maximum was attained much later in the test. Loose agglomerates could not store much energy internally in any of the tests even after extensive straining and flattening of the agglomerate. The capacity for storing energy in the loose agglomerate increased if the loading rate was reduced. This was different than the case of the dense[1] agglomerate in which double impact and diametrical compression tests, although having very different loading rates, achieved about the same (maximum) amount of energy stored prior to fracture (see Fig. 9.12).

Compared to the dense agglomerates, the platen forces were much lower. In the free-fall impact test the platen force attained an absolute maximum of about 0.75 mN, which was over 20 times lower than the maximum attained in the free-fall impact test of the dense[1] agglomerate for the same impact velocity (see Fig. 9.17 compared to Fig. 9.7). For each of the three types of test the platen force increased much more slowly for the loose agglomerate than for the dense agglomerates. It is also noted that the evolution of the platen force in Fig. 9.17 shows extensive fluctuations, which are only partly due to the fact that the plot was drawn to a much smaller scale than the ones for the dense agglomerates, Fig. 9.7 and 9.13.

The work input for the loose agglomerate, Fig. 9.19, was very low up to 1.3% strain. The diametrical compression test was the least efficient in flattening the agglomerate as it needed the most work input for achieving the same nominal strain - see Fig. 9.19. It is interesting that the trend of the evolution in the work input was closer to the trend observed for the dense[2] agglomerate (which had the highest contact density) prior to fracture (Fig. 9.14) rather than the trend exhibited by the dense[1] agglomerate before fracture, which was almost linear (Fig. 9.8).

Figure 9.20 shows the evolution of the total number of particles in the largest surviving cluster in the three types of tests. Unlike the behaviour of the dense agglomerates (Fig. 9.10) the free-fall impact test was not the one to produce the most debris from the very beginning

of the test. Up to 4% strain the double impact test was the one which resulted in the largest amount of debris and only at strains above 5.5% was the free-fall impact test the most "productive" in the detachment of debris (Fig. 9.20). As in the case of the dense agglomerates, the loose agglomerate suffered the lowest attrition in the diametrical compression test.

Having seen the differences in the evolution of the forces on the platens it is a little surprising to find that the flattening of the loose agglomerate did not vary with loading rate and type of test, as was the case with the dense agglomerates. Figure 9.21 clearly shows that, the evolution of the total number of particles in contact with the platen/s was very similar for the three tests. The slight exception was the end of the free-fall impact test, where the flattening increased with very little additional nominal straining (Fig. 9.21).

9.4 FRAGMENT SIZE DISTRIBUTIONS

Many workers have tried to quantify the degree of sample fragmentation obtained in various tests. They use sieves to categorise the fragments according to their size and then they usually weigh the categories separately. Only rarely do laboratory workers weigh every fragment obtained. For free-fall impact tests, they normally plot the mass of fragments undersize against the fragment size to provide fragment size distribution plots (generally Gates-Gaudin-Schuman log-log plots).

For a test in which the specimen fractures into a relatively low number of large fragments, workers have found that the typical log-log size distribution plot consists of two almost straight lines with different slopes. The first line, of low slope, represents the small fragments, the debris, or the *complement*. The second, steeper line represents the large fragments, or the *residue*. Arbiter et al (1969) plotted the fragment size distributions for each of the three types of test that they carried out on sand-cement agglomerates - free-fall impact, double impact and diametrical compression.

9.4.1 Free-Fall Impact Tests

The plot in Fig. 9.22 shows the fragment size distributions obtained for the dense[1] agglomerate in four free-fall impact tests using various impact velocities of 0.1 m/s (that caused agglomerate rebound), 0.2 and 0.3 m/s (that resulted in agglomerate fracture/fragmentation), and 0.9 m/s (causing agglomerate shattering). The cumulative normalised mass undersize is plotted versus the fragment size relative to the initial agglomerate size. In Fig. 9.22 m_0 is the total mass of the agglomerate (at the start of the test) and m_f is the mass of the fragments under a certain size. As in the laboratory where

sieves are used, the size of a fragment is represented by its maximum dimension, which is the diameter of its circumscribing sphere, denoted D_f. The diameter of the circumscribing sphere of the agglomerate at the start of the test is denoted as D_0.

The trends of the distributions shown in Fig. 9.22 are very similar to the ones obtained by Arbiter et al (1969) in their free-fall impact tests on sand-cement agglomerates (see Fig. 14 and 15 in Arbiter et al, 1969). The results are also similar to most results of free-fall impact laboratory tests published in the literature: the higher the impact velocity, the larger the mass of small fragments obtained. The mass of debris increased with increasing impact velocity. The gradients of the lines representing the debris are not very different for all the four tests. The gradients of the lines representing the residue varied depending on the number of large fragments obtained.

The data representing the debris can be fitted with a power law having the form

$$m_f/m_0 = k\,(D_f/D_0)^n \tag{9.1}$$

where m_f/m_0 is the mass of fragments undersize normalised to the initial mass of the agglomerate, D_f/D_0 is the diameter of the circumscribed sphere of the fragment normalised to the initial diameter of the agglomerate, and n the exponent of debris distribution. It can be seen from Fig. 9.22 that for the input velocities producing fracture/fragmentation (0.2 and 0.3 m/s), the exponent n does not change. This indicates that in the case of fracture/fragmentation, as in the free-fall impact laboratory tests of Arbiter et al (1969), the exponent is insensitive to the impact velocity, energy input and pattern of fragmentation. For the dense[1] agglomerate n was found to be 0.5. For their sand-cement agglomerates, Arbiter et al (1969) found $n \approx 0.25$. It is possible that the difference is due to the much more coarse structure of the simulated agglomerate.

The work of Arbiter et al (1969) suggests that the prefactor k varies with the square of the impact velocity V (V^2 is also called the specific impact energy). The plot in Fig. 9.23 presents the cumulative mass undersize (m_f/m_0) of the debris against $V^2\,(D_f/D_0)^{0.5}$ for the three tests that did not cause agglomerate shattering. The fact that all the points are situated on the same straight line demonstrates that, the following correlation is valid

$$m_f/m_0 = \lambda\, V^2\,(D_f/D_0)^n \tag{9.2}$$

and, for the data shown in Fig. 9.23, $\lambda \approx 4$.

Figure 9.24 presents the size distribution of all the fragments obtained in five different free-fall impact tests on the dense[2] agglomerate. In general, the trends were similar to the ones

obtained for the dense[1] agglomerate (Fig. 9.22). However, as more debris was obtained for the same impact velocity, the prefactor k was higher. Also the exponent of debris distribution was larger for the dense[2] agglomerate, i.e. $n = 0.7$.

For the three tests causing fracture, Fig. 9.25 shows the cumulative mass undersize of fragments plotted against $V^2 (D_f/D_0)^{0.7}$. The reasonably good fit with the straight line shows that, for the dense[2] agglomerate, also the exponent does not vary significantly with impact velocity, energy input and pattern of fragmentation. From Fig. 9.25 the value of λ for the dense[2] agglomerate is approximately 14, which is 3.5 times larger than the value obtained for the dense[1] agglomerate.

Arbiter et al (1969) suggested that λ is a function of the material properties of the sample. From free-fall impact test simulations on FCC agglomerates having interface energies varying from 0.2 to 4.0 J/m^2, Kafui (1996) found that λ is directly related to the Dupre energy of adhesion Γ (or interface energy), and that there exists a power law relationship between Γ and λ. Kafui (1996) found that λ decreases with increasing interface energy. In this thesis the two dense agglomerates tested in free-fall impact had the same interface energy (Γ=2.0 J/m^2) but different contact density (the dense[2] agglomerate had a 14.6% larger mechanical coordination number than the dense[1] agglomerate, Tables 6.1 and 7.1). The little higher contact density resulted in 3.5 larger λ in the dense[2] agglomerate. Therefore, at a first glance, the work carried out in this thesis suggests that varying contact density has a different qualitative effect than varying the interface energy, if it is considered that both these parameters increase the "strength" of the agglomerate. From the values of λ one can conclude that the dense[1] agglomerate is "stronger" than the dense[2] agglomerate. Many results from the simulations also suggest that the dense[1] agglomerate is "stronger", as it fractured at higher nominal strains and it usually attained higher values of stored elastic energy (see the maximum attained values of the average normal contact force in double impact and diametrical compression for the same loading-rate (see Tables 9.2 and 9.3) than the dense[2] agglomerate.

It is clearly demonstrated by results obtained from the free-fall impact tests on the two dense agglomerates that λ (in the relationship (9.2)) varies not just with the interface energy, but also with the contact density of the agglomerate. More research work is needed to find out the exact relationship between λ and an agglomerate's contact density.

Overall, the correlations for the free-fall impact tests, presented in Figs. 9.22 - 9.25, of the two dense agglomerates were as good as the correlations found by Arbiter et al (1969) on their sand-cement agglomerates (see Arbiter et al, 1969, Fig. 17) and by Kafui (1996) in his face-centred-cubic agglomerate simulations.

9.4.2 Double Impact Tests

For double impact tests causing only local damage with some debris, the state of the agglomerate at the end of the test was used to determine the fragment size distribution. In order to obtain the fragment size distributions in the double impact tests causing fracture, the impacting platen was usually arrested shortly after the primary fracture, similar to the procedure used by Arbiter et al (1969) in their double impact tests.

The fragment size distributions for the weak-dense agglomerate in tests using the same platen mass (100 times heavier than the agglomerate) but different impact velocities are illustrated in Fig. 9.26. For the test with V = 1.0 m/s, two distributions are presented depending on the moment in the test when the impacting platen was arrested: (a) when the force attained its maximum value on the top (impacting) platen, (b) just after the total force on the platens attained its maximum. Similar to the results obtained for free-fall impact tests at various impact velocities, the mass of the debris was larger for tests with higher impact velocities or higher energy input. The exponent n of debris distribution for the two tests with the highest impact velocity (1.0 m/s) was 0.25 - same as the one obtained by Arbiter et al (1969) for their sand-cement agglomerates (note that, for this high impact velocity, the exponent n did not vary when the impacting platen was arrested at different moments during tests of same impact velocity). Different than the results obtained for free-fall tests, one can see that the exponent n varied considerably with impact velocity in the double impact tests, even if only tests causing fracture were considered.

Apart from varying the impact velocity, in the double impact tests, the impact kinetic energy can also be varied by changing the mass of the impacting platen. For the weak-dense agglomerate, Fig. 9.27 presents the fragment size distributions obtained from four tests with the same impact velocity (0.04 m/s) but different platen masses. The test in which the top platen velocity was maintained constant at 0.04 m/s is also presented in the figure. Unlike the comparison for different impact velocities (Fig. 9.26 for double impact and Fig. 9.22 and 9.24 for free-fall impact), varying the mass of the impacting platen did not result in a significant increase in the amount of debris for tests in which the agglomerate fractured. Moreover, varying only the mass of the impacting platen produced no change in the exponent of the debris distribution. The results obtained from the test in which the platen velocity was constant are situated in between the ones obtained from the other two tests causing fracture (see Fig. 9.27). Both Figs. 9.26 and 9.27 demonstrate that, for tests causing fracture, the impact velocity has a much more significant effect on the resulting fragment size distribution than the mass of the impacting platen.

The state at the very end of a test (when the fragmentation process stops naturally, long after the moment of primary fracture) was used in the free-fall impacts for obtaining the fragment

size distribution. The situation is more complicated in the case of the double impact tests, as the impacting platen had to be arbitrarily arrested. (In tests in which the agglomerate fractures, the double impact test cannot be continued indefinitely because this will result in crushing of the fractured agglomerate.) In laboratory tests, workers (e.g. Arbiter et al, 1969) arrested the impacting platen immediately after they observed "signs" of primary fracture, i.e. the drop in the platen force. They were not, however, concerned with the fact that it is very important to determine the exact moment when primary fracture occurs. The simulated tests have revealed that the precise moment when the impacting platen was arrested after fracture makes a lot of a difference to the resulting fragment size distribution.

For the same agglomerate and initial test conditions, three slightly different ways of "controlling" the impacting platen after fracture were selected for comparison. In the first simulation the platen was arrested immediately after the primary fracture moment (determined with precision by observing the distribution of the particle velocity vectors - see section 7.3). In the second simulation the impacting platen was arrested a little while after the primary fracture moment when the total force on the platens had dropped. What was different in the third simulation compared to the second one was that the impacting platen was not just halted but also removed. This last procedure is the most similar to the one followed in laboratory double impact tests (see Arbiter et al, 1969). Figure 9.28 presents the fragment size distribution for the three slightly different simulations on the same dense[1] agglomerate and initial test conditions (0.2 m/s impact velocity, platen mass equal to the agglomerate mass). The large differences in the amount of debris, and significant variation in the exponent for the simulations in which the platen was arrested at different moments after primary fracture are evident. The findings show that, in the laboratory, the fragment size distribution for double impact tests is not entirely reliable information, as it very much depends on the precise moment when the impacting platen is arrested (and whether it is removed from the agglomerate).

Although the three resulting fragment size distributions in Fig. 9.28 were obtained for the same agglomerate fractured in the same test, a significant difference in the amount of debris can be observed. Returning to section 9.1, the slightly more debris produced in the free-fall impact test compared to the double impact test (0.2 m/s impact velocity, see Fig. 9.4) appears now to be less significant, as more debris particles would certainly result in the double impact test soon after the top platen was taken off the agglomerate.

9.4.3 Comparisons Between All Three Types Of Test

A comparison in terms of fragment size distributions was also carried out for the three types of test in which the dense[1] agglomerate fractured primarily into two large fragments (see also section 9.2.1) - the free-fall impact test of 0.2 m/s impact velocity, the double impact

test of 0.02 m/s impact velocity and the diametrical compression test with a platen velocity of 10 mm/min. Figure 9.29 shows the results of this comparison which compares well with a similar comparison carried out on sand-cement agglomerates by Arbiter et al, 1969 (see their Fig. 16). The same conclusion can be reached as the one drawn by Arbiter et al (1969): the diametrical compression tests always produce less debris than the double impact and free-fall impact tests. However, in contrast to the conclusions of Arbiter et al (1969), the exponent n of the debris distribution was not insensitive to the particular type of test performed on the agglomerate, but it seemed to be the same only for the low-velocity double impact and diametrical compression tests (Fig. 9.29).

9.5 INPUT ENERGY CONSIDERATIONS

There is special interest, especially in comminution applications, to relate the energy input to the subsequent degree of breakage.

9.5.1 Free-Fall Impact Tests

Table 9.1 presents the approximate energy input to primary fracture and the maximum average normal contact force in 11 of the free-fall impact tests carried out on the two strong-dense agglomerates. The input energy to fracture was taken to be the difference between the impact kinetic energy and the kinetic energy of all the particles at the moment of fracture. Other energies were considered to be negligible (for example the energy due to gravity potential up to the fracture moment was only around 0.12 nJ). The free-fall impact test simulations were halted when not much was occurring in terms of damage and debris ratios. In most of the tests, the total particle kinetic energy at this point was not quite zero.

The table suggests that there is an impact velocity below which the free-fall impact test cannot produce fracture as not enough strain energy is stored in the agglomerate. One can observe in Table 9.1 that the dense[2] agglomerate fractures after attaining a peak average normal contact force of 13.79 μN, whereas the dense[1] agglomerate does not fracture after attaining a higher peak (of 15.36 μN). This indicates that the dense[2] agglomerate is more brittle, as it can fracture at lower levels of elastic stored energy than the dense[1] agglomerate. Additionally, the minimum input energy for producing fracture of the dense[2] agglomerate was more than 60% lower than the minimum input energy required by the dense[1] agglomerate (see Table 9.1).

From the point of view of producing fracture, the most efficient free-fall impact tests are the ones in which most of the impact kinetic energy has been consumed by the moment of fracture (i.e. the input energy to fracture is almost equal to the impact kinetic energy). For

example, 91% of the impact kinetic energy was used by the fracture moment in the 0.1785 m/s impact velocity test on the dense[1] agglomerate, whereas even more, 94%, was used in the 0.12 m/s impact velocity test on the dense[2] agglomerate - see Table 9.1. For higher impact velocities, although the input energy to fracture was higher it increased much less than the increase in impact kinetic energy. For example, for the impact velocity of 0.3 m/s, only 55% of the impact kinetic energy was used up to the fracture moment in both the strong dense agglomerates. Tests with higher impact velocities "consumed" more energy until the fracture moment due to the higher dissipation of energy in the larger contact damage zones. Higher impact velocities therefore led to extensive fracturing and shattering of the dense agglomerates.

9.5.2 Double Impact Tests

The impact kinetic energy in the double impact tests is less significant than in free-fall impact tests, especially in tests in which the top platen is arrested at fracture or in tests in which the kinetic energy of the impacting platen becomes higher than the impact kinetic energy (when the platen is much heavier than the agglomerate). Table 9.2 presents the work input (input energy) to primary fracture and the maximum average normal contact force in twelve of the double impact tests carried out on the three dense agglomerates.

In order to produce primary fracture, for the same impact velocity of 0.04 m/s, the weak-dense agglomerate needed 19% less work input for a 6.726 times heavier impacting platen (see test {4} compared to test {3} in Table 9.2). More work input (44%) was needed for almost the same impact kinetic energy in the test when the impact velocity was 2.5 times higher (see test {6} compared to test {4} in Table 9.2). For higher impact velocities and the same platen mass, more work input was needed up to the moment of fracture (see test {6} compared to test {3} in Table 9.2). However, a different behaviour was observed for very high velocities (1.0 m/s). If the impacting platen was arrested at only 0.26% nominal strain, the work input up to that moment (which was about half that in the other tests) - was sufficient for producing the break-up of the agglomerate into two large fragments (see test {7} compared to tests {3-6} in Table 9.2). It follows that the most efficient (least energy-consuming) breakage processes are obtained if the impact velocity is very high. However, if the aim is to obtain two or three strong large fragments, lower velocities and heavy impacting platens are more appropriate - see test {4} in Table 9.2.

It appears that in the double impact test there is a minimum amount of input energy required to break a particular agglomerate. It was found that a work input of 20 nJ was not sufficient to break the weak-dense agglomerate, but was more than enough to fracture the dense[1] agglomerate. For the same impact velocity (of 0.1 m/s) and impact kinetic energy (557.57 nJ), the weak-dense agglomerate needed 3.4 times more work input until the primary

fracture moment than the dense[1] agglomerate (see Table 9.2). This must be related to the fact that the dense[1] agglomerate was able to store 4.3 times more elastic strain energy than the weak-dense agglomerate.

Lower impact velocities are more efficient for producing the fracturing of the dense agglomerates. For the same impact kinetic energy but 10 times higher impact velocity, the dense[1] agglomerate needed 23% more energy input up to the moment of primary fracture (see test {11} compared to test {9} in Table 9.2). The dense[2] agglomerate certainly behaved the most brittle, requiring only half the work input up to the primary fracture moment for the same impact velocity and platen mass compared to the dense[1] agglomerate - see test {12} compared to test {9} in Table 9.2.

9.5.3 Diametrical Compression Tests

Table 9.3 presents the work input (input energy) to primary fracture and the maximum average normal contact force in the two diametrical compression tests carried out on the dense agglomerates. For the same loading rate, primary fracture in the dense[2] agglomerate occurred at 57% less strain than in the dense[1] agglomerate. Also the work input by the moment of primary fracture was almost 70% lower in the dense[2] agglomerate, indicating that fracture at lower nominal strains reduces the energy input requirement.

9.5.4 Comparisons

Comparing Tables 9.1, 9.2 and 9.3 it appears that the impact tests can be the most efficient in producing fracture of the dense agglomerates. The lowest impact velocity producing fracture results in 2-3 large fragments and it only consumes 16.16 nJ (in the case of the dense[1] agglomerate) and 6.25 nJ (in the case of the dense[2] agglomerate) by the moment of primary fracture. Overall, for low impact velocities, it can be observed that the energy utilisation is better in impact than compression testing. If clean fracture with strong large fragments is not required, high impact velocities in the double impact test appear to be the more efficient than low ones (see the 1.0 m/s impact velocity when the impacting platen was arrested, for the weak-dense agglomerate). Diametrical compression is the most appropriate test for obtaining the "strongest" large fragments from an agglomerate and the least amount of debris.

Arbiter et al (1969) made a comparison between two impact tests with the same input energy to fracture: a free-fall impact test and a double impact test in which the platen mass was about half the mass of the agglomerate. From the data presented in the paper it appears that the impact velocity in the free-fall impact test was approximately twice that in the double impact test and the impact kinetic energy was about eight times higher. The result was, however,

approximately the same: the size distribution of the debris (see Arbiter et al, 1969, Fig. 16) was almost identical for the two tests. Arbiter et al (1969) defined the breakage efficiency in terms of the mass of fragments below a certain size per unit energy input. They essentially concluded that double impact and free-fall impact tests result in the same breakage efficiency for the debris if the same amount of energy is input.

A similar comparison between the two types of impact tests was also carried out in this project. It can be observed from Tables 9.1 and 9.2 that the same amount of energy (16.15 nJ) was input to primary fracture in both the free-fall impact test of 0.1785 m/s impact velocity and the double impact test of 0.02 m/s (with a platen that was 100 times heavier than the agglomerate). Although having an 8.9 times higher impact velocity, the free-fall impact test provided 20% less impact kinetic energy than the double impact test. However, the large difference in impact velocity was crucial: at fracture the free-fall impact test had produced 74% more broken bonds and four times more debris. Figure 9.30 shows the comparison in fragment size distributions for the two tests. It is evident from the graph that the quantity of debris is much higher in the free-fall impact test. It is concluded from this comparison that the same energy input to fracture is not a sufficient condition for obtaining similar results in free-fall impact and double impact tests, as the laboratory tests of Arbiter et al (1969) appear to suggest.

Two other tests had almost the same energy input to primary fracture: the free-fall impact test of 0.2 m/s and the double impact test 0.2 m/s impact velocity that had a platen mass equal to the mass of the agglomerate (see Tables 9.1 and 9.2). Although the input energy to fracture was slightly larger for the double impact test, the free-fall impact test resulted in a little more debris (Fig. 9.4). However, the agreement improved if the impacting platen was taken off the agglomerate after fracture (see Fig. 9.28 and paragraph 9.4.2.). Figure 9.31 presents the fragment size distributions for the two impact tests and illustrates that the size distribution of the debris was almost identical. The results of the simulation suggest that only for the same impact velocity, the same initial kinetic energy and the same mass of the impacting body will the size distribution of the debris be the same.

From their laboratory tests Arbiter et al (1969) reported that the diametrical compression test required about half the energy to initiate fracture than the free-fall impact test. The input energy (to fracture) of their diametrical compression test was lower than the input energy in all the impact (free-fall impact and double impact) tests presented in their paper. The situation was different in the simulation tests presented in this thesis. The work input to primary fracture in the diametrical compression test was larger than the energy input to primary fracture in the impact tests. The difference in the results could lie in the fact that the primary fracture in the tests reported by Arbiter et al (1969) consisted of over four large fragments, whereas the comparison in this thesis was more of "like with like". On the other hand, it was

not very clear from the paper how the energy input was calculated for each different type of test. In the simulations the diametrical compression tests produced a significantly smaller amount of debris than the free-fall impact and double impact tests (as in the tests of Arbiter et al, 1969), but not because a smaller energy was input to fracture moment, as Arbiter et al (1969) concluded, but because of the very low rate of loading (velocity).

It has been seen that between 800-1600 bonds were broken at the primary fracture of each of the two strong dense agglomerates in each of the three types of test causing fracture in two or three large fragments. However, one could observe that the breakage of only about 300-400 of these bonds were sufficient for separating the two large fragments. It results that only about 7%-20% of the bonds broken up to the moment of primary fracture were really necessary to break for agglomerate fracture, that a damage of about 0.03 would usually be sufficient for producing the separation of the agglomerate into two large fragments. Furthermore, the total work done only in breaking the 800-1600 bonds lost by the moment of primary fracture is much lower than the total work "consumed" (input) by the primary fracture moment. The work that went into the inelastic deformation of the agglomerate (at the interface/s with the platen/s) is therefore significant. In laboratory diametrical compression tests on limestone pellets, Kapur and Fuerstenau (1967) calculated the work done in the "compression" (compaction) of the material in the contact cones before fracture for different loading-rates (0.5-10 mm/min) and agglomerate sizes (from 8 to 20 mm). Unexpectedly, they found no obvious correlation between this work and the loading-rate or agglomerate diameter. The simulations on the dense agglomerates revealed that the work done in the local plastic deformation zones increases with loading-rate in all three types of test.

9.6 WAVE PROPAGATION AND LOAD TRANSMISSION

9.6.1 Wave Propagation

Although quasi-static conditions are usually assumed for simplifying the theoretical analysis of real phenomena, the dynamic effects cannot always be disregarded. An external load on a sample induces an internal state of stress which is continuously changing. Apart from elastic, kinetic, gravity-potential, and dissipated energies, a quota of the input energy is transformed into vibrational energy - the energy of wave propagation. The more dynamic the load, the larger is the vibrational energy (see Hunter, 1957) and the more this influences the behaviour of the sample. Waves have usually very little effect on the behaviour of samples subjected to slow diametrical compression tests, but may significantly influence their behaviour in high-velocity impact and fast loading tests.

When external forces are applied to a sample, different waves are generated and propagate, with finite velocities, from the loaded region into the sample (Timoshenko, 1958). These waves can be longitudinal (moving along the load direction, also called dilatational waves), transverse (moving perpendicular on the load direction, also called distortion, lateral or shear waves), surface Rayleigh (moving in a thin surface layer, at interfaces or free boundaries), recompression (generated by the propagation of cracks), or rearrangement waves (in some non-homogeneous and particulate materials). All the load-transfer types of waves created in a loaded sample are superimposed into what is called stress waves which transform the sample from one state of stress to another state. As well as velocity, magnitude and direction of wave propagation, the attenuation (dissipation) of waves is also important. Waves dissipate fast in plastic-deforming samples and transmit fast in elastic ones.

Some workers found that waves caused or aided the breakage of various brittle solid samples in impact tests, especially when the impact velocities were very high. Although waves certainly influence the agglomerate failure process, the propagation of waves was not analysed in detail in this thesis because it was not found to be a significant factor in the agglomerate fracture process. There are several reasons for this. Apart from the fact that the impact velocities were not that high, the simulated samples were not solids but agglomerates, which behave inelastically. The inelasticity and internal discontinuities of agglomerates are known to attenuate the intensity of the vibrational energy. Although the wave propagation occurring inside a constituent particle is similar to the wave propagation in a solid sphere, within agglomerates waves dissipate considerably because they reflect and refract whenever they meet a particle-particle interface (Rossmanith and Shukla, 1982). Only a part of the wave is transmitted through the contact to an adjacent particle. As time elapses after the initiation of the very first wave, more waves are formed (due to particle-particle impacts and wave reflections) and superimposed. Shukla and Rossmanith (1986) and Rossmanith and Shukla (1982) closely analysed the transmission of waves across contacts and along different particle-particle zig-zag propagation pathways. They showed that the more angular and the longer the wave propagation-path, the lower the wave speed and the larger the energy dissipation.

The speed of wave propagation depends mainly on the material properties. In this thesis the propagation velocity of the longitudinal wave through a constituent particle was of about 8902 m/s (corresponding to solid glass material). However, the wave propagation velocity through the agglomerates was expected to be much lower, as an agglomerate as a whole presents a discontinuous structure and exhibits inelastic behaviour. In an impact test, the impact velocity determines the magnitude of longitudinal wave. The propagation velocity of the longitudinal wave through the agglomerate mainly depends on the arrangement of the particles. For granular bars composed of face-centre-cubic arrays of steel spheres (3.175 mm diameter) Duffy and Mindlin (1957) determined the longitudinal wave velocity to be

400-600 m/s. Using dynamic photoelasticity and high-speed photography, Rossmanith and Shukla (1982) calculated the propagation velocity of waves through a two-dimensional randomly packed column of discs having negligible bond forces. The discs were 25 mm in diameter made of polyester (Homalite 100). At a depth of 50 mm the propagation velocity of the longitudinal wave was found to be 700 m/s, and at 100 mm depth it had reduced to 500 m/s.

In this thesis, the time required for the longitudinal (compression) wave to reach the agglomerate pole opposite to the one impacted can be estimated by analysing the evolution of the state of the interparticle bonds. Figure 9.32 presents the evolution of the number of the compressive interparticle contact forces up to 20 μs in five free-fall impact tests on the dense[1] and dense[2] agglomerates. Until the longitudinal wave reaches the top pole of the agglomerate it is a compressive wave and, therefore, turns the tensile contacts which are approximately oriented in the direction of propagation into compressive contacts. This process can be observed in Fig. 9.32, where the total number of compressive contacts is initially increasing (up to about 2 μs). At the moment when the longitudinal (compressive) wave reaches the top pole, it turns tensile and reflects back towards the impacted pole. On its way back the longitudinal wave, now tensile, converts some of the compressive contacts into tensile contacts. It is very likely that this is why, in Fig. 9.32, the number of compressive contacts starts decreasing after reaching a maximum at about 2 μs (for both dense agglomerates). The first peak in the evolution of the total number of compressive contacts could therefore, in free-fall impact tests, correspond to the moment when the longitudinal wave is reflected from the top pole of the agglomerate. Based on this assumption, the average propagation velocity of the longitudinal wave was approximately 550 m/s.

It is noted that the estimated propagation velocity agrees reasonably well with the conclusions of Duffy and Mindlin (1957) and Rossmanith and Shukla (1982). However, there were two main differences between the conditions in the simulations and the laboratory tests: the size of the constituent particles and the bond force. The diameter of the particles in the simulated agglomerates was about 50 and 400 times smaller than the diameter of the constituent particles in the tests of Duffy and Mindlin (1957) and Rossmanith and Shukla (1982) respectively. This should have resulted in a much higher attenuation of the propagation velocity of the longitudinal waves in the simulated tests. However, the much stronger bonds in the simulated tests reduced the attenuation of the propagation velocity of the waves. The interface energy at the interparticle contacts was negligible in the laboratory tests, especially when compared to that used in the simulations (2 J/m^2). In their tests on model assemblies, Saad et al (1994) showed that longitudinal waves propagate faster if the interparticle contacts are stronger.

In particulate materials the speed of wave propagation depends on the material and size of the constituent particles and on the distribution and number of interparticle contacts, but also on the nature of the contacts. Furthermore, in particulate material, the wave velocity is not constant but decreases at every contact it passes through.

In various laboratory tests (see Shockey et al, 1974) the speed of crack propagation was empirically found to depend on the speed of the longitudinal wave propagation: the maximum crack propagation velocity was usually found to be three times lower than the wave propagation velocity. In Chapter 8 it was shown that the velocity of any fracture crack is not constant but varies during the fracture process. However, the average velocity of a fracture crack in the free-fall impact tests on the two strong-dense agglomerates was 2-9 times lower than the average propagation velocity of the longitudinal wave, which agrees reasonably well with the experimental findings reported in the literature.

Some workers have shown that the longitudinal waves have a major contribution to the failure of impacted solid samples. Gildemeister and Schönert (1972) and Schönert (1979) believed that some of their impacted PMMA discs failed from a crack initiated in the middle of the hemisphere opposite to the one impacted due to the propagation of the longitudinal wave. From a theoretical treatment of the impact of an elastic sphere, Gildemeister and Schönert (1972) showed that only the longitudinal wave could have produced, after reflecting from the opposite pole, the crack initiation leading to failure because the reflected longitudinal wave was tensile and more concentrated. From the results presented in Chapter 8 and 6 on dense agglomerates that fractured in free-fall impact tests one could observe that all the bonds which broke prior to 3 μs were situated in the impacted region by the platen. At 3 μs the agglomerate was still in the local failure stage, long before the start of the fracture process. This indicates that the longitudinal wave created at the moment of impact which reflected at about 2 μs could not have initiated the fracture of the dense agglomerates, as Gildemeister and Schönert (1972) suggested. Furthermore, the front of the longitudinal wave did not appear to provide any significant contribution to the local failure of the agglomerate around the impact zone since most of the local bond breakage occurred after the wave had passed through the impact region.

Figure 9.33 presents the evolution of the damage ratio in four free-fall impact tests on the dense[1] agglomerate. For impact velocities producing fracture, the breakage of bonds immediately after the reflection of the longitudinal wave (from 2 to 4 μs in Fig. 9.33) occurred mostly around the impacted region by the platen. Figure 9.34 presents the evolution of the platen force in four free-fall impact tests on the dense[1] agglomerate. For impact velocities producing fracture the force on the platen attained a maximum value between 3.5 and 5 μs. This also indicates that the local failure at the impact zone was concluded during the final propagation phase of the longitudinal reflected wave. The

situation was slightly different for the free-fall impact test of higher impact velocity (0.9 m/s) which resulted in shattering of the agglomerate. The maximum force on the platen (Fig. 9.34) occurred just after the reflection of the longitudinal wave, indicating that the local contact zone failed earlier in the shattering test. It can be observed in Fig. 9.33 that the most rapid increase in the damage ratio in the shattering test occurred between 1.5 μs and 3.5 μs. This suggests that the propagation of the reflected tensile longitudinal wave must have contributed to the extensive randomly distributed breakage of bonds in the agglomerate.

Impacting solid specimens on a target at a high velocity, Schönert (1979) observed recompression waves which were generated from cracks that developed in the impact zone. He concluded that recompression waves run out from the surfaces of propagating cracks, interact with the other waves and attenuate the stress pulse. For rocks Shockey et al (1974) also claimed that recompression waves may influence the fracture/fragmentation behaviour. It appears that the recompression waves developed during the fracture processes in the simulations were too small to influence the fracture behaviour of the agglomerates. This was mainly because the crack propagation velocity was almost an order of magnitude lower (see Table 8.1) than in the laboratory tests in which the presence of recompression waves was observed (e.g. Schönert, 1979, reported a crack propagation velocity of 1000-2000 m/s).

The contact density of the loose agglomerate was significantly less than that of the dense agglomerates. Consequently, it was much more tortuous for the wave propagation. The more angular wave propagation paths resulted in more dissipation of vibrational energy compared to the dense agglomerates. The energy dissipation associated with the longitudinal wave was also affected by the particle rearrangement observed in the loose agglomerate. The propagation velocity of the longitudinal wave in the loose agglomerate could not be determined from the evolution of the number of compressive contacts. It seems that the attenuation was so large that the longitudinal wave induced no change in the number of compressive contacts during the free-fall impact tests. Under load, the low contact density resulted in local particle rearrangements which produced rearrangement waves which superimposed on the other propagating waves, complicating the process. Evidence of the particle rearrangement process (which lasted throughout the test) is provided by the fluctuations observed in the evolution of the force developed on platens (see Fig. 9.17 for example). The rearrangement process was also responsible for the small fluctuation in the evolution of the number of compressive contact forces. Rossmanith and Shukla (1982) noted that the rearrangement waves in their dynamic experiments on granular material propagated with very low effective speed and left behind a different distribution of load paths and particle locations. However, more simulations on the loose agglomerate are required to confirm these observations.

9.6.2 Load Transmission

Rossmanith and Shukla (1982) showed that, in particulate material, dynamic load transfer and wave propagation is similar to the transfer and distribution of static loads. In photoelastic experiments on discs they showed that particulate material exhibits discontinuous behaviour under both dynamic and static applied forces due to the manner in which waves propagate. Endley and Peyrot (1977) studied the load transfer in granular media for static problems. They found that, in a random distribution of particles, the applied load will search for the shortest and most direct transmission path. Whereas in the case of a homogeneous sphere the load transfer path would be linear, there usually are more zig-zag paths in agglomerates. For certain (regular) arrangements of particles and certain directions of load, the transmission path can be linear and exactly along the direction of the applied load. This was demonstrated in the diametrical compression test on the face-centre-cubic agglomerate reported in Chapter 5 - see Fig. 5.19. For polydisperse random agglomerates the load transfer will be along transmission paths which are to some extent angular, depending on the positioning of particles and number of contacts (see for example Figs. 7.49 and 7.50). Endley and Peyrot (1977) showed that the less angular a zig-zag path, the more load the chain of particles will be able to carry.

From the simulations it was found that the density of bonds significantly affects the distribution and transmission of load through the agglomerates. Apart from the fact that the zig-zag transmission paths were less angular in the dense agglomerates, there were also many more load transfer paths formed in the dense agglomerates (Figs. 6.55 and 7.49) than in the loose agglomerate (Figs. 6.57, 7.50 and 7.67). This would appear to have had a significant effect on the different behaviour observed in the dense and loose agglomerates. In the dense agglomerates load was transmitted radially from the contact zones (Fig. 6.55 and 7.49), along reasonably linear trajectories depending on the actual particle arrangement. Having fewer bonds, the loose agglomerate developed fewer load-transmission paths than the dense agglomerates and, in particular, especially lacked the radial ones (see Fig. 6.57 and 7.50a). In particulate media, stress and load distribution are directly related to the stored elastic energy within the sample. The elastic strain energy is stored at interparticle contacts. The larger the sum of the compressive forces developed at the contacts carrying the load at any moment in time, the larger is the elastic energy stored by the agglomerate. The dense agglomerates, possessing more interparticle contacts than the loose agglomerate, have a higher potential for storing energy.

During a test, images showing only the interparticle contacts that transmitted compressive forces larger than a certain value could provide a good indication of the evolution of stored energy. A large number of contacts would indicate a larger amount of stored energy, whereas the location of these contacts carrying the largest load would identify where most of

the stored energy resides within the agglomerate at that moment in the test. For example, Fig. 6.62 and 7.59 indicate that the elastic strain energy stored at that particular moment in the test was concentrated in the agglomerate-platen regions.

Similar to the propagation of waves, it is more difficult to transmit load through particulate material than through solids. The attenuation of load is significant even through a straight chain of particles. The load transfer, as well as the wave propagation, is very much a time-dependent process. At different moments during the simulations the configuration of the load transmission paths was slightly different. This is partly due to the variation of the force on platen/s and partly due to the local rearrangements of the particles. When contacts in the load-transmitting chains break or slide, the particles in the path will tend to rearrange and relocate. Very slight local displacements can lead to load transmission along different pathways. In the loose agglomerates, this process is more pronounced and often generated a rearrangement wave that considerably altered the configuration of the load transmission-paths.

It was found in the simulations presented in Chapters 5-8 that the load transmission determines the mode of failure. The transmission of the load exactly along the loaded diameter in the FCC agglomerate (see Fig. 5.19) enabled the internal storage of energy which finally produced the fracture of the agglomerate. In tests where the agglomerates fractured (Chapters 5-8) the increase in the load (platen force) produced an increase in the load-transmission zone but no increase in the agglomerate-platen contact area. Just before the force on the platen/s attained a maximum value, the load-transmission zone extended to the centre of the agglomerate (see Fig. 6.55 and 7.49). At this point the fracture process was started and ended with agglomerate breakage during the unloading phase. In tests in which the dense agglomerates shattered, the increased applied load produced a larger load-transmission zone which resulted in breakage of many more bonds earlier in the test.

In the case of the loose agglomerate, the load produced flattening of the agglomerate at the contacts with the platens. The increasing agglomerate-platen contact area resulted in a distorted (extremely flattened) shape of the agglomerate. This created a few extra zig-zag transmission paths along the loading direction that encouraged the crushing of the agglomerate (Fig. 7.50 and 7.67). The continuous local buckling of the parallel transmission paths caused repeated particle rearrangements and finally crushing of the loose agglomerate.

The behaviour in the three types of tests simulated was found to depend mainly on the amount and rate of energy input into the agglomerate. In tests in which the loading rate was low, the load had time to transmit from the agglomerate-platen zone and, as a result, the local stresses were lower and fewer bonds were broken. The amount of local damage and debris was larger for higher loading rates. In the limit, for very high loading rates, the damage

extended all over the agglomerate soon after the load had been transmitted across the full extent of the agglomerate.

9.7 DISCUSSION ABOUT DAMAGE PROCESSES

In all three types of tests, agglomerate failure started from the zones of contact with the platens where the contact forces were largest throughout the test. The first bonds to be broken and first debris particles to be detached always occurred close to the platens.

9.7.1 Damage Prediction

It was found from the simulations that observations of the load transmission can help to predict, step by step, the evolution of damage (bond breakage) during the test. The most accurate predictions, however, are restricted to the loading stage of the tests. The best way of identifying the contacts carrying significant load is to examine images showing only the contacts carrying the largest compressive forces.

In the dense agglomerates, the largest contact compressive forces at the beginning of a test are concentrated in the neighbourhood of the platens. This is also the place where bonds start to break (see Fig. 7.68 and state{1} in Figs. 8.2, 8.5 and 8.7). Later, the largest compressive forces tend to spread farther, both radially and along the direction of the loaded diameter - as does the breakage of bonds (see state{2} in Figs. 8.2, 8.5 and 8.7). The image in Fig. 9.35 presents the compressive contact forces higher than 0.047 mN at the moment when the platen force was maximum (at t=4.4 μs, 8.9 μs before the moment of fracture) in the free-fall impact test with an impact velocity of 0.2 m/s. The orientation of each contact force line corresponds to the direction of the resultant force at the contact. It can be seen that only some of the interparticle contacts transmit significant load: those whose directions run approximately radially from the point of impact. Figure 9.36 shows the broken bonds in the space lattice for the same test but after an additional 1.2 μs. From Figs. 9.35 and 9.36 one can note that the contacts which have broken at t=5.6 μs are located in almost exactly the same region as the contacts that were carrying load at t=4.4 μs.

For velocities causing shattering, the platen forces are higher and more contacts are transmitting the load sooner. Figure 9.37 shows the compressive contact forces higher than 0.047 mN at t=2.6 μs when the platen force was a maximum in the free-fall impact test with 0.9 m/s impact velocity. It is noted that almost all the bonds are carrying load throughout the agglomerate. Figure 9.38 presents the broken bonds in the space lattice at t=4.0 μs (1.4 μs later) for the same test. One can also see that the breakage of bonds occurred all over the agglomerate (see Fig. 9.38 compared to Fig. 9.37).

Although the location of the largest contact forces can be correlated with the local (even when extensive) damage, they do not provide indications of the location of the fracture surfaces. This indicates that the driving mechanism of bond breakage within the local damage zones is different than the one which results in breaking bonds to form fracture surfaces. The bonds in the damage zones break due to the large compressive contact forces, due to the relative lateral displacements of the particles forming these contacts. The interparticle contacts that break are not the ones carrying the large compressive forces but the others, which are located in between them and which usually have directions perpendicular to the directions of the contacts bearing the large compressive forces (see Fig. 9.36 and 9.38). In contrast, the main cause of breakage for the bonds that break to create the propagation of fracture is, as shown in Chapter 8, the tensile hoop stress.

9.7.2 Contact Damage

The contact damage refers to the broken bonds and, sometimes, debris detachment from the agglomerate-platen contact regions. For the same velocity in the free-fall impact test, the dense[2] agglomerate having the largest contact density exhibited larger damage zones than the dense[1] agglomerate. The loose agglomerate (having the lowest contact density) exhibited the smallest contact damage zones. These indicate that, at least within certain limits, lower contact densities result in smaller damage zones by the agglomerate-platen interfaces. Higher contact densities confer elasticity to an agglomerate and therefore, these findings are consistent with the observations from some laboratory tests. Schönert (1979) and other workers have shown that the more elastic materials exhibit more local damage in the form of a finely-fragmented cone at the agglomerate-platen interface, whereas the more inelastic-behaving materials exhibit a larger but undestroyed cone at the interface (see Fig. 9 in Schönert, 1979). On the other hand, the fact that the weak-dense agglomerate exhibited larger damage zones than the dense[1] agglomerate indicates that lower interface energies also result in larger local damage zones, as weaker bonds are much easier to break. Furthermore, higher loading rates also increase the volume of the local damage region in all the three types of tests because the load has less time to transmit into the agglomerate and thus the local intensity of the stresses is higher, resulting in more broken bonds locally. Laboratory tests show similar results.

There were three different phases in the evolution of the local damage by the agglomerate-platen interfaces: before the fracture process, during the fracture process and after the fracture process. The first phase is when most of the bonds in the immediate vicinity of the platens were broken. Furthermore, this was the phase that preceded and prepared the initiation of the fracture process in tests in which the agglomerates fractured. The damage zone/s were found to play an important role in fracture initiation and development. As

inferred by some workers from laboratory data (e.g. Arbiter et al, 1969, Schönert, 1979, Ghadiri et al, 1990, Salman et al, 1994) fracture initiates from these plastic zones as they are pushed like wedges into the agglomerate and generate the hoop tensile stresses causing fracture.

The breakage of bonds by the platen during this first phase (see Fig. 7.68 and state{1} in Figs. 8.2, 8.5 and 8.7). was similar to the random development of microcracks in indentation tests on heterogeneous samples of alumina with a grain size greater than 15 μm - see Fig. 2.b in Lawn et al (1994) and Fig. 3. and 4.d-f in Guiberteau et al (1994). The directions of the broken bonds were randomly distributed similar to the variation in the orientation of the microcracks produced in the indentation tests beneath the contact area. The general cause of microcrack formation was the compressive loading but the local stress which actually produced each microcrack was the shear stress (see Fig. 7 in Guiberteau et al, 1994). In the case of agglomerates also, local shear stresses generated by the compressive load were one cause of bond breakage. The load forced some particles to slide and thus produce breakage of contact between particles that were pulled apart along the direction of that contact. Figure 9.39a shows a two-dimensional schematical view of this mechanism. The applied load pushes particle A in between particles B and C producing breakage of the contact between B and C. However, most bond breakage in the damage zones in the simulations occurred due to the behaviour of the zig-zag paths carrying load. Some bonds were lost due to the fact that these chains were compressed and strained more than the surrounding material. Others broke due to the slight buckling of the chains - see Fig. 9.39b illustrating a two-dimensional schematical view of the two mechanisms. In grey are marked the particles belonging to the paths that transmit load. The load-transmission path on the right hand side of Fig. 9.39b is strained and thus particle J is displaced downwards a little. This displacement breaks particle J's contact with particle K, as this does not displace. The load-transmission chain on the left hand side buckles to the left and thus breaks the contacts with particles H and M. The buckling also forces particle F to displace to the left and thus to break its contact with the stationary particle E. Figure 9.39b also indicates how the buckling of the chain can create a contact - the one between particles N and L. In the loose agglomerates the columns carrying load are more widely spaced and have an accentuated zig-zag pattern. This leads to a more severe buckling mechanism in loose agglomerates causing more rearrangement of particles. Compared to dense agglomerates, these rearrangements can typically result in almost equal amounts of both broken bonds and newly-formed bonds.

The average velocity of the development of the local damage zones before fracture varied with the type of test; it increased with the loading rate and with the interface energy of the agglomerate, but it was found to be lower for agglomerates of higher contact density - see column (5) in Table 8.1. The fastest development of the damage zone was experienced by the dense[2] agglomerate in the free-fall impact tests, whereas the lowest velocities of

damage advance was exhibited in diametrical compression tests. Compared to the overall average velocity of crack propagation, the speed at which the damage zone extended was higher only in the free-fall impact tests on the dense[1] agglomerate and in the double impact test on the weak-dense agglomerate - see columns (10) and (5) in Table 8.1. In the diametrical compression test on the dense[1] agglomerate the propagation velocity of bond breakage in the damage zones was almost five times lower than the average propagation velocity of the fracture crack.

During the fracture process (phase two in the evolution of local damage) the damage zone did not increase significantly in volume and in the number of microcracks (broken bonds) created as most of the input energy was used to propagate cracks. However, the development of the local damage zone was intense in phase three, after primary fracture. For the dense agglomerates, the shape of the contact damage zone just after the fracture moment was approximately conical, as reported for many laboratory tests. However, most laboratory tests described the shape of the damage zone at the end of the test and not at the moment of fracture. From fracture onwards the damage zone in the dense agglomerates increased in size by spreading laterally to modify the shape of the zone from conical to more like an hemisphere by the end of simulation. The appearance was similar to the damage zones in the diametrical compression and free-fall impact tests reported by Gildemeister and Schönert (1976), Santurbano and Fairhurst (1991), and Kelly and Macmillan (1986). The shape was also similar to the roughly hemispherical damage zones in the tests reported by Lawn et al (1994) and Guiberteau et al (1994) (using spherical indenters on homogeneous material of grain size larger than 15 μs). The density of broken bonds in the local damage zone also increased after fracture. Although the load decreased considerably after fracture, the continued development of local damage occurred mainly because the agglomerate was broken up into large fragments which started to separate from each other, creating more space for the damage zone. Additionally, the relatively sharp edges of the "fresh" large fragments could not survive long even when the platen forces were low.

9.7.3 General Damage

Bonds broke at the interface zones, all over the agglomerate volume (in tests resulting in the shattering/crushing of the loose and dense agglomerates) and/or along fracture and crack surfaces. It was shown that in dense agglomerates bonds seemed to break mainly due to the large interparticle contact forces and to the hoop tensile stresses created by the "pushing" of the agglomerate-platen contact damage zone/s towards the centre of the agglomerate. In contrast, the loose agglomerate had much fewer bonds from the very start (see Fig. 6.3) and much smaller interparticle contact forces and thus the bonds broke under a different mechanism. The very low solid fraction and the fact that most particles in the loose agglomerate only hold one bond (see Fig. 6.3) suggests that, from the very start, the loose

agglomerate was made up of many weak clusters of particles. Moreover, most of these clusters were connected with one or very few bonds to other clusters, and thus they could easily displace and break-off from the agglomerate. The more "freedom of movement" of the small and weak clusters within the loose agglomerate was the main cause of bond breakage in the loose agglomerate.

9.7.4 Process Of Debris Detachment

The debris detachment process always started from the agglomerate-platen interface regions in the case of the dense agglomerates (Figs. 6.4, 6.18b and 7.6), and occurred a little after the process of bond breakage. This was expected, as the bond breakage in the contact zone was more intense at the core than near to the surface of the agglomerate (Fig. 7.68) where debris particles could detach. After the fracture moment, debris also started to detach from between the large fragments (see Figs. 6.22a, 7.14 and 7.53). Additionally, further loading of the large fragments after agglomerate fracture resulted in erosion of the irregular edges and corners of these fragments (see Fig. 6.56).

For agglomerates which shattered or crushed, debris detachment also started near the local damage regions (Figs. 6.32a,b and 7.19). The internal weakening, through extensive bond breakage, occurred much faster and with much less flattening for the dense agglomerates compared to the loose agglomerate. However, the process of debris detachment was prolonged for both types of agglomerates. Instead of being explosive, shattering was more like a rapid wear process that gradually transformed the entire agglomerate into debris. For both types of agglomerates, debris particles were detached from the surface of the agglomerate inwards (see Figs. 6.32, 6.33, 6.50, 6.52, 6.43 and 6.54). For tests of high impact velocities on the dense agglomerates, the impacted half of the agglomerate was the first to be transformed into debris (see Fig. 6.33a, 7.19 and 7.20). The loose agglomerate started to lose particles from the contact zones also, see Fig. 6.83.a., 6.86.c, but debris was also detached from the surface of the agglomerate - see Fig. 6.32a,b, 6.33b, 7.47 and 7.48.

Agglomerate	impact velocity [m/s]	impact kinetic energy [nJ]	kinetic energy at primary fracture [nJ]	approximately imput energy to primary fracture [nJ]	maximum average normal contact force [μN]
dense[1]	0.10	5.58	---	---	15.36
	0.1785	17.76	1.61	16.15	22.08
	0.20	22.30	3.37	18.93	18.22
	0.30	50.18	22.72	27.46	21.65
	0.90	451.60	391.8	59.80	74.39
dense[2]	0.10	4.61	---	---	12.99
	0.12	6.64	0.39	6.25	13.79
	0.15	10.37	1.49	8.88	17.51
	0.20	18.44	5.48	12.95	19.41
	0.30	41.49	18.8	22.69	29.23

Table 9.1 Energy parameters in free-fall impact tests on dense agglomerates

Agglomerate		impact velocity [m/s]	mass platen times heavier than mass agglomerate	impact kinetic energy [nJ]	work input to primary fracture [nJ]	maximum average normal contact force [μN]
weak-dense	{1}	0.01	100	5.58	---	7.11
	{2}	0.04	20	17.84	---	7.96
	{3}	0.04	100	89.21	50.5	9.08
	{4}	0.04	672.6	599.25	41.4	8.84
	{5}	0.04	(–)	---	45.9	8.36
	{6}	0.10	100	557.57	59.0	7.35
	{7}	1.0	100	55757	24.4	23.03
	{8}	1.0	100	55757	82.6	23.03
dense[1]	{9}	0.02	100	22.30	16.15	28.72
	{10}	0.10	100	557.57	17.40	31.79
	{11}	0.20	1	22.30	19.88	32.83
dense[2]	{12}	0.20	100	18.44	8.60	22.51

Table 9.2 Energy parameters in double impact tests on dense agglomerates

Agglomerate	velocity of platen [mm/min]	work input to primary fracture [nJ]	maximum average normal contact force [μN]
dense[1]	10	30.49	28.72
dense[2]	10	9.56	26.79

Table 9.3 Energy parameters in diametrical compression tests on dense agglomerates

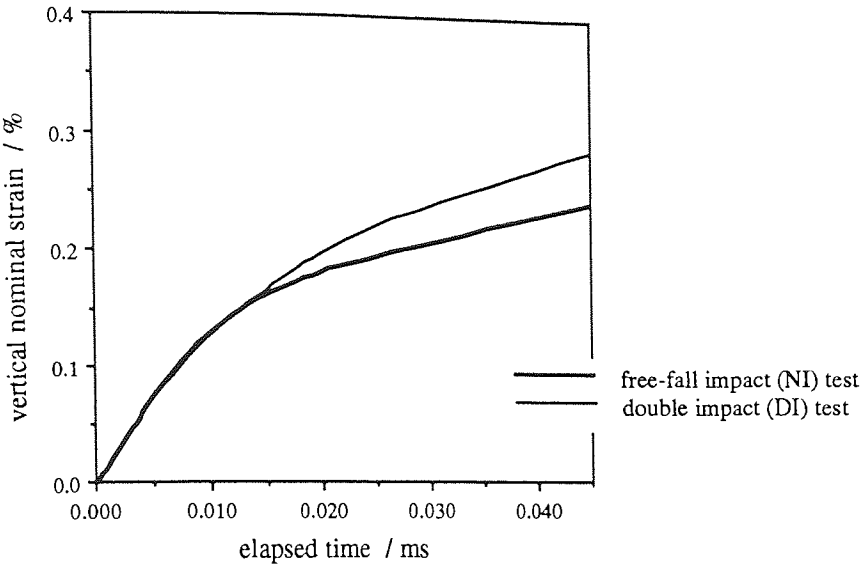

Fig. 9.1 Evolution of the vertical nominal strain of the agglomerate for free-fall and double impact tests, dense[1] agglomerate, V=0.2 m/s

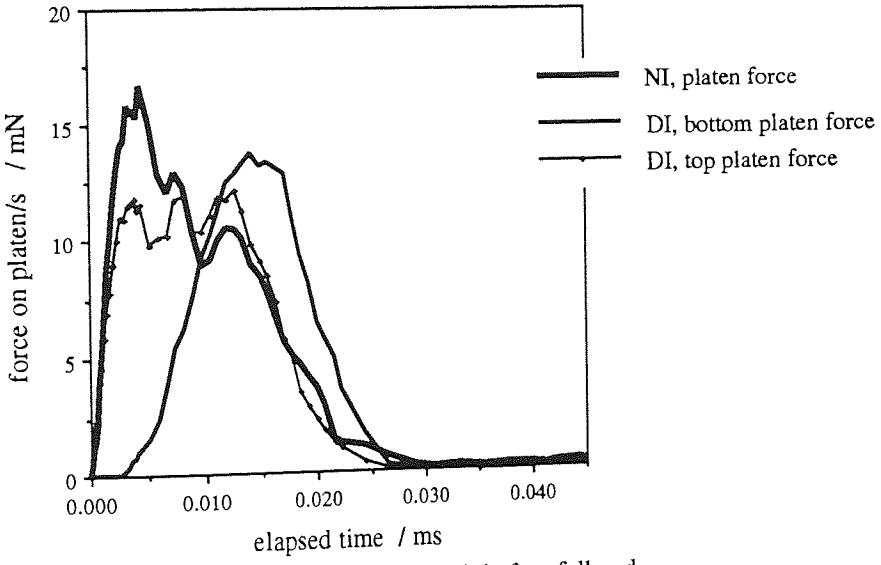

Fig. 9.2 Evolution of force on platen/s in free-fall and double impact tests, dense[1] agglomerate, V=0.2 m/s

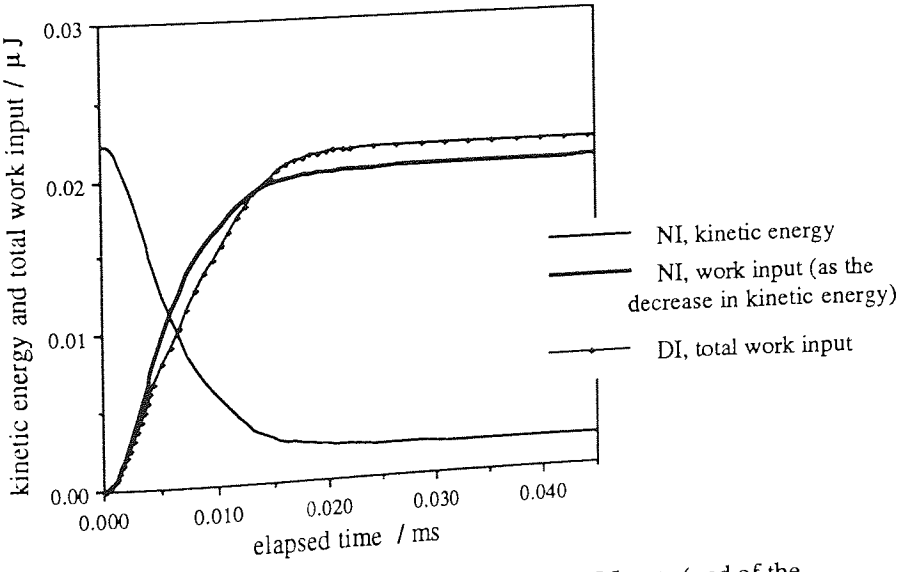

Fig. 9.3 Evolution of the total work input in NI and DI tests (and of the kinetic energy for the NI test), dense[1] agglomerate, V=0.2 m/s

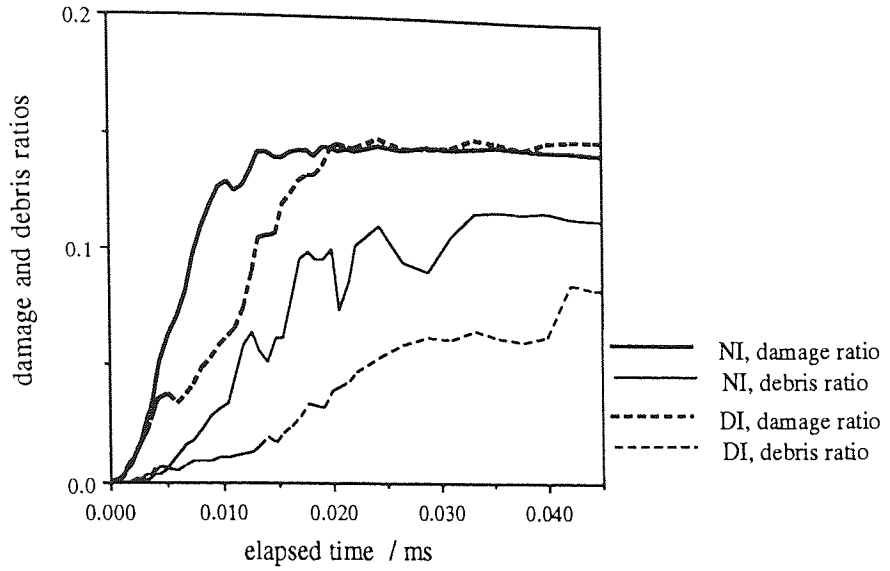

Fig. 9.4 Evolution of damage and debris ratios for free-fall impact (NI) and double impact (DI) tests, dense[1] agglomerate, V=0.2 m/s

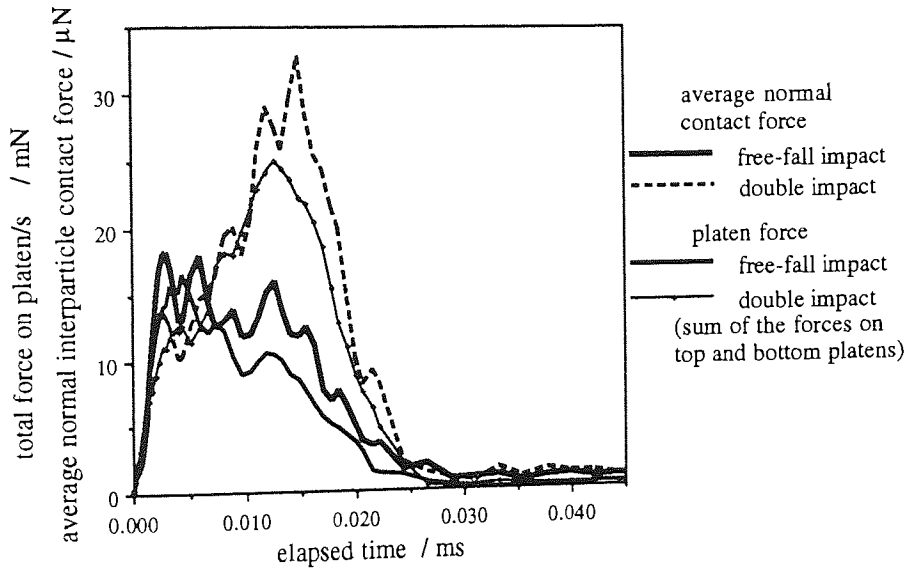

Fig. 9.5 Evolution of average normal contact force and platen force in free-fall and double impact tests, dense[1] agglomerate, V=0.2 m/s

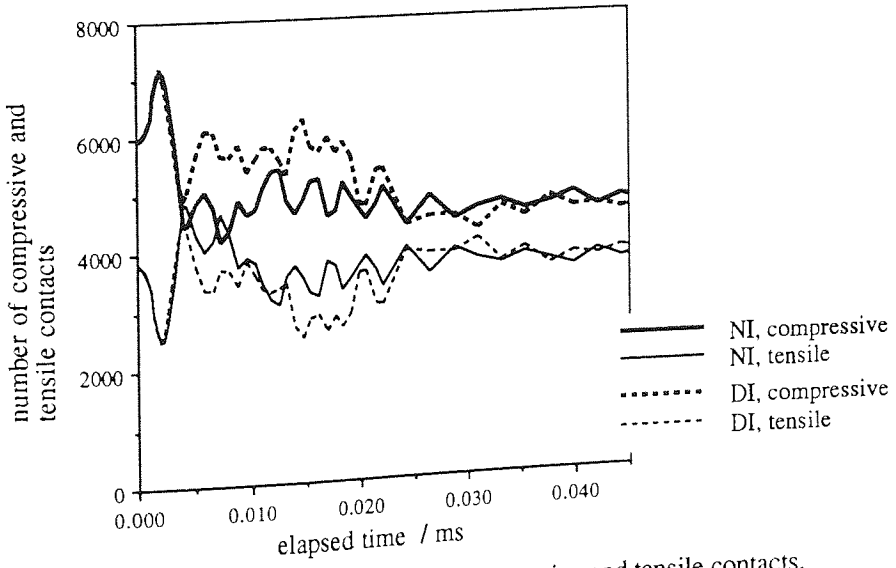

Fig. 9.6 Evolution of total number of compressive and tensile contacts, free-fall and double impact tests, dense (1) aggomerate, V=0.2 m/s

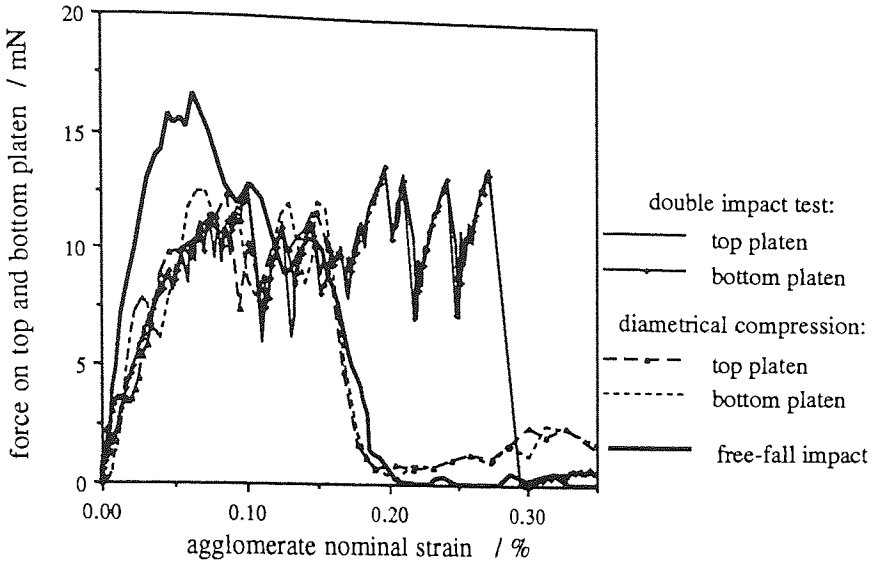

Fig. 9.7 Evolution of platen forces, free-fall impact (V=0.2 m/s), double impact (V=0.02 m/s) and diametrical compression (V=10 mm/min) tests, dense[1] agglomerate

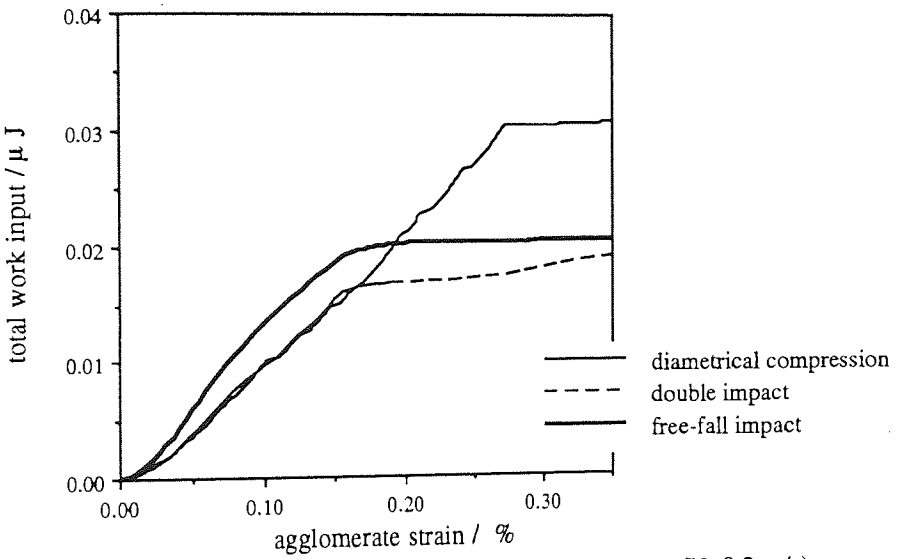

Fig. 9.8 Evolution of total work input in free-fall impact (V=0.2 m/s), double impact (V=0.02 m/s) and diametrical compression (V=10 mm/min) tests, dense[1] agglomerate

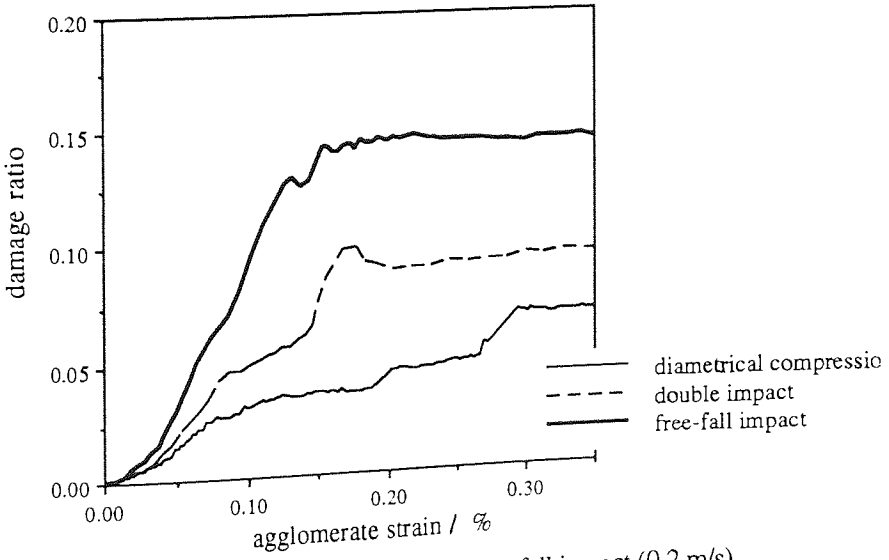

Fig. 9.9 Evolution of damage ratio in free-fall impact (0.2 m/s), double impact (V=0.02 m/s) and diametrical compression (V=10 mm/min) tests, dense[1] agglomerate

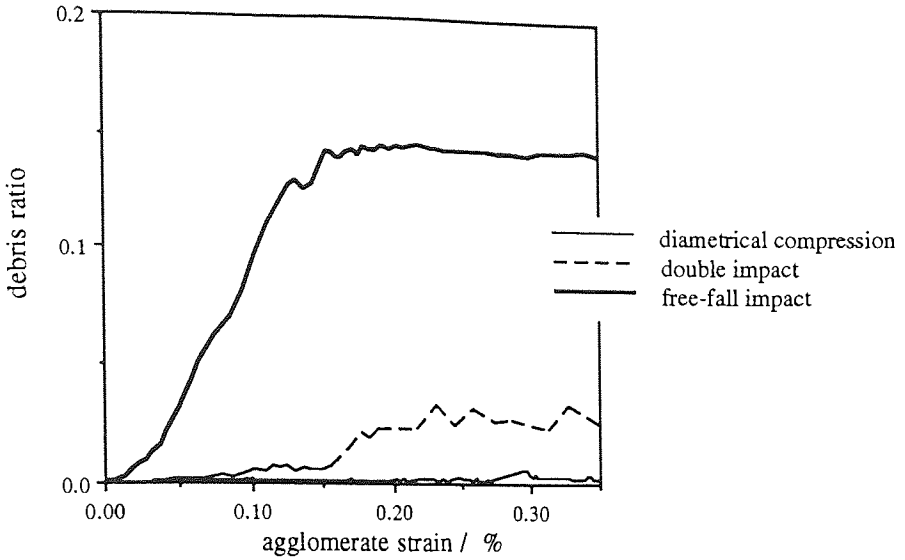

Fig. 9.10 Evolution of debris ratio in free-fall impact (0.2 m/s), double impact (V=0.02 m/s) and diametrical compression (V=10 mm/min) tests, dense[1] agglomerate

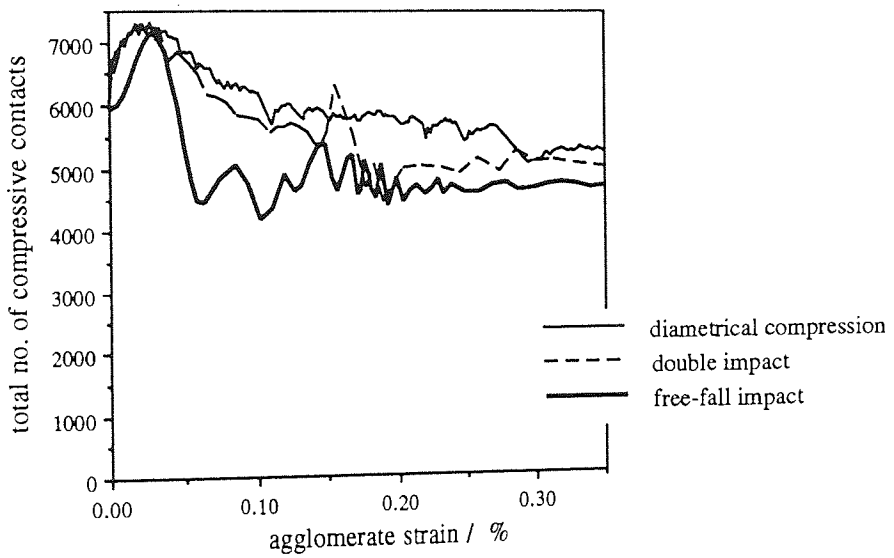

Fig. 9.11 Evolution of total number of compressive interparticle contacts in free-fall impact (0.2 m/s), double impact (V=0.02 m/s) and diametrical compression (V=10 mm/min) tests, dense[1] agglomerate

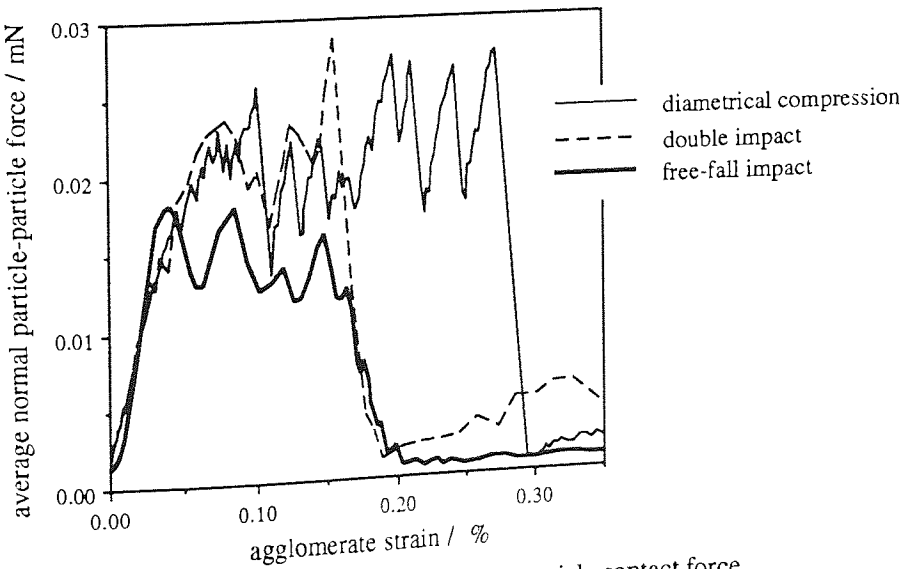

Fig. 9.12 Evolution of the average normal interparticle contact force, free-fall impact (V=0.2 m/s), double impact (V=0.02 m/s) and diametrical compression (V=10 mm/min), dense[1] agglomerate

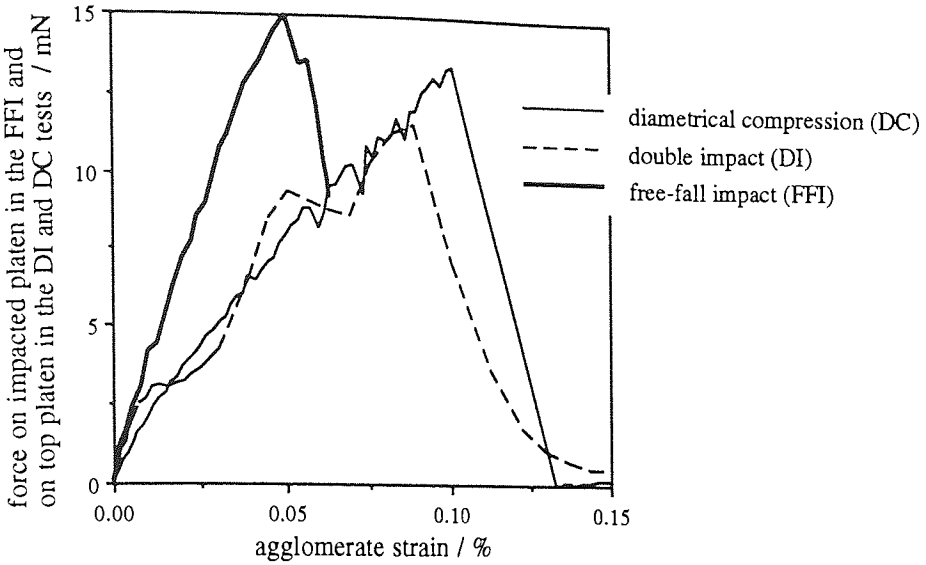

Fig. 9.13 Evolution of platen force, free-fall impact (V=0.12 m/s), double impact (V=0.02 m/s) and diametrical compression (V=10 mm/min), dense[2] agglomerate

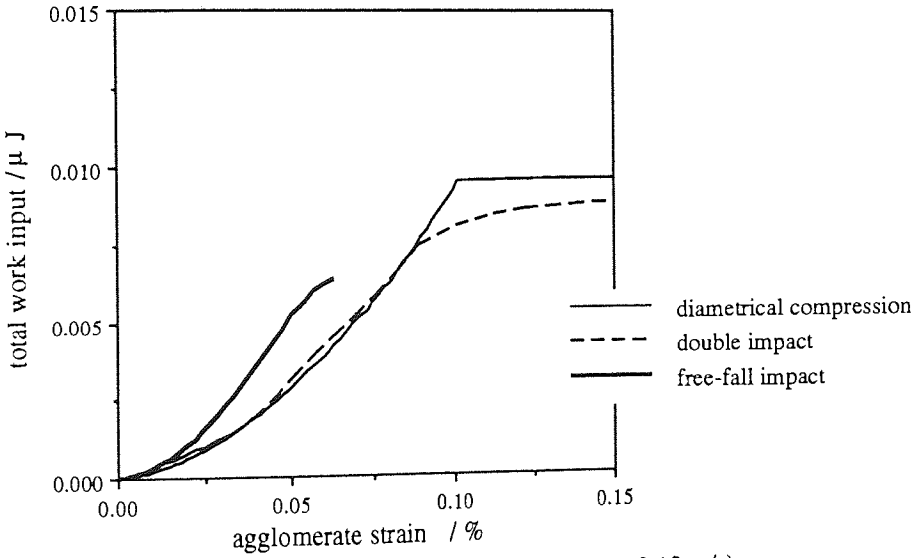

Fig. 9.14 Evolution of work input, free-fall impact (V=0.12 m/s), double impact (V=0.02 m/s) and diametrical compression (V=10 mm/min), dense[2] agglomerate

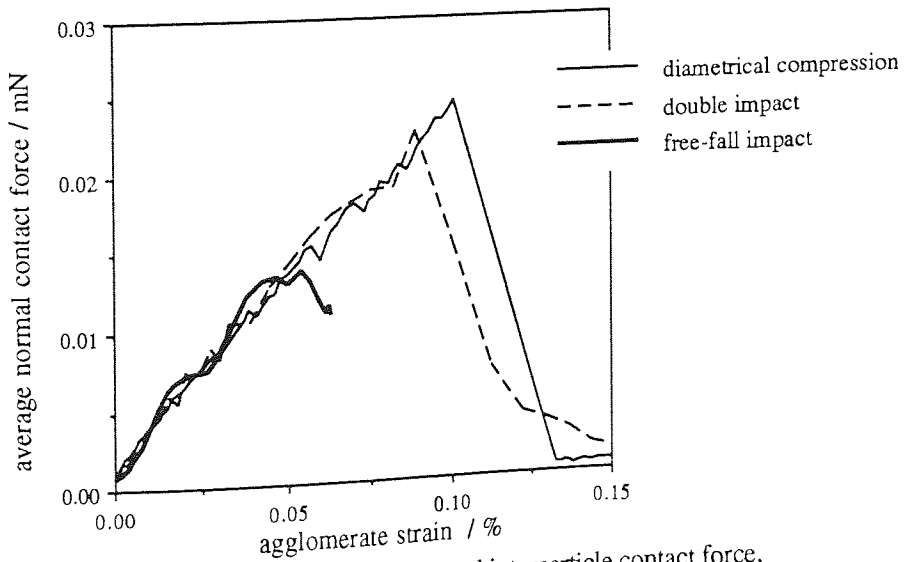

Fig. 9.15 Evolution of average normal interparticle contact force, free-fall impact (V=0.12 m/s), double impact (V=0.02 m/s) and diametrical compression (V=10 mm/min), dense[2] agglomerate

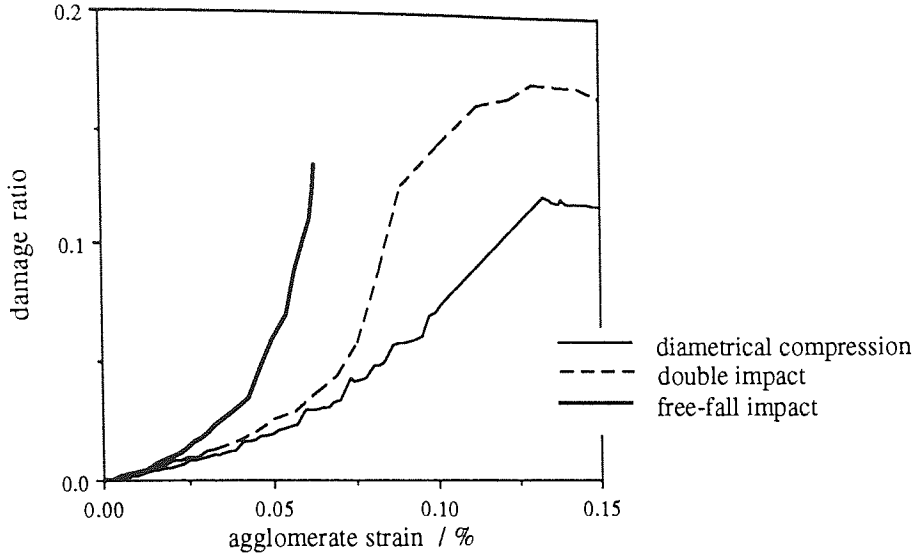

Fig. 9.16 Evolution of damage ratio, free-fall impact (V=0.12 m/s), double impact (V=0.02 m/s) and diametrical compression (V=10 mm/min), dense[2] agglomerate

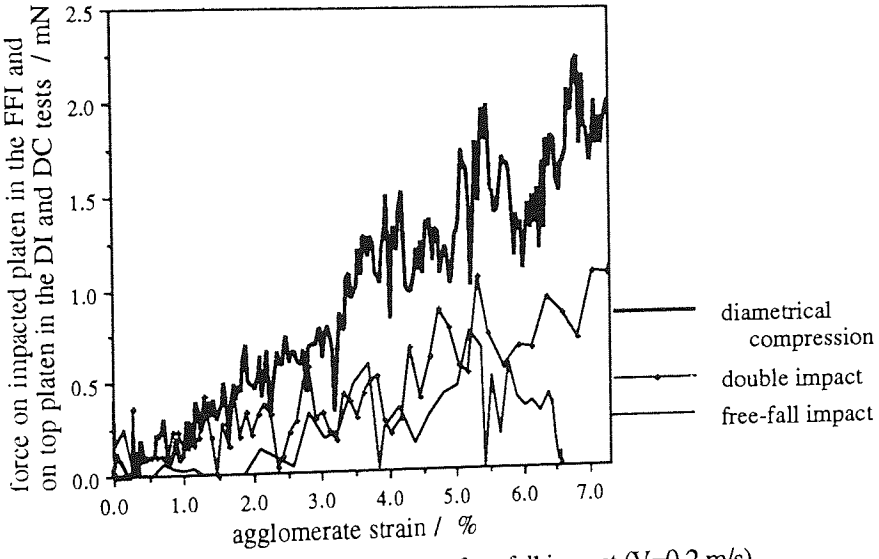

Fig. 9.17 Evolution of platen force, free-fall impact (V=0.2 m/s), double impact (V=0.02 m/s) and diametrical compression (V=180 mm/min), loose agglomerate

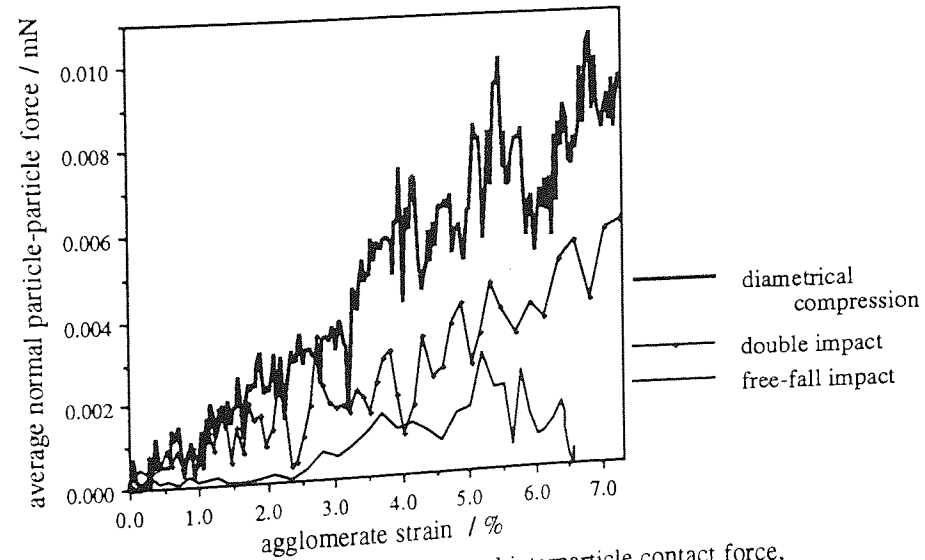

Fig. 9.18 Evolution of the average normal interparticle contact force, free-fall impact (V=0.2 m/s), double impact (V=0.02 m/s) and diametrical compression (V=180 mm/min), loose agglomerate

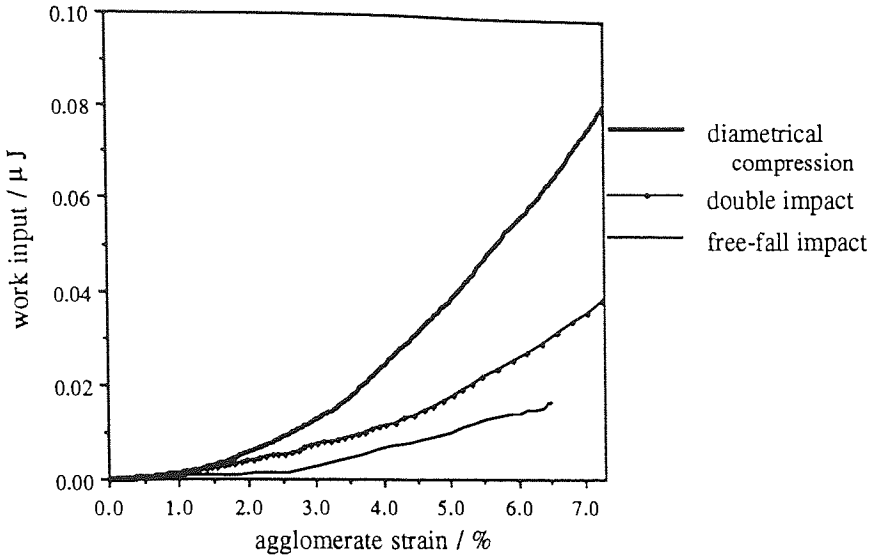

Fig. 9.19 Evolution of work input, free-fall impact (V=0.2 m/s), double impact (V=0.02 m/s) and diametrical compression (V=180 mm/min) tests, loose agglomerate

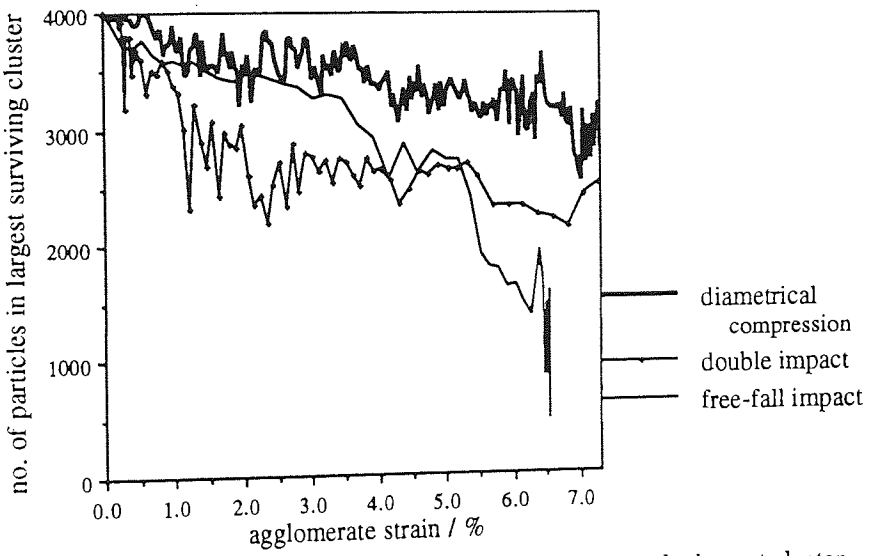

Fig. 9.20 Evolution of number of particles belonging to the largest cluster, free-fall impact (V=0.2 m/s), double impact (V=0.02 m/s) and diametrical compression (V=180 mm/min) tests, loose agglomerate

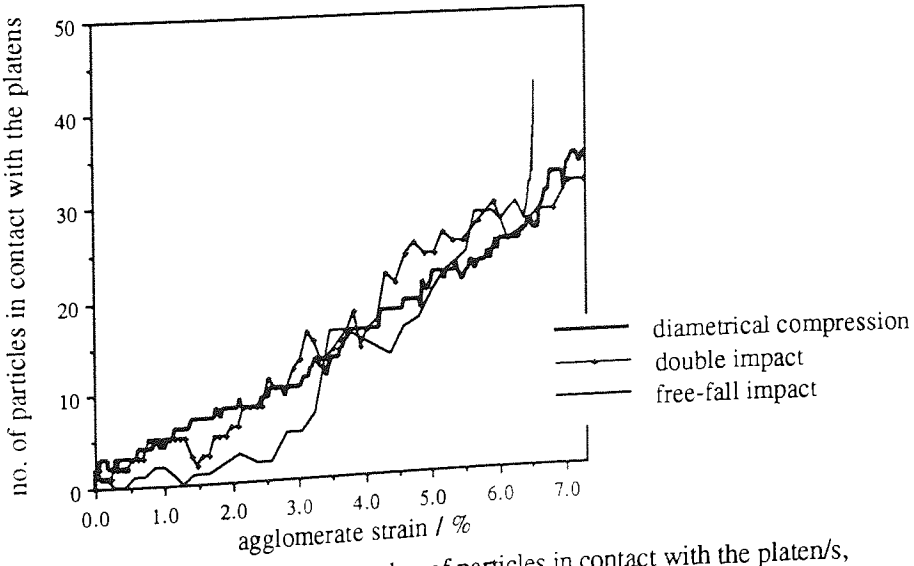

Fig. 9.21 Evolution of total number of particles in contact with the platen/s, free-fall impact (V=0.2 m/s), double impact (V=0.02 m/s) and diametrical compression (V=180 mm/min) tests, loose agglomerate

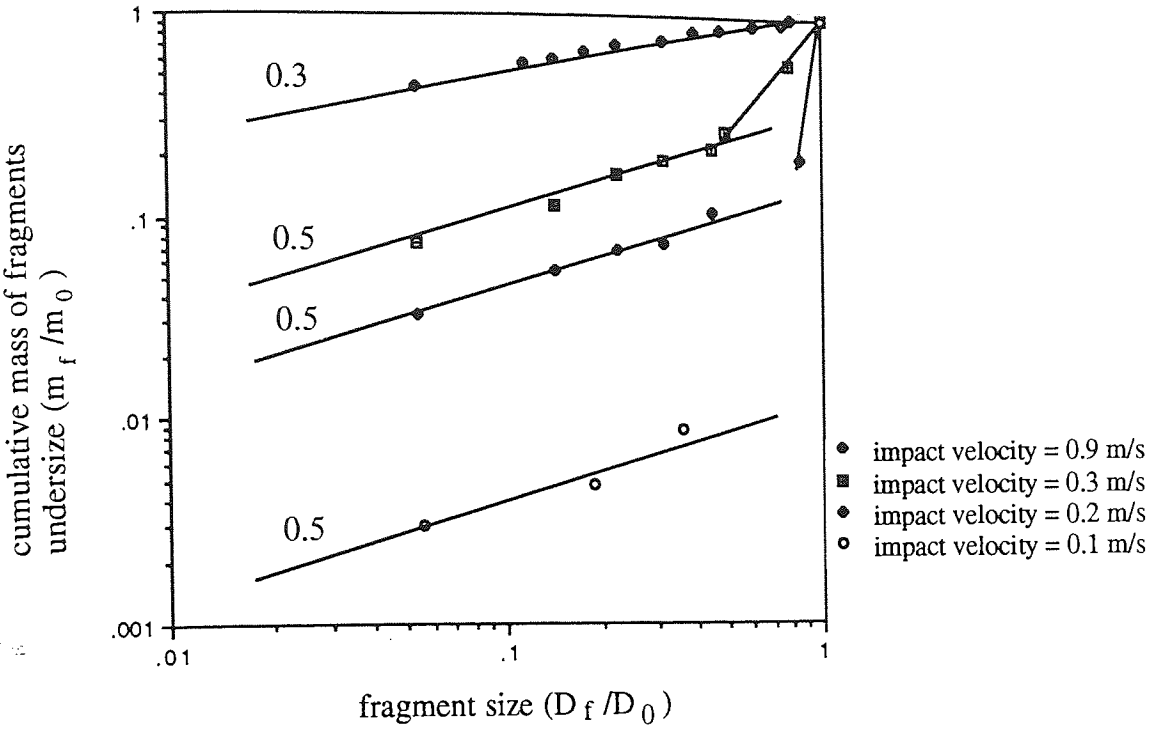

Fig. 9.22 Size distribution of all the fragments in four different free-fall impact tests, dense[1] agglomerate

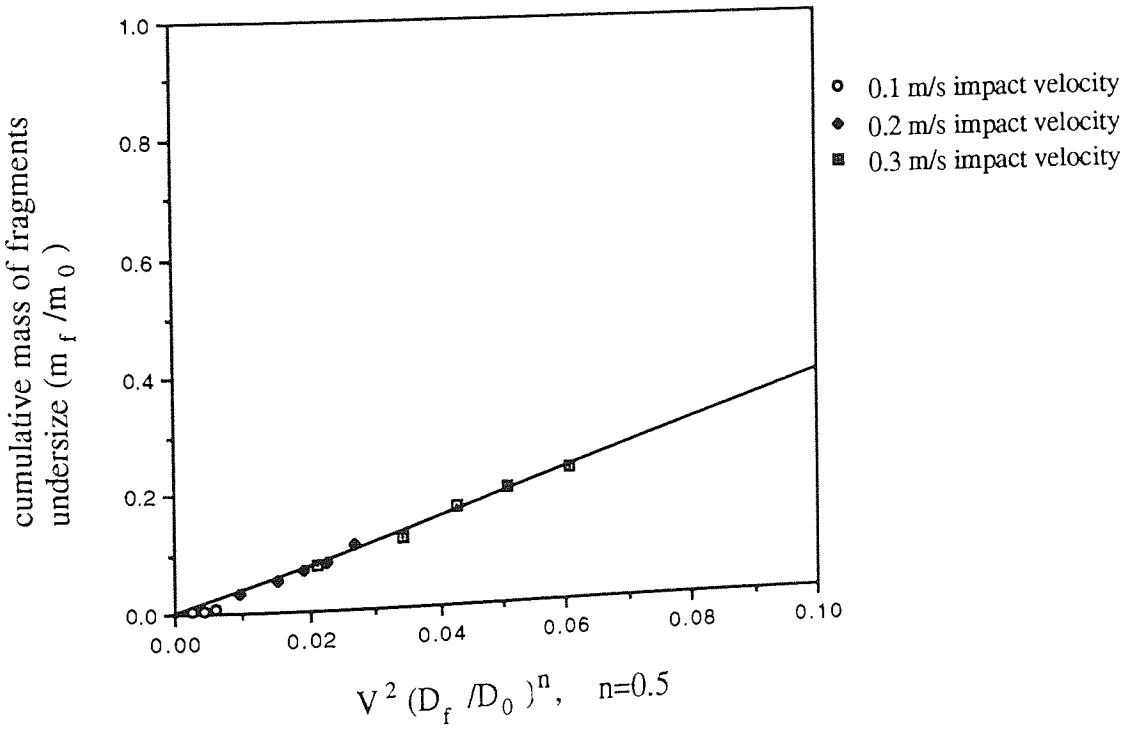

Fig. 9.23 Size distribution of the complement in three different free-fall impact tests, dense[1] agglomerate

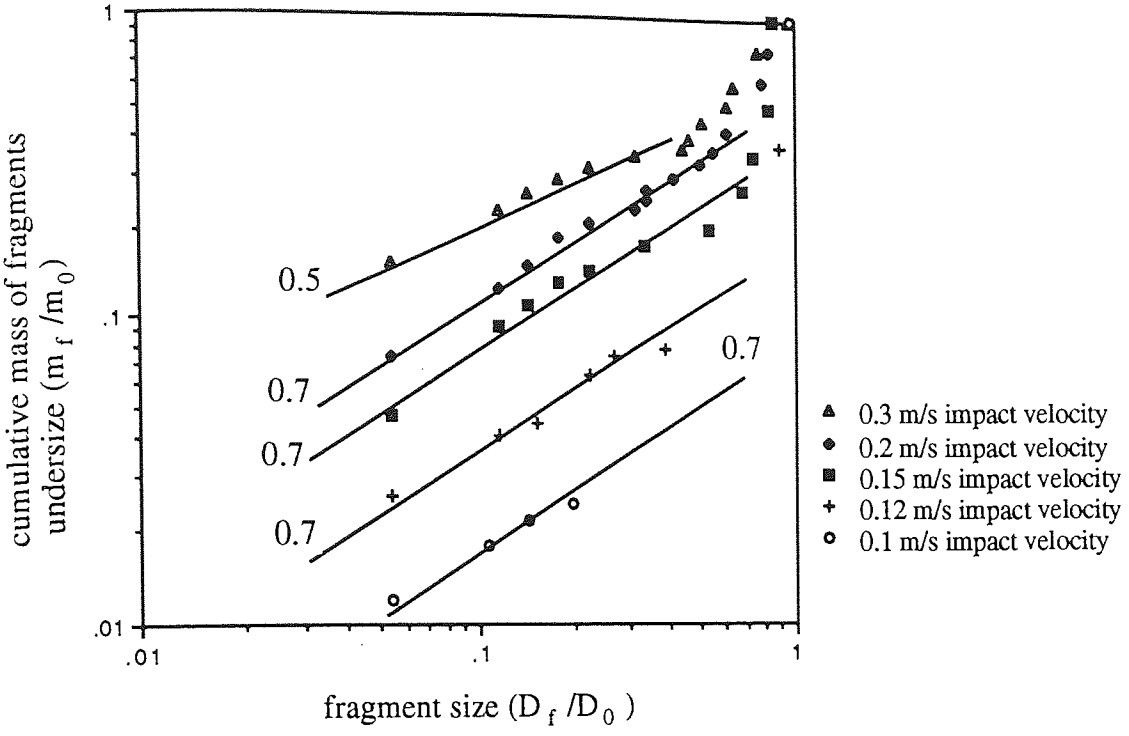

Fig. 9.24 Size distribution of all fragments in five different free-fall impact tests, dense[2] agglomerate

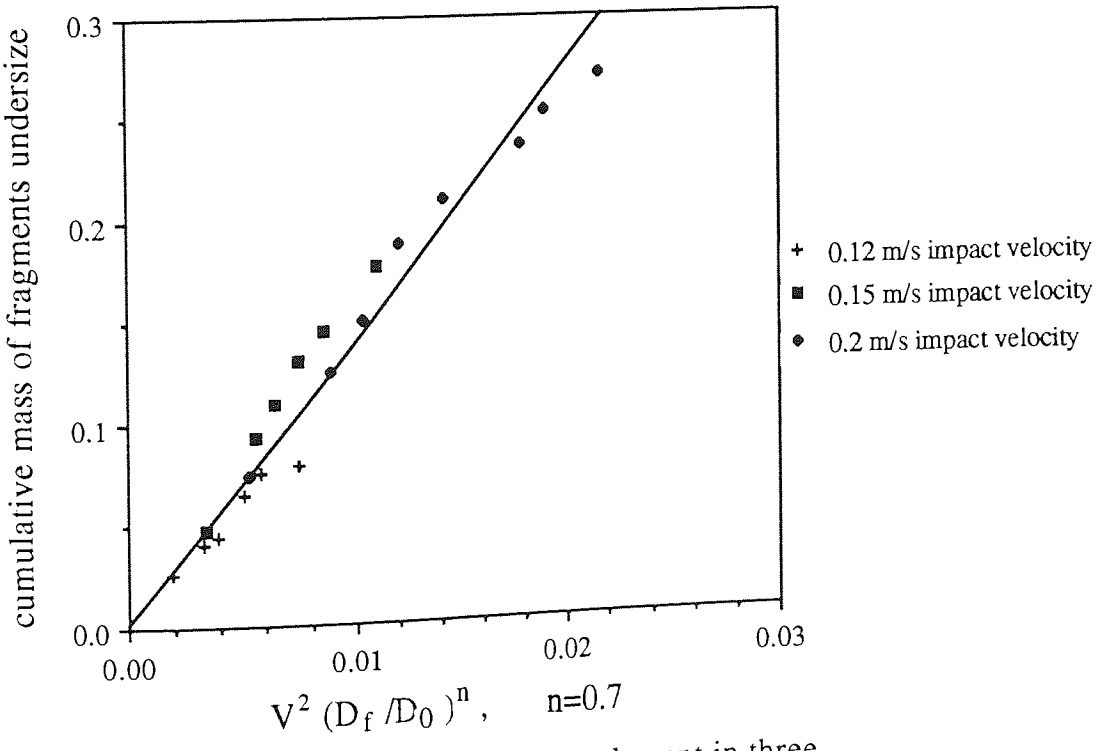

Fig. 9.25 Size distribution of the complement in three different free-fall impact tests, dense[2] agglomerate

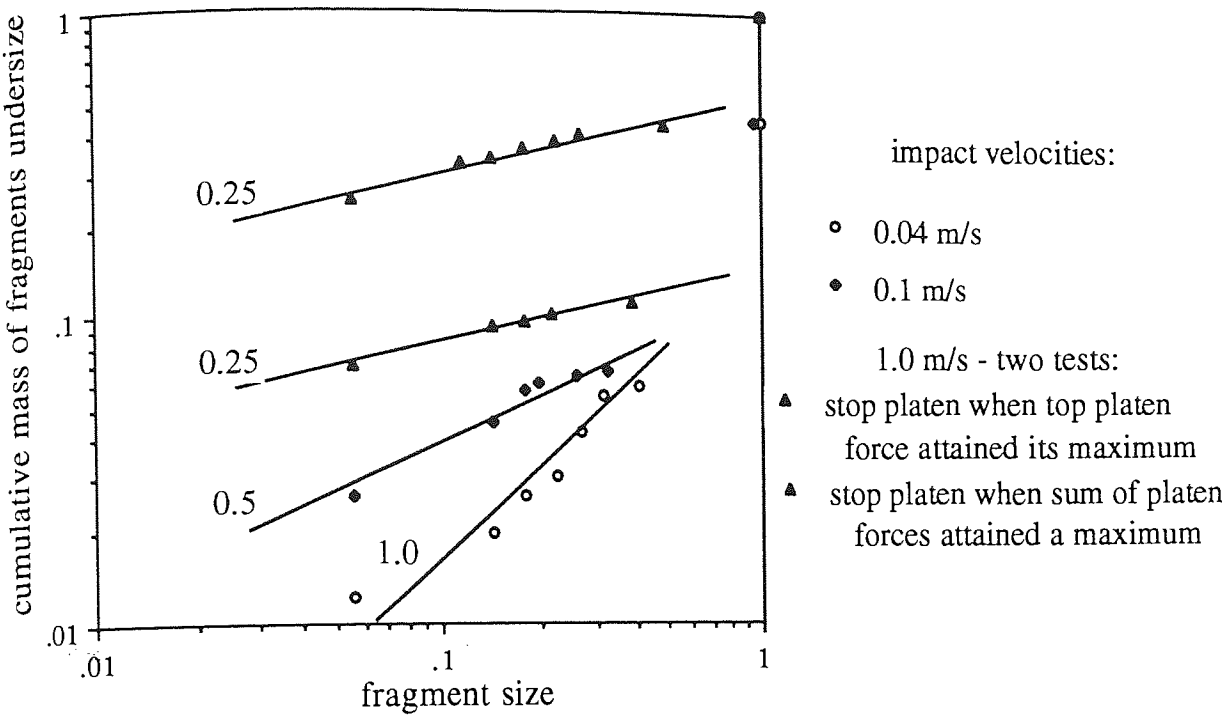

Fig. 9.26 Size distribution of all fragments in three different double impact tests where the impacting platen was 100 times heavier than the agglomerate, weak-dense agglomerate

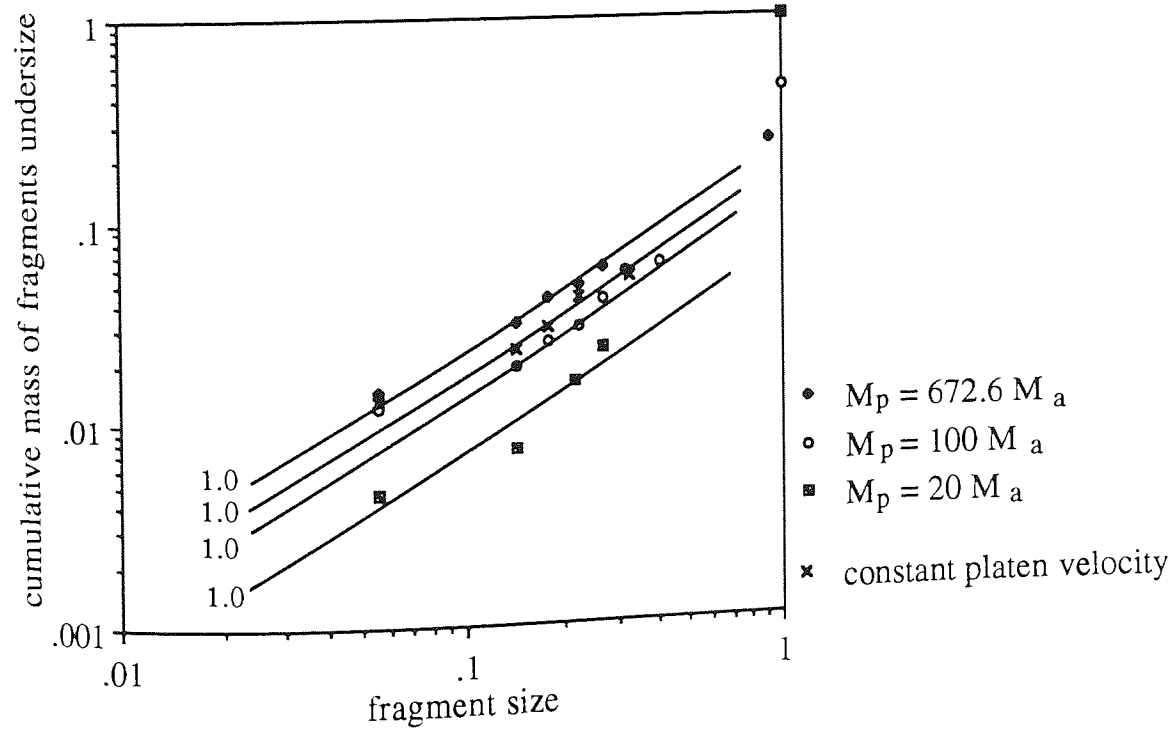

Fig. 9.27 Fragment size distributions for four double impact tests having the same impact velocity of 0.04 m/s, weak-dense agglomerate

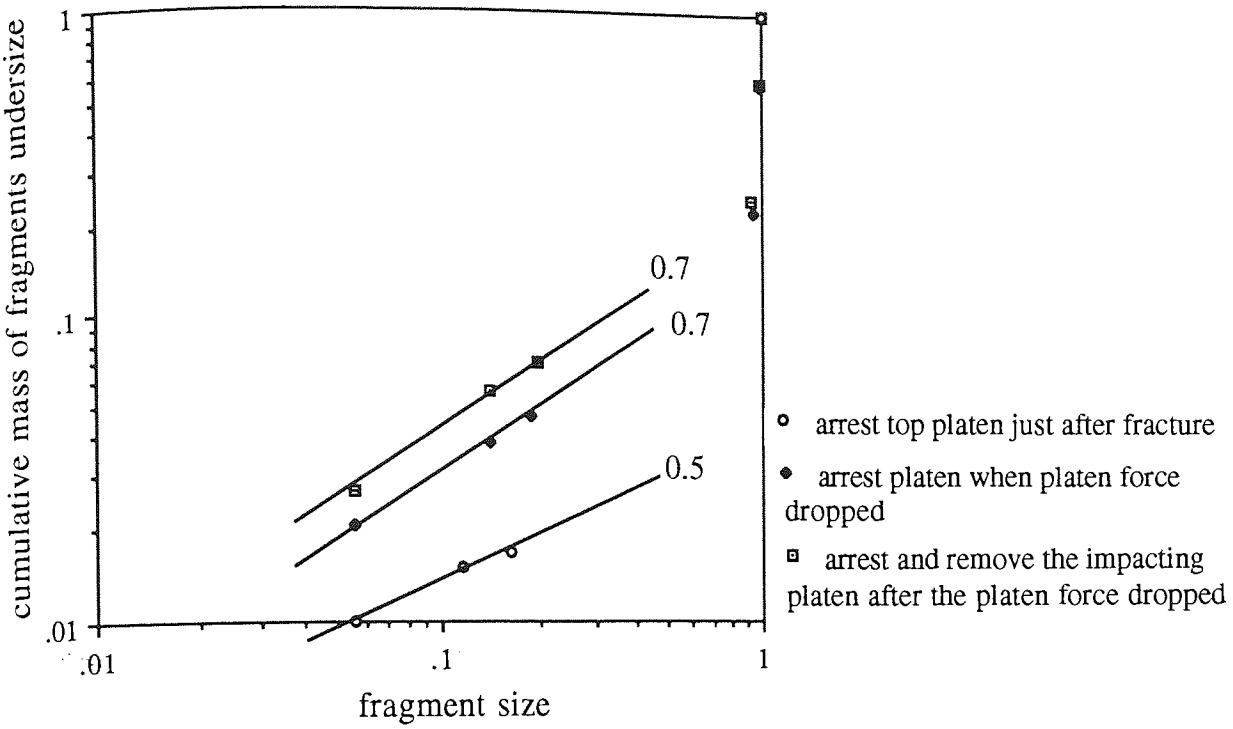

Fig. 9.28 Fragment size distributions for a double impact test depending on when and how the impacting platen was arrested, V=0.2 m/s, dense[1] agglomerate

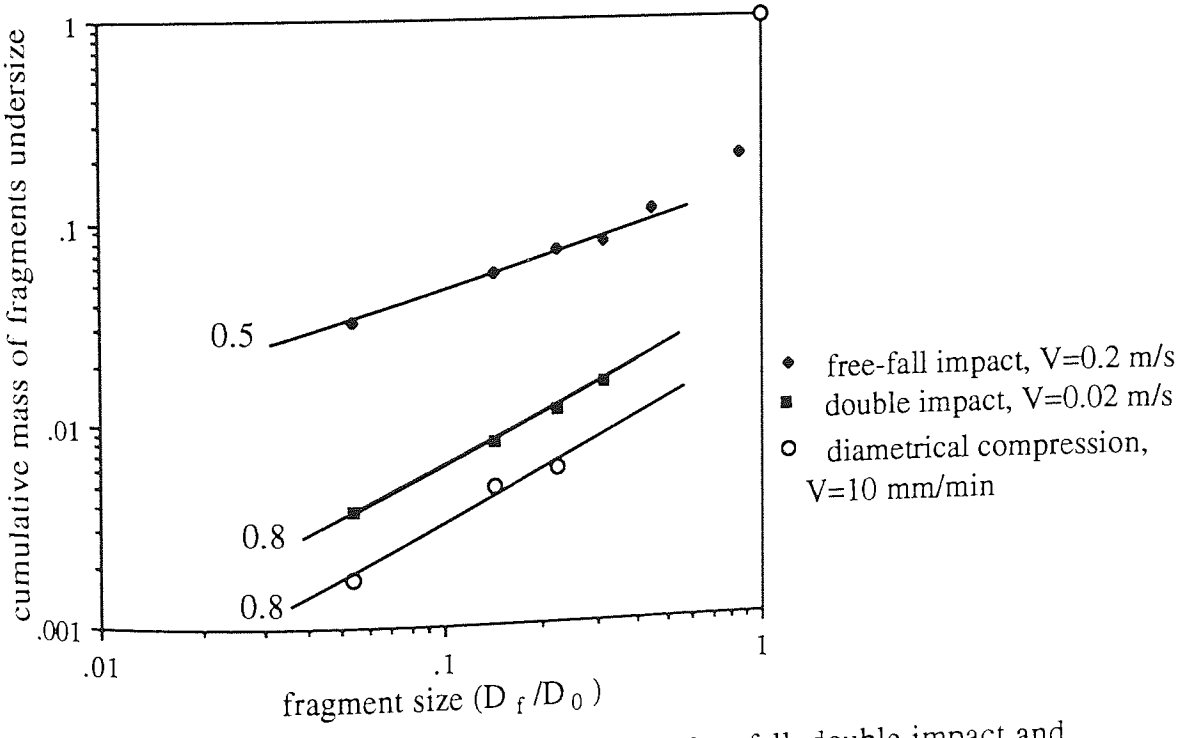

Fig. 9.29 Fragment size distributions for the free-fall, double impact and diametrical compression tests that experienced primary fracture into two approximately hemispherical fragments, dense[1] agglomerate

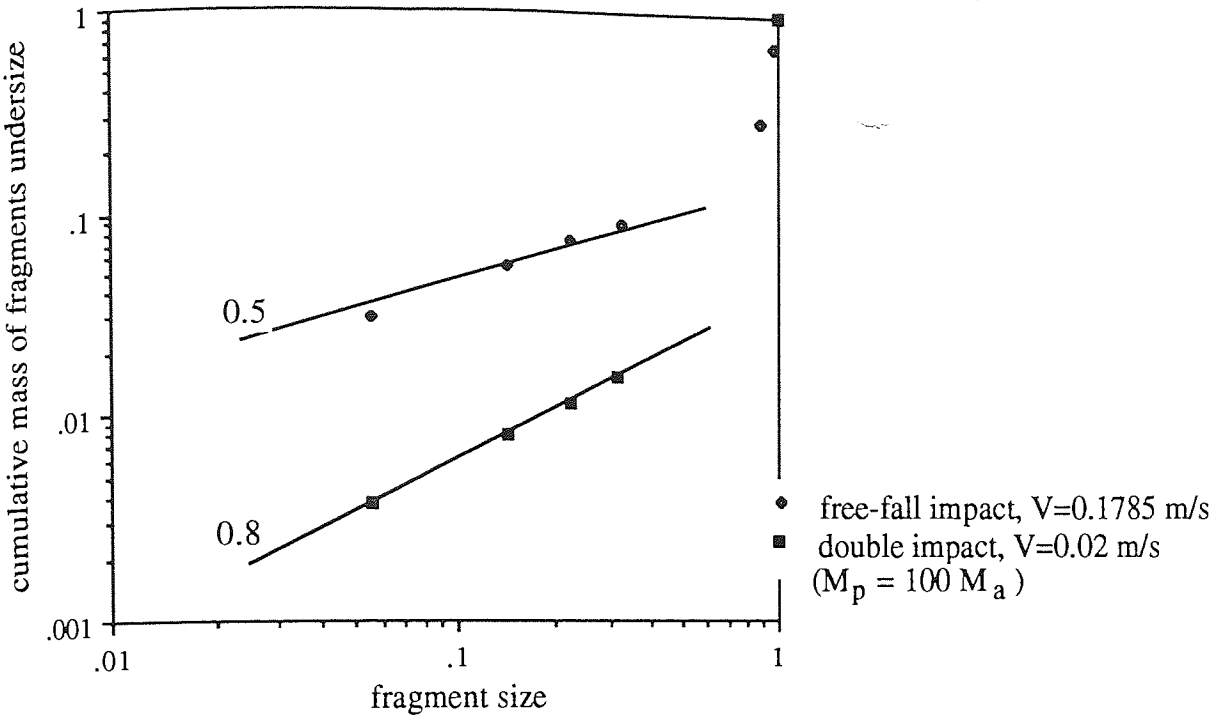

Fig. 9.30 Fragment size distributions for the free-fall and double impact tests having the same energy consumed at fracture, dense[1] agglomerate

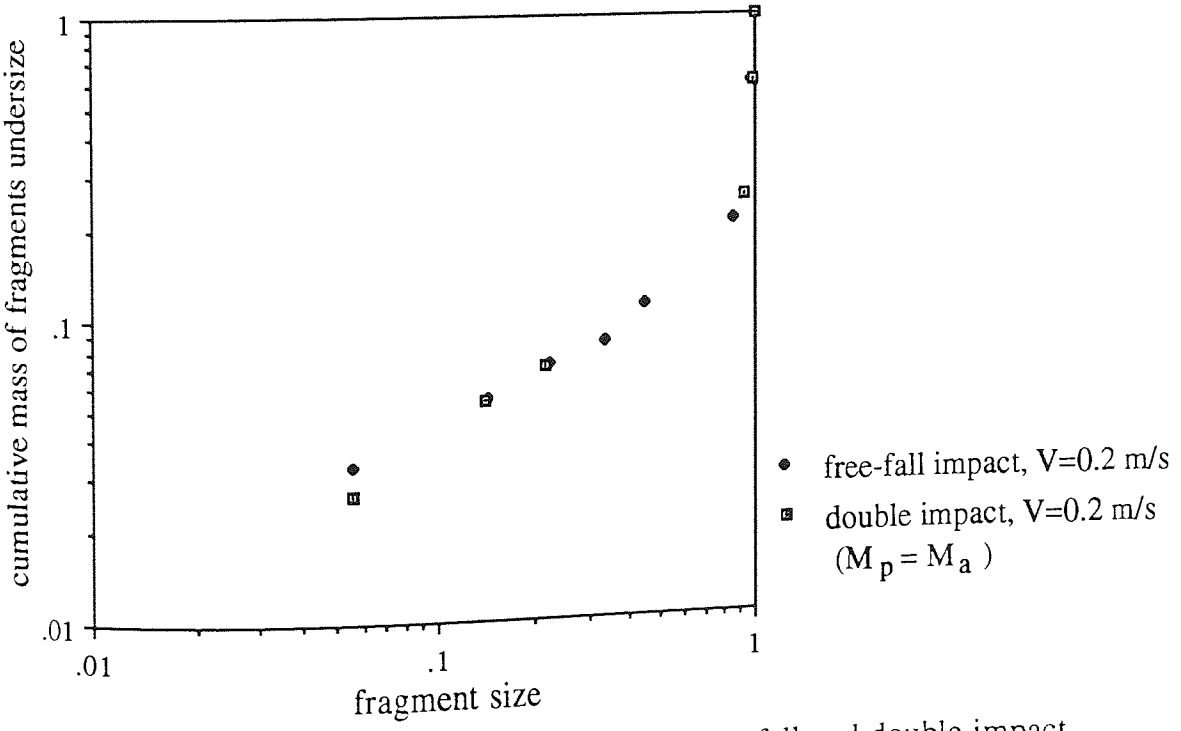

Fig. 9.31 Fragment size distributions for the free-fall and double impact tests of same input velocity (of 0.2 m/s) and mass of impacting platen equal to mass of agglomerate, dense[1] agglomerate

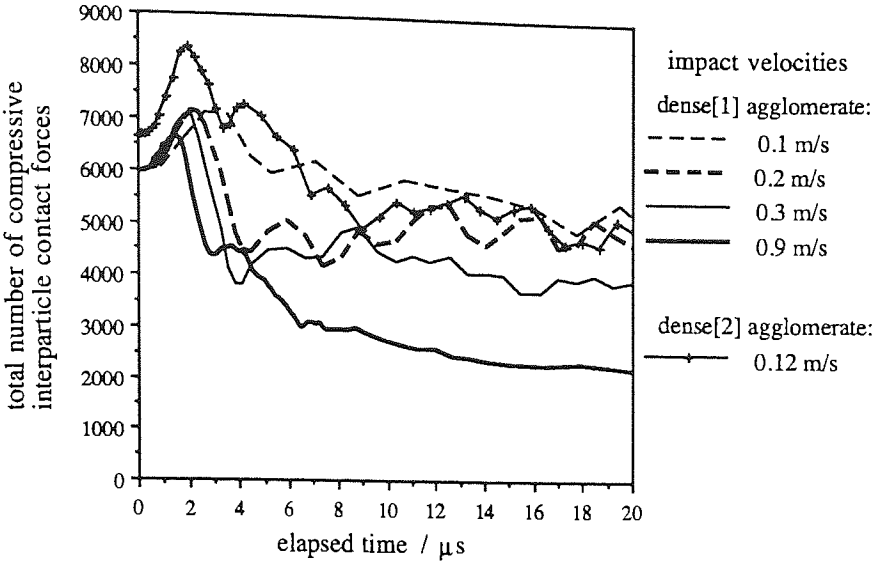

Fig. 9.32 Evolution of the total number of compressive forces in five free-fall impact tests, dense[1] and dense[2] agglomerates

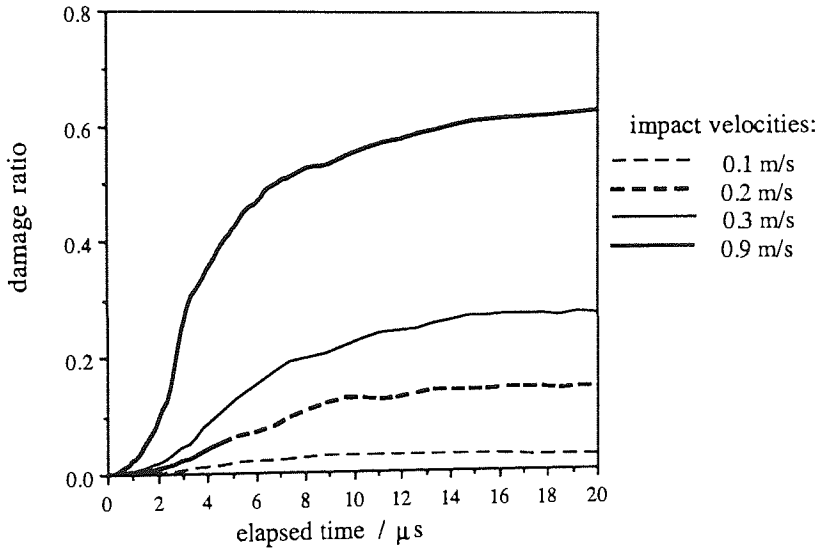

Fig. 9.33 Evolution of damage ratio in four free-fall impact tests, dense[1] agglomerate

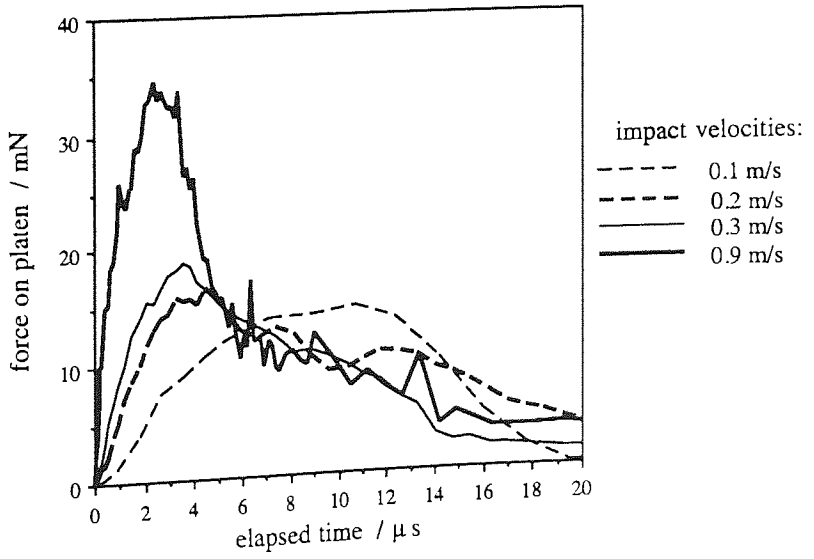

Fig. 9.34 Evolution of the platen force in four free-fall impact tests, dense[1] agglomerate

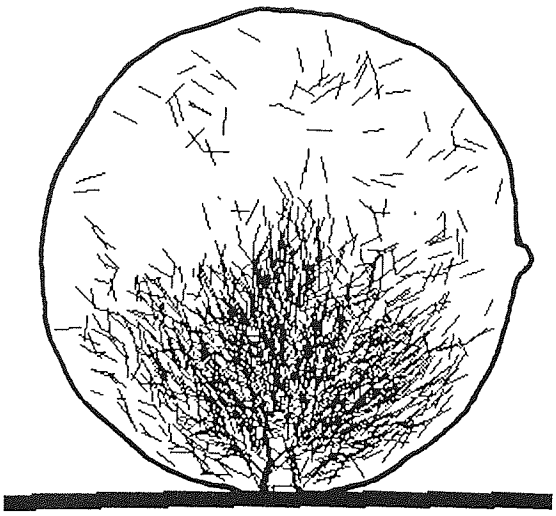

Fig. 9.35 The 1384 compressive contact forces higher than 0.047 mN at the moment when the platen force was a maximum, free-fall impact, dense[1] agglomerate, V=0.2 m/s, t=4.4 μs, view from front.

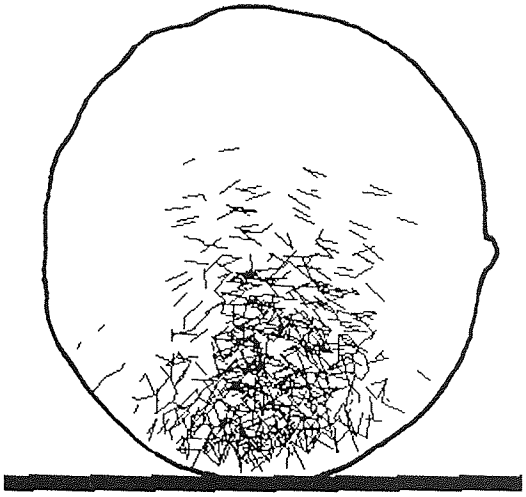

Fig. 9.36 The 689 broken bonds in the space lattice, free-fall impact, dense[1] agglomerate, V=0.2 m/s, t=5.6 μs, view from front.

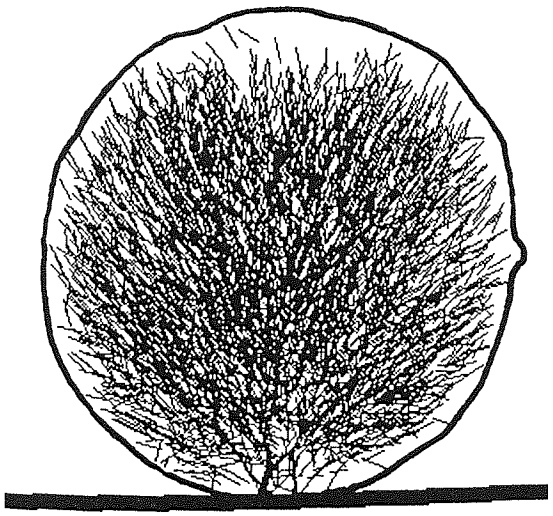

Fig. 9.37 The 3968 compressive contact forces higher than 0.047 mN at the moment when the platen force was a maximum, free-fall impact, dense[1] agglomerate, V=0.9 m/s, t=2.6 μs, view from front.

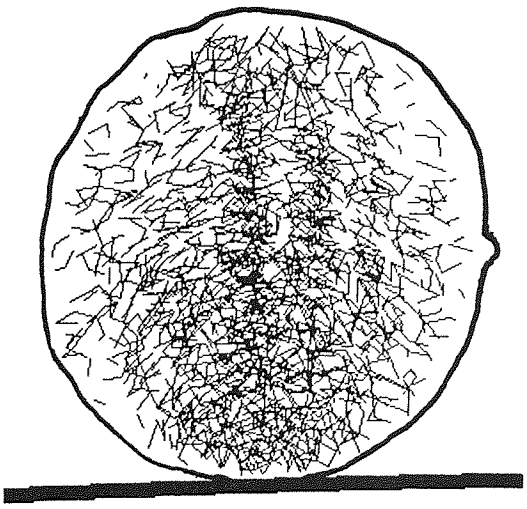

Fig. 9.38 The 1960 broken bonds in the space lattice, free-fall impact, dense[1] agglomerate, V=0.9 m/s, t=4.0 μs, view from front.

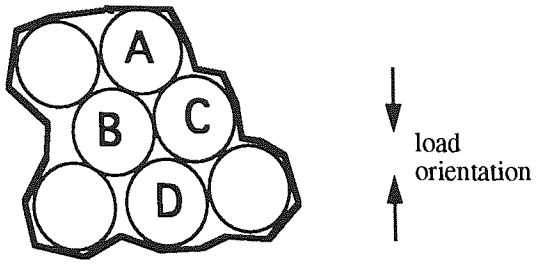

(a) Bond breakage due to the sliding of particles (the contact between particles B and C). The applied load pushes particle A in between particles B and C which causes the breakage of the contact between them.

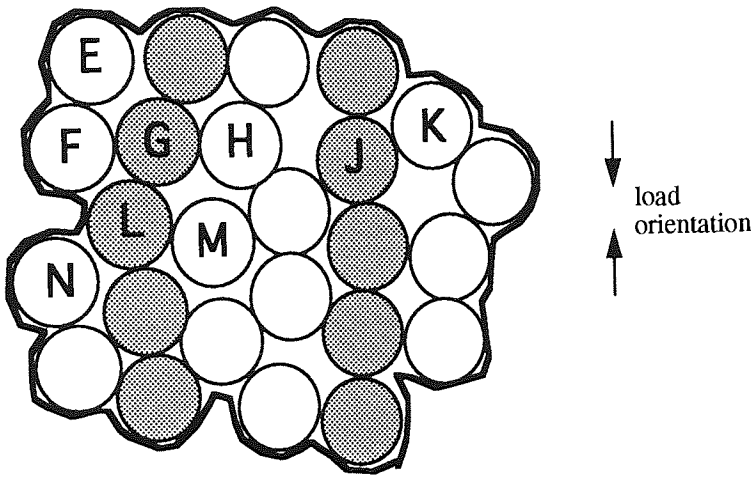

(b) Bond breakage due to the compression of load-bearing chains (the contact between particles J and K) and the buckling of chains (the contacts between particles G and H, L and M, E and F). The particles belonging to the compressively loaded chains are marked grey.

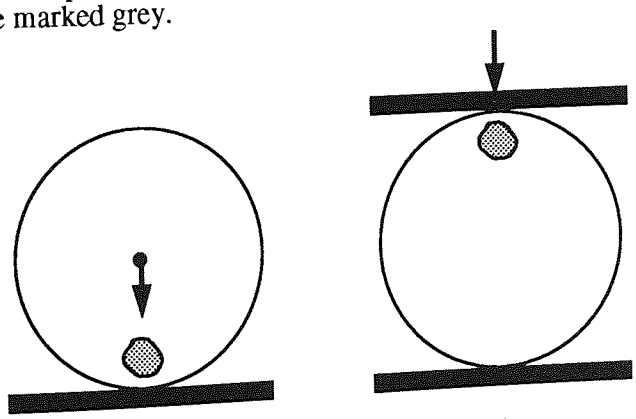

(c) (d)

Fig. 9.39 Simplified two-dimensional schemes showing some bond breakage mechanisms encountered in the formation of the local damage zone close to the agglomerate-platen interface. The images in **(a)** and **(b)** present zones "taken" from a two-dimensional agglomerate under free-fall impact, **(c)**, double impact or diametrical compression, **(d)**.

CHAPTER 10

CONCLUSIONS, LIMITATIONS AND FUTURE WORK

10.1 INTRODUCTION

The review of the laboratory experiments presented in Chapters 2, 3 and 4 has indicated that due to their discrete nature the behaviour of agglomerates is very complex and differs from the behaviour of solid specimens. In this project the failure of the agglomerates subjected to impact and diametrical compression has been examined in detail using computer simulation. Although all the findings presented in this thesis are based on computer simulated experiments it has been demonstrated in Chapters 6, 7, 8 and 9 that the tests carried out yielded good, reliable and realistic data. The most significant findings are summarised in this chapter, followed by comments on limitations and suggestions for further work.

Continuing the computer simulation research work of others, this project proved once more that the program TRUBAL is a valuable tool for investigating granular material behaviour. This time the enhanced TRUBAL software was employed to analyse in-depth aspects (the micromechanics) of agglomerate failure that could not and cannot (yet) be investigated in laboratory tests. Certain aspects, such as the step-by-step evolution of the fracture surface, have never ever been observed before in three dimensions. Some measurements, such as the ones that revealed the variation of the fracture crack velocity during the fracture process, would also be very difficult to obtain in the laboratory testing of small agglomerates. Simulations also have the great advantage that exactly the same agglomerate can be used in a multitude of tests. This is impossible in laboratory testing where very "similar" agglomerates need to be used and statistical averages of the results obtained have to be carried out. However, this project demonstrated that very small "differences" in the samples lead to different behaviour in the same test (for instance due to a different fracture pattern induced). The laboratory workers can, therefore, never be quite sure why some agglomerates fractured in different ways.

10.2 FRACTURING OF THE DENSE AGGLOMERATES

Most of the effort in this project was directed towards examining in detail the fracture of the dense agglomerates. As in most laboratory tests, the dense agglomerates primarily fractured into two or three large fragments, irrespective of the type of test. The primary fracture surfaces were not planar, but were approximately oriented along the loading direction. For higher impact velocities, secondary fractures occurred in such a way that the higher the impact velocity the more fragments were obtained.

Fracture in this project was always preceded by local plastic deformation adjacent to the agglomerate-platen interface/s. The loading stage began with the development of plastic damage zone/s which advanced from the loaded surface/s towards the centre of the agglomerate. The particles in the damage zones were heavily compressed and, as a result, they were displaced and progressively separated from each other - following a complex mechanism. This resulted in the irreversible local deformation of the agglomerate, similar to the typical laboratory-observed plastic deformation of particulate material. The interparticle sliding and the random breakage of bonds was found to be similar to the formation of random microcracks observed in indentation tests (for materials with the same range of grain-sizes).

The fracture process was long - it commenced in the last part of the loading stage, when cracks initiated and started to develop, and completed in the second part of the unloading phase, when the agglomerate was essentially broken into a number of large fragments. Cracks initiated from the damage zones and propagated towards the centre of the agglomerate. They could be observed as microcracks developing along several half-diametral meridional planes. At the very end of loading (and start of unloading), when several large cracks had reached the agglomerate centre, a "selection" process took place. As a result of the selection process only two or three large cracks developed further - through additional microcrack formation and microcrack coalescence. The propagation of these selected cracks from the core towards the equatorial line of the agglomerate concluded with the fracture of the agglomerate along the planes of these "fracture" cracks. An apparent "healing process" commenced at the end of the fracture process: the non-fracturing large cracks closed and, as a result, the broken bonds along them re-adhered. On the other hand, the continuation of loading resulted in additional bond breakage - to actually propagate some of the old abandoned cracks or to create and propagate new ones - and, finally, in secondary fractures. The overall shape of the damage zones at the end of a test resulting in fracture was a cone for free-fall impact tests and an apple-stub for diametrical compression or double impact tests (see the lines representing the bonds broken by the end of the test in Fig. 6.11a and Fig. 7.52).

Although the large cracks could be easily distinguished from the microcracks, there was no clear crack front, as a few interparticle contacts usually broke ahead of the approximate crack front. This may be a particularity of coarse-grained agglomerates. Calculations of the propagation velocity of the fracture crack (average crack front) revealed that there are large variations during the fracture process. Fracture was found to accelerate during the final part of the fracture process in the confined-agglomerate tests (diametrical compression and double impact). On the other hand, the propagation of the fracture crack was slowing down all through the fracture process in the free-fall impact tests (see Table 8.1). The fracture

crack's propagation was found to be stable until the very final interval just before the fracture moment.

From their impact and diametrical compression tests on a large number of "clone" spheres, Salman et al (1994) inferred that more fracture planes indicate that fracture occurred in steps, that secondary fractures follow a primary fracture. It is now confirmed from simulation tests that this is true. It is also true that secondary fractures often occur very close in time after the primary fracture, this obviously being the reason why the "stepped" character of breakage is so difficult to observe in laboratory tests.

In all three types of test, the effective energy necessary for producing the fracture surface was found to be much lower than the input energy to the fracture moment. Most of the input energy was dissipated during loading due to the irreversible deformation of the material in the agglomerate-platen contact damage zone/s. No significant energy-absorbing "failure process zone" ahead of the crack front was identified. The primary fracture occurred during the largest drop in the platen force and in the stored elastic energy, showing that part of the stored energy was used in the final stage of the fracture process.

Several important conclusions pertinent to the fracture of coarse-grained agglomerates emerged from the simulations. Firstly, the primary fracture of the agglomerates tested in this project was semi-brittle and the fracture mode was tensile (mode I). The main driving force of fracture was the tensile (hoop) stresses, a fact best illustrated by the particle velocity field around the moment of fracture. After the fracture moment, the large fragments just created started suddenly to move in opposite directions, perpendicular to the loading direction. However, the results of this project clearly indicate that diametrical compression tests cannot be used for determining the tensile strength of agglomerates.

Another important conclusion is that the fracture of dense agglomerates, in all three types of test, initiates from the platen region/s and not from the centre of the agglomerate. There was no indication that some pre-existing flaws would induce a stress concentration (large interparticle contact forces) around them. The initial positioning of the particles within the agglomerate relative to the point of loading played an important role in "deciding" the location of the first few created large cracks. The pre-existing flaw population was not found to affect the selection of the fracture surface from the existing large cracks. Instead, the ultimate location of the primary fracture surface strongly depended on the rate of loading, on the interface energy and on the type of test.

No other known analysis of fracture in three dimensions revealed the way in which the fracture cracks propagate along the fracture surface of spherical samples. When the fracture cracks originate from adjacent to the platen/s (as in the three types of test analysed in this

project), one would assume that the fracture cracks propagate either radially or linearly from the agglomerate-platen interface. However, the work in this project revealed that, at least for agglomerates, the propagation of the fracture cracks is more complex - see the schematic evolution presented in Fig. 8.23 for the free-fall impact test and in Fig. 8.24 for the diametrical compression and low-velocity double impact tests.

10.3 LOCAL DAMAGE OF AGGLOMERATES

In impact tests of sufficiently low impact velocity and/or small falling mass the agglomerates exhibited only local damage by the end of the simulation. The damage zone was located adjacent to the agglomerate-platen interface/s and was very similar to the one developed at the beginning of the tests causing agglomerate fracture. The local interparticle sliding and bond breakage produced minute local rearrangements of particles, resulting in the local irreversible deformation of the agglomerate. Within the damage zone, the loose agglomerate suffered much less local microcrack formation (bond breakage), but more rearrangements of particles than the dense agglomerates.

In the case of the free-fall impact test, apart from deforming at the zone of impact, the dense agglomerates also rebounded from the platen. In contrast, the loose agglomerate did not rebound from the platen, this revealing its more plastic behaviour. The dense agglomerate having the highest contact density had the highest coefficient of restitution, this indicating that higher contact densities lead to more elastic behaviour.

10.4 SHATTERING OF AGGLOMERATES

The shattering of dense and loose agglomerates in impact tests was a long process for both dense and loose agglomerates. Shortly after the beginning of the test, the dispersed distribution of the large compressive interparticle contact forces showed that the load transmitted rapidly over the entire volume of the agglomerate. This was different than in the tests causing fracture, where the load only managed to transmit to the centre of the agglomerate, within a certain volume adjacent to the agglomerate-platen interface/s (see section 9.7.1). A little later, the high stresses (compressive contact forces) caused the breaking of a significant number of bonds all over the agglomerate, which prompted particles to separate from each other and from the agglomerate. Instead of being sudden, the debris detachment was a gradual process. The zones closer to the impacted agglomerate pole were the first ones to be transformed into debris. However, the debris maintaining the contact between the platen/s and agglomerate was only freed after the termination of loading (when the platen force/s approached zero).

10.5 DEBRIS DETACHMENT AND FRAGMENT SIZE DISTRIBUTION

The computer simulated tests permitted easy monitoring of the precise evolution of debris detachment during a test, such as observing exactly when, during the damage process, debris started to detach, or when most of the debris was detached. It also allowed a comparison of the evolution of the debris detachment in different test types on the same agglomerate. A new parameter was defined to represent the debris: the debris ratio (see section 6.2.2). At any moment in a test, the debris ratio is the ratio of the debris (complement) mass to the initial mass of the agglomerate.

In tests where the agglomerates suffered only local damage a relatively low amount of debris detached, usually from the external surface of the damage zone. At the other extreme, in shattering tests, the entire agglomerate was usually reduced to debris. The debris detachment started from the external surface of the agglomerate inwards, and was similar to a corrosion process.

For the agglomerates that fractured, the exact distribution of debris and other resulting fragments at the end of tests was more closely investigated. For the same agglomerate, the diametrical compression test was found to produce the least amount of debris for the same number of resulting large fragments. For the free-fall impact tests, the simulation results led to a similar conclusion as the one obtained from laboratory tests by Arbiter et al (1969): the exponent of the debris distribution (see section 9.4) is insensitive to the input velocity, energy input and pattern of fragmentation. In the case of double impact tests it was discovered that varying the mass of the impacting platen leaves the exponent unchanged and leads to very slight differences in the fragment size distributions. However, the impact velocity was found to have a much more significant effect on both the exponent and the amount of debris. A novel finding was that, on the same agglomerate, the free-fall and double impact tests exhibited the same fracture size distributions (and presented almost similar evolutions of the work input and damage ratio) only if the impact velocities were the same and the mass of agglomerate was equal to the mass of the impacting platen (see Chapter 9).

10.6 GENERAL CONSIDERATIONS AND OVERALL CONCLUSIONS

The enhanced TRUBAL code allowed a very detailed analysis of each simulated test. The parameters monitored included the precise evolution of work input, platen force, agglomerate velocity and kinetic energy, impacting platen velocity, every and all particle velocities, nominal strain, damage ratio and interparticle forces.

A very important conclusion derived from this project (see Chapters 5-8) is that an agglomerate cannot fracture if it cannot store a certain amount of elastic energy internally. The dense agglomerates suffered only local failure (without fracture) if the energy stored internally was not sufficient. On the other hand, the loose-packed agglomerate could not be fractured in any of the types of test because, as observed in the test simulations, it could not store elastic energy internally. Most of the input energy in the loose agglomerate was dissipated during the irreversible deformation of the agglomerate.

From all the tests simulated it can be concluded that brittleness is directly proportional to the interface energy, solid fraction, contact density and load-rate. The dense agglomerate having the highest contact density behaved in the most brittle manner in all three types of test.

The loose agglomerate behaved as a particle system consisting of many small and medium-sized clusters connected to each other with very few bonds. This made the loose agglomerate very "debris-prone" (it broke very easily into debris). In the loose agglomerate the debris detachment started from the very start of the test. In contrast, the dense agglomerates behaved much closer to solid samples than the loose agglomerate. The platen force (and the internally stored energy) increased sharply from the very start of test in the dense agglomerates. Cracks developed along certain internal surfaces and thus attempted to fracture the agglomerate into large and medium-sized fragments. The dense agglomerates had a tendency to break-up into many medium-sized fragments even in the tests causing shattering (they finally disintegrated due to the extensive bond breakage). The loose agglomerate suffered much larger irreversible deformations compared to the dense agglomerates. The behaviour was so different from that of dense agglomerates in all three types of test that it is clear that further research is required to clarify some of the observations made in this thesis.

10.7 LIMITATIONS AND FUTURE WORK

As in many other doctorate theses having an interesting and challenging research subject, the main real limitation encountered in this project was time! The answer to a question triggers an increasing list of further questions. There is a lot of truth in the saying: "The more we discover, the more we realise how much more still remains to be discovered".

The results presented in this thesis are directly relevant to coarse-grained agglomerates consisting of spherical particles (of about 60 μm diameter) that can only suffer elastic deformations. However, most of the agglomerates in real-life are made of particles that are not perfect spheres and that also suffer plastic deformations at the interparticle contacts. Aston's Particulate Materials research group have developed, very recently, two new versions of TRUBAL: one that handles plastic deformation at interparticle contacts and the

other that allows ellipsoidal-shaped particles. The enhancements now permit future work to find out how and to what extent do contact plastic deformation and non-spherical particle shape change the agglomerate behaviour under compression and impact testing. An imperative topic for future work is the simulation of medium-grained and fine-grained agglomerates, to see what changes will the size and total number of particles have on the behaviour of agglomerates. With the computer speed and memory doubling almost on a yearly basis, computers fast enough to simulate agglomerates of millions of constituent particles will soon become more affordable. It is possible that fine-grained agglomerates would behave much closer to solid samples than the coarse-grained agglomerates, and that the large fluctuations in the evolution of platen/s force (and other parameters) observed for coarse-grained agglomerates will disappear.

The laboratory research of Shipway and Hutchings (1993a,b) showed that spherical solid samples behave very differently in the case of elastic or plastic platens. As the platens used in this project were perfect elastic, several simulations of each of the three test types, this time using plastic platens, would be a possible follow-up research work. Although the plastic platens would lead to less local damage and debris detachment, it is not expected that they would produce significant changes in the failure behaviour of agglomerates.

Following one of the most important conclusions of this thesis, future research on coarse-grained agglomerates should attempt to relate the minimum elastic energy that an agglomerate has to be able to store for producing fracture to the particle diameter, agglomerate size, interface energy, solid fraction and contact density. This research could yield very useful results which would help to predict the work input necessary for the fracture of an agglomerate. Another alternative would be to find the threshold contact density, solid fraction and interface energy necessary for an agglomerate to fracture in diametrical compression; this information would then be used in different industrial applications.

In diametrical compression tests, the location of the fracture surface depends on the exact orientation of the agglomerate respective to the direction of loading. An interesting follow-up to the research carried out in this project would be to carry out compression tests with more than two points of loading on the agglomerates. This would certainly complicate the fracture process and be more relevant to the fracture of agglomerates in die compaction tests, for example. Having a sufficiently high-speed computer, an excellent project would be to simulate agglomerate beds in compression. By comparing the results with the ones from this project, one would be able to clarify whether simple diametrical compression tests (or maybe slow double impact tests) were relevant to the behaviour of agglomerates when compressed in beds.

More test simulations would be useful to find the precise effect of the contact density on the behaviour and fracture size distribution of agglomerates. The effect of the impact velocity on the fracture size distribution for the double impact test also needs more investigation. According to this project's results, it seems likely that further work could lead to exactly pin-point how double impact testing can replace free-fall impact testing. This would be of valuable practical interest, as there are many situations when it is more convenient to perform double impact rather than free-fall impact tests.

The interface energy in this project's agglomerates was uniform. An interesting and innovative exploration would be to produce and test agglomerates having non-uniform interface energy. Research in this area could find a way to produce much "stronger" agglomerates by trying to prevent them from fracturing - for example by creating stronger bonds in certain particular locations of the agglomerate. Using higher interface energy for the bonds close to the external surface of the agglomerate would certainly reduce attrition, but would it also alter significantly the agglomerate's behaviour under impact and compression testing? Another interesting formula would be to produce and test agglomerates having stronger bonds along three perpendicular diameters, as this would certainly impose resistance towards the hoop tensile stresses that cause fracturing.

A topic for further work in the area of impact tests would be to carry out oblique impact tests and to re-impact impacted agglomerates. This would model more realistically the impact phenomena that agglomerates suffer in real processing operations. In oblique impacts a short research project could determine the threshold impact angle under which agglomerates only suffer local damage (without fracturing).

Further exploration of the tests carried out could quantify exactly where the input energy is going during the tests. It could also examine in more detail the wave propagation within agglomerate and the exact way in which it influences the failure behaviour in the case of very high loading-rates.

REFERENCES

Abdel-Ghani, M., Petrie, J.G., Seville, J.P.K., Clift, R. and Adams, M.J. **(1991)** - Mechanical properties of cohesive particulate solids, *Powder Technol.*, **65**, 113-123.

Adams, M.J. **(1985)** - The strength of particulate solids, *J. Powder Bulk Solids Technol.*, **9**, 15-20.

Adams, M.J. and Perchard, V. **(1985)** - The cohesive forces between particles with interstitial liquid, *I. Chem. E. Symp. Series*, [91], 147-160.

Adams, M.J., Mullier, M.A., Seville, J.P.K. and Williams, J.G. **(1989)** - A fracture mechanics approach to the breakage of agglomerated particulate solids, *Powders and Grains (ed. Biarez and Gourves)*, Balkema, Rotterdam.

Akazawa, T. **(1953)** - Tension test method for concrete, *Union Test. Res. Lab. Mat. Structures*, [16, Nov.], 13-23.

Arbiter, N., Harris, C.C. and Stamboltzis, G.A. **(1969)** - Single fracture of brittle spheres, *Trans. Soc. Min. Eng. AIME*, **244**, 118-130.

Ashton, M.D., Cheng, D.C.-H., Farley, R. and Valentin, F.H.H. **(1965)** - *Rheol. Acta*, **4**, 206-218.

Bemrose, C.R. and Bridgwater, J. **(1987)** - A review of attrition test methods, *Powder Technol.*, **49**, 97-126.

Bennison, S.J. and Lawn, B.R. **(1989)** - Flaw tolerance in ceramics with rising crack resistance characteristics, *J. Mat. Sci.*, **24**, 3169-3175.

Bergstrom, B.H., Sollenberger, C.L. and Mitchell, W. Jr. **(1961)** - Energy aspects of single particle crushing, *Trans. Soc. Min. Eng. AIME*, **220**, 367-372.

Bergstrom, B.H. and Sollenberger, C.L. **(1961)** - Kinetic energy effect in single particle crushing, *Trans. Soc. Min. Eng. AIME*, **220**, 373-379.

Bond, F.C. **(1952)** - The third theory of comminution, *Trans. AIME*, **193**, 484.

British Materials Handling Board **(1987)** - Particle Attrition - State-of-the-Art Review, *Ser. Bulk Mat. Handl.*, **5**, Trans. Tech. Public.

Brecker, J.N. **(1974)** - The fracture strength of abrasive grains, *Trans. ASME, Series B, J. Eng. for Industry*, **96**, 1253-1257.

Breval, E., Jennings, J.S., Komarneni, S., Macmillan, N.H. and Lunghofer, E.P. **(1987)** - Microstructure, strength and environmental degradation of proppants, *J. Mat. Sci.*, **22**, 2124-2134.

Britten, J.R. and Pilpel, N. **(1978)** - Effects of temperature on the tensile strength of pharmaceutical powders, *J. Pharm. Pharmacol.*, **30**, 673-677.

Cai, H., Kalceff, M.A. and Lawn, B.R. **(1994)** - Deformation and fracture of mica-containing glass-ceramics in Hertzian contacts, *J. Mater. Res.*, **9**, [3], 762-770.

Capes, C.E. **(1970/71)** - Efflorescence and the drying of agglomerates, *Powder Technol.*, **4**, 77-82.

Capes, C.E. **(1971/72)** - The correlation of agglomerate strength with size, *Powder Technol.*, **5**, 119-125.

Carneiro, F.L.L.B., Barcellos, A. **(1953)** - Tensile strength of concretes, *Union Test. Res. Lab. Mat. Structures*, [13, March], 103-107.

Chantikul, P., Bennison, S.J. and Lawn, B.R. **(1990)** - Role of grain size in the strength and R-curve properties of alumina, *J. Am. Ceram. Soc.*, **73**, [8], 2419-2427.

Chapman, G.P. **(1968)** - The cylinder splitting test (with particular reference to concrete made with different natural aggregates), *Concrete*, **2**, [2], 77-85.

Charles, R.J. **(1957)** - Energy-size reduction relationships in comminution, *Trans. Soc. Min. Eng. AIME*, **208**, 80-88.

Charles and De Bruyn **(1956)** - Energy transfer by impact, *Trans. Soc. Min. Eng. AIME*, **205**, 47-53.

Chantikul, P., Bennison, S.J. and Lawn, B.R. **(1990)** - Role of grain size the strength and R-curve properties of alumina, *J. Am. Ceram. Soc.*, 73, [8, 2419-2427.

Chaudhri, M.M. **(1985)** - High-speed photographic investigations of the dynamic localised loading of some oxide glasses, *Strength of Inorganic Glass (ed. C.R. Kurkjian, Plenum Press)*, New York and London, 87-109.

Cheng, D.C.-H. **(1968)** - The tensile strength of powders, *Chem. Eng. Sci.*, **23**, 1405-1420.

Cleaver, J.A.S. and Ghadiri, M. **(1993)** - Impact attrition of sodium carbonate monohydrate crystals, *Powder Technol.*, 76, 15-22.

Colback, P.S.B. **(1966)** - An analysis of brittle fracture initiation and propagation in the Brazilian test, *Proc. Cong. Int. Soc. Rock Mech.*, Lisbon, 385-391.

Cook, R.F., Fairbanks, C.J., Lawn, B.R. and Mai, Y.-W. **(1987)** - Crack resistance by interface Bridging: Its role in determining strength characteristics, *J. Mater. Res.*, 2 [3], 345-356.

Crabtree, D.D., Kinasevich, R.S., Mular, A.L., Meloy, T.P., Fuerstenau, D.W. **(1964)** - Mechanisms of size reduction in comminution systems: Part I. Impact, abrasion, and chipping grinding, *Trans. Soc. Min. Eng.*, (June), 201-206.

Cundall, P.A. **(1971)** - A computer model for simulating progressive large scale movements in blocky rock systems, *Proc. Symp. Int. Soc. Rock Mech.*, Nacy II, Art. 8.

Cundall, P.A. and Strack, O.D.L. **(1979a)** - The distinct element method as a tool for research in granular media, *Report to the National Sci. Foundation: Part II, Dept. Civil Mineral Eng.*, University of Minnesota.

Cundall, P.A. and Strack, O.D.L. **(1979b)** - A discrete numerical model for granular assemblies, *Geotechnique*, **29**, 47-65.

Darvell, B.W. **(1990)** - Uniaxial compression tests and the validity of indirect tensile strength, *J. Mat. Sci.*, **25**, 757-780.

Dean, W.R., Sneddon, I.M. and Parsons, H.W. **(1952)** - The distribution of stress in a decelerating elastic sphere (Based on A.R.D. Theoretical Report, June, 1944), *Selected Gov. Res. Rep.: Strength and Testing of Materials: Part II: Testing Methods and Test Results*, London: H.M.S.O., 212-234.

Dexter, A.R. **(1975)** - J. Terramechanics, **12**, [1], 3-14.

Doelker, E., Mordier, D., Kopp, S. **(1989)** - Relevance of various mechanical strength measurements of pharmaceutical compressed tablets, *Powders and Grains (ed. Biarez and Gourves)*, Balkema, Rotterdam, 411-416.

Duffy, J. and Mindlin, R.D. **(1957)** - Stress-strain relations and vibrations of a granular medium, *J. of Appl. Mech. (Dec.)*, 585-593.

Endley, S.N. and Peyrot, A.H. **(1977)** - Load distribution in granular media, *J. Eng. Mech. Div., Proceedings ASCE*, 99-111.

Ennis, B.J., Green, J. and Davies, R. **(1994)** - The legacy of neglect in the U.S., *Chem. Eng. Progress, (April)*, USA.

Esezobo, S. and Pilpel, N. **(1976)** - Some formulation factors affecting the tensile strength, disintegration and dissolution of uncoated oxytetracycline tablets, *J. Pharm. Pharmacol.*, **28**, 8-16.

Fairhurst, C. **(1964)** - On the validity of the Brazilian test for brittle materials, *Int. J. Rock Mech. Mining Sci.*, **1**, 535-546.

Fell, J.T. and Newton, J.M. **(1970)** - Determination of Tablet Strength by the Diametral-Compression Test, *J. Pharm. Sci.*, **59**, [5], 688-691.

Ferracane J.L. and Greener E.H. **(1986)** - The effect of resin formulation on the degree of conversion and mechanical properties of dental restorative resins, *J. Biomed. Mat. Research*, **20**, 121-131.

Fisher, R.A. **(1926)** - On the capillary forces in an ideal soil; correction of formulae given by W.B. Haines, *J. Agricult. Sci.*, **16**, 492-505.

Freiman, S.W., Hench, L.L. **(1972)** - Effect of crystallization on the mechanical properties of Li2O-SiO2 glass-ceramics, *J. Am. Ceram. Soc.*, **55**, 86-89.

Frocht, M. M. **(1948)** - *Photoelasticity, Wiley*, New York (vol. I and II).

Frocht, M.M. and Guernsey, F. **(1952)** - A special investigation to develop a general method for three-dimensionsl photoelastic stress analysis, *Contract No. NAW-5959, Natnl. Adv. Comm. for Aeronautics Technical Note 2822.*

Gaudin, A.M. and Hukki, R.T. **(1946)** - Principles of comminution: Size and surface distribution, *Trans. Soc. Min. Eng. AIME*, **169**, 67.

Gaudin, A.M. and Melloy T.P. **(1962)** - *Trans. Soc. Min. Eng. AIME*, **223**, 40.

Ghadiri, M., Arteaga, P. and Cheung, W. **(1990)** - Impact attrition of particulate solids, *Proc. of Second World Congress on Particle Technol. (Sept.)*, Tokyo, Japan.

Gildemeister, H.H. and Schönert, K. **(1972)** - Brechnung zur Wellenausbreitung in Kugeln und Bruchphänomene in Kreisscheiben bei Prallbeanspruchung, *Dechema Monographie*, **69**, 233-267.

Gildemeister, H.H. and Schönert, K. **(1976)** - Bruchpaenomene und Spannungsfeld in prallbeanspruchten Kugeln, *Dechema Monographie*, **79**, 131-149.

Gilvarry, J.J. **(1961)** - Fracture of brittle solids. I. Distribution function for fragment size in single fracture (Theoretical), *J. Appl. Phys.*, **32**, [3], 391-399.

Gilvarry, J.J. and Bergstrom, B.H. **(1961a)** - Fracture and comminution of brittle solids. I. (Theory and experiment), *Trans. Soc. Min. Eng. AIME*, **220**, 380-389.

Gilvarry, J.J. and Bergstrom, B.H. **(1961b)** - Fracture of brittle solids. II. Distribution function for fragment size in single fracture (Experimental), *J. Appl. Phys.*, **32**, [3], 400-410.

Grady, D.E. **(1990)** - Particle size statistics in dynamic fragmentation, *J. Appl. Phys.*, **68**, [12], 6099-6105.

Griffith, A.A. **(1920)** - The Phenomena of rupture and flow in solids, *Phil. Trans. Royal Soc.*, London, **221**, 163-198.

Guiberteau, F., Padture, N.P. and Lawn, B.R. **(1994)** - Effect of grain size on hertzian contact damage in alumina, *J. Am. Ceram. Soc.*, **77**, [7], 1825-18231.

Hadas, A., Wolf, D. **(1984)** - Soil aggregates and clod strength dependence on size, cultivation, and stress load rates, *Soil Sci. Soc. Am. J.*, **48**,1157-1164.

Hertz, H. **(1895)** - *Gesammelte Werke - Vol. 1*, Leipzig, 174-196.

Hertzberg, R.W. **(1976)** - *Deformation And Fracture Mechanics Of Engineering Materials*, Wiley, New York.

Hess, W. and Schönert, K. **(1981)** - Brittle-plastic transition in small particles, *Proc. Powtech Conf. (March 1981)*, Birmingham, Particle Technol., EFCE Event no. 241, D/1/1 - D2/1/9.

Hiramatsu, Y.and Oka, Y. **(1966)** - Determination of the tensile strength of rock by a compression test of an irregular test piece, *Int. J. Rock Mech. Min. Sci.*, **3**, 89-90.

Hogue, C. and Newland, D. **(1994)** - Efficient computer simulation of moving granular particles, *Powder Technol.*, 51-66.

Hondros, G. **(1959)** - The evaluation of Poisson's ratio and the modulus of materials of a low tensile resistance by the Brazilian (indirect tensile) test with particular reference to concrete, *Australian J. Appl. Sci.*, **10**, 243-268.

Hunter, S.C. **(1957)** - Energy absorbed by elastic waves during impact, *J. Mech. Phys. Solids*, **5**, 162-171.

Inglis, C.E. **(1913)** - Stresses in a plate due to the presence of cracks and sharp corners, *Trans. Inst. of Naval Architects*, **55**, 219-242.

Irwin, G.R. **(1958)** - *Handbuch Der Physik*, **VI**, Springer-Verlag, Heilderberg.

Jaeger, J.C. **(1967)** - Failure of rocks under tensile conditions, *Int. J. Rock Mech. and Mining Sci.*, **4**, 219-227.

Jarosz, P.J. and Parrott E.L. **(1982)** - Factors influencing axial and radial tensile strengths of tablets, *J. Pharm. Sci.*, **71**, [6], 607-614.

Jarosz, P.J. and Parrott E.L. **(1983)** - Comparison of granule strength and tablet tensile strength, *J. Pharm. Sci.*, **72**, [5], 530-534.

Johnson, K.L., Kendall, K. and Roberts, A.D. **(1971)** - Surface energy and the contact of elastic solids, *Proc. Roy. Soc. London*, **A324**, 301-313.

Kapur, P.C. and Fuerstenau, D.W. **(1967)** - Dry strength of pelletized spheres, *J. Am. Ceram. Soc.*, **50**, [1], 14-18.

Kafui, K.D. and Thornton, C. **(1993)** - Computer simulated impacts of agglomerates, *"Powders & Grains 93" - Proc. 2nd Int. Conf. on Micromech. Granular Media (Birmingham, July 1993, ed. Thornton, C.)*, Balkema, Rotterdam, 401-406.

Kafui, K.D. and Thornton, C. **(1994)** - Agglomerate fracture/fragmentation, *Proc. First Particle Technology Forum, Vol. 2, AIChE (Denver, Aug. 1994)*, USA, 184-189.

Kafui, K.D. and Thornton, C. **(1995)** - Some aspects of silo discharge: Computer simulations, *Proc. Conf. "PARTEC 95" 3rd Europ. Symp. - Storage And Flow Of Particulate Solids, (Nurnberg, March 1995)*, Germany, 379-388.

Kafui, K.D. **(1996)** - personal communication, paper to be submitted to *Powder Technol.*

Keller, D.L., Converse, H.H., Hodges, T.O. and Chung, D.S. **(1972)** - Corn kernel damage due to high velocity impact, *Trans. ASAE*, 330-332.

Kelly, A. and Macmillan, N.H. **(1986)** - *Strong Solids ("Monographs on the Physics and Chemistry of Materials" Series), Oxford Science Publications*, 3rd ed.

Kendall K. **(1987)** - Relevance of contact mechanics to powders - elasticity, friction and agglomerate strength, *Tribol. in Particulate Technol. (ed. Briscoe, B. J. and Adams, M. J.)*, Adam Hilger, Bristol, 110-122.

Kendall **(1988)** - Agglomerate strength, *Powder Metallurgy*, **31**, [1], 28-31.

Kendall, K. and Weihs, T.P. **(1992)** - Adhesion of nanoparticles within spray-dried agglomerates, *J. Phys. D: Appl. Phys.*, **25**, A3-A8.

Kendall, K., Alford, N.McN. and Birchall J.D. **(1987)** - Elasticity of particle assemblies as a measure of the surface energy of solids, *Proc. Roy. Soc.*, London, **A412**, 269-283.

Kienzler, R. and Schmitt, W. **(1990)** - On single-particle comminution; numerical analysis of compressed spheres, *Powder Technol.*, **61**, 29-38.

Kirk, I.W. and McLeod, H.E. **(1967)** - Cottonseed rupture from static energy and impact velocity, *Trans. ASAE*, 217-219.

Kobayashi, R. **(1965)** - Mechanical properties of rocks under the action of high-speed loads, *2nd report, Nippon. Kogyo Kaishi.*, **81**, 595.

Krishnayya, A.V.G. and Eisenstein, Z. **(1974)** - Brazilian tensile test for soils, *Canadian Geotechnical J.*, **11**, 632-642.

Kschinka, B.A., Perrella, S., Nguyen, H. and Bradt, R.C. **(1986)** - Strengths of glass spheres in compression, *J. Am. Ceram. Soc.*, **69**, [6], 467-472.

Lam, K.K. and Newton, J.M. **(1991)** - Investigation of applied compression on the adhesion of powders to a substrate surface, *Powder Technol.*, **65**, 167-175.

Lautenschlager, E.P., Jacobs, J.J., Marshall, G.W. and Meyer Jr., P.R. **(1976)** - Mechanical properties of bone cements containing large doses of antibiotic powders, *J. Biomed. Mat. Res.*, **10**, 929-938.

Lawn, B.R. **(1985)** - Indentation: deformation and fracture processes, *Strength of Inorganic Glass (ed. C.R. Kurkjian, Plenum Press)*, New York and London, 67-86.

Lawn, B.R. **(1993)** - *Fracture of Brittle Solids, 2nd ed.*, Cambridge University Press.

Lawn, B.R., Padture, N.P., Guiberteau, F. and Cai, H. **(1994)** - A model for microcrack initiation and propagation beneath Herzian contacts in polycrystalline ceramics, *Acta Metall. Mater.*, **42**, [5], 1683-1693.

Lawn, B.R. and Marshall, D.B. **(1979)** - Hardness, toughness, and brittleness: an indentation analysis, *J. Am. Ceram. Soc.*, **62**, [7-8], 347-350.

Lawn, B.R. and Wilshaw, T.R. **(1975)** - Review. Indentation fracture: principles and applications, *J. Mat. Sc.*, **10**, 1049-1081.

Lian, C., Thornton, C. and Adams, M.J. **(1993a)** - A theoretical study of liquid bridge forces and stability between two rigid spherical bodies, *J. Colloid and Interface Sci.*, **161**, 138-147.

Lian, C., Thornton, C. and Adams, M.J. **(1993b)** - Effect of liquid bridge forces on agglomerate collisions, *"Powders and Grains 93": Proc. 2nd Int. Conf. on Micromech. of Granular Media (Birmingham, July 1993, ed. Thornton, C.)*, Balkema, Rotterdam, 59-64.

Lian, G. **(1994)** - Computer simulation of moist agglomerate collisions, *PhD Thesis*, Aston University, UK.

Louvier, F.J., Calderwood, D.L. **(1967)** - Breakage of milled rice at different free fall heights, *Proc. of the Anual Meeting of the SW Region of the ASAE (April 27-28)*, Stillwater, Oklahoma.

Lur'e, A.I. **(1964)** - *Three-Dimensional Problems Of The Theory Of Elasticity*, Interscience-Wiley, New York, 361-367.

Mai, Y.-W. and Lawn, B.R. **(1987)** - Crack-interface grain bridging as a fracture resistance mechanism in ceramics: II, Theoretical fracture mechanics model, *J. Am. Ceram. Soc.*, **70**, [4], 289-294.

Marion, R. and Johnstone, J.K. **(1977)** - A parametric study of the diametrical compression test for ceramics, *Ceramic Bulletin*, **56**, [11], 998-1002.

Mellor, M., Hawkes, I. **(1971)** - Measurement of tensile strength by diametrical compression of discs and annuli, *Eng. Geology*, **5**, 173-225.

Mecholsky, J.J., Passoja, D.E., Feinberg-Ringel, K.S. **(1989)** - Quantitative analysis of brittle fracture surfaces using fractal geometry, *J. Am. Ceram. Soc.*, **72**, [1], 60-65.

Meyers, M.A. and Meyers, P.P. **(1984)** - Compressive strength of iron-ore agglomerates, *Trans. Soc. Mining Eng. of AIME*, **274**, 1875-1884.

Meyers, M.A. and Tantevee, T. **(1986)** - Stress induced in iron-ore pellets by hydrogen reduction, *Metall. Trans. B*, **17B**, (March), 217-227.

Mindlin, R.D, Deresiewicz, H. **(1953)** - Elastic spheres in contact under varying oblique forces, *J. Appl. Mech.*, **20**, 327-344.

Mitchell, N.B. **(1961)** - The indirect tension test for concrete, *Mat. Res. and Stand.*, **1**, (Oct.), 780-788.

Newitt, D.M., Conway-Jones, J.M. **(1958)** - A contribution to the theory and practice of granulation, *Trans. Inst. Chem. Eng.*, **36**, 422-442.

Newton, J.M., Rowley, G., Fell, J.T., Peacock, D.G. and Ridgway K. **(1971)** - Computer analysis of the relation between tablet strength and compaction pressure, *J. Pharm. Pharmacol.*, **23**, 195S-201S.

Ning, Z. and Thornton, C. **(1993)** - Elastic-plastic impact of fine particles with a surface, *"Powders and Grains 93" - Proc. 2nd Int. Conf. on Micromech. of Granular Media (ed. Thornton, C., Birmingham, July 1993)*, Balkema, Rotterdam, 33-38.

Ning **(1995)** - Elasto-plastic impact of fine particles and fragmentation of small agglomerates, *PhD Thesis*, Aston University, UK.

Oka, Y. and Majima, H. **(1970)** - A theory of size reduction involving fracture mechanics, *Canadian Metall. Quarterly*, **9**, [2], 429-439.

Orowan, E. **(1949)** - Fracture and strength of solids, *Rep. Prog. Phys.*, [12].

Pandey, P. and Singh, D.P. **(1986)** - Deformation of a rock in different tensile tests, *Eng. Geology*, **22**, 281-292.

Patel, C.I. and Staniford, J.N. **(1987)** - Determination of the apparent failure viscosity of tablets, *J. Pharm. Pharmacol.*, **39**, 647-650.

Pauw, O.G. and Mare, M.S. **(1988)** - The determination of optimum impact-breakage routes for an ore, *Powder Technol.*, **54**, 3-13.

Peltier, R. **(1954)** - Theoretical investigation of the Brazilian test, *Union Test. Res. Lab. Mat. Structures (RILEM)*, [19].

Perry, J.S., Hall, C.W. **(1965)** - Mechanical properties of pea beans under impact loading, *Trans. of the ASAE*, 191-193.

Pietsch, W.B. **(1969)** - *Canadian J. Chem. Eng.*, **47**, 403.

Pietsch, W. **(1991)** - *Size Enlargement By Agglomeration*, Wiley, 19-111.

Potapov, A.V. and Campbell, C.S. **(1994)** - Computer simulation of impact-induced particle breakage, *Powder Technol.*, **81**, 207-216.

Rees, J.E. and Shotton, E. **(1969)** - The effect of dimensions on the compaction properties of sodium chloride, *J. Pharm. Pharmacol.*, **21**, 731-743.

Ridgway, K. **(1970)** - Testing tablets by diametral crushing, *Pharm. J.*, **205**, (Dec.), 709-712.

Rogowski, A.S. **(1964)** - Strength of soil aggregates, *PhD Thesis*, Iowa State University of Sci. and Technol., Ames, Iowa, USA.

Rogowski, A.S., Moldenhauer, W.C. and Kirkham, D. **(1968)** - Rupture parameters of soil aggregates, *Soil Sci. Soc. America: Proc.*, **32**, 720-724.

Rogowski, A.S. and Kirkham, D. **(1976)** - Strength of soil aggregates: influence of size, density and clay and organic matter content (1), Mededelingen Faculteit, Landbouwwetenschappen RijksUniversiteit, Gent, Belgium, 41, 85-100.

Rossmanith, H.P. and Shukla, R.I. **(1982)** - Photoelastic investigation of dynamic load transfer in granular media, *Acta Metallica*, [42], 211-225.

Rudnick, A., Hunter, A.R. and Holden, F.C. **(1963)** - An analysis of the diametral-compression test, *Mat. Res. and Standard*, (April), 283-289.

Rumpf, H. **(1961)** - *Int. Symposion (ed. W.A. Knepper)*, U.S. Steel Corporation, Philadelphia.

Rumpf, H. **(1962)** - The strength of granules and agglomerates, *Agglomeration (ed. W.A. Knepper)*, New York, 379-418.

Rumpf, H. **(1990)** - *Particle Technology*, Chapman and Hall, London.

Rumpf, H. and Schönert, K. **(1972)** - Die Bruchenscheinungen in Kugeln bei elastischen sowie plastischen Verformungen durch Druckbeanspruchung, *Dechema Monographie*, **69**, 51-85.

Saad, M., Shukla, A., Sienkiewicz, F., Zhang, Z. and Gautam, A. **(1994)** - Wave propagation in saturated and cemented granular materials, *Proc. Int. Conf. on Mech. and Statistical Physics of Particulate Mat. (org. by Instit. for Mech. and Mat., 8-10 June 1994)*, Univ. of Calif., La Jolla, California.

Salman, A.D., Szabo, M., Angyal, I. and Verba, A. **(1988)** - Particle degradation, *Periodica Polytechnica: Mech. Eng.*, **32**, [3-4], 233-251.

Salman, A.D., Gorham, D.A. and Verba, A. **(1994)** - A study of solid particle failure under normal and oblique impact, *Proc. 8th Int. Conf. on Erosion by Liquid and Solid Impact, (September 1994)*, Cambridge.

Santurbano, R. and Fairhurst, C. **(1991)** - Fracture mechanics in the context of rock crushing: Preliminary experimental results concerning the impact of limestone spheres, *Rock Mech. as Multidisciplinary Sci. (ed. Roegiers)*, Balkema, Rotterdam, 441-449.

Sammis, C.G. and Ashby, M.F. **(1986)** - The failure of brittle porous solids under compressive stress states, *Acta Metall.*, **34**, [3], 511-526.

Savkoor, A.R. and Briggs, G.A.D. **(1977)** - The effect of tangential force on the contact of elastic solids in adhesion, *Proc. Roy. Soc.*, London, **A356**, 103-114.

Schönert, K. **(1973)** - Single particle crushing of polymers, *Harold Heywood Memorial Symp.*, Loughborough University of Technology.

Schönert, K. **(1972)** - Role of fracture physics in understanding comminution phenomena, *Trans. Soc. Min. Eng., AIME*, **252**, (March), 21-26.

Schönert, K. **(1979)** - Aspects of the physics of breakage relevant to comminution, *Fourth Tewksbury Symp.: Fracture at Work, University of Melbourne (ed. D.S. Mansell and G.H. Vasey, Feb.)*, Melbourne, 3.1-3.30.

Schubert, H. **(1975)** - Tensile strength of agglomerates, *Powder Technol.*, **11**, 107-119.

Schubert, H., Hermann, W. and Rumpf, H. **(1975)** - Deformation behaviour of agglomerates under tensile stresses, *Powder Technol.*, **11**, 121-131.

Shaw, M.C, Braiden, P.M. and DeSalvo, G.J. **(1975)** - The disc test for brittle materials, *J. Eng. for Industry*, **97**, (Febr.), 77-87.

Shipway, P.H. and Hutchings, I.M. **(1993a)** - Fracture of brittle spheres under compression and impact loading. I. Elastic stress distributions, *Phil. Mag. A*, **67**, [6], 1389-1404.

Shipway, P.H. and Hutchings, I.M. **(1993b)** - Fracture of brittle spheres under compression and impact loading. II. Results for lead-glass and sapphire spheres, *Phil. Mag. A*, **67**, [6], 1405-1421.

Shipway, P.H. and Hutchings, I.M. **(1993c)** - Attrition of brittle spheres by fracture under compression and impact loading, *Powder Technol.*, **76**, 23-30.

Shinohara, K. and Capes, C.E. **(1979)** - Effect of distributed loading on stress patterns in discoidal agglomerates during the diametrical compression test, *Powder Technol.*, **24**, 179-186.

Shinohara, K., Capes, C.E. and Fouda, A.E. **(1982)** - A theoretical model of the effect of distributed loading on the tensile strength of agglomerates as measured in the diametrical compression test, *Powder Technol.*, **32**, 163-171.

Shockey, D.A., Curran, D.R., Seaman, L., Rosenberg, J.T. and Petersen, C.F. **(1974)** - Fragmentation of rock under dynamic loads, *Int. J. Rock Mech. Sci. and Geomech. Abstr.*, **11**, 303-317.

Shotton, E. and Ganderton, D. **(1960)** - The strength of compressed tablets, *J. Pharm. Pharmacol.*, **12**, 87T-96T.

Shukla, A. and Rossmanith, H.P. **(1986)** - Dynamic photoelastic investigation of wave propagation and energy transfer across contacts, *J. Strain Analysis*, **21**, [4], 213-218.

Sikong, L., Hashimoto, H. and Yashima, S. **(1990)** - Breakage behaviour of fine particles of brittle minerals and coals, *Powder Technol.*, **61**, 51-57.

Singh, D. and Shetty, D.K. **(1989)** - Fracture toughness of polycrystalline ceramics in combined mode I and mode II loading, *J. Am. Ceram. Soc.*, **72**, [1], 78-84.

Steier, K. and Schönert, K. **(1972)** - Verformung und Bruchphänomene unter Druckbeanspruchung von sehr kleinen Körnern aus Kalkstein, Quartz und Polystyrol, *Dechema Monographien*, **69**, 167-192.

Sternberg, E. and Rosenthal, F. **(1952)** - The elastis sphere under concentrated loads, *J. Appl. Mech.*, **19**, 413-421.

Strack, O.D.L. and Cundall, P.A. **(1978)** - The distinct element method as a tool for research in granular media, *Report to the National Sci. Foundation: Part I, Dept. Civil Mineral Eng., University of Minnesota.*

Stroh, A.N. **(1954)** - The formation of cracks as a result of plastic flow - I, *Proc. Roy. Soc. A*, London, 404-414.

Stroh, A.N. **(1955)** - The formation of cracks as a result of plastic flow - II, *Proc. Roy. Soc. A*, London, 548-560.

Swanson, P.L., Fairbanks, C.J., Lawn, B.R., Mai, Y.-W. and Hockey, B.J. **(1987)** - Crack-interface grain bridging as a fracture resistance mechanism in ceramics: I, Experimental study on alumina, *J. Am. Ceram. Soc.*, **70**, [4], 279-289.

Tabor, D. **(1987)** - *Adhesion of Solids, Tribol. in Particulate Technol. (ed. Briscoe, B. J. and Adams, M. J.)*, Adam Hilger, Bristol, 206-219.

Tanaka, K., Yamamoto, H., Yumoto, S. and Ichnose, T. **(1985)** - Crush strength of spherical ferrite carriers, *J. Mat. Sci. Letters*, **4**, 184-186.

Thornton, C. **(1991)** - Interparticle sliding in the presence of adhesion, *J. Phys. D: Appl. Phys.*, **24**, 1942-1946.

Thornton and Sun **(1993)** - Axisymmetric compression of 3D polydisperse system of spheres, *"Powders & Grains 93" - Proc. 2nd Int. Conf. on Micromech. Granular Media (Birmingham, July 1993, ed. Thornton, C.)*, Balkema, Rotterdam,129-134.

Thornton, C., Yin, K.K. and Adams, M.J. **(1996)** - Numerical simulation of the impact fracture and fragmentation of agglomerates, *J. Phys. D: Appl. Phys.*, **29**, 424-435.

Tilly, G.P. and Wendy, S. **(1970)** - The interaction of particle and material behaviour in erosion processes, *Wear*, **16**, 447.

Timoshenko, S. **(1958)** - Strength of Materials, Part II: Advanced Theory and Problems, *(Third ed., Van Nostrand Reinhold Company)*, New York.

Timoshenko, S.P. and Goodier, J.N. **(1951)** - Theory of elasticity, *McGraw-Hill*, New York.

Tsunakawa, H. and Aoki, R. **(1972)** - *Kagaku Kogaku*, **36**, 281-286.

Uuemois, H. and Kleis, I. **(1975)** - A critical analysis of erosion problems which have been little studied, *Wear*, **31**, 359.

Van der Zwaag, S. and Hagan, J.T. **(1985)** - Deformation prpcess in silica and different soda-lime glasses under conical indentations, *Strength of Inorganic Glass (ed. C.R. Kurkjian, Plenum Press)*, New York and London, 147.

Vardar, Ö, Finnie, I. **(1975)** - An analysis of the Brazilian disk fracture test using the Weibull probabilistic treatment of brittle strength, *Int. J. of Fracture*, **11**, [3], 495-508.

Verall, R.J. **(1976)** - A sphere compression test for measuring the mechanical properties of dental composite materials, *J. of Dentistry*, **4**, 11-14.

Weibull, W. **(1951)** - A statistical distribution function of wide applicability, *J. Appl. Mech.*, **18**, 293-297.

Wijk, G. **(1978)** - Some new theoretical aspects of indirect measurements of the tensile strength of rocks, *Int. J. Rock Mech., Mining Sci. and Geomech. Abstr.*, **15**, 149-160.

Wong, J.Y., Laurich-McIntyre, S.E., Khaund, A.K. and Bradt, R.C. **(1987)** - Strength of green and fired spherical aluminosilicate aggregates, *J. Am. Ceram. Soc.*, **70**, 785-91.

Wright, P.J.F. **(1955)** - Comments on an indirect tensile test on concrete cylinders, *Mag. Concrete Res.*, **7**, [20], 87-96.

Wu, J., Mai, Y.-W. and Yee, A.F. **(1994)** - Fracture toughness and fracture mechanisms of polybutylene-terephthalate/ploycarbonate/impact-modifier blends - part III, *J. Mat. Sci.*, **29**, 4510-4522.

Wynnyckyj, J.R. **(1985)** - The correlation between the strength factor and the true tensile strength of agglomerate spheres, *Canadian J. Chem. Eng.*, **63**, [4, Aug.], 591-597.

Yin, K.K. **(1992)** - *Numerical modelling of agglomerate degradation, PhD Thesis*, Aston University, UK.

York, P. and Pilpel, N. **(1973)** - The tensile strength and compression behaviour of lactose, four fatty acids, and their mixtures in relation to tableting, *J. Pharm. Pharmacol.*, **25**, 1P-11P.

Young, Z., Hanson, M.T. and Kovacevic, R. **(1994)** - Topological measure of brittle fragmentation, *Internat. J. Solids Struct.*, **31**, [3], 391-415.

Zeleny, R.A. **(1957)** - A study of the dissipation of energy in single particle crushing, *PhD Thesis*, University of Minnesota, USA.

APPENDIX A

TRUBAL SIMULATION SOFTWARE PROGRAM

A.1 THEORETICAL BASIS OF TRUBAL

A.1.1 Evolution Of TRUBAL And The Distinct Element Method

TRUBAL is a simulation software developed in FORTRAN by Peter Cundall (see Strack and Cundall, 1978 and Cundall and Strack, 1979a,b) to model the behaviour of particulate/granular media. The program TRUBAL was first utilised as a simulation tool with the aim of establishing micromechanical constitutive laws for granular materials. Cundall continuously enhanced and used TRUBAL for different granular media modelling problems. With Cundall's 1989 version of TRUBAL, perfect elastic spherical particles could be created in a cubic work-space and Newton's second law of motion was used by the program to determine particle displacements. The Distinct Element Method embedded in TRUBAL uses a time-dependent finite difference scheme to model the progressive movement of each particle. At a contact, the normal forces are transmitted between two particles according to Hertzian theory, whereas the tangential contact forces were transmitted according to a linear spring model. The program was also endowed with a two-dimensional mode option - for which it could also produce visualisations.

In parallel with Cundall's work, other groups of researchers have used, or enhanced and used the TRUBAL software. However, after 1989, most improvements to the TRUBAL software and the largest volume of simulation work has been carried out at Aston University. The main three current versions of TRUBAL at Aston are TRUBAL-DRY, TRUBAL-WET and TRUBAL-PLASTIC.

The Distinct Element Method (DEM) is at the very core of the TRUBAL software. It provides the effective facility to simulate the behaviour of particulate material by means of cyclic, step-by-step displacement of particles. The length of time between two consecutive cycles - called a time-step - is very small (usually 0.03 μs in this project) - so that some theoretical approximations are negligible within this duration. However, the theoretical approximations do not "add up" giving larger (non-acceptable) approximations after large numbers of cycles, as the DEM actually successively displaces particles and does new calculations after each cycle.

Newton's second law of motion is employed in TRUBAL for determining the movement of particles and walls within each time-step. To model the particle-particle and particle-platen interaction, different contact mechanics theories are used in TRUBAL (Aston versions), including theories of Hertz (1895), Mindlin and Deresiewicz (1953), Johnson et al (1971), Savkoor and Briggs (1977), Thornton (1991), Johnson (1985) - for dry agglomerates, and Adams and Perchard (1985), Lian et al (1993) - for wet agglomerates.

A.1.2 Newton's Second Law Of Motion

Within a calculation cycle of duration Δt, Newton's equations of motion for a particle are:

$$F_i - F_d = \frac{m \cdot \Delta v_i}{\Delta t} \qquad \text{(for translational motion)} \qquad \text{(A.1)}$$

$$M_i - M_d = \frac{I \cdot \Delta \omega_i}{\Delta t} \qquad \text{(for rotational motion)} \qquad \text{(A.2)}$$

where the damping force $F_d = ß_g \times v_i$, the damping moment $M_d = ß_g \times \omega_i$, i = 1,2,3 are indicators for the X, Y and Z directions, F_i is the out-of-balance force on the particle

(resultant force acting on it), M_i is the out-of-balance moment of particle, v_i and ω_i are the translational and rotational velocities, β_g is the global damping coefficient, I is the rotational moment of inertia of the spherical particle and m is the particle's mass. The velocity increments Δv_i and $\Delta\omega_i$ of each particle are obtained by solving (A.1) and (A.2) with a finite difference method. The translational and rotational displacement increments Δx_i and respective $\Delta\Phi_i$ of each particle are determined using the simple relations:

$$\Delta x_i = v_i \times \Delta t \tag{A.3}$$

$$\Delta\Phi_i = \omega_i \times \Delta t \tag{A.4}$$

A.1.3 Contact Forces Between Dry Elastic Particles In The Absence Of Adhesion

THE NORMAL CONTACT FORCE

TRUBAL knows that a contact between two spherical particles of radii R_1 and R_2 exists if the distance between the centres of the two particles is less than the sum of their radii. The overlap (relative approach) between the two particles is easily calculated, as the coordinates of the particles are known.

According to Hertz, the induced contact force due to the relative approach α is:

$$N = \frac{4}{3} E^* (R^* \times \alpha^3)^{\frac{1}{2}} \tag{A.5}$$

where $1/R^* = 1/R_1 + 1/R_2$, (A.6)

$$\frac{1}{E^*} = \frac{1-\nu_1^2}{E_1} + \frac{1-\nu_2^2}{E_2} \tag{A.7}$$

E_1, ν_1, respective E_2, ν_2 are the Young's modulus and Poisson's ratio of the two particles.

Following (A.5), if $\Delta\alpha$ is the increment of the relative approach of the particles within one calculation cycle, the induced increment in the normal contact force is:

$$\Delta N = 2\, E^* \times a \times \Delta\alpha \tag{A.8}$$

where a is the radius of the contact area:

$$a^2 = \alpha \times R^* \tag{A.9}$$

THE TANGENTIAL CONTACT FORCE

If there is no surface energy, the tangential force at the contact between two particles is determined using the theory of Mindlin and Deresiewicz (1953). A relative slip is produced at the contact of two surfaces if they are subjected to an increasing tangential displacement $\Delta\delta$. The slip is initiated at the perimeter and progresses inward over an annular area of the contact surface. The incremental tangential displacement $\Delta\delta$ produces an increment ΔT in the tangential contact force - which depends on the loading history and on the normal contact force's variation, as follows:

$$\Delta T = 8\, G^* a\, \Theta_k\, \Delta\delta + (-1)^k \mu\, \Delta N\, (1 - \Theta_k) \quad (A.10)$$

where $\Theta k = 1$, for $|\Delta T| < \mu\, \Delta N$ (no slip solution). (A.11)

Otherwise,

$$\Theta_k{}^3 = 1 - (T + \mu\, \Delta N) / \mu\, N \quad \text{if } k=0 \quad (A.12.a)$$

$$\Theta_k{}^3 = 1 - ((-1)^k\, (T-T_k) + 2\mu\, \Delta N) / 2\mu\, N \quad \text{if } k=1 \text{ and } k=2, \quad (A.12.b)$$

(partial slip solution)

where k = 0,1,2 represents the loading path (virgin loading, unloading, reloading respectively), $\Delta\delta$ is the increment of the contacting particles' tangential displacement, μ is the friction coefficient,

$$1/G^* = (2-\nu 1)/G1 + (2-\nu 2)/G2 \quad (A.13)$$

and $T_k = T_k - (-1)^k\, \mu\, \Delta N.$ (A.14)

After each cycle, T_k needs updating with the new value of the normal contact force increment ΔN using (A.14).

A.1.4 Contact Forces Between Dry Elastic Particles (With Adhesion)

THE NORMAL CONTACT FORCE

When surface energy is considered, the contact force in the direction normal to the contact area is modelled according to JKR theory - see (Johnson et al, 1971). A relative approach $\Delta\alpha$ between the contacting adhering particles leads to an increment in the normal contact force as follows:

$$\Delta N = 6E^* a \left(\frac{\sqrt{N_1} - \sqrt{N_c}}{3\sqrt{N_1} - \sqrt{N_c}} \right) \Delta\alpha \quad (A.15)$$

where N_1 is the effective normal force (the Hertz's force to cause the same contact area of radius a), and $N_c = 3\, \pi\, \gamma\, R^*$ is the pull-off force due to the surface energy γ of the adhering contacting particles.

THE TANGENTIAL CONTACT FORCE

The model for determining the tangential contact force for two adhering particles was developed by Thornton (1991), following the theories of Mindlin and Deresiewicz (1953) and Savkoor and Briggs (1977). Here, the increment ΔT in the tangential contact force, due to the incremental tangential displacement $\Delta\delta$, depends again on the loading history but also on the tangential force's magnitude compared to the normal force. At the start, an increasing tangential force tends to reduce the contact area (peeling). The incremental tangential force ΔT is calculated with Mindlin's no-slip solution:

$$\Delta T = 8\, G^*\, a_r\, \Delta\delta \quad (A.16)$$

where a_r is the radius of the reduced contact area determined as:

$$a_r^3 = 3R^* \frac{N + 2N_c \pm \sqrt{4N \times N_c + 4N_c^2 - \frac{T^2 \times E^*}{4G^*}}}{4E^*} \qquad (A.17)$$

The peeling mechanism is complete only when T reaches the critical value

$$T_c = 4\sqrt{\frac{G^*(NN_c \times N_c^2)}{E^*}} \qquad (A.18)$$

The contact area has been reduced to

$$a_p = \left[\frac{3R^*}{4E^*}(N + 2N_c)\right]^{\frac{1}{3}} \qquad (A.19)$$

If the tangential force at the end of peeling $T=T_C$ is greater than the sliding force, the tangential force should fall immediately to the value of the sliding force. If $T=T_C$ is smaller than the sliding force, a subsequent slip annulus starts to spread inwards over the contact area. The tangential force is then determined using the Mindlin and Deresievicz (1953) partial-slip solution - equations (A.10) and (A.12), with N replaced by $N + 2\ N_C$.

A.2 TRUBAL'S LOGIC AND INCORPORATED PRINCIPLES

The software program TRUBAL is written in FORTRAN computer language and it is organised into a large number of subroutines (see Fig. 3.1). The main structure of TRUBAL at Aston University is the same as it was in 1979 when its development was accomplished by Peter Cundall. The alterations carried out at Aston over the last 4 years were either incorporated into existing software subroutines or consisted of the addition of new subroutines.

An efficient and fast algorithm incorporated in TRUBAL eases the detection of new particle-particle and particle-wall contacts. The time-step magnitude is realistically determined according to the Rayleigh wave propagation speed, whereas contact and global damping are calculated from dashpot models.

A.2.1 Contact Searching - The Grid Of Boxes System

After each cycle particles and platens/walls have to be moved to new positions. As a result, TRUBAL has to check if there are any new particle-particle or particle-platen contacts formed. For a large number of particles, this search for possible contacts would take too much computing time, as the coordinates of each particle would have to be compared with the coordinates of all the other particles and walls. Based on the fact that a particle can only make a new contact with a particle or platen which lies in its vicinity, a contact detection scheme (as part of the Distinct Element Method) was embedded in TRUBAL. From the very first command issued, the simulation's working space is divided into a lattice of cubic boxes, the size of each box being larger than the diameter of each particle. When particles and walls are created (generated), they are mapped into boxes, so that each particle will map into at least one box of the lattice. Later, when the program searches for whether a particle should have new contacts, it goes through the boxes information and knows to check only the particles and platens lying in the boxes into which a circumscribing cube maps.

A.2.2 Time Step Calculation

The time step, or the duration of a cycle, is realistically calculated by TRUBAL at the very start of simulation, based on the velocity with which Rayleigh waves propagate through an elastic body. The critical time step Δt_C - representing the highest frequency of Rayleigh wave

propagation through an agglomerate of spherical particles - is determined by the smallest particle of radius R_{min}:

$$\Delta t_c = \frac{\pi R_{min}}{\alpha}\sqrt{\frac{\rho}{G}} \qquad (A.20)$$

where $a \approx 0.1631\ \nu + 0.876605$, ρ is the particle density, G the shear modulus of particles and ν the Poisson's ratio. A fraction of the critical time-step is normally used in the simulations.

A.2.3 Main Memory: Linked-Lists Arrays

Due to the cyclic advancement of a simulation, TRUBAL needs to store the parameters determined in a cycle for use in the calculations of a subsequent cycle. For storage TRUBAL uses a main memory which actually is a group of arrays connected through pointers. Each array stores data relative to a particular aspect of the simulation: the *particle array* only stores information concerning each spherical particle (particle type, coordinates, displacement increments, velocities, out-of-balance forces and moments etc); the *wall array* contains data about each wall (wall type, velocities, forces on walls, forces and velocities set by servo, displacement increments etc); the *box array* stores information about lattice boxes (where particles and walls are mapped); the *contact array* contains data about the particle-particle and particle-wall contacts (normal and tangential contact forces, displacements, stiffnesses, surface energy, contact area's radius etc). When, at a particular moment, a user issues the command to save the state of a simulation, almost all the data existing in the main memory at that moment is saved into a file. This file can be re-opened and re-used by TRUBAL at a later date, to continue the simulation, to plot images or to print results.

The fact that TRUBAL uses linked lists and many pointers makes it more complicated (complex) and risky but, on the other hand, saves a lot of precious computing time and storage space. Nevertheless, great care has to be taken any time when changes are made to the TRUBAL code.

A.2.4 Energy Dissipation

TRUBAL is equipped with five realistic ways of dissipating energy: contact and global damping, friction, adhesive peeling and, in TRUBAL-WET only, viscous resistance of liquid bridges. Contact damping, or stiffness-proportional damping, is modelled by a dashpot and represents the dissipation of energy through the solid particles. Global damping, or mass-proportional damping, is modelled as dashpots that connect all particles to the axis of reference; it operates in the form of Rayleigh damping.

A.3 ON HOW TRUBAL WORKS, EVOLUTION OF SIMULATIONS

TRUBAL is a powerful simulation tool; it can be used for creating agglomerates, testing agglomerates, recording data, and plotting images at any moment during testing (see several examples of using TRUBAL-ACI in Appendix B).

At the very start (see Fig. 5.1. and Appendix B), the program reads the first command line - which, as discussed, is either typed on-line by the user or taken from the batch input data file (a list of commands). For a new simulation, TRUBAL creates the workspace, divides it into a lattice of boxes and initialises all the simulation's parameters. For a restart simulation, TRUBAL reads the file where the state was saved and restores (re-loads in its memory) all the simulation's parameters from there. In the case of a new simulation, TRUBAL also processes the subsequent command lines which usually provide the new simulation's initial parameters (characteristics of particles etc) and the walls positions (if the case), and specify where to create/generate the particles (see Appendix B). After particle creation/generation, TRUBAL automatically maps particles and walls into lattice boxes.

At the CYCLE command (see Appendix B), TRUBAL effectively starts the simulation and carries out cyclic computations. At first it calculates the forces and moment increments for each particle, then their accelerations, velocities and displacements. The next step is to move particles and walls/platens to their new positions. As a consequence of having new coordinates, particles and walls need to be re-boxed. TRUBAL then carries out a search for new particle-particle or particle-wall contacts. A subsequent step consists in resolving the contacts - by determining the relative displacement of each pair of two particles in contact and then calculating the normal forces, radius of contact, tangential forces, etc.

During a simulation, TRUBAL automatically prints some information in "trubal.out", "kw.out" and, when requested, (see Appendix B) also in other output files or on the screen. The graphic facilities are usually employed after carrying out the test simulations. States saved during test simulations should be restarted and appropriate plotting commands should be used for obtaining different images (see Appendix B) .

Appendix B is a manual provided for future users of the TRUBAL-ACI program wishing to carry out agglomerate testing simulations. Sections B.1 - B.8 provide details on most of the commands that can be issued with TRUBAL-ACI. The description of the data that is automatically stored during simulations in the program's main arrays (particle, wall and contact arrays) can be found in section B.9. Section B.10 provides 4 typical data files that were used in simulating the tests presented in this thesis; values specified for the various parameters are given.

APPENDIX B

TRUBAL-ACI USER MANUAL

TRUBAL is a software program written in FORTRAN to enable the simulation of granular/particulate systems. This user manual only presents the procedures and commands needed by the variant TRUBAL-ACI for the simulation of diametrical compression, double impact and free-fall or simple impact of agglomerates.

B.1 INTRODUCTION

The TRUBAL-ACI software program was prepared to run on IBM RS/6000 workstations. The executable file is created from the compilation of eight files of FORTRAN code.

For the TRUBAL-ACI to be able to run, a file called "**trubal.dir**" should exist in the current working directory. From the very start, TRUBAL-ACI will check the contents of this file for to determine the mode in which it should operate. If this file contains the word "BATCH", the program will operate in indirect (batch) mode. It will take its input from the command file "**trubal.dat**" and place its output in the "**trubal.out**" file. If "**trubal.dir**" contains the word "TERM", the user will have to interact directly (command by command) with TRUBAL. The software program will expect input from the keyboard and will send its output to the screen. Input and output redirection can directly be used in this case to take input from and send output to specified files.

In this project TRUBAL-ACI was only used in the indirect mode, as this was considered to be the most reliable. As a consequence, only the procedures connected with this mode will be presented in the following paragraphs. All the commands presented should be written in the "**trubal.dat**" command file. The file "**trubal.dat**" should always start with a START or RESTART command. Examples of command files can be found in section B.10.

TRUBAL-ACI will not run if any of the 19 output-data files having the extension "**.out**" exist in the working directory. This is because new files with these names are created by default at any TRUBAL-ACI run. All files with the extension "**.out**" should be removed from the working directory (or renamed) before each TRUBAL-ACI run.

When parameters (usually indicated by < > brackets) are arranged horizontally for a command, they must all be given except for optional parameters, denoted by square [ ] brackets. Parameters arranged vertically after a command denote the selection of options that may be given : any or all of these parameters may be given in any order. For example **Print B C I** will print the particles, contacts and general information respectively. Parameters that start with a lower-case stand for numbers: e.g. <nball> may be given as 100 and <a> may be given as 1.2e-7. Parameters and commands that start with an upper-case letter and are not enclosed by < > brackets should be typed literally (either in upper- or lower-case). The commands and option names may be typed in full, or truncated to the first three letters. For example, the command **PRINT CONTACTS** may be given as PRI CON, PRINT CONT or any other variation. Parameters may be separated by any number of spaces, commas, brackets or slashes.

The newly introduced commands and options to commands (that distinguishes TRUBAL-ACI from other existing TRUBAL versions at Aston) will be presented underlined (e.g. PLOT CFORCES).

The commands are divided into 7 main groups, according to their scope of usage. Only the commands in sections B.4, B.5 and B.6 are presented in alphabetical order. Most commands have options; presented below are only the commands and options used in this project.

B.2 START, RESTART AND STOP COMMANDS

Any simulation job (preparation, test, or image plot) with TRUBAL has to start with a START or RESTART command and stop with a STOP command.

START x_{max} y_{max} z_{max} **nbox nball nwall [Log]**

This command (or the **RESTART** command) must be the first one given to TRUBAL. The parameters x_{max}, y_{max} and z_{max} are the maximum dimensions of the working box volume in the x, y and z directions, respectively.
nbox is the number of boxes requested for the grid network, and **<nball>** is the maximum number of particles that may be needed. There is no problem if fewer particles are subsequently generated: the purpose of the **START** command is to allocate enough memory to hold all the required boxes and particles. The parameter **<nwall>** indicates the maximum number of walls that may be needed. The optional keyword **<Log>** turns the "log" facility on immediately: i.e. output is echoed to the output file "**trubal.out**" unless redirected.

STOP

Stops the program. The current state of the problem is not saved automatically. Use the **SAVE** command to do that before issuing the stop command.

RESTART [Filename]

A previously-saved problem is restored from the file **{Filename}**. If a file name is not given, a default file name of "**save.old**" is assumed. The command **RESTART** may only be given as the first command of a run or as the first command after a **NEW** command.

NEW

The program returns to the point at which it expects a **START** or **RESTART** command. The data for the current problem is lost from memory.

B.3 AUXILIARY COMMANDS

Several auxiliary commands were developed within this project to aid main commands: the sole purpose of these commands is to input different parameters needed by new options in the main commands.

FFF <a> <b> <c> <n>

FFO <a> <b> <n>

FFT <n> <m>

FRN <n>

Default for all these auxiliary commands' parameters is 0.0 (which must be specified).

On issuing them on their own, the above commands have usually no effect on a TRUBAL run. All these commands should therefore only be issued just before main commands, for example:
FFF 0.0 0.0 12.0 0
PLOT VELOCITY.
Whereas **<n>** and **<m>** should be inputted as integers, **<a>**, **<b>** and **<c>** should be given as real numbers. Information about what **<a>**, **<b>**, **<c>**, **<n>** and **<m>** represent

can be found at the relevant main commands that need them (usually plotting commands, as PLOT CLUSTERS, PLOT FORCES, etc).

B.4 CREATION AND PREPARATION OF AGGLOMERATES AND PLATENS/WALLS

AGGLOMERATE nagg x_c y_c z_c r_a

Defines a circular or spherical region of radius r_a centred at (x_c, y_c, z_c) in which particles are to be generated for the agglomerate number **nagg** (refer to the **AGENERATE** and **RGENERATE** commands); **nagg** takes values of 1 or 2 since a maximum of two circular/spherical agglomerates can be handled by the program at the moment.

AGENERATE isize mtyp nagg x_o y_o z_o dx dy dz

Particles of size type **isize** and material type **mtyp** are automatically generated in such a way that the lowest particle is at (x_o, y_o, z_o) and the others are placed at the specified incremental distance of **dx, dy, dz** in each of the coordinate directions from each other. nagg is the number of the agglomerate. Only particles which fall inside the specified region for the agglomerate (refer to the **AGGLOMERATE** command) are accepted. If no region was specified, the whole working region specified by (x_{max}, y_{max}, z_{max}) in the **START** command is filled with particles. This command is useful for generating regular packings.

DWALL [P d a b c] [V v_x v_y v_z] [M mtyp] [SE f v_{max} g]

This command creates a wall. In the first form, a plane wall which extends over the dimension of the working space is created. **P** defines a plane wall representing the equation ax + by + cz = d. Only walls parallel to one of the three planes x-y, y-z and x-z are handled in at the moment. This means that only one of the parameters a, b,c is non-zero for any wall. For a non-zero **a** for example, the ratio **d/a** then gives the x-intercept of a 'y-z' wall. In the 2-d case which handles only walls parallel to either the Ox or Oy axis, the equation reduces to **ax + by = d**, but a value of zero must still be specified for **c**. **V** gives the translational velocity of the wall (v_x, v_y, v_z) and **M** indicates the wall material type mtyp. The selection **SE** introduces servo control for the wall. **f** is the desired normal force on the wall. v_{max} is the maximum normal velocity allowed for the wall and **g** is the servo gain.

CREATE x y z v_x v_y v_z q_x q_y q_z isize mtyp

A sphere is created at location (x,y,z) with size type **isize** and material type **mtyp**. The x, y and z linear and angular velocity components for the sphere are given as v_x, v_y, v_z, q_x, q_y, q_z respectively. Currently, TRUBAL allows 10 size-types and 5 material-types. If the created particle overlaps existing particles, it is rejected.

RGENERATE <n> isize mtyp nagg
SEED <n>

<n> particles of size type **isize** and material type **mtyp** are randomly generated in a region previously specified by the **AGGLOMERATE** command or by default in the region specified in the **START** command. No effort is made to fit particles into gaps between other particles. If a candidate particle overlaps an existing particle, it is rejected and another is tried. Before issuing this command, a radius must already have been defined for the size type **isize.**

If several sizes of particles are to be combined in an assembly, the larger ones should be generated first since it is easier to fit small particles into gaps. **nagg** indicates the

agglomerate number for which the particles are generated - up to two agglomerates are handled at the moment. In the second form of the command **RGE SEED <n>**, no particles are generated, but the random number generator produces **<n>** numbers which are discarded. This is useful for obtaining different spatially-distributed samples with the same particles size distribution.

B.5 SPECIFYING PARTICLE AND PLATENS/WALL PROPERTIES

Particle material type, particle size type and wall material type were specified by particle and wall creation command respectively. Some platen/wall properties are mandatory introduced in their creation command (e.g. wall mass, see previous paragraph).

AWALL <n> [**P** d a b c] [**V** v_x v_y v_z] [**M** mtyp] [**SE** f v_{max} g]

This command alters the position (**P**), velocity (**V**) or material type (**M**) of wall **<n>**. **SE** sets the servo control for the wall. See **DWALL** command for the definition of the parameters. **P**, **V**, **M** and **SE** are all selectable but the wall number **<n>** must be logically specified.

COHESION gamma mtyp

gamma is entered as the surface energy for particles of material type **mtyp**.

DAMPING frac freq imass istiff iswitch

Damping is specified in terms of the Rayleigh damping parameters: **frac** is the fraction of critical damping at the modal frequency **freq**. Rayleigh damping involves mass-proportional (global) damping and stiffness-proportional (contact) damping: the former may be switched off by giving **imass** as 1, and the latter by giving **istiff** as 1. Otherwise these parameters should be set to zero for full Rayleigh damping. The contact damping must, however, never be switched off in simulations. The damping parameters are specified for particle-to-particle contact if **iswitch** is given as 1 and for particle-to-wall contact if **iswitch** is given as 0.

DENSITY <d> mtyp

<d> is taken as the mass density of all particles of material type **mtyp**.

FRACTION <f>

The fraction of critical time-step is set to **<f>**. The critical time step (Δt_{crit}) is based on the Rayleigh wave speed. The time it takes for the wave to traverse each particle is computed and the minimum of these times is used as (Δt_{crit}). The default value of **<f>** is 1.0 and if numerical instability is suspected, the value of **<f>** should be reduced.

FRICTION amu mtyp

The friction coefficient is set to **amu** for particles or walls of material type **mtyp**. For two different material types in contact, the smaller of the two coefficients is used in the program.

GRAVITY gx gy gz

Gravitational accelerations are prescribed for each of the coordinate directions. If **gx**, **gy** and **gz** are entered as equal quantities, a centripetal gravity field of the specified value is simulated (having as centre the existing particles or agglomerate's centre of mass). The centripetal gravity field is used in the agglomerate preparation process. (Note that gravity is not meaningful when full periodic boundaries are in effect.)

PRA **<v>** **<mtyp>**

Specifies the Poisson ratio value <v> for material-type **<mtyp>**.

RADIUS **<r>** **<isize>**

<r> is enered as the radius of particles of size type **<isize>**.

VELOCITY v_{1x} v_{1y} v_{1z} **ivd**
v_{1x} v_{1y} v_{1z} v_{2x} v_{2y} v_{2z} **ivd**

This command is used to specify the velocity of a particle or particles in an agglomerate. The parameters v_{1x}, v_{1y}, v_{1z} specify the x, y and z components of the desired velocity for particles in the first agglomerate, and where there are two agglomerates, v_{2x}, v_{2y}, v_{2z} specify the velocity components for the second agglomerate's particles. The parameter ivd is used to indicate whether the agglomerate(s) is (are) being impacted (**ivd**=1) or not (**ivd**=0). In the former case, a flag is set in the program which ensures that any secondary contacts formed after impact use a base value of surface energy (of 0.03 J/m2) corresponding to van der Waal's forces of attraction only. The flag can also be set by issuing the new command **CHF**.

YMD **<ymod>** **<mtyp>**

Specifies a Young's modulus value **<ymod>** for all particles of material-type **<mtyp>**.

2-D

This command causes **TRUBAL** to operate in two-dimensional mode. The particles are still regarded as spheres, but they are constrained to move in the xOy plane only. Although the equations of motion are truncated to two dimensions, the force-displacement calculation (subroutine HFORD) still operates in three dimensions. This could be modified to improve running speed. In 2-d mode, the generation routine sets the z coordinate of all particles to the same value - corresponding to the centre of the box volume in the z direction. Only one box should be specified in the z direction, although **TRUBAL** will not complain if more are requested.

3-D

This command brings TRUBAL-ACI back in the three-dimensional mode.

B.6 TEST SIMULATIONS

Using TRUBAL-ACI, simulations of diametrical compression, double impact and free-fall impact tests can be carried out and closely monitored. Each test is dynamic and thus simulated as a succession (sequence) of thousands and thousands of cycles. No test simulation is possible without issuing the CYCLE command.

CYCLE **<n>**

The program is set to execute **<n>** calculation cycles.

TCYCLE **<n>**

Same as the CYCLE command but it does not run several initialising subroutines. It is better and faster to use TCYCLE command, and to leave CYCLE command just for the start of simulation and for cycling just after a state has been saved (see the examples in Appendix B).

GRID **ed11 ed22 ed33 ed12 ed23 ed31**

The strain-rates e11, e22, e33, e12, e23, e31, of periodic space are set. Note that the strain rates e23 and e31 are not used although they should be entered in the **GRID** command as zero. The components e11, e22 and e33 cause the periodic volume to change shape. However the component e12 does not distort the periodic volume in shear; rather there is a step in x or z displacement between the bottom y-boundary and the top y-boundary. This step in shear is printed out when the **PRINT GRID** command is given.

ISET <k> <iadd>

The integer **<k>** is inserted into the main memory array IA(I) at address **<iadd>**. Great caution is needed when using this command.

LOG **ON**
OFF

The command **LOG ON** causes all commands, comments, error messages, etc., to be reproduced on a file **"trubal.out"**. The command **LOG OFF** suppresses this echo function, except for output from the **PRINT** command.

RESET

Accumulated rotations are set to zero. This has no effect on the mechanical behaviour, since only incremental rotations are used in the calculation. Note that the rotations are simply the summations, over time, of the incremental rotations.

RSET **<r> <iadd>**

The real number **<r>** is inserted into the main memory array IA(I) at the address **<iadd>**. Great caution is needed when using this command.

SAVE **[Filename]**

The current problem (simulation) state is saved in the file **Filename**. If a file name is not given, a default file name **"save.new"** is assumed. If a file name is specified that already exists, the existing data is over-written. The saved state records all positions, velocities, forces, options and so on, at a given stage in a run; it corresponds to a "snapshot" at a single point in time. The **SAVE** command does not record the sequence of commands used to reach a state.

ZERO **<izf>**

Sets the particle velocities (translational and rotational) to zero. If **<izf>** is given as 1, in all subsequent cycles, the particle velocities are set to zero after each cycle. Use **<izf>** = 0 to over-ride this.

B.7 DATA OUTPUT

Some simulation data is output automatically, while carrying out simulations - into files "trubal.out" and "kw.out". Using printing commands, additional simulation data can be printed in "trubal.out", other output files and/or on the screen.

Most commands used to output data consist of over two words, the first of them being PRINT. For inputting parameters for certain options, some printing commands need auxiliary commands to be issued just before them.

PRINT DATA

This command outputs various information into 18 output files and on the screen:
- into file "**d0.out**": cycle from start, vertical displacement of bottom platen [m], vertical displacement of top platen [m], vertical position of bottom platen [m], vertical position of top platen [m], agglomerate's minimum coordinates (OX, OY and OZ components) [m], agglomerate's maximum coordinates (OX, OY and OZ components) [m];
- into file "**d1.out**": cycle from start, total number of contacts, agglomerate's coordination number, agglomerate's porosity, agglomerates maximum dimension along the OX, OY and OZ axis [m], agglomerate's strain along the OX, OY and OZ axis [%], total kinetic energy of particles [J/m^2], average normal contact force [N];
- into file "**d2.out**": cycle from start, resultant force on bottom platen [N], resultant force on top platen [N], average compressive contact force [N], average tensile contact force [N], maximum compressive contact force [N], maximum (in absolute value) tensile contact force [N], work input by the top platen [J], velocity of the top platen (along OY axis) [m/s], average particle velocities along OX, OY and OZ axis [m/s];
- into file "**d3.out**": cycle from start, total number of contacts, number of particles in the largest cluster, number of particles in the second largest cluster, number of particles in the third largest cluster, number of particles in the fourth largest cluster, number of singlets, number of doublets, number of triplets, number of quadruplets, maximum particle velocity [m/s], average particle velocity [m/s], number of clusters consisting of over 2 particles, number of clusters consisting of over 1 particle (non-singlets), elapsed time [s], work done in breaking contacts [J], damage ratio;
- into file "**d5.out**": cycle from start, number of "peeled" contacts, percentage of peeled contacts [%], number of spinning particles, percentage of spinning particles [%], top platen's kinetic energy [J];
- into file "**d6.out**": cycle from start, total work done by normal contact forces [J], total work done by tangential contact forces [J], total particle kinetic energy of translation [J], total particle kinetic energy of rotation [J], energy dissipated by contact damping [J], energy dissipated by global damping [J], total work done by normal particle-particle contact forces [J], total work done by tangential particle-particle contact forces [J], work dissipated by adhesive peeling [J], total work done by normal particle-platen contact forces [J], total work done by tangential particle-platen contact forces [J];
- into file "**d6_.out**": cycle from start, work dissipated in tangential particle-particle sliding [J], work dissipated in tangential particle-particle microslip [J], work dissipated in particle-particle pre-peeling [J], work dissipated in adhesive peeling [J], work dissipated in tangential particle-platen sliding [J], work dissipated in tangential particle-platen microslip [J], work dissipated in particle-platen pre-peeling [J], energy released through gravity potential [J], energy dissipated by contact damping of normal forces [J] and energy dissipated by contact damping of tangential forces [J];
- into file "**d7.out**": cycle from start, total number of contacts, total contacts with platens, contacts with bottom platen, contacts with top platen, number of tensile contacts, number of compressive contacts, vertical force on bottom platen [N], vertical force on top platen [N], strain of platens [%], elapsed time [s], damage ratio, work inputted by the bottom platen [J], work inputted by the top platen [J], total work inputted by platens [J];
- into file "**d9.out**": cycle from start, cumulated resultant forces on platens [N], resultant force on bottom platen [N], resultant force on top platen [N], OX component of force on bottom platen [N], OY component of force on bottom platen [N], OZ component of force on bottom platen [N], OX component of force on top platen [N], OY component of force on top platen [N], OZ component of force on top platen [N], OY component of force on bottom platen [N]*, OY component of force on bottom platen [N]*; (* these forces are calculated differently: by summing up the particle-platen contact forces);
- into file "**d11.out**": total number of compressive forces and their distribution in 20 bands of magnitude, the minimum compressive force [N] and the maximum compressive force [N];

- into file "**d12.out**": total number of tensile forces and their distribution in 20 bands of magnitude, the minimum compressive force [N] and the maximum tensile force [N];
- into file "**d21.out - d25.out**": cycle from start, the individual values of the normal particle-platens contact forces (maximum of 24 with each platen) [N];
- on the screen: cycle from start, total number of contacts, total kinetic energy of particles [J], number of contacts with bottom platen, number of contacts with top platen, number of compressive contacts, number of tensile contacts, vertical force on bottom platen [N], vertical force on top platen [N], strain of agglomerate along OX and OY [%], number of particles in largest cluster, number of particles in second largest cluster, number of singlets, maximum particle velocity [m/s], average particle velocity [m/s], platen velocity (for diametrical compression and double impact) or agglomerate velocity (for free-fall impact) along OY (loading axis) [m/s], total work inputted by platens [J];

PRINT DISPLACEMENTS

Outputs into file "**d4.out**" the following information about each particle: particle number, translational displacements (OX, OY and OZ components) [m], angular displacements, angular velocity, number of contacts with other particles, number of contacts with platens (usually maximum 1), number of peeled contacts, particle radius [m], and indication if particle is allowed to spin (if allowed flag will be $\neq 0$).

PRINT PPP

This command should be issued at the very start of a simulation, as it initialises (to 0.0 usually) many of the data that is to be later printed into the files "**d1.out - d25.out**" (using command PRINT DATA).

The following printing commands output simulation data for the particular state (problem) into the file "**trubal.out**". Several keywords may be given on the same line (e.g. PRINT BALLS CHD INFO). To reduce the amount of output, the **WINDOW** command may be given prior to the **Print** command.

PRINT BALLS

Outputs detailed information about particles (data from the particle array).

PRINT CHD

Outputs information about the contact forces.

PRINT CHISTORY

Outputs general information about particle-particle contacts.

PRINT CLUSTER

Outputs information about clusters.

PRINT CONTACTS [**All**]

Outputs detailed information about contacts. The optional keyword {**All**} requests that all contacts are printed, rather than just those taking load, which is the default.

PRINT ENERGY

Outputs information about most energies of interest.

PRINT ENTRIES

Outputs information about boxes.

PRINT GRID

Outputs information about size of the periodic cell.

PRINT INFO

Outputs summary general information.

PRINT GINFO
Outputs more detailed general simulation information.

PRINT MAP
Outputs all the data stored in the memory map.

PRINT PARTITIONS
Outputs information about the stress partitions.

PRINT STRESS
Outputs information about the stress tensor.

FFO 0.0 0.0 <n>
PRINT BDA
Outputs, for each particle, the data stored in the particle array at position **<n>**.

FFO 0.0 0.0 <n>
PRINT WDA
Outputs, for each platen/wall, the data stored in the wall array at position **<n>**.

FFO 0.0 <b> <n>
PRINT CDA
Outputs, for each contact, the data stored in the contact array at position **<n>**. For <b> = 1.0 it prints information about all contacts, whereas for **<b>** = 4.0 it only prints information about broken contacts (gaps, actually). For **<b>** = 2.0 it only prints information about all compressive contacts, and for **<b>** = 3.0 it only prints information about all tensile contacts.
Section B.9 presents details about the data stored in the particle, wall and contact arrays.

B.8 PLOTTING OF IMAGES

Most commands used to output data consist of over two words, the first of them being **PLOT**. For inputting parameters for certain options, some effective plotting commands need auxiliary commands to be issued just before them. The plotting commands produce either 2-d (xOy) or 3-d graphic images using the "Personal GraPHIGS" graphics package for IBM RS/6000 workstations.

The commands used in plotting of images are presented in three main groups: main commands, commands for analysing slices, commands for analysing the fracture surface, commands for analysing certain clusters.

Enhancements have been carried out for all plotting subroutines so that the important simulation data corresponding to each plot (such as data file used, simulation cycle, the numbers of particles, state used, contacts, forces, velocities, displacements, etc.) to be printed on the plot, next to the image.

For obtaining a clearer "feel" of a 3-D image, it was decided in this project that actually there is a need for minimum 3 plots to be produced - usually a view from front, one from right and one from top (see Fig. B.1. showing the typical agglomerate simulated and the three axes of coordinates, and Fig. B.2. presenting a typical three-view-plot image).

B.8.1 Main Commands

¤ *Plotting all particles:*

PLOT BALLS
Plots all the particles as spheres (3-d) or shaded circles (2-d).

PLOT CIRCLES

Plots the particles as wireframe spheres (3-d) or unshaded circles (2-d).

¤ *Plotting clusters colour-coded according to their size (best for distinguishing debris):*

PLOT CLUSTERS **[<n1> <n2>]**
[Bak]

Plots different fragments and debris in different colours to help identify the fragmentation pattern. The default colours for plotted clusters (best suited for distinguishing debris) will be as follows:

- red - for clusters having over 200 particles
- green - for clusters having 36 - 200 particles
- pink - for clusters having 21 - 35 particles
- dark blue - for clusters having 9 -20 particles
- dark blue - for clusters having 5 - 8 particles
- yellow - for clusters having 3 - 4 particles
- black - for clusters having 1 - 2 particles (singlets and doublets)

If the optional parameters **<n1>** and **<n2>** are given, only fragments having a number of particles between **<n1>** and **<n2>** are plotted, otherwise all fragments are displayed. By specifying **<n1>** = **<n2>**, a fragment of a specific size can be displayed. The optional keyword **Bak** specifies that only particles in the cluster which carry the largest contact forces (relative to a force level scaled to the current maximum force) are displayed.

¤ *Plotting specified clusters colour-coded according to their size (best suited for distinguishing between up to 5 specified clusters):*

FFF <a> <b> <c> 100000
FFO <d> <e> 100000
PLOT CLUSTERS

Plots specified fragments and debris in different colours to help identify the fragmentation pattern. To specify a cluster, the total number of particles contained in it should be known and entered. Up to 5 clusters can be entered as fractional parameters for parameters **<a>**, **<b>**, **<c>**, **<d>**, and **<e>**. There are 5 options with this command group:

•(1) For 1 specified cluster, i.e.

FFF <a> 0.0 0.0 100000
PLOT CLUSTERS

parameter **<a>** should actually be the number of particles in the cluster. The clusters will be coloured as follows:

- red - for the specified cluster, having **<a>** particles
- green - for clusters having over 36 particles
- pink - for clusters having 21 - 35 particles
- dark blue - for clusters having 9 -20 particles
- dark blue - for clusters having 5 - 8 particles
- yellow - for clusters having 3 - 4 particles
- black - for clusters having 1 - 2 particles (singlets and doublets)

•(2) For 2 specified clusters, i.e.

FFF <a> <b> 0.0 100000
PLOT CLUSTERS

parameters **<a>** and **<b>** should actually be the numbers of particles in the first and second specified clusters. This option is best suited for agglomerates fractured in two large clusters. The clusters will be coloured as follows :

- red - for the first specified cluster, having **<a>** particles
- green - for the second specified cluster, having **<b>** particles
- pink - for clusters having over 21 particles
- dark blue - for clusters having 9 -20 particles
- dark blue - for clusters having 5 - 8 particles
- yellow - for clusters having 3 - 4 particles

- black - for clusters having 1 - 2 particles (singlets and doublets)

•(3) For 3 specified clusters, i.e.

FFF <a> <b> <c> 100000

PLOT CLUSTERS

parameters **<a>**, **<b>** and **<c>** should actually be the numbers of particles in the first second, and third specified clusters. This option is best suited for agglomerates fractured in three large clusters. The clusters will be coloured as follows :

- red - for the first specified cluster, having **<a>** particles
- green - for the second specified cluster, having **<b>** particles
- pink - for the third specified cluster, having **<c>** particles
- dark blue - for clusters having over 21 particles
- dark blue - for clusters having 9 - 20 particles
- yellow - for clusters having 3 - 8 particles
- black - for clusters having 1 - 2 particles (singlets and doublets)

•(4) For 4 specified clusters, i.e.

FFF <a> <b> <c> 100000

FFO <d> 0.0 0.0 100000

PLOT CLUSTERS

parameters **<a>**, **<b>**, **<c>** and **<d>** should actually be the numbers of particles in the first second, third and fourth specified clusters. This option is best suited for agglomerates fractured in four large clusters. The clusters will be coloured as follows:

- red - for the first specified cluster, having **<a>** particles
- green - for the second specified cluster, having **<b>** particles
- pink - for the third specified cluster, having **<c>** particles
- dark blue - for the fourth specified cluster, having **<d>** particles
- dark blue - for clusters having over 20 particles
- yellow - for clusters having 3 - 20 particles
- black - for clusters having 1 - 2 particles (singlets and doublets)

•(5) For 5 specified clusters, parameters **<a>**, **<b>**, **<c>**, **<d>** and <e> should actually be the numbers of particles in the first second, third, fourth and fifth specified clusters. The clusters plotted will be coloured as follows :

- red - for the first specified cluster, having **<a>** particles
- green - for the second specified cluster, having **<b>** particles
- pink - for the third specified cluster, having **<c>** particles
- dark blue - for the fourth specified cluster, having **<d>** particles
- dark blue - for the fifth specified cluster, having **<e>** particles
- yellow - for clusters having over 4 particles
- black - for clusters having 1 - 4 particles (singlets and doublets)

¤ *Plotting contacts and distinguishing between new, broken, existing, sliding, peeled and readhered contacts:*

PLOT CND [NEW] [DEL] [EXI] [SLI] [PEL] [REA] [ALL]

Plots the connection diagram. This is a plot that results from comparing two states of the agglomerate and identifying contacts which are present in both states as existing contacts (**EXI**), contacts which are present in the new state but not in the old as new contacts (**NEW**) and contacts in the old state which are not in the new state as broken contacts (**DEL**). Sliding contacts at that moment are also identified if the **SLI** option is specified. Re-adhered contacts are plotted by option **REA**, whereas peeled contacts are given by option **PEL**. Note that re-adhered contacts include the new contacts. There usually are some readhered contacts that are already peeled. The **ALL** option will print the new, broken, existing and sliding contacts. The centres of particles with these contacts are joined with lines of different colours to yield the connection diagram. The colours used for the contacts are the following: existing - green, broken - red, new - yellow, sliding - dark blue, peeled - black and readhered - light blue.

¤ *Distinguishing the locations of the broken contacts in top views:*

PLOT CND DEL

This command is usually issued for obtaining a top view of the broken contacts in the agglomerate (as the platens are not asked to be plotted). For a clearer image, the contacts broken in the bottom half of agglomerate are automatically coloured black, while the contacts broken in the top half are coloured red.

FFF 0.0 4.0 0.0 0
PLOT CND DEL

Same as the above, but 4 coloured sections are used instead of two: red, green, dark blue and black (top of top half, bottom of top half, top of bottom half and bottom of bottom half).

¤ *Plotting contacts as dots or "crack"-lines:*

FFT <a> 0
PLOT CND .....

Plots the connection diagram similar to the above, but not showing contacts as lines uniting the centres particle (but as dots or "crack"-lines).
•(1) For **<a>** = 1, plots the contact diagram with contacts marked as dots instead of lines uniting centres of particles in contact.
•(2,3,4) For **<a>** = 2, **<a>** = 3 or **<a>** = 4, plots the contact diagram with contacts drawn as "crack"-lines, i.e. lines perpendicular on the direction passing through the centres of particles in contact. **<a>** = 2 is for front view, **<a>** = 3 is for right view, and **<a>** = 4 is for top view.

¤ *Plotting the broken contacts colour-coded according to their gap magnitude - useful for analysing the "crack opening" process:*

FFF <a> 3.0 <c> 99
PLOT CND DEL

Plots the broken contacts distinguishing between the actual magnitudes of the interparticle gaps. **<a>** represents the maximum gap magnitude (in meters); its value is automatically displayed on the screen any time the command PLOT CND is issued. The number **<c>** is the ratio of minimum gap magnitude (for a certain colour) to the maximum gap magnitude. Largest gaps are plotted in black, medium gaps in red and smallest gaps in green colour.

¤ *Plotting the already peeled contacts at the start of a simulation with the PLOT CND PEL command:*

APEL
PLOT CND PEL

Plots the contacts peeled during the simulation (as in the main PLOT CND command already discussed) plus the contacts that were already peeled at the start of simulation.

¤ *Plotting the final average particle displacements vectors:*

PLOT DISPLACEMENTS

Plots the particles' displacements. This is a plot that results from comparing two states of the agglomerate and identifying the initial and final positions of particles centres. Initial and final position for each particle are joined with a line symbolising the average displacement vector; the direction of the vector is marked with a distinct coloured (red) dot.

¤ *Colour-coding particle displacements according to their magnitude:*

FFF <a> <b> <c> <n>
PLOT DISPLACEMENTS

Same as above but 3 colour bands and line thickness are used to distinguish between different displacement magnitudes. **<a>** and **<b>** are the ratios of the minimum displacements (to be plotted in the first and second bands) to the maximum displacement's magnitude. **<a>** should be given larger than **<b>**. If **<c>** = 0.0 the plot uses the default thickness. If **<c>** ≠ 0.0, the value of **<c>** will be a thickness coefficient (multiplier) and the value of parameter **<n>** will trigger one of the following 5 options:

- (1) For **<n>** = 1 lines in first band (representing largest displacements) will be plotted three times thicker than lines in third band.
- (2) For **<n>** = 2 lines in first band (representing largest displacements) will be plotted four times thicker than lines in third band.
- (3) For **<n>** = 10000 only displacements in the first and third band of magnitude will be plotted.
- (4) For **<n>** = 20000 only displacements in the first band of magnitude will be plotted.
- (5) For **<n>** = 30000 only displacements in the third band of magnitude will be plotted.

¤ *Plotting all the interparticle contact forces, distinguishing between compressive and tensile:*

PLOT FORCES

Plots contact forces as lines oriented in the direction of the force. Compressive and tensile forces are identified with different colours (green and red respectively). The thickness of each force line is proportional to the magnitude of the contact force (scaled to the current maximum force).

¤ *Plotting only the largest interparticle contact forces, distinguishing between compressive and tensile:*

FFO <a> <b> 0
PLOT FORCES

Plots only contact forces larger than a certain value. The maximum compressive and tensile forces are first determined. **<a>** is ratio of the smallest compressive force plotted to the maximum compressive force, whereas **<b>** is ratio of the smallest tensile force plotted to the maximum tensile force.

FFO <a> <b> <n>
PLOT FORCES

Plots only the largest contact forces: **<n>** compressive contact forces and **<n>** tensile contact forces (the largest ones). **<a>** and **<b>** are entered just as estimated values for the ratios of the largest **<n>** compressive/tensile forces plotted to the maximum compressive/tensile force. The actual values for these two ratios are automatically determined by TRUBAL-ACI and printed on the plot (by the image).

¤ *Plotting all the interparticle compressive contact forces:*

PLOT CFORCES

Same as PLOT FORCES, but only plots the compressive contact forces (green).

¤ *Plotting only the largest compressive contact forces:*

FFO <a> 0.0 0
PLOT CFORCES

Plots only compressive contact forces larger than a certain value. The maximum compressive forces are first determined. **<a>** is ratio of the smallest compressive force plotted to the maximum compressive force.

FFO <a> 0.0 <n>
PLOT CFORCES

Plots only the **<n>** largest compressive contact forces. **<a>** is entered just as an estimated value for the ratio of the largest **<n>** compressive forces plotted to the maximum compressive force. The actual values for the ratio is automatically determined by TRUBAL-ACI and printed on the plot.

¤ *Plotting all the interparticle tensile contact forces:*

PLOT TFORCES

Same as PLOT FORCES, but only plots the tensile contact forces (red).

¤ *Plotting only the largest tensile contact forces:*

FFO 0.0 <b> 0
PLOT TFORCES

Plots only tensile contact forces larger than a certain value. The maximum tensile forces are first determined. **<b>** is ratio of the smallest tensile force plotted to the maximum tensile force.

FFO 0.0 <b> <n>
PLOT TFORCES

Plots only the **<n>** largest tensile contact forces. **<b>** is entered just as an estimated value for the ratio of the largest **<n>** tensile forces plotted to the maximum tensile force. The actual values for the ratio is automatically determined by TRUBAL-ACI and printed on the plot.

¤ *Plotting contacts colour-coded according to the force they are carrying:*

FFO 0.0 0.0 500000
FFF <a> <b> <c> 20
PLOT FORCES or PLOT CFORCES or PLOT TFORCES

This command group is able (through colour-coding) to distinguish between compressive and tensile contacts and between different magnitudes of resultant contact forces. **<a>, <b>** and **<c>** are ratios to the maximum contact force used to colour-code contacts (in 4 bands) according to the magnitude of the force they are carrying (the contcts carrying the largest force are represented in red).

¤ *Plotting all velocity vectors of particles:*

PLOT VELOCITIES

Plots all velocity vectors of particles, scaled down from the value of the maximum velocity value. The vector's directions are coloured green, whereas the vector's arrow is marked with a red dot.

¤ *Plotting all velocity vectors of particles with the possibility of scaling:*

FFF 0.0 0.0 <a> 0
PLOT VELOCITY

Plots all velocity vectors of particles same as above, but the parameter <a> allows the user to scale up or down the plotted lengths of velocity vectors. The default value for <a> is 3.0.

¤ *Colour-coding velocity vectors according to their direction and sense:*

FRN <n>
PLOT VELOCITIES

Plots all velocity vectors of particles same as above, but using more colours, to easier distinguish their direction and sense. Default for **<n>** is 11 (one colour only). See Section B.6 for how this command group helps to identify the large fragments (in the largest cluster) by using a proper choice of the **<n>** parameter (for simulation states after fracture). There are 5 options for specifying the **<n>** parameter:

•(1) For **<n>** = 0, the velocity vectors having the sense towards the negative OX axis will be colour-coded light blue; all the other ones will be colour-coded green.

•(2) For **<n>** = 5, the velocity vectors having the sense towards the negative OZ axis will be colour-coded light blue; all the other ones will be colour-coded green.

•(3) For **<n>** = 2, the velocity vectors having the sense towards the negative OY axis will be colour-coded light blue; all the other ones will be colour-coded green.

•(4) For **<n>** = 1, the velocity vectors having the sense towards the negative OX axis and positive OZ axis will be colour-coded light blue; all the other ones will be colour-coded green.

•(5) For **<n>** = 4, the velocity vectors having the sense towards the negative OX axis and negative OZ axis will be colour-coded light blue; all the other ones will be colour-coded green.

•(6) For **<n>** = 3, the velocity vectors will be colour-coded in 4 distinct colours, according to their direction and sense relative to the 4 principal quadrants of the plane xOz. (This option can be used to identify fracture in 4 large fragments).

¤ *Plotting all the platens:*

PLOT WALLS

Plots all the existing platens/walls as black finite planes with green edges.

¤ *Plotting only certain platens:*

WNO <n> <m>
PLOT WALLS

Same as above, but plots only specified platens. **<n>** and **<m>** are parameters for entering the platens to be plotted (their order of creation number). For instance, WNO 2 3 / PLOT WALLS will plot the 2nd and 3rd created platens.

¤ *Combined command: plotting both particles and the interparticle contact forces:*

PLOT CFB

This actually is an overlap plot of PLOT BALLS and PLOT FORCES (see the comments on the two main commands).

B.8.2 Commands For Analysing Slices Through An Agglomerate

FFO <a> <b> n
PLOT CND .....

Plots different contacts (see the main PLOT CND command) residing in an agglomerate slice, rather than for the whole agglomerate. The volume of the slices is determined by "cutting" the agglomerate with two parallel planes and "throwing away" the particles not residing between the planes. Parameters **<a>** and **<b>** must represent the planes' coordinates (measured from agglomerate's centre, but in opposite directions). As the two parallel "slicing" planes are parallel with one of the three axes of coordinates, there are three cases for slice plots:

•(1)For **<n>** = 1, plots slices created by planes parallel to the vertical yOz plane of coordinates.

•(2)For **<n>** = 2, plots slices created by planes parallel to the horizontal xOz plane of coordinates.

•(3)For **<n>** = 3, plots slices created by planes parallel to the vertical yOx plane of coordinates.

Examples:

FFO <a> <b> 3
PLOT CND
This plots a typical middle slice from the agglomerate obtained with two planes parallel to the vertical yOx plane of coordinates: a plane through the back half of agglomerate (at distance **<a>** from its centre) and a plane through the front half of agglomerate (at distance **<b>** from its centre).

FFO <a> 1000.0 3
PLOT CND
This plots an end (back) slice from the agglomerate obtained with a plane parallel to the vertical yOx plane of coordinates ("cutting" a slice from the back half of agglomerate).

FFO <a> 1000.0 3
PLOT CND
This plots a slice from the agglomerate obtained with two planes parallel to the vertical yOx plane of coordinates: a diametral plane and a plane through the back half of agglomerate.

FFO 1000.0 0.0 3
PLOT CND
This plots the front half of the agglomerate only (obtained by slicing the agglomerate with a diametral plane parallel to the vertical yOx plane of coordinates).

B.8.3 Commands For Analysing Fracture

Some agglomerates under diametrical compression, double impact or free-fall impact tests break up into large fragments. The exact moment of breakage can be easily observed by analysing the PLOT VELOCITIES image: the velocities of particles in any large fragment should be almost parallel (showing that all particles in fragment move in the same direction). The problem is that, generally, large fragments only completely separate into large clusters long after the breakage moment - making difficult to follow the fracture mechanism. Due to interlocking, particles in a large fragment may maintain, for quite long duration after fracture, several contacts with another large fragment. A technique for identifying, separating and analysing large fragments is, therefore, needed in TRUBAL. The procedure was devised and developed in this project and is described below.

Using PLOT VELOCITIES images, the exact moment of breakage should be determined. Using the FRN <n> / PLOT VELOCITIES command group (see section B.8.1), the fragments can be identified by observing the vector colour-coding. Information about the fragments should then be saved into a file "**particles.sav**". This is done automatically by using the

SAP

command after restarting the state at which agglomerate broke up.

Having the "**particles.sav**" file in the working directory, the fracture behaviour of agglomerate can be analysed by simply restarting any state (before or after the fracture moment) and issuing the command:

GEP

The **GEP** command only loads the information existing in the "**particles.sav**" file for use later (when issuing the commands below) in order to distinguish which particles belong to the future (or already existing) large fragments.

Note: after issuing the SAP and GEP commands, the FRN command should not be used (as the parameter it would enter is already known).

¤ *Plotting contacts on the fracture surface:*

FFF <a> <b> 0.0 300
PLOT CND

Plots only the interparticle contacts (colour-coded according to their history - see main PLOT CND command) on the fracture surface. There are a total of 4 options:

•(1) For **<b>** ≠ 5.0 and **<a>** = 10.0, plots all contacts that initially existed between the two largest fragments: e.g. existing (green), broken (red).

•(2) For **<b>** ≠ 5.0 and **<a>** = 11.0, plots all contacts that initially existed between the two largest fragments: plus the contacts between the analysed (left) large fragment and debris.

•(3) For **<b>** = 5.0 and **<a>** = 10.0, similar to (1) but does not plot the contacts still bridging the two large fragments at the reference (fracture) state.

•(4) For **<b>** = 5.0 and **<a>**= 11.0, similar to (2) but does not plot the contacts still bridging the two large fragments at the reference (fracture) state.

•(5) For **<a>**= 1.0 similar as above, but plots all contacts that initially existed between the two largest clusters.

•(5) For **<a>**= 2.0 similar as above, but plots all contacts that initially existed between the three largest clusters.

¤ *Plotting contacts on the fracture surface colour-coded according to the force they are carrying:*

FFO 0.0 0.0 500000
FFF <a> <b> <c> <n>
PLOT FORCES or PLOT CFORCES or PLOT TFORCES

This command group plots only the contacts on the fracture surface and is able (through colour-coding) to distinguish between compressive and tensile contacts and between different magnitudes of normal and tangential (compressive) contact forces. **<a>**, **<b>** and **<c>** are ratios to the maximum contact force used to colour-code contacts according to the magnitude of the force they are carrying (the contcts carrying the largest force are represented in red). Depending on the choice of parameter **<n>**, there are 6 options:

•(1) For <n> = 10 plots contacts on the fracture surface colour-coded according to the magnitude of their normal compressive force.

•(2) For <n> = 11 plots contacts on the fracture surface colour-coded according to the magnitude of their tangential compressive force.

•(3) For <n> = 10 plots contacts on the fracture surface colour-coded according to the magnitude of the ratio between their tangential and normal compressive forces.

•(4) For <n> = 12 plots contacts on the fracture surface colour-coded according to whether they are tensile or compressive.

•(5) For <n> = 13 is similar to option (1) but also plots the readhered contacts on the fracture surface.

•(6) For <n> = 1 plots contacts between the largest two clusters colour-coded according to the magnitude of their normal compressive force.

¤ *Plotting particles on the fracture surface:*

FFF <a> <b> <c> <n>
PLOT BALLS

Options (2a)-(5b) below only work if commands **SAP** and **GEP** were used in advance - see (*) - and if the agglomerate is to break into two large fragments. Option (1) needs the command PRINT CLUSTER to be declared in advance.

There are a total of 8 options, according to the specified values for a, b, c, and n:

•(1) For <n> = 200000 and <a> = 10.0 plots the largest two fragments (in red and green).

•(2a,b)For <n> = 200000, <a> = 1.0, <m> ≠ 1 and <m> ≠ 2 plots only the largest fragment on left (in red) and the particles on the fracture surface with other colours, as follows:

•(2a) for <b> ≠ 1.0, <b> ≠ 2.0 and <b> ≠ 3.0 plots particles on the fracture surface in contact with the other large cluster in green (existing) and black (broken);
•(2b) for <b> = 3 same as (2a) but additionally plots the particles on the fracture surface in contact with the debris in light blue (existing) and dark blue (broken).

•(3a,b)For <n> = 200000, <a> = 1.0, <m> = 1 plots the largest fragment on the left (in red), the debris (in yellow) and the particles on the fracture surface with other colours, as follows:

•(3a) for <b> ≠1.0, <b> ≠ 2.0 and <b> ≠ 3.0 plots particles on the fracture surface in contact with the other large cluster in green (existing) and black (broken);
•(3b) for <b> = 3 same as (2a) but additionally plots the particles on the fracture surface in contact with the debris in light blue (existing) and dark blue (broken).

•(4)For <n> = 200000, <a> = 1.0, <b> ≠ 1.0, <b> ≠ 2.0 and <b> ≠ 3.0, and <m> = 2 plots:
- the largest fragment on the left (in red),
- the debris as singlets and doublets (in yellow), triplets and quadruplets (in light blue), debris-clusters having between 5-20 particles (in dark blue) and debris-clusters having over 5 particles (in pink)
- the particles on the fracture surface in contact with the other large cluster in green (existing) and black (broken).

•(5a) For <c> = 1 similar to (2a) but does not plot the particles on the fracture surface which had contacts with the other large cluster at the reference state.
•(5b) For <c> = 2 similar to (2b) but does not plot the particles on the fracture surface which had contacts with the other large cluster at the reference state.

¤ *Separating the large fragments:*

Many times it is useful to clearly separate the large fragments resulting from the breakage of an agglomerate. To achieve this, the large fragments will have to be "artificially" moved away from each other.

PLOT CLUSTER .....
FRN <n>
BLOW <b> <m>

This command group will artificially move apart large fragments with a displacement = **DM** × **r**, where **r** is the average particle radius and **DM** is a displacement multiplier - that has to be entered as <b>. The choice of <n> for identifying the large fractures was already discussed in section B.8.1 and at the start of this section. Depending on the value of <m> there are two options:

•(1) For <m> ≠ 200000 the large fragments are just moved apart along the OX axis.
•(2) For <m> = 200000 the large fragments are moved apart in the xOz plane according to their velocity vectors (direction and sense).

After moving the large fragments apart, any plotting command can be used.

¤ *Analysing the largest fragments and the fracture surface at a certain moment without initially using the SAP and GEP commands:*

If there is no need for an evolutionary analysis, the agglomerate's largest fragments and the fracture surface can be analysed at any moment (state of simulation) without initially using the SAP and GEP commands. It is sufficient to issue the PRINT CLUSTERS command beforehand (to identify the largest existing clusters) and the FRN <n> / PLOT VELOCITIES commands group (to identify the largest fragments in the largest cluster). The following groups of commands can be used:

PRINT CLUSTERS
FRN <n>
PLOT VELOCITIES
FFF <a> <b> <c> 400
PLOT CND

Plots only the interparticle contacts on the fracture surface with their history (see main PLOT CND command - existing in green, broken in red, etc)

PRINT CLUSTERS
FRN <n>
PLOT VELOCITIES
FFF <a> <b> 0.0 200
PLOT CND

Plots all the interparticle contacts on the fracture surface, even if they existed and were broken before the start of simulation.

B.8.4 Commands For Analysing Certain Clusters

¤ *Plotting images of only certain clusters:*

PLOT CLUSTERS .....
CLF
PLOT VELOCITIES ..... , or
CLF
PLOT FORCES ....., or
CLF
PLOT CFORCES ...., or
CLF
PLOT TFORCES ....., or
CLF
PLOT DISPLACEMENTS.

To analyse the velocities or forces of only a certain part of the agglomerate, the certain part should be first identified and plotted with the command PLOT CLUSTERS ..... The new command **CLF** will set a flag only for the particles to be plotted. PLOT VELOCITIES, PLOT FORCES, PLOT CFORCES, PLOT TFORCES and PLOT DISPLACEMENTS can be then issued for plotting velocities, forces or displacements only for the selected particles.

B.9 DATA STORED IN TRUBAL'S PARTICLE, WALL AND CONTACT ARRAYS

For each particle, the PARTICLE ARRAY contains the following information:
P(1) - position vector : x component
P(2) - position vector : y component
P(3) - position vector : z component
P(4) - accumulated displacement : x component
P(5) - accumulated displacement : y component
P(6) - accumulated displacement : z component
P(7) - velocity vector : x component
P(8) - velocity vector : y component
P(9) - velocity vector : z component
P(10) - angular position : about x axis
P(11) - angular position : about y axis
P(12) - angular position : about z axis
P(13) - accumulated angular displacement : about x axis
P(14) - accumulated angular displacement : about y axis
P(15) - accumulated angular displacement : about z axis
P(16) - angular velocity : about x axis

P(17) - angular velocity : about y axis
P(18) - angular velocity : about z axis
P(19) - force sum : x component
P(20) - force sum : y component
P(21) - force sum : z component
P(22) - moment sum : about x axis
P(23) - moment sum : about y axis
P(24) - moment sum : about z axis
P(25) - size and material type stored as one (= itypm+64*ityps)
P(26) - number to identify to which large fragment the particle belongs
P(27) - applied particle force : x component | used in original for
P(28) - applied particle force : y component | specific tests
P(29) - applied particle force : z component | by Cundall
P(30) - identifies to which agglomerate the particle belongs (1 or 2)

For each platen/wall, the WALL ARRAY contains the following information:
W(1) - D | parameters in plane wall equations
W(2) - A | Ax + By + Cz = D
W(3) - B |
W(4) - C | (for the 2-d case, C=0.0)
W(5) - Normal force set by servo control for the wall
W(6) - Maximum normal velocity of the wall set by servo
W(7), W(8), W(9) -Wall velocity : x,y,z component
W(10) - empty
W(11) - measured normal force on the wall
W(12) - Code indicating wall type (1 for plane)
W(13) - mass of wall
W(14) - GAIN or servo control mechanism
W(15), W(16), W(17) - wall displacement increment - x,y,z components
W(18) - empty
W(19), W(20, W(21) - wall force - x,y,z components
W(22), W(23), W(24) - empty
W(25) - wall material type
W(26) - W(40) - empty

For each contact, the CONTACT ARRAY contains the following information:
C(1), C(2), C(3) - tangential force components
C(4) - normal force
C(5) and C(6) - addresses of the two balls comprising the contact
C(7), C(8), C(9) - tangential displacement components
C(10) - tangential displacement
C(11) - resultant tangential force
C(12) - T* (T-star) - the unloading point (historical maximum tangential force)
C(13) - T** (T-double star) - the reloading point (historical minimum tangential force)
C(14) - DD - cumulated value by which the system has fallen short of its equivalent point on a normal force curve
C(15) - peeling force
C(16) - value of γ - specific surface energy
C(17) - contact radius
C(18) - flag which indicates the direction of tangential loading
C(19) - empty
C(20) - flag used to determine when work done in breaking contact is to be calculated
C(21) - normal contact stiffness
C(22) - tangential contact stiffness
C(23) - link pointing to the next contact in the list

B.10 EXAMPLES OF COMMAND FILES USED IN THIS PROJECT

Create the random dense[1] agglomerate:

START 0.0014 0.0014 0.0014 64 4500 4 LOG
*
YMD 7.0E10 1
YMD 7.0E10 2
PRATIO 0.30 1
PRATIO 0.30 1
DENSITY 2.65E3 1
DENSITY 2.65E3 2
FRICTION 0.35 1
FRICTION 0.35 2
*
radius 0.315e-4 1
radius 0.310e-4 1
radius 0.300e-4 1
radius 0.295e-4 1
radius 0.290e-4 1
radius 0.285e-4 1
rgen seed 8000
agg 0.0008 0.00072 0.0008 0.00067
*
*Generate the 16 (largest) particles of radius R_1:
rgen 16 1 1 1
*Generate the 196 particles of radius R_2:
rgen 196 2 1 1
*Generate the 920 particles of radius R_3:
rgen 230 3 1 1
rgen 230 3 1 1
rgen 230 3 1 1
rgen 100 3 1 1
rgen 90 3 1 1
rgen 40 3 1 1
*Generate the 1596 particles of radius R_4:
rgen 70 4 1 1
rgen 30 4 1 1
.....
*Generate the 920 particles of radius R_5:
rgen 30 5 1 1
rgen 30 5 1 1
.....
*Generate the 236 particles of radius R_6:
rgen 6 6 1 1
rgen 5 6 1 1
.....
*Generate the 920 particles of radius R_7:
rgen 2 7 1 1
rgen 2 7 1 1
.....
*Save the 4000 created particles:
save S_4000DRY
*
*Introduce centripetal gravity and cycle to bring all particles together:
GRAVITY 9.8 9.8 9.8
CYCLE 1000
CYCLE 1000
.....

*Gradually introduce interface energy while taking off the centripetal gravity
*(also introduce global and contact damping and reduce the time-step):
FRACTION 0.01
DAMPING 0.3 0.5 0 0 1
COHESION 0.01 1
GRAVITY 9.5 9.5 9.5
CYCLE 1000
CYCLE 1000
.....
COHESION 0.03 1
GRAVITY 9.1 9.1 9.1
CYCLE 1000
CYCLE 1000
.....
.....
COHESION 1.0 1
GRAVITY 0.0 0.0 0.0
CYCLE 1000
CYCLE 1000
.....
*Bring damping to normal:
DAMPING 0.5 0.5 1 0 0
DAMPING 0.1 0.5 1 0 1
CYCLE 1000
CYCLE 1000
.....
FRACTION 1.0
*Save the dense[1] agglomerate:
save RM4T1A.
STOP

Free-fall impact test of the dense[1] agglomerate ("RM4T1A."), V=0.2 m/s:

RESTART RM4T1A.
*
*Print initial information and reset parameters for the output files:
print ginfo cluster data sss
FRO
*
*Set a fraction of the time-step:
FRACTION 0.1
*
*Place the agglomerate in a gravitational field:
GRAVITY 0.0 -9.8 0.0
*
*Create the bottom platen at a very small distance from the agglomerate:
DWALL P 1.900650E-04 0.0 1.0 0.0 M 2
*
*Set the vertically downwards velocity of the agglomerate:
VELOCITY 0.0 -0.2 0.0 1
*
FFO 0.0 0.0 100
*
CYCLE 1
print cluster data
TCYCLE 50
print cluster data
TCYCLE 50
print cluster data

.....
* save state in files:
save SI5_0
.....
(continue up to 105,000 cycles)
.....
TCYCLE 1500
print cluster data ginfo
STOP

The test was re-run several times for saving the state of simulation at important moments (e.g at the moment when the platen force was a maximum, at the primary fracture moment).

Double impact test of the dense[1] agglomerate ("RM4T1A."), V=0.02 m/s, $M_p = 100\ M_a$:

RESTART RM4T1A.
print ginfo cluster data sss
FRO
VELOCITY 0.0 0.0 0.0 1
*
*Set a fraction of the time-step:
FRACTION 0.6
*
**Place the agglomerate in a gravitational field:*
GRAVITY 0.0 -9.8 0.0
*
*Create the top platen at a timestep distance from the agglomerate:
DWALL P 1.307620E-03 0.0 1.0 0.0 M 2
*Create bottom platen to almost "touch" the agglomerate:
DWALL P 1.900806E-04 0.0 1.0 0.0 M 2
*
*Specify the mass of the top platen and
*set the vertically downwards velocity of the top platen:
AWALL 1 MASS 1.11514E-4 VELOCITY 0.0 -0.02 0.0
*
FFO 0.0 0.0 100
*
CYCLE 1
print cluster data
TCYCLE 50
print cluster data
TCYCLE 50
print cluster data
.....
* save state in files:
save SDI4_0
.....
(continue up to 180,000 cycles)
.....
TCYCLE 3000
print cluster data ginfo
STOP

The test was re-run several times for saving the state in simulation at important moments.

Diametrical compression test of the dense[2] agglomerate ("RSD1A"), V=10 mm/min:

RESTART RSD1A
print ginfo cluster data sss
FRO
FRACTION 1.0
GRAVITY 0.0 -9.8 0.0
*
* Make sure the agglomerate is stationary:
VELOCITY 0.0 0.0 0.0 1
*
*Create top and bottom platens to almost "touch" the agglomerate:
DWALL P 1.2403395E-03 0.0 1.0 0.0 M 2
DWALL P 1.8927367E-04 0.0 1.0 0.0 M 2
*
*Give a velocity of 0.000166666 m/s (half the velocity specified
*in the PPIE G001 Standard) to the top platen
AWALL 1 VELOCITY 0.0 -0.000166666 0.0
*
FFO 0.0 0.0 5000
*
CYCLE 1
print cluster data
TCYCLE 5000
print cluster data
TCYCLE 5000
print cluster data
.....
* save state in files every 50,000 cycles:
save RSDC2_0
.....
(continue up to 400,000 cycles)
.....
TCYCLE 5000
print cluster data ginfo
STOP

The test was re-run several times for saving the state in simulation at important moments.